FERTILIZATION IN THE SPOTLIGHT: DYNAMICS AND MECHANISMS OF SPERM-EGG INTERACTION

EDITED BY: Enrica Bianchi, Maria Jiménez-Movilla and Amber R. Krauchunas
PUBLISHED IN: Frontiers in Cell and Developmental Biology

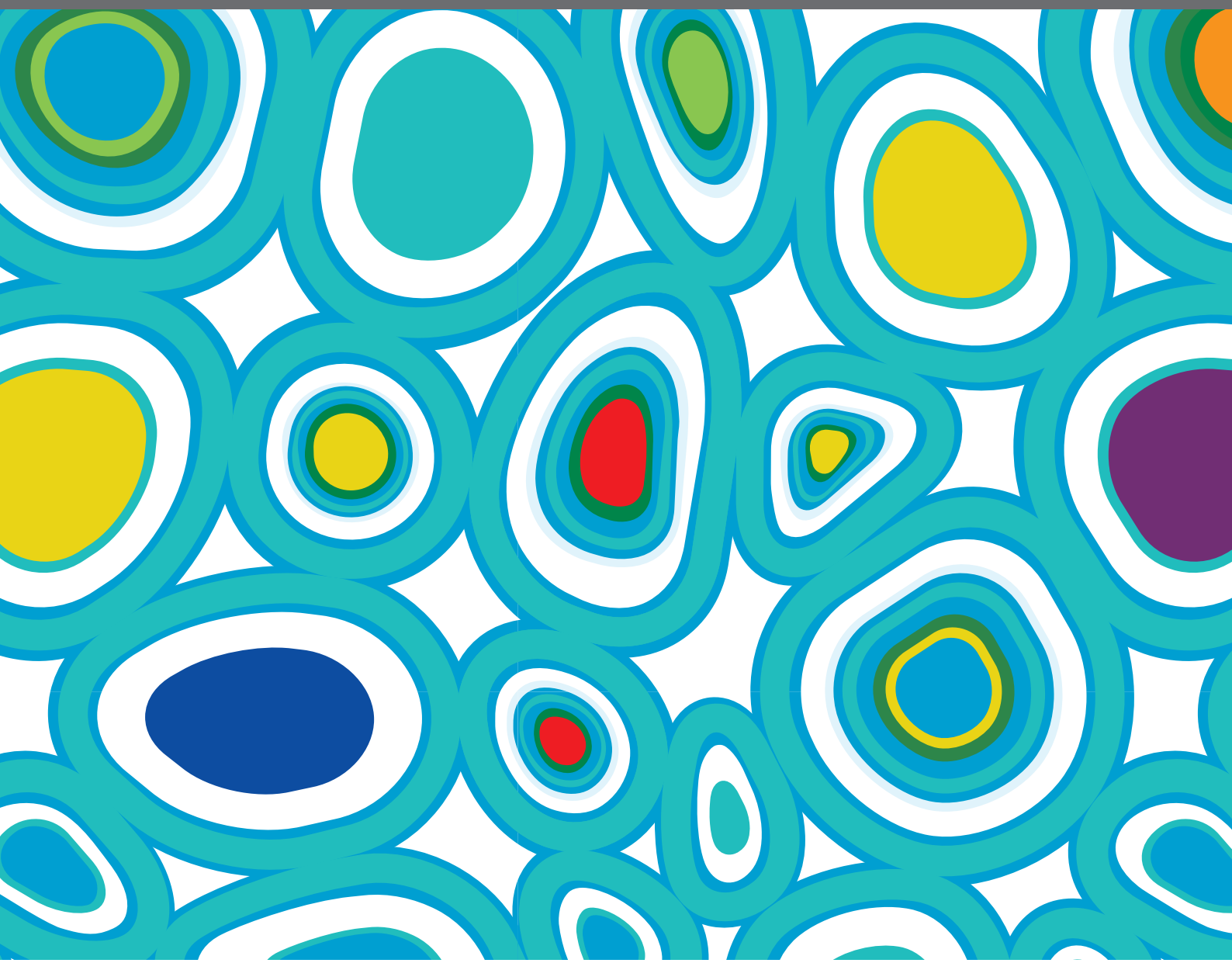

frontiers Research Topics

ISSN 1664-8714
ISBN 978-2-83250-278-5
DOI 10.3389/978-2-83250-278-5

About Frontiers

Frontiers is more than just an open-access publisher of scholarly articles: it is a pioneering approach to the world of academia, radically improving the way scholarly research is managed. The grand vision of Frontiers is a world where all people have an equal opportunity to seek, share and generate knowledge. Frontiers provides immediate and permanent online open access to all its publications, but this alone is not enough to realize our grand goals.

Frontiers Journal Series

The Frontiers Journal Series is a multi-tier and interdisciplinary set of open-access, online journals, promising a paradigm shift from the current review, selection and dissemination processes in academic publishing. All Frontiers journals are driven by researchers for researchers; therefore, they constitute a service to the scholarly community. At the same time, the Frontiers Journal Series operates on a revolutionary invention, the tiered publishing system, initially addressing specific communities of scholars, and gradually climbing up to broader public understanding, thus serving the interests of the lay society, too.

Dedication to Quality

Each Frontiers article is a landmark of the highest quality, thanks to genuinely collaborative interactions between authors and review editors, who include some of the world's best academicians. Research must be certified by peers before entering a stream of knowledge that may eventually reach the public - and shape society; therefore, Frontiers only applies the most rigorous and unbiased reviews.
Frontiers revolutionizes research publishing by freely delivering the most outstanding research, evaluated with no bias from both the academic and social point of view. By applying the most advanced information technologies, Frontiers is catapulting scholarly publishing into a new generation.

What are Frontiers Research Topics?

Frontiers Research Topics are very popular trademarks of the Frontiers Journals Series: they are collections of at least ten articles, all centered on a particular subject. With their unique mix of varied contributions from Original Research to Review Articles, Frontiers Research Topics unify the most influential researchers, the latest key findings and historical advances in a hot research area! Find out more on how to host your own Frontiers Research Topic or contribute to one as an author by contacting the Frontiers Editorial Office: frontiersin.org/about/contact

FERTILIZATION IN THE SPOTLIGHT: DYNAMICS AND MECHANISMS OF SPERM-EGG INTERACTION

Topic Editors:
Enrica Bianchi, University of York, United Kingdom
Maria Jiménez-Movilla, University of Murcia, Spain
Amber R. Krauchunas, University of Delaware, United States

Citation: Bianchi, E., Jiménez-Movilla, M., Krauchunas, A. R., eds. (2022). Fertilization in the Spotlight: Dynamics and Mechanisms of Sperm-Egg Interaction. Lausanne: Frontiers Media SA. doi: 10.3389/978-2-83250-278-5

Table of Contents

frontiers | Frontiers in Cell and Developmental Biology

TYPE Editorial
PUBLISHED 08 September 2022
DOI 10.3389/fcell.2022.993865

OPEN ACCESS

EDITED AND REVIEWED BY
Shao-Chen Sun,
Nanjing Agricultural University, China

*CORRESPONDENCE
Enrica Bianchi,
enrica.bianchi@york.ac.uk
Maria Jimenez-Movilla,
mariajm@um.es
Amber R. Krauchunas,
arkrauch@udel.edu

SPECIALTY SECTION
This article was submitted to Molecular and Cellular Reproduction, a section of the journal Frontiers in Cell and Developmental Biology

RECEIVED 14 July 2022
ACCEPTED 03 August 2022
PUBLISHED 08 September 2022

CITATION
Bianchi E, Jimenez-Movilla M and Krauchunas AR (2022), Editorial: Fertilization in the spotlight: Dynamics and mechanisms of sperm-egg interaction.
Front. Cell Dev. Biol. 10:993865.
doi: 10.3389/fcell.2022.993865

Editorial: Fertilization in the spotlight: Dynamics and mechanisms of sperm-egg interaction

Enrica Bianchi[1]*, Maria Jimenez-Movilla[2]* and Amber R. Krauchunas[3]*

[1]Department of Biology, Hull York Medical School, York Biomedical Research Institute, University of York, York, United Kingdom, [2]Department of Cell Biology and Histology, Faculty of Medicine, University of Murcia, IMIB, Murcia, Spain, [3]Department of Biological Sciences, University of Delaware, Newark, DE, United States

KEYWORDS

fertilization, sperm, egg, gamete interaction, cell fusion, acrosome

Editorial on the Research Topic
Fertilization in the spotlight: Dynamics and mechanisms of sperm- egg interaction

Fertilization has intrigued scientists for centuries and is of great interest to the general public for its wider implications in human health. Undeniably, outstanding progress has been made but many questions remain to be answered. The purpose of this Research Topic was to highlight the variety of molecular mechanisms underlying gamete interaction in sexually reproducing species and to draw attention to the long-standing open questions of fertilization.

Unicellular and multicellular species use fertilization to ensure the formation of a unique new organism that is genetically distinct from their parents. Two purposefully developed cells collectively named gametes (sperm and eggs in multicellular organisms) meet either in the external environment or in internal organs, bind to one another and fuse together to generate a viable progeny.

Thanks to decades of research we now have the ability to manipulate gametes *in vitro* and *in vivo* and to successfully achieve *in vitro* fertilization in humans as well as in many other species (Carroll, 2018). Our knowledge of the molecular mechanisms governing the sperm-egg interaction has greatly increased particularly with the advent of genetically modified animal models which contributed to identify molecules that are essential for fertilization. Among the breakthroughs of the last decade are the discovery of the first binding pair essential for mammalian fertilization (Juno and Izumo1) (Bianchi et al., 2014), and the identification of the first fusogen (a protein that induces cell fusion) named Hap2/GCS1 in plants and unicellular organisms (Johnson et al., 2004; Mori et al., 2006; von Besser et al., 2006; Liu et al., 2008). Investigations in organisms as different as C. elegans, Zebrafish, Abalone, Sea urchin (Krauchunas et al., 2016; Raj et al., 2017; Deneke and Pauli, 2021; Wessel et al., 2021)

and mammals (Bianchi and Wright, 2020) are contributing to identifying novel proteins involved in sperm-egg recognition and to unravel the dynamics of these interactions.

Even today, knowledge about the molecular mechanisms that produce the capacity of recognition, union and fusion between the two cells, the oocyte and the spermatozoa, is still very scarce and any solid contribution can help to unravel the molecular puzzle that is the origin of the zygote. On the side of spermatozoa, the research conducted by Wang et al. identified Chromosome 1 open reading frame 56 (C1orf56) to be a SLeX-binding sperm protein. They showed that purified C1orf56 from spermatozoa bound to human zona pellucida (ZP) and immunofluorescence staining localized C1orf56 to the acrosomal region of capacitated spermatozoa, a region that binds ZP. Moreover, they found that C1orf56 is relocated from the equatorial region to the acrosomal region after capacitation suggesting that C1orf56 may have functions after ZP-binding and acrosome reaction.

Two contributions unravel the role of IZUMO1 and SPACA6 using mutant sperm lacking these fusion-related genes previously demonstrated in a mouse model. The research conducted by Matsumara et al. show here that Izumo1 KO male rats are infertile due to fertilization defects. However, unlike in mice, Izumo1 knockout rat spermatozoa failed to bind to the oolemma. Moreover, reanalysis of the Izumo1 KO mice shows the percentage of the oolemma bound acrosome-reacted spermatozoa was drastically decreased in the Izumo1 KO mice compared with WT, indeed suggesting that IZUMO1 is required for binding the acrosome-reacted spermatozoa to oolemma prior to fusion. Of note, it was reported that the acrosome-reacted spermatozoa hardly bind to the JUNO KO eggs in mice (Bianchi et al., 2014). Intriguingly, this study found that, unlike sperm lacking Izumo1, sperm lacking the novel fusion-related genes Fimp, Sof1, Spaca6, or Tmem95 bind to the oolemma after the acrosome reaction. All together these data suggest that these proteins could be involved in different molecular pathways to regulate binding and/or fusion since all of them are essential to complete fertilization. The original article published by Binner et al. using the Zebrafish model shows that Spaca6 knockout males are sterile. While sperm lacking Spaca6 have normal morphology and are motile, Spaca6-deficient sperm fail to bind to the egg and therefore cannot complete fertilization. This is in contrast to murine sperm lacking SPACA6, which was reported to be able to bind but unable to fuse with oocytes (Barbaux et al., 2020; Noda et al., 2020). Moreover, here they show that Spaca6 regulates Dcst2 protein levels and interestingly, recent work in mice has shown that SPACA6 levels are decreased in sperm lacking IZUMO1, DCST1 and/or DCST2 (Inoue et al., 2021). Then authors suggest that Spaca6 may contribute to forming and/or stabilizing a multi-factor complex on the sperm membrane that regulates both binding and fusion.

The study conducted by Gonzalez-Brusi et al. identified by mass spectrometry a list of 41 sperm proteins that were pulled down with TMEM95 and none of them were sperm proteins known to play a role in fertilization, suggesting an independent role of TMEM95 in fertilization. Between these lists, they propose OLFR601 protein as a candidate to collaborate with TMEM95, as OLFR601 is allocated to the acrosomal region and may mediate affinity for an odorant involved in fertilization. However, Olfr601 disruption did not impair the sperm fertilization ability, suggesting that its function may be redundant with that of other sperm proteins. Nevertheless, more studies are needed to further investigate the complex functions of those newly identified fusion-related molecules.

Regarding the oocyte side, in silico docking analysis by Stepanenko et al. for blocking JUNO-IZUMO1 interaction identifies two molecules, Z786028994 and Z1290281203, that show fertilization inhibitory effect in both an *in vitro* fertilization assay in mice and an *in vitro* penetration of human sperm into hamster oocytes. The accumulation of sperm cells in the perivitelline space of eggs treated with molecules Z786028994 and Z1290281203 suggests that the fertilization failure seen by these two molecules is a result of inhibition of sperm–egg fusion. However, none of the molecules significantly affected the binding of JUNO and IZUMO1 using AVEXIS. Therefore, until further research is performed, the mechanism of action of these IVF inhibitors remains unclear.

In this Research Topic, three research articles focus on cellular characteristics of sperm that contribute to the sperm's fertilizing ability. Giaccagli et al. examined the relationship between mitochondrial activity and fertilizing ability of the sperm. Their results indicate that there is a rise in mitochondrial membrane potential during sperm capacitation and this mitochondrial activity is important for both *in vitro* and *in vivo* fertilization at the step of zona pellucida penetration. Ma et al. tested the role of Toll-like receptor 2 (TLR2) for sperm function and similarly concluded that TLR2 plays a role in sperm interactions with the zona pellucida and suggest that TLR2 contributes to acrosomal exocytosis in response to zona pellucida attachment. Structural analysis of acrosomal exocytosis was carried out by Leung et al. with the use of cryoelectron tomography to visualize acrosomal exocytosis in pig sperm. In addition to observing a heterogenous population of vesicles and paracrystalline patches surrounding the fully acrosome-reacted sperm, this study shows that the post-acrosomal plasma membrane becomes densely packed with membrane protein densities that were not present in unreacted cells.

To fully understand sperm-egg interactions we need to not only investigate the molecular and cellular aspects of the gametes, but to examine the evolution of reproductive genes. Two original research articles and one review in this Research Topic highlight the importance of gene duplication and diversification of sperm-expressed genes in different taxa. Carlisle et al. carried out a detailed evolutionary genomic analysis in abalone and discovered duplications of lysin and sp18 ancestral to abalone. Interestingly, they did not find evidence of recent duplications of egg coat proteins suggesting that it is not duplications on the egg side that are driving duplication and diversification of the sperm acrosomal proteins in *H. tuberculata*. Transcriptomic and proteomic analyses were carried out by Wilburn et al. to provide a molecular description of salamander gametes. Their data reveal that the sperm express paralogs of pheromone proteins suggesting these protein families

have been co-opted for multiple reproductive functions through gene duplication and rapid evolution. In addition, gene duplication and repeat domain expansion in the evolution of fertilization proteins such as Izumo, Juno, DCST, and ZP domains is reviewed by Rivera and Swanson.

Four additional reviews round out this spotlight on sperm-egg interactions. Brukman et al. review the fusexin class of fusogens within the context of structure, mechanism of action, and gamete fusion. Pinello and Clark review gamete fusion and the role of HAP2/GCS1 in *Chlamydomonas reinhardtii* and *Tetrahymena thermophila* as well as discuss the possibility of HAP2/GCS1 as a candidate for transmission-blocking vaccine development against parasitic protists. Gonzalez et al. review the role of CRISP proteins in fertility and different stages of the fertilization process discussing both genetic and non-genetic studies to dissect the functions of this protein family. Finally, Saito and Sawada review sperm-egg interactions and self/nonself-recognition at the level of the egg coat in ascidians.

The broad range of subjects in this research topic show the great effort of the scientific community in elucidating the still elusive mechanisms of fertilization. We believe that the collaboration of researchers working on various aspects of sperm-egg interaction is instrumental to unravel the molecular cascades orchestrating this event in different species and to overcome the experimental limitations of investigating gamete biology.

Author contributions

All authors listed have made a substantial, direct, and intellectual contribution to the work and approved it for publication.

Funding

Project PID 2020-114109GB-I00 to MJ-M, funded by the Spanish Ministry of Science and Innovation and FEDER funds from the European Union. EB was funded by the Biotechnology and Biological Sciences Research Council, United Kingdom (Grant BB/T006390/1).

Acknowledgments

We would like to thank all the authors and reviewers that contributed their research and expertise to this Research Topic.

Conflict of interest

The authors declare that the research was conducted in the absence of any commercial or financial relationships that could be construed as a potential conflict of interest.

Publisher's note

References

Barbaux, S., Ialy-Radio, C., Chalbi, M., Dybal, E., Homps-Legrand, M., Do Cruzeiro, M., et al. (2020). Sperm SPACA6 protein is required for mammalian Sperm-Egg Adhesion/Fusion. *Sci. Rep.* 10, 5335. doi:10.1038/s41598-020-62091-y

Bianchi, E., Doe, B., Goulding, D., and Wright, G. J. (2014). Juno is the egg Izumo receptor and is essential for mammalian fertilization. *Nature* 508, 483–487. doi:10.1038/nature13203

Bianchi, E., and Wright, G. J. (2020). Find and fuse: Unsolved mysteries in sperm–egg recognition. *PLoS Biol.* 18, e3000953. doi:10.1371/journal.pbio.3000953

Carroll, M. (2018). The road to 1978: A brief history of fertility research. *Biochem. (Lond).* 40, 4–7. doi:10.1042/BIO04003004

Deneke, V. E., and Pauli, A. (2021). The fertilization enigma: How sperm and egg fuse. *Annu. Rev. Cell. Dev. Biol.* 37, 391–414. doi:10.1146/annurev-cellbio-120219-021751

Inoue, N., Hagihara, Y., and Wada, I. (2021). Evolutionarily conserved sperm factors, DCST1 and DCST2, are required for gamete fusion. *eLife* 10, e66313. doi:10.7554/eLife.66313

Johnson, M. A., von Besser, K., Zhou, Q., Smith, E., Aux, G., Patton, D., et al. (2004). Arabidopsis hapless mutations define essential gametophytic functions. *Genetics* 168, 971–982. doi:10.1534/genetics.104.029447

Krauchunas, A. R., Marcello, M. R., and Singson, A. (2016). The molecular complexity of fertilization: Introducing the concept of a fertilization synapse. *Mol. Reprod. Dev.* 83, 376–386. doi:10.1002/mrd.22634

Liu, Y., Tewari, R., Ning, J., Blagborough, A. M., Garbom, S., Pei, J., et al. (2008). The conserved plant sterility gene HAP2 functions after attachment of fusogenic membranes in Chlamydomonas and Plasmodium gametes. *Genes. Dev.* 22, 1051–1068. doi:10.1101/gad.1656508

Mori, T., Kuroiwa, H., Higashiyama, T., and Kuroiwa, T. (2006). GENERATIVE CELL SPECIFIC 1 is essential for angiosperm fertilization. *Nat. Cell. Biol.* 8, 64–71. doi:10.1038/ncb1345

Noda, T., Lu, Y., Fujihara, Y., Oura, S., Koyano, T., Kobayashi, S., et al. (2020). Sperm proteins SOF1, TMEM95, and SPACA6 are required for sperm–oocyte fusion in mice. *Proc. Natl. Acad. Sci. U. S. A.* 117, 11493–11502. doi:10.1073/pnas.1922650117

Raj, I., Sadat Al Hosseini, H., Dioguardi, E., Nishimura, K., Han, L., Villa, A., et al. (2017). Structural basis of egg coat-sperm recognition at fertilization. *Cell.* 169, 1315–1326.e17. doi:10.1016/j.cell.2017.05.033

von Besser, K., Frank, A. C., Johnson, M. A., and Preuss, D. (2006). Arabidopsis HAP2 (GCS1) is a sperm-specific gene required for pollen tube guidance and fertilization. *Development* 133, 4761–4769. doi:10.1242/dev.02683

Wessel, G. M., Wada, Y., Yajima, M., and Kiyomoto, M. (2021). Bindin is essential for fertilization in the sea urchin. *Proc. Natl. Acad. Sci. U. S. A.* 118, e2109636118. doi:10.1073/pnas.2109636118

frontiers in Cell and Developmental Biology

ORIGINAL RESEARCH
published: 20 July 2021
doi: 10.3389/fcell.2021.700396

Identification of Sialyl-Lewis(x)-Interacting Protein on Human Spermatozoa

Ying Wang[1,2†], Weie Zhao[1,3†], Si Mei[1,4], Panyu Chen[3], Tsz-Ying Leung[1,5], Cheuk-Lun Lee[1,5], William S. B. Yeung[1,5], Jian-Ping Ou[1,6], Xiaoyan Liang[3*] and Philip C. N. Chiu[1,5*]*

[1] Department of Obstetrics and Gynecology, Queen Mary Hospital, The University of Hong Kong, Hong Kong, Hong Kong, [2] Department of Obstetrics and Gynecology, Center of Reproductive Medicine, Peking University Third Hospital, Beijing, China, [3] The Sixth Affiliated Hospital of Sun Yat-sen University, Guangzhou, China, [4] Department of Physiology, Medical College, Hunan University of Chinese Medicine, Changsha, China, [5] Shenzhen Key Laboratory of Fertility Regulation, Department of Obstetrics and Gynecology, The University of Hong Kong-Shenzhen Hospital, Shenzhen, China, [6] Center for Reproductive Medicine, The Third Affiliated Hospital, Sun Yat-sen University, Guangzhou, China

OPEN ACCESS

Edited by:
Amber R. Krauchunas, University of Delaware, United States

Reviewed by:
Pavla Postlerová, Institute of Biotechnology (ASCR), Czechia
Eveline Litscher, Icahn School of Medicine at Mount Sinai, United States

***Correspondence:**
Philip C. N. Chiu
pchiucn@hku.hk
Xiaoyan Liang
liangxy2@mail.sysu.edu.cn
Jian-Ping Ou
oujp3@mail.sysu.edu.cn

† These authors have contributed equally to this work

Specialty section:
This article was submitted to Molecular and Cellular Reproduction, a section of the journal Frontiers in Cell and Developmental Biology

Received: *26 April 2021*
Accepted: *28 June 2021*
Published: *20 July 2021*

Citation:
Wang Y, Zhao W, Mei S, Chen P, Leung T-Y, Lee C-L, Yeung WSB, Ou J-P, Liang X and Chiu PCN (2021) Identification of Sialyl-Lewis(x)-Interacting Protein on Human Spermatozoa. Front. Cell Dev. Biol. 9:700396. doi: 10.3389/fcell.2021.700396

Capacitated spermatozoa initiate fertilization by binding to the zona pellucida (ZP). Defective spermatozoa-ZP binding causes infertility. The sialyl-Lewis(x) (SLeX) sequence is the most abundant terminal sequence on the glycans of human ZP glycoproteins involving in spermatozoa-ZP binding. This study aimed to identify and characterize the SLeX-binding proteins on human spermatozoa. By using affinity chromatography followed by mass spectrometric analysis, chromosome 1 open reading frame 56 (C1orf56) was identified to be a SLeX-binding protein of capacitated spermatozoa. The acrosomal region of spermatozoa possessed C1orf56 immunoreactive signals with intensities that increased after capacitation indicating translocation of C1orf56 to the cell surface during capacitation. Treatment with antibody against C1orf56 inhibited spermatozoa-ZP binding and ZP-induced acrosome reaction. Purified C1orf56 from capacitated spermatozoa bound to human ZP. A pilot clinical study was conducted and found no association between the percentage of capacitated spermatozoa with C1orf56 expression and *in vitro* fertilization (IVF) rate in assisted reproduction treatment. However, the percentage of C1orf56 positive spermatozoa in the acrosome-reacted population was significantly ($P < 0.05$) lower in cycles with a fertilization rate < 60% when compared to those with a higher fertilization rate, suggesting that C1orf56 may have functions after ZP-binding and acrosome reaction. A larger clinical trial is needed to determine the possible use of sperm C1orf56 content for the prediction of fertilization potential of sperm samples.

Keywords: zona pellucida, human spermatozoa, sialyl-Lewis(x), C1orf56, fertilization rate

INTRODUCTION

Human oocytes are surrounded by a ∼7–20 μm thick porous cellular extracellular matrix termed zona pellucida (ZP), which is the main player in spermatozoa-oocyte interactions and species-specific fertilization. Spermatozoa-ZP binding is the first event in fertilization. Defective spermatozoa-ZP binding leads to infertility and is an important cause of reduced fertilization rates

in assisted reproduction (Liu and Baker, 2000). A meta-analysis has shown high predictive power of spermatozoa-ZP binding on fertilization outcome (Oehninger et al., 2000). Defective spermatozoa-ZP binding is more frequent for men with abnormal semen parameters, especially those with severe teratozoospermia and oligozoospermia (Liu and Baker, 2004). Despite the importance of spermatozoa-ZP interaction, the mechanisms regulating the process are unclear partly due to failure in the identification of ZP receptor(s) on human spermatozoa.

Human ZP is composed of four glycoproteins namely ZP glycoprotein 1 (ZP1), ZP2, ZP3, and ZP4 (Chiu et al., 2014). Glycan chains are found on the asparagine (N-linked) and serine/threonine (O-linked) residues of these ZP glycoproteins. We have identified sialyl-Lewis(x) (SLeX) [NeuAcα2–3Galβ1-4(Fucα1–3)GlcNAc] as the most abundant terminal sequence on the N-linked glycans of human ZP (Pang et al., 2011). Human oocyte–spermatozoon binding involves both protein-protein and protein-glycans interactions (Chiu et al., 2014; Gupta, 2021).

Recent transgenic mice studies suggested that ZP2 is the primary ligand for human sperm binding to ZP (Baibakov et al., 2012; Avella et al., 2014, 2016). Human spermatozoa bind to and penetrate the ZP of oocytes from transgenic mice carrying the four human ZP glycoproteins in place of the three mouse ZP glycoproteins (Baibakov et al., 2012). When human ZP2 is absent from these mice, human spermatozoa rarely bind to the oocytes (Avella et al., 2014). It is noted that the human spermatozoa take 180–240 min to bind onto the mouse ZP containing human ZP2 (Baibakov et al., 2012), which was much longer than 15–60 min for binding to human ZP (Plachot et al., 1986; Morales et al., 1994). The slower binding kinetics could be due to inappropriate glycosylation of human ZP2 in the mice, consistent with differential interaction of human spermatozoa to recombinant human ZP2 and native ZP2 with different glycosylation (Chiu et al., 2014; Gupta, 2021).

Several glycoconjugates have been associated with human spermatozoa-ZP binding (Chiu et al., 2014; Gupta, 2021). For example, glycoconjugates terminated with the SLeX sequences or antibodies against the sequence inhibited the spermatozoa-ZP binding (Pang et al., 2011). Synthesized highly complex triantennary N-glycans with SLeX moieties have increased inhibitory activities (Chinoy and Friscourt, 2018). Spermatozoa-SLeX interaction has been used to capture human spermatozoa in a microfluidic system for forensic investigation (Inci et al., 2018; Deshmukh et al., 2020). The ZP glycans may take part in direct interaction with the sperm ZP receptors or may provide the proper tertiary structure that maximizes the availability of the ZP glycoproteins to their receptors on spermatozoa.

The identity of human sperm ZP receptor(s) is controversial (Gupta, 2018; Tumova and Zigo, 2021). Several human sperm carbohydrate-binding proteins have been proposed (Chiu et al., 2007b). However, antibodies against and competitors/substrates of these molecules fail to completely block spermatozoa-ZP binding and/or ZP-induced acrosome reaction, suggesting that they are not solely mediating spermatozoa-ZP binding. The objective of this study was to identify and characterize the human sperm SLeX-binding proteins.

MATERIALS AND METHODS

Semen and Oocyte Samples

The Ethics Committee of the University of Hong Kong/Hospital Authority Hong Kong West Cluster approved the research protocol. Informed consent was obtained from patients who donated their semen and oocyte samples for research use. Human spermatozoa were collected by masturbation from patients attending the infertility clinic at the Queen Mary Hospital and the Family Planning Association, Hong Kong (Mei et al., 2019). Only semen samples with normal semen parameters according to the World Health Organization (2010) criteria (strict criteria >4%, volume >1.5 ml, total sperm number $>39 \times 10^6$ per ejaculate, concentration $>15 \times 10^6$/ml, total motility >40%, progressive motility >32%, and vitality >58%) were used. Spermatozoa were processed by density gradient centrifugation using AllGrad (LifeGlobal, Brussels, Belgium) and resuspended in Earle Balanced Salt Solution (EBSS; Flow Laboratories, Irvine, United Kingdom) supplemented with 0.3% bovine serum albumin (BSA), 0.3 mmol/l sodium pyruvate, 0.16 mmol/l penicillin-G, 0.05 mmol/l streptomycin sulfate, and 14 mmol/l sodium bicarbonate (all from Sigma, St Louis, MO, United States) (EBSS/0.3% BSA) to a concentration of 2×10^6 spermatozoa/ml. Capacitated spermatozoa were prepared by a 3-h incubation in EBSS supplemented with 3% BSA as previously described (Chiu et al., 2010).

For the pilot clinical study, semen samples were collected from men whose female partner underwent conventional IVF treatment at the Sixth affiliated Hospital of the Sun Yat-sen University, Guangzhou, China. The research protocol of the study was approved by the Ethics Committee of the Sun Yat-sen University. Semen samples were prepared by density gradient centrifugation followed by a standard swim-up procedure World Health Organization (2010). Briefly, 1 mL EBSS/0.3%BSA medium was gently layered over the processed spermatozoa pellet in a sterile 15 mL centrifuge tube after density gradient centrifugation. The tube was inclined at 45° and incubated for 1 h at 37°C. The upper 0.5 mL medium was collected for IVF treatment and the remaining sperm suspension was used for experimentation. After washing with EBSS/0.3%BSA once, the final sperm pellet was resuspended in 1 mL EBSS/0.3%BSA. The motility and morphology of the spermatozoa were then determined.

Human oocytes were collected from the Assisted Reproduction Program at the Queen Mary Hospital, Hong Kong. Unfertilized metaphase II oocytes from couples who underwent intracytoplasmic sperm injection were collected and stored in an oocyte storage buffer at 4°C. The oocyte storage buffer contained 1.5 M $MgCl_2$, 0.1% polyvinyl pyrrolidone (PVP) and 40 mM HEPES with pH 7.2.

Determination of Sperm Viability

Sperm viability was determined by the trypan blue exclusion staining. Processed spermatozoa (2×10^5) and trypan blue dye were mixed in a 1:1 ratio to a final volume of 12 μL. The mixture was placed on a glass slide for 3 min before examination

under a light microscope with 400 × magnification. Viable spermatozoa were transparent without staining, whereas non-viable spermatozoa were stained blue. At least 200 spermatozoa were randomly counted to evaluate the sperm viability of the sample.

Determination of Sperm Motility

The Hobson sperm tracker system (Hobson Tracking Systems Ltd., Sheffield, United Kingdom) was used to determine the sperm motility parameters in all the experiments except the clinical study. The set-up parameters of the system and the procedures were described previously (Huang et al., 2013). Each measurement was performed on a warmed microscope stage at 37°C. Five hundred spermatozoa per sample in randomly selected fields were evaluated to determine (1) average path velocity (VAP, μm/s), (2) curvilinear velocity (VCL, μm/s), (3) straight-line velocity (VSL, μm/s), (4) beat cross frequency (BCF, Hz), (5) amplitude of lateral head displacement (ALH, μm), (6) mean linearity (LIN, VSL/VCL), (7) straightness (STR, VSL/VAP), (8) percentage hyperactivation (HYP), and (9) percentage progressive motility (VAP $\geq$ 25 μm/s). All samples were processed in triplicate.

Manual sperm motility counting based on the WHO recommended protocol (World Health Organization, 2010) was also used. In manual counting, 2×10^5 processed spermatozoa were added on a glass slide and observed under a light microscope at 400 × magnification. At least 200 spermatozoa were counted randomly. Their motilities were divided into three classes according to the WHO criteria (World Health Organization, 2010), namely progressive motile (PR), non-progressive motile (NP) and immotile (IM). PR were spermatozoa moving actively, either linearly or in a large circle. NP were those exhibiting all other patterns of motility and without progression; IM were those without movement. In this study, total motility referred to the sum of PR and NP spermatozoa. The WHO reference value of total motility is >40%. For comparison purposes, the samples were divided into a high motility group and a low motility group when their total motility was >40% and ≤40%, respectively.

Determination of Sperm Morphology

Diff-Quik staining was used to determine sperm morphology. In general, 10 μL of semen was smeared on a glass slide, air-dried at room temperature and placed successively in the Diff-Quik fixative (Microptic S.L., Barcelona, Spain) for 10 s, the Diff-Quik solution I for 15 s, and the Diff-Quik solution II for 15 s at room temperature. The slides were then placed under running water to remove excess stain and air-dried at room temperature. The morphology of spermatozoa was determined under a light microscope at 1,000 × magnification. For each sample, 200 spermatozoa in randomly selected fields were counted. Only spermatozoa with both head and tail seen were assessed. The samples were considered normal when the percentage of spermatozoa with normal morphology as defined by strict criteria (World Health Organization, 2010) was >4%.

Hemizona Binding Assay

The hemizona binding assay was performed as described (Yao et al., 1998). Unfertilized oocytes were micro-bisected into two identical hemizona. Each hemizonae was incubated with 2×10^5 spermatozoa/mL in a 100 μL droplet of EBSS/0.3%BSA under mineral oil for 3 h at 37°C in an atmosphere of 5% CO_2. After incubation, the loosely bound spermatozoa were removed by several washes with EBSS/0.3% BSA and the numbers of tightly bound spermatozoa on the outer surface of the hemizona were counted. The results are expressed as hemizona index (HZI), which is the ratio of the number of bound spermatozoa in the test droplet to that in the control droplet × 100.

Determination of Ionophore and ZP-Induced Acrosome Reaction

Purification of solubilized ZP was performed as described (Chiu et al., 2010). Briefly, the ZP was separated from the oocytes under a microscope and heat-solubilized at 70°C in 5 mM NaH_2PO_4 buffer (pH 2.5) for 90 min. Capacitated spermatozoa at a concentration of 2×10^6 spermatozoa/ml were incubated with solubilized ZP (1 μg/ml, 60 min) or ionophore A23187 (2.5 μM, 30 min) at 37°C in an atmosphere of 5% CO_2 in air (Chiu et al., 2008a). The acrosomal status of the treated spermatozoa was then evaluated.

Determination of Acrosomal Status

The percentage of capacitated spermatozoa was assayed by chlortetracycline staining (CTC) as described (Chiu et al., 2005). The capacitation status of 200 spermatozoa were evaluated under a fluorescence microscope (Zeiss, Oberkochen, Germany) at × 630 magnification. Five CTC staining patterns of the sperm head were identified (Chiu et al., 2005). CTC4 pattern (uniform head fluorescence) was the main capacitated pattern.

Fluorescein isothiocyanate-labeled *Pisum sativum* (FITC-PSA) (Sigma, St Louis, MO, United States) was used to determine acrosome reaction. Processed spermatozoa (0.5×10^6) were fixed in 300 μl of 95% ethanol and dried on slides before staining with Hoechst 33258 [Pentahydrate (bis-Benzimide); Sigma] and 2 μg/20 μL FITC-PSA in PBS for 30 min. The slides were then washed, mounted in glycerol containing 0.2 M n-propyl gallate (Sigma), and observed under a fluorescent microscope (Zeiss). At least 200 spermatozoa were randomly selected and counted under the microscope with 400 × magnification. Acrosome-reacted spermatozoa were defined as those without Hoechst and FITC-PSA staining or with FITC-PSA staining at the equatorial segment only. The filter set used for CTC and FITC-PSA staining consisted of an excitation filter BP 450-490, a chromatic beam splitter FT510 and a barrier filter LP520.

Purification of Sialyl-Lewis(x) Binding Protein

Sialyl-Lewis(x) -binding proteins on the plasma membrane of capacitated spermatozoa were identified by our established chromatographic method using SLeX-BSA neoglycoprotein affinity column followed by mass spectrometric analysis as described (Chiu et al., 2007a; Lee et al., 2011). In brief,

capacitated spermatozoa (100×10^6) were washed thrice in EBSS. Non-integral, peripheral membrane-associated proteins on spermatozoa were removed by incubation of the washed spermatozoa in 1 M NaCl in PBS with gentle stirring for 10 min at 25°C as described (Chiu et al., 2007a). The spermatozoa were then collected by centrifugation at $600 \times g$ for 10 min before extraction of the sperm plasma membrane proteins by the ProteoExtract Native Membrane Protein Extraction Kit (Merck, Kenilworth, NJ, United States) according to the manufacturer's instructions. The insoluble fraction was discarded after centrifugation at $15{,}000 \times g$ for 40 min. The supernatant was diluted in a solution of MOPS-NaOH buffer (pH 7.3) containing 0.2% Triton X-100 and 6 mM $MnCl_2$. SLeX-BSA (Dextra, Reading, United Kingdom) conjugated sepharose beads (GE Healthcare) were used to precipitate the SLeX-binding protein from the extracted membrane protein fractions. Lewis(x) (LeX)-BSA, which did not bind to human spermatozoa (Chiu et al., 2012) was used as a control.

Tryptic In-Solution Digestion

The purified SLeX-binding proteins were precipitated in precooled acetone and collected as a pellet after centrifugation at $16{,}000 \times g$ for 10 min followed by removal of the supernatant. Trypsin digestion of the pellets was performed as described (Ye et al., 2015). The digestion was terminated by acidification with 1% trifluoroacetic acid. The supernatant was then saved until use.

Two-Dimensional Liquid Chromatography With Tandem Mass Spectrometry

The Proteomic Laboratory for System Biology Research (Baptist University, Hong Kong, People's Republic of China) performed 2D LC-MS/MS analyses on the purified samples. The liquid chromatographic separation was conducted in a nano-liquid chromatography system (Dionex UltiMate 3000 Nano-LC System; Dionex). For the first dimension, two buffers were used to set up a gradient for separation: buffer A was 20% acetonitrile/10 mM potassium dihydrogen phosphate, pH 3.0; buffer B was buffer A plus 0.5 M potassium chloride. Peptides were injected into a 50×1.0 mm polysulfoethyl A strong cation exchange column (Poly LC Inc.) and eluted at a flow rate of 30 μL/min with increasing salt concentrations (100% buffer A and 0% buffer B from 0 to 10 min; 70% buffer A and 30% buffer B from 10 to 40 min; 65% buffer A and 35% buffer B from 40 to 45 min, 0% buffer A, and 100% buffer B from 45 to 50 min). Fractions were collected every 5 min.

The 2D LC separation was performed in the same nano-LC system with a reverse-phase column (Pepmap C18, 75 μm × 150 mm; Dionex). Two buffers were used for this step: buffer C was 0.05% trifluoroacetic acid and buffer D was 80% ACN/0.04% trifluoroacetic acid. Each fraction from the strong cation exchange column was injected into a reversed-phase column with a 100-min linear gradient (a 90-min gradient from 0 to 35% buffer D; 5 min from 35% buffer D to 50% buffer D; and a 5-min holding at 90% buffer D). Matrix-assisted laser desorption ionization (MALDI) spot was applied every 30 s, and the MS/MS analysis was performed in a Bruker Autoflex III MALDI Tandem Time-of-Flight (MALDI TOF/TOF) Mass Spectrometer (Bruker Daltonics).

Analysis of MS Data

Mascot (version 2.2.04[1]) was used to identify the peptides. Each MS/MS spectrum was searched against the Human IPI Protein Database 3.71. Proteins were considered to be successfully identified when the total Mascot score reached 65 or above.

Expression and Localization of Sperm C1orf56

Uncapacitated and capacitated spermatozoa (2×10^6) were extracted by SDS, resolved by 10% SDS-PAGE and blotted on polyvinylidene difluoride membranes. Western blotting was performed using a rabbit polyclonal anti-chromosome 1 open reading frame 56 (C1orf56) antibody (0.1 μg/mL; Sigma). Anti-beta-tubulin antibody (Sigma) was used to determine sample loading. Quantification of protein bands normalized with respect to the tubulin control was carried out with the Image J 1.49 software[2].

For immunostaining and cytometry analysis, human spermatozoa were mildly fixed in 0.5% paraformaldehyde for 10 min at room temperature (Chiu et al., 2008b) followed by incubation with polyclonal anti-C1orf56 antibody (1 μg/mL; Sigma) overnight at 4°C. The bound antibodies were detected by the Alexa Fluor 488/555-conjugated goat anti-rabbit IgG (Invitrogen, CA, United States). For simultaneous staining, the slides were washed, further immersed for 1 min in ice-cold methanol for cell permeabilization and incubated with FITC-PSA for 9 min following our established protocol (Chiu et al., 2008b). After washing, the spermatozoa were examined under a fluorescence microscope (Zeiss) with 600 × magnification or a flow cytometer (BD FACSCanto II Analyzer; BD Biosciences). The flow cytometry data were evaluated with the use of the Flowjo software (Tree Star).

Effects of Anti-C1orf56 Antibody on Sperm Functions

Capacitated spermatozoa (2×10^6/mL) were pre-incubated in medium supplemented with functional blocking anti-C1orf56 antibody (0.01, 0.1 or 1 μg/mL; Sigma) at 37°C in a 5% CO_2 atmosphere for 1 h. Isotypic-matched antibody (non-specific rabbit IgG; Invitrogen) was used as control. The spermatozoa were washed with fresh EBSS/0.3% BSA before evaluation of their viability and motility, acrosomal status, ZP-induced acrosome reaction and ZP binding capacity as described above. To study the effect of anti-C1orf56 antibody treatment on the binding capabilities of the capacitated spermatozoa to SLeX, capacitated spermatozoa (5×10^7) were incubated with 0.5 μM Alexa Fluor-594 labeled SLeX-BSA in the presence of 1 μg/ml anti-C1orf56 antibody for 120 min followed by the flow cytometry analysis.

[1] http://www.matrixscience.com

[2] http://imagej.nih.gov/ij/index.html

Purification of C1orf56 on Human Spermatozoa

C1orf56 on human spermatozoa was purified by immuno-affinity chromatography. To prepare the anti-C1orf56 affinity column, cyanogen bromide activated Sepharose 4 Fast Flow gel beads (GE Healthcare) were swelled in the swelling buffer (1 mM HCl) for 30 min, and washed with 10 gel volumes of the same buffer. Antibody coupling was done by incubation of 1 mg of anti-C1orf56 antibodies (Sigma) with 0.5 mL of swelled cyanogen bromide beads in coupling buffer overnight at 4°C with gentle shaking. The coupled affinity column was then washed with blocking buffer (0.2 M glycine, pH 8.0) before further blocking in the same buffer overnight at 4°C. The blocked affinity column was then washed successively with the coupling buffer and the acetate buffer (0.1 M sodium acetate, 0.5 M NaCl, and pH 4.0) for four times. Finally, the affinity column was washed twice with Tris-buffered saline (TBS: 25 mM Tris, 3 mM KCl, and 140 mM NaCl, pH 7.4; USB corporation, Cleveland, OH, United States) and kept at 4°C until use.

The extracted membrane proteins (see above) of capacitated spermatozoa (5×10^7) were loaded onto the anti-C1orf56 antibody coated Sepharose column and washed successively by TBS, 1 M NaCl with 1% isopropyl alcohol, 10 mM ammonium acetate with 0.1% isopropyl alcohol (pH 5.0), and TBS. The bound C1orf56 was eluted with 0.1% trifluoroacetic acid. The concentration of the purified C1orf56 was determined by a protein assay kit (Bio-Rad, Hercules, CA, United States). The purity of C1orf56 was checked by SDS-PAGE and western blotting.

Binding of C1orf56 to Zona Pellucida

Purified C1orf56 was labeled with Alexa Fluor-594® (Alexa Fluor 594 Protein Labeling Kit; Molecular Probes). Matched hemizona were incubated with 1 μg/mL labeled C1orf56 in the presence or absence of the anti-C1orf56 neutralizing antibody (Sigma) for 3 h at 37°C in an atmosphere of 5% CO_2. The binding was then observed under a fluorescence microscope.

Ovarian Stimulation and *in vitro* Fertilization

Couples attending the infertility clinic at the Sixth Affiliated Hospital of Sun Yat-sen University from January, 2016 to March, 2017 were recruited in this study. The standard gonadotrophin-releasing hormone agonist long protocol was used. Conventional insemination was performed 4 h after oocyte retrieval, and the fertilization check was conducted after 16–18 h. Normal fertilization was indicated by the appearance of two pronuclei (2PN). Fertilization rate was defined as the number of 2PN zygotes observed divided by the total number of inseminated oocytes × 100.

Data Analyses

All values were expressed as mean ± standard error of the mean (SEM). For all experiments, the non-parametric rank sum test for comparisons was used to identify differences between groups. If the data were normally distributed, parametric Student *t*-test was used as the posttest. The data were analyzed by SPSS 20.0 (IBM) and P-value < 0.05 was considered as statistically significant.

RESULTS

Identification of Potential SLeX-Binding Proteins

Mass spectrometry analysis of the SLeX-BSA affinity purified sperm membrane fraction identified a total of 59 proteins with Mascot protein score higher than 65[3]. Proteins were selected for studies when they were absent in the LeX-BSA (Dextra) affinity purified fraction and when they had been reported to be present only in human sperm head region. Only 4 proteins met these criteria. They were chromosome 1 open reading frame 56 (C1orf56), ZP-binding protein 1 (ZPBP1), heat shock-related 70 kDa protein 2 (HSPA2) and sperm acrosome membrane-associated protein 1 (SPACA 1) (**Figure 1**). ZPBP1 (Lin et al., 2007), HSPA2 (Huszar et al., 2000), and SPACA1 (Hao et al., 2002) are known to be involved in spermatozoon-oocyte interaction. In this report, C1orf56 was investigated for its role in spermatozoa-ZP interaction.

Presence of C1orf56 in Human Spermatozoa

The percentage of capacitated spermatozoa increased from 16.86 ± 3.0% to 61.43 ± 4.8% ($N = 10$) (**Supplementary Figure 1**) after capacitation, as demonstrated by chlortetracycline staining (Chiu et al., 2005). The anti-C1orf56 antibody recognized a major protein band of size ∼39 kDa in the human sperm extract (**Figure 2**). Densitometric analysis of Western blot (**Figure 2A**) showed the presence of a comparable amount of C1orf56 in the uncapacitated and capacitated spermatozoa. Another band of 65 kDa was also found which might represent the non-specific binding of the antibodies to the albumin which were abundant in the sperm culture medium. Similar observation on the sperm C1orf56 expression was found in flow cytometric analysis (**Figure 2B**); the percentage of uncapacitated and capacitated spermatozoa with positive C1orf56 immunoreactivities were 19.6 ± 4.6% and 17.5 ± 4.2%, respectively.

Immunostaining for C1orf56 was performed on non-permeabilized uncapacitated, capacitated and acrosome reacted spermatozoa (**Figure 3**). Most uncapacitated C1orf56-positive spermatozoa (69.2 ± 4.8%) exhibited immunoreactive signals on the equatorial region. After capacitation, strong signals were observed in the acrosomal region (18.1 ± 3.3%). Calcium ionophore treatment significantly induced acrosome reaction of the capacitated spermatozoa (7.62 ± 1.9% vs. 45.82 ± 7.8%; $N = 5$) (**Supplementary Figure 1**). The fluorescence signals on the acrosomal region became much weaker after ionophore-induced acrosome reaction (**Figure 3B**). This observation was further confirmed by simultaneous staining with antibody against C1orf56 and FITC-PSA (**Supplementary Figure 2**). The observation suggests translocation of C1orf56 to sperm surface during capacitation, which is lost after acrosome reaction.

[3]https://doi.org/10.25442/hku.14677797.v1

IPI00550533 Mass: 37259 Score: 115 Queries matched: 7 emPAI: 0.29
Tax_Id=9606 Gene_Symbol=C1orf56 Isoform 1 of Uncharacterized protein C1orf56

Query	Observed	Mr(expt)	Mr(calc)	Delta	Miss	Score	Expect	Rank	Peptide
2317	422.9000	843.7854	842.4974	1.2881	0	7	24	6	R.VGALSQLR.T
6328	652.3000	1302.5854	1302.6568	-0.0713	0	60	0.00029	1	R.FIANSQEPEIR.L 6341
8504	788.3000	1574.5854	1574.7536	-0.1682	0	42	0.018	1	R.ELPSATPNTAGSSSTR.F 8505
11828	880.0000	2636.9782	2637.2002	-0.2220	1	53	0.00034	1	R.SSAINEEDGSSEEGVVINAGKDSTSR.E 11829

IPI00013006 Mass: 40971 Score: 104 Queries matched: 11 emPAI: 0.36
Tax_Id=9606 Gene_Symbol=ZPBP Zona pellucida-binding protein 1

Query	Observed	Mr(expt)	Mr(calc)	Delta	Miss	Score	Expect	Rank	Peptide
3426	517.8000	1033.5854	1033.5808	0.0046	0	19	5.1	1	K.IVGSTSFPVK.A
6828	675.8000	1349.5854	1349.7092	-0.1237	0	32	0.23	1	R.FFNQQVEILGR.R 6827
7582	480.3000	1437.8782	1436.7558	1.1223	0	24	1.1	1	K.SPHVLCVTQQLR.N 7566
9466	883.4000	1764.7854	1763.8519	0.9336	0	30	0.25	1	R.NAELIDPSFQWYGPK.G 9465
10272	978.3000	1954.5854	1954.7794	-0.1940	0	37	0.0088	1	K.CPECCVICSPGSYNPR.D 10273 10274 10279

IPI00007702 Mass: 70263 Score: 103 Queries matched: 12 emPAI: 0.20
Tax_Id=9606 Gene_Symbol=HSPA2 Heat shock-related 70 kDa protein 2

Query	Observed	Mr(expt)	Mr(calc)	Delta	Miss	Score	Expect	Rank	Peptide
2827	465.8000	929.5854	929.5004	0.0850	0	19	5.3	1	R.VCNPIISK.L
5112	614.8000	1227.5854	1227.6207	-0.0353	0	32	0.23	1	K.VEIIANDQGNR.T 5113
5365	627.8000	1253.5854	1252.6088	0.9767	0	1	2.7e+002	2	R.FEELNADLFR.G
6452	658.3000	1314.5854	1314.6455	-0.0601	0	21	2.3	1	K.NALESYTYNIK.Q
7937	744.3000	1486.5854	1486.6940	-0.1086	0	44	0.012	1	R.TTPSYVAFTDTER.L 7938 7939
8952	830.4000	1658.7854	1658.8879	-0.1024	0	45	0.0082	1	R.IINEPTAAAIAYGLDK.K
9116	846.3000	1690.5854	1690.7183	-0.1329	0	15	5.5	1	K.STAGDTHLGGEDFDNR.M 9114
10775	703.0000	2105.9782	2106.0633	-0.0851	1	1	1.9e+002	7	R.FEELNADLFRGTLEPVEK.A

IPI00008910 Mass: 32693 Score: 88 Queries matched: 9 emPAI: 0.21
Tax_Id=9606 Gene_Symbol=SPACA1 Sperm acrosome membrane-associated protein 1

Query	Observed	Mr(expt)	Mr(calc)	Delta	Miss	Score	Expect	Rank	Peptide
7729	731.3000	1460.5854	1460.6970	-0.1115	0	68	4.2e-005	1	K.FTVYTSSELQMR.R 7730
7733	731.3000	1460.5854	1459.6977	0.8878	0	17	6.2	1	R.EVILTNGCPGGESK.C 7731 7732
8055	752.8000	1503.5854	1503.7165	-0.1311	0	17	4.8	1	K.ASTPEVQSEQSSVR.Y
10664	692.3000	2073.8782	2073.9790	-0.1008	0	14	8.4	1	R.GPTDCGWGKPISESLESVR.L 10663
11839	661.8000	2643.1709	2643.2850	-0.1141	1	8	22	1	R.KESHPLAFECDTLDNNEIVATIK.F

FIGURE 1 | Identification of SLeX/LeX-binding proteins from sperm membrane protein extracts using SLeX/LeX-BSA affinity chromatography followed by MALDI-TOF-MS/MS. Sperm membrane protein extracts were purified by membrane protein extraction kit (ProteoExtract native membrane protein Extraction Kit; Merck). Each MS/MS spectrum was searched against the Human IPI Protein Database 3.71.

Anti-C1orf56 Antibody inhibited Spermatozoa-Zona Pellucida and -SLeX Binding

Treatment with anti-C1orf56 antibody at a concentration of 1 μg/ml significantly ($P < 0.05$) decreased the number of capacitated spermatozoa bound onto hemizona (**Figure 4A**) when compared to the untreated control spermatozoa or those treated with isotypic-matched antibody. The treatment also suppressed spermatozoa-SLeX binding (**Figure 5**) and ZP-induced acrosome reaction of capacitated spermatozoa (**Figure 4B**) significantly. The antibody at the concentration used did not affect sperm viability, motility and acrosomal status (**Supplementary Figures 3–5**).

Purified C1orf56 Bound to Human Zona Pellucida

C1orf56 with molecular size ∼39 kDa was significantly enriched from spermatozoa by affinity chromatography (**Figure 6A**). Fluorescence-labeled C1orf56 bound to the ZP of human oocytes specifically (**Figure 6B**). There were impurities in the partially purified C1orf56 fraction as demonstrated by SDS-PAGE. The impurities may be due to non-specific interaction of the cyanogen bromide activated Sepharose 4 with other proteins eluted together with C1orf56 during purification (Kennedy and Barnes, 1980). In order to demonstrate the specific action of c1orf56 on binding to ZP, we included a control study using neutralizing antibody against c1orf56 (**Figure 6B**). The bound signal diminished in the presence of the neutralizing antibody. To increase the purity of the isolated C1orf56, further purification steps, such as ion exchange chromatography, and gel filtration, were required.

The Relationship Between C1orf56 Surface Expression and Fertilization Rates

The association of C1orf56 surface expression with fertilization rate (FR) was investigated. Flow cytometry analysis was used to detect the surface expression of C1orf56 in spermatozoa. In this analysis, the samples were divided into a high FR group with fertilization rate is ≥60% and a low FR group with fertilization rate <60%. There was no significant difference in the percentage of capacitated spermatozoa with surface C1orf56 expression between the high and the low FR group ($P > 0.05$, **Figure 7A**). In the acrosome reacted spermatozoa population (**Figure 7B**), there

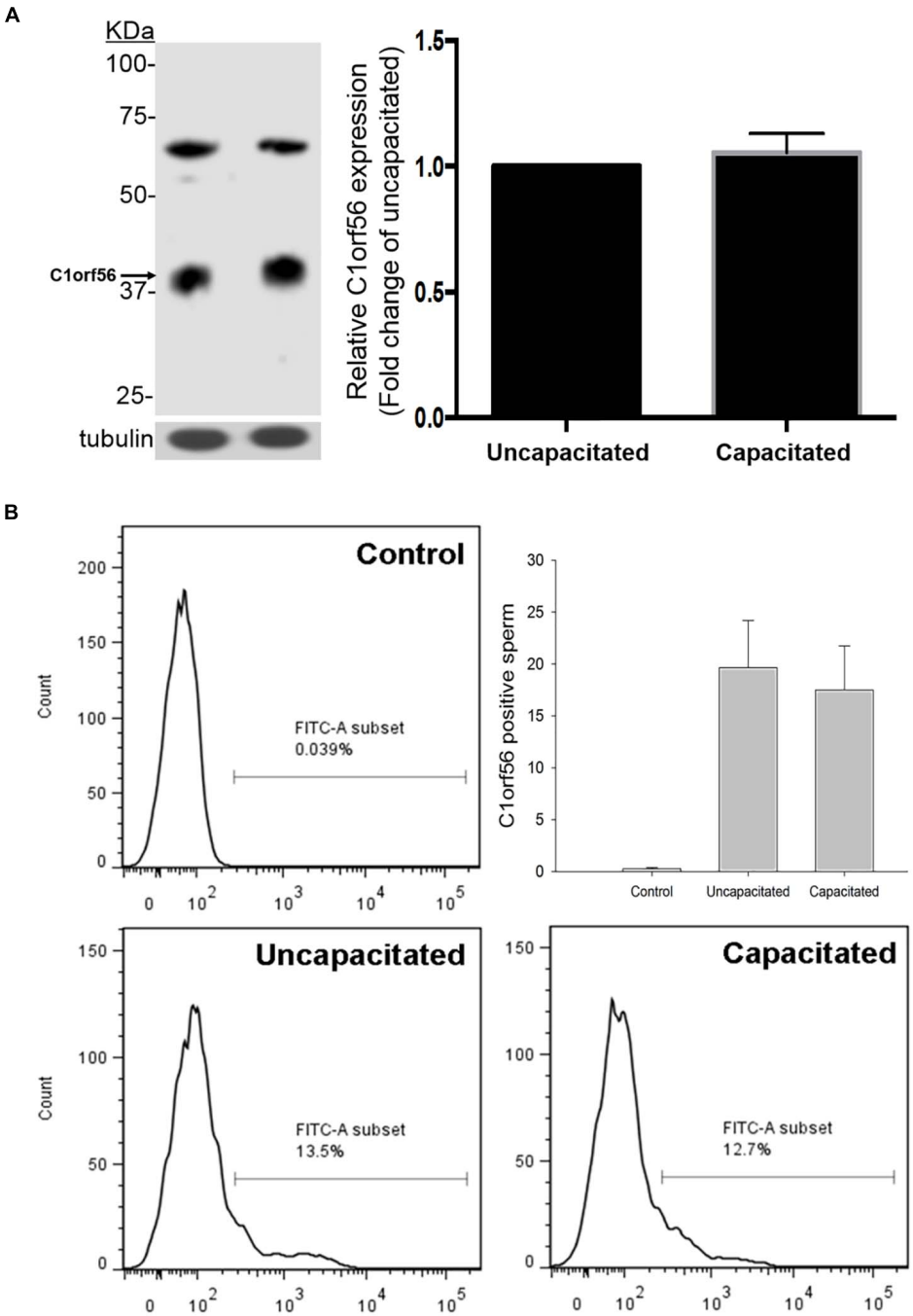

FIGURE 2 | Uncapacitated and capacitated spermatozoa possess similar levels of C1orf56 expression. **(A)** Washed spermatozoa (2×10^6) were lysed and resolved in 10% SDS-PAGE followed by Western blotting using anti-C1orf56 antibody. Sample loading was revealed by anti-tubulin antibody. Semi-quantitative comparison of C1orf56 expression between uncapacitated and capacitated sperm samples in Western blotting was also shown. **(B)** Flow cytometry analysis of the C1orf56 surface expression on uncapacitated and capacitated sperm. Spermatozoa were first incubated with 1 μg/mL anti-C1orf56 antibody or isotypic-matched antibody from the same species (control) followed by Alexa Fluor-488 fluorescence-conjugated secondary antibody. All data are represented as mean ± standard error of the mean (SEM) ($N = 5$).

was a significantly lower C1orf56 expression in the low FR group when compared to the high FR group.

The relationship between the C1orf56 expression and sperm motility and morphology were also studied. When the samples were divided into a high motility group (Total motility >40%) and a low motility group (total motility ≤40%), there was no difference between the two groups (**Supplementary Figure 6**). Similarly, there was no difference in both the

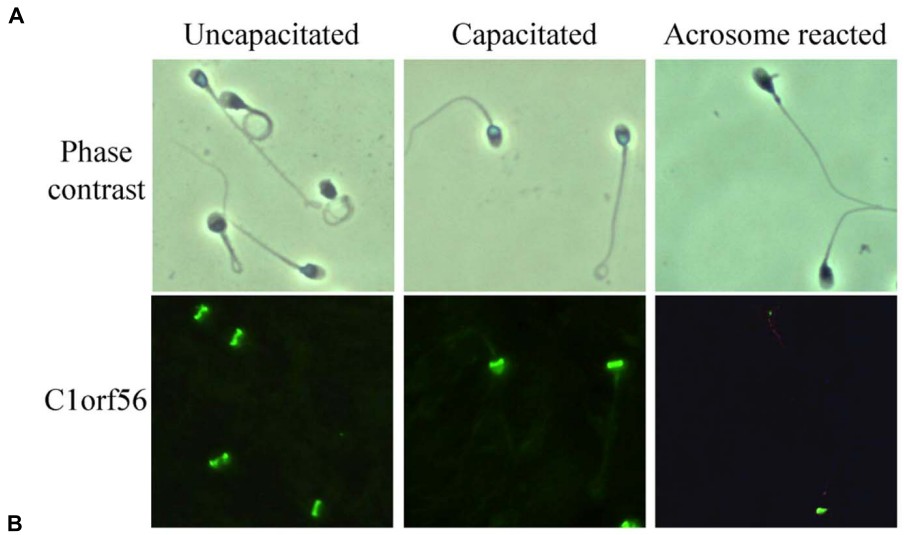

B

Treatment	A-E+	A+E+	A-E-
UN	69.2 ± 4.8	7.3 ± 1.2	22.5 ± 2.4
CAP	61.2 ± 5.3	18.1 ± 3.3*	19.7 ± 1.6
AR	53.3 ± 5.4	4.4 ± 1.0	38.6 ± 2.9

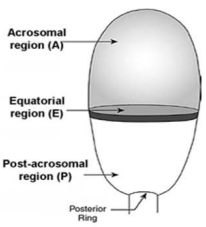

FIGURE 3 | Acrosomal region of human spermatozoa possesses strong C1orf56 immunoreactivity after capacitation. **(A)** C1orf56 immunoreactivities were visualized using Alexa Fluor 488-conjugated secondary antibody. Three staining patterns were observed in the C1orf56-positive sperm: (A–E+): Focal signals over the equatorial region; (A+E+): Strong signals over both the equatorial and acrosomal regions; (A–E–): No staining signal on sperm head. All the results shown are representative of five replicate experiments. **(B)** Percentage of C1orf56-positive sperm with A–E+, A+E+, or A–E– staining patterns. 200 C1orf56-positive sperm in randomly selected fields were determined under a fluorescence microscope after immunostaining. All data are represented as mean ± standard error of the mean (SEM). *$P < 0.05$ when compared the percentages of A+E+ staining pattern of C1orf56 in capacitated (CAP) sperm with uncapacitated (UN) or acrosome reacted (AR) sperm. A, acrosomal region; E, equatorial region, $N = 10$.

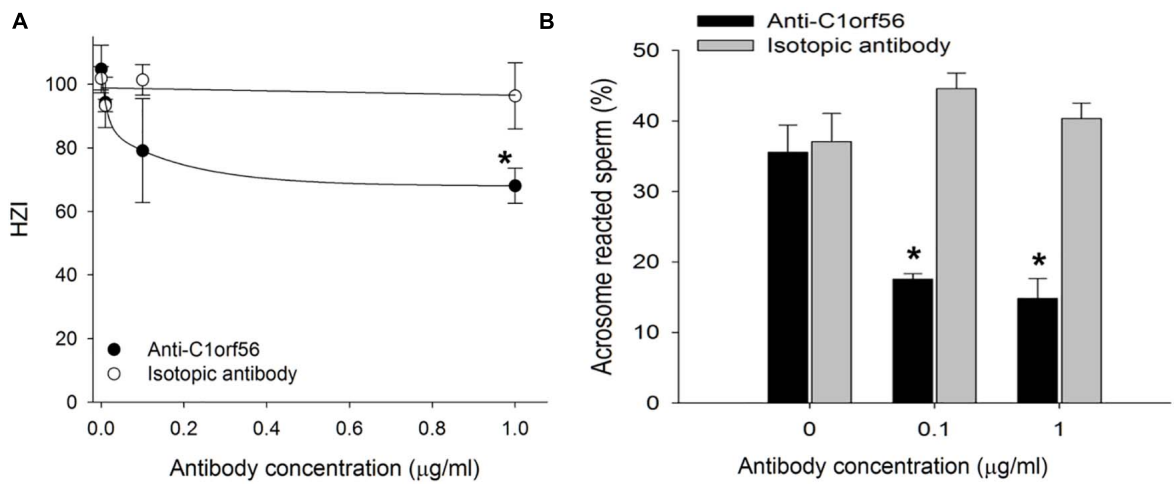

FIGURE 4 | Anti-C1orf56 antibody inhibits spermatozoa-ZP interaction. Capacitated spermatozoa were incubated in culture medium supplemented with different concentrations of anti-C1orf56 antibody. The **(A)** ZP-binding capacity and **(B)** solubilized ZP-induced acrosome reaction of the sperm were then determined by hemizona assay and FITC-PSA staining, respectively. Hemizona binding index (HZI) was the ratio of the number of bound spermatozoa on the test hemizona to that on the control hemizona times 100. *$P < 0.05$ when compared with the corresponding control with isotypic matched antibody.

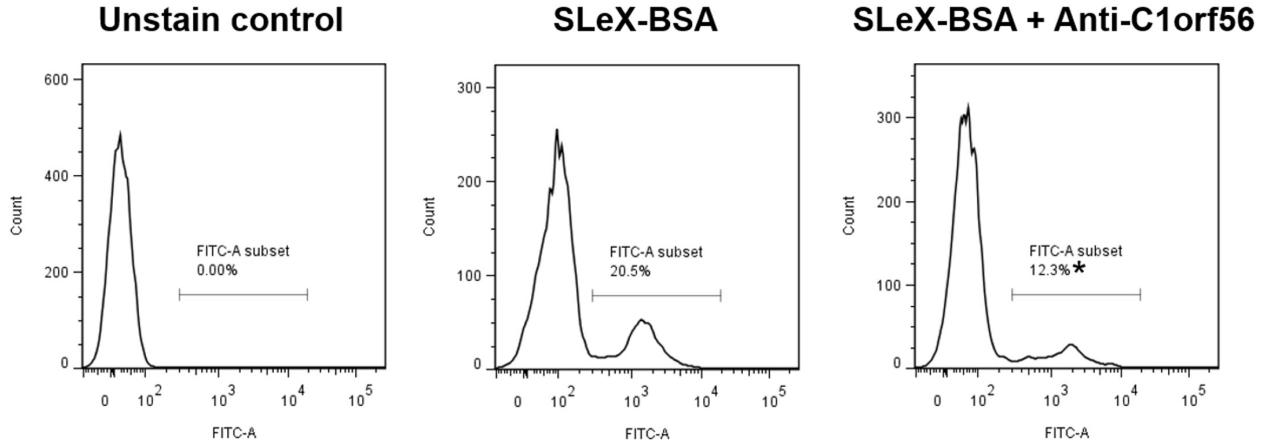

FIGURE 5 | Anti-C1orf56 antibody inhibits spermatozoa-SLeX binding. Capacitated sperm were incubated with 0.5 μM Alexa Fluor-594 labeled SLeX-BSA in the presence or absence of 1 μg/ml anti-C1orf56 antibody for 120 min followed by the flow cytometry analysis. The results shown are representative of three replicate experiments. *$P < 0.05$ when compared with the control without anti-C1orf56 antibody.

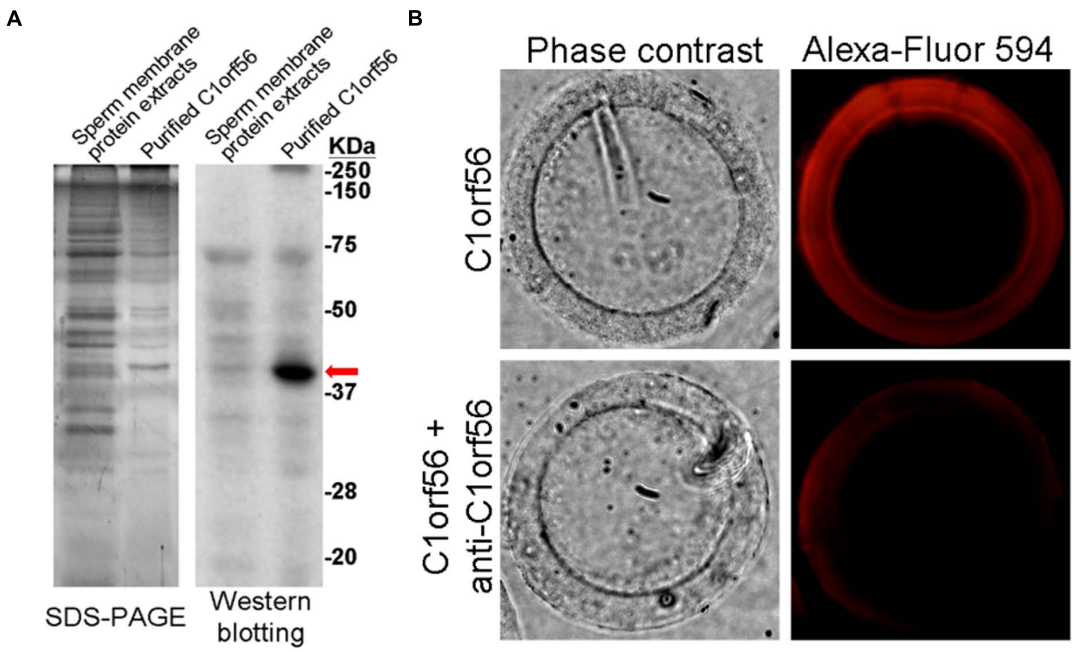

FIGURE 6 | Binding of purified C1orf56 to human ZP. **(A)** C1orf56 was partially purified from membrane protein extracts of capacitated spermatozoa by anti-C1orf56 immuno-affinity chromatography. The purity of the purified proteins (arrow) was checked by SDS-PAGE and Western blotting. **(B)** Purified C1orf56 was labeled with Alexa Fluor-594 labeling kit (Invitrogen). Matching hemizona were incubated with the 1 μg/mL labeled C1orf56 in the presence or absence of polyclonal anti-C1orf56 neutralizing antibody. The results shown are representative of three replicate experiments.

capacitated and the acrosome reacted subpopulation between samples with percentages of normal form >4% and ≤4% (**Supplementary Figure 7**).

DISCUSSION

Using an affinity chromatography with SLeX as a bait, four potential SLeX-binding proteins, including chromosome 1 open reading frame 56 (C1orf56), was identified to be the SLeX-binding proteins of capacitated spermatozoa. The contribution of C1orf56 to spermatozoa-ZP interaction was further demonstrated by the binding of purified C1orf56 to the ZP as well as the inhibitory effect of anti-C1orf56 antibody on spermatozoa-ZP interaction.

This is the first study on localization and function of C1orf56 in human spermatozoa. C1orf56 was identified in a human sperm proteomic study (Wang et al., 2013). Immunohistochemical

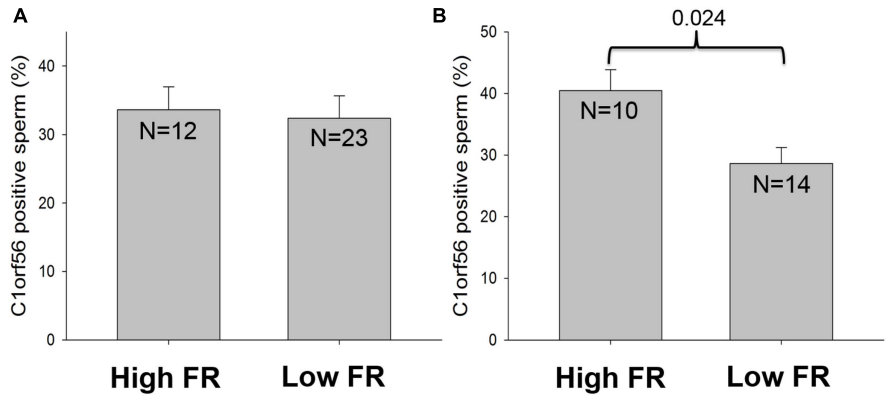

FIGURE 7 | The relationship between C1orf56 expression and fertilization rate. C1orf56 surface expression is determined on **(A)** capacitated spermatozoa and **(B)** acrosome reacted spermatozoa by flow cytometry. Data was classified and analyzed according to the fertilization rate (FR), which is divided into high FR group ($FR \geq 60\%$) and low FR group ($FR < 60\%$).

staining of human testicular tissue shows strong C1orf56 immunoreactivities only in cells of the seminiferous tubules (The Human Protein Altas[4]), suggesting a role of C1orf56 in sperm functions. Consistently, we demonstrated that human sperm surface C1orf56 is involved in spermatozoa-ZP binding.

Derived from three observations: (1) Immunofluorescence staining localized C1orf56 to the acrosomal region of capacitated spermatozoa, a region that binds ZP (Chiu et al., 2008b); (2) Anti-C1orf56 antibody suppressed spermatozoa-SLeX and spermatozoa-ZP binding and ZP-induced acrosome reaction; and (3) Purified C1orf56 from spermatozoa bound to human ZP. The mechanism by which C1orf56 regulates spermatozoa-SLeX binding is unknown. Bioinformatics analysis using a motif scan program revealed that C1orf56 contains a thrombospondin type-1 (TSP1) repeat profile known to be involved in the binding of multiple matrix glycoproteins and proteoglycans (Adams and Tucker, 2000). The possible involvement of TSP1 repeats on ZP binding needs further investigation.

According to the contact mechanics theory (Kozlovsky and Gefen, 2012), a high density of sperm ZP receptors on the sperm head is required to provide sufficient biochemical binding forces for efficient spermatozoa-ZP interaction counteracting the propulsive forces generated by the swimming spermatozoa. Despite the theoretical need of a large number of ZP receptors on spermatozoa for fertilization, their identities are controversial. Several candidate carbohydrate-binding proteins such as fucosyltransferase-5 (Chiu et al., 2007b), sperm agglutination antigen-1 (Diekman et al., 1997), alpha-D-mannosidase (Tulsiani et al., 1990), and galactosyltransferase (Shur et al., 1998), have been proposed as the putative receptors on human spermatozoa. The failure of genetic ablation of these potential molecules in affecting male fertility in animal models, and the inability of antibodies against and competitors/substrates of these molecules to completely block human spermatozoa-ZP binding and/or ZP-induced acrosome reaction, suggest that they are not the sole mediator of spermatozoa-ZP binding and that there are multiple sperm receptors for the ZP glycoproteins (Wassarman, 1999; Wassarman et al., 2001; Avella et al., 2013). Consistently, anti-C1orf56 antibody alone could not completely block spermatozoa-ZP binding.

Apart from C1orf56, three other SLeX-binding proteins were identified in this study. ZPBP1 (Lin et al., 2007) and SPACA1 (Hao et al., 2002) are involved in spermatozoon-oocyte interaction in animals, but there are no similar studies on human spermatozoa. HSPA2 is a testis-enriched member of the heat shock protein family. In humans, HSPA2 facilitates the assembly and/or presentation of ZP-interacting protein complexes on the sperm surface (Nixon et al., 2015). Interestingly, the HSPA2-associated ZP-interacting complex undergoes a capacitation-associated translocation to the outer leaflet of the sperm surface (Nixon et al., 2015). Reduced expression of HSPA2 from the human sperm proteome reduces the capacity for spermatozoa-oocyte recognition and fertilization after assisted reproduction treatment (Huszar et al., 2000). These data support a multi-molecular structures of the sperm ZP receptor(s) that are assembled during capacitation.

A human sperm ZP receptor complex has been identified. It composes of arylsulfatase A (ARSA), sperm adhesion molecule 1 (SPAM1) and HSPA2 (Redgrove et al., 2013). During capacitation, the complex is translocated to the sperm acrosomal region. ARSA mediates sperm-ZP interaction, SPAM1 is involved in the dispersal of cumulus matrix, and while HSPA2 organizes other proteins in the complex to be on the sperm surface (Asquith et al., 2004; Redgrove et al., 2012, 2013). Another sperm ZP receptor complex composing of galactosyltransferase (GalT) and SED1 has been reported (Shur et al., 2006). In this complex, GalT recognizes the ZP glycans while SED1 mediates the initial docking of the spermatozoa with the ZP to facilitate the GalT-ZP interaction. The relationship between C1orf56 and other sperm-ZP interacting proteins remains to be investigated.

The present results showed that C1orf56 expression is relocated from the equatorial region to the acrosomal region after capacitation. Capacitation involves lipid remodeling with rearrangement of glycoproteins on the sperm plasma

[4]http://www.proteinatlas.org/ENSG00000143443/normal

membrane (Gadella et al., 2008; Fraser, 2010). The mechanism for the protein relocation is unknown. The lipids in the plasma membranes are organized as compact structures with microdomains termed lipid rafts, which are small, heterogeneous, highly dynamic, sterol and sphingolipid-enriched membrane domains formed through protein, and lipid interaction for cell adhesion and signaling (Harris and Siu, 2002; Lajoie et al., 2009). During capacitation, efflux of cholesterol induces aggregation of lipid raft microdomains into a large membrane raft (Aoki et al., 2005; van Gestel et al., 2005; Selvaraj et al., 2007). After capacitation, the uniform localization of lipid rafts in uncapacitated spermatozoa is replaced by a pattern of confinement with lipid rafts enriched with proteins known to take part in spermatozoa-ZP binding (Nixon and Aitken, 2009; Wang et al., 2020). There is also an increased presence of lipid rafts on the acrosomal region of the sperm plasma membrane (Nixon et al., 2009). These data indicate that the lipid rafts serve as a dynamic platform for relocation of proteins on the sperm plasma membrane during capacitation.

Our results demonstrated diminishment of C1orf56 immunoreactivities after acrosome reaction. The observation is highly suggestive that C1orf56 is present mainly on the plasma membrane, which is lost after acrosome reaction.

CONCLUSION

Standard semen analysis provides limited information on sperm fertilizing capacity. Defective spermatozoa-ZP interaction can still occur in 13% men with normal semen analysis (Chiu et al., 2014). Until now, there is no simple method to identify spermatozoa with defective spermatozoa-ZP interaction. The present study tested the possibility of using C1orf56 expression on spermatozoa in predicting fertilization in clinical IVF. No difference in the C1orf56 expression on capacitated spermatozoa between the high FR group and the low FR group was found. The lack of difference between the two groups is likely due to the presence of multiple ZP receptors (Wassarman, 1999; Gadella et al., 2008; Fraser, 2010; Chiu et al., 2014) and reduction in one of them can be compensated by others. On the other hand, the C1orf56 level in the acrosome reacted spermatozoa was positively associated with fertilization rates. The observation suggests that C1orf56 may have functions after ZP-binding and acrosome reaction. However, the sample size in this study is small and a follow-up study with larger sample size is needed to confirm the observation.

Although assisted reproduction with intracytoplasmic sperm injection can improve fertilization, the cost and the associated risks of the micromanipulation procedure may not justify men with mild fertilization problems to undergo such treatment (Bhattacharya et al., 2001). To improve the clinical management of these men, it is important to diagnose defective ZP interaction with a reliable test before the commencement of assisted reproduction treatment. The determination of sperm ZP receptor can be a simple test for prediction of the fertilization potential of sperm samples in the future.

DATA AVAILABILITY STATEMENT

The mass spectrometry data is available at HKU Data Repository: https://doi.org/10.25442/hku.14677797.v1.

ETHICS STATEMENT

The studies involving human participants were reviewed and approved by Ethics Committee of the University of Hong Kong/Hospital Authority Hong Kong West Cluster. The patients/participants provided their written informed consent to participate in this study.

AUTHOR CONTRIBUTIONS

YW, WZ, and SM: acquisition of data, analysis of data, and drafting the manuscript. PC and T-YL: analysis of data and critically revising the article. C-LL: analysis of data, critically revising the article, and teaching the technique. WY, J-PO, XL, and PC: study design, critically revising the article, and final approval of the version to be published. All authors have read and agreed to the published version of the manuscript.

FUNDING

This work was supported in part by the Hong Kong Research Grant Council Grant (17116417), Hong Kong Health and Medical Research Fund (07182446), Sanming Project of Medicine in Shenzhen (81801447), and the High Level-Hospital Program, Health Commission of Guangdong Province, China (HKUSZH201902041).

SUPPLEMENTARY MATERIAL

The Supplementary Material for this article can be found online at: https://www.frontiersin.org/articles/10.3389/fcell.2021.700396/full#supplementary-material

REFERENCES

Adams, J. C., and Tucker, R. P. (2000). The thrombospondin type 1 repeat (TSR) superfamily: diverse proteins with related roles in neuronal development. *Dev. Dyn.* 218, 280–299. doi: 10.1002/(SICI)1097-0177(200006)218:2<280::AID-DVDY4<3.0.CO;2-0

Aoki, V. W., Liu, L., and Carrell, D. T. (2005). Identification and evaluation of a novel sperm protamine abnormality in a population of infertile males. *Hum. Reprod.* 20, 1298–1306. doi: 10.1093/humrep/deh798

Asquith, K. L., Baleato, R. M., McLaughlin, E. A., Nixon, B., and Aitken, R. J. (2004). Tyrosine phosphorylation activates surface chaperones facilitating sperm-zona recognition. *J. Cell Sci.* 117(Pt 16), 3645–3657. doi: 10.1242/jcs.01214

Avella, M. A., Baibakov, B. A., Jimenez-Movilla, M., Sadusky, A. B., and Dean, J. (2016). ZP2 peptide beads select human sperm in vitro, decoy mouse sperm in vivo, and provide reversible contraception. *Sci. Transl. Med.* 8:336ra360. doi: 10.1126/scitranslmed.aad9946

Avella, M. A., Baibakov, B., and Dean, J. (2014). A single domain of the ZP2 zona pellucida protein mediates gamete recognition in mice and humans. *J. Cell Biol.* 205, 801–809. doi: 10.1083/jcb.201404025

Avella, M. A., Xiong, B., and Dean, J. (2013). The molecular basis of gamete recognition in mice and humans. *Mol. Hum. Reprod.* 19, 279–289. doi: 10.1093/molehr/gat004

Baibakov, B., Boggs, N. A., Yauger, B., Baibakov, G., and Dean, J. (2012). Human sperm bind to the N-terminal domain of ZP2 in humanized zonae pellucidae in transgenic mice. *J. Cell Biol.* 197, 897–905. doi: 10.1083/jcb.201203062

Bhattacharya, S., Hamilton, M. P., Shaaban, M., Khalaf, Y., Seddler, M., Ghobara, T., et al. (2001). Conventional in-vitro fertilisation versus intracytoplasmic sperm injection for the treatment of non-male-factor infertility: a randomised controlled trial. *Lancet* 357, 2075–2079. doi: 10.1016/s0140-6736(00)05179-5

Chinoy, Z. S., and Friscourt, F. (2018). Chemoenzymatic synthesis of asymmetrical multi-antennary N-glycans to dissect glycan-mediated interactions between human sperm and oocytes. *Chemistry* 24, 7970–7975. doi: 10.1002/chem.201800451

Chiu, P. C., Chung, M. K., Koistinen, R., Koistinen, H., Seppala, M., Ho, P. C., et al. (2007a). Cumulus oophorus-associated glycodelin-C displaces sperm-bound glycodelin-A and -F and stimulates spermatozoa-zona pellucida binding. *J. Biol. Chem.* 282, 5378–5388. doi: 10.1074/jbc.M607482200

Chiu, P. C., Chung, M. K., Koistinen, R., Koistinen, H., Seppala, M., Ho, P. C., et al. (2007b). Glycodelin-A interacts with fucosyltransferase on human sperm plasma membrane to inhibit spermatozoa-zona pellucida binding. *J. Cell Sci.* 120(Pt 1), 33–44. doi: 10.1242/jcs.03258

Chiu, P. C., Chung, M. K., Tsang, H. Y., Koistinen, R., Koistinen, H., Seppala, M., et al. (2005). Glycodelin-S in human seminal plasma reduces cholesterol efflux and inhibits capacitation of spermatozoa. *J. Biol. Chem.* 280, 25580–25589. doi: 10.1074/jbc.M504103200

Chiu, P. C., Lam, K. K., Lee, C. L., Huang, V. W., Wong, B. S., Zhao, W., et al. (2012). Adrenomedullin enhances the progressive motility and zona pellucida-binding capacity of spermatozoa from normozoospermic but not asthenozoospermic men. *Mol. Reprod. Dev.* 79:76. doi: 10.1002/mrd.21398

Chiu, P. C., Lam, K. K., Wong, R. C., and Yeung, W. S. (2014). The identity of zona pellucida receptor on spermatozoa: an unresolved issue in developmental biology. *Semin. Cell Dev. Biol.* 30, 86–95. doi: 10.1016/j.semcdb.2014.04.016

Chiu, P. C., Wong, B. S., Chung, M. K., Lam, K. K., Pang, R. T., Lee, K. F., et al. (2008a). Effects of native human zona pellucida glycoproteins 3 and 4 on acrosome reaction and zona pellucida binding of human spermatozoa. *Biol. Reprod.* 79, 869–877 doi: 10.1095/biolreprod.108.069344

Chiu, P. C., Wong, B. S., Lee, C. L., Lam, K. K., Chung, M. K., Lee, K. F., et al. (2010). Zona pellucida-induced acrosome reaction in human spermatozoa is potentiated by glycodelin-A via down-regulation of extracellular signal-regulated kinases and up-regulation of zona pellucida-induced calcium influx. *Hum. Reprod.* 25, 2721–2733. doi: 10.1093/humrep/deq243

Chiu, P. C., Wong, B. S., Lee, C. L., Pang, R. T., Lee, K. F., Sumitro, S. B., et al. (2008b). Native human zona pellucida glycoproteins: purification and binding properties. *Hum. Reprod.* 23, 1385–1393. doi: 10.1093/humrep/den047

Deshmukh, S., Inci, F., Karaaslan, M. G., Ogut, M. G., Duncan, D., Klevan, L., et al. (2020). A confirmatory test for sperm in sexual assault samples using a microfluidic-integrated cell phone imaging system. *Forensic. Sci. Int. Genet.* 48:102313. doi: 10.1016/j.fsigen.2020.102313

Diekman, A. B., Westbrook-Case, V. A., Naaby-Hansen, S., Klotz, K. L., Flickinger, C. J., and Herr, J. C. (1997). Biochemical characterization of sperm agglutination antigen-1, a human sperm surface antigen implicated in gamete interactions. *Biol. Reprod.* 57, 1136–1144. doi: 10.1095/biolreprod57.5.1136

Fraser, L. R. (2010). The "switching on" of mammalian spermatozoa: molecular events involved in promotion and regulation of capacitation. *Mol. Reprod. Dev.* 77, 197–208. doi: 10.1002/mrd.21124

Gadella, B. M., Tsai, P. S., Boerke, A., and Brewis, I. A. (2008). Sperm head membrane reorganisation during capacitation. *Int. J. Dev. Biol.* 52, 473–480. doi: 10.1387/ijdb.082583bg

Gupta, S. K. (2018). The human egg's zona pellucida. *Curr. Top. Dev. Biol.* 130, 379–411. doi: 10.1016/bs.ctdb.2018.01.001

Gupta, S. K. (2021). Human zona pellucida glycoproteins: binding characteristics with human spermatozoa and induction of acrosome reaction. *Front. Cell Dev. Biol.* 9:619868. doi: 10.3389/fcell.2021.619868

Hao, Z., Wolkowicz, M. J., Shetty, J., Klotz, K., Bolling, L., Sen, B., et al. (2002). SAMP32, a testis-specific, isoantigenic sperm acrosomal membrane-associated protein. *Biol. Reprod.* 66, 735–744. doi: 10.1095/biolreprod66.3.735

Harris, T. J., and Siu, C. H. (2002). Reciprocal raft-receptor interactions and the assembly of adhesion complexes. *Bioessays* 24, 996–1003. doi: 10.1002/bies.10172

Huang, V. W., Zhao, W., Lee, C. L., Lee, C. Y., Lam, K. K., Ko, J. K., et al. (2013). Cell membrane proteins from oviductal epithelial cell line protect human spermatozoa from oxidative damage. *Fertil Steril* 99, 1444–1452.e23. doi: 10.1016/j.fertnstert.2012.11.056

Huszar, G., Stone, K., Dix, D., and Vigue, L. (2000). Putative creatine kinase M-isoform in human sperm is identifiedas the 70-kilodalton heat shock protein HspA2. *Biol. Reprod.* 63, 925–932. doi: 10.1095/biolreprod63.3.925

Inci, F., Ozen, M. O., Saylan, Y., Miansari, M., Cimen, D., Dhara, R., et al. (2018). A novel on-chip method for differential extraction of sperm in forensic cases. *Adv. Sci. (Weinh)* 5:1800121. doi: 10.1002/advs.201800121

Kennedy, J. F., and Barnes, J. A. (1980). Assessment of the use of cyanogen bromide-activated Sepharose in analytic and preparative immunoadsorption. *Int. J. Biol. Macromol* 2, 289–296. doi: 10.1016/0141-8130(80)90047-1

Kozlovsky, P., and Gefen, A. (2012). The relative contributions of propulsive forces and receptor-ligand binding forces during early contact between spermatozoa and zona pellucida of oocytes. *J. Theor. Biol.* 294, 139–143. doi: 10.1016/j.jtbi.2011.11.002

Lajoie, P., Goetz, J. G., Dennis, J. W., and Nabi, I. R. (2009). Lattices, rafts, and scaffolds: domain regulation of receptor signaling at the plasma membrane. *J. Cell Biol.* 185, 381–385. doi: 10.1083/jcb.200811059

Lee, C. L., Chiu, P. C., Pang, P. C., Chu, I. K., Lee, K. F., Koistinen, R., et al. (2011). Glycosylation failure extends to glycoproteins in gestational diabetes mellitus: evidence from reduced alpha2-6 sialylation and impaired immunomodulatory activities of pregnancy-related glycodelin-A. *Diabetes* 60, 909–917. doi: 10.2337/db10-1186

Lin, Y. N., Roy, A., Yan, W., Burns, K. H., and Matzuk, M. M. (2007). Loss of zona pellucida binding proteins in the acrosomal matrix disrupts acrosome biogenesis and sperm morphogenesis. *Mol. Cell Biol.* 27, 6794–6805. doi: 10.1128/MCB.01029-07

Liu, D. Y., and Baker, H. W. (2000). Defective sperm-zona pellucida interaction: a major cause of failure of fertilization in clinical in-vitro fertilization. *Hum. Reprod.* 15, 702–708. doi: 10.1093/humrep/15.3.702

Liu, D. Y., and Baker, H. W. (2004). High frequency of defective sperm-zona pellucida interaction in oligozoospermic infertile men. *Hum. Reprod.* 19, 228–233. doi: 10.1093/humrep/deh067

Mei, S., Chen, P., Lee, C. L., Zhao, W., Wang, Y., Lam, K. K. W., et al. (2019). The role of galectin-3 in spermatozoa-zona pellucida binding and its association with fertilization in vitro. *Mol. Hum. Reprod.* 25, 458–470. doi: 10.1093/molehr/gaz030

Morales, P., Vigil, P., Franken, D. R., Kaskar, K., Coetzee, K., and Kruger, T. F. (1994). Sperm-oocyte interaction: studies on the kinetics of zona pellucida binding and acrosome reaction of human spermatozoa. *Andrologia* 26, 131–137. doi: 10.1111/j.1439-0272.1994.tb00774.x

Nixon, B., and Aitken, R. J. (2009). The biological significance of detergent-resistant membranes in spermatozoa. *J. Reprod. Immunol.* 83, 8–13. doi: 10.1016/j.jri.2009.06.258

Nixon, B., Bielanowicz, A., McLaughlin, E. A., Tanphaichitr, N., Ensslin, M. A., and Aitken, R. J. (2009). Composition and significance of detergent resistant membranes in mouse spermatozoa. *J. Cell Physiol.* 218, 122–134. doi: 10.1002/jcp.21575

Nixon, B., Bromfield, E. G., Dun, M. D., Redgrove, K. A., McLaughlin, E. A., and Aitken, R. J. (2015). The role of the molecular chaperone heat shock protein A2 (HSPA2) in regulating human sperm-egg recognition. *Asian J. Androl.* 17, 568–573. doi: 10.4103/1008-682X.151395

Oehninger, S., Franken, D. R., Sayed, E., Barroso, G., and Kolm, P. (2000). Sperm function assays and their predictive value for fertilization outcome in IVF therapy: a meta-analysis. *Hum. Reprod. Update* 6, 160–168. doi: 10.1093/humupd/6.2.160

Pang, P. C., Chiu, P. C., Lee, C. L., Chang, L. Y., Panico, M., Morris, H. R., et al. (2011). Human sperm binding is mediated by the sialyl-Lewis(x) oligosaccharide on the zona pellucida. *Science* 333, 1761–1764. doi: 10.1126/science.1207438

Plachot, M., Junca, A. M., Mandelbaum, J., Cohen, J., Salat-Baroux, J., and Da Lage, C. (1986). Timing of in-vitro fertilization of cumulus-free and cumulus-enclosed human oocytes. *Hum. Reprod.* 1, 237–242. doi: 10.1093/oxfordjournals.humrep.a136392

Redgrove, K. A., Anderson, A. L., McLaughlin, E. A., O'Bryan, M. K., Aitken, R. J., and Nixon, B. (2013). Investigation of the mechanisms by which the molecular chaperone HSPA2 regulates the expression of sperm surface receptors involved in human sperm-oocyte recognition. *Mol. Hum. Reprod.* 19, 120–135. doi: 10.1093/molehr/gas064

Redgrove, K. A., Nixon, B., Baker, M. A., Hetherington, L., Baker, G., Liu, D. Y., et al. (2012). The molecular chaperone HSPA2 plays a key role in regulating the expression of sperm surface receptors that mediate sperm-egg recognition. *PLoS One* 7:e50851. doi: 10.1371/journal.pone.0050851

Selvaraj, V., Buttke, D. E., Asano, A., McElwee, J. L., Wolff, C. A., Nelson, J. L., et al. (2007). GM1 dynamics as a marker for membrane changes associated with the process of capacitation in murine and bovine spermatozoa. *J. Androl.* 28, 588–599. doi: 10.2164/jandrol.106.002279

Shur, B. D., Evans, S., and Lu, Q. (1998). Cell surface galactosyltransferase: current issues. *Glycoconj. J.* 15, 537–548.

Shur, B. D., Rodeheffer, C., Ensslin, M. A., Lyng, R., and Raymond, A. (2006). Identification of novel gamete receptors that mediate sperm adhesion to the egg coat. *Mol. Cell Endocrinol.* 250, 137–148. doi: 10.1016/j.mce.2005.12.037

Tulsiani, D., Skudlarek, M., and Orgebin-Crist, M. (1990). Human sperm plasma menbranes possess alpha-D-mannosidase activity but no galactosyltransferase activity but no falactosyltransferase activity. *Biol. Reprod.* 42, 843–858. doi: 10.1095/biolreprod42.5.843

Tumova, L., and Zigo, M. (2021). Ligands and receptors involved in the sperm-zona pellucida interactions in mammals. *Cells* 10:133. doi: 10.3390/cells10010133

van Gestel, R. A., Brewis, I. A., Ashton, P. R., Helms, J. B., Brouwers, J. F., and Gadella, B. M. (2005). Capacitation-dependent concentration of lipid rafts in the apical ridge head area of porcine sperm cells. *Mol. Hum. Reprod.* 11, 583–590. doi: 10.1093/molehr/gah200

Wang, D., Cheng, L., Xia, W., Liu, X., Guo, Y., Yang, X., et al. (2020). LYPD4, mouse homolog of a human acrosome protein, is essential for sperm fertilizing ability and male fertility†. *Biol. Reprod.* 102, 1033–1044. doi: 10.1093/biolre/ioaa018

Wang, G., Wu, Y., Zhou, T., Guo, Y., Zheng, B., Wang, J., et al. (2013). Mapping of the N-linked glycoproteome of human spermatozoa. *J. Proteome Res.* 12, 5750–5759. doi: 10.1021/pr400753f

Wassarman, P. (1999). Mammalian fertilization: molecular aspects of gamete adhesion, exocytosis, and fusion. *Cell* 96, 175–183.

Wassarman, P., Jovine, L., and Litscher, E. (2001). A profile of fertilization in mammals. *Nat. Cell. Biol.* 3, 59–64.

World Health Organization (2010). *Laboratory Manual for the Examination and Processing of Human Semen*. Geneva: World Health Organization, 7–113.

Yao, Y. Q., Chiu, C. N., Ip, S. M., Ho, P. C., and Yeung, W. S. (1998). Glycoproteins present in human follicular fluid that inhibit the zona-binding capacity of spermatozoa. *Hum. Reprod.* 13, 2541–2547. doi: 10.1093/humrep/13.9.2541

Ye, H., Hill, J., Gucinski, A. C., Boyne, M. T. II, and Buhse, L. F. (2015). Direct site-specific glycoform identification and quantitative comparison of glycoprotein therapeutics: imiglucerase and velaglucerase alfa. *AAPS J.* 17, 405–415. doi: 10.1208/s12248-014-9706-4

Conflict of Interest: The authors declare that the research was conducted in the absence of any commercial or financial relationships that could be construed as a potential conflict of interest.

frontiers in Cell and Developmental Biology

ORIGINAL RESEARCH
published: 26 October 2021
doi: 10.3389/fcell.2021.767161

Capacitation-Induced Mitochondrial Activity Is Required for Sperm Fertilizing Ability in Mice by Modulating Hyperactivation

María Milagros Giaccagli[1], Matías Daniel Gómez-Elías[1], Jael Dafne Herzfeld[1], Clara Isabel Marín-Briggiler[2], Patricia Sara Cuasnicú[1], Débora Juana Cohen[1] and Vanina Gabriela Da Ros[1]*

[1] Laboratorio de Mecanismos Moleculares de la Fertilización, Instituto de Biología y Medicina Experimental (IByME-CONICET), Buenos Aires, Argentina, [2] Laboratorio de Biología Celular y Molecular de la Reproducción, Instituto de Biología y Medicina Experimental (IByME-CONICET), Buenos Aires, Argentina

To become fully competent to fertilize an egg, mammalian sperm undergo a series of functional changes within the female tract, known as capacitation, that require an adequate supply and management of energy. However, the contribution of each ATP generating pathway to sustain the capacitation-associated changes remains unclear. Based on this, we investigated the role of mitochondrial activity in the acquisition of sperm fertilizing ability during capacitation in mice. For this purpose, the dynamics of the mitochondrial membrane potential (MMP) was studied by flow cytometry with the probe tetramethylrhodamine ethyl ester (TMRE). We observed a time-dependent increase in MMP only in capacitated sperm as well as a specific staining with the probe in the flagellar region where mitochondria are confined. The MMP rise was prevented when sperm were exposed to the mitochondrial uncoupler carbonyl cyanide m-chlorophenyl hydrazine (CCCP) or the protein kinase A (PKA) inhibitor H89 during capacitation, indicating that MMP increase is dependent on capacitation and H89-sensitive events. Results showed that whereas nearly all motile sperm were TMRE positive, immotile cells were mostly TMRE negative, supporting an association between high MMP and sperm motility. Furthermore, CCCP treatment during capacitation did not affect PKA substrate and tyrosine phosphorylations but produced a decrease in hyperactivation measured by computer assisted sperm analysis (CASA), similar to that observed after H89 exposure. In addition, CCCP inhibited the *in vitro* sperm fertilizing ability without affecting cumulus penetration and gamete fusion, indicating that the hyperactivation supported by mitochondrial function is needed mainly for *zona pellucida* penetration. Finally, complementary *in vivo* fertilization experiments further demonstrated the fundamental role of mitochondrial activity for sperm function. Altogether, our results show the physiological relevance of mitochondrial functionality for sperm fertilization competence.

Keywords: mitochondria, capacitation, hyperactivation, fertilization, sperm

OPEN ACCESS

Edited by:
Maria Jiménez-Movilla, University of Murcia, Spain

Reviewed by:
Marc Yeste, University of Girona, Spain
Lonny Ray Levin, Cornell University, United States

****Correspondence:***
Débora Juana Cohen
deborajcohen@gmail.com

Specialty section:
This article was submitted to Molecular and Cellular Reproduction, a section of the journal Frontiers in Cell and Developmental Biology

Received: *30 August 2021*
Accepted: *08 October 2021*
Published: *26 October 2021*

Citation:
Giaccagli MM, Gómez-Elías MD, Herzfeld JD, Marín-Briggiler CI, Cuasnicú PS, Cohen DJ and Da Ros VG (2021) Capacitation-Induced Mitochondrial Activity Is Required for Sperm Fertilizing Ability in Mice by Modulating Hyperactivation. Front. Cell Dev. Biol. 9:767161. doi: 10.3389/fcell.2021.767161

Abbreviations: BSA, bovine serum albumin; CASA, computer-assisted sperm analysis; CCCP, carbonyl cyanide 3-chlorophenylhydrazone; COCs, cumulus–oocyte complexes; DAPI, 4′,6-diamidine-2′-phenylindole dihydrochloride; DMSO, dimethyl sulfoxide; MFI, mean fluorescence intensity; MMP, mitochondrial membrane potential; OXPHOS, oxidative phosphorylation; PKA, protein kinase A; TMRE, tetramethylrhodamine, ethyl ester; ZP, *zona pellucida*.

INTRODUCTION

Mammalian fertilization is a complex process that involves different sequential interactions between the spermatozoon and the egg. As this interplay occurs in the oviduct, sperm must reach it from the semen deposit site in the vagina or uterus, depending on the species (Yanagimachi, 1994). During this transport, sperm experience a series of functional and structural modifications collectively known as capacitation (Chang, 1951; Austin, 1952). These changes are molecularly triggered by the entry of HCO_3^- and Ca^{2+}, which activate protein kinase A (PKA)-dependent signaling cascades leading to phosphorylation of proteins, increase in intracellular pH and hyperpolarization of the plasma membrane potential (reviewed in Puga Molina et al., 2018). Capacitation can be mimicked *in vitro* in a defined medium containing HCO_3^-, Ca^{2+}, a cholesterol acceptor (commonly serum albumin) and energy sources (Yanagimachi, 1994). The two functional consequences of this process are the ability to undergo acrosome reaction, essential for sperm to penetrate and fuse with the egg (Yanagimachi, 1994), and the development of hyperactivation, critical for sperm to swim through the oviductal fluid, detach from the isthmus reservoir and penetrate the envelopes that surround the egg (Demott and Suarez, 1992; Suarez and Dai, 1992; Yanagimachi, 1994; Stauss et al., 1995; Brukman et al., 2016). Taken together, the acquisition of the capacitation status is mandatory for the cells to become fertilization competent.

Sperm motility disorders are one of most relevant causes of male infertility (Nowicka-bauer and Nixon, 2020; Shahrokhi et al., 2020; Tu et al., 2020). Understanding the cellular and molecular mechanisms involved in flagellar movement is required to improve diagnosis and treatment of the associated pathologies. Although the etiology of these disorders is known only in few cases, it could be associated with structural or functional sperm defects, such as dysregulation of specific signaling pathways or energy production (Nowicka-bauer and Nixon, 2020; Shahrokhi et al., 2020; Tu et al., 2020). In view of this, research has been carried out to elucidate the individual contribution of each energy metabolic pathways, glycolysis and oxidative phosphorylation (OXPHOS), occurring in the sperm tail (Fawcett, 1975; Bunch et al., 1998; Eddy, 2006; Krisfalusi et al., 2006; Balbach et al., 2020), to sustain motility. However, the results obtained so far in different species are controversial. In humans, whereas several studies revealed that glucose, the main glycolytic substrate, plays a key role in supplying ATP for motility, others showed the importance of OXPHOS for motility and sperm function (reviewed in Ruiz-Pesini et al., 2007; Boguenet et al., 2021). This controversy might be partially attributed to differences in the experimental conditions used in each case. In addition, it can also be due to an often disregard for the facts that glycolysis both requires ATP to start the process, contrary to OXPHOS, and it is usually a prerequisite for OXPHOS (Ramalho-Santos et al., 2009; Barbagallo et al., 2020). In this sense, a functional association between these two pathways has been recently described in sperm (Tourmente et al., 2015; Balbach et al., 2020). Therefore, besides not reaching a consensus, there is no direct evidence showing an association between these energy metabolic pathways and sperm fertilizing ability in humans due to ethical limitations, reinforcing research using animal models.

In mice, knockout studies showed that glycolysis (Miki et al., 2004; Odet et al., 2008; Danshina et al., 2010), rather than OXPHOS (Narisawa et al., 2002; Nayernia et al., 2002), is essential for sustaining sperm motility and male fertility. In addition, whereas several glycolytic (i.e., glucose, fructose, and mannose) and non-glycolytic (i.e., lactate and pyruvate) substrates maintained sperm motility (Mukai and Okuno, 2004; Goodson et al., 2012), only glucose and mannose were able to support hyperactivation (Goodson et al., 2012). Despite this, using an extracellular flux analyzer, it has recently been shown that mouse sperm enhance both glycolysis and OXPHOS to sustain the energy demand increase during capacitation (Balbach et al., 2020). However, in that case, capacitation was induced through a pharmacological stimulation of PKA, opening the possibility that these energy providing pathways could be differently regulated under physiological conditions. Therefore, fertilization assays to evaluate whether the provenance of ATP is relevant for acquisition of motility and fertilization competence remain necessary.

Considering the above findings and that mitochondrial metabolism is superior to glycolysis in terms of ATP production, the aim of this study was to determine the role of mitochondrial activity in the acquisition of sperm fertilizing ability during capacitation in mice. Here, we show the dynamics of the mitochondrial membrane potential (MMP; also referred in the literature as $\Delta\Psi m$) during capacitation, which reflects the cellular capacity to produce ATP by OXPHOS and, therefore, it is used as an indicator of mitochondrial activity (Nicholls and Ward, 2000). Our study was performed with the cationic lipophilic dye tetramethylrhodamine, ethyl ester (TMRE) that had not been widely used for evaluation of sperm quality (Marchetti et al., 2004; Losano et al., 2017), despite several of its attractive characteristics, such as low mitochondrial toxicity, its single-channel fluorescence is simple to analyze and it can be combined with other probes for multiparametric staining (Nicholls and Ward, 2000; Marchetti et al., 2004). In addition, we analyzed the relevance of mitochondrial function not only for hyperactivation but also for *in vitro* and *in vivo* sperm fertilizing ability.

MATERIALS AND METHODS

Animals

Hybrid (C57BL/6xBALB/c) F1 male (age: 3–6 months) and female (age: 45 days–4 months) mice were housed in the animal facility at IBYME-CONICET (Buenos Aires, Argentina) and maintained with food and water *ad libitum* in a temperature-controlled room (21–23°C) with light:dark (12:12 h, lights on: 7:00 AM) cycle. Approval for the study protocol was obtained from the Institutional Animal Care and Use Committee of Instituto de Biología y Medicina Experimental (N° 08/2021). Experiments involving animals were performed in accordance with the Guide for Care and Use of Laboratory Animals published by the National Institutes of Health.

Reagents

Reagents and chemicals were purchased from Sigma-Aldrich (St Louis, MO), unless otherwise indicated.

Sperm Capacitation

Mouse sperm were recovered by incising the cauda epididymis in 300 μl of capacitation medium containing 99.3 mM NaCl, 2.7 mM KCl, 1.8 mM $CaCl_2.2H_2O$, 0.3 mM $Na_2H_2PO_4.2H_20$, 0.5 mM $MgCl_2.2H_2O$, 25 mM $NaHCO_3$, 5.6 mM glucose, 24.4 mM lactate and 0.5 mM pyruvate, and supplemented with 0.3% (w/v) bovine serum albumin (BSA), pH: 7.3–7.5 ("swim-out") (Da Ros et al., 2008). Aliquots of the suspension were added to 300 μl of capacitation medium containing either carbonyl cyanide 3-chlorophenylhydrazone (CCCP), H89 (Cayman Chemical, Ann Arbor, MI) or dimethyl sulphoxide (DMSO; Baker, Phillipsburg, NJ), as vehicle (< 1% v/v), to give a final concentration of 5–10 × 10^6 cells/ml. Sperm suspensions were then incubated for 90 min at 37°C in an atmosphere with 5% (v/v) CO_2 in air.

Mitochondrial Membrane Potential Determination

For MMP analysis by flow cytometry, the "swim out" procedure was carried out in a BSA-free medium. As this medium does not support mouse sperm capacitation (Visconti et al., 1995, 1999), it is considered to be non-capacitating. Aliquots of the sperm suspension were added to 200 μl of BSA-free medium or of capacitation medium containing CCCP (concentration range: 5–80 μM), H89 (20 μM) or DMSO. After different time periods of incubation (0, 40, 70 min) sperm were loaded with 0.1 μM TMRE (Invitrogen Carlsbad, CA) and incubated for 20 additional minutes. Samples were washed to remove the excess of probe by centrifugation at 725 ×*g* for 3 min, resuspended in the BSA-free medium, and exposed without permeabilization to 0.02 μg/ml 4′,6-diamidine-2′-phenylindole dihydrochloride (DAPI; Invitrogen) just before measurement to assess cell viability (see experiment annotation example in Lee et al., 2008). Fluorescence was detected using a BD FACSCantoTM II analyzer (BD Biosciences, East Rutherford, NJ) following the manufacturer's indications. DAPI and TMRE fluorescence was collected using the Pacific Blue (450/50) and PE (585/42) filters, respectively. One technical replicate (20000 measured events) was performed for each treatment in each independent experiment. After acquisition, fluorescence compensation and data analysis were performed by FlowJo 10 software (FlowJo LLC, Ashland, OR). The overall gating strategy used is shown in the corresponding Figure and its legend. Results are presented as mean fluorescence intensity (MFI) for TMRE and percentage of cells showing high TMRE signal.

For localization studies, sperm treated with CCCP (20 μM) or DMSO were loaded with 0.1 μM TMRE and 15 μg/ml Hoechst 33342 (Invitrogen), and incubated to complete the 90 min period. Micrographs were obtained from living sperm samples seeded in polylysine (0.1 mg/ml) coverslips and observed under an Olympus IX83 Spinning Disk microscope (Olympus Corp., Tokyo, Japan) (× 600).

Protein Phosphorylation Assessment

After capacitation in the presence of CCCP (concentration range: 5–60 μM) or DMSO, protein phosphorylation was assessed as previously reported (Da Ros et al., 2008; Weigel Muñoz et al., 2018). Sperm suspensions were washed with PBS, resuspended in Laemmli sample buffer (Laemmli, 1970), then boiled for 5 min and centrifuged at 2.000 ×*g*. The supernatants were boiled again in the presence of 70 mM 2-β-mercaptoethanol, and solubilized proteins (corresponding to 5 × 10^6 sperm/lane) were separated by SDS-PAGE (7.5% polyacrylamide) and transferred onto nitrocellulose. After blocking with 2% skim milk in PBS-Tween, the membranes were probed with either anti-phospho-PKA substrate (1:1000; clone 9624, Cell Signaling Technology, Danvers MA) or anti-phosphotyrosine antibody (1:1000; clone 4G10; Merck MilliPore, Burlington, MA). Next, the membranes were incubated with the corresponding peroxidase-conjugated secondary antibody (1:4000; Vector Laboratories, Burlingame, CA). The immunoreactive proteins were detected by ECL Western blotting kit (Thermo Fisher, Waltham, MA) and images captured with G:BOX GENI (Syngene, Synoptics Ltd, Cambridge, England) according to the manufacturer's instructions. For quantification, the pixels of each lane in the images were calculated using the ImageJ software.[1] Each value was relativized to the one of the phospho-hexokinase (116 kDa) band of the same lane, as this protein is constitutively Tyr-phosphorylated (Kalab et al., 1994; Visconti et al., 1996), and then normalized to the control lane (CAP, see figure legend) of each blot. For this purpose, the phospho-PKA substrate blots were stripped and further probed with the anti-phosphotyrosine antibody to detect the phospho-hexokinase band in the same samples.

Simultaneous Evaluation of Motility and Mitochondrial Membrane Potential

Twenty min before the end of capacitation, sperm were loaded with 0.1 μM TMRE and 15 μg/ml Hoechst 33342 (Invitrogen), and incubated to complete the 90 min period. Samples were then washed, resuspended in fresh medium, mounted in pre-warmed slides and observed under a Nikon Optiphot microscope (Nikon, Tokyo, Japan) equipped with epifluorescence optics (× 500). Sperm were scored motile or immotile and as TMRE positive or negative depending on the presence of a bright red staining in the midpiece of the flagellum.

Motility Assessment by Computer Assisted Sperm Analysis

After 90 min-capacitation in the presence of CCCP (concentration range: 10–60 μM), H89 (20 μM) or DMSO, sperm aliquots (15 μl) were placed between pre-warmed slides and cover slips (22 × 22 mm) to create a chamber with 30 μm depth, and were examined at 37°C using Sperm Class Analyzer® system (SCA v.6.2.0.1., Microptic SL, Barcelona, Spain). Drifting was set in 25 μm/s. At least 200 sperm distributed in a minimum of 10 different microscope fields were evaluated (30 frames acquired at 60 Hz for each measurement). The

[1] http://imagej.nih.gov/ij

following parameters were assessed: curvilinear velocity (VCL, μm/s), straight line velocity (VSL, μm/s), average path velocity (VAP, μm/s), linearity (LIN,%), straightness (STR,%), wobble (WOB,%), amplitude of lateral head displacement (ALH, μm) and beat cross frequency (BCF, Hz). Sperm were considered hyperactivated when presenting VCL $\geq$ 271 μm/s, LIN $<$ 50% and ALH $\geq$ 3.5 μm. These custom cutoffs were selected based on our experience (Brukman et al., 2016) and previously reported recommendations (Bray et al., 2005).

In vitro Fertilization Assays

Gamete interaction assays were carried out as previously reported (Da Ros et al., 2008). Briefly, female mice were superovulated by an injection of eCG (5 UI, Syntex, Buenos Aires, Argentina), followed by hCG (5 UI, Syntex) 48 h later. Cumulus-oocyte complexes (COCs) were collected from the oviducts 13–14 h after hCG administration and pooled. When needed, cumulus cells were removed by incubating the COCs in 0.3 mg/ml hyaluronidase (type IV) for 3–5 min. In some cases, the *zona pellucida* (ZP) was dissolved by treating the eggs with acid Tyrode solution (pH 2.5) for 10–20 s (Nicolson et al., 1975). Sperm were incubated for 90 min in the capacitation medium with different concentrations of CCCP (concentration range: 20–60 μM) or DMSO. After that, sperm were washed, and resuspended in a fresh medium for insemination.

COCs and ZP-intact eggs were inseminated with a final concentration of 1–5 $\times$ 10^5 cells/ml and gametes co-incubated for 3 h at 37°C in an atmosphere of 5% (v/v) CO_2 in air. Eggs were then fixed with 2% (w/v) paraformaldehyde in PBS, washed, stained with 10 μg/ml Hoechst 33342, mounted on slides and finally analyzed under the epifluorescence microscope ($\times$ 250). For fusion assays, ZP-free eggs were inseminated with a final concentration of 1–5 $\times$ 10^4 cells/ml and gametes co-incubated for 1 h under the same incubation conditions as stated above. Eggs were then fixed with 2.5% glutaraldehyde (Baker), stained with 1% aceto-carmine solution and observed under the microscope ($\times$ 400). In all cases, eggs were considered fertilized when at least one decondensing sperm nucleus or two pronuclei were observed in the egg cytoplasm.

Cumulus Penetration Assay

After sperm incubation in the presence of CCCP (concentration range: 5–60 μM), H89 (20 μM) or DMSO, cumulus penetration assays were performed as previously described (Ernesto et al., 2015). Briefly, sperm were stained with 5 μg/ml Hoechst 33342, and used to inseminate the COCs (final concentration: 1–2.5 $\times$ 10^4 sperm/ml). Gametes were co-incubated for 15 min at 37°C in an atmosphere of 5% (v/v) CO_2 in air. COCs were then washed, fixed with 2% (w/v) paraformaldehyde and the number of sperm within the cumulus was determined under the epifluorescence microscope ($\times$ 250).

Intrauterine Insemination

Intrauterine insemination assays were performed as previously described (Curci et al., 2021). Briefly, female mice were superovulated by an injection of eCG, followed by hCG 46 h later. Nine h later, females were anesthetized with ketamine (100 mg/kg, Holliday- Scott SA, Buenos Aires, Argentina)—xilacine (10 mg/kg, Richmond Vet Farma SA, Buenos Aires, Argentina), and both uterine horns were surgically exposed. Then, sperm suspensions (1–10 $\times$ 10^7 sperm/ml) preincubated with different concentrations of CCCP (range: 20–60 μM) or DMSO for 20 min were injected into the uterine horns using one for CCCP-treated sperm and the contralateral for control sperm. After surgery, females were placed on a warm pad until complete recovery. Fifteen h later, COCs were collected from the *ampulla,* and incubated in KSOM medium (Erbach et al., 1994), scoring the percentage of 2-cell embryos 24 h later. Embryos were then transferred to a fresh KSOM medium drop to evaluate the development to the blastocyst stage on day 4 after insemination.

Statistical Analysis

Calculations were performed using the Prism 80.0 software (GraphPad Software, La Jolla, CA). Data was analyzed by one- or two-way analysis of the variance (ANOVA) after checking data normality (Shapiro-Wilk test) and homoscedasticity (Spearman's test for two-way ANOVA or Brown-Forsythe test for one-way ANOVA). Transformations were performed when assumptions were violated. One-way ANOVA followed by Fisher's LSD post-test was used for determining the effect of CCCP on MMP (except % of sperm TMRE+), kinematic parameters (except linearity index), hyperactivation, and *in vitro* and *in vivo* sperm fertilizing ability. Two-way ANOVA followed by Fisher's LSD post-test was used for determining the MMP dynamics during capacitation and the simultaneous evaluation of MMP and motility. Data represents the mean ± SEM of independent experiments. In cases where the assumptions remained unfulfilled, the non-parametric Kruskal-Wallis test followed by Dunn's post-test was used for determining the effect of CCCP on MMP (% of sperm TMRE+), sperm cumulus penetration ability and linearity index. Data represents the median with interquartile range. In all cases, differences were considered significant at a level of $p < 0.05$.

RESULTS

Assessment of Mitochondrial Membrane Potential Dynamics During Sperm Capacitation

To study the role of mitochondrial activity in the acquisition of sperm fertilizing ability in mice, we first evaluated its dynamics during capacitation. For these experiments, we measured MMP in sperm using the probe TMRE that emits high fluorescence in living cells when it is sequestered by active mitochondria with high MMP (Nicholls and Ward, 2000). As this dye had not been previously used in mouse sperm, initial experiments were carried out to set up the proper concentration and incubation time for MMP determination (data not shown). After this, epididymal sperm were incubated under capacitating or non-capacitating (BSA-free) conditions for different periods of time, then loaded with TMRE, and finally analyzed for fluorescence intensity by flow cytometry (**Figure 1A**). Results showed that,

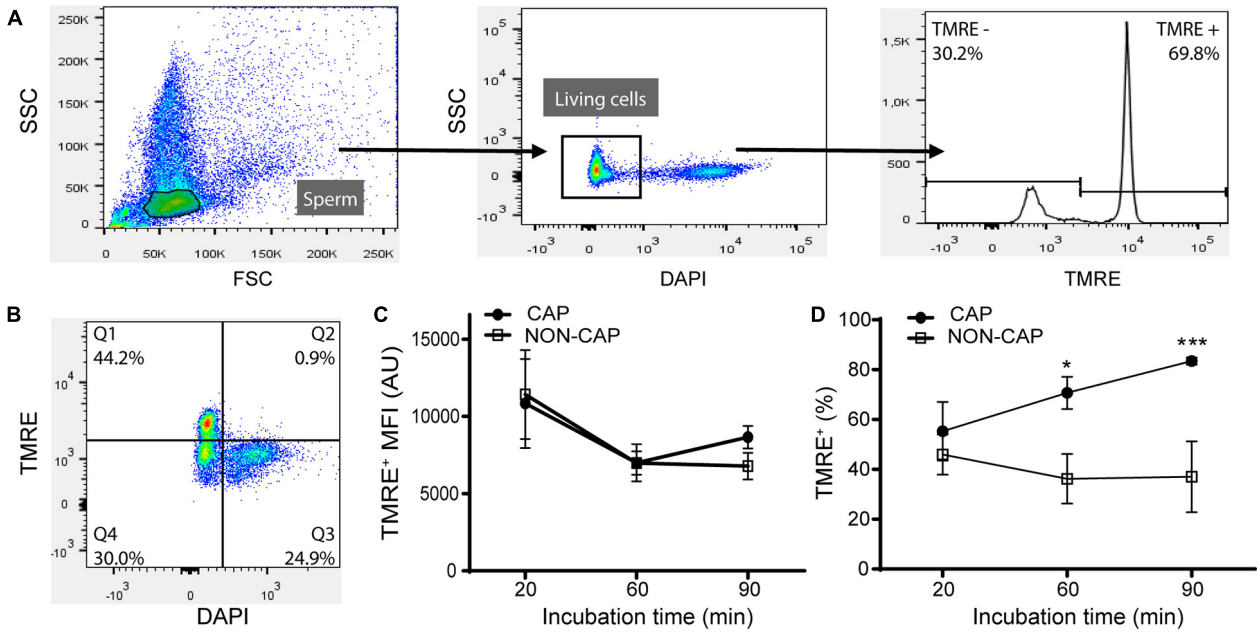

FIGURE 1 | Determination of mitochondrial membrane potential by flow cytometry during mouse sperm capacitation. Epididymal mouse sperm were incubated under non-capacitating or capacitating conditions, loaded with TMRE, and fluorescence was measured by flow cytometry. **(A)** Gating strategy used in the analysis: sperm were selected on a forward (FSC) and side scatter (SSC) plot (left panel) and, then, DAPI negative (living) cells (center panel) were further gated to determine the percentage of TMRE+ and TMRE− cells (right panel). Representative data of capacitated sperm is shown. **(B)** A representative image of a TMRE and DAPI scatter plot showing that only living cells present TMRE staining (Q1). **(C)** Mean fluorescence intensity (MFI) from capacitated (CAP) and non-capacitated (NON-CAP) TMRE + sperm at different incubation times. **(D)** Percentage of CAP and NON-CAP TMRE + sperm at different incubation times. Results are expressed as mean ± SEM. $n = 5$. $^{*}p < 0.05$, $^{***}p < 0.001$.

as expected, only living cells presented TMRE staining (DAPI negative cells) (**Figure 1B**). In addition, the MFI of the TMRE positive population remained similar under both incubation conditions and constant over time (**Figure 1C**). On the other hand, the percentage of TMRE positive cells gradually increased during capacitation, tripling the value of the non-capacitated ones at the end of the incubation (3.2 ± 0.7 times, $n = 5$) (**Figure 1D**). The fact that at time = 20 min no differences in MMP values were observed between incubations with or without BSA, and that the time-dependent increase in MMP dynamics along capacitation was observed even in the presence of BSA (**Figure 1D**), argues against the possibility that the difference in TMRE between non-capacitating and capacitating conditions is only caused by a different dye solubility or loading due to the presence of BSA. Altogether, these data support that during capacitation, cells undergo mitochondrial activation.

To further validate the use of TMRE to measure MMP in mouse sperm, flow cytometry experiments were repeated on sperm incubated during capacitation with different concentrations of the mitochondrial OXPHOS uncoupler, CCCP. Under these conditions, a dose-dependent decrease in both the MFI of the TMRE positive population (**Figure 2A**) and the percentage of TMRE positive cells (**Figure 2B**) was observed, which was significant from 10 μM CCCP. Viability controls using DAPI revealed that CCCP did not affect the percentage of living cells at any of the tested concentrations (**Figure 2C**). Subsequent fluorescence microscopy studies in capacitated cells showed TMRE signal only in the midpiece of the flagellum (**Figure 2D** left panels), consistent with the localization of mitochondria (Fawcett, 1975; Eddy, 2006; Gervasi et al., 2018). Accordingly, in CCCP-treated samples, sperm without TMRE staining were observed (**Figure 2D** right panels).

As the above results supporting the use of TMRE to assess sperm MMP dynamics, revealed an increase in this parameter during capacitation, two different strategies were undertaken to further analyze the association between mitochondrial activity and capacitation. In the first case, we evaluated whether the increase in MMP depends on capacitation-associated signaling pathways. For this purpose, sperm were incubated in the capacitation medium in the presence of H89, which blocks the capacitation-induced PKA signaling cascade, and MMP was determined by flow cytometry. Sperm incubated under capacitating conditions in the presence of CCCP or vehicle (capacitated sperm) were used as controls. Contrary to capacitated sperm, cells exposed to H89 or CCCP showed no increase in the percentage of cells exhibiting TMRE staining at the end of incubation (**Figure 3A**), with similar percentages of sperm viability among groups and time periods (**Figure 3B**). As a second approach, we investigated whether the increase in MMP was required for the occurrence of capacitation-associated signaling pathways leading to protein phosphorylation. To this end, sperm were incubated under capacitating conditions with different concentrations of CCCP, and the phosphorylation of proteins normally observed during

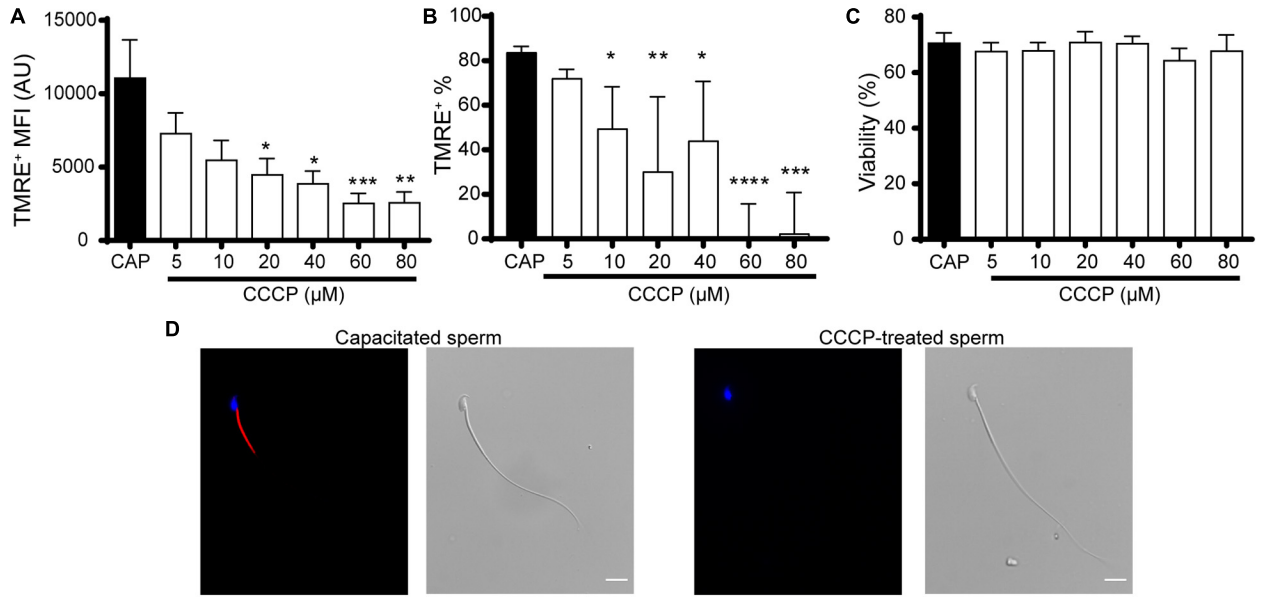

FIGURE 2 | Validation of TMRE as a probe for the analysis of mitochondrial membrane potential in mouse sperm. Epididymal sperm were incubated in the capacitation medium containing CCCP (5–80 μM) or DMSO (capacitated sperm, CAP), loaded with TMRE, and at 90 min of total incubation fluorescence was measured by flow cytometry. The following parameters were scored: **(A)** Mean fluorescence intensity (MFI). **(B)** Percentage of TMRE+ sperm. **(C)** Percentage of sperm viability. Results are expressed as mean ± SEM in **(A,C)** and median with interquartile range in **(B)**. In all cases, at least 3 independent experiments were performed. $^{*}p < 0.05$, $^{**}p < 0.01$, $^{***}p < 0.001$, $^{****}p < 0.0001$. **(D)** Representative fluorescence and phase-contrast microscopy images showing TMRE (red) and Hoechst 33342 (blue) staining patterns of capacitated (left) and CCCP-treated (right) sperm. $n = 3$. Bar = 10 μm.

capacitation (Visconti et al., 1995; Krapf et al., 2010) was assessed by Western blotting. Results showed no statistically significant differences in the capacitation-associated increase in either PKA substrates or tyrosine phosphorylations at any of the conditions tested (**Figures 3C,D**). Altogether, these results show that the increase in MMP is dependent on capacitation and H89-sensitive events, and that the PKA signaling cascade is not affected by mitochondrial disruption.

Relevance of Capacitation-Induced Mitochondrial Activity for Motility

In order to unveil an association between mitochondrial activity and motility in capacitated sperm, we simultaneously evaluated both variables in the same cell by microscopy. Whereas motility was subjectively recorded as motile or immotile in a bright field, high MMP was evaluated with TMRE by fluorescent staining. Results revealed that nearly all cells within the motile capacitated sperm population (98.1 ± 1.1%, $n = 3$) exhibited TMRE labeling (**Figure 4A**). In addition, immotile cells were mostly TMRE negative (71.1 ± 2.8%, $n = 3$) (**Figure 4A**). These observations support a strong association between high MMP and motility in capacitated sperm. Furthermore, objective analysis of motility by Computer assisted sperm analysis (CASA) showed that sperm treated with CCCP during capacitation exhibited a significant decrease in several of the kinematic parameters (**Supplementary Table 1**) as well as in the percentage of hyperactivation from 20 μM CCCP (**Figure 4B**) compared to control capacitated cells. Of note, there was no statistically significant difference between the effect produced by CCCP at 40 or 60 μM and H89 on hyperactivation (**Figure 4B**). Altogether, these results argue in favor of a role of mitochondrial activity in the development of hyperactivation during capacitation.

Relevance of Capacitation-Induced Mitochondrial Activity for *in vitro* Sperm Fertilizing Ability

To fully understand whether the rise in mitochondrial activity during capacitation is necessary for sperm to become fertilization competent, *in vitro* fertilization studies were carried out. For these experiments, sperm incubated under capacitating conditions with different concentrations of CCCP were washed, resuspended in fresh medium, and used to inseminate either ZP-free eggs, ZP-intact eggs or eggs surrounded by both the cumulus and the ZP (COCs). Results obtained using ZP-free eggs to evaluate gamete fusion showed similar fertilization rates among all treatments (**Figure 5A**). In contrast, in both approaches using eggs with ZP (with or without cumulus cells), a significant decrease in fertilization rates was observed for CCCP-treated sperm compared to controls without CCCP (**Figures 5B,C**). Interestingly, whereas for ZP-intact assays 20 μM CCCP was enough to produce a significantly negative effect, in cumulus-intact assays 40 μM was needed, supporting the already proposed beneficial effect of cumulus cells for capacitation and/or fertilization (Yanagimachi, 1994; Da Ros et al., 2008). Altogether, these results indicate that mitochondrial function is required for the acquisition of sperm fertilizing ability in

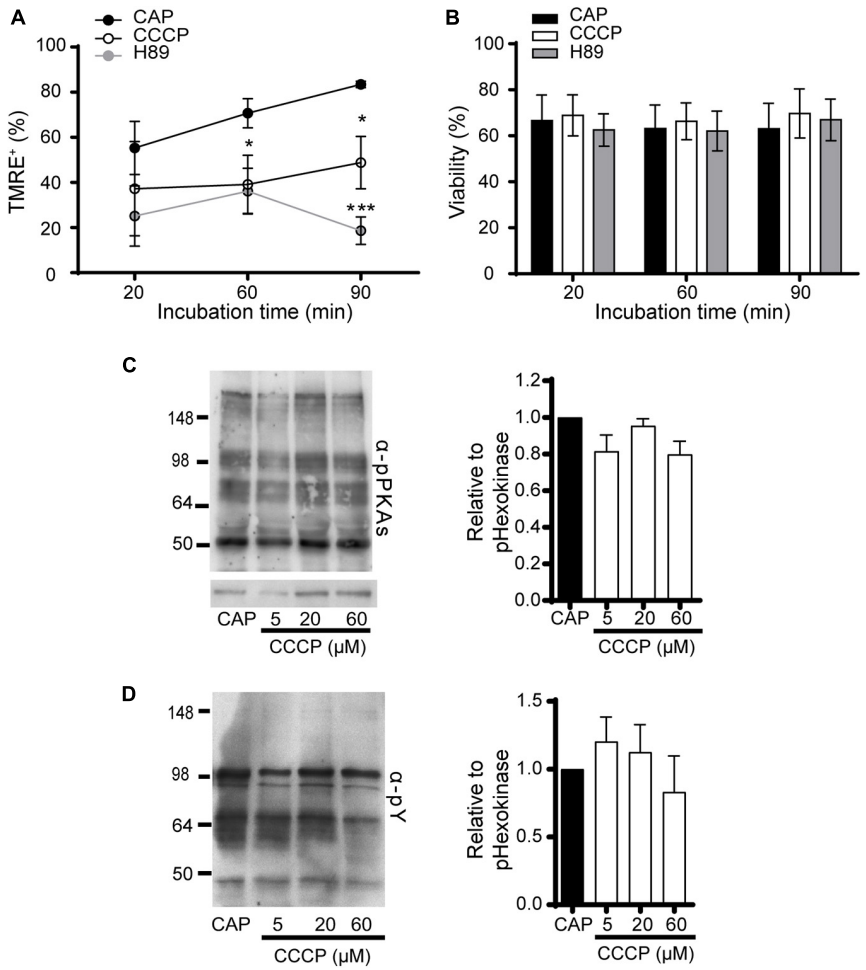

FIGURE 3 | Association between the increase in mitochondrial activity and capacitation in mouse sperm. **(A,B)** Epididymal sperm were incubated in the capacitation medium containing CCCP (20 μM), H89 (20 μM) or DMSO (capacitated sperm, CAP), loaded with TMRE, and fluorescence was measured by flow cytometry. The following parameters were scored: **(A)** Percentage of sperm exhibiting TMRE + signal. **(B)** Percentage of viability from experiments shown in **(A)**. Results are expressed as mean ± SEM. $n = 5$. $^{*}p < 0.05$, $^{***}p < 0.001$. **(C,D)** Epididymal sperm were incubated in the capacitation medium containing CCCP (5–60 μM) or DMSO (capacitated sperm, CAP), and analyzed by Western blotting for phosphorylation **(C)** in PKA substrates (α-pPKAs) and **(D)** in tyrosine residues (α-pY). Representative blots are shown on the left. Right panels correspond to quantification graphs of each phosphorylation normalized to CAP. At least 3 independent experiments were performed.

mice in a step previous to gamete fusion. Considering our observations showing that mitochondrial activity is necessary for hyperactivation and that this type of motility is required for penetration of the egg envelopes (Suarez and Dai, 1992; Yanagimachi, 1994; Stauss et al., 1995; Brukman et al., 2016), we next investigated whether the fertilization impairments observed were due to a failure in egg coat penetration. For this purpose, we performed cumulus penetration assays where CCCP-exposed sperm and controls (capacitated sperm and H89-treated sperm) were stained with Hoechst 33342 and used to inseminate COCs, recording the number of fluorescent sperm heads inside the *cumulus oophorus* 15 min later. Of note, the CCCP and H89 concentrations used were those that had produced an inhibitory effect on hyperactivation (see **Figure 4B**). As shown in **Figure 5D**, whereas few sperm were capable of penetrating the cumulus mass when incubated in the presence of H89, higher and similar numbers were observed for those incubated with CCCP as well as for capacitated control cells. These results do not support a role of mitochondria in the ability of sperm to penetrate the *cumulus oophorus*, indicating that hyperactivation induced by mitochondrial activity is mainly needed for ZP penetration.

Relevance of Capacitation-Induced Mitochondrial Activity for *in vivo* Sperm Fertilizing Ability

Based on the above *in vitro* observations, we next explored the relevance of mitochondrial function *in vivo*. As a proof of concept of this hypothesis, intrauterine inseminations in superovulated females were performed with sperm pre-treated with different concentrations of CCCP, and the fertilization rates were then analyzed. Results revealed a significant progressive decrease in

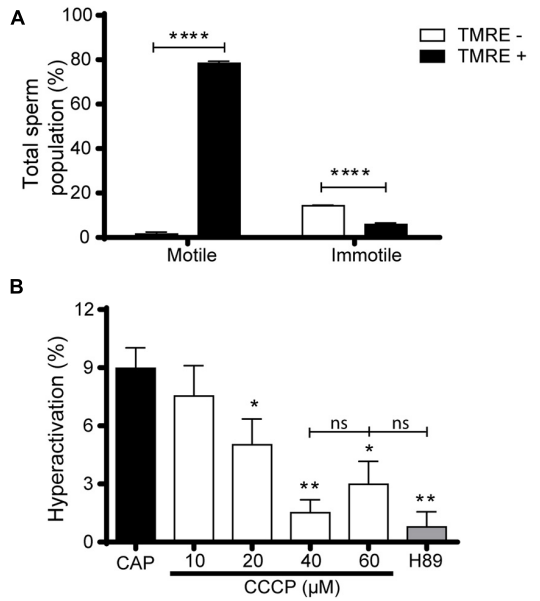

FIGURE 4 | Association between the increase in mitochondrial activity and motility in mouse sperm. **(A)** Epididymal sperm were incubated under capacitating conditions, loaded with TMRE, and motility as well as TMRE staining were simultaneously analyzed by microscopy to calculate the percentage of motile and immotile sperm with or without TMRE signal (TMRE+ and TMRE-, respectively). $n = 3$ **(B)** Epididymal sperm were incubated in the capacitation medium containing CCCP (10–60 μM), or H89 (20 μM) or DMSO (capacitated sperm, CAP), and the percentage of hyperactivation in motile sperm determined by CASA. At least 4 independent experiments were performed. In all cases, results are expressed as mean ± SEM; $^{*}p < 0.05$, $^{**}p < 0.01$, $^{****}p < 0.0001$.

the *in vivo* percentage of fertilized eggs as CCCP concentration increased, with a significant effect at 60 μM (**Figure 6**). For the few fertilized eggs obtained from CCCP-treated sperm, embryonic development was allowed to continue *in vitro*, observing normal blastocysts (data not shown). Altogether, these results show the key role of mitochondria function for not only the *in vitro* but also *in vivo* fertilizing ability of mouse sperm.

DISCUSSION

In the current study, mouse sperm mitochondrial activity was studied in depth in order to evaluate its dynamics during capacitation and its role for the acquisition of sperm fertilizing ability. Our principal contribution relies on the fact that mouse sperm capacitation is accompanied by a rise in mitochondrial activity which is required for hyperactivation and penetration of the egg envelope, likely the ZP rather than the *cumulus oophorus*. Complementary *in vivo* fertilization experiments further demonstrated the relevance of mitochondrial activity for sperm function, emphasizing the physiological importance of mitochondrial functionality for sperm fertilization competence.

Early studies of mitochondrial activity in mouse sperm were focused on O_2 consumption reporting a constant or a declined rate during capacitation (Boell, 1985; Fraser and Lane, 1987). On the other hand, recent works have shown an increase during capacitation in both OXPHOS, determined by an extracellular flux analyzer (Balbach et al., 2020), and MMP, analyzed by flow cytometry using JC-1 (Yang et al., 2020), a probe widely used despite its complexities and false results (Perry et al., 2011). However, none of these techniques allows the simultaneous determination of mitochondrial activity and viability in a single cell. In this sense, our study provides several advantages in the approach designed to overcome this limitation. First, we measured MMP by using TMRE, a probe that has never been used before in mouse sperm despite enabling multiparametric staining (Nicholls and Ward, 2000; Marchetti et al., 2004). This characteristic of the dye led us to assess MMP and viability in single sperm by flow cytometry. Second, our approach allowed us to perform these measurements in the presence of HCO_3^-, the physiological activator of capacitation. This is particularly relevant when considering recent reports showing an increase in glycolysis and OXPHOS during mouse sperm capacitation induced by pharmacological PKA activators (Balbach et al., 2020), although a lower glucose consumption was then observed under those conditions (Hidalgo et al., 2020). Therefore, our study is the first to evaluate MMP dynamics in single living sperm undergoing capacitation in physiological conditions.

Our results revealed a gradual increase in the number of sperm cells with high MMP during capacitation, in contraposition to the constant number observed when cells were incubated under non-capacitating conditions. The statistical difference between both conditions was observed around 1 h, suggesting that the rise in mitochondrial function in mouse sperm might be related to a mid or late event of the capacitation process. Interestingly, the lack of BSA in the presence of HCO_3^- in the capacitation medium (BSA-free or non-capacitating medium) precluded that increase, possibly due to the described role of this protein in the activation of HCO_3^-/PKA signaling pathway (Osheroff et al., 1999; Visconti et al., 1999). This effect is different to that observed under the same incubation conditions when glucose consumption was the endpoint measurement (Hidalgo et al., 2020), revealing different regulatory mechanisms for each energy metabolic pathway, and thus the importance of directly measuring MMP in mouse sperm. The fact that the TMRE fluorescence intensity of the positive cells did not change with the incubation conditions suggests that mitochondrial activation during capacitation is an "all-or-nothing" process within each sperm.

Specificity of the TMRE staining was further confirmed by the restricted localization of its fluorescence to the midpiece of the flagellum, the region in which mitochondria are confined in sperm (Fawcett, 1975; Eddy, 2006; Gervasi et al., 2018). Finally, the observation that the addition of CCCP to the capacitation medium abrogated the rise in MMP, both in flow cytometry and microscopy studies, validated the use of TMRE for MMP evaluation in mouse sperm. Of note, the collapse of mitochondrial activity induced by CCCP did not compromise sperm viability, at least during the time period analyzed, although mitochondrial activity disturbance is often associated with apoptosis in other cell types (Boguenet et al., 2021). Altogether, our observations support a role of mitochondrial function along the capacitation process. Therefore, besides the increase in

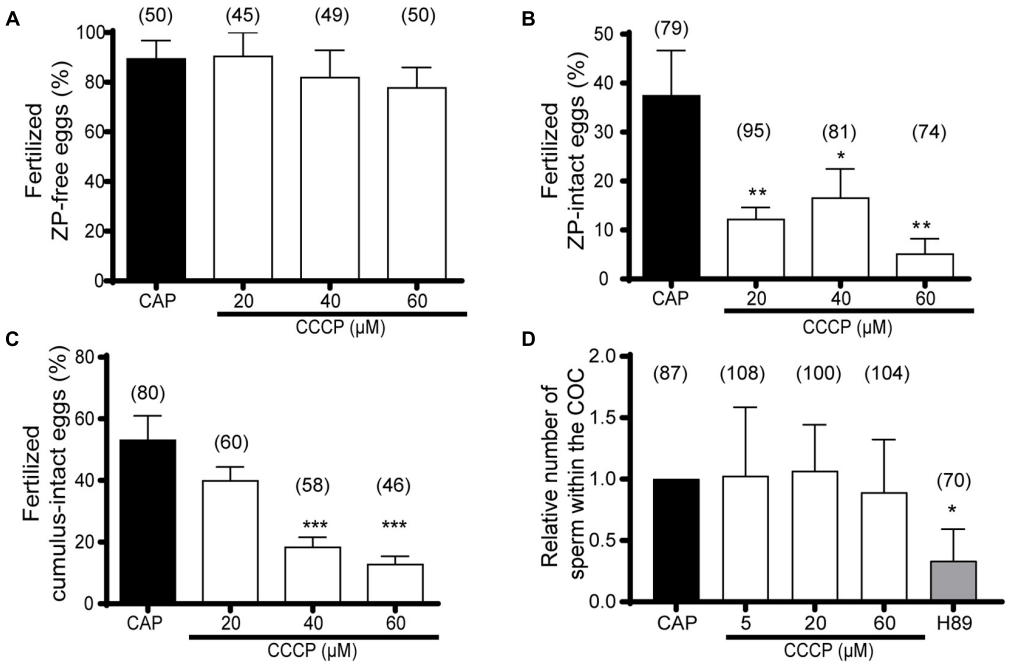

FIGURE 5 | Relevance of mitochondrial activity on mouse sperm *in vitro* fertilizing ability. **(A–C)** Epididymal sperm were incubated in the capacitation medium containing CCCP (20–60 μM) or DMSO (capacitated sperm, CAP), and used to inseminate **(A)** ZP-free eggs ($n = 4$), **(B)** ZP-intact eggs ($n = 5$) or **(C)** cumulus-intact eggs ($n = 4$). The percentage of fertilized eggs was determined in all cases. **(D)** Epididymal sperm were incubated in the capacitation medium containing CCCP (5–60 μM), H89 (20 μM), or DMSO (capacitated sperm, CAP), loaded with Hoechst 33342, and used to inseminate cumulus-intact eggs. After 15 min, the number of bright sperm heads within the cumulus matrix was determined. Results representing the relative numbers to the capacitated group are shown ($n = 6$). In brackets is indicated the total number of analyzed eggs per treatment. Results are expressed as mean ± SEM for **(A–C)** and median with interquartile range for **(D)**. $^{*}p < 0.05$, $^{**}p < 0.01$, $^{***}p < 0.001$.

intracellular pH and hyperpolarization of the plasma membrane potential, among others (reviewed in Puga Molina et al., 2018), the MMP rise represents another hallmark of capacitation that could be used as a new biomarker of this process in mouse sperm. Moreover, the successful setup of the TMRE measurement will undoubtedly be useful to further understand sperm physiology by analyzing MMP and other capacitation-induced parameters (i.e., pH increase), simultaneously, in single-cell approaches.

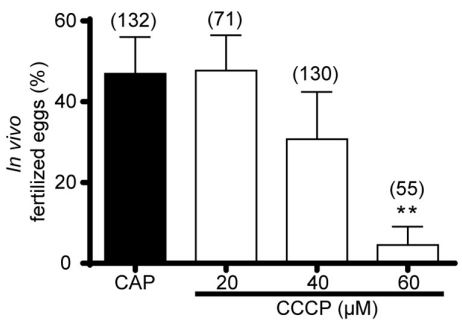

FIGURE 6 | Relevance of mitochondrial activity on mouse sperm *in vivo* fertilizing ability. Epididymal sperm in a non-capacitating concentration were incubated in the capacitation medium containing CCCP (20–60 μM) or DMSO (capacitated sperm, CAP), and used to inseminate superovulated females. After 15 h, COCs were collected from the *ampulla*, and incubated in KSOM medium, scoring the percentage of 2-cell embryos 24 h later. Results are expressed as mean ± SEM. At least 4 independent experiments were performed in which one or more females per treatment were included. In brackets is indicated the total number of analyzed eggs per treatment. $^{**}p < 0.01$.

Our experiments aimed to investigate the crosstalk between energy metabolic and signaling pathways during capacitation showed that the observed rise in mitochondrial functionality required at least the activation of the PKA signaling pathway. These results are consistent with the mentioned report showing an increase in mitochondrial activity after the downstream stimulation of HCO_3^--induced sAC (Balbach et al., 2020), jointly supporting an involvement of the HCO_3^-/sAC/PKA pathway in mitochondrial activity during mouse sperm capacitation. The other approach used to study this crosstalk showed that there is no significant effect of CCCP on PKA substrate phosphorylation, an expected result considering that this phosphorylation is an early event of capacitation (Krapf et al., 2010; Battistone et al., 2013) whereas the increase in mitochondrial activity was observed around 1 h of capacitation. In addition, similar results were obtained for tyrosine phosphorylation, in line with previous reports (Travis et al., 2001; Goodson et al., 2012; Balbach et al., 2020), indicating that mitochondrial function may not be essential to sustain phosphorylation of sperm proteins. Therefore, this led us to conclude that other energy metabolic pathways should be sufficient to support these phosphorylations.

Considering the conflict around the relevance of mitochondrial activity for mouse sperm motility (Mukai and Okuno, 2004; Goodson et al., 2012; Takei et al., 2014), we assessed simultaneously, in the same cell, if the increase in MMP was linked to the motility status of the capacitated cells. Our findings showing that motile sperm exclusively exhibited TMRE staining whereas the immotile cells were predominantly TMRE negatives, support a strong association between mitochondrial function and motility in mouse capacitated sperm. The very small number of immotile sperm displaying TMRE signal might be attributed to residual fluorescence of previously motile sperm. To our knowledge, this is the first study that simultaneously monitors both the occurrence of an energy metabolic pathway and a functional sperm parameter in a single cell subjected to capacitation. Of note, although previous studies showed no association between mitochondrial function and sperm motility (Mukai and Okuno, 2004; Takei et al., 2014), no references were made to whether sperm were incubated or not under capacitating conditions, particularly about the presence of BSA in the medium, which seems to be required for mitochondrial activity according to our results. Moreover, when we objectively analyzed motility after capacitation by CASA, several kinematic parameters as well as the percentage of hyperactivated sperm decreased in the groups exposed to CCCP in comparison to the capacitated control, supporting a role for mitochondrial function in the acquisition and/or maintenance of hyperactivation. Our data showing that sperm mitochondrial disruption results in normal protein phosphorylation with a reduced hyperactivation, reveals that this type of motility implies more than the activation of the phosphorylation pathway, including molecular mechanisms that depend on mitochondrial activity (Ramalho-Santos et al., 2009). Their precise contribution to hyperactivation requires further investigation. Interestingly, Goodson et al. (2012) showed that the addition of glucose or mannose, contrary to pyruvate and lactate, in the capacitation medium supported hyperactivation, suggesting a role for glycolysis over mitochondrial metabolism in this type of motility. A possible explanation to merge their and our results might be that hyperactivation depends on both pathways as suggested by the facts that: (1) hyperactivation is sustained in the presence of glucose (Goodson et al., 2012), condition in which both glycolysis and mitochondria are active, considering the recent reported link between both metabolic pathways (Tourmente et al., 2015; Balbach et al., 2020), and (2) hyperactivation is diminished when only one of these pathways is active (Goodson et al., 2012 and present results), i.e., in the presence of pyruvate only mitochondria are functional, and in the presence of CCCP only glycolysis is active.

Having observed a role of mitochondrial functionality in capacitation, we then evaluated whether this was relevant for the acquisition of sperm fertilizing ability. *In vitro* gamete fusion assays revealed that mitochondrial activity during capacitation was not required for sperm to fuse with the egg, reinforcing previous observations precluding the requirement of hyperactivation for this step of gamete interaction (Yanagimachi, 1994; Ren et al., 2001; Xie et al., 2006). On the other hand, *in vitro* fertilization studies demonstrated the need of mitochondrial function during capacitation for sperm to penetrate the egg coats. In line with our results, Balbach et al. (2020) have recently reported higher fertilization rates of cumulus-intact eggs when sperm were capacitated in the presence of both glucose and pyruvate than the mere presence of only one of them, suggesting that both glycolysis and mitochondrial metabolism are contributing, possibly to a different extent, to the development of not only hyperactivation but also the sperm fertilizing ability. In this regard, and considering that hyperactivation is required for egg envelope penetration (Suarez and Dai, 1992; Yanagimachi, 1994; Stauss et al., 1995; Brukman et al., 2016), our results support the idea that the low fertilization rates of sperm exposed to CCCP were linked to the observed defects in hyperactivation. The fact that CCCP-treated sperm were able to penetrate the *cumulus oophorus* supports a role of mitochondrial activity-induced hyperactivation mainly in the ZP penetration step. Interestingly, H89-exposed sperm, exhibiting similar hyperactivation defects than CCCP-treated sperm, produced lower cumulus penetration rates. Therefore, the flagellar movement assigned in both cases as hyperactivation by CASA was functionally different, suggesting that physiologically relevant motility still cannot be measured by current methods and, therefore, the development of alternative overcoming approaches for its determination, such as 3D high-resolution flagellar tracking (Nandagiri et al., 2021), might be needed. Alternatively, the requirement of hyperactivation, as determined by CASA, for sperm penetration of the cumulus matrix might need some revision (Suarez and Dai, 1992; Brukman et al., 2016).

Taking into account that the *in vitro* capacitation conditions may differ from those encountered by sperm in their transit through the female reproductive tract, in particular considering that the availability of nutrients and its concentrations *in vivo* are poorly defined, performing *in vivo* studies was critical to determine the physiological relevance of our *in vitro* findings. Our results from intrauterine insemination experiments revealed the need of mitochondrial function for sperm to fertilize the egg *in vivo* as well as the availability of oxidizable substrates in the female reproductive tract. Although the use of CCCP in these experiments is regarded as a proof of concept to study mitochondrial function under physiological conditions, this type of *in vivo* approach is unique in terms of the potentiality of discovering similarities and disparities between *in vitro* and *in vivo* capacitation. In this sense, different CCCP concentrations between both conditions were needed to obtain a significant effect in the fertilizing ability of sperm. Besides this, we could not assess whether the *in vivo* effect was attributable to the one observed *in vitro* in ZP penetration or, additionally, to another hyperactivation-dependent event such as swimming through the oviductal fluid (Demott and Suarez, 1992; Suarez and Dai, 1992; Yanagimachi, 1994; Stauss et al., 1995; Brukman et al., 2016) due to the lack of appropriate tools to study sperm migration. In line with this, an association between mitochondrial dysfunctionality and male infertility as a result of a diminished sperm motility has been reported for several knockout models (VPS13A, Tppp2, Gykl1, and Gk2) (Chen et al., 2017; Nagata et al., 2018; Zhu et al., 2019).

It has been postulated that whereas glycolysis is used for activities requiring quick and local increases of ATP, OXPHOS is a more efficient source of ATP over time (Zecchin et al., 2015). Therefore, considering the high demand on ATP sperm have in their long journey through the female reproductive tract to accomplish fertilization in the *ampulla,* it is tempting to speculate that *in vivo* sperm may utilize both metabolic pathways in response to the different extracellular energy substrates to produce ATP. In view of this, more innovative strategies are still needed to be developed in order to fully understand how sperm metabolism could shift *in vivo* between glycolysis and OXPHOS.

In humans, MMP has been postulated as a predictive marker of sperm fertilization ability in both natural conception and *in vitro* fertilization (reviewed in Ramalho-Santos et al., 2009; Boguenet et al., 2021). However, the precise role of mitochondrial activity in human sperm is hampered primarily by ethical issues concerning research with human eggs. In the present study, we explored this in the mouse model which, in spite of presenting some differences in the molecular mechanisms underlying capacitation compared to human (Puga Molina et al., 2018; Boguenet et al., 2021), is the best approach that can be used to study gamete interaction *in vitro* and *in vivo*. In view of this, our findings demonstrating that *in vivo* sperm fertilizing ability is dependent on mitochondrial activity could help to understand sperm physiology and might serve as the basis for future studies focusing on the mitochondria as a target for contraception development and/or for diagnosis and treatment of fertility disorders.

DATA AVAILABILITY STATEMENT

The raw data supporting the conclusions of this article will be made available by the authors, without undue reservation.

ETHICS STATEMENT

The animal study was reviewed and approved by Institutional Animal Care and Use Committee of Instituto de Biología y Medicina Experimental.

AUTHOR CONTRIBUTIONS

MG, MG-E, and JH performed all experiments. CM-B collaborated with CASA evaluation. MG, DC, and VD designed the experiments, analyzed the results, and wrote the manuscript. PC contributed intellectual content in the experimental design and the discussion of results. All authors read, corrected, and approved the final manuscript.

FUNDING

This study was partially supported by National Agency for Scientific and Technological Promotion (ANPCyT) grants (PICT 2015-555 to VD and PICT 2017-668 to DC and VD).

ACKNOWLEDGMENTS

We would like to thank laboratory members for their helpful comments. We greatly acknowledge Rene Baron and Williams Foundations.

SUPPLEMENTARY MATERIAL

The Supplementary Material for this article can be found online at: https://www.frontiersin.org/articles/10.3389/fcell.2021.767161/full#supplementary-material

REFERENCES

Austin, C. R. (1952). The capacitation of the Mammalian Sperm. *Nature* 170, 328–329.

Balbach, M., Gervasi, M. G., Hidalgo, D. M., Visconti, P. E., Levin, L. R., and Buck, J. (2020). Metabolic changes in mouse sperm during capacitation. *Biol. Reprod.* 4, 791–801. doi: 10.1093/biolre/ioaa114

Barbagallo, F., La Vignera, S., Cannarella, R., Aversa, A., Calogero, A. E., and Condorelli, R. A. (2020). Evaluation of Sperm Mitochondrial Function: a Key Organelle for Sperm Motility. *J. Clin. Med.* 9:363. doi: 10.3390/jcm9020363

Battistone, M. A., Da Ros, V. G., Salicioni, A. M., Navarrete, F. A., Krapf, D., Visconti, P. E., et al. (2013). Functional human sperm capacitation requires both bicarbonate-dependent PKA activation and down-regulation of Ser/Thr phosphatases by Src family kinases. *Mol. Hum. Reprod.* 19, 570–580. doi: 10.1093/molehr/gat033

Boell, E. J. (1985). Oxygen consumption of mouse sperm and its relationship to capacitation. *J. Exp. Zool.* 234, 105–116. doi: 10.1002/jez.1402340113

Boguenet, M., Bouet, P. E., Spiers, A., Reynier, P., and May-Panloup, P. (2021). Mitochondria: their role in spermatozoa and in male infertility. *Hum. Reprod. Update* 27, 697–719. doi: 10.1093/humupd/dmab001

Bray, C., Son, J. H., Kumar, P., and Meizel, S. (2005). Mice deficient in CHRNA7, a subunit of the nicotinic acetylcholine receptor, produce sperm with impaired motility. *Biol. Reprod.* 73, 807–814. doi: 10.1095/biolreprod.105.042184

Brukman, N. G., Miyata, H., Torres, P., Lombardo, D., Caramelo, J. J., Ikawa, M., et al. (2016). Fertilization defects in sperm from Cysteine-rich secretory protein 2 (Crisp2) knockout mice: implications for fertility disorders. *Mol. Hum. Reprod.* 4, 240–251. doi: 10.1093/molehr/gaw005

Bunch, D. O., Welch, J. E., Magyar, P. L., Eddy, E. M., and O'Brien, D. A. (1998). Glyceraldehyde 3-phosphate dehydrogenase-S protein distribution during mouse spermatogenesis. *Biol. Reprod.* 58, 834–841. doi: 10.1095/biolreprod58.3.834

Chang, M. (1951). Fertilizing capacity of spermatozoa deposited into the fallopian tubes. *Nature* 168, 697–698. doi: 10.1038/168697b0

Chen, Y., Liang, P., Huang, Y., Li, M., Zhang, X., Ding, C., et al. (2017). Glycerol kinase-like proteins cooperate with Pld6 in regulating sperm mitochondrial sheath formation and male fertility. *Cell Discov.* 3:17030. doi: 10.1038/celldisc.2017.30

Curci, L., Carvajal, G., Sulzyk, V., Gonzalez, S. N., and Cuasnicú, P. S. (2021). Pharmacological Inactivation of CatSper Blocks Sperm Fertilizing Ability Independently of the Capacitation Status of the Cells: implications for Non-hormonal Contraception. *Front. Cell Dev. Biol.* 9:686461. doi: 10.3389/fcell.2021.686461

Da Ros, V. G., Maldera, J. A., Willis, W. D., Cohen, D. J., Goulding, E. H., Gelman, D. M., et al. (2008). Impaired sperm fertilizing ability in mice lacking Cysteine-RIch Secretory Protein 1 (CRISP1). *Dev. Biol.* 320, 12–18. doi: 10.1016/j.ydbio.2008.03.015

Danshina, P. V., Geyer, C. B., Dai, Q., Goulding, E. H., Willis, W. D., Kitto, G. B., et al. (2010). Phosphoglycerate kinase 2 (PGK2) is essential for sperm function and male fertility in mice. *Biol. Reprod.* 82, 136–145. doi: 10.1095/biolreprod.109.079699

Demott, R. P., and Suarez, S. S. (1992). Hyperactivated sperm progress in the mouse oviduct. *Biol. Reprod.* 46, 779–785. doi: 10.1095/biolreprod46.5.779

Eddy, E. (2006). "The Spermatozoon," in *Knobil and Neill's Physiology of Reproduction*, ed. J. D. Neil (New York: Elsevier), 3–54.

Erbach, G. T., Lawitts, J. A., Papaioannou, V. E., and Biggers, J. D. (1994). Differential growth of the mouse preimplantation embryo in chemically defined media. *Biol. Reprod.* 50, 1027–1033. doi: 10.1095/biolreprod50.5.1027

Ernesto, J. I., Weigel Muñoz, M., Battistone, M. A., Vasen, G., Martínez-López, P., Orta, G., et al. (2015). CRI SP1 as a novel CatSper regulator that modulates sperm motility and orientation during fertilization. *J. Cell Biol.* 210, 1213–1224. doi: 10.1083/jcb.201412041

Fawcett, D. W. (1975). The mammalian spermatozoon. *Dev. Biol.* 2, 394–436. doi: 10.1016/0012-1606(75)90411-x

Fraser, L. R., and Lane, M. R. (1987). Capacitation- and fertilization- related alterations in mouse sperm oxygen consumption. *J. Reprod. Fertil.* 81, 385–393. doi: 10.1530/jrf.0.0810385

Gervasi, M. G., Xu, X., Carbajal-Gonzalez, B., Buffone, M. G., Visconti, P. E., and Krapf, D. (2018). The actin cytoskeleton of the mouse sperm flagellum is organized in a helical structure María Gracia Gervasi. *J. Cell Sci.* 131:jcs215897. doi: 10.1242/jcs.215897

Goodson, S. G., Qiu, Y., Sutton, K. A., Xie, G., Jia, W., and O'Brien, D. A. (2012). Metabolic substrates exhibit differential effects on functional parameters of mouse sperm capacitation. *Biol. Reprod.* 87:75. doi: 10.1095/biolreprod.112.102673

Hidalgo, D. M., Romarowski, A., Gervasi, M. G., Navarrete, F., Balbach, M., Salicioni, A. M., et al. (2020). Capacitation increases glucose consumption in murine sperm. *Mol. Reprod. Dev.* 87, 1037–1047. doi: 10.1002/mrd.23421

Kalab, P., Visconti, P., Leclerc, P., and Kopf, G. S. (1994). P95, the Major Phosphotyrosine-Containing Protein in Mouse Spermatozoa, Is a Hexokinase With Unique Properties. *J. Biol. Chem.* 269, 3810–3817. doi: 10.1016/s0021-9258(17)41932-6

Krapf, D., Arcelay, E., Wertheimer, E. V., Sanjay, A., Pilder, S. H., Salicioni, A. M., et al. (2010). Inhibition of Ser/Thr phosphatases induces capacitation-associated signaling in the presence of Src kinase inhibitors. *J. Biol. Chem.* 285, 7977–7985. doi: 10.1074/jbc.M109.085845

Krisfalusi, M., Miki, K., Magyar, P. L., and O'Brien, D. A. (2006). Multiple glycolytic enzymes are tightly bound to the fibrous sheath of mouse spermatozoa. *Biol. Reprod.* 75, 270–278. doi: 10.1095/biolreprod.105.049684

Laemmli, U. K. (1970). Cleavage of structural proteins during the assembly of the head of bacteriophage T4. *Nature* 228, 726–734. doi: 10.1038/227680a0

Lee, J. A., Spidlen, J., Boyce, K., Cai, J., Crosbie, N., Dalphin, M., et al. (2008). MIFlowCyt: the Minimum Information about a Flow Cytometry Experiment. *Cytometry A* 73, 926–930. doi: 10.1002/cyto.a.20623.MIFlowCyt

Losano, J. D. A., Angrimani, D. S. R., Dalmazzo, A., Rui, B. R., Brito, M. M., Mendes, C. M., et al. (2017). Effect of mitochondrial uncoupling and glycolysis inhibition on ram sperm functionality. *Reprod. Domest. Anim.* 52, 289–297. doi: 10.1111/rda.12901

Marchetti, C., Jouy, N., Leroy-Martin, B., Defossez, A., Formstecher, P., and Marchetti, P. (2004). Comparison of four fluorochromes for the detection of the inner mitochondrial membrane potential in human spermatozoa and their correlation with sperm motility. *Hum. Reprod.* 19, 2267–2276. doi: 10.1093/humrep/deh416

Miki, K., Qu, W., Goulding, E. H., Willis, W. D., Bunch, D. O., Strader, L. F., et al. (2004). Glyceraldehyde 3-phosphate dehydrogenase-S, a sperm-specific glycolytic enzyme, is required for sperm motility and male fertility. *Proc. Natl. Acad. Sci. U. S. A.* 101, 16501–16506. doi: 10.1073/pnas.0407708101

Mukai, C., and Okuno, M. (2004). Glycolysis plays a major role for adenosine triphosphate supplementation in mouse sperm flagellar movement. *Biol. Reprod.* 71, 540–547. doi: 10.1095/biolreprod.103.026054

Nagata, O., Nakamura, M., Sakimoto, H., Urata, Y., Sasaki, N., Shiokawa, N., et al. (2018). Mouse model of chorea-acanthocytosis exhibits male infertility caused by impaired sperm motility as a result of ultrastructural morphological abnormalities in the mitochondrial sheath in the sperm midpiece. *Biochem. Biophys. Res. Commun.* 503, 915–920. doi: 10.1016/j.bbrc.2018.06.096

Nandagiri, A., Gaikwad, A. S., Potter, D. L., Nosrati, R., Soria, J., O'bryan, M. K., et al. (2021). Flagellar energetics from high-resolution imaging of beating patterns in tethered mouse sperm. *Elife* 10:e62524. doi: 10.7554/ELIFE.62524

Narisawa, S., Hecht, N. B., Goldberg, E., Boatright, K. M., Reed, J. C., and Millán, J. L. (2002). Testis-Specific Cytochrome c -Null Mice Produce Functional Sperm but Undergo Early Testicular Atrophy. *Mol. Cell. Biol.* 22, 5554–5562. doi: 10.1128/mcb.22.15.5554-5562.2002

Nayernia, K., Adham, I. M., Burkhardt-Göttges, E., Neesen, J., Rieche, M., Wolf, S., et al. (2002). Asthenozoospermia in Mice with Targeted Deletion of the Sperm Mitochondrion-Associated Cysteine-Rich Protein (Smcp) Gene. *Mol. Cell. Biol.* 22, 3046–3052. doi: 10.1128/mcb.22.9.3046-3052.2002

Nicholls, D. G., and Ward, M. W. (2000). Mitochondrial membrane potential and neuronal glutamate excitotoxicity: mortality and millivolts. *Trends Neurosci.* 23, 166–174. doi: 10.1016/s0166-2236(99)01534-9

Nicolson, G. L., Yanagimachi, R., and Yanagimachi, H. (1975). Ultrastructural localization of lectin-binding sites on the zonae pellucide and plasma membranes of mamalian eggs. *J. Cell Biol.* 66, 263–274. doi: 10.1083/jcb.66.2.263

Nowicka-bauer, K., and Nixon, B. (2020). Molecular changes induced by oxidative stress that impair human sperm motility. *Antioxidants* 9:134. doi: 10.3390/antiox9020134

Odet, F., Duan, C., Willis, W. D., Goulding, E. H., Kung, A., Eddy, E. M., et al. (2008). Expression of the gene for mouse lactate dehydrogenase C (Ldhc) is required for male fertility. *Biol. Reprod.* 79, 26–34. doi: 10.1095/biolreprod.108.068353

Osheroff, J. E., Visconti, P. E., Valenzuela, J. P., Travis, A. J., Alvarez, J., and Kopf, G. S. (1999). Regulation of human sperm capacitation by a cholesterol efflux-stimulated signal transduction pathway leading to protein kinase A-mediated up-regulation of protein tyrosine phosphorylation. *Mol. Hum. Reprod.* 5, 1017–1026. doi: 10.1093/molehr/5.11.1017

Perry, S. W., Norman, J. P., Barbieri, J., Brown, E. B., and Gelbard, H. A. (2011). Mitochondrial membrane potential probes and the proton gradient: a practical usage guide. *Biotechniques* 50, 98–115. doi: 10.2144/000113610

Puga Molina, L. C. P., Balestrini, P. A., Marín-Briggiler, C. I., Romarowski, A., and Buffone, M. G. (2018). Molecular basis of human sperm capacitation. *Front. Cell Dev. Biol.* 6:72. doi: 10.3389/fcell.2018.00072

Ramalho-Santos, J., Varum, S., Amaral, S., Mota, P. C., Sousa, A. P., and Amaral, A. (2009). Mitochondrial functionality in reproduction: from gonads and gametes to embryos and embryonic stem cells. *Hum. Reprod. Update* 15, 553–572. doi: 10.1093/humupd/dmp016

Ren, D., Navarro, B., Perez, G., Jackson, A. C., Hsu, S., Shi, Q., et al. (2001). A sperm ion channel required for sperm motility and male fertility. *Nature* 413, 603–609. doi: 10.1038/35098027

Ruiz-Pesini, E., Díez-Sánchez, C., López-Pérez, M. J., and Enríquez, J. A. (2007). The Role of the Mitochondrion in Sperm Function: is There a Place for Oxidative Phosphorylation or Is This a Purely Glycolytic Process?. *Curr. Top. Dev. Biol.* 77, 3–19. doi: 10.1016/S0070-2153(06)77001-6

Shahrokhi, S. Z., Salehi, P., Alyasin, A., Taghiyar, S., and Deemeh, M. R. (2020). Asthenozoospermia: cellular and molecular contributing factors and treatment strategies. *Andrologia* 52:e13463. doi: 10.1111/and.13463

Stauss, C. R., Votta, T. J., and Suarez, S. S. (1995). Sperm motility hyperactivation facilitates penetration of the hamster zona pellucida. *Biol. Reprod.* 53, 1280–1285. doi: 10.1095/biolreprod53.6.1280

Suarez, S. S., and Dai, X. (1992). Hyperactivation enhances mouse sperm capacity for penetrating viscoelastic media. *Biol. Reprod.* 46, 686–691. doi: 10.1095/biolreprod46.4.686

Takei, G. L., Miyashiro, D., Mukai, C., and Okuno, M. (2014). Glycolysis plays an important role in energy transfer from the base to the distal end of the flagellum in mouse sperm. *J. Exp. Biol.* 217, 1876–1886. doi: 10.1242/jeb.090985

Tourmente, M., Villar-Moya, P., Rial, E., and Roldan, E. R. S. (2015). Differences in ATP generation via glycolysis and oxidative phosphorylation and relationships with sperm motility in mouse species. *J. Biol. Chem.* 290, 20613–20626. doi: 10.1074/jbc.M115.664813

Travis, A. J., Jorgez, C. J., Merdiushev, T., Jones, B. H., Dess, D. M., Diaz-Cueto, L., et al. (2001). Functional Relationships between Capacitation-dependent Cell Signaling and Compartmentalized Metabolic Pathways in Murine Spermatozoa. *J. Biol. Chem.* 276, 7630–7636. doi: 10.1074/jbc.M006217200

Tu, C., Wang, W., Hu, T., Lu, G., Lin, G., and Tan, Y. Q. (2020). Genetic underpinnings of asthenozoospermia. *Best Pract. Res. Clin. Endocrinol. Metab.* 34:101472. doi: 10.1016/j.beem.2020.101472

Visconti, P. E., Bailey, J. L., Moore, G. D., Pan, D., Olds-Clarke, P., and Kopf, G. S. (1995). Capacitation of mouse spermatozoa. I. Correlation between the capacitation state and protein tyrosine phosphorylation. *Development* 121, 1129–1137.

Visconti, P. E., Galantino-Homer, H., Ning, X., Moore, G. D., Valenzuela, J. P., Jorgez, C. J., et al. (1999). Cholesterol Efflux-mediated Signal Transduction in Mammalian Sperm. *J. Biol. Chem.* 274, 3235–3242. doi: 10.1074/jbc.274.5.3235

Visconti, P. E., Olds-Clarke, P., Moss, S. B., Kalab, P., Travis, A. J., De Las Heras, M., et al. (1996). Properties and localization of a tyrosine phosphorylated form of hexokinase in mouse sperm. *Mol. Reprod. Dev.* 43, 82–93. doi: 10.1002/(SICI)1098-2795(199601)43:1<82::AID-MRD11<3.0.CO;2-6

Weigel Muñoz, M., Battistone, M. A., Carvajal, G., Maldera, J. A., Curci, L., Torres, P., et al. (2018). Influence of the genetic background on the reproductive phenotype of mice lacking Cysteine-RIch Secretory Protein 1 (CRISP1). *Biol. Reprod.* 99, 373–383. doi: 10.1093/biolre/ioy048/4898003

Xie, F., Garcia, M. A., Carlson, A. E., Schuh, S. M., Babcock, D. F., Jaiswal, B. S., et al. (2006). Soluble adenylyl cyclase (sAC) is indispensable for sperm function and fertilization. *Dev. Biol.* 296, 353–362. doi: 10.1016/j.ydbio.2006.05.038

Yanagimachi, R. (1994). "The physiology of reproduction," in *Knobil and Neill's Physiology of Reproduction*, eds E. Knobil and J. D. Neill (New York, NY: Raven Press), 189–317.

Yang, Q., Wen, Y., Wang, L., Peng, Z., Yeerken, R., Zhen, L., et al. (2020). Ca2+ ionophore A23187 inhibits ATP generation reducing mouse sperm motility and PKA-dependent phosphorylation. *Tissue Cell* 66:101381. doi: 10.1016/j.tice.2020.101381

Zecchin, A., Stapor, P. C., Goveia, J., and Carmeliet, P. (2015). Metabolic pathway compartmentalization: an underappreciated opportunity?. *Curr. Opin. Biotechnol.* 34, 73–81. doi: 10.1016/j.copbio.2014.11.022

Zhu, F., Yan, P., Zhang, J., Cui, Y., Zheng, M., Cheng, Y., et al. (2019). Deficiency of TPPP2, a factor linked to oligoasthenozoospermia, causes subfertility in male mice. *J. Cell. Mol. Med.* 23, 2583–2594. doi: 10.1111/jcmm.14149

Conflict of Interest: The authors declare that the research was conducted in the absence of any commercial or financial relationships that could be construed as a potential conflict of interest.

Publisher's Note: All claims expressed in this article are solely those of the authors and do not necessarily represent those of their affiliated organizations, or those of the publisher, the editors and the reviewers. Any product that may be evaluated in this article, or claim that may be made by its manufacturer, is not guaranteed or endorsed by the publisher.

frontiers in Cell and Developmental Biology

ORIGINAL RESEARCH
published: 10 December 2021
doi: 10.3389/fcell.2021.765673

Membrane Remodeling and Matrix Dispersal Intermediates During Mammalian Acrosomal Exocytosis

Miguel Ricardo Leung[1,2], *Ravi Teja Ravi*[1], *Bart M. Gadella*[3] *and Tzviya Zeev-Ben-Mordehai*[1,2]*

[1]Bijvoet Centre for Biomolecular Research, Utrecht University, Utrecht, Netherlands, [2]The Division of Structural Biology, Wellcome Centre for Human Genetics, The University of Oxford, Oxford, United Kingdom, [3]Department of Farm and Animal Health and Biomolecular Health Sciences, Faculty of Veterinary Medicine, Utrecht University, Utrecht, Netherlands

To become fertilization-competent, mammalian sperm must undergo a complex series of biochemical and morphological changes in the female reproductive tract. These changes, collectively called capacitation, culminate in the exocytosis of the acrosome, a large vesicle overlying the nucleus. Acrosomal exocytosis is not an all-or-nothing event but rather a regulated process in which vesicle cargo disperses gradually. However, the structural mechanisms underlying this controlled release remain undefined. In addition, unlike other exocytotic events, fusing membranes are shed as vesicles; the cell thus loses the entire anterior two-thirds of its plasma membrane and yet remains intact, while the remaining nonvesiculated plasma membrane becomes fusogenic. Precisely how cell integrity is maintained throughout this drastic vesiculation process is unclear, as is how it ultimately leads to the acquisition of fusion competence. Here, we use cryoelectron tomography to visualize these processes in unfixed, unstained, fully hydrated sperm. We show that paracrystalline structures within the acrosome disassemble during capacitation and acrosomal exocytosis, representing a plausible mechanism for gradual dispersal of the acrosomal matrix. We find that the architecture of the sperm head supports an atypical membrane fission–fusion pathway that maintains cell integrity. Finally, we detail how the acrosome reaction transforms both the micron-scale topography and the nanoscale protein landscape of the sperm surface, thus priming the sperm for fertilization.

Keywords: acrosome reaction, mammalian sperm, membrane fusion, cryo-elecron tomography, fertilization

OPEN ACCESS

Edited by:
Enrica Bianchi,
University of York, United Kingdom

Reviewed by:
Mariano G. Buffone,
CONICET Instituto de Biología y Medicina Experimental (IBYME), Argentina
María José Gómez-Torres,
University of Alicante, Spain

***Correspondence:**
Tzviya Zeev-Ben-Mordehai
z.zeev@uu.nl

Specialty section:
This article was submitted to Molecular and Cellular Reproduction, a section of the journal Frontiers in Cell and Developmental Biology

Received: *27 August 2021*
Accepted: *19 October 2021*
Published: *10 December 2021*

Citation:
Leung MR, Ravi RT, Gadella BM and Zeev-Ben-Mordehai T (2021) Membrane Remodeling and Matrix Dispersal Intermediates During Mammalian Acrosomal Exocytosis. Front. Cell Dev. Biol. 9:765673. doi: 10.3389/fcell.2021.765673

INTRODUCTION

Mammalian sperm must reside in the female reproductive tract for several hours before they are able to fertilize the egg. During this time, sperm undergo a plethora of biochemical changes collectively called capacitation (Bailey, 2010; Aitken and Nixon, 2013; Gervasi and Visconti, 2016). The discovery of this phenomenon was crucial to the development of *in vitro* fertilization (Austin, 1951; Chang, 1951, Chang, 1959). Capacitation is characterized by cholesterol efflux, phospholipase activation, and altered membrane fluidity, along with a multitude of biochemical changes (Nolan and Hammerstedt, 1997; Travis and Kopf, 2002; Harrison and Gadella, 2005; Bailey, 2010). Together, these changes render sperm capable of undergoing the acrosome reaction, a unique exocytotic event that is an absolute requirement for sperm to become fusion-competent (Yanagimachi, 1981) (**Figure 1A**).

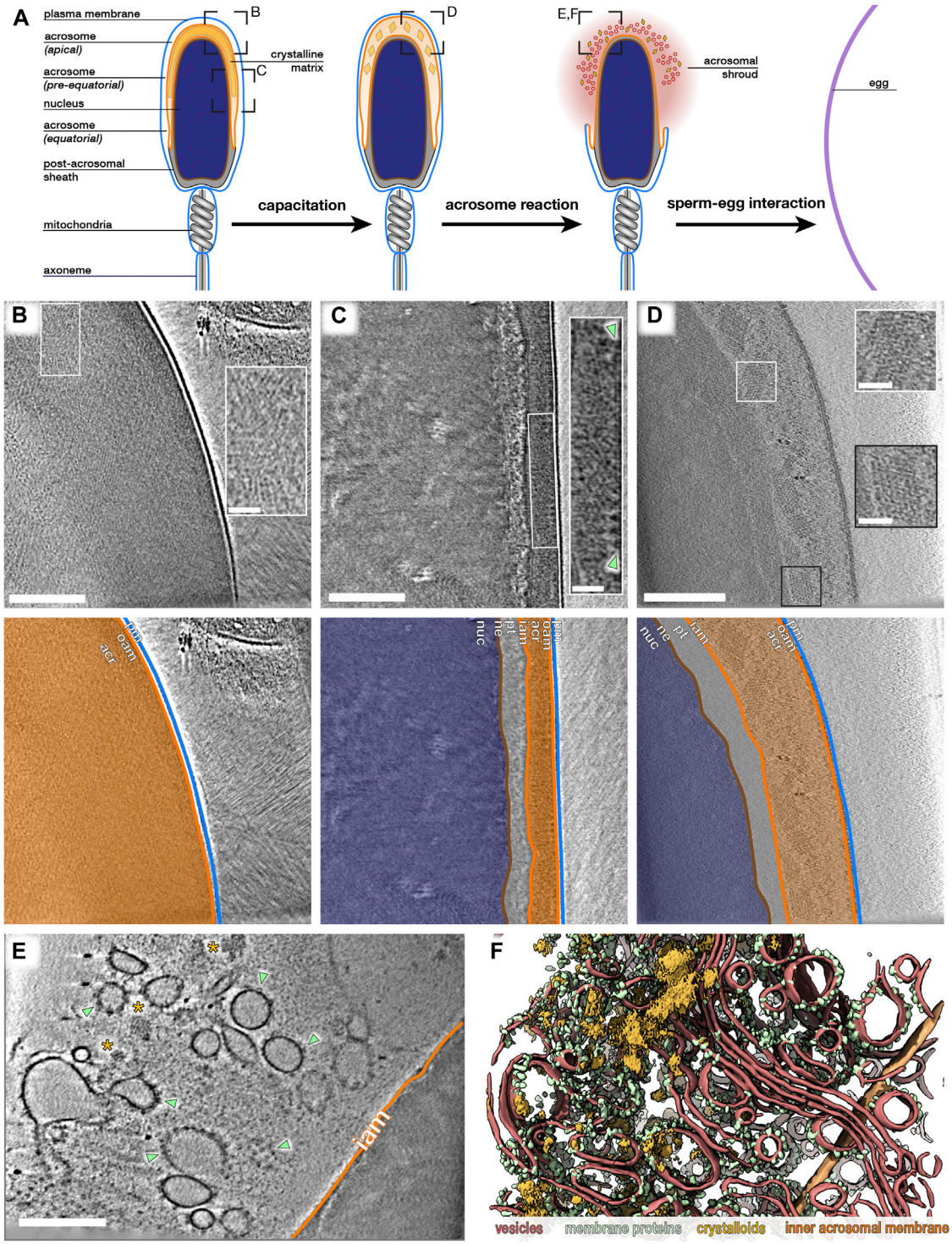

FIGURE 1 | The paracrystalline fraction of the acrosomal matrix progressively disassembles during acrosomal exocytosis. **(A)** Schematic diagram illustrating the morphological changes that mammalian sperm undergo in the female reproductive tract, simulated in this study *in vitro*. Boxed regions indicate approximate locations where data in **(B–F)** were acquired. **(B,C)** Computational slices through Volta phase plate cryo-tomograms of noncapacitated sperm thinned by cryo-focused ion beam milling. Note how the acrosome is dense even in thinned samples. Insets show regions with large paracrystalline patches. Large membrane protein densities are visible on the luminal surface of the outer acrosomal membrane (green arrowheads in inset). **(D)** Computational slice through a defocus-contrast cryotomogram of a sperm cell whose acrosome had swollen after incubation in capacitating media for ~2 h. Note the decondensation of the acrosome and the prominent paracrystalline patches (insets). **(E,F)** Computational slice **(E)** and corresponding three-dimensional reconstruction **(F)** of the acrosomal shroud. The cell was incubated in capacitating media for ~2 h and treated with calcium ionophore for ~30 min. Note the paracrystalline patches (asterisks in **E**, goldenrod in **F**) and membrane protein-decorated vesicles (green arrowheads in **E**, green in **F**). Vesicle membranes are shown in red, and the inner acrosomal membrane is shown in orange. Scale bars: 250 nm; insets: 50 nm Color scheme: orange—outer and inner acrosomal membrane, red—vesiculated plasma and outer acrosomal membranes, green—membrane protein densities, goldenrod—paracrystalline patches.

The acrosome is a large regulated secretory vesicle overlying the anterior two-thirds of the nucleus; its crucial role in mammalian fertilization manifests in the fact that malformation of the acrosome causes infertility in both humans and mice. Three distinct segments of the acrosome can be defined based on their positions along the sperm head (**Figure 1A**): the apical segment extends beyond the nucleus and forms the most anterior region of the acrosome; the principal or pre-equatorial segment forms the major part of the acrosome; and the equatorial segment delimits the posterior part of the acrosome. During acrosomal exocytosis, the plasma membrane fuses with the outer acrosomal membrane at multiple points. This destabilizes the acrosome and liberates its contents, which include several proteins implicated in either penetrating through or binding to the egg vestments (Foster and Gerton, 2016).

Acrosomal exocytosis is not an all-or-nothing event but instead involves the gradual dispersal of vesicle cargo (Hardy et al., 1991; Kim, Foster and Gerton, 2001; Kim and Gerton, 2003). Biochemical analyses defined two classes of acrosome contents: a soluble fraction that is released shortly after the onset of the acrosome reaction, and a matrix fraction that disperses more slowly. Consistent with this, conventional electron microscopy (EM) studies showed discrete zones within the acrosome, including paracrystalline material that extends across large areas of the vesicle in sperm from several mammalian species including the rat (Phillips, 1972), rabbit (Courtens, Courot and Fléchon, 1976; Olson and Winfrey, 1994; Fléchon, 2016), ram, and bull (Courtens, Courot and Fléchon, 1976). However, the structural changes in the acrosomal matrix that mediate differential release of acrosome contents remain undefined.

Another distinctive feature of acrosomal exocytosis is the lack of membrane recycling. The plasma membrane and the outer acrosomal membrane are shed as vesicles, so the sperm head loses a large portion of its limiting membrane while the remainder becomes fusogenic. Acrosome vesiculation has been studied extensively with classical EM (Barros et al., 1967; Russell et al., 1979; Jamil and White, 1981; Nagae et al., 1986; Stock and Fraser, 1987; Yudin et al., 1988; Flaherty and Olson, 1991; Zanetti and Mayorga, 2009; Sosa et al., 2015), identifying acrosome swelling and membrane docking as clear intermediates leading to exocytosis (Zanetti and Mayorga, 2009; Tsai et al., 2010; Sosa et al., 2015). However, the membrane remodeling pathways that ensure the cell remains intact throughout this dramatic vesiculation process remain undefined.

Here, we use cryoelectron tomography (cryo-ET) to image sperm undergoing *in vitro* capacitation and acrosome exocytosis. Cryo-ET provides three-dimensional information about rare events in unfixed, unstained, fully hydrated samples, and thus in close to native conditions (Ng and Gan, 2020). We show that the paracrystalline component of the acrosomal matrix gradually dissolves during acrosomal exocytosis, explaining the differential release previously observed. We also find that the defined ultrastructural organization of the sperm head facilitates a unique fission–fusion mechanism that maintains cell integrity despite drastic membrane vesiculation. We demonstrate that acrosome exocytosis also facilitates massive membrane protein relocalization onto the post-acrosomal plasma membrane, building a platform for interaction with the egg.

RESULTS

In Uncapacitated Sperm, the Plasma Membrane (PM) and the Outer Acrosomal Membrane (OAM) are Closely Apposed Along the Entire Acrosome

We plunge-froze sperm from highly fertile, commercial artificial insemination pigs (*Sus scrofa domestica*) and imaged them using cryo-ET. In intact uncapacitated sperm, the plasma membrane (PM) and the outer acrosomal membrane (OAM) are closely apposed along the entire acrosome (**Figures 1B,C**; **Supplementary Figure S1**). The PM and the OAM are ~8–10 nm apart and lie parallel to each other until the equatorial segment of the acrosome, where the vesicle tapers (**Supplementary Figure S1D–F**). This differs from many classical EM images of uncapacitated sperm, in which the PM and OAM appear wavy with estimated interbilayer distances of >10 nm (Zanetti and Mayorga, 2009; Tsai et al., 2010; Sosa et al., 2015), and demonstrates the benefits of using cryo-ET to visualize acrosomal exocytosis.

The Paracrystalline Fraction of the Acrosomal Matrix Progressively Disassembles During Exocytosis

We sought to determine how the internal organization of the acrosome changes during acrosomal exocytosis. We first imaged acrosome contents in intact uncapacitated sperm cells thinned to ~150–200 nm with cryo-focused ion beam (cryo-FIB) milling (Marko et al., 2006; Rigort et al., 2012). Even after thinning and imaging with the Volta phase plate (VPP) (Danev et al., 2014; Fukuda et al., 2015), the acrosome lumen was still very dense (**Figures 1B,C**). Nonetheless, we observed large patches of paracrystalline material in both the apical and pre-equatorial regions of the acrosome (insets in Figures 1B,C), similar to the structures observed in rat sperm (Phillips, 1972), rabbit sperm (Olson and Winfrey, 1994), and ram sperm (Fléchon, 2016).

To visualize acrosomal exocytosis, we imaged sperm incubated in capacitating media (containing calcium, bicarbonate, and bovine serum albumin) for ~2 h and subsequently treated with calcium ionophore A23187. These protocols are known to induce boar sperm capacitation and acrosome reaction (Tsai et al., 2007; Boerke et al., 2014), which we also confirmed through phosphotyrosine staining and fluorescent lectin staining, respectively (**Supplementary Figure S2**). Following treatment, fully acrosome-reacted sperm could be readily targeted in low-magnification cryo-EM projection images (**Supplementary Figure S3**). These cells were surrounded by a cloud of vesicles (the acrosomal shroud) (**Supplementary Figure S3A**), and their apical regions had become very thin due to the loss of the acrosome (**Supplementary Figure S3B**), allowing us to image them without cryo-FIB milling. We note that acrosomal shrouds

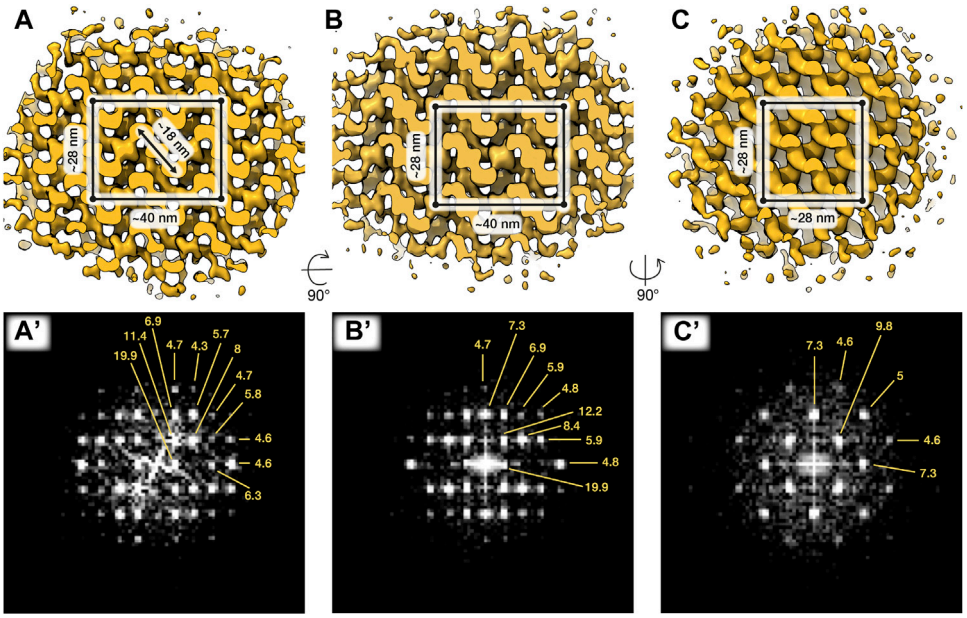

FIGURE 2 | *In situ* structures of paracrystalline patches from capacitated sperm. Three orthogonal isosurface views **(A–C)** and corresponding Fourier transforms **(A'–C')** of a subtomogram average of 87 × 87 × 87 nm paracrystalline patch from swollen acrosomes of boar sperm incubated in capacitating media for ~2 h. The putative tetragonal body-centered unit cell is annotated in **(A–C)**. Averages were generated from ~1,400 particles from 2 cells.

tend to remain associated with sperm heads despite several pipetting and dilution steps before imaging. In our analyses, we excluded sperm in which the plasma membrane peeled off at the equatorial/post-acrosomal regions, which would likely result in loss of cell integrity and thus in cell death (**Supplementary Figures S3C, D**).

We found that the acrosomal shroud consists of a highly heterogeneous population of vesicles that are decorated with membrane proteins (**Figures 1E,F**). Interspersed between these vesicles are the contents of the acrosome, including striking paracrystalline patches that were heterogeneous in size and shape (ionophore: 12/13 tomograms, each from a different cell, from three different animals) (**Figure 1E**; **Supplementary Figure S4**). We also observed paracrystalline patches in acrosomal shrouds of sperm stimulated with progesterone (5/5 tomograms, each from a different cell, from one animal), which has been shown to stimulate the acrosome reaction in human sperm (Harper et al., 2006).

To follow the paracrystalline patches during intermediate stages of exocytosis, we imaged cells incubated in capacitating media without ionophore treatment. Paracrystalline patches were readily visible in swollen acrosomes (**Figure 1D**), where they had already begun to dissociate into smaller fragments. We then used subtomogram averaging to resolve the structure of the paracrystalline patches at a resolution of ~30–40 Å (**Figure 2**). We chose to average from capacitated sperm since the surrounding material was too dense in uncapacitated sperm. The patches were also larger in capacitated sperm than in the shrouds of acrosome-reacted sperm, which facilitated averaging by increasing particle numbers. Our averages reveal that the paracrystalline patches adopt a tetragonal body-centered crystal lattice with apparent unit cell dimensions a = 28 nm, b = 28 nm, and c = 40 nm.

Taken together, our data indicate that the paracrystalline patches in the acrosomal shroud result from disassembly of an initial larger superstructure. The paracrystalline fraction may thus represent the core of the acrosomal matrix, acting as a structural scaffold onto which soluble components of the acrosome are anchored. Their progressive disassembly may represent a mechanism for controlled release of acrosome contents that appears to be conserved across mammals.

An Atypical Membrane Fission-Fusion Pathway Maintains Cell Integrity at the Equatorial Segment

We then sought to trace membrane remodeling intermediates involved in capacitation and acrosomal exocytosis. Sperm within an ejaculate are inherently variable (Buffone, Hirohashi and Gerton, 2014), which precludes a strictly timepoint-based assessment of the reaction coordinate. We instead imaged several cells from several different animals (**Supplementary Table S1**), analyzed the dataset for membrane remodeling intermediates that we could observe consistently, and ordered these stages relative to one another (**Figures 3**, **4**).

We captured a range of intermediates already in capacitated sperm without ionophore stimulation (**Figure 3**), including acrosome swelling, membrane docking, and membrane destabilization (**Supplementary Figure S5**). Acrosome swelling is one of the earliest stages of acrosomal exocytosis (Zanetti and Mayorga, 2009; Sosa et al., 2015) and indeed was observed even in capacitated cells (Boerke et al., 2014). Swelling is associated with decondensation of acrosomal contents, but our tomograms reveal that decondensation is not uniform. Specifically, a dense core

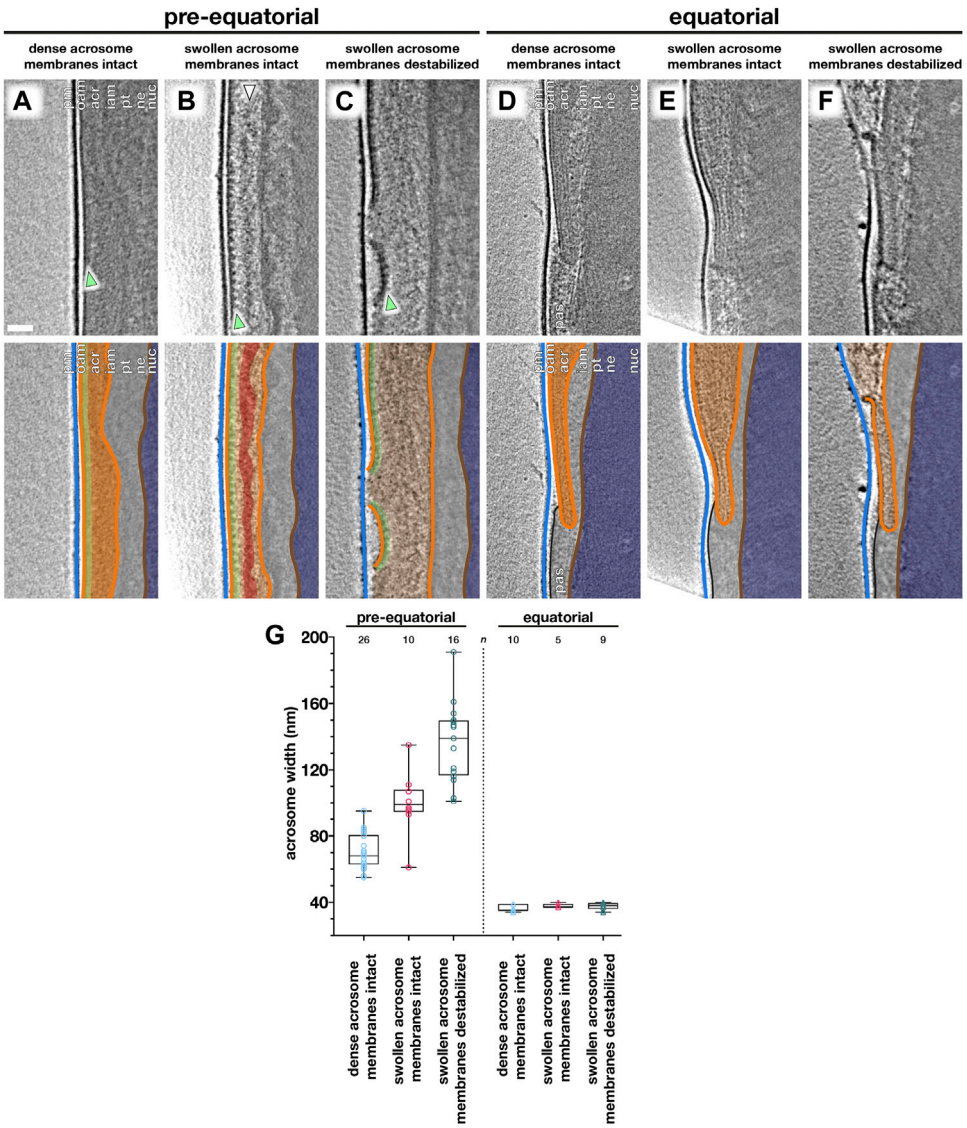

FIGURE 3 | Acrosome swelling is associated with membrane destabilization in capacitated sperm. **(A–F)** Computational slices (top panels) and schematic annotations (bottom panels) of Volta phase plate cryotomograms of the pre-equatorial **(A–C)** and equatorial **(D–F)** region of sperm before **(A,D)** or after (B–C, E–F) a ~2-h incubation in capacitating media without ionophore stimulation. Note the rows of membrane protein densities on the outer acrosomal membrane (green arrowheads in A–C) and the streak of acrosomal matrix that remains condensed during acrosome swelling (white arrowhead in **B**). **(G)** Measurements of acrosomal width at the pre-equatorial (left) and equatorial (right) regions in sperm showing various states of acrosome swelling and membrane destabilization. For each tomogram, acrosome width was measured as the distance between the outer and inner acrosomal membranes at three different locations. Every data point represents the average of these three measurements for the relevant tomogram. Each tomogram is from a different cell (*n* indicates the number of tomograms used for analysis). The boxes indicate the median and interquartile range, while the whiskers indicate the minimum and maximum values. Scale bar: 50 nm. Labels: pm, plasma membrane; oam, outer acrosomal membrane; acr, acrosome; iam, inner acrosomal membrane; pt, perinuclear theca; ne, nuclear envelope; nuc, nucleus; pas, post-acrosomal sheath. Color scheme: blue—plasma membrane, orange—outer and inner acrosomal membranes, green—membrane protein densities, red—condensed acrosomal material, light gray—perinuclear theca and post-acrosomal sheath, brown—nuclear envelope, dark blue—nucleus.

remains near the center of the vesicle (white arrowhead in **Figure 3B**), which is continuous with a thin streak of electron-dense material sandwiched between the OAM and the IAM at the end of the acrosome (white arrowhead in **Figure 4B**). Decondensation also improves contrast in the acrosome, making visible large membrane protein densities on the luminal surface of the OAM (green arrowhead in **Figures 3B,C**). These structures are also visible in VPP tomograms of FIB-milled uncapacitated sperm (green arrowheads in **Figure 1B** inset and **Figure 3A**). The OAM proteins form rows of teeth-like densities, each extending ~14 nm into the OAM lumen and spaced ~18 nm from its neighbors.

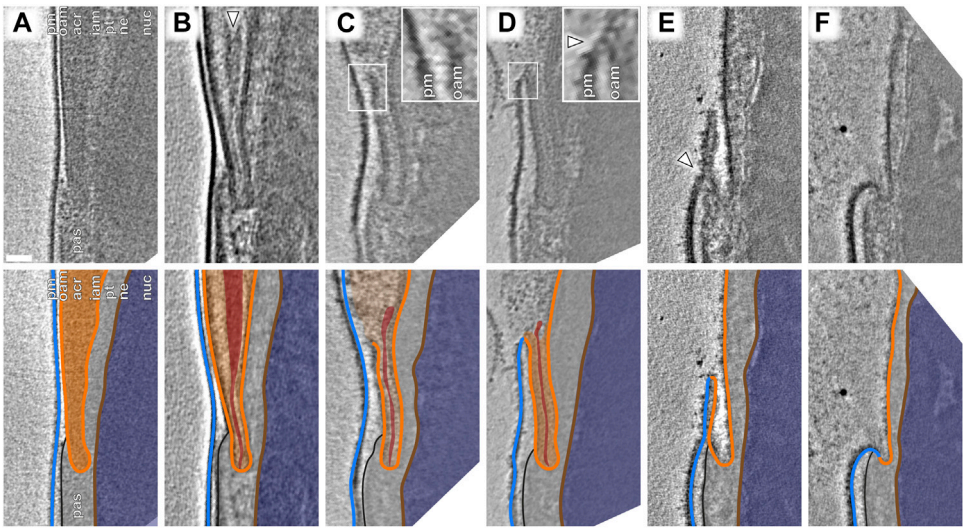

FIGURE 4 | An atypical membrane fission–fusion pathway maintains cell integrity at the equatorial region. **(A–F)** Computational slices (top panels) and corresponding schematic annotations (bottom panels) of Volta phase plate cryotomograms of the equatorial region of sperm incubated for ~2 h in capacitating media without **(A–D)** and with **(E,F)** subsequent ~30-min ionophore stimulation. In **(B)**, the white arrowhead indicates condensed material at the core of the acrosome that is continuous with a thin streak of electron-dense material in the equatorial segment. In **(C)**, the inset shows the point of OAM rupture immediately anterior to the equatorial region. In **(D)**, the inset shows that the OAM has fused (white arrowhead) with the overlying PM at this location. Scale bar: 50 nm. Labels: pm, plasma membrane; oam, outer acrosomal membrane; acr, acrosome; iam. inner acrosomal membrane; pt, perinuclear theca; ne, nuclear envelope; nuc, nucleus; pas, post-acrosomal sheath. Color scheme: blue—plasma membrane, orange—outer and inner acrosomal membranes, red—condensed acrosomal material, light gray—perinuclear theca and post-acrosomal sheath, brown—nuclear envelope, dark blue—nucleus.

We could further distinguish between two stages of acrosome swelling: one in which the acrosome swells but the overlying membranes are still intact (**Figures 3B,E**), and another in which the OAM already destabilizes (**Figures 3C,F**). OAM destabilization is characterized by local membrane rupture (**Figures 3C,F**; **Figure 4C**; **Supplementary Figure S5G–L**). OAM rupture was associated with the extent of acrosome swelling; in cells with ruptured OAMs, the acrosome had swollen to nearly twice its original width (136 ± 24 nm vs. 71 ± 11 nm, with an intermediate value of 100 ± 18 nm in cells with swollen acrosomes but intact membranes) (**Figure 3G**). In contrast, the width of the equatorial segment did not change significantly even in cells with ruptured OAMs (acrosome swollen, membranes destabilized: 38 ± 2 nm; acrosome swollen, membranes intact: 38 ± 1 nm; uncapacitated sperm with dense acrosome, membranes intact: 36 ± 2 nm). Notably, OAM rupture occurred just anterior to the equatorial segment, on average 260 ± 80 nm from the end of the acrosome (mean ± s.d., 8 tomograms, each from a different cell) (**Figure 3F**).

Focusing on the equatorial segment, we observed an atypical membrane fission–fusion pathway that mediates resealing of the sperm head (**Figure 4**). The ruptured end of the OAM fuses with the overlying PM (**Figures 4C,D**; **Supplementary Figure S5J–L**), and after this fusion event, the electron-dense streak also diffuses, leaving a hairpin-shaped membrane (**Figure 4E**, **Supplementary Figure S6A–B**). This hairpin-shaped membrane then constricts and buds off just anterior to the post-acrosomal sheath (**Figure 4E**, arrowhead), yielding the characteristic morphology of acrosome-reacted cells (**Figure 4F**, **Supplementary Figure S6C**).

Acrosomal Exocytosis Transforms the Molecular Landscape of the Sperm Plasma Membrane

After loss of the acrosome, the inner acrosomal membrane (IAM) is the new limiting membrane of the apical segment of the sperm cell (**Figure 1E**). The PM overlying the equatorial/post-acrosomal segment remains intact and is now continuous with the IAM (**Figure 5**). Segmentation of high-contrast tomograms acquired with a VPP revealed that the PM forms a "sheath" around the post-acrosomal region (**Figure 5D**, **Supplementary Figure S6**). Our tomograms also showed tubulovesicular projections overlying the equatorial segment (**Figure 5D**, **Supplementary Figure S6**). These tubular membranes are consistent with those observed by freeze-fracture EM (Aguas and da Silva, 1989). Thus, the acrosome reaction remodels the overall topography of the sperm surface.

We then compared the post-acrosomal segment in uncapacitated versus acrosome-reacted sperm (**Figures 5B,E**; **Supplementary Figure S7**). Inspecting the PM overlying the post-acrosomal sheath reveals major differences in protein decoration. In unreacted cells, the post-acrosomal PM is relatively smooth, with only a few small protein densities protruding from the membrane (**Figure 5B**, **Supplementary Figures S7A–C**) (14/14 tomograms, each from a different cell, from six different animals). In contrast, the post-acrosomal PM was densely packed with membrane protein densities in ~80% of

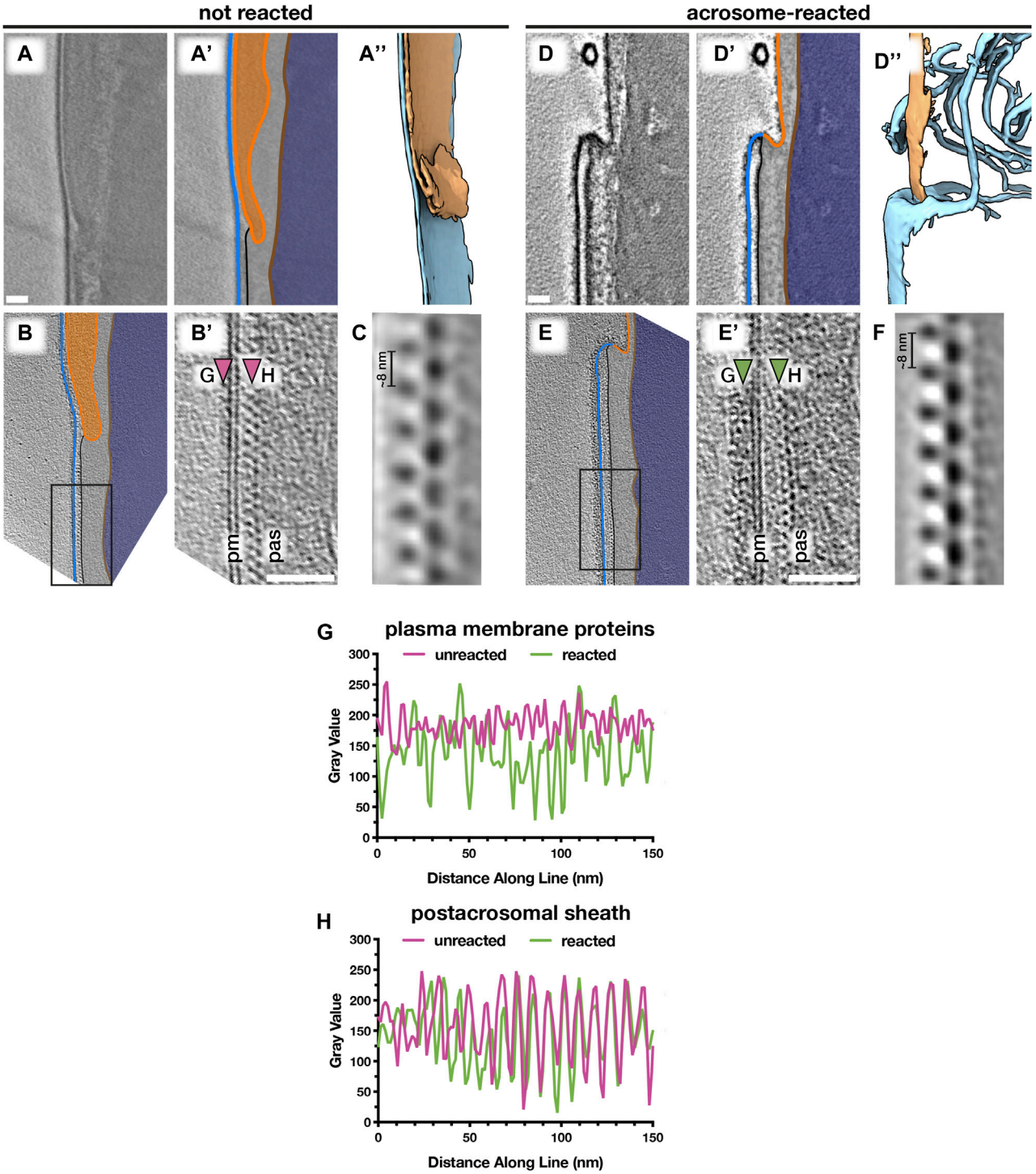

FIGURE 5 | Acrosomal exocytosis transforms the molecular landscape of the sperm plasma membrane. Comparing the post-acrosomal plasma membrane in unreacted **(A–C)** versus acrosome-reacted **(D–F)** reveals major differences in membrane protein decoration. **(A,D)** Computational slices **(A and A',D and D')** and corresponding three-dimensional reconstructions **(A'',D'')** of VPP cryotomograms illustrating how acrosomal exocytosis remodels the topography of the equatorial region. **(B,E)** Computational slices through defocus-contrast cryotomograms illustrating how the post-acrosomal plasma membrane becomes densely packed with membrane proteins after acrosomal exocytosis. **(C,F)** Subtomogram averages of the post-acrosomal sheath from unreacted **(C)** and acrosome-reacted **(F)** cells. **(G,H)** Exemplary linescans illustrating changes in membrane protein density after the acrosome reaction **(G)**, as well as the lack of noticeable change in the post-acrosomal sheath **(H)**. Linescans were taken at the approximate locations marked by arrowheads in **(B') and (E')**. Scale bars: 50 nm. Labels: pm, plasma membrane; pas, post-acrosomal sheath. Color scheme: blue—plasma membrane, orange—outer and inner acrosomal membranes, light gray—perinuclear theca and post-acrosomal sheath, brown—nuclear envelope, dark blue—nucleus.

tomograms of acrosome-reacted cells (30/37 tomograms, each from a different cell, from five different animals) (**Figures 5E,G**; **Supplementary Figures S7D–F**). These densities do not appear to be ordered, which suggests that they represent a range of different conformations, proteins, or protein complexes. Thus, the acrosome reaction results in massive membrane protein relocalization that alters the molecular landscape of the sperm surface.

We then used subtomogram averaging to define the substructure of the post-acrosomal sheath in more detail (**Figures 5C,F**). The peripheral layer of the post-acrosomal sheath, immediately underlying the PM, consists of a multilayered structure with an ~8-nm repeating unit. Our averages reveal that neither the substructure nor the overall organization of the post-acrosomal sheath changes noticeably after acrosomal exocytosis, which is consistent with measurements directly from tomograms (**Figure 5H**). Similarly, the distance between the PM and the post-acrosomal sheath remains relatively unchanged (unreacted: 15 ± 2 nm, reacted: 18 ± 3 nm).

DISCUSSION

Gradual Disassembly of the Paracrystalline Matrix may Represent a Mechanism for Controlled Release of Acrosome Contents

Leading up to and during acrosomal exocytosis, acrosome contents disperse at rates dependent on their partitioning into either soluble or particulate fractions. The particulate fraction, also known as the acrosomal matrix, disperses gradually in a process dependent on alkalization and proteolytic self-digestion (Buffone et al., 2008). However, we do not understand the underlying structural transitions in the acrosomal matrix that regulate the dispersal of acrosomal contents. Studies of acrosomal matrix dispersal are often performed on guinea pig sperm, which have large acrosomes partitioned into subdomains easily visible by transmission EM (Flaherty and Olson, 1988; Hardy et al., 1991; Olson and Winfrey, 1994; Kim, Foster and Gerton, 2001). Here, we use cryo-ET to show that the acrosome is structurally compartmentalized also in boar sperm (**Figure 1**), which have comparatively thin acrosomes and no obvious subdomains when viewed by conventional EM (Buffone et al., 2008).

Specifically, we find an extensive Paracrystalline fraction in the boar sperm acrosome. Although Paracrystalline structures have been demonstrated previously in acrosomes of other mammals, they were not followed throughout capacitation and acrosomal exocytosis. Our data now show that the Paracrystalline fraction begins to disassemble during capacitation (**Figure 1D**) and continues to do so during acrosomal exocytosis, resulting in small patches scattered among the vesicles of the acrosomal shroud (**Figures 1E,F**). Gradual disassembly of the Paracrystalline matrix thus represents a plausible mechanism for controlled release of acrosome contents. Refining this model will require further studies aimed at determining the nature of the Paracrystalline fraction—for instance, whether it represents a scaffolding structure or a storage phase for inactive enzymes. The subtomogram averages we present here (**Figure 2**) can help toward this goal by providing constraints on the molecular dimensions of candidate proteins.

Cryo-ET Reveals how Capacitation-Associated Membrane Destabilization Relates to the Membrane Fission–Fusion Processes Involved in Acrosomal Exocytosis

Our observations suggest that acrosome swelling relates directly to membrane destabilization (**Figure 3**), which is likely caused by an increase in membrane tension in addition to known changes in membrane composition mediated by cholesterol efflux and phospholipase activation (Aitken and Nixon, 2013; Asano, Nelson-Harrington and Travis, 2013). A role for swelling-dependent membrane destabilization is also supported by observations that hyper-osmotic conditions inhibit the acrosome reaction (Bielfeld, Jeyendran and Zaneveld, 1993) and that lysophosphatidylcholine, a positive curvature amphiphile that reduces the energetic barrier for membrane rupture (Glushakova et al., 2005), promotes the reaction (Parrish et al., 1988; de Lamirande, Leclerc and Gagnon, 1997). Meanwhile, the equatorial region is stabilized by the electron-dense core of the acrosome (**Figures 3D–F**) and the post-acrosomal region likewise stabilized by the post-acrosomal sheath. Thus, the precise organization of the sperm head facilitates the rupture–fusion pathway that maintains cell integrity despite destabilization and vesiculation of the rest of the acrosome (**Figure 4**).

The intermediates we observe do not appear to fit the canonical fusion-by-hemifusion pathway; instead, the presence of membrane edges is reminiscent of the rupture–insertion pathway (Chlanda et al., 2016; Haldar et al., 2019). Whether fusion proceeds via hemifusion or via rupture–insertion depends on membrane spontaneous curvature and hence on lipid composition, with the rupture–insertion pathway strongly favoring cholesterol-poor bilayers (Chlanda et al., 2016; Haldar et al., 2019). This may be particularly relevant given that one of the molecular signatures of capacitation is cholesterol efflux.

Acrosomal exocytosis transforms the molecular landscape of the sperm plasma membrane

Acrosomal exocytosis is an absolute requirement for mammalian sperm to fuse with the egg (Yanagimachi, 1981). Fluorescence microscopy has shown that as a result of the acrosome reaction, Izumo1 relocalizes onto the plasma membrane, allowing it to interact with its oocyte-borne partner, Juno, to mediate sperm-egg adhesion (Satouh et al., 2012). However, the Izumo1–Juno interaction is not sufficient to mediate membrane fusion (Bianchi et al., 2014). Our understanding of sperm–egg fusion is hampered by the fact that, beyond the translocation of Izumo1, we know very little about what happens to the molecular landscape of the sperm surface after the acrosome reaction.

Here, we show that acrosomal exocytosis transforms both the micron-scale topography and the molecular landscape of the

sperm surface (**Figure 5**). We find that the post-acrosomal plasma membrane becomes heavily decorated with membrane protein densities. Such changes may be due to the relocalization of membrane proteins, similar to the phenomenon observed by freeze-fracture EM for the acrosomal cap region (Aguas and da Silva, 1989), or to the binding of liberated acrosomal proteins to pre-existing receptors. The post-acrosomal membrane protein densities do not appear to be ordered, which suggests that they represent a range of different conformations, proteins, or protein complexes. Indeed, in addition to Izumo1, there are now a number of proteins on mammalian sperm that are known to be essential for sperm–egg binding and fusion (Inoue et al., 2005; Fujihara et al., 2020; Lamas-Toranzo et al., 2020; Noda et al., 2020). Our results therefore complement the emerging view that mammalian sperm–egg fusion involves several molecular species acting in concert. Our study also opens avenues for future work into how these various players are organized on the sperm membrane at the nanoscale.

MATERIALS AND METHODS

Sperm Washing, Capacitation, and Acrosome Reaction

Freshly ejaculated pig (*Sus scrofa domestica*) semen was purchased from an artificial insemination company (AIM Varkens KI, Veghel, Nederland). Semen was typically diluted in Beltsville thawing solution (BTS: 205 mM glucose, 20.4 mM NaCl, 5.4 mM KCl, 15 mM $NaHCO_3$, 3.4 mM EDTA) and stored at 18°C until use. Sperm were used within 1 day of delivery. Sperm were gently layered onto a discontinuous gradient consisting of 2 ml 70% Percoll overlaid with 4 ml of 35% Percoll (GE Healthcare), both in 1X HEPES-buffered saline (HBS: 20 mM HEPES, 137 mM NaCl, 10 mM glucose, 2.5 mM KCl, 1% kanamycin, pH 7.6). Pelleted cells were washed once in 1X DPBS (Sigma), resuspended in 1 ml of 1X DPBS, and counted.

Capacitation and acrosome reaction protocols were based on methods previously validated for pig sperm (Tsai et al., 2007). Washed sperm were resuspended in 1X TALP (20 mM HEPES, 90 mM NaCl, 21.7 mM sodium lactate, 5 mM glucose, 3.1 mM KCl, 1 mM sodium pyruvate, 0.4 mM $MgSO_4$, 0.3 mM NaH_2PO_4, 2 mM $CaCl_2$, 15 mM $NaHCO_3$, 100 µg/ml kanamycin, 0.3% w/v fatty acid-free BSA (Sigma), pH 7.4) at concentrations in the range of 10–20 × 10^6 cells/ml. Sperm were allowed to capacitate for between 2 and 2.5 h at 37°C, 5% CO_2. In order to stimulate the acrosome reaction more rapidly and in a larger percentage of cells, calcium ionophore A23187 (Sigma) was added to capacitated cells to a final concentration of 5 or 3 µM. Cells were incubated for either a further 30 min (for ionophore) at 37°C, 5% CO_2. As a supplementary experiment to verify the presence of paracrystalline patches using another AR inducer, we also imaged cells stimulated with progesterone (Sigma) at a final concentration of 3 µM.

For flow cytometry, cells were first washed with 1X DPBS and their concentration adjusted to 30–50 × 10^6 cells/ml. Sperm were then stained with propidium iodide (LifeTechnologies) and with PNA-FITC (Sigma), both at a final concentration of 1 µg/ml. Sperm were then diluted 1/100 to 0.3–0.5 × 10^6 cells/ml and analyzed using a BD FACSCanto II flow cytometer. Viable, acrosome-reacted cells were defined as those in the PI^-FITC^+ quadrant of the cytogram.

To assess capacitation, cells were stained with antibodies against phosphorylated tyrosine. Either uncapacitated or capacitated sperm cells were allowed to settle in 8-well ibidi µ-slides for 15 min, after which paraformaldehyde was added to a final concentration of 4%. After 30 min of fixation, cells were washed with PBS and subsequently permeabilized with 0.5% Triton X-100 in PBS for 15 min. Cells were then washed with PBS three times, then blocked overnight at 4°C with 1% BSA in PBS with 0.05% Tween 20 (PBS-T). After blocking, cells were incubated with primary antibody (anti-phosphotyrosine clone 4G10 diluted 1:200 in PBS-T + 1% BSA) for 2 h at room temperature (RT). Cells were washed in PBS three times and incubated with secondary antibody (goat antimouse AlexaFluor-488 diluted 1:100 in PBS-T + 1% BSA) for 1 h at RT. Cells were again washed with PBS three times, and nuclei were counterstained with Hoechst 33342 for 30 min in PBS. After three final PBS washes, FluorSave mounting medium was added to the wells. Slides were imaged using a CorrSight microscope (ThermoFisher) operating in the spinning disk mode.

Cryo-EM Grid Preparation

Typically, 3 µl of a suspension containing either 1–3x10^6 cells/ml (for whole cell tomography) or 20–30 × 10^6 cells/ml (for cryo-FIB milling) was pipetted onto either glow-discharged Quantifoil R 2/1 200-mesh holey carbon or Quantifoil 200-mesh lacey carbon grids. One microliter of a suspension of BSA-conjugated gold beads (Aurion) was added, and the grids then blotted manually from the back (opposite the side of cell deposition) for ~3 s (for whole cell tomography) or ~5–6 s (for cryo-FIB milling) using a manual plunge-freezer (MPI Martinsried). Grids were immediately plunged into either liquid ethane or a liquid ethane–propane mix (37% ethane) (Tivol et al., 2008), cooled to liquid nitrogen temperature. Grids were stored under liquid N_2 until imaging.

Cryo-Focused Ion Beam Milling

Grids were mounted into modified Autogrids (FEI) for mechanical support. Clipped grids were loaded into an Aquilos (FEI) dual-beam cryo-focused ion beam/scanning electron microscope (cryo-FIB/SEM). All SEM imaging was performed at 2 kV and 13 pA, whereas FIB imaging for targeting was performed at 30 kV and 10 pA. Milling was typically performed with a stage tilt of 18°, so lamellae were inclined 11° relative to the grid. Each lamella was milled in four steps: an initial rough mill at 1 nA beam current, an intermediate mill at 300 pA, a fine mill at 100 pA, and a polishing step at 30 pA. Lamellae were milled with the wedge pre-milling method described in Schaffer et al. (2017) and with stabilizing expansion segments described in Wolff et al. (2019).

Tilt Series Acquisition

Tilt series was acquired on either a Talos Arctica (FEI) operating at 200 kV or a Titan Krios (FEI) operating at 300 kV, both

equipped with a postcolumn energy filter (Gatan) in zero-loss imaging mode with a 20-eV energy-selecting slit. All images were recorded on a K2 Summit direct electron detector (Gatan) in either counting or super-resolution mode with dose fractionation. Tilt series was collected using SerialEM (Mastronarde, 2005) at a target defocus of between −4 and −6 μm (conventional defocus-contrast) or between −0.5 and −1.5 μm (for tilt series acquired with the Volta phase plate). Tilt series were typically recorded using either strict or grouped dose-symmetric schemes either spanning ±56° in 2° increments or ±54° in 3° increments, with total dose limited to ~100 $e^{-}/Å^{2}$.

Tomogram Reconstruction

Frames were aligned either post-acquisition using Motioncor2 1.2.1 (Zheng et al., 2017) or on-the-fly using Warp (Tegunov and Cramer, 2019). Frames were usually collected in counting mode; when super-resolution frames were used, they were binned 2X during motion correction. Tomograms were reconstructed in IMOD (Kremer et al., 1996) using weighted back-projection, with a SIRT-like filter (Zeng, 2012) applied for visualization and segmentation. Defocus-contrast tomograms were CTF-corrected in IMOD using *ctfphaseflip,* while VPP tomograms were left uncorrected.

Tomogram Segmentation

Tomogram segmentation was generally performed semiautomatically. Initial segmentation was performed using the neural network-based TomoSeg package in EMAN 2.21. Segmentation was then refined manually in either Avizo 9.2.0 (FEI) or Chimera 1.12. Membrane distance measurements were performed using built-in functions in Avizo 9.2.0.

Subtomogram Averaging of Paracrystalline Patches

Subtomogram averaging with missing wedge compensation was performed using PEET 1.13.0 (Nicastro et al., 2006; Heumann et al., 2011). Alignments were performed first on 4x-binned data, after which aligned positions and orientations were transferred to 2x-binned data using scripts shared by Dr. Daven Vasishtan.

Particle positions were seeded by generating a three-dimensional grid of points in paracrystalline patches using the *gridInit* program. All particle orientations were randomized and initial alignments allowed for full rotational searches around all axes. To ensure consistency, two independent initial alignments were performed, each using a randomly selected particle from a separate tomogram as an initial reference. Since alignments converged on a similar structure, alignments were continued. The dataset was cleaned by 1) removing all particles with a cross-correlation value less than one standard deviation above the mean (which removed poorly aligning particles such as those at the edges of paracrystalline patches) and by 2) removing overlapping particles. The orientations of the remaining particles were again randomized and another alignment performed. After a final particle cleanup by classification, a final restricted alignment run was performed. Averages presented in the manuscript were filtered to the estimated resolution based on the Fourier shell correlation (FSC) at a cutoff of 0.5 (Nicastro et al., 2006).

Measurements and Quantification

All measurements were performed on ~20-nm-thick central tomographic slices. Acrosomal width was measured manually in IMOD as the distance between the outer and inner acrosomal membranes. For each tomogram, three measurements were recorded at different locations to account for slight variations in the shape of the acrosome. Linescans for measurement of the post-acrosomal sheath were performed in Fiji v 2.0.0-rc-69/1.52p.

SIGNIFICANCE

Mammalian sperm must undergo a complex series of biochemical and morphological changes in the female reproductive tract in order to become fertilization-competent. These changes culminate in acrosomal exocytosis, during which multiple membrane fusions destabilize the acrosomal vesicle and liberate its contents, which include proteins implicated in penetrating and binding to the egg vestments. Here, we use cryoelectron tomography to visualize acrosomal exocytosis intermediates in unfixed, unstained sperm. Our results suggest structural bases for how gradual dispersal of acrosome contents is regulated, as well as for how the cell remains intact after losing much of its plasma membrane. We also show that acrosomal exocytosis transforms both the micron-scale topography and the nanoscale molecular landscape of the sperm surface, thus priming it for interaction and fusion with the egg. These findings yield important insights into sperm physiology and contribute to our understanding of the fundamental yet enigmatic process of mammalian fertilization.

DATA AVAILABILITY STATEMENT

The original contributions presented in the study are included in the article/**Supplementary Material**, further inquiries can be directed to the corresponding author. Subtomogram averages of paracrystalline patches from capacitated boar sperm have been deposited to the Electron Microscopy Data Bank (EMDB) with deposition number: EMD-13877.

AUTHOR CONTRIBUTIONS

ML and RR prepared samples for cryo-EM. ML, RR, and TZ-B-M collected and analyzed cryo-ET data. ML, RR, BG, and TZ-B-M wrote the manuscript.

FUNDING

This work was funded by NWO Start-Up Grant 740.018.007 to TZ-B-M, and ML is supported by a Clarendon Fund-Nuffield Department of Medicine Prize Studentship.

ACKNOWLEDGMENTS

The authors thank Dr. M Vanevic for excellent computational support, and Dr. SC Howes, Ingr. CTWM Schneijdenberg and JD Meeldijk for managing and maintaining the Utrecht University EM Square facility. The authors also thank S Leemans and L Teeuwen for their help with sperm preparation in initial stages of the project. This work benefitted from access to the Netherlands Center for Electron Nanoscopy (NeCEN) with support from operators Dr. RS Dillard and Dr. CA Diebolder and IT support from B Alewijnse.

SUPPLEMENTARY MATERIAL

The Supplementary Material for this article can be found online at: https://www.frontiersin.org/articles/10.3389/fcell.2021.765673/full#supplementary-material

Supplementary Figure S1 | The plasma membrane and the outer acrosomal membrane are closely spaced even in noncapacitated sperm. **(A–C)** Low-magnification high-dose cryo-EM projection images of noncapacitated boar sperm heads. Digital zooms show close apposition between the plasma membrane and the outer acrosomal membrane at the apical **(i)**, pre-equatorial **(ii)**, and equatorial **(iii)** regions. **(D–F)** Left panels show three-dimensional reconstructions of the plasma membrane and the outer acrosomal membrane at the apical **(D)**, pre-equatorial **(E)**, and equatorial **(f)** regions. The plasma membrane is colored based on distance from the outer acrosomal membrane, which is shown as a cutaway view in orange. Right panels show corresponding histograms of intermembrane distances. Scale bars: **(A–C)** 1 μm; digital zooms: 250 nm Labels: pm, plasma membrane; oam, outer acrosomal membrane; pas, post-acrosomal sheath.

Supplementary Figure S2 | Flow-cytometric assessment of acrosome reaction efficiency. **(A,B)** Flow cytograms of noncapacitated sperm **(A)** and sperm stimulated to acrosome react with ionophore A23187 **(B)**. **(C)** Proportion of viable acrosome-reacted sperm (PI^-, $PNA\text{-}FITC^+$) as assessed by flow cytometry. Bar graphs show mean ± standard deviation and summarize three independent experiments on three separate animals. **(D)** Fluorescence microscopy-based assessment of the tyrosine phosphorylation response in capacitated pig sperm.

Supplementary Figure S3 | Distinguishing acrosome-reacted sperm from membrane-disrupted sperm in low-magnification cryo-EM projection images. Low-magnification high-dose cryo-EM projection images of acrosome-reacted **(A,B)** and membrane-disrupted **(C,D)** sperm. Note how acrosome-reacted sperm successfully re-seal at the equatorial/post-acrosomal region (**A–B**, white arrows in digital zooms); in contrast, membrane-disrupted sperm have also lost the plasma membrane overlying the post-acrosomal sheath (**C–D**, black arrows in digital zooms). Also note how the apical region becomes very thin in acrosome-reacted cells; in contrast, membrane-disrupted sperm retain an acrosomal ghost around their heads. Scale bars: (**A–D)** 1 μm; digital zooms: 250 nm Labels: pm, plasma membrane; oam, outer acrosomal membrane; iam, inner acrosomal membrane; pas, post-acrosomal sheath; nuc, nucleus; shroud, acrosomal shroud Color scheme: blue—plasma membrane, orange—inner acrosomal membrane, black—post-acrosomal sheath, red—acrosomal shroud.

Supplementary Figure S4 | Additional examples of paracrystalline patches in the acrosomal shroud of acrosome-reacted cells. Computational slices through Volta phase plate cryotomograms of the acrosomal shroud collected at the apical region of sperm stimulated to undergo acrosomal exocytosis with either calcium ionophore **(A,B)** or progesterone **(C,D)**. The boundary of the cell, which is now delimited by the inner acrosomal membrane (iam), is traced in orange. Note the presence of paracrystalline patches (asterisks) of varying shapes and sizes in all tomograms. Scale bars: 250 nm Labels: iam, inner acrosomal membrane; nuc, nucleus.

Supplementary Figure S5 | Additional examples of membrane remodeling intermediates observed in sperm incubated in capacitating media without ionophore stimulation. Computational slices through cryotomograms of sperm with **(A–C)** swollen acrosomes and intact membranes; **(D–F)** swollen acrosomes and locally docked membranes (insets); and **(G–L)** profusely swollen acrosomes and destabilized membranes at the pre-equatorial **(G–I)** and equatorial regions **(J–L)**. Tomograms in **(A,B,D,I,J, and L)** were acquired with the Volta phase plate, while tomograms in **(C,E,F,G,H, and K)** were acquired with defocus-contrast. Scale bars: 100 nm Labels: pm, plasma membrane; oam, outer acrosomal membrane; iam, inner acrosomal membrane; pt, perinuclear theca; pas, post-acrosomal sheath; nuc, nucleus Color scheme: blue—plasma membrane, orange—outer and inner acrosomal membranes, green—membrane protein densities, gray—perinuclear theca and post-acrosomal sheath, brown—nuclear envelope, dark blue—nucleus.

Supplementary Figure S6 | Additional examples of the remodeled topography of acrosome-reacted cells. **(A–C)** Computational slices and **(A'–C')** corresponding three-dimensional reconstructions of Volta phase plate cryotomograms of acrosome-reacted sperm. Scale bar: 250 nm Labels: pm, plasma membrane; iam, inner acrosomal membrane; pas, post-acrosomal sheath; ne, nuclear envelope; nuc, nucleus Color scheme: blue—plasma membrane, orange—inner acrosomal membrane, black—post-acrosomal sheath, brown—nuclear envelope.

Supplementary Figure S7 | Additional examples of membrane protein relocalization onto the post-acrosomal plasma membrane of acrosome reacted cells. Computational slices through cryotomograms of the equatorial/post-acrosomal region in uncapacitated, noncapacitated **(A–C)**, and acrosome-reacted **(D–F)** sperm. The change in membrane protein decoration (arrowheads in **D–F**) is seen consistently even in three different imaging conditions: intermediate-magnification defocus contrast **(A,D)**, high-magnification defocus contrast **(B,E)**, and high-magnification Volta phase plate contrast **(C,F)**. Scale bars: 100 nm Labels: pm, plasma membrane; acr, acrosome; pas, post-acrosomal sheath; ne, nuclear envelope; nuc, nucleus Color scheme: blue—plasma membrane, orange—outer and inner acrosomal membranes, gray—perinuclear theca and post-acrosomal sheath, brown—nuclear envelope, dark blue—nucleus.

Supplementary Table S1 | Dataset summary reporting number of tomograms in the dataset representing each membrane remodeling intermediate.

REFERENCES

Aguas, A. P., and da Silva, P. P. (1989). Bimodal Redistribution of Surface Transmembrane Glycoproteins during Ca2+-dependent Secretion (Acrosome Reaction) in Boar Spermatozoa. *J. Cell Sci* 93 (Pt 3), 467–479. doi:10.1242/jcs.93.3.467

Aitken, R. J., and Nixon, B. (2013). Sperm Capacitation: A Distant Landscape Glimpsed but Unexplored. *Mol. Hum. Reprod.* 19 (12), 785–793. doi:10.1093/molehr/gat067

A.P. Harrison, R., and Gadella, B. M. (2005). Bicarbonate-induced Membrane Processing in Sperm Capacitation. *Theriogenology* 63 (2), 342–351. doi:10.1016/j.theriogenology.2004.09.016

Asano, A., Nelson-Harrington, J. L., and Travis, A. J. (2013). Phospholipase B Is Activated in Response to Sterol Removal and Stimulates Acrosome Exocytosis in Murine Sperm. *J. Biol. Chem.* 288 (39), 28104–28115. doi:10.1074/jbc.M113.450981

Austin, C. (1951). Observations on the Penetration of the Sperm into the Mammalian Egg. *Aust. Jnl. Bio. Sci.* 4 (4), 581. doi:10.1071/BI9510581

Bailey, J. L. (2010). Factors Regulating Sperm Capacitation. *Syst. Biol. Reprod. Med.* 56 (5), 334–348. doi:10.3109/19396368.2010.512377

Barros, C., Bedford, J. M., Franklin, L. E., and Austin, C. R. (1967). Membrane Vesiculation as a Feature of the Mammalian Acrosome reactionThe Journal of Cell Biology. *Rockefeller Univ. Press* 34 (3), C1–C5. doi:10.1083/jcb.34.3.C1

Bianchi, E., Doe, B., Goulding, D., and Wright, G. J. (2014). Juno Is the Egg Izumo Receptor and Is Essential for Mammalian Fertilization. *Nature* 508 (7497), 483–487. doi:10.1038/nature13203

Bielfeld, P., Jeyendran, R. S., and Zaneveld, L. J. D. (1993). Andrology: Osmo-Sensitivity of the Human Sperm Acrosome Reaction. *Hum. Reprod.* 8 (8), 1235–1239. doi:10.1093/oxfordjournals.humrep.a138233

Boerke, A., van der Lit, J., Lolicato, F., Stout, T. A. E., Helms, J. B., and Gadella, B. M. (2014). Removal of GPI-Anchored Membrane Proteins Causes Clustering of Lipid Microdomains in the Apical Head Area of Porcine Sperm. *Theriogenology* 81 (4), 613–624. doi:10.1016/j.theriogenology.2013.11.014

Buffone, M. G., Foster, J. A., and Gerton, G. L. (2008). The Role of the Acrosomal Matrix in Fertilization. *Int. J. Dev. Biol.* 52 (5–6), 511–522. doi:10.1387/ijdb.072532mb

Buffone, M. G., Hirohashi, N., and Gerton, G. L. (2014). Unresolved Questions Concerning Mammalian Sperm Acrosomal Exocytosis1. *Biol. Reprod.* 90 (5), 1–8. doi:10.1095/biolreprod.114.117911

Chang, M. C. (1959). Fertilization of Rabbit Ova *In Vitro*. *Nature* 184 (4684), 466–467. doi:10.1038/184466a0

Chang, M. C. (1951). Fertilizing Capacity of Spermatozoa Deposited into the Fallopian Tubes. *Nature* 168 (4277), 697–698. doi:10.1038/168697b0

Chlanda, P., Mekhedov, E., Waters, H., Schwartz, C. L., Fischer, E. R., Ryham, R. J., et al. (2016). The Hemifusion Structure Induced by Influenza Virus Haemagglutinin Is Determined by Physical Properties of the Target Membranes. *Nat. Microbiol.* 1 (6), 16050. doi:10.1038/nmicrobiol.2016.50

Courtens, J. L., Courot, M., and Fléchon, J. E. (1976). The Perinuclear Substance of Boar, Bull, Ram and Rabbit Spermatozoa. *J. Ultrastruct. Res.* 57 (1), 54–64. doi:10.1016/S0022-5320(76)80054-8

Danev, R., Buijsse, B., Khoshouei, M., Plitzko, J. M., and Baumeister, W. (2014). Volta Potential Phase Plate for In-Focus Phase Contrast Transmission Electron Microscopy. *Proc. Natl. Acad. Sci.* 111 (44), 15635–15640. doi:10.1073/pnas.1418377111

de Lamirande, E., Leclerc, P., and Gagnon, C. (1997). Capacitation as a Regulatory Event that Primes Spermatozoa for the Acrosome Reaction and Fertilization. *Mol. Hum. Reprod.* 3 (3), 175–194. doi:10.1093/molehr/3.3.175

Flaherty, S. P., and Olson, G. E. (1988). Membrane Domains in guinea Pig Sperm and Their Role in the Membrane Fusion Events of the Acrosome Reaction. *Anat. Rec.* 220 (3), 267–280. doi:10.1002/ar.1092200307

Flaherty, S. P., and Olson, G. E. (1991). Ultrastructural Analysis of the Acrosome Reaction in a Population of Single guinea Pig Sperm. *Anat. Rec.* 229 (2), 186–194. doi:10.1002/ar.1092290205

Fléchon, J.-E. (2016). The Acrosome of Eutherian Mammals. *Cell Tissue Res* 363 (1), 147–157. doi:10.1007/s00441-015-2238-0

Foster, J. A., and Gerton, G. L. (2016). "The Acrosomal Matrix," in *Advances in Anatomy, Embryology, and Cell Biology*, 15–33. doi:10.1007/978-3-319-30567-7_2

Fujihara, Y., Lu, Y., Noda, T., Oji, A., Larasati, T., Kojima-Kita, K., et al. (2020). Spermatozoa Lacking Fertilization Influencing Membrane Protein (FIMP) Fail to Fuse with Oocytes in Mice. *Proc. Natl. Acad. Sci. USA* 117 (17), 9393–9400. doi:10.1073/pnas.1917060117

Fukuda, Y., Laugks, U., Lučić, V., Baumeister, W., and Danev, R. (2015). Electron Cryotomography of Vitrified Cells with a Volta Phase Plate. *J. Struct. Biol.* 190 (2), 143–154. doi:10.1016/j.jsb.2015.03.004

Gervasi, M. G., and Visconti, P. E. (2016). Chang's Meaning of Capacitation: A Molecular Perspective. *Mol. Reprod. Dev.* 83 (10), 860–874. doi:10.1002/mrd.22663

Glushakova, S., Yin, D., Li, T., and Zimmerberg, J. (2005). Membrane Transformation during Malaria Parasite Release from Human Red Blood Cells. *Curr. Biol.* 15 (18), 1645–1650. doi:10.1016/j.cub.2005.07.067

Haldar, S., Mekhedov, E., McCormick, C. D., Blank, P. S., and Zimmerberg, J. (2019). Lipid-dependence of Target Membrane Stability during Influenza Viral Fusion. *J. Cell Sci.* 132 (4), jcs218321. doi:10.1242/jcs.218321

Hardy, D. M., Oda, M. N., Friend, D. S., and Huang, T. T. F. (1991). A Mechanism for Differential Release of Acrosomal Enzymes during the Acrosome Reaction. *Biochem. J.* 275 (3), 759–766. doi:10.1042/bj2750759

Harper, C. V., Barratt, C. L. R., Publicover, S. J., and Kirkman-Brown, J. C. (2006). Kinetics of the Progesterone-Induced Acrosome Reaction and its Relation to Intracellular Calcium Responses in Individual Human Spermatozoa1. *Biol. Reprod.* 75 (6), 933–939. doi:10.1095/biolreprod.106.054627

Heumann, J. M., Hoenger, A., and Mastronarde, D. N. (2011). Clustering and Variance Maps for Cryo-Electron Tomography Using Wedge-Masked Differences. *J. Struct. Biol.* 175 (3), 288–299. doi:10.1016/j.jsb.2011.05.011

Inoue, N., Ikawa, M., Isotani, A., and Okabe, M. (2005). The Immunoglobulin Superfamily Protein Izumo Is Required for Sperm to Fuse with Eggs. *Nature* 434 (7030), 234–238. doi:10.1038/nature03362

Jamil, K., and White, I. G. (1981). Induction of Acrosomal Reaction in Sperm with Lonophore A23187 and Calcium. *Arch. Androl.* 7, 283–292. doi:10.3109/01485018108999319

Kim, K.-S., Foster, J. A., and Gerton, G. L. (2001). Differential Release of Guinea Pig Sperm Acrosomal Components during Exocytosis1. *Biol. Reprod.* 64 (1), 148–156. doi:10.1095/biolreprod64.1.148

Kim, K.-S., and Gerton, G. L. (2003). Differential Release of Soluble and Matrix Components: Evidence for Intermediate States of Secretion during Spontaneous Acrosomal Exocytosis in Mouse Sperm☆. *Developmental Biol.* 264 (1), 141–152. doi:10.1016/J.YDBIO.2003.08.006

Lamas-Toranzo, I., Hamze, J. G., Bianchi, E., Fernández-Fuertes, B., Pérez-Cerezales, S., Laguna-Barraza, R., et al. (2020). TMEM95 Is a Sperm Membrane Protein Essential for Mammalian Fertilization. *eLife* 9, 1–18. doi:10.7554/eLife.53913

L. Zeng, G. (2012). A Filtered Backprojection Algorithm with Characteristics of the Iterative Landweber Algorithm. *Med. Phys.* 39 (2), 603–607. doi:10.1118/1.3673956

Marko, M., Hsieh, C., Moberlychan, W., Mannella, C. A., and Frank, J. (2006). Focused Ion Beam Milling of Vitreous Water: Prospects for an Alternative to Cryo-Ultramicrotomy of Frozen-Hydrated Biological Samples. *J. Microsc.* 222 (1), 42–47. doi:10.1111/j.1365-2818.2006.01567.x

Mastronarde, D. N. (2005). Automated Electron Microscope Tomography Using Robust Prediction of Specimen Movements. *J. Struct. Biol.* 152 (1), 36–51. doi:10.1016/j.jsb.2005.07.007

Nagae, T., Yanagimachi, R., Srivastava, P. N., and Yanagimachi, H. (1986). Acrosome Reaction in Human Spermatozoa*. *Fertil. Sterility* 45 (5), 701–707. doi:10.1016/S0015-0282(16)49344-1

Ng, C. T., and Gan, L. (2020). Investigating Eukaryotic Cells with Cryo-ET. *MBoC* 31 (2), 87–100. doi:10.1091/mbc.E18-05-0329

Nicastro, D., Schwartz, C., Pierson, J., Gaudette, R., Porter, M. E., and McIntosh, J. R. (2006). The Molecular Architecture of Axonemes Revealed by Cryoelectron Tomography. *Science* 313 (5789), 944–948. doi:10.1126/science.1128618

Noda, T., Lu, Y., Fujihara, Y., Oura, S., Koyano, T., Kobayashi, S., et al. (2020). Sperm Proteins SOF1, TMEM95, and SPACA6 Are Required for Sperm–oocyte Fusion in Mice. *Proc. Natl. Acad. Sci. USA* 117 (21), 11493–11502. doi:10.1073/pnas.1922650117

Nolan, J. P., and Hammerstedt, R. H. (1997). Regulation of Membrane Stability and the Acrosome Reaction in Mammalian Sperm. *FASEB j.* 11 (8), 670–682. doi:10.1096/fasebj.11.8.9240968

Olson, G. E., and Winfrey, V. P. (1994). Structure of Acrosomal Matrix Domains of Rabbit Sperm. *J. Struct. Biol.* 112 (1), 41–48. doi:10.1006/jsbi.1994.1005

Parrish, J. J., Susko-Parrish, J., Winer, M. A., and First, N. L. (1988). Capacitation of Bovine Sperm by Heparin1. *Biol. Reprod.* 38 (5), 1171–1180. doi:10.1095/biolreprod38.5.1171

Phillips, D. M. (1972). Substructure of the Mammalian Acrosome. *J. Ultrastruct. Res.* 38 (5–6), 591–604. doi:10.1016/0022-5320(72)90092-5

Rigort, A., Bauerlein, F. J. B., Villa, E., Eibauer, M., Laugks, T., Baumeister, W., et al. (2012). Focused Ion Beam Micromachining of Eukaryotic Cells for Cryoelectron Tomography. *Proc. Natl. Acad. Sci.* 109 (12), 4449–4454. doi:10.1073/pnas.1201333109

Russell, L., Peterson, R., and Freund, M. (1979). Direct Evidence for Formation of Hybrid Vesicles by Fusion of Plasma and Outer Acrosomal Membranes during the Acrosome Reaction in Boar Spermatozoa. *J. Exp. Zool.* 208 (1), 41–55. doi:10.1002/jez.1402080106

Satouh, Y., Inoue, N., Ikawa, M., and Okabe, M. (2012). Visualization of the Moment of Mouse Sperm-Egg Fusion and Dynamic Localization of IZUMO1. *J. Cell Sci.* 125 (21), 4985–4990. doi:10.1242/jcs.100867

Schaffer, M., Mahamid, J., Engel, B. D., Laugks, T., Baumeister, W., and Plitzko, J. M. (2017). Optimized Cryo-Focused Ion Beam Sample Preparation Aimed at *In Situ* Structural Studies of Membrane Proteins. *J. Struct. Biol.* 197 (2), 73–82. doi:10.1016/j.jsb.2016.07.010

Sosa, C. M., Pavarotti, M. A., Zanetti, M. N., Zoppino, F. C. M., De Blas, G. A., and Mayorga, L. S. (2015). Kinetics of Human Sperm Acrosomal Exocytosis. *oup* 21 (3), 244–254. doi:10.1093/molehr/gau110

Stock, C. E., and Fraser, L. R. (1987). The Acrosome Reaction in Human Sperm from Men of Proven Fertility. *Hum. Reprod.* 2 (2), 109–119. doi:10.1093/oxfordjournals.humrep.a136494

Tegunov, D., and Cramer, P. (2019). Real-time Cryo-Electron Microscopy Data Preprocessing with Warp. *Nat. Methods* 16 (11), 1146–1152. doi:10.1038/s41592-019-0580-y

Tivol, W. F., Briegel, A., and Jensen, G. J. (2008). An Improved Cryogen for Plunge Freezing. *Microsc. Microanal* 14 (5), 375–379. doi:10.1017/S1431927608080781

Travis, A. J., and Kopf, G. S. (2002). The Role of Cholesterol Efflux in Regulating the Fertilization Potential of Mammalian Spermatozoa. *J. Clin. Invest.* 110 (6), 731–736. doi:10.1172/JCI1639210.1172/jci0216392

Tsai, P.-S., Garcia-Gil, N., van Haeften, T., and Gadella, B. M. (2010). How Pig Sperm Prepares to Fertilize: Stable Acrosome Docking to the Plasma Membrane. *PLoS ONE* 5 (6), e11204. doi:10.1371/journal.pone.0011204

Tsai, P.-S., Tsai, P.-S., De Vries, K. J., Tsai, P.-S., De Vries, K. J., De Boer-Brouwer, M., et al. (2007). Syntaxin and VAMP Association with Lipid Rafts Depends on Cholesterol Depletion in Capacitating Sperm Cells. *Mol. Membr. Biol.* 24 (4), 313–324. doi:10.1080/09687860701228692

Wolff, G., Limpens, R. W. A. L., Zheng, S., Snijder, E. J., Agard, D. A., Koster, A. J., et al. (2019). Mind the gap: Micro-expansion Joints Drastically Decrease the Bending of FIB-Milled Cryo-Lamellae. *J. Struct. Biol.* 208 (3), 107389. doi:10.1016/j.jsb.2019.09.006

Yanagimachi, R. (1981). "Mechanisms of Fertilization in Mammals," in *Fertilization and Embryonic Development* in Vitro. Editors L. Mastroianni and J. D. Biggers (Boston, MA: Springer), 81–182. doi:10.1007/978-1-4684-4016-4_6

Yudin, A. I., Gottlieb, W., and Meizel, S. (1988). Ultrastructural Studies of the Early Events of the Human Sperm Acrosome Reaction as Initiated by Human Follicular Fluid. *Gamete Res.* 20 (1), 11–24. doi:10.1002/mrd.1120200103

Zanetti, N., and Mayorga, L. S. (2009). Acrosomal Swelling and Membrane Docking Are Required for Hybrid Vesicle Formation during the Human Sperm Acrosome Reaction1. *oup* 81 (2), 396–405. doi:10.1095/biolreprod.109.076166

Conflict of Interest: The authors declare that the research was conducted in the absence of any commercial or financial relationships that could be construed as a potential conflict of interest.

Publisher's Note: All claims expressed in this article are solely those of the authors and do not necessarily represent those of their affiliated organizations, or those of the publisher, the editors and the reviewers. Any product that may be evaluated in this article, or claim that may be made by its manufacturer, is not guaranteed or endorsed by the publisher.

frontiers in Cell and Developmental Biology

REVIEW
published: 14 December 2021
doi: 10.3389/fcell.2021.800351

Cysteine-Rich Secretory Proteins (CRISP) are Key Players in Mammalian Fertilization and Fertility

*Soledad N. Gonzalez, Valeria Sulzyk, Mariana Weigel Muñoz and Patricia S. Cuasnicu**

Instituto de Biología y Medicina Experimental (IByME-CONICET), Ciudad Autónoma de Buenos Aires, Buenos Aires, Argentina

Mammalian fertilization is a complex process involving a series of successive sperm-egg interaction steps mediated by different molecules and mechanisms. Studies carried out during the past 30 years, using a group of proteins named CRISP (Cysteine-RIch Secretory Proteins), have significantly contributed to elucidating the molecular mechanisms underlying mammalian gamete interaction. The CRISP family is composed of four members (i.e., CRISP1-4) in mammals, mainly expressed in the male tract, present in spermatozoa and exhibiting Ca^{2+} channel regulatory abilities. Biochemical, molecular and genetic approaches show that each CRISP protein participates in more than one stage of gamete interaction (i.e., cumulus penetration, sperm-ZP binding, ZP penetration, gamete fusion) by either ligand-receptor interactions or the regulation of several capacitation-associated events (i.e., protein tyrosine phosphorylation, acrosome reaction, hyperactivation, etc.) likely through their ability to regulate different sperm ion channels. Moreover, deletion of different numbers and combination of *Crisp* genes leading to the generation of single, double, triple and quadruple knockout mice showed that CRISP proteins are essential for male fertility and are involved not only in gamete interaction but also in previous and subsequent steps such as sperm transport within the female tract and early embryo development. Collectively, these observations reveal that CRISP have evolved to perform redundant as well as specialized functions and are organized in functional modules within the family that work through independent pathways and contribute distinctly to fertility success. Redundancy and compensation mechanisms within protein families are particularly important for spermatozoa which are transcriptionally and translationally inactive cells carrying numerous protein families, emphasizing the importance of generating multiple knockout models to unmask the true functional relevance of family proteins. Considering the high sequence and functional homology between rodent and human CRISP proteins, these observations will contribute to a better understanding and diagnosis of human infertility as well as the development of new contraceptive options.

Keywords: sperm, egg, gamete, fertilization, fertility, CRISP

OPEN ACCESS

Edited by:
Enrica Bianchi,
University of York, United Kingdom

Reviewed by:
Naokazu Inoue,
Fukushima Medical University, Japan
Elizabeth Grace Bromfield,
The University of Newcastle, Australia

****Correspondence:***
Patricia S. Cuasnicu
pcuasnicu@gmail.com

Specialty section:
This article was submitted to Molecular and Cellular Reproduction, a section of the journal Frontiers in Cell and Developmental Biology

Received: *22 October 2021*
Accepted: *15 November 2021*
Published: *14 December 2021*

Citation:
Gonzalez SN, Sulzyk V, Weigel Muñoz M and Cuasnicu PS (2021) Cysteine-Rich Secretory Proteins (CRISP) are Key Players in Mammalian Fertilization and Fertility. Front. Cell Dev. Biol. 9:800351. doi: 10.3389/fcell.2021.800351

Abbreviations: CatSper, cation channel of sperm; COC, cumulus-oocyte complexes; CRISP, Cysteine Rich Secretory Proteins; QKO, quadruple knockout; TKO, triple knockout; TRPM8, transient receptor potential membrane 8; RyR, ryanodine receptor; ZP, zona pellucida.

INTRODUCTION

In mammals, sperm that leave the testes are not capable of recognizing and fertilizing the egg. In order to acquire fertilizing competence, sperm must undergo several physiological changes during their transit through the male and female reproductive tracts, known as sperm maturation (Robaire and Hinton, 2015) and sperm capacitation (Chang, 1951; Austin, 1952), respectively. Whereas sperm maturation occurs during epididymal transit and confers sperm the ability to move progressively and to fertilize the egg, sperm capacitation takes place while sperm are ascending through the female tract towards the oviduct and allows sperm to undergo both the acrosome reaction, an exocytotic event that occurs in the head, and to develop a vigorous flagellar movement termed hyperactivation. Both the acrosome reaction and hyperactivation are essential for the gamete interaction process that occurs in the oviductal ampulla and which involves several coordinated and successive stages (i.e., cumulus penetration, zona pellucida (ZP) sperm-ZP binding, ZP penetration, gamete fusion) (Florman and Fissore, 2015).

For more than 30 years, our laboratory has been dedicated to elucidate the molecular mechanisms involved in the mammalian fertilization process using as a model the evolutionarily conserved Cysteine-RIch Secretory Protein (CRISP) family, a group of highly homologous proteins enriched mainly in the mammalian reproductive tract and the venom of reptiles (Mochca-Morales et al., 1990; Yamazaki and Morita, 2004; Gibbs and O'Bryan, 2007). The CRISP family, together with the Antigen-5 and the Pathogenesis Related-1 proteins, forms the CAP superfamily of proteins found in a wide range of organisms including humans. The tertiary structure of CAP proteins shows a remarkable conservation despite significant phylogenetic distance between organisms, suggesting that these proteins may be involved in common and essential biological processes (Gibbs et al., 2008). CRISP proteins (Mw 20–30 kDa) are characterized by the presence of sixteen conserved cysteines, ten of which are located in the C-terminal region or cysteine-rich domain (CRD), which is connected by a hinge region to the plant pathogenesis-related 1 (PR-1) domain located in the N-terminus (Guo et al., 2005; Gibbs et al., 2008). Whereas the N-terminal domain was proposed to be involved in cell-cell adhesion and fusion (Maeda et al., 1998; Ellerman et al., 2006) as well as in amyloid-type aggregation and/or oligomerization (Sheng et al., 2019; Sheng et al., 2021), the C-terminal domain showed the ability to regulate various ion channels (i.e., Cyclic Nucleotide Gated (CNGs), Ryanodine (RyR), Transient Receptor Potential ion channel Member 8 (TRPM8), Cation channel of Sperm (CatSper), etc.) (Yamazaki et al., 2002; Gibbs et al., 2006, 2011; Ernesto et al., 2015). In mammals, four CRISP proteins have been identified, mainly expressed in the male reproductive tract. The following sections describe their functional roles during the fertilization process as well as their relevance for animal fertility.

EVIDENCE ON THE RELEVANCE OF CRISP PROTEINS FOR FERTILIZATION AND FERTILITY THROUGH THE USE OF NON-GENETIC APPROACHES

CRISP1

CRISP1, the first member of the family, was identified in the rat epididymis and originally named DE (Cameo and Blaquier, 1976). It is an androgen-dependent glycoprotein that associates with the sperm plasma membrane during epididymal transit (Kohane et al., 1980a, 1980b; Garberi et al., 1982; Eberspaecher et al., 1995) with two different affinities (Cohen et al., 2000a). Whereas a major loosely bound population is released during capacitation, acting as a decapacitating factor and preventing a premature capacitation in the male tract (Cohen et al., 2000a; Roberts et al., 2003), a minor, strongly bound population, remains in sperm after capacitation, migrates from the dorsal region of the acrosome to the equatorial segment concomitant with the acrosome reaction and participates in gamete interaction (Rochwerger et al., 1992; Cohen et al., 2000b). Biochemical and molecular approaches revealed that CRISP1 plays a role in both sperm binding to the ZP and gamete fusion through its binding to complementary sites located in the ZP and the egg plasma membrane (oolemma), respectively (Rochwerger et al., 1992; Cohen et al., 2000b; Busso et al., 2007a). Considering that gamete fusion involves a first stage of sperm binding to the oolemma followed by a subsequent step of fusion between the sperm and egg plasma membranes, it is interesting to note that CRISP1 was found to participate in a step subsequent to sperm binding to the oolemma and leading to gamete fusion through a small region of only 12 amino acid residues that resides in an evolutionary conserved region of the whole CRISP family called Signature 2 (Ellerman et al., 2006). It is important to mention that the human homologue (hCRISP1) (Haendler et al., 1993; Hayashi et al., 1996; Krätzschmar et al., 1996), like its rodent counterpart, is also expressed in the epididymis, binds to human sperm with two different affinities and participates in both sperm binding to the ZP and gamete fusion through complementary sites localized in the human egg (Cohen et al., 2001; Maldera et al., 2014). In this regard, whereas evidence showed that ZP3 acts as a ZP binding site for CRISP1 (Maldera et al., 2014), the identity of binding sites for CRISP proteins involved in gamete fusion remains unknown. Although originally described in males, CRISP1 is also expressed along the female reproductive tract (Reddy et al., 2008) including the cumulus cells that surround the egg where it also plays a role in gamete interaction and, more specifically, in cumulus penetration, through its ability to modulate sperm motility and orientation (Ernesto et al., 2015).

Interestingly, electrophysiological studies revealed that CRISP1 also exhibits the ability to regulate TRPM8, a thermo sensitive Ca^{2+} channel located in both the sperm head and tail

plasma membranes, and proposed to regulate the progesterone- and ZP-induced acrosome reaction (Martínez-López et al., 2010; Ernesto et al., 2015) as well as CatSper, the main sperm Ca^{2+} channel located in the principal piece of the tail and essential for sperm hyperactivation and male fertility (Ren et al., 2001; Sun et al., 2017). In this regard, although several inhibitors of CatSper have been described (Rennhack et al., 2018), to our knowledge, CRISP1 is the only physiological blocker of CatSper described so far.

The first evidence of the potential relevance of CRISP1 not only for fertilization but also for fertility was observed when male and female rats were immunized with either native or recombinant CRISP1. This strategy produced high levels of antibodies and a significant decrease in fertility in both sexes without eliciting pathological effects (Cuasnicu et al., 1990; Perez Martinez et al., 1995; Ellerman et al., 1998, 2008; Muñoz et al., 2012). These results, later supported by plasmid based contraceptive vaccines encoding mouse CRISP1 (Luo et al., 2012, 2016), constitute a strong proof of concept that blocking epididymal protein CRISP1 by immunological or pharmacological means, may lead to an effective male contraceptive. Moreover, immunization of non-human primates with hCRISP1 also produced specific antibodies that enter the male reproductive tract, recognize the native protein on sperm and remain associated with the ejaculated cells without eliciting effects on sperm number, morphology and motility, excluding deleterious effects of the immune response on the testes and/or the epididymis (Ellerman et al., 2010). This, together with the inhibitory effect of anti-hCRISP1 antibodies on both human sperm-ZP interaction and gamete fusion (Cohen et al., 2001; Maldera et al., 2014), supports CRISP1 as a promising contraceptive target in men. Thus, CRISP1 seems to fulfill many of the criteria to be considered an attractive target for contraception as it is an epididymal protein localized in the surface of mammalian sperm being accessible to immunological or drug attack, it has key functional roles in fertilization (i.e gamete interaction and CatSper regulation), it is relevant for fertility, and it has a functional homologue in humans.

CRISP2

CRISP2, initially identified as testicular protein-1 (TPX-1) (Kasahara et al., 1989), is a non-glycosylated protein expressed almost exclusively in the testis in an androgen independent manner (Haendler et al., 1997) and present in germ cells of numerous species (i.e., guinea pig (Hardy et al., 1988), rat (Maeda et al., 1998; O'Bryan et al., 1998), mouse (Kasahara et al., 1989; Mizuki et al., 1992), human (Kasahara et al., 1989), horse (Giese et al., 2002) and boar (Vadnais et al., 2008)). CRISP2 localizes in the surface of spermatogenic cells (Maeda et al., 1998) and within the sperm acrosome (O`Bryan et al., 2001; Nimlamool et al., 2013), neck and outer dense fibers of the tail (O'Bryan et al., 1998, 2001). Like CRISP1, CRISP2 also relocalizes to the equatorial segment after acrosome reaction (Cuasnicu et al., 2016). However, while CRISP1 migrates to the equatorial segment, CRISP2 is released from the acrosome and then associates to the surface of the equatorial segment (Busso et al., 2005; Busso et al., 2007a; Muñoz et al., 2012; Nimlamool et al., 2013). Interestingly, recent results showed that under native, non-reducing conditions, CRISP2 formed oligomers both in the tail and the head but with different molecular weights and different biochemical properties (Zhang et al., 2021). Although a slight expression of CRISP2 has been observed in the ovary (Reddy et al., 2008) the relevance of this observation is still unknown.

Structure and function studies revealed that while the N-terminal domain of CRISP2 exhibits cell to cell adhesion properties (Maeda et al., 1999), the C-terminal domain is able to regulate Ca^{2+} RyR channels (Gibbs et al., 2006). Considering that both RyR (Harper et al., 2004) and CRISP2 are located in the neck and that the Ca^{2+} released from intracellular stores at the neck is involved in sperm hyperactivation (Chang and Suarez, 2011), it is likely that CRISP2 modules sperm hyperactivation by regulating RyR controlling intracellular Ca^{2+} stores. As previously described for CRISP1, CRISP2 located in the equatorial segment of acrosome reacted sperm (Busso et al., 2005, 2007b; Muñoz et al., 2012; Nimlamool et al., 2013) also participates in gamete fusion through its interaction with egg plasma membrane complementary sites (Busso et al., 2005; Busso et al., 2007b). Interestingly, competition studies indicate that CRISP2 binds to the same egg complementary sites that CRISP1 (Busso et al., 2007b), suggesting that CRISP2 may cooperate with CRISP1 during gamete fusion. Whereas this cooperation might be due to a synergistic action of each individual protein, the possibility cannot be excluded that these two proteins could eventually form a complex (i.e., dimers and/or oligomers) to achieve that role, consistent with the reported oligomeric properties of CRISP family members (Zhang et al., 2021). Human CRISP2 (Kasahara et al., 1989) was also found to be present within the sperm acrosome and tail and to participate in gamete fusion through complementary sites in the human egg plasma membrane (Busso et al., 2005).

In contrast to the significant inhibition of fertility observed in animals injected with CRISP1 (Ellerman et al., 1998, 2010), immunization of male and female rats with recombinant CRISP2 raised specific antibodies in both sexes without affecting animal fertility (Muñoz et al., 2012), consistent with the internal localization of CRISP2. Interestingly however, evidence indicates that aberrant CRISP2 expression is associated with human fertility problems. Patients with azoospermia or oligoasthenoteratospermia (Du et al., 2006) or with asthenospermia (Jing et al., 2011; Heidary et al., 2019) syndromes exhibit lower expression of CRISP2 than fertile man (Gholami et al., 2020). Moreover, a correlation was found between CRISP2 expression and low sperm progressive motility, abnormal sperm morphology and infertility, suggesting that the lower expression of CRISP2 in these patients could be due to a post-transcriptional regulation process mediated by miR27 b (Zhou et al., 2015). In agreement with the observations in humans, recent studies revealed a positive correlation between CRISP2 expression levels and boar fertility and that sperm CRISP2 has the potential to serve as a fertility biomarker (Gao et al., 2021).

CRISP3

CRISP3, originally described in mice salivary glands (Haendler et al., 1993) and in human neutrophil granules (Kjeldsen et al.,

1996), is expressed in an androgen-dependent manner (Schwidetzky et al., 1995; Haendler et al., 1997) and, unlike the other members of the CRISP family, shows a wider expression distribution including exocrine glands such as pancreas and prostate (Kratzschmar et al., 1996), organs with immunological roles such as the thymus and spleen and, at lower levels, the epididymis, seminal vesicle, ovary and uterus (Kratzschmar et al., 1996; Schambony et al., 1998; Evans et al., 2015). In humans, CRISP3 was described in several tissues and differences in its expression are associated with different pathologies such as prostate cancer (Kosari et al., 2002; Bjartell et al., 2007; Noh et al., 2016), breast cancer (Tang et al., 2020), Sjögren's syndrome (Laine et al., 2007), varicocele (Belardin et al., 2019), prostatitis and endometriosis (Grande et al., 2017), among others. Two forms of human CRISP3 (i.e. glycosylated and non-glycosylated) were described along the male reproductive tract (Ubdy et al., 2005) and found to bind to human sperm with different affinities (Da Ros et al., 2015). While the glycosylated form is weakly bound and released during capacitation, the non-glycosylated form is tightly bound and remains on the spermatozoa even after the acrosome reaction (Da Ros et al., 2015), similarly to the two populations described for CRISP1. CRISP3 was also found to be present in horse seminal plasma and to prevent the interaction between polymorphonuclear cells and spermatozoa in the uterus (Doty et al., 2011), supporting a possible role in sperm protection during their transit through the female reproductive tract. However, little information exists about the relevance of CRISP3 for fertilization (Da Ros et al., 2015) and fertility (Hamann et al., 2007). Although no specific role of CRISP3 in ion channel regulation has been reported, the low levels of this protein in lacrimal and salivary gland secretion of patients with Sjögren's syndrome (Tapinos et al., 2002; Laine et al., 2007) together with the altered ion concentrations reported in these glands (Enger et al., 2014) known to be relevant for their functionality (Konttinen et al., 2006), support the idea that CRISP3 may influence the ion concentration of these glands, likely through an ion channel regulatory ability.

CRISP4

CRISP4 is an androgen-dependent protein almost exclusively synthesized in the epididymis and not expressed in the female reproductive tract (Jalkanen et al., 2005; Reddy et al., 2008; Turunen et al., 2012). Like CRISP1, epididymal CRISP4 associates with sperm during maturation (Jalkanen et al., 2005; Nolan et al., 2006). However, differently from CRISP1, CRISP4 is strongly bound to sperm and remains on the cells even after the acrosome reaction, lacking a loosely bound population (Weigel Muñoz et al., 2019). Patch-clamp of murine testicular sperm revealed that the CRD domain of CRISP4 has the ability to inhibit TRPM8 without affecting capacitation-associated parameters (i.e., sperm tyrosine phosphorylation or progesterone-induced acrosome reaction) (Gibbs et al., 2011). These observations together with the lack of a loosely bound population support a role for CRISP4 in gamete interaction rather than as a decapacitating factor as previously proposed for CRISP1. The first evidence on the involvement of CRISP4 in sperm-egg interaction emerged when two different groups developed the CRISP4 null mice and will be described in the following section (Gibbs et al., 2011; Turunen et al., 2012). Interestingly, mice fed a high-fat diet present a decline in sperm motility and fertilization in part from the disruption of epididymal CRISP4 expression and secretion (Borges et al., 2017). Rodent CRISP4 was found to exhibit high homology with epididymal hCRISP1, even higher than that between the rodent and human CRISP1 protein, suggesting that CRISP4 represents the rodent counterpart of hCRISP1 (Jalkanen et al., 2005; Nolan et al., 2006; Arevalo et al., 2020). However, subsequent observations showing the involvement of CRISP4 in gamete interaction led to propose that hCRISP1 is the equivalent to the combination of rodent CRISP1 and CRISP4 (Gibbs et al., 2011; Maldera et al., 2014).

In summary, the reported observations indicate that CRISP proteins exhibit a high sequence, structural and functional homology being involved in different stages of the fertilization process. To better analyze their functional roles as well as their relevance for fertility, our laboratory and others have generated several knockout models for CRISP family members (i.e., single, double and multiple knockouts) which exhibit different phenotypes described in detail in the following section.

EVIDENCE ON THE RELEVANCE OF CRISP PROTEINS FOR FERTILIZATION AND FERTILITY THROUGH THE USE OF KNOCKOUT MODELS

Single Knockout Models

Crisp1$^{-/-}$

In addition to the immunization studies showing the need of CRISP1 for fertility and, as another approach to study the relevance of this protein for fertility, our laboratory developed the CRISP1 knockout mice which represented the first knockout animal for a CRISP family member (Da Ros et al., 2008). Surprisingly, animal fertility was not affected in either male or female mice (Da Ros et al., 2008; Ernesto et al., 2015), and the same results were later obtained in knockout male mice for CRISP1 generated in different genetic backgrounds (Hu et al., 2018; Weigel Muñoz et al., 2018), revealing that blocking the protein in an adult animal by immunization differs from deleting the gene, an approach that allows functional compensation of the lacking molecule during animal development. Nevertheless, in spite of their normal fertility, knockout males showed sperm with clear defects to interact with the ZP and to fuse with the egg (Da Ros et al., 2008), consistent with the previously proposed roles of CRISP1 in fertilization (Rochwerger et al., 1992; Busso et al., 2007a). Comparison of phenotypes in CRISP1 knockout mice of different genetic background revealed new roles for CRISP1 in hyperactivation development, sperm motility, progesterone-induced acrosome reaction and cAMP/PKA signaling pathway (Weigel Muñoz et al., 2018). Interestingly, whereas defects in gamete interaction, hyperactivation and cAMP/PKA signaling seem to withstand the genetic contexts, progesterone-induced acrosome reaction, motility and tyrosine phosphorylation defects were clearly dependent on the genetic background of the mutant

animals (Weigel Muñoz et al., 2018), indicating that the phenotype observed in CRISP1 null males is not entirely controlled by the mutation at *Crisp1* locus but it is modulated by the genetic context. Of note, in spite of the Ca^{2+} channel regulatory activity described for CRISP1 (Ernesto et al., 2015), intracellular Ca^{2+} levels seem to be normal in *Crisp1*$^{-/-}$ sperm (Weigel Muñoz et al., 2018). Given the reported ability of CRISP1 to affect both CatSper currents and intracellular Ca^{2+} levels (Ernesto et al., 2015), it is possible that the lack of CRISP1 produces a Ca^{2+} deregulation which is compensated by other CRISP family members and, thus, not reflected in the total concentration of the cation within the cell (Weigel Muñoz et al., 2018). In addition to our observations in males, the availability of CRISP1 knockout females confirmed that CRISP1 is also expressed along the female reproductive tract (i.e., uterus, oviduct and ovary), including the cumulus cells that surround the egg (Ernesto et al., 2015) where CRISP1 was proposed to orient sperm by regulating hyperactivation through its ability to inhibit CatSper (Ernesto et al., 2015).

Crisp2$^{-/-}$

The proposed role of CRISP2 in gamete interaction (Busso et al., 2005; 2007b) together with the reported association between fertility defects and aberrant expression of CRISP2 in humans (Du et al., 2006; Jing et al., 2011; Zhou et al., 2015) led our laboratory to generate CRISP2 knockout mice. However, as observed for CRISP1, males lacking CRISP2 were fertile under controlled laboratory conditions (Brukman et al., 2016) supporting the existence of a functional compensation of the lacking molecule by other members of the family. Nevertheless, fertility evaluation under more demanding conditions such as the use of *Crisp2*$^{-/-}$ males subjected to unilateral vasectomy to reduce sperm number in the ejaculate (Judd et al., 1997), showed a significant decrease in fertility rates compared to controls (Brukman et al., 2016). Consistent with this, a slight subfertility was observed in CRISP2 knockout males generated in a different genetic background (Lim et al., 2019), indicating that CRISP2 is indeed necessary for optimal fertility.

Apart from the relevance of CRISP2 for fertility, the analysis of CRISP2 knockout animals allowed a better understanding of the role of this protein in sperm physiology. *In vivo* studies revealed that unilaterally vasectomized *Crisp2*$^{-/-}$ mice also showed lower levels of fertilized eggs in the ampulla, confirming that fertilization defects were responsible for the lower fertility rates observed in these mice (Brukman et al., 2016). In addition, whereas no differences in *in vivo* fertilization were observed when mutant males were mated with natural estrus females, significantly lower *in vivo* fertilization rates were observed for *Crisp2*$^{-/-}$ males mated with hormone-stimulated females that ovulate a higher number of eggs compared to estrus females, representing a more demanding condition for mutant sperm (Brukman et al., 2016). According to these results, it is clear that whereas control males could deal with different *in vivo* modifications, *Crisp2*$^{-/-}$ males could not. These observations may be extrapolated to humans where the subfertility of an individual can or cannot be detected depending on the fertility status of the partner.

In addition to the *in vivo* fertilization defects, CRISP2 knockout sperm exhibited defects to fertilize ZP-free eggs *in vitro* (Brukman et al., 2016), consistent with the reported role of CRISP2 in gamete fusion through egg plasma membrane complementary sites in both rodents and humans (Busso et al., 2005; 2007b). However, a more pronounced decrease in fertilization rates was observed when *in vitro* experiments were performed using eggs surrounded by the cumulus and/or the ZP, supporting a role for CRISP2 in penetration of the egg coats. In agreement with this, a lower number of *Crisp2*$^{-/-}$ sperm was observed within the cumulus mass during cumulus penetration assays, and hyperactivated motility was significantly lower in mutant sperm (Brukman et al., 2016). Subsequent studies supported that these motility defects could be due to a stiffness of the midpiece in CRISP2 mutant sperm that impairs hyperactivation development and thus, egg coat penetration (Lim et al., 2019; Curci et al., 2020). Different from *Crisp1*$^{-/-}$ animals, sperm lacking CRISP2 exhibit a clear dysregulation of Ca^{2+} homeostasis (Brukman et al., 2016) that could explain the molecular mechanisms underlying the capacitation-associated defects in the mutant cells. In this regard, recent results in CRISP2 knockout mice support the idea that ion channel regulation by CRISP proteins controls energy flows powering the axonema (Nandagiri et al., 2021). Moreover, CRISP1, CRISP2, and CRISP4 have been proposed to be required to optimize sperm flagellum waveform (Gaikwad et al., 2021).

Together, our *in vivo* and *in vitro* results reveal that CRISP2 knockout mice exhibit clear fertilization deficiencies likely linked to defects in hyperactivation development and intracellular Ca^{2+} regulation, supporting that fertilization defects may be underlying the fertility disorders observed in men with aberrant expression of CRISP2. Of note, the finding that reproductive defects in CRISP2 knockout mice are masked by conventional mating, becoming evident under more demanding conditions, highlights the relevance of using different experimental approaches to analyze male fertility.

Crisp3$^{-/-}$

In contrast to the rest of the CRISP family members, there is little information on the relevance of CRISP3 for fertilization and fertility. Although a recent work reports that *Crisp3*$^{-/-}$ males were fertile, no further details on the reproductive phenotype of these animals were provided (Volpert et al., 2020). In this regard, the phenotype exhibited by mice lacking both *Crisp1* and *Crisp3* (see below) does not support a critical role for CRISP3 in fertilization.

Crisp4$^{-/-}$

Crisp4 single knockout males were also found to be fertile even when generated using different strategies and genetic backgrounds (Gibbs et al., 2011; Turunen et al., 2012; Carvajal et al., 2018; Hu et al., 2018). As mentioned above, the availability of CRISP4 knockout mice allowed the study of the participation of CRISP4 in the fertilization process which had not been studied before. *Crisp4*$^{-/-}$ males exhibited normal fertilization rates in eggs recovered from the ampulla of superovulated females (Carvajal et al., 2018), indicating that *Crisp4*$^{-/-}$ sperm, differently from

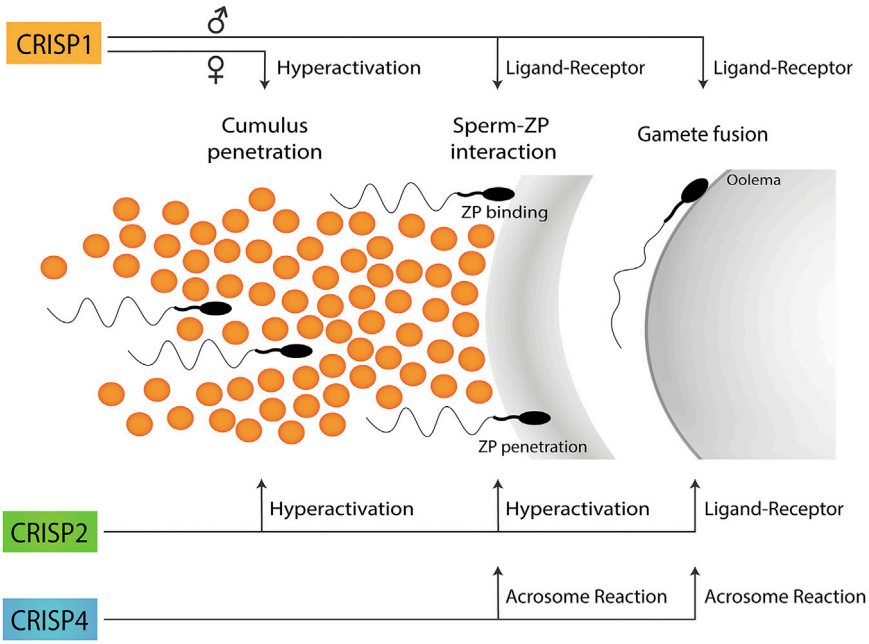

FIGURE 1 | Participation of CRISP proteins in different steps of the fertilization process. Epididymal CRISP1 was reported to participate in both sperm-ZP binding and gamete fusion through ligand-receptor interactions whereas cumulus CRISP1 was proposed to play a role in cumulus penetration by orienting sperm through its ability to modulate sperm hyperactivation. Testicular CRISP2 was reported to be involved in both cumulus and ZP penetration through its ability to regulate sperm hyperactivation as well as in gamete fusion through ligand-receptor interactions. Finally, CRISP4 was reported to play a role in sperm-ZP interaction as well as in gamete fusion consistent with its ability to regulate the acrosome reaction. No information is still available on the functional roles of CRISP3 in gamete interaction. A schematic sperm representation is included.

Crisp2$^{-/-}$ cells, are able to fertilize control eggs even in demanding conditions such as those produced by the presence of a high number of eggs in the ampulla. However, sperm lacking CRISP4 exhibited a severely affected ability to fertilize cumulus oocyte complexes as well as ZP-intact and ZP-free eggs under *in vitro* conditions (Carvajal et al., 2018). In this regard, whereas there are reports on the involvement of CRISP4 in sperm-ZP binding (Turunen et al., 2012), subsequent assays showing that CRISP4 mutant sperm were able to penetrate the cumulus cells and bind to the ZP together with the lack of accumulation of sperm in the perivitelline space support that fertilization defects in this colony may also reside at ZP penetration (Carvajal et al., 2018). Although sperm lacking CRISP4 did not exhibit defects in hyperactivation, the lower levels of progesterone induced-acrosome reaction observed in these cells compared to controls (Carvajal et al., 2018) could well explain their impaired ability to penetrate ZP-intact eggs as the acrosome reaction is essential for egg coat penetration (Yanagimachi, 1994). Interestingly, whereas a significant (Gibbs et al., 2011) or complete (Turunen et al., 2012; Carvajal et al., 2018) inhibition of progesterone-induced acrosome reaction was observed in all CRISP4 knockout models (Gibbs et al., 2011; Turunen et al., 2012; Carvajal et al., 2018), normal percentages of acrosome reacted sperm were observed in response to calcium ionophore, a non-physiological inductor of the acrosome reaction (Turunen et al., 2012), suggesting that CRISP4 might regulate the acrosome reaction by affecting calcium transport while not affecting the successive stages after calcium influx has occurred. Considering that the recombinant CRISP4 CRD domain has shown to be able to inhibit TRPM8 Ca^{2+} channel (Gibbs et al., 2011), it is possible that a modification in intracellular Ca^{2+} concentration would be responsible for the altered capacitated-sperm parameters observed in *Crisp4*$^{-/-}$ sperm. Acrosome reaction defects observed in all knockout models might also contribute to the impaired gamete fusion ability of CRISP4 knockout sperm as only acrosome-reacted sperm are able to fuse with the oolemma. Nevertheless, the possibility that CRISP4 mediates gamete fusion through a ligand-receptor interaction as previously observed for epididymal CRISP1 cannot be excluded.

Taken together, the results obtained using single knockout models support the participation of each CRISP protein in more than one stage of fertilization and the involvement of more than one CRISP in each stage of the fertilization process either by ligand-receptor interactions or by regulating different functional events (i.e., acrosome reaction, hyperactivation, etc.) (**Figure 1**), likely through their ability to regulate different sperm Ca^{2+} channels (**Figure 2**).

However, in spite of the critical roles of CRISP proteins in different stages of fertilization, all single knockout animals were fertile, supporting the existence of functional overlapping or redundancy among CRISP family members. In this regard, the development of mutant mice has revolutionized the reproductive field showing that only a small number of the proteins previously known to play an essential role in the fertilization process were

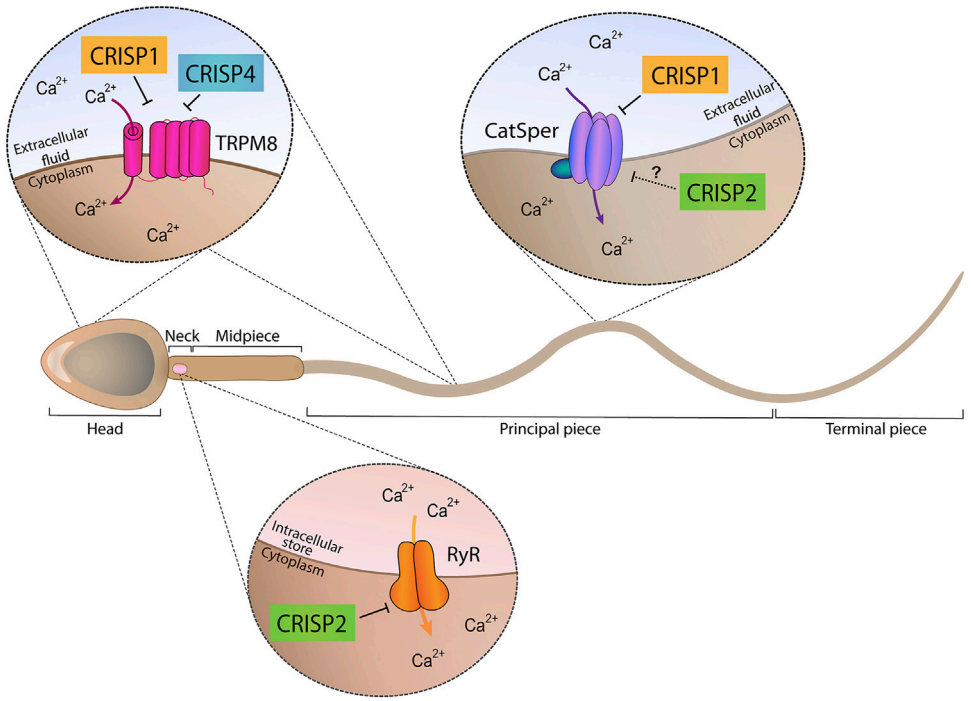

FIGURE 2 | Ion channel regulatory abilities of CRISP proteins. Epididymal proteins CRISP1 and CRISP4 (located in the head and tail plasma membrane) were found to regulate TRPM8 channel present in both sperm head and tail plasma membranes and proposed to be involved in acrosome reaction regulation. In addition, epididymal CRISP1 was found to exhibit the ability to regulate CatSper, located in the principal piece of the tail and involved in hyperactivation development. Testicular CRISP2 (located within the sperm head, neck and tail) was found to regulate Ryanodine Receptors (RyR) known to be present in the neck and to control intracellular Ca^{2+} stores. A schematic sperm representation is included.

indeed essential for fertility in mice (Miyata et al., 2016). A possible explanation for these observations may be the existence of functional redundancy among protein members of the same family which could partially or totally compensate for each other's loss, contributing to strengthening reproductive success. Such a mechanism becomes especially important in sperm which are transcriptionally and translationally silent cells. Based on this, animals simultaneously lacking more than one CRISP were generated and characterized. The following sections describe the different phenotypes observed for doubles, triples and quadruples knockout mice for *Crisp* family genes.

Double Knockout Models

Crisp2$^{-/-}$*/Crisp4*$^{-/-}$

The fact that *Crisp2* and *Crisp4* are located in different chromosomes together with the availability of CRISP2 and CRISP4 single knockout colonies, led our laboratory to generate double *Crisp2*$^{-/-}$*/Crisp4*$^{-/-}$ mice by natural mating (Curci et al., 2020). Analysis of animal fertility revealed that, in spite of the participation of both proteins in key stages of the fertilization process, males lacking both proteins were fertile under normal laboratory conditions (Curci et al., 2020). Nevertheless, when *Crisp2*$^{-/-}$*/Crisp4*$^{-/-}$ males were mated under more demanding conditions such as using superovulated females, a clear decrease in *in vivo* fertilization rates was observed compared to controls and to either *Crisp2* or *Crisp4* single mutant males (Curci et al., 2020). Consistent with this and with the reported roles of CRISP2 and CRISP4 in different stages of the fertilization process, *Crisp2*$^{-/-}$*/Crisp4*$^{-/-}$ sperm showed severe *in vitro* fertilization defects likely due to the combination of the capacitation-associated defects observed in sperm from each single knockout model (i.e. impaired tyrosine phosphorylation, progesterone-induced acrosome reaction and hyperactivation development). Although the reasons for the normal fertility of these mutant animals is still unknown, it is possible that the lack of epididymal CRISP4 is partially compensated by the presence of CRISP1, the other epididymal CRISP family member.

Crisp1$^{-/-}$*/Crisp4*$^{-/-}$

Both CRISP1 and CRISP4 are expressed in the epididymis in high concentrations (Eberspaecher et al., 1995; Krätzschmar et al., 1996), bind to sperm during epididymal transit and participate in sperm-ZP interaction and gamete fusion (Da Ros et al., 2008; Carvajal et al., 2018), supporting the idea that they could compensate for each other to ensure fertility success. This led to the generation of two different models of males lacking both CRISP1 and CRISP4 (Carvajal et al., 2018; Hu et al., 2018). While Hu et al. (2018) found no differences in fertility between mutant and control mice, concluding that epididymal CRISP are not absolutely required for male fertility, observations from our

laboratory showed that *Crisp1*$^{-/-}$/*Crisp4*$^{-/-}$ colony exhibited a clear disruption of fertility (Carvajal et al., 2018). Differences in the genetic background and/or environmental conditions might explain the different phenotypes observed in the two studies. The impaired fertility of *Crisp1*$^{-/-}$/*Crisp4*$^{-/-}$ revealed, for the first time, the relevance of CRISP proteins for fertility and confirmed the existence of compensatory mechanisms among CRISP family members. In this way, whereas in *Crisp2*$^{-/-}$/*Crisp4*$^{-/-}$ mice, CRISP4 could be partially compensated by the presence of epididymal CRISP1, it is likely that the simultaneous lack of the two epididymal proteins in *Crisp1*$^{-/-}$/*Crisp4*$^{-/-}$, cannot be compensated by the remaining family members (i.e., CRISP2 and CRISP3).

Analysis of subfertile *Crisp1*$^{-/-}$/*Crisp4*$^{-/-}$ males showed they exhibited an immature epididymal epithelium and abnormal luminal acidification, contributing to a better understanding of the fine-tuning mechanisms underlying epididymal sperm maturation (Carvajal et al., 2018). Interestingly, fertility rates correlated with the percentages of fertilized oocytes recovered from the oviduct, supporting the idea that fertility impairment in these mutant mice are mainly due to *in vivo* fertilization defects. This idea was supported by the *in vitro* fertilization studies showing that *Crisp1*$^{-/-}$/*Crisp4*$^{-/-}$ mutant sperm exhibited a lower ability to fertilize oocytes either with or without their coats, consistent with the reported roles for CRISP1 and CRISP4 in sperm-ZP interaction and gamete fusion (Cohen et al., 2000b; Busso et al., 2007a; Carvajal et al., 2018). Subsequent studies showed that sperm fertilizing defects might be due to a failure of mutant sperm to undergo a normal capacitation process as judged by the clear alterations in capacitation-associated sperm parameters such as protein tyrosine phosphorylation, progesterone-induced acrosome reaction and hyperactivation (Carvajal et al., 2018; Hu et al., 2018). Considering the abnormal epididymal epithelium and luminal acidification, it is likely that sperm functional defects occur as a consequence of a defective sperm maturation process.

Crisp1$^{-/-}$/*Crisp3*$^{-/-}$

The *Crisp1*$^{-/-}$/*Crisp3*$^{-/-}$ colony was generated by CRISPR-Cas 9 technology (Wang et al., 2013; Curci et al., 2020). Analysis of animal fertility showed that these mutant males were subfertile, indicating that the absence of CRISP1 in combination with either CRISP4 or CRISP3 unveils the important role of CRISP proteins for optimal fertility. However, differently to what it was observed in the *Crisp1*$^{-/-}$/*Crisp4*$^{-/-}$ double knockout animals, normal levels of fertilization rates were observed when the eggs were recovered from the ampulla of control females mated with *Crisp1*$^{-/-}$/*Crisp3*$^{-/-}$ males (Curci et al., 2020), supporting that fertility inhibition in this colony occurred as a consequence of post-fertilization defects. Subsequent studies showed that male subfertility was associated, at least in part, with a failure of fertilized eggs to reach the blastocyst stage, revealing the relevance of CRISP1 and CRISP3 for early embryo development and supporting the impact of paternal factors in this process. It remains to be clarified whether impaired embryo development occurs as a consequence of a delayed *in vivo* fertilization. Interestingly in this regard, examination of ejaculated sperm within the uterus of control mated females showed that whereas control sperm were moving freely in the uterine fluid, *Crisp1*$^{-/-}$/*Crisp3*$^{-/-}$ sperm were mostly inmotile and forming aggregates within a viscous uterine fluid (Curci et al., 2020). This phenotype might be associated with an alteration of the reported ability of CRISP proteins to form amyloid-like structures (Sheng et al., 2019) known to trap damaged sperm within the uterus (Roan et al., 2017) and/or with coagulation/liquefaction defects within the uterus (Magdaleno et al., 1997; Udby et al., 2002) due to the lack of CRISP3 in the seminal plasma. These sperm motility defects within the uterus could be responsible for sperm transport deficiencies that, finally, lead to a delayed fertilization and embryo development defects in this colony. Nevertheless, we cannot exclude the possibility that embryo development deficiencies are due to sperm epididymal maturation and/or capacitation defects reported to affect embryonic development (Orgebin-Crist et al., 1967; Conine et al., 2018; Navarrete et al., 2019).

Multiple (Triple and Quadruple) Knockout Models

The normal fertility and the subfertility of the different single and double knockout models support a functional compensation of the lacking proteins by the remaining members of the family that led to the generation of multiple knockout models lacking more than two *Crisp* genes simultaneously (Curci et al., 2020). Triple knockout (TKO) male mice lacking *Crisp1*, *Crisp2*, and *Crisp3* genes as well quadruple knockout (QKO) males deficient in the four CRISP members showed a dramatic inhibition in their fertility with an average of less than one born pup and a high proportion of sterile males (Curci et al., 2020) revealing, for the first time, the essential role of CRISP proteins for animal fertility. In this case, the severe fertility phenotype in TKO and QKO males was accompanied by significantly lower *in vivo* fertilization rates in the ampulla compared to controls which could be due to sperm transport and/or gamete interaction defects. Consistent with the fact that multiple knockout mice lack *Crisp1* and *Crisp3* genes, TKO and QKO ejaculated sperm were also mostly inmotile within the uterine fluid and trapped into aggregates in a very viscous fluid as previously described for the *Crisp1*$^{-/-}$/*Crisp3*$^{-/-}$ colony.

Besides motility defects at uterine level, sperm migration studies revealed that TKO and QKO sperm were capable of reaching the lower oviduct but exhibited clear defects in migrating within the organ (Curci et al., 2020). Although oviductal migration defects for *Crisp1*$^{-/-}$/*Crisp3*$^{-/-}$cannot be excluded, the normal *in vivo* fertilization rates observed for this colony does not favor this possibility. These observations support that oviductal migration defects in multiple knockout mice are likely due to the midpiece rigidity phenotype observed in ejaculated TKO and QKO (Lim et al., 2019; Curci et al., 2020) but not in *Crisp1*$^{-/-}$/*Crisp3*$^{-/-}$ sperm, associated with the lack of *Crisp2* and leading to defects in hyperactivation known to be required for detaching sperm from the isthmus epithelium.

In addition to these *in vivo* observations, *in vitro* fertilization studies revealed that TKO and QKO sperm had serious deficiencies in their ability to fertilize COC and ZP-intact eggs

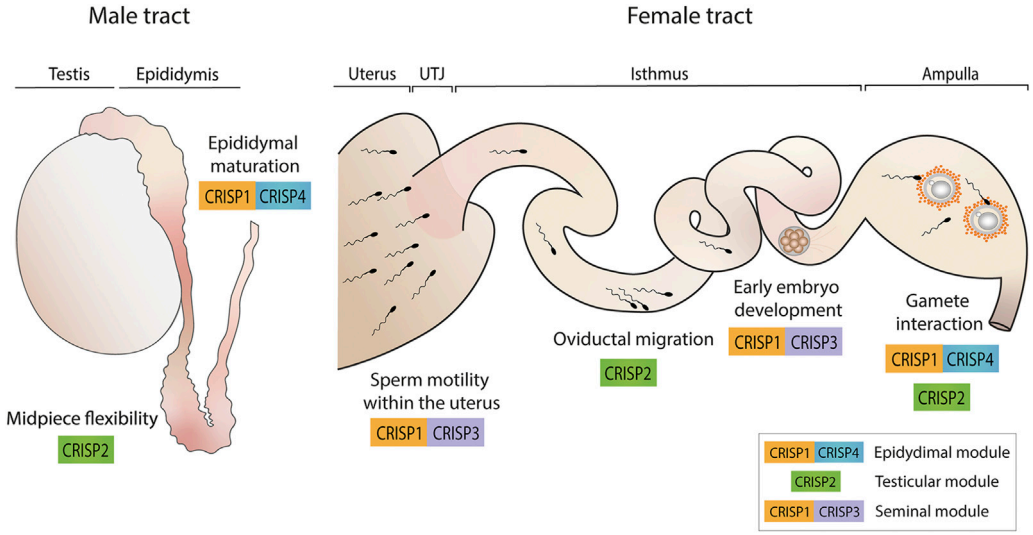

FIGURE 3 | CRISP functional modules and their roles in male and female reproductive tracts. Epididymal CRISP1 and CRISP4 (epididymal module) were found to be involved in sperm maturation as well as in gamete interaction. Testicular CRISP2 (testicular module) was reported to be required for the development of sperm midpiece flexibility critical for hyperactivation and, thus, for oviductal sperm migration and gamete interaction. Finally, CRISP1 and CRISP3 (seminal module) were found to be essential for maintaining sperm motility within the uterus and for early embryo development. A schematic sperm representation is included.

with no accumulation of sperm in the perivitelline space, indicating that fertilization failure could be attributed mostly to sperm defects to interact with the egg coats. This was further supported by the significantly lower levels of both hyperactivation and acrosome reaction observed in multiple mutant sperm. Hyperactivation failure could explain the impairment of both oviductal migration and egg coat penetration observed in multiple KO sperm (Curci et al., 2020). The finding that QKO but not TKO were unable to fertilize ZP-free eggs together with gamete fusion rates in TKO sperm that did not differ from those observed for *Crisp1*$^{-/-}$ or *Crisp2*$^{-/-}$ single knockout sperm argues against the involvement of CRISP3 in gamete fusion and reveals a key role of CRISP4 in this event supported by the low gamete fusion rates observed in those knockout models lacking *Crisp4* (i.e., *Crisp4*$^{-/-}$, *Crisp1*$^{-/-}$/*Crisp4*$^{-/-}$, *Crisp2*$^{-/-}$/*Crisp4*$^{-/-}$) (Carvajal et al., 2018). Although the mechanisms underlying CRISP4 involvement in gamete fusion are still under investigation, they could be linked to CRISP4 interaction with egg complementary sites as observed for both CRISP1 (Rochwerger et al., 1992; Da Ros et al., 2008) and CRISP2 (Busso et al., 2007b) and/or the reported involvement of CRISP4 in the acrosome reaction (Gibbs et al., 2011; Turunen et al., 2012; Carvajal et al., 2018) known to be essential for gamete fusion (Yanagimachi, 1994). Interestingly, the finding that QKO males did not exhibit a stronger fertility phenotype compared to that observed for TKO males, supports the notion that *in vivo* fertilization failure is mainly due to sperm defects in those events that precede gamete fusion such as sperm migration within the oviduct and penetration of the egg coats.

Consistent with the ability of CRISP proteins to regulate Ca^{2+} channels and the relevance of this cation for most sperm functional events, QKO sperm did not show the characteristic intracellular Ca^{2+} increase that occurs during sperm capacitation, indicating that multiple mutant sperm exhibit a dysregulation of Ca^{2+} homeostasis that probably reflects the final balance of the individual contribution of each CRISP to Ca^{2+}regulation. Finally, multiple mutant males exhibited clear embryo development defects as those previously described for the *Crisp1*$^{-/-}$/*Crisp3*$^{-/-}$colony (Curci el al., 2020).

Collectively, analysis of the different phenotypes observed in single, double and multiple knockout models showed that the subfertility of *Crisp1* and *Crisp3* males is associated with both the presence of inmotile sperm within the uterus and embryo development failure. As expected, these defects were also observed in infertile TKO and QKO males lacking *Crisp1* and *Crisp3*. However, besides these deficiencies, TKO and QKO mice exhibit sperm with midpiece rigidity due to the additional lack of testicular CRISP2 which affects hyperactivation and, thus, both oviductal migration and gamete interaction due to the critical role of this vigorous motility for detachment of sperm from the isthmus and egg coat penetration (Yanagimachi, 1994; Florman and Fissore, 2015). Finally, the few TKO and QKO sperm that might reach the ampulla exhibit severe gamete interaction defects due to egg coat penetration deficiencies generated by the lack of *Crisp2* and both sperm-ZP binding and gamete fusion failure associated with the lack of epididymal *Crisp1* and *Crisp4* genes.

The finding that mice lacking three or four CRISP proteins exhibit more severe phenotypes than single or double CRISP knockout mice supports the idea that the combined mutations of *Crisp* members lead to disruption of multiple independent pathways. Similar results were observed for the sperm β-defensin protein family since animals were fertile when lacking one individual gene, subfertile when lacking two or three genes (Zhang et al., 2018) and completely infertile when nulling the whole family member expression (Zhou et al., 2013).

CONCLUSION AND PERSPECTIVES

Biochemical, cellular and genetic approaches revealed that CRISP proteins play key functional roles in the successive stages of the fertilization process (i.e., cumulus penetration, sperm-ZP binding, ZP penetration, gamete fusion) through different mechanisms that include ligand-receptor interactions as well as regulation of several capacitation-associated events (i.e., acrosome reaction, hyperactivation, etc.), likely through their ability to regulate different Ca^{2+} channels. Moreover, results showed that CRISP are involved not only in gamete interaction but also in previous and subsequent steps such as sperm migration within the female tract and early embryo development. Collectively, it can be concluded that CRISP proteins are essential for male fertility due to a combination of different functional roles during the fertilization process. These findings also support the use of CRISP proteins for contraception, opening the possibility of targeting CRISP activity at different levels.

Evidence supports the idea that CRISP proteins have evolved to perform redundant as well as specialized functions to ensure fertility success and are organized in functional modules within the family that work through independent pathways and contribute distinctly to fertility success (**Figure 3**). In this way, whereas epididymal CRISP1 and CRISP4 (epididymal module) are critical for epididymal sperm maturation, play similar roles in gamete interaction and can compensate for each other, testicular CRISP2 and seminal CRISP3 appear to have specific functions not compensated by the remaining CRISP family members. Whereas CRISP2 (testicular module) showed to be critical for the development of sperm midpiece flexibility that occurs during epididymal maturation and, thus, for oviductal sperm migration and egg coat penetration, CRISP3, together with CRISP1 (seminal module), seems to be needed for maintaining sperm motility within the uterus as well as for early embryo development.

Redundancy and compensatory mechanisms like those observed within the CRISP protein family are particularly important in the case of spermatozoa which are transcriptionally and translationally inactive cells and carry several protein families (i.e., ADAMs, defensins, CRISP, etc.) to guarantee their functionality. This emphasizes the importance of generating multiple knockout of family genes since single knockout models might be masking the true functional relevance of family proteins.

Considering the high sequence and functional homology between rodent and human CRISP proteins, it is likely that the same redundant and specific mechanisms operate within the human CRISP family giving rise to the same functional modules (i.e., epididymal CRISP1, testicular CRISP2 and seminal CRISP3). Furthermore, as the three hCRISP genes are located very close to each other within the same chromosome, it is possible that a single rearrangement in that region is responsible for some cases of unexplained infertility due to the simultaneous absence of more than one human CRISP protein, supporting the relevance of our observations for the diagnosis and treatment of human infertility as well as for the development of new non-hormonal contraceptive options.

AUTHOR CONTRIBUTIONS

SG, MWM, VS, and PC participated in manuscript writing and editing. VS and PC designed all schematic figures. PC conceived the manuscript and coordinated all the activities.

FUNDING

The work described in this review was partially supported by the National Research Council (CONICET) grant (PIP 2015-149) and the National Agency for Scientific and Technological Promotion (ANPCyT) grant (PICT 2015-471) to PC.

REFERENCES

Arévalo, L., Brukman, N. G., Cuasnicú, P. S., and Roldan, E. R. S. (2020). Evolutionary Analysis of Genes Coding for Cysteine-RIch Secretory Proteins (CRISPs) in Mammals. *BMC Evol. Biol.* 20, 67. doi:10.1186/s12862-020-01632-5

Austin, C. R. (1952). The 'Capacitation' of the Mammalian Sperm. *Nature* 170, 326. doi:10.1038/170326a0

Belardin, L., Camargo, M., Intasqui, P., Antoniassi, M., Fraietta, R., and Bertolla, R. (2019). Cysteine-rich Secretory Protein 3: Inflammation Role in Adult Varicocoele. *Andrology* 7, 53–61. doi:10.1111/andr.12555

Bjartell, A. S., Al-Ahmadie, H., Serio, A. M., Eastham, J. A., Eggener, S. E., Fine, S. W., et al. (2007). Association of Cysteine-Rich Secretory Protein 3 and Beta-Microseminoprotein with Outcome after Radical Prostatectomy. *Clin. Cancer Res.* 13, 4130–4138. doi:10.1158/1078-0432.CCR-06-3031

Borges, B. C., Garcia-Galiano, D., da Silveira Cruz-Machado, S., Han, X., Gavrilina, G. B., Saunders, T. L., et al. (2017). Obesity-Induced Infertility in Male Mice Is Associated with Disruption of Crisp4 Expression and Sperm Fertilization Capacity. *Endocrinology* 158, 2930–2943. doi:10.1210/en.2017-00295

Brukman, N. G., Miyata, H., Torres, P., Lombardo, D., Caramelo, J. J., Ikawa, M., et al. (2016). Fertilization Defects in Sperm from Cysteine-Rich Secretory Protein 2 (Crisp2) Knockout Mice: Implications for Fertility Disorders. *Mol. Hum. Reprod.* 22, 240–251. doi:10.1093/molehr/gaw005

Busso, D., Cohen, D. J., Hayashi, M., Kasahara, M., and Cuasnicú, P. S. (2005). Human Testicular Protein TPX1/CRISP-2: Localization in Spermatozoa, Fate after Capacitation and Relevance for Gamete Interaction. *Mol. Hum. Reprod.* 11, 299–305. doi:10.1093/molehr/gah156

Busso, D., Cohen, D. J., Maldera, J. A., Dematteis, A., and Cuasnicu, P. S. (2007). A Novel Function for CRISP1 in Rodent Fertilization: Involvement in Sperm-Zona Pellucida Interaction. *Biol. Reprod.* 77, 848–854. doi:10.1095/biolreprod.107.061788

Busso, D., Goldweic, N. M., Hayashi, M., Kasahara, M., and Cuasnicú, P. S. (2007). Evidence for the Involvement of Testicular Protein CRISP2 in Mouse Sperm-Egg Fusion. *Biol. Reprod.* 76, 701–708. doi:10.1095/biolreprod.106.056770

Cameo, M. S., and Blaquier, J. A. (1976). Androgen-controlled Specific Proteins in Rat Epididymis. *J. Endocrinol.* 69, 47–55. doi:10.1677/joe.0.0690047

Carvajal, G., Brukman, N. G., Weigel Muñoz, M., Battistone, M. A., Guazzone, V. A., Ikawa, M., et al. (2018). Impaired Male Fertility and Abnormal Epididymal Epithelium Differentiation in Mice Lacking CRISP1 and CRISP4. *Sci. Rep.* 8, 17531. doi:10.1038/s41598-018-35719-3

Chang, H., and Suarez, S. S. (2011). Two Distinct Ca(2+) Signaling Pathways Modulate Sperm Flagellar Beating Patterns in Mice. *Biol. Reprod.* 85, 296–305. doi:10.1095/biolreprod.110.089789

Chang, M. C. (1951). Fertilizing Capacity of Spermatozoa Deposited into the Fallopian Tubes. *Nature* 168, 697–698. doi:10.1038/168697b0

Cohen, D. J., Ellerman, D. A., Busso, D., Morgenfeld, M. M., Piazza, A. D., Hayashi, M., et al. (2001). Evidence that Human Epididymal Protein ARP Plays a Role in Gamete Fusion through Complementary Sites on the Surface of the Human Egg. *Biol. Reprod.* 65, 1000–1005. doi:10.1095/biolreprod65.4.1000

Cohen, D. J., Ellerman, D. A., and Cuasnicú, P. S. (2000). Mammalian Sperm-Egg Fusion: Evidence that Epididymal Protein DE Plays a Role in Mouse Gamete Fusion. *Biol. Reprod.* 63, 462–468. doi:10.1095/biolreprod63.2.462

Cohen, D. J., Rochwerger, L., Ellerman, D. A., Morgenfeld, M. M., Busso, D., and Cuasnicú, P. S. (2000). Relationship between the Association of Rat Epididymal Protein "DE" with Spermatozoa and the Behavior and Function of the Protein. *Mol. Reprod. Dev.* 56, 180–188. doi:10.1002/(SICI)1098-2795(200006)56:2<180:AID-MRD9>3.0.CO;2-4

Conine, C. C., Sun, F., Song, L., Rivera-Pérez, J. A., and Rando, O. J. (2018). Small RNAs Gained during Epididymal Transit of Sperm Are Essential for Embryonic Development in Mice. *Dev. Cel* 46, 470–e3. doi:10.1016/j.devcel.2018.06.024

Cuasnicu, P. S., Da Ros, V. G., Weigel Muñoz, M., and Cohen, D. J. (2016). "Acrosome Reaction as a Preparation for Gamete Fusion,". *Sperm Acrosome Biogenesis and Function during Fertilization, Advances in Anatomy, Embryology and Cell Biology*. Editor M. G. Buffone (Springer), 220. Chapter 9.

Cuasnicú, P. S., Conesa, D., and Rochwerger, L. (1990). "Potential Contraceptive Use of an Epididymal Protein that Participates in Fertilization," in *Gamete Interaction. Prospects for Immunocontraception*. Editors N. J Alexander, D. Griffin, J. M Spieler, and G. M Waites (New York): Wiley-Liss), 143–153.

Curci, L., Brukman, N. G., Weigel Muñoz, M., Rojo, D., Carvajal, G., Sulzyk, V., et al. (2020). Functional Redundancy and Compensation: Deletion of Multiple Murine Crisp Genes Reveals Their Essential Role for Male Fertility. *FASEB J.* 34, 15718–15733. doi:10.1096/fj.202001406r

Da Ros, V. G., Maldera, J. A., Willis, W. D., Cohen, D. J., Gelman, D. M., Rubinstein, M., et al. (2008). Impaired Sperm Fertilizing Ability in Mice Lacking Cysteine-RIch Secretory Protein 1 (CRISP1). *Dev. Biol.* 320, 12–18. doi:10.1016/j.ydbio.2008.03.015

Da Ros, V. G., Muñoz, M. W., Battistone, M. A., Brukman, N. G., Carvajal, G., Curci, L., et al. (2015). From the Epididymis to the Egg: Participation of CRISP Proteins in Mammalian Fertilization. *Asian J. Androl.* 17, 711–715. doi:10.4103/1008-682x.155769

Doty, A., Buhi, W. C., Benson, S., Scoggin, K. E., Pozor, M., Macpherson, M., et al. (2011). Equine CRISP3 Modulates Interaction between Spermatozoa and Polymorphonuclear Neutrophils. *Biol. Reprod.* 85, 157–164. doi:10.1095/biolreprod.110.084491

Du, Y., Huang, X., Li, J., Hu, Y., Zhou, Z., and Sha, J. (2006). Human Testis Specific Protein 1 Expression in Human Spermatogenesis and Involvement in the Pathogenesis of Male Infertility. *Fertil. Steril* 85, 1852–1854. doi:10.1016/j.fertnstert.2005.11.064

Eberspaecher, U., Roosterman, D., Krätzschmar, J., Haendler, B., Habenicht, U. F., Becker, A., et al. (1995). Mouse Androgen-dependent Epididymal Glycoprotein CRISP-1 (DE/AEG): Isolation, Biochemical Characterization, and Expression in Recombinant Form. *Mol. Reprod. Dev.* 42, 157–172. doi:10.1002/mrd.1080420205

Ellerman, D. A., Brantúa, V. S., Martínez, S. P., Cohen, D. J., Conesa, D., and Cuasnicú, P. S. (1998). Potential Contraceptive Use of Epididymal Proteins: Immunization of Male Rats with Epididymal Protein DE Inhibits Sperm Fusion Ability. *Biol. Reprod.* 59, 1029–1036. doi:10.1095/biolreprod59.5.1029

Ellerman, D. A., Busso, D., Maldera, J. A., and Cuasnicú, P. S. (2008). Immunocontraceptive Properties of Recombinant Sperm Protein DE: Implications for the Development of Novel Contraceptives. *Fertil. Steril* 89, 199–205. doi:10.1016/j.fertnstert.2007.02.025

Ellerman, D. A., Cohen, D. J., Weigel Muñoz, M., Da Ros, V. G., Ernesto, J. I., Tollner, T. L., et al. (2010). Immunologic Behavior of Human Cysteine-Rich Secretory Protein 1 (hCRISP1) in Primates: Prospects for Immunocontraception. *Fertil. Steril* 93, 2551–2556. doi:10.1016/j.fertnstert.2010.01.075

Ellerman, D. E., Cohen, D. J., Da Ros, V. G., Morgenfeld, M. M., Busso, D., and Cuasnicú, P. S. (2006). Sperm Protein "DE" Mediates Gamete Fusion through an Evolutionarily Conserved Site of the CRISP Family. *Dev. Biol.* 297, 228–237. doi:10.1016/j.ydbio.2006.05.013

Enger, T. B., Aure, M. H., Jensen, J. L., and Galtung, H. K. (2014). Calcium Signaling and Cell Volume Regulation Are Altered in Sjögren's Syndrome. *Acta Odontol Scand.* 72, 549–556. doi:10.3109/00016357.2013.879995

Ernesto, J. I., Weigel Muñoz, M., Battistone, M. A., Vasen, G., Martínez-López, P., Orta, G., et al. (2015). CRISP1 as a Novel CatSper Regulator that Modulates Sperm Motility and Orientation during Fertilization. *J. Cel Biol* 210, 1213–1224. doi:10.1083/jcb.201412041

Evans, J., D'Sylva, R., Volpert, M., Jamsai, D., Merriner, D. J., Nie, G., et al. (2015). Endometrial CRISP3 Is Regulated throughout the Mouse Estrous and Human Menstrual Cycle and Facilitates Adhesion and Proliferation of Endometrial Epithelial Cells. *Biol. Reprod.* 92, 99. doi:10.1095/biolreprod.114.127480

Florman, H. M., and Fissore, R. A. (2015). "Fertilization in Mammals," in *Knobil and Neill's Physiology of Reproduction*. Editors T. M Plant and A. J Zeleznik (Massachusetts): Elsevier/Academic Press), 149–196.

Gaikwad, A. S., Nandagiri, A., Potter, D. L., Nosrati, R., O'Connor, A. E., Jadhav, S., et al. (2021). CRISPs Function to Boost Sperm Power Output and Motility. *Front Cel Dev Biol* 9, 693258. doi:10.3389/fcell.2021.693258

Gao, F., Wang, P., Wang, K., Fan, Y., Chen, Y., Chen, Y., et al. (2021). Investigation into the Relationship between Sperm Cysteine-Rich Secretory Protein 2 (CRISP2) and Sperm Fertilizing Ability and Fertility of Boars. *Front. Vet. Sci.* 8, 653413. doi:10.3389/fvets.2021.653413

Garberi, J. C., Fontana, J. D., and Blaquier, J. A. (1982). Carbohydrate Composition of Specific Rat Epididymal Protein. *Int. J. Androl.* 5, 619–626. doi:10.1111/j.1365-2605.1982.tb00296.x

Gholami, D., Salman Yazdi, R., Jami, M. S., Ghasemi, S., Sadighi Gilani, M. A., Sadeghinia, S., et al. (2020). The Expression of Cysteine-Rich Secretory Protein 2 (CRISP2) and miR-582-5p in Seminal Plasma Fluid and Spermatozoa of Infertile Men. *Gene* 730, 144261. doi:10.1016/j.gene.2019.144261

Gibbs, G. M., and O'Bryan, M. K. (2007). Cysteine Rich Secretory Proteins in Reproduction and Venom. *Soc. Reprod. Fertil. Suppl.* 65, 261–267.

Gibbs, G. M., Orta, G., Reddy, T., Koppers, A. J., Martínez-López, P., de la Vega-Beltràn, J. L., et al. (2011). Cysteine-rich Secretory Protein 4 Is an Inhibitor of Transient Receptor Potential M8 with a Role in Establishing Sperm Function. *Proc. Natl. Acad. Sci. U S A.* 108, 7034–7039. doi:10.1073/pnas.1015935108

Gibbs, G. M., Roelants, K., and O'Bryan, M. K. (2008). The CAP Superfamily: Cysteine-Rich Secretory Proteins, Antigen 5, and Pathogenesis-Related 1 Proteins-Rroles in Reproduction, Cancer, and Immune Defense. *Endocr. Rev.* 29, 865–897. doi:10.1210/er.2008-0032

Gibbs, G. M., Scanlon, M. J., Swarbrick, J., Curtis, S., Gallant, E., Dulhunty, A. F., et al. (2006). The Cysteine-Rich Secretory Protein Domain of Tpx-1 Is Related to Ion Channel Toxins and Regulates Ryanodine Receptor Ca2+ Signaling. *J. Biol. Chem.* 281, 4156–4163. doi:10.1074/jbc.M506849200

Giese, A., Jude, R., Kuiper, H., Raudsepp, T., Piumi, F., Schambony, A., et al. (2002). Molecular Characterization of the Equine Testis-specific Protein 1 (TPX1) and Acidic Epididymal Glycoprotein 2 (AEG2) Genes Encoding Members of the Cysteine-Rich Secretory Protein (CRISP) Family. *Gene* 299, 101–109. doi:10.1016/s0378-1119(02)01018-1

Grande, G., Vincenzoni, F., Milardi, D., Pompa, G., Ricciardi, D., Fruscella, E., et al. (2017). Cervical Mucus Proteome in Endometriosis. *Clin. Proteomics* 14, 7. doi:10.1186/s12014-017-9142-4

Guo, M., Teng, M., Niu, L., Liu, Q., Huang, Q., and Hao, Q. (2005). Crystal Structure of the Cysteine-Rich Secretory Protein Stecrisp Reveals that the Cysteine-Rich Domain Has a K+ Channel Inhibitor-like Fold. *J. Biol. Chem.* 280, 12405–12412. doi:10.1074/jbc.M413566200

Haendler, B., Habenicht, U. F., Schwidetzky, U., Schüttke, I., and Schleuning, W. D. (1997). Differential Androgen Regulation of the Murine Genes for Cysteine-Rich Secretory Proteins (CRISP). *Eur. J. Biochem.* 250, 440–446. doi:10.1111/j.1432-1033.1997.0440a.x

Haendler, B., Krätzschmar, J., Theuring, F., and Schleuning, W. D. (1993). Transcripts for Cysteine-Rich Secretory Protein-1 (CRISP-1; DE/AEG) and the Novel Related CRISP-3 Are Expressed under Androgen Control in the Mouse Salivary Gland. *Endocrinology* 133, 192–198. doi:10.1210/endo.133.1.8319566

Hamann, H., Jude, R., Sieme, H., Mertens, U., Töpfer-Petersen, E., Distl, O., et al. (2007). A Polymorphism within the Equine CRISP3 Gene Is Associated with Stallion Fertility in Hanoverian Warmblood Horses. *Anim. Genet.* 38, 259–264. doi:10.1111/j.1365-2052.2007.01594.x

Hardy, D. M., Huang, T. T., Driscoll, W. J., Tung, K. K., and Wild, G. C. (1988). Purification and Characterization of the Primary Acrosomal Autoantigen of guinea Pig Epididymal Spermatozoa. *Biol. Reprod.* 38, 423–437. doi:10.1095/biolreprod38.2.423

Harper, C. V., Barratt, C. L., and Publicover, S. J. (2004). Stimulation of Human Spermatozoa with Progesterone Gradients to Simulate Approach to the Oocyte. Induction of [Ca(2+)](i) Oscillations and Cyclical Transitions in Flagellar Beating. *J. Biol. Chem.* 279, 46315–46325. doi:10.1074/jbc.M401194200

Hayashi, M., Fujimoto, S., Takano, H., Ushiki, T., Abe, K., Ishikura, H., et al. (1996). Characterization of a Human Glycoprotein with a Potential Role in Sperm-Egg Fusion: cDNA Cloning, Immunohistochemical Localization, and Chromosomal Assignment of the Gene (AEGL1). *Genomics* 32, 367–374. doi:10.1006/geno.1996.0131

Heidary, Z., Zaki-Dizaji, M., Saliminejad, K., and Khorramkhorshid, H. R. (2019). Expression Analysis of the CRISP2, CATSPER1, PATE1 and SEMG1 in the Sperm of Men with Idiopathic Asthenozoospermia. *J. Reprod. Infertil.* 20, 70–75.

Hu, J., Merriner, D. J., O'Connor, A. E., Houston, B. J., Furic, L., Hedger, M. P., et al. (2018). Epididymal Cysteine-Rich Secretory Proteins Are Required for Epididymal Sperm Maturation and Optimal Sperm Function. *Mol. Hum. Reprod.* 24, 111–122. doi:10.1093/molehr/gay001

Jalkanen, J., Huhtaniemi, I., and Poutanen, M. (2005). Mouse Cysteine-Rich Secretory Protein 4 (CRISP4): a Member of the Crisp Family Exclusively Expressed in the Epididymis in an Androgen-dependent Manner. *Biol. Reprod.* 72, 1268–1274. doi:10.1095/biolreprod.104.035758

Jing, X., Xing, R., Zhou, Q., Yu, Q., Guo, W., Chen, S., et al. (2011). Expressions of Cysteine-Rich Secretory Protein 2 in Asthenospermia. *Zhonghua Nan Ke Xue* 17, 203–207.

Judd, J. E., Berndtson, W. E., and Castro, A. C. (1997). Extragonadal Sperm Reserves, Sperm-Depletion Rates, Numbers of Sperm Per Mating, and Fertility with Successive Matings by Intact or Unilaterally Vasectomized Rats. *J. Androl.* 18, 698–707.

Kasahara, M., Gutknecht, J., Brew, K., Spurr, N., and Goodfellow, P. N. (1989). Cloning and Mapping of a Testis-specific Gene with Sequence Similarity to a Sperm-Coating Glycoprotein Gene. *Genomics* 5, 527–534. doi:10.1016/0888-7543(89)90019-0

Kjeldsen, L., Cowland, J. B., Johnsen, A. H., and Borregaard, N. (1996). SGP28, a Novel Matrix Glycoprotein in Specific Granules of Human Neutrophils with Similarity to a Human Testis-specific Gene Product and a Rodent Sperm-Coating Glycoprotein. *FEBS Lett.* 380, 246–250. doi:10.1016/0014-5793(96)00030-0

Kohane, A. C., Cameo, M. S., Piñeiro, L., Garberi, J. C., and Blaquier, J. A. (1980). Distribution and Site of Production of Specific Proteins in the Rat Epididymis. *Biol. Reprod.* 23, 181–187. doi:10.1095/biolreprod23.1.181

Kohane, A. C., González Echeverría, F. M., Piñeiro, L., and Blaquier, J. A. (1980). Interaction of Proteins of Epididymal Origin with Spermatozoa. *Biol. Reprod.* 23, 737–742. doi:10.1095/biolreprod23.4.737

Konttinen, Y. T., Porola, P., Konttinen, L., Laine, M., and Poduval, P. (2006). Immunohistopathology of Sjögren's Syndrome. *Autoimmun. Rev.* 6, 16–20. doi:10.1016/j.autrev.2006.03.003

Kosari, F., Asmann, Y. W., Cheville, J. C., and Vasmatzis, G. (2002). Cysteine-rich Secretory Protein-3: a Potential Biomarker for Prostate Cancer. *Cancer Epidemiol. Biomarkers Prev.* 11, 1419–1426.

Krätzschmar, J., Haendler, B., Eberspaecher, U., Roosterman, D., Donner, P., and Schleuning, W. D. (1996). The Human Cysteine-Rich Secretory Protein (CRISP) Family. Primary Structure and Tissue Distribution of CRISP-1, CRISP-2 and CRISP-3. *Eur. J. Biochem.* 236, 827–836. doi:10.1111/j.1432-1033.1996.t01-1-00827.x

Laine, M., Porola, P., Udby, L., Kjeldsen, L., Cowland, J. B., Borregaard, N., et al. (2007). Low Salivary Dehydroepiandrosterone and Androgen-Regulated Cysteine-Rich Secretory Protein 3 Levels in Sjögren's Syndrome. *Arthritis Rheum.* 56, 2575–2584. doi:10.1002/art.22828

Lim, S., Kierzek, M., O'Connor, A. E., Brenker, C., Merriner, D. J., Okuda, H., et al. (2019). CRISP2 Is a Regulator of Multiple Aspects of Sperm Function and Male Fertility. *Endocrinology* 160, 915–924. doi:10.1210/en.2018-01076

Luo, J., Yang, J., Cheng, Y., Li, W., Yin, T. L., Xu, W. M., et al. (2012). Immunogenicity Study of Plasmid DNA Encoding Mouse Cysteine-Rich Secretory Protein-1 (mCRISP1) as a Contraceptive Vaccine. *Am. J. Reprod. Immunol.* 68, 47–55. doi:10.1111/j.1600-0897.2012.01117.x

Luo, J., Liu, X. L., Zhang, Y., Wang, Y. Q., Xu, W. M., and Yang, J. (2016). The Immunogenicity of CRISP1 Plasmid-Based Contraceptive Vaccine Can Be Improved when Using Chitosan Nanoparticles as the Carrier. *Am.J.Reprod.Immunol.* 75, 643–653. doi:10.1111/aji.12513

Maeda, T., Nishida, J., and Nakanishi, Y. (1999). Expression Pattern, Subcellular Localization and Structure-Ffunction Relationship of Rat Tpx-1, a Spermatogenic Cell Adhesion Molecule Responsible for Association with Sertoli Cells. *Dev. Growth Differ.* 41, 715–722. doi:10.1046/j.1440-169x.1999.00470.x

Maeda, T., Sakashita, M., Ohba, Y., and Nakanishi, Y. (1998). Molecular Cloning of the Rat Tpx-1 Responsible for the Interaction between Spermatogenic and Sertoli Cells. *Biochem. Biophys. Res. Commun.* 248, 140–146. doi:10.1006/bbrc.1998.8918

Magdaleno, L., Gasset, M., Varea, J., Schambony, A. M., Urbanke, C., Raida, M., et al. (1997). Biochemical and Conformational Characterisation of HSP-3, a Stallion Seminal Plasma Protein of the Cysteine-Rich Secretory Protein (CRISP) Family. *FEBS Lett.* 420, 179–185. doi:10.1016/s0014-5793(97)01514-7

Maldera, J. A., Weigel Muñoz, M., Chirinos, M., Busso, D., G E Raffo, F., Battistone, M. A., et al. (2014). Human Fertilization: Epididymal hCRISP1 Mediates Sperm-Zona Pellucida Binding through its Interaction with ZP3. *Mol. Hum. Reprod.* 20, 341–349. doi:10.1093/molehr/gat092

Martínez-López, P., Treviño, C. L., De la Vega-Beltrán, J. L., De Blas, G., Monroy, E., Beltrán, C., et al. (2010). TRPM8 in Mouse Sperm Detects Temperature Changes and May Influence the Acrosome Reaction. *J. Cel Physiol.* 226, 1620–1631. doi:10.1002/jcp.22493

Miyata, H., Castaneda, J. M., Fujihara, Y., Yu, Z., Archambeault, D. R., Isotani, A., et al. (2016). Genome Engineering Uncovers 54 Evolutionarily Conserved and Testis-Enriched Genes that Are Not Required for Male Fertility in Mice. *Proc. Natl. Acad. Sci. U S A.* 113, 7704–7710. doi:10.1073/pnas.1608458113

Mizuki, N., Sarapata, D. E., Garcia-Sanz, J. A., and Kasahara, M. (1992). The Mouse Male Germ Cell-specific Gene Tpx-1: Molecular Structure, Mode of Expression in Spermatogenesis, and Sequence Similarity to Two Non-mammalian Genes. *Mamm. Genome* 3, 274–280. doi:10.1007/BF00292155

Mochca-Morales, J., Martin, B. M., and Possani, L. D. (1990). Isolation and Characterization of Helothermine, a Novel Toxin from *Heloderma horridum* Horridum (Mexican Beaded Lizard) Venom. *Toxicon* 28, 299–309. doi:10.1016/0041-0101(90)90065-f

Muñoz, M. W., Ernesto, J. I., Bluguermann, C., Busso, D., Battistone, M. A., Cohen, D. J., et al. (2012). Evaluation of Testicular Sperm CRISP2 as a Potential Target for Contraception. *J. Androl.* 33, 1360–1370. doi:10.2164/jandrol.112.016725

Nandagiri, A., Gaikwad, A. S., Potter, D. L., Nosrati, R., Soria, J., O'Bryan, M. K., et al. (2021). Flagellar Energetics from High-Resolution Imaging of Beating Patterns in Tethered Mouse Sperm. *Elife* 10, e62524. doi:10.7554/elife.62524

Navarrete, F. A., Aguila, L., Martin-Hidalgo, D., Tourzani, D. A., Luque, G. M., Ardestani, G., et al. (2019). Transient Sperm Starvation Improves the Outcome of Assisted Reproductive Technologies. *Front. Cel Dev Biol* 7, 262. doi:10.3389/fcell.2019.00262

Nimlamool, W., Bean, B. S., and Lowe-Krentz, L. J. (2013). Human Sperm CRISP2 Is Released from the Acrosome during the Acrosome Reaction and Re-associates at the Equatorial Segment. *Mol. Reprod. Dev.* 80, 488–502. doi:10.1002/mrd.22189

Noh, B. J., Sung, J. Y., Kim, Y. W., Chang, S. G., and Park, Y. K. (2016). Prognostic Value of ERG, PTEN, CRISP3 and SPINK1 in Predicting Biochemical Recurrence in Prostate Cancer. *Oncol. Lett.* 11, 3621–3630. doi:10.3892/ol.2016.4459

Nolan, M. A., Wu, L., Bang, H. J., Jelinsky, S. A., Roberts, K. P., Turner, T. T., et al. (2006). Identification of Rat Cysteine-Rich Secretory Protein 4 (Crisp4) as the Ortholog to Human CRISP1 and Mouse Crisp4. *Biol. Reprod.* 74, 984–991. doi:10.1095/biolreprod.105.048298

O'Bryan, M. K., Loveland, K. L., Herszfeld, D., McFarlane, J. R., Hearn, M. T., and De Kretser, D. M. (1998). Identification of a Rat Testis–specific Gene Encoding a Potential Rat Outer Dense Fibre Protein. *Mol. Reprod. Dev.* 50, 313–322. doi:10.1002/(sici)1098-2795(199807)50:3<313:aid-mrd7>3.0.co;2-m

O'Bryan, M. K., Sebire, K., Meinhardt, A., Edgar, K., Keah, H. H., Hearn, M. T. W., et al. (2001). Tpx-1 Is a Component of the Outer Dense Fibers and Acrosome of

Rat Spermatozoa. *Mol. Rep. Dev.* 58, 116–125. doi:10.1002/1098-2795(200101)58:1<116:aid-mrd14>3.0.co;2-8

Orgebin-Crist, M-C., Brantley, E. B., and Hart, J. R. (1967). Maturation of Spermatozoa in the Rabbit Epididymis: Fertilizing Ability and Embryonic Mortality in Does Inseminated with Epididymal Spermatozoa. *Ann. Biol. Anim. Biochim. Biophys.* 7, 373–389. doi:10.1051/rnd:19670403

Perez Martinez, S., Conesa, D., and Cuasnicú, P. S. (1995). Potential Contraceptive Use of Epididymal Proteins: Evidence for the Participation of Specific Antibodies against Rat Epididymal Protein DE in Male and Female Fertility Inhibition. *J. Reprod. Immunol.* 29, 31–45. doi:10.1016/0165-0378(95)00927-d

Reddy, T., Gibbs, G. M., Merriner, D. J., Kerr, J. B., and O'Bryan, M. K. (2008). Cysteine-rich Secretory Proteins Are Not Exclusively Expressed in the Male Reproductive Tract. *Dev. Dyn.* 237, 3313–3323. doi:10.1002/dvdy.21738

Ren, D., Navarro, B., Perez, G., Jackson, A. C., Hsu, S., Shi, Q., et al. (2001). A Sperm Ion Channel Required for Sperm Motility and Male Fertility. *Nature* 413, 603–609. doi:10.1038/35098027

Rennhack, A., Schiffer, C., Brenker, C., Fridman, D., Nitao, E. T., Cheng, Y. M., et al. (2018). A Novel Cross-Species Inhibitor to Study the Function of CatSper Ca2+ Channels in Sperm. *Br. J. Pharmacol.* 175, 3144–3161. doi:10.1111/bph.14355

Roan, N. R., Sandi-Monroy, N., Kohgadai, N., Usmani, S. M., Hamil, K. G., Neidleman, J., et al. (2017). Semen Amyloids Participate in Spermatozoa Selection and Clearance. *Elife* 6, e24888. doi:10.7554/eLife.24888

Robaire, B., and Hinton, B. T. (2015). *"The Epididymis," in Knobil and Neill's Physiology of Reproduction*: *Two-Volume Set*. Editors A. J. Zeleznik and T. M. Plant. 4th Edn (Amsterdam: Elsevier), Vol. 1, 691–771.

Roberts, K. P., Wamstad, J. A., Ensrud, K. M., and Hamilton, D. W. (2003). Inhibition of Capacitation-Associated Tyrosine Phosphorylation Signaling in Rat Sperm by Epididymal Protein Crisp-1. *Biol. Reprod.* 69, 572–581. doi:10.1095/biolreprod.102.013771

Rochwerger, L., Cohen, D. J., and Cuasnicú, P. S. (1992). Mammalian Sperm-Egg Fusion: the Rat Egg Has Complementary Sites for a Sperm Protein that Mediates Gamete Fusion. *Dev. Biol.* 153, 83–90. doi:10.1016/0012-1606(92)90093-v

Schambony, A., Gentzel, M., Wolfes, H., Raida, M., Neumann, U., and Töpfer-Petersen, E. (1998). Equine CRISP-3: Primary Structure and Expression in the Male Genital Tract. *Biochim. Biophys. Acta* 1387, 206–216. doi:10.1016/s0167-4838(98)00122-8

Schwidetzky, U., Haendler, B., and Schleuning, W. D. (1995). Isolation and Characterization of the Androgen-dependent Mouse Cysteine-Rich Secretory Protein-3 (CRISP-3) Gene. *Biochem. J.* 309 (Pt 3), 831–836. doi:10.1042/bj3090831

Sheng, J., Olrichs, N. K., Geerts, W. J., Li, X., Rehman, A. U., Gadella, B. M., et al. (2019). Zinc Binding Regulates Amyloid-like Aggregation of GAPR-1. *Biosci. Rep.* 39, BSR20182345. doi:10.1042/BSR20182345

Sheng, J., Gadella, B. M., Olrichs, N. K., Kaloyanova, D. V., and Helms, J. B. (2021). The Less Conserved Metal-Binding Site in Human CRISP1 Remains Sensitive to Zinc Ions to Permit Protein Oligomerization. *Sci. Rep.* 11, 5498. doi:10.1038/s41598-021-84926-y

Sun, X. H., Zhu, Y. Y., Wang, L., Liu, H. L., Ling, Y., Li, Z. L., et al. (2017). The Catsper Channel and its Roles in Male Fertility: a Systematic Review. *Reprod. Biol. Endocrinol.* 15, 65. doi:10.1186/s12958-017-0281-2

Tang, W., Guo, X., Niu, L., Song, D., Han, B., and Zhang, H. (2020). Identification of Key Molecular Targets that Correlate with Breast Cancer through Bioinformatic Methods. *J. Gene Med.* 22, e3141. doi:10.1002/jgm.3141

Tapinos, N. I., Polihronis, M., Thyphronitis, G., and Moutsopoulos, H. M. (2002). Characterization of the Cysteine-Rich Secretory Protein 3 Gene as an Early-Transcribed Gene with a Putative Role in the Pathophysiology of Sjögren's Syndrome. *Arthritis Rheum.* 46, 215–222. doi:10.1002/1529-0131(200201)46:1<215:AID-ART10024>3.0.CO;2-M

Turunen, H. T., Sipilä, P., Krutskikh, A., Toivanen, J., Mankonen, H., Hämäläinen, V., et al. (2012). Loss of Cysteine-Rich Secretory Protein 4 (Crisp4) Leads to Deficiency in Sperm-Zona Pellucida Interaction in Mice. *Biol. Reprod.* 86, 1–8. doi:10.1095/biolreprod.111.092403

Udby, L., Bjartell, A., Malm, J., Egesten, A., Lundwall, A., Cowland, J. B., et al. (2005). Characterization and Localization of Cysteine-Rich Secretory Protein 3 (CRISP-3) in the Human Male Reproductive Tract. *J. Androl.* 26, 333–342. doi:10.2164/jandrol.04132

Udby, L., Cowland, J. B., Johnsen, A. H., Sørensen, O. E., Borregaard, N., and Kjeldsen, L. (2002). An ELISA for SGP28/CRISP-3, a Cysteine-Rich Secretory Protein in Human Neutrophils, Plasma, and Exocrine Secretions. *J. Immunol. Methods* 263, 43–55. doi:10.1016/s0022-1759(02)00033-9

Vadnais, M. L., Foster, D. N., and Roberts, K. P. (2008). Molecular Cloning and Expression of the CRISP Family of Proteins in the Boar. *Biol. Reprod.* 79, 1129–1134. doi:10.1095/biolreprod.108.070177

Volpert, M., Furic, L., Hu, J., O'Connor, A. E., Rebello, R. J., Keerthikumar, S., et al. (2020). CRISP3 Expression Drives Prostate Cancer Invasion and Progression. *Endocr. Relat. Cancer* 27, 415–430. doi:10.1530/ERC-20-0092

Wang, H., Yang, H., Shivalila, C. S., Dawlaty, M. M., Cheng, A. W., Zhang, F., et al. (2013). One-step Generation of Mice Carrying Mutations in Multiple Genes by CRISPR/Cas-mediated Genome Engineering. *Cell* 153, 910–918. doi:10.1016/j.cell.2013.04.025

Weigel Muñoz, M., Batisttone, M. A., Carvajal, G., Maldera, J. A., Curci, L., Torres, P., et al. (2018). Influence of the Genetic Background on the Reproductive Phenotype of Mice Lacking Cysteine-RIch Secretory Protein 1 (CRISP1). *Biol. Rep.* 99, 373–383. doi:10.1093/biolre/ioy048

Weigel Muñoz, M., Carvajal, G., Curci, L., Gonzalez, S. N., and Cuasnicu, P. S. (2019). Relevance of CRISP Proteins for Epididymal Physiology, Fertilization, and Fertility. *Andrology* 7, 610–617. doi:10.1111/andr.12638

Yamazaki, Y., Brown, R. L., and Morita, T. (2002). Purification and Cloning of Toxins from Elapid Venoms that Target Cyclic Nucleotide-Gated Ion Channels. *Biochemistry* 41, 11331–11337. doi:10.1021/bi026132h

Yamazaki, Y., and Morita, T. (2004). Structure and Function of Snake Venom Cysteine-Rich Secretory Proteins. *Toxicon* 44, 227–231. doi:10.1016/j.toxicon.2004.05.023

Yanagimachi, R. (1994). "Mammalian Fertilization,". *The Physiology Of Reproduction*. Editors E. Knobil and J. D. Neill., 189–317.

Zhang, C., Zhou, Y., Xie, S., Yin, Q., Tang, C., Ni, Z., et al. (2018). CRISPR/Cas9-mediated Genome Editing Reveals the Synergistic Effects of β-defensin Family Members on Sperm Maturation in Rat Epididymis. *FASEB J.* 32, 1354–1363. doi:10.1096/fj.201700936R

Zhang, M., Bromfield, E. G., Veenendaal, T., Klumperman, J., Helms, J. B., and Gadella, B. M. (2021). Characterization of Different Oligomeric Forms of CRISP2 in the Perinuclear Theca versus the Fibrous Tail Structures of Boar Spermatozoa. *Biol. Reprod.* 26, ioab145. doi:10.1093/biolre/ioab145

Zhou, J. H., Zhou, Q. Z., Lyu, X. M., Zhu, T., Chen, Z. J., Chen, M. K., et al. (2015). The Expression of Cysteine-Rich Secretory Protein 2 (CRISP2) and its Specific Regulator miR-27b in the Spermatozoa of Patients with Asthenozoospermia. *Biol. Reprod.* 92, 28–29. doi:10.1095/biolreprod.114.124487

Zhou, Y. S., Webb, S., Lettice, L., Tardif, S., Kilanowski, F., Tyrrell, C., et al. (2013). Partial Deletion of Chromosome 8 β-defensin Cluster Confers Sperm Dysfunction and Infertility in Male Mice. *Plos Genet.* 9, e1003826. doi:10.1371/journal.pgen.1003826

Conflict of Interest: The authors declare that the research was conducted in the absence of any commercial or financial relationships that could be construed as a potential conflict of interest.

Publisher's Note: All claims expressed in this article are solely those of the authors and do not necessarily represent those of their affiliated organizations, or those of the publisher, the editors, and the reviewers. Any product that may be evaluated in this article, or claim that may be made by its manufacturer, is not guaranteed or endorsed by the publisher.

frontiers in Cell and Developmental Biology

ORIGINAL RESEARCH
published: 03 January 2022
doi: 10.3389/fcell.2021.806982

The Sperm Protein Spaca6 is Essential for Fertilization in Zebrafish

Mirjam I. Binner†, Anna Kogan†‡, Karin Panser, Alexander Schleiffer, Victoria E. Deneke and Andrea Pauli**

Research Institute of Molecular Pathology (IMP), Vienna BioCenter (VBC), Campus-Vienna-Biocenter 1, Vienna, Austria

OPEN ACCESS

Edited by:
Enrica Bianchi, University of York, United Kingdom

Reviewed by:
Sandrine Barbaux, Institut National de la Santé et de la Recherche Médicale (INSERM), France
Yuhkoh Satouh, Gunma University, Japan
Andrew Singson, Rutgers, The State University of New Jersey, United States

***Correspondence:**
Victoria E. Deneke
victoria.deneke@imp.ac.at
Andrea Pauli
andrea.pauli@imp.ac.at

†Present address:
Anna Kogan, Department of Biochemistry, University of Oxford, Oxford, United Kingdom

‡These authors have contributed equally to this work

Specialty section:
This article was submitted to Molecular and Cellular Reproduction, a section of the journal Frontiers in Cell and Developmental Biology

Received: *01 November 2021*
Accepted: *07 December 2021*
Published: *03 January 2022*

Citation:
Binner MI, Kogan A, Panser K, Schleiffer A, Deneke VE and Pauli A (2022) The Sperm Protein Spaca6 is Essential for Fertilization in Zebrafish. Front. Cell Dev. Biol. 9:806982. doi: 10.3389/fcell.2021.806982

Fertilization is a key process in all sexually reproducing species, yet the molecular mechanisms that underlie this event remain unclear. To date, only a few proteins have been shown to be essential for sperm-egg binding and fusion in mice, and only some are conserved across vertebrates. One of these conserved, testis-expressed factors is SPACA6, yet its function has not been investigated outside of mammals. Here we show that zebrafish *spaca6* encodes for a sperm membrane protein which is essential for fertilization. Zebrafish *spaca6* knockout males are sterile. Furthermore, Spaca6-deficient sperm have normal morphology, are motile, and can approach the egg, but fail to bind to the egg and therefore cannot complete fertilization. Interestingly, sperm lacking Spaca6 have decreased levels of another essential and conserved sperm fertility factor, Dcst2, revealing a previously unknown dependence of Dcst2 expression on Spaca6. Together, our results show that zebrafish Spaca6 regulates Dcst2 levels and is required for binding between the sperm membrane and the oolemma. This is in contrast to murine sperm lacking SPACA6, which was reported to be able to bind but unable to fuse with oocytes. These findings demonstrate that Spaca6 is essential for zebrafish fertilization and is a conserved sperm factor in vertebrate reproduction.

Keywords: fertilization, zebrafish, sperm-egg interaction, gamete, sperm, reproduction

INTRODUCTION

Fertilization is an essential process which ensures reproductive success and species survival. Multiple events, such as sperm migration through the female reproductive tract, sperm activation, gamete fusion and egg activation are necessary for fertility and contribute to the formation of a new organism (Bianchi and Wright, 2016; Stein et al., 2020; Deneke and Pauli, 2021). Despite its critical role, little is known about the molecular mechanisms mediating fertilization, particularly sperm-egg interaction and fusion.

In recent years, several proteins have been shown to be essential for sperm-egg interaction in mammals. Most notably, mammalian testis-expressed IZUMO1 and its receptor JUNO on the egg membrane (oolemma) form a complex which is needed for binding of the two gametes prior to fusion (Inoue et al., 2013; Bianchi and Wright, 2016). *Izumo1* knockout (KO) sperm can penetrate the zona pellucida (ZP), a glycoprotein coat surrounding the mammalian oocyte, but fail to fuse with the oolemma (Inoue et al., 2005). CD9, an integral membrane protein expressed on the oolemma, has also been shown to be required for gamete fusion (Kaji et al., 2000; le Naour et al., 2000; Miyado et al., 2000). Furthermore, other sperm factors—fertilization influencing membrane protein (FIMP), sperm-oocyte fusion required 1 (SOF1), transmembrane protein 95 (TMEM95), sperm acrosome associated 6 (SPACA6) and the DC-STAMP-like domain-containing proteins DCST1 and

DCST2—have been shown to be required for sperm-egg fusion in mice (Barbaux et al., 2020; Lamas-Toranzo et al., 2020; Noda et al., 2020; Nado et al., 2021; Inoue et al., 2021). Despite the many factors shown to be necessary for sperm-egg fusion, the combination of these factors appears not to be sufficient to drive fusion in a heterologous system. Noda and others expressed the essential sperm factors involved in fusion, including IZUMO1, in HEK293T cells and observed that HEK293T cells were able to bind but were unable to fuse to ZP-free eggs, indicating the possible need for additional molecules that are involved in this process (Inoue et al., 2013; Noda et al., 2020). Despite these recent advances, the molecular mechanisms of gamete fusion and the interplay between the various sperm and egg factors remain unclear.

Zebrafish has recently emerged as a model organism to study vertebrate fertilization due to its genetic tractability, access to a large number of gametes and external fertilization. The first factor that was discovered to be essential in zebrafish fertilization was Bouncer—a short three-finger-type protein anchored to the egg membrane (Herberg et al., 2018). *Bouncer*$^{-/-}$ females are sterile and sperm is unable to bind to Bouncer-deficient eggs, suggesting that Bouncer is involved in sperm-egg membrane binding (Herberg et al., 2018). Interestingly, the mammalian homolog of Bouncer is SPACA4, which is present in sperm and is involved in penetrating the zona pellucida (Fujihara et al., 2021). Moreover, we have shown that DCST1 and DCST2 are also necessary for zebrafish fertilization (Noda et al., 2021). However, while in mice *Dcst1* and *Dcst2* KO sperm can bind to, but rarely fuse with oocytes (Inoue et al., 2021; Noda et al., 2021), zebrafish *dcst1/2* KO sperm already show defects in sperm-egg binding (Noda et al., 2021). Therefore, zebrafish represents an interesting model system for the study of fertilization; despite the presence of mammalian fertilization factors in fish (Dcst1/2, Bouncer/SPACA4), the currently characterized factors show functional divergence in the fertilization process (Fujihara et al., 2021; Noda et al., 2021). Elucidating the role of conserved fertilization factors in both mammalian and non-mammalian vertebrate species will help to uncover common themes as well as distinct functionalities. Here, we investigate the role of Spaca6 in fertilization in zebrafish.

RESULTS

Spaca6 is a Conserved Testis-Expressed Membrane Protein

To study the role of Spaca6 in zebrafish fertilization, we first identified the full-length *spaca6* mRNA and protein sequence in zebrafish. *Spaca6* has two gene annotations in the most recent zebrafish genome release (GRCz11): a predicted protein-coding gene containing 7 exons (NCBI: XM_021466914.1) and a predicted non-protein coding gene containing 8 exons (ENSEMBL: ENSDART00000155083.2). In addition to the difference in exon numbers, we noticed that the predicted NCBI protein-coding annotation lacked the N-terminus including the signal peptide, which is present in mammalian SPACA6 homologs (Noda et al., 2020). To identify the sequence of the full-length *spaca6* transcript that is expressed in testis, we isolated RNA from wild-type zebrafish testes and amplified a 954-nt region from cDNA that contained an extended Spaca6 N-terminus and a total of 9 exons. Indeed, coverage tracks derived from RNA sequencing (Herberg et al., 2018; Noda et al., 2021) show expression peaks that align to the mapped transcript as well as specific expression of Spaca6 in testis (**Figure 1A**, **Supplementary Figure S1A**), as has been previously reported in mammals (Barbaux et al., 2020; Noda et al., 2020).

The full-length zebrafish *spaca6* transcript (GeneID: 101885333; NM_001397778.1) encodes for a 318-amino acid single-pass membrane protein that resembles mammalian SPACA6 proteins in their sequence and predicted tertiary structure (**Figures 1B,C**). It contains an N-terminal signal peptide, followed by an extracellular region containing an alpha-helical domain (extracellular domain, ECD) and an immunoglobulin (Ig) fold domain, a transmembrane domain and a short cytoplasmic domain (**Figure 1B**). Alignment of Spaca6 protein sequences from different vertebrates shows that Spaca6 is conserved in its amino acid sequence and secondary structure elements (**Figure 1B**, **Supplementary Figure S1B**).

Similar to mouse SPACA6, whose extracellular region has been shown to closely resemble that of IZUMO1 (Nishimura et al., 2016), Alphafold2 (Jumper et al., 2021) predicts the extracellular domain of zebrafish Spaca6 to fold into a four-helix bundle followed by an Ig-like domain comprised of beta sheets (**Figure 1C**). In order to taxonomically map Spaca6 homologues, we performed iterative BLASTP searches. This revealed that—similar to Izumo1—Spaca6 homologs are present across vertebrates, while proteins containing a DC-STAMP-like domain, such as Dcst1 and Dcst2, show a much broader distribution across both vertebrates and invertebrates (**Figure 1D**). Together, the conservation of Spaca6 across vertebrates and predicted similarities in tertiary structure with the mammalian homologs motivated us to assess the functional role of Spaca6 in zebrafish.

Spaca6 is Essential for Male Fertility in Zebrafish

Using CRISPR/Cas9-mediated mutagenesis, we generated zebrafish lacking Spaca6 protein. To this end, gRNAs were designed to target the third and fourth exons of the full-length *spaca6* gene. A mutant harboring an 86-bp deletion was recovered, which resulted in the introduction of a premature stop codon (**Figure 2A**, **Supplementary Figures S1C,D**). To test whether Spaca6 is required for fertilization in zebrafish, we assessed the fertilization rates of wild-type, heterozygous and homozygous KO fish (**Figures 2B,C**). While *spaca6*$^{+/-}$ males had fertilization rates comparable to wild type, *spaca6*$^{-/-}$ males were sterile (**Figure 2C**). Consistent with the expression of Spaca6 exclusively in the male germline (**Supplementary Figure S1A**), *spaca6*$^{-/-}$ females were fertile (**Figure 2C**), revealing that Spaca6 is only required for male fertility. To confirm that the observed fertilization defect of *spaca6*$^{-/-}$ males was caused by the absence of Spaca6 protein, we generated a rescue line that ubiquitously

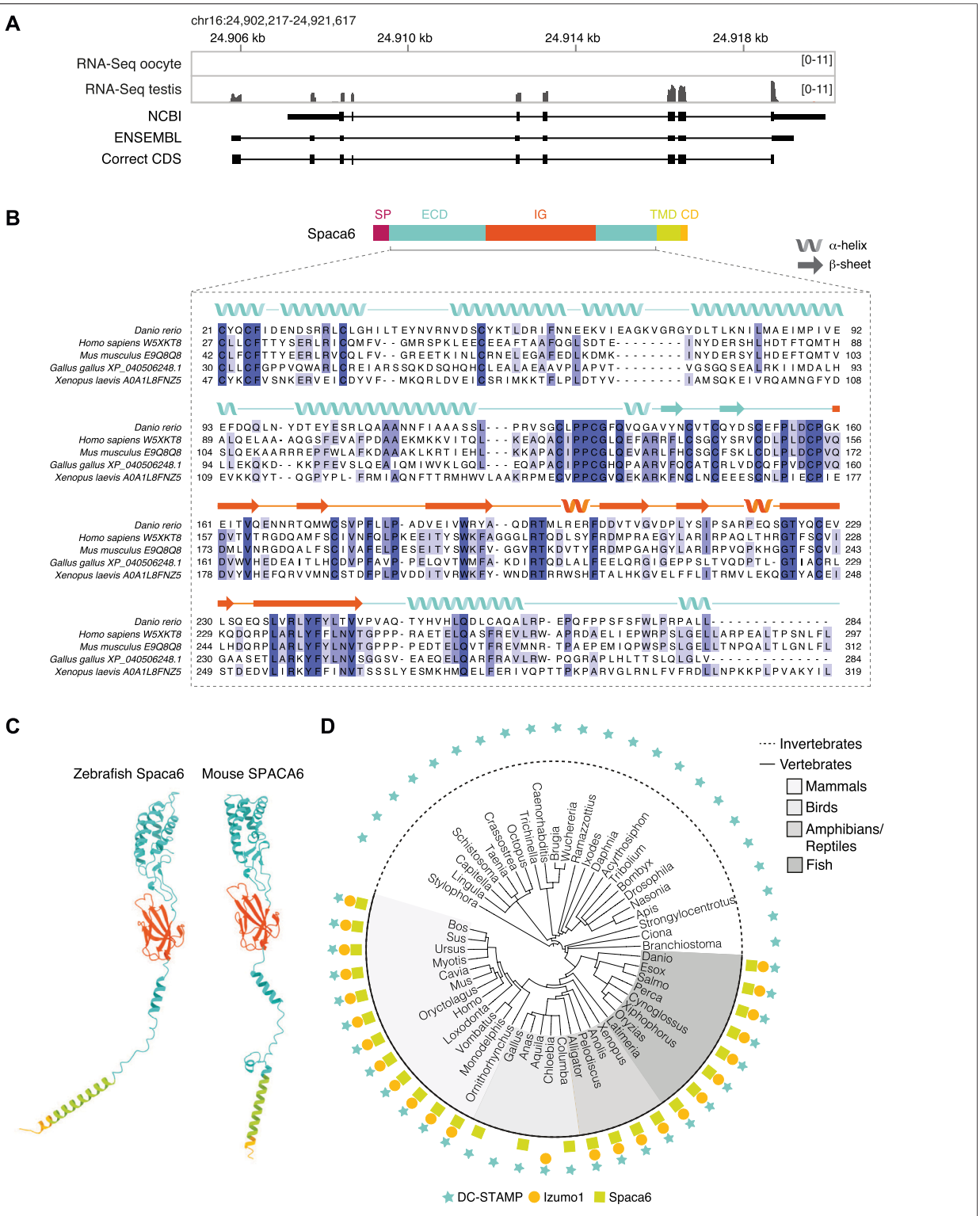

FIGURE 1 | Identification of Spaca6 in zebrafish. **(A)**. Expression and genomic features of zebrafish *spaca6*. Coverage tracks for RNA sequencing data from oocyte and testis aligned with ENSEMBL (ENSDART00000155083.2) and NCBI (XM_021466914.1) annotations as well as the full-length, newly identified testis coding DNA sequence (correct CDS). Genomic coordinates are based on GRCz11. **(B)**. Protein domain structure of full-length Spaca6 and sequence alignment of the mature extracellular region of selected vertebrate Spaca6 proteins. Secondary structure prediction of the zebrafish Spaca6 protein sequence is depicted above the sequence alignment (coil: alpha-helix; arrow: beta-sheet). The extracellular domain (ECD) is shown in blue, while the Immunoglobulin-like domain (IG) is shown in orange. SP, signal peptide; TMD, Transmembrane domain; CD, Cytoplasmic domain. **(C)**. Tertiary structure predictions of mouse and zebrafish Spaca6. Protein folding

(*Continued*)

FIGURE 1 | predictions of mature Spaca6 (lacking the signal peptide sequence) were performed using AlphaFold2 (Jumper et al., 2021). Extracellular domain, blue; Ig-like domain, orange; Transmembrane domain, green; Cytoplasmic domain, yellow. **(D)**. Taxonomic tree of DC-STAMP-like proteins, Izumo1 and Spaca6 across vertebrates and invertebrates. DC-STAMP-like proteins (blue star) are conserved both in vertebrates and invertebrates; Izumo1 (orange circle) and Spaca6 (green square) are conserved only in vertebrates.

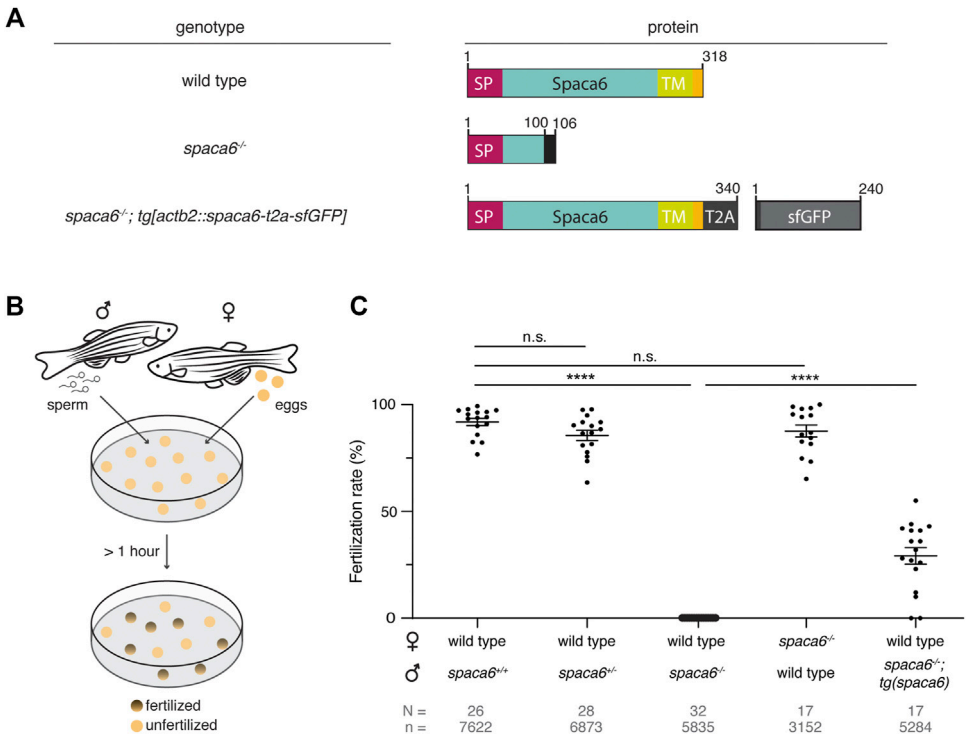

FIGURE 2 | Zebrafish Spaca6 is essential for male fertility. **(A)**. Diagrams of Spaca6 proteins made in wild-type, *spaca6*$^{-/-}$ and rescue [*spaca6*$^{-/-}$; *tg*(*actb2:spaca6-t2a-GFP*)] zebrafish lines. An 86-nt deletion in the *spaca6*$^{-/-}$ line leads to a retained sequence from intron two and a premature stop-codon, resulting in a dysfunctional truncated protein (translated part of the intron is shown in black). In the rescue line, a SGGSG spacer and a part of the viral T2A protein result in a C-terminal 23-aa addition. The amino acid position is given above the scheme. Signal peptide (SP), red; Extracellular domain, blue; Transmembrane domain (TM), green; Cytoplasmic domain, yellow. **(B)**. Scheme of a mating assay performed to quantify fertilization rates. Fish and gametes are not drawn to scale. **(C)**. Quantification of fertilization rates. Fertilization rates were calculated by counting the number of embryos that developed beyond the one-cell stage. ****, $p < 0.0001$ (Mann-Whitney test); n.s, not significant; error bars, standard deviation (SD); *N* = number of crosses; *n* = number of embryos.

expresses Spaca6 in a *spaca6*$^{-/-}$ background [*spaca6*$^{-/-}$; *tg*(*actb2:spaca6-T2A-GFP*)], hereafter referred to as *spaca6*$^{-/-}$; tg(*spaca6*). Transgenic Spaca6 partially rescued the fertilization defect of *spaca6* KO males (**Figure 2C**), suggesting that the fertility defect is indeed due to a lack of Spaca6.

Spaca6 KO Sperm is Motile but Fails to Bind to the Egg Membrane

To functionally dissect the fertilization defect in *spaca6*$^{-/-}$ males, we first assessed whether mutant sperm were morphologically normal. Differential interference contrast (DIC) images did not show any gross morphological differences between *spaca6*$^{-/-}$ and wild-type sperm (**Figure 3A**). Furthermore, *spaca6*$^{-/-}$ and wild-type sperm had a similar sperm head size and tail length (**Figure 3B**). In addition, we reasoned that another parameter that may affect sperm fertilizing ability is sperm motility. However, both wild-type and mutant sperm showed comparable motility and directed displacement (**Figures 3C,D**, **Supplementary Movie S1**). Therefore, the fertilization defect of *spaca6* KO sperm is neither due to morphological defects nor due to an inability of sperm to undergo activation and forward movement.

We next tested whether *spaca6* KO sperm is able to approach the micropyle, a funnel-shaped structure within the egg coat that serves as the only sperm entry point in fish (Hart and Donovan, 1983; Wolenski and Hart, 1987; Yanagimachi et al., 2013). In zebrafish, the micropyle measures 30 µm in diameter at the surface and gradually tapers off until it reaches the oolemma. This final inner canal is 2.3 µm in diameter and is therefore only able to accommodate a single sperm head (Hart and Donovan, 1983; Wolenski & Hart, 1987). Wild-type and *spaca6*$^{-/-}$ sperm were added to wild-type eggs and a time-lapse of sperm

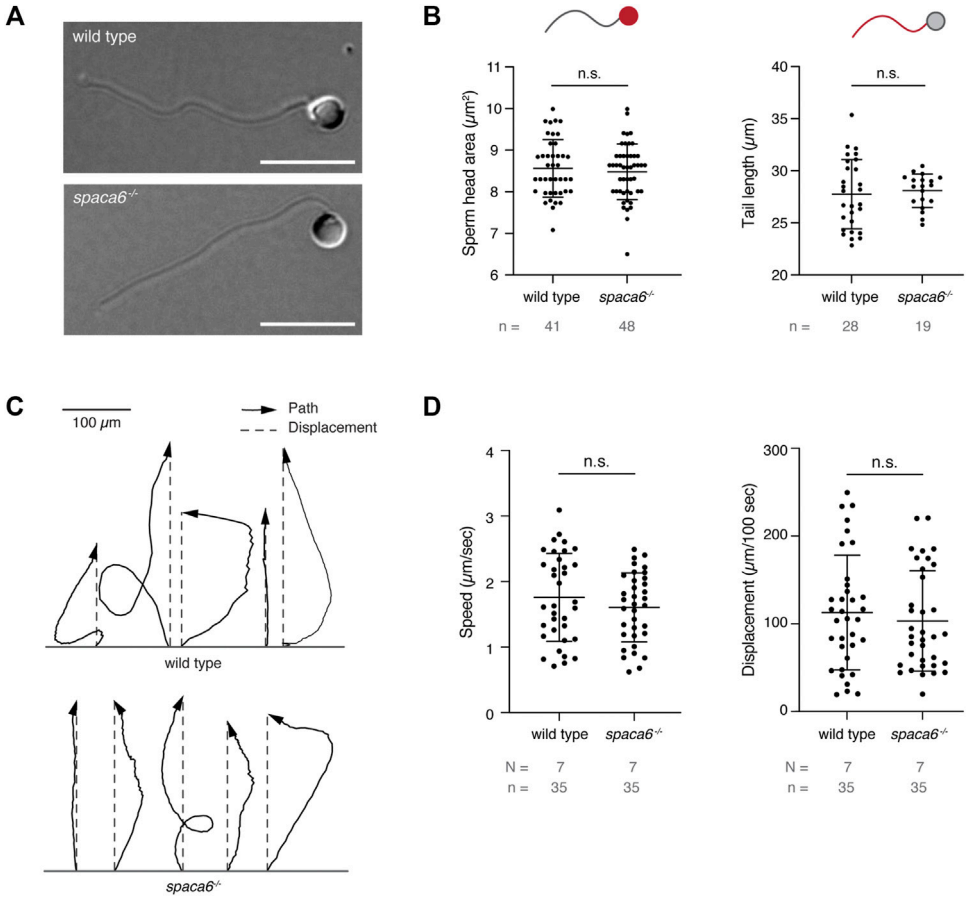

FIGURE 3 | *Spaca6* KO sperm is morphologically normal and motile. **(A).** Representative differential interference contrast (DIC) images of wild-type and *spaca6*$^{-/-}$ sperm. Scale bar = 10 µm. **(B)**. Measurements of the head area (left) and tail length (right) of wild-type and *spaca6*$^{-/-}$ sperm. n.s, not significant (Mann-Whitney test, $p > 0.05$); error bars, SD; *n* = number of sperm. **(C).** Representative tracks of wild-type and *spaca6*$^{-/-}$ sperm. Tracks (black arrows) were rotated and aligned at their origin. The relative displacement (grey dashed line) is overlaid. **(D)**. Sperm speed and displacement (per 100 s). n.s, not significant (Mann-Whitney test, $p > 0.05$); error bars, SD; *N* = number of independent experiments; *n* = number of sperm.

approaching the micropyle region was recorded. Both wild-type and mutant sperm were able to reach the micropyle within the same time-frame [number of times sperm successfully approached the micropyle out of the total number of recorded events: 7/9 (wild-type sperm) and 5/6 (*spaca6*$^{-/-}$ sperm)] (**Figure 4A**, **Supplementary Movie S2**). Although *spaca6*$^{-/-}$ sperm drifted away after a few minutes (**Figure 4A**, **Supplementary Movie S2**), we conclude that *spaca6*$^{-/-}$ sperm was able to approach and enter the micropyle similar to wild-type sperm. To test whether *spaca6*$^{-/-}$ sperm may be defective in egg binding, we performed a sperm binding assay that we had previously established (Herberg et al., 2018; Noda et al., 2021). This assay reports the ability of sperm to stably adhere to the oolemma, which is a requirement for the subsequent fusion of sperm and egg. In short, wild-type eggs were activated with water and manually dechorionated to expose the entire egg surface. Sperm was then added and sperm binding rates were recorded via time-lapse imaging. As observed in the sperm approach assay, *spaca6*$^{-/-}$ sperm was able to reach the egg, but failed to stably bind to the egg surface (**Figure 4B**, **Supplementary Movie S3**). This was in contrast to wild-type sperm, which was able to stably bind to the egg surface for at least 1 minute (**Figure 4C**, **Supplementary Movie S3**). It is worth pointing out that a fraction of the total number of bound wild-type sperm may have not only bound but also fused to the oolemma. While our current assay does not allow us to distinguish bound from potentially already fused sperm, our observation that *spaca6*$^{-/-}$ sperm did not adhere nor showed evidence of prolonged transient interaction with the oolemma indicates that *spaca6*$^{-/-}$ sperm is already defective in binding to oolemma. Therefore, we conclude that Spaca6 is required for sperm to stably adhere to the egg plasma membrane in zebrafish.

Dcst2 Levels Are Reduced in *spaca6* KO Sperm

Recent work in mice has shown that SPACA6 levels are decreased in sperm lacking IZUMO1, DCST1 and/or DCST2 (Inoue et al., 2021), suggesting that these essential fertility factors may co-regulate each other. To investigate whether this regulation holds

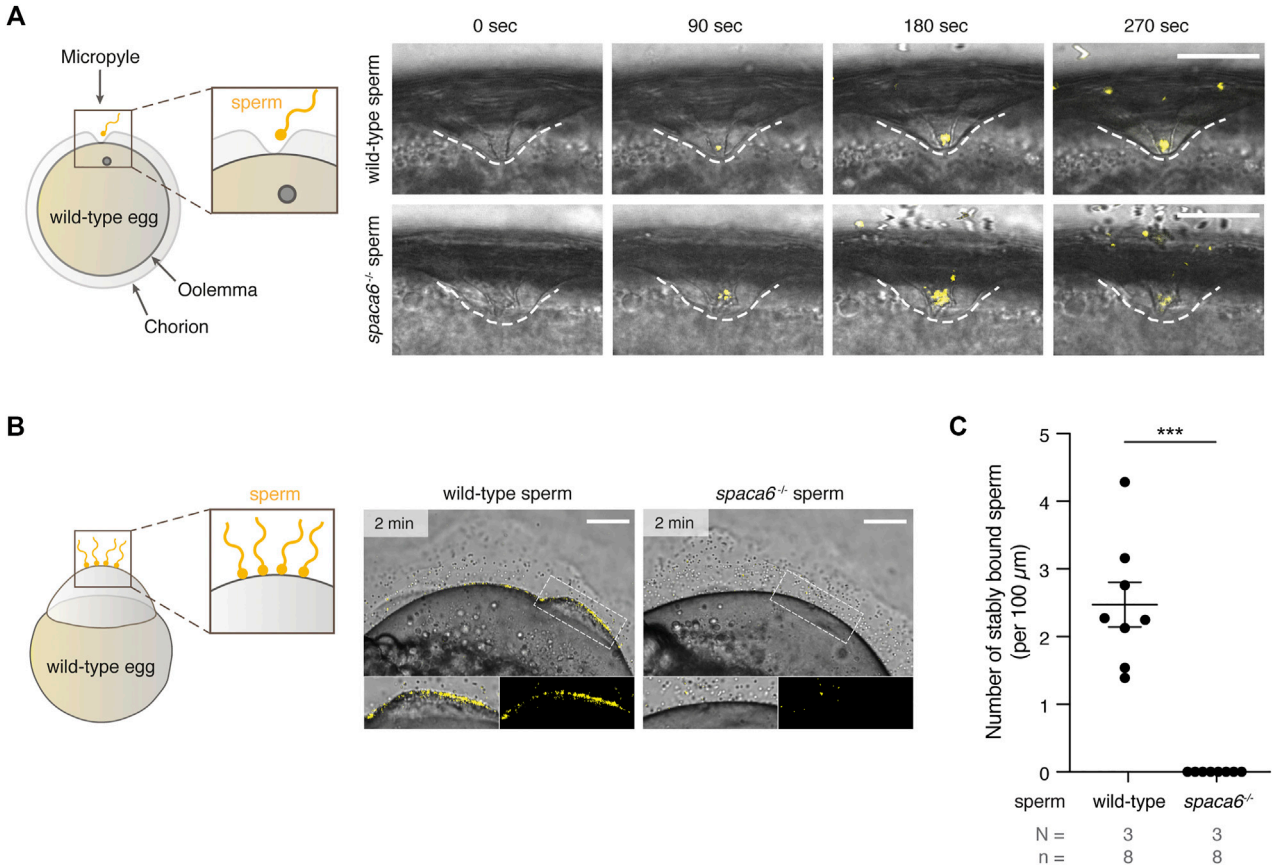

FIGURE 4 | Zebrafish Spaca6 is essential for sperm-egg binding. **(A)**. Time-lapse images of sperm approaching the micropyle of wild-type eggs. Left: Experimental setup. Right: Representative time series of MitoTracker-labeled wild-type (top) and *spaca6*$^{-/-}$ (bottom) sperm (yellow) approaching the micropyle (white dashed lines). Scale bar = 50 µm. **(B)**. Sperm binding assay. Left: Experimental setup. Wild-type and *spaca6*$^{-/-}$ sperm were labeled with MitoTracker (yellow) and subsequently incubated with activated and dechorionated wild-type eggs. Right: Representative images of wild-type (top) and *spaca6*$^{-/-}$ (bottom) sperm binding to the surface of the egg 2 min after sperm addition. The boxed region is shown at higher magnification below. Scale bar = 100 µm. **(C)**. Quantification of sperm binding. Binding of sperm to the egg was quantified by assessing the number of stably bound sperm per 100 µm over a period of 2 min. Wild-type sperm were frequently found bound to the oolemma. ***, $p < 0.001$ (Mann-Whitney test); error bars, SD; *N* = number of independent experiments; *n* = number of sperm.

true reciprocally, we measured Dcst2 protein levels and localization in *spaca6*$^{-/-}$ sperm, using an antibody recognizing zebrafish Dcst2 (Noda et al., 2021). Dcst2 levels were significantly decreased in *spaca6*$^{-/-}$ sperm, as revealed by immunoblotting (**Figures 5A,B**, **Supplementary Figure S2**) and immunofluorescence imaging, which showed a reduction of Dcst2-positive foci around the sperm plasma membrane (**Figure 5C**). The decrease in Dcst2 levels was partially restored in sperm of the *spaca6*$^{-/-}$; tg(*spaca6*) rescue line, which is consistent with the partial rescue of fertility (**Figure 2B**). Our data therefore suggests that Spaca6 regulates Dcst2 protein levels.

DISCUSSION

Our results show that testis-expressed Spaca6 is essential for zebrafish fertilization. We make two major findings: 1) In zebrafish, the absence of Spaca6 leads to a disruption in the sperm's binding ability to the egg surface and 2) the levels of another key fertilization factor, Dcst2, depend on the presence of Spaca6.

Our study shows that Spaca6 has an essential role in fertilization outside of mammals. Even though Spaca6 is conserved among vertebrates (**Figures 1B–D**), the step at which fertilization stalls in the absence of Spaca6 differs between zebrafish and mice. Mouse *Spaca6* KO sperm can penetrate the zona pellucida and bind to the oolemma, but fail to fuse with the egg (Barbaux et al., 2020; Noda et al., 2020). In contrast, our findings in zebrafish reveal that zebrafish sperm lacking Spaca6 is already unable to bind to the egg membrane, and is thus required in a step before fusion can take place.

On a molecular level the observed difference could possibly be reconciled from mouse experiments involving IZUMO1. One possibility is that mouse *Spaca6* KO sperm is still able to bind to the oocyte due to the presence of IZUMO1, thereby providing a redundant role in sperm adhesion to the egg. In support of this notion, IZUMO1 protein levels as well as IZUMO1 relocation

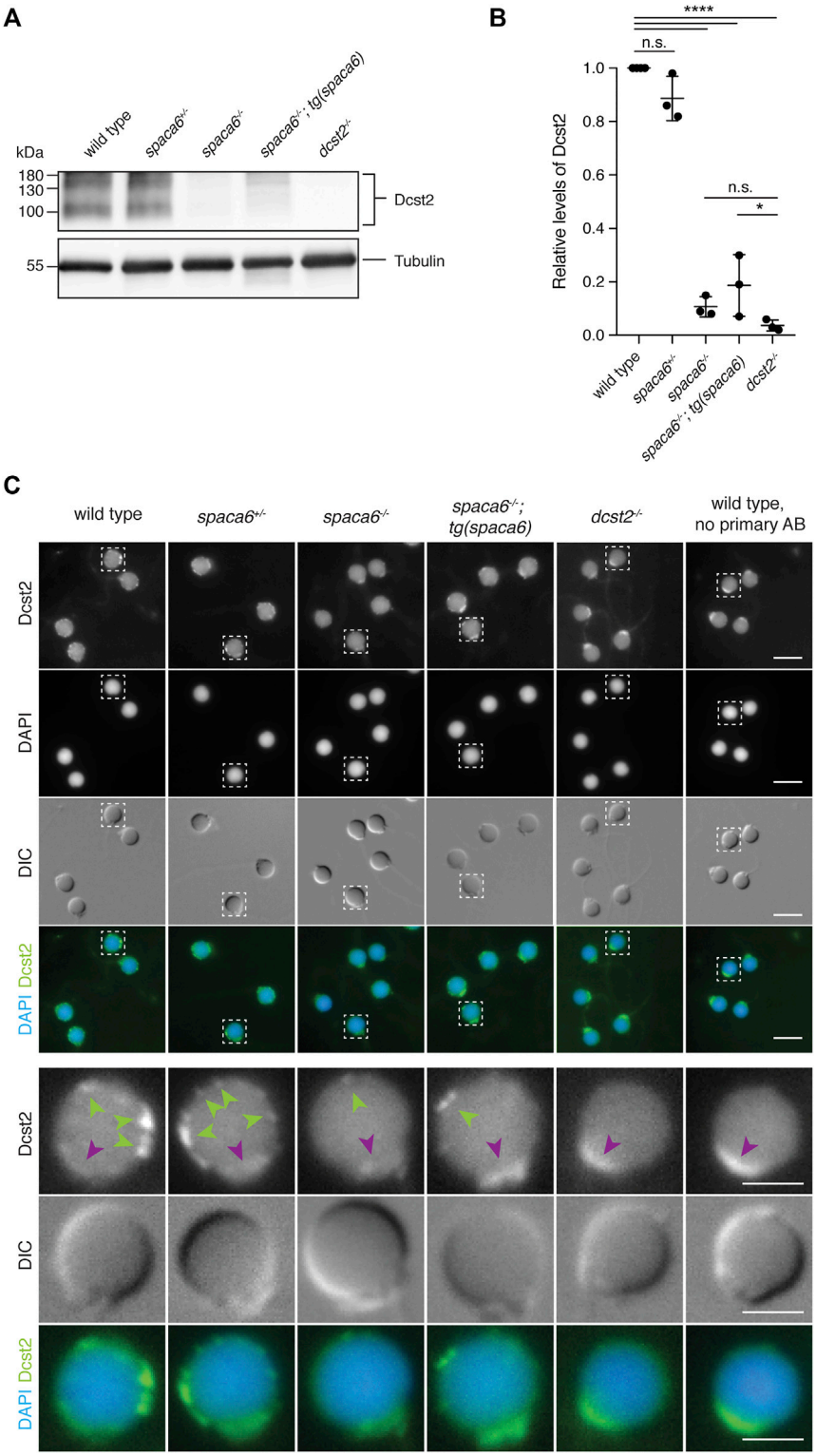

FIGURE 5 | Dcst2 levels are reduced in zebrafish *spaca6* KO sperm. **(A)**. Immunoblot of sperm samples of different genotypes probed with antibodies against zebrafish Dcst2. Zebrafish Dcst2 is predicted to be a glycoprotein, resulting in a wider area of detected signal. Tubulin protein levels of the same blot are shown as loading control. The uncropped immunoblot is shown in **Supplementary Figure S2**. **(B)**. Quantification of sperm Dcst2 levels of different genotypes based on three independent immunoblots. Values were compared to tubulin levels and normalized to wild type. Statistical significance was calculated using one-way ANOVA and multiple comparisons analysis: n.s, not significant ($p > 0.05$; ****, $p < 0.0001$; *, $p = 0.045$). **(C).** Immunofluorescent images of Dcst2 protein in sperm heads of different

(*Continued*)

FIGURE 5 | genotypes. Upper panels: Overview images (scale bar = 5 μm). Lower panels: Higher magnification images of an individual exemplary sperm head (boxed in the upper panels) for each genotype (scale bar = 2 μm). Sperm were stained with DAPI (blue) to visualize nuclei and antibodies against zebrafish Dcst2 (green). Dcst2 localizes to distinct foci around the sperm head membrane (green arrowheads in the lower panels) in wild-type, *spaca6*$^{+/-}$ and tg(*spaca6*)-rescued sperm. Autofluorescence of the sperm midpiece appears as a uniform signal in the Dcst2 channel (magenta arrowhead).

during the acrosome reaction were reported to be normal in *Spaca6* KO sperm (Barbaux et al., 2020; Inoue et al., 2021). Moreover, IZUMO1 was shown to be sufficient for cells to bind to the oocyte (Inoue et al., 2013; Noda et al., 2020), suggesting that one major role of IZUMO1 is to enable sperm to adhere to the egg surface. Although zebrafish have an Izumo1 ortholog (**Figure 1C**), its mammalian binding partner on the egg surface, JUNO, appears to be absent in fish (Grayson, 2015). Izumo1's presence may therefore not be sufficient to mediate binding between the two gametes in fish. Future experiments exploring the role of Izumo1 in zebrafish fertilization as well as potential co-regulation of Spaca6 and Izumo1 will help elucidate the molecular mechanisms in fish and mammalian systems alike.

Direct evidence that essential sperm factors co-regulate each other was recently reported in mice (Inoue et al., 2021). Inoue and others showed that sperm lacking IZUMO1, DCST1 and/or DCST2 had undetectable levels of SPACA6 protein, which suggested that SPACA6 levels are dependent on the presence of each of these factors. Interestingly, SPACA6 protein levels were restored when IZUMO1 was transgenically expressed in *Izumo1* KO sperm, but not when DCST1/2 were expressed in *Dcst1/2* KO sperm, even though fertilization was rescued. One possibility is that SPACA6 levels were undetectable in the rescue but high enough for fertilization to be restored. Another possibility is that the role of SPACA6 can be by-passed by transgenic expression of DCST1/2, suggesting an indirect role of SPACA6 in fertilization. Our data shows that in zebrafish, transgenic expression of Spaca6 results in a partial rescue of fertilization (**Figure 2C**), which is correlated with a partial restoration of Dcst2 levels (**Figure 5**). However, it is currently unclear whether this partial rescue in fertilization is due to insufficient levels of Spaca6, Dcst1/2 or both. Together, this study and studies in mice point towards a co-regulation of SPACA6 and DCST1/2. Inoue et al. demonstrated that DCST1/2 regulates the levels of SPACA6 (Inoue et al., 2021), and we show that zebrafish Dcst2 levels depend on the presence of Spaca6 (**Figure 5**). Whether these factors act purely as stabilization factors or whether they also play a role in sperm-egg interaction remains to be tested. Further studies characterizing the molecular co-regulation of these factors will be necessary to understand their role in protein stability, binding and fusion.

In conclusion, Spaca6 is a conserved factor essential for fertilization in vertebrates, but its molecular function still remains unclear. Judging from the current data, there are several possible explanations to reconcile the role of Spaca6. Since Dcst2 levels are disrupted in *spaca6* KO sperm in zebrafish, Spaca6 may serve as a stabilization factor. While this idea has not yet been tested experimentally in mammals, loss of DCST1/2 protein levels in mammalian *Spaca6* KO sperm would provide direct evidence for a conserved role of Spaca6 across vertebrates in stabilizing Dcst1/2. Alternatively, due to Spaca6's structural similarity to Izumo1 (Nishimura et al., 2016)—a well-known adhesion factor - and the inability of *spaca6* KO sperm to bind to the egg surface in zebrafish, Spaca6 could be involved in sperm-egg adhesion, which may or may not depend on its regulation of Dcst1/2. In this context, studies of its potential interaction partner(s) on the egg membrane in zebrafish and mice might identify new fertilization factors on the egg. Finally, the notion of a membrane complex needed for binding and fusion has been previously proposed (Barbaux et al., 2020; Noda et al., 2020). Spaca6 may contribute to forming and/or stabilizing such a multi-factor complex on the sperm membrane that regulates both binding and fusion. Further investigation of the co-regulation and potential interaction between Spaca6, Dcst1/2, Izumo1 and other known essential fertilization factors may help elucidate the mechanism of gamete fusion on a molecular level.

MATERIALS AND METHODS

Zebrafish Husbandry

Zebrafish (*Danio rerio*) were raised according to standard protocols (28°C water temperature, 14/10 h light/dark cycle). TLAB fish were generated by crossing AB and natural variant TL (Tupfel Longfin) zebrafish and used as wild type for all experiments. The generation of zebrafish *spaca6* KO fish is described below. The *dcst2*$^{-/-}$ zebrafish line has been described previously (Noda et al., 2021). All fish experiments were conducted according to Austrian and European guidelines for animal research and approved by the Amt der Wiener Landesregierung, Magistratsabteilung 58—Wasserrecht.

Identification of the Full-Length Zebrafish Spaca6 Sequence

Current gene annotations for zebrafish *spaca6* (NCBI *Danio rerio* Annotation release 106: XM_021466914.1, seven exons; and ENSEMBL release 104: BX539313.2-201, ENSDART00000155083.2, eight exons) were found in the Genome Browser (http://genome.ucsc.edu) using the zebrafish genome release (GRCz11). To obtain the correct, full-length sequence for zebrafish Spaca6, wild-type zebrafish testis cDNA was used for amplifying a region predicted to encompass the full-length protein sequence (primers used for PCR: Spaca6_CDS_F: GCTACTTGTTCTTTTTGCAGGATCCGCCACCATGTTTGT GTTTATTGCAAAAC and Spaca6_CDS_R: ACACTCCTGATC CTCCTGAGAATTCGGCTGGATTAGAAACGTTG). The amplified region was cloned and subsequently sequence-verified (submitted to NCBI as GeneID:101885333; NM_001397778.1). Published RNA sequencing data from adult tissues (Herberg et al., 2018; Noda et al., 2021) was used to analyse *spaca6* gene expression levels in various adult tissues and

to examine the coverage tracks across spaca6 in testis and oocytes using the Integrative Genomics Viewer (IGV) (http://software.broadinstitute.org/software/igv/).

Taxonomic Tree of Spaca6, Izumo1 and DC-STAMP-like Proteins and Analysis of Spaca6 Protein Structure and Conservation

Spaca6 orthologs were collected in a series of NCBI blast searches starting with human SPACA6 (sp|W5XKT8|SACA6_HUMAN) and zebrafish Spaca6 (ref|XP_021322589.1|) from the UniProt reference proteomes or NCBI non redundant (nr) protein database applying significant E-value thresholds (1e-05) (Altschul, 1997; Schoch et al., 2020; Bateman et al., 2021). Sequences of the DC-STAMP protein family, including human DCST1, DCST2, DC-STAMP, and OC-STAMP, were identified in a Hidden Markov Model (HMM) search using the PFAM DC-STAMP model against UniProt reference proteomes databases applying significant E-value thresholds (<0.01) (Eddy, 1998; El-Gebali et al., 2019). Izumo1 protein family members were identified using the PFAM IZUMO HMM search tool, covering the amino-terminal conserved region of human IZUMO1 (21–165, sp|Q8IYV9|IZUM1_HUMAN) in the UniProt reference proteomes databases (E-value < 0.01). In addition, an extended region of IZUMO1 (corresponding to human 1–219) was used and searched for with NCBI blastp in the NCBI nr database (E-value < 0.001). Out of the full set of 453 taxa containing either DC-STAMP, Izumo1 or Spaca6 proteins, 52 representative animal species were selected, and a taxonomic tree was retrieved using the NCBI Taxonomy CommonTree tool (Schoch et al., 2020). The tree visualization was performed in iTOL v6 (Letunic and Bork, 2021).

The protein sequence alignment of vertebrate Spaca6 amino acid sequences was performed using the Muscle alignment tool (http://www.drive5.com/muscle/, version 3.8.31) and visualized with Jalview (Waterhouse et al., 2009). The percentage of sequence identity of the mature Spaca6 protein of different vertebrate species was derived using the Percent Identity Matrix from Clustal Omega (Sievers et al., 2011).

The protein domain predictions for zebrafish Spaca6 and mouse SPACA6 (Uniprot ID: E9Q8Q8) were obtained from InterPro (Blum et al., 2021). Additionally, the Ig-like domain annotation was derived from previously published data for mouse IZUMO1 and SPACA6 (Nishimura et al., 2016). Secondary and tertiary protein structure predictions were obtained using AlphaFold2 (Jumper et al., 2021). The mouse SPACA6 model (Identifier: AF-E9Q8Q8-F) was already predicted, whilst the zebrafish Spaca6 tertiary structure was modeled using the newly identified Spaca6 amino acid sequence without the signal peptide.

Generation of *spaca6* KO Zebrafish

Spaca6 KO fish were generated by Cas9-mediated mutagenesis. Two guide RNAs (sgRNAs) targeting the third and fourth exons of the full-length *spaca6* gene were generated according to published protocols (Gagnon et al., 2014) by oligo annealing followed by T7 polymerase-driven *in vitro* transcription (gene-specific targeting oligos: spaca6_1_gRNA: TAATACGACTCA CTATAGGCGGCCTCAAGCCTGCCCAGGTTTTAGAGC TAGAAATAGCAAG and spaca6_2_gRNA: TAATACGACTCA CTATAGGTCTGGATGTTTGCCCCCATGGTTTTAGAGCTA GAAATAGCAAG; common tracer oligo AAAAGCACCGAC TCGGTGCCACTTTTTCAAGTTGATAACGGACTAGCCTTA TTTTAACTTGCTATTTCTAGCTCTAAAAC). Cas9 protein and *spaca6* sgRNAs were co-injected into the cell of one-cell stage TLAB embryos. Putative founder fish were outcrossed to TLAB wild-type fish. A founder fish carrying a germline mutation in the *spaca6* gene was identified by a size difference in the *spaca6* PCR amplicon in a pool of embryo progeny (primers: spaca6_gt_F: GCAGAGAAATCTTGATTG GAGG and spaca6_gt_R: AAGCAGACCAGTATACAATTT TTGC). Embryos from this founder fish were raised to adulthood. Amplicon sequencing of adult fin-clips identified the 86-nt deletion, which results in a frameshift mutation and a premature stop codon in intron 2 (GRCz11: Chr16:24,907,548). Genotyping of *spaca6* mutant fish was performed by PCR using primers: spaca6_gt_F and spaca6_gt_R. Detection of the deletion was performed by standard gel electrophoresis using a 4% agarose gel. Homozygous *spaca6*$^{-/-}$ fish were generated by outcrossing *spaca6*$^{+/-}$ fish to wild-type fish and then incrossing *spaca6*$^{+/-}$ fish from the next generation.

Generation of Zebrafish Expressing Transgenic Spaca6

The full-length *spaca6* coding sequence, including the *spaca6* signal peptide, the extracellular region and transmembrane and intracellular domains, was amplified by PCR from cDNA derived from adult zebrafish testis (Spaca6_CDS_F and Spaca6_CDS_R) and subcloned by Gibson cloning (Gibson et al., 2009) into a vector for Tol2-mediated transgenesis along with a *SG-linker-T2A-sfGFP* sequence inserted in frame immediately before the stop-codon of the *spaca6* sequence (resulting vector: pMTB Tol2 -*actb2*-promoter—*spaca6*—*SG-linker-T2A-sfGFP* SV40UTR). Zebrafish lines expressing transgenic Spaca6 were generated by injecting the *spaca6* expression construct with *Tol2* mRNA into *spaca6*$^{+/-}$ zebrafish embryos (15 ng/µl of the plasmid in RNase-free water, 35 ng/µl *Tol2* mRNA, 0.083% phenol red solution [Sigma-Aldrich]), following standard procedures. Injected embryos with high expression of sfGFP at 1 day post fertilization were raised to adulthood. Putative founder fish were crossed to *spaca6*$^{-/-}$ or *spaca6*$^{+/-}$ fish and the progeny was screened for fluorescence, raised to adulthood and genotyped using primers spaca6_gt_F and spaca6_gt_R to identify adult fish lacking endogenous *spaca6*. *Spaca6*$^{-/-}$ male fish expressing transgenic *spaca6* [*spaca6*$^{-/-}$; tg(*spaca6*)] were crossed to wild-type females in order to quantify fertilization rates and assess functionality of the construct.

Quantification of *in vivo* Fertilization Rates in Zebrafish

The evening prior to mating, male and female fish were separated in breeding cages (one male and one female per cage). The next

morning, male and female fish were allowed to mate. Eggs were collected and kept at 28°C in E3 medium (5 mM NaCl, 0.17 mM KCl, 0.33 mM $CaCl_2$, 0.33 mM $MgSO_4$, 0.00001% Methylene blue). The rate of fertilization was assessed approximately 3 h post laying. By this time, fertilized embryos have developed to ~1000-cell stage embryos, while unfertilized eggs resemble one-cell stage embryos. Direct comparisons were made between siblings of different genotypes [wild type; *spaca6*$^{-/-}$; *spaca6*$^{+/-}$; *spaca6*$^{-/-}$ tg(*actb2:spaca6-t2a-GFP*)].

Assessment of Sperm Morphology

To collect wild-type or mutant sperm, male zebrafish were anesthetized using 0.1% tricaine. Sperm was collected with a glass capillary from the urogenital opening and immediately fixed with 3.7% formaldehyde at 4°C for 20 min. Sperm were spun onto an adhesive slide using a CytoSpin 4 (Thermo Fisher Scientific) at 1,000 rpm for 5 min followed by permeabilization with ice-cold methanol for 5 min and a wash with 0.1% Tween in 1x PBS (PBST). After mounting using VECTASHIELD Antifade with DAPI (Vector Laboratories), sperm were imaged with an Axio Imager.Z2 microscope (Zeiss) with an oil immersion 63x/1.4 Plan-Apochromat DIC objective.

Assessment of Sperm Motility

Sperm were isolated from 1 to 2 wild-type and mutant male fish and kept in 100 µl Hank's saline (0.137 M NaCl, 5.4 mM KCl, 0.25 mM Na_2HPO_4, 1.3 mM $CaCl_2$, 1 mM $MgSO_4$, and 4.2 mM $NaHCO_3$) containing 0.5 µM MitoTracker Deep Red FM (Molecular Probes) for >10 min on ice. Sperm (approximately 5,000 sperm/µl) were activated using E3 medium in a 1:4 dilution and placed onto a 10 µm thick chamber slide (Leja counting chamber, SC 10–01–04-B). Sperm motility was imaged 30 s after activation using an Axio Imager.Z2 microscope (Zeiss) and a 10x/0.3 plan-neofluar objective using darkfield. Sperm tracks were analyzed using Fiji with the "manual tracking" plugin (Cordelieres, 2005). Sperm that were present in the movie for more than 30 timeframes were tracked for as many frames as possible. Coordinates of the sperm cells were used to calculate average sperm speed and displacement. Sperm displacement was calculated by measuring the distance between the first and the last coordinates (normalized by 100 timeframes).

Imaging of Zebrafish Sperm Approach

Sperm were isolated from 2 to 4 wild-type and mutant male fish and kept in 150 µl Hank's saline containing 0.5 µM MitoTracker Deep Red FM (Molecular Probes) for >10 min on ice. Unactivated, mature eggs were then isolated from a wild-type female. To prevent activation, eggs were kept in sorting medium (Leibovitz's medium, 0.5% BSA, pH 9.0) at room temperature. Eggs were kept in place using a petri dish with cone-shaped agarose molds (1.5% agarose in sorting medium) filled with sorting medium. Imaging was performed with a LSM800 Examiner Z1 upright system (Zeiss) with a 20x/1.0 plan-apochromat water dipping objective. Before sperm addition, sorting media was removed and 1 ml of E3 medium carefully added close to the egg. 3 µl of stained spermatozoa (approximately 150,000—300,000 sperm) was added as close to the egg as possible during image acquisition. The resulting time-lapse movies were analyzed using Fiji. Timestamps were calculated beginning with the addition of sperm to the eggs.

Imaging and Analysis of Zebrafish Sperm-Egg Binding

Sperm were isolated from 2 to 4 wild-type and mutant male fish and kept in 200 µl Hank's saline containing 0.5 µM MitoTracker Deep Red FM (Molecular Probes) on ice. Unactivated, mature eggs were squeezed from a wild-type female fish and activated by addition of E3 medium. After 10 min, 1–2 eggs were manually dechorionated using forceps and one egg was transferred to a cone-shaped 2% agarose-coated imaging dish with E3 medium. After focusing on the egg plasma membrane, the objective was briefly lifted to add 2–5 µl of stained sperm (approximately 200,000–250,000 sperm). Imaging was performed with a LSM800 Examiner Z1 upright system (Zeiss) using a 20x/0.3 Achroplan water dipping objective. Images were acquired until sperm were no longer motile (5 min). To analyze sperm-egg binding, stably bound sperm were counted. Sperm were counted as bound when they remained in the same position for at least 2 min following a 90-s period in which they activated and approached the egg. Data was plotted as the number of sperm bound per 100 µm of egg membrane for 2 minutes.

Sperm Immunocytochemistry

Sperm from zebrafish males was collected in 3.7% formaldehyde diluted in Hank's saline solution and stored on ice for 20 min to 1 h. Sperm was pelleted by centrifugation at 850 rpm for 3 min, and the fixative was replaced with Hank's saline. Sperm was spun onto an adhesive slide with a CytoSpin 4 (Thermo Fisher Scientific) at 800 rpm for 3 min. Slides were briefly washed once in 1x PBS, and the sperm was permeabilized in 0.25% Tween in 1x PBS for 30 min before blocking with 10% normal goat serum (Invitrogen) and 40 µg/ml BSA in PBST for at least 1 h. Slides were then incubated with mouse anti-zebrafish-Dcst2 antibody in blocking buffer (1:650; (Noda et al., 2021)) overnight at 4°C in a humidified chamber. After several washes with PBST, slides were incubated with goat anti-mouse IgG Alexa Fluor 488 secondary antibody (1:380, Thermo Fisher Scientific) for 1 h, washed several times with PBST and finally once with 1x PBS. After mounting using VECTASHIELD Antifade with DAPI (Vector Laboratories), sperm was imaged with an Axio Imager.Z2 microscope (Zeiss) using an oil immersion 100x/1.4 plan-apochromat objective. Widefield sperm images were processed for each genotype using Fiji by adjusting image brightness and contrast without clipping of intensity values.

Western Blotting of Sperm Samples

For western blot analysis, sperm from 3-6 males was sedimented at 3,000 rpm for 3.5 min. The supernatant was replaced with RIPA buffer (50 mM Tris-HCl [pH 7.5], 150 mM NaCl, 1 mM $MgCl_2$, 1% NP-40, 0.5% sodium deoxycholate, 1 × complete protease inhibitor [Roche]) including 1% SDS. After preparation of all samples, 1 U/µl benzonase (Merck) was added, and samples were incubated for 30 min at room temperature. Samples were then mixed with 4 × Laemmli buffer containing β-mercaptoethanol and boiled at 95°C for 5 min. After SDS-

PAGE, samples were wet-transferred onto a nitrocellulose membrane. Total protein was visualized by Ponceau staining before blocking with 5% milk powder in 0.1% Tween in 1 × TBS (TBST). Membranes were incubated in primary mouse anti-zebrafish-Dcst2 antibody [1:500; (Noda et al., 2021)] overnight at 4°C, then washed with TBST before HRP-conjugated secondary antibody [1:10.000 (115–036–062, Dianova)] incubation for 1 h. Membranes were washed several times in TBST before HRP activity was visualized using Clarity Western ECL Substrate (BioRad) on a ChemiDoc (BioRad). For visualizing Tubulin levels, membranes were stripped using Restore Western Blot Stripping Buffer (Thermo Fisher Scientific) before washing, blocking and incubation with mouse anti-alpha-Tubulin antibody [1:20.000 (T6074, Merck)] and proceeding with secondary antibody staining and detection as described above.

To assess relative Dcst2 protein amounts, average intensities of Dcst2-specific bands were quantified in Fiji on three independent immunoblots for each genotype relative to tubulin levels, which was used as loading control. Values were then normalized to the levels of wild-type sperm.

DATA AVAILABILITY STATEMENT

The original contributions presented in the study are included in the article/**Supplementary Material**, further inquiries can be directed to the corresponding authors.

ETHICS STATEMENT

The animal study was reviewed and approved by the Amt der Wiener Landesregierung, Magistratsabteilung 58—Wasserrecht; Vienna, Austria.

AUTHOR CONTRIBUTIONS

VD and AP conceived the study; MB, AK, and KP designed, performed and analyzed experiments with contributions from VD, AP, and AS performed the phylogenetic analysis; VD and AP coordinated and supervised the project; all authors contributed to writing the manuscript.

FUNDING

This research was funded by the Research Institute of Molecular Pathology (IMP), Boehringer Ingelheim, the Austrian Academy of Sciences, FFG (Headquarter grant FFG-852936), the FWF START program (Y 1031-B28) to AP, the HFSP Career Development Award (CDA00066/2015) and the HFSP Young Investigator Award to AP, EMBO-YIP funds to AP, and an HFSP post-doctoral fellowship to VD. The funders had no role in study design, data collection and analysis, decision to publish, or preparation of the manuscript. For the purpose of Open Access, the author has applied a CC BY public copyright license to any Author Accepted Manuscript (AAM) version arising from this submission.

ACKNOWLEDGMENTS

We thank the team of the Biooptics facility at the Vienna Biocenter, in particular Pawel Pasierbek and Thomas Lendl, for support with microscopy and image analysis; the animal facility personnel from the IMP for taking excellent care of zebrafish; Anna Bandura for help with genotyping; Juraj Ahel for providing the AlphaFold2 script; Maria Novatchkova for help with RNA sequencing analysis; Andreas Blaha and Sara Berent for valuable help with the sperm morphology assay; and the entire Pauli lab for fruitful discussions.

SUPPLEMENTARY MATERIAL

The Supplementary Material for this article can be found online at: https://www.frontiersin.org/articles/10.3389/fcell.2021.806982/full#supplementary-material

REFERENCES

Altschul, S. (1997). Gapped BLAST and PSI-BLAST: a New Generation of Protein Database Search Programs. *Nucleic Acids Res.* 25, 3389–3402. doi:10.1093/nar/25.17.3389

Barbaux, S., Ialy-Radio, C., Chalbi, M., Dybal, E., Homps-Legrand, M., do Cruzeiro, M., et al. (2020). Sperm SPACA6 Protein Is Required for Mammalian Sperm-Egg Adhesion/Fusion. *Sci. Rep.* 10, 5335. doi:10.1038/s41598-020-62091-y

Bateman, A., Martin, M.-J., Orchard, S., Magrane, M., Agivetova, R., Ahmad, S., et al. (2021). UniProt: the Universal Protein Knowledgebase in 2021. *Nucleic Acids Res.* 49, D480–D489. doi:10.1093/nar/gkaa1100

Bianchi, E., and Wright, G. J. (2016). Sperm Meets Egg: The Genetics of Mammalian Fertilization. *Annu. Rev. Genet.* 50, 93–111. doi:10.1146/ANNUREV-GENET-121415-121834

Blum, M., Chang, H.-Y., Chuguransky, S., Grego, T., Kandasaamy, S., Mitchell, A., et al. (2021). The InterPro Protein Families and Domains Database: 20 Years on. *Nucleic Acids Res.* 49, D344–D354. doi:10.1093/nar/gkaa977

Cordelieres, F. (2005). *Manual Tracking*. Available at: https://imagej.nih.gov/ij/plugins/track/track.html(Accessed October 28, 2021).

Deneke, V. E., and Pauli, A. (2021). The Fertilization Enigma: How Sperm and Egg Fuse. *Annu. Rev. Cel Dev. Biol.* 37, 391–414. doi:10.1146/ANNUREV-CELLBIO-120219-021751

Eddy, S. R. (1998). Profile Hidden Markov Models. *Bioinformatics* 14, 755–763. doi:10.1093/bioinformatics/14.9.755

El-Gebali, S., Mistry, J., Bateman, A., Eddy, S. R., Luciani, A., Potter, S. C., et al. (2019). The Pfam Protein Families Database in 2019. *Nucleic Acids Res.* 47, D427–D432. doi:10.1093/nar/gky995

Fujihara, Y., Herberg, S., Blaha, A., Panser, K., Kobayashi, K., Larasati, T., et al. (2021). The Conserved Fertility Factor SPACA4/Bouncer Has Divergent Modes of Action in Vertebrate Fertilization. *Proc. Natl. Acad. Sci. USA* 118, e2108777118. doi:10.1073/pnas.2108777118

Gagnon, J. A., Valen, E., Thyme, S. B., Huang, P., Ahkmetova, L., Pauli, A., et al. (2014). Efficient Mutagenesis by Cas9 Protein-Mediated Oligonucleotide Insertion and Large-Scale Assessment of Single-Guide RNAs. *PLoS ONE* 9, e98186. doi:10.1371/journal.pone.0098186

Gibson, D. G., Young, L., Chuang, R.-Y., Venter, J. C., Hutchison, C. A., and Smith, H. O. (2009). Enzymatic Assembly of DNA Molecules up to Several Hundred Kilobases. *Nat. Methods* 6, 343–345. doi:10.1038/nmeth.1318

Grayson, P. (2015). Izumo1 and Juno: the Evolutionary Origins and Coevolution of Essential Sperm-Egg Binding Partners. *R. Soc. Open Sci.* 2, 150296. doi:10.1098/rsos.150296

Hart, N. H., and Donovan, M. (1983). Fine Structure of the Chorion and Site of Sperm Entry in the Egg ofBrachydanio. *J. Exp. Zool.* 227, 277–296. doi:10.1002/jez.1402270212

Herberg, S., Gert, K. R., Schleiffer, A., and Pauli, A. (2018). The Ly6/uPAR Protein Bouncer Is Necessary and Sufficient for Species-specific Fertilization. *Science* 361, 1029–1033. doi:10.1126/science.aat7113

Inoue, N., Ikawa, M., Isotani, A., and Okabe, M. (2005). The Immunoglobulin Superfamily Protein Izumo Is Required for Sperm to Fuse with Eggs. *Nature* 434, 234–238. doi:10.1038/nature03362

Inoue, N., Hamada, D., Kamikubo, H., Hirata, K., Kataoka, M., Yamamoto, M., et al. (2013). Molecular Dissection of IZUMO1, a Sperm Protein Essential for Sperm-Egg Fusion. *Development (Cambridge)* 140, 3221–3229. doi:10.1242/dev.094854

Inoue, N., Hagihara, Y., and Wada, I. (2021). Evolutionarily Conserved Sperm Factors, DCST1 and DCST2, Are Required for Gamete Fusion. *eLife* 10, e66313. doi:10.7554/eLife.66313

Jumper, J., Evans, R., Pritzel, A., Green, T., Figurnov, M., Ronneberger, O., et al. (2021). Highly Accurate Protein Structure Prediction with AlphaFold. *Nature* 596, 583–589. doi:10.1038/s41586-021-03819-2

Kaji, K., Oda, S., Shikano, T., Ohnuki, T., Uematsu, Y., Sakagami, J., et al. (2000). The Gamete Fusion Process Is Defective in Eggs of Cd9-Deficient Mice. *Nat. Genet.* 24, 279–282. doi:10.1038/73502

Lamas-Toranzo, I., Hamze, J. G., Bianchi, E., Fernández-Fuertes, B., Pérez-Cerezales, S., Laguna-Barraza, R., et al. (2020). TMEM95 Is a Sperm Membrane Protein Essential for Mammalian Fertilization. *eLife* 9, e53913. doi:10.7554/eLife.53913

le Naour, F., Rubinstein, E., Jasmin, C., Prenant, M., and Boucheix, C. (2000). Severely Reduced Female Fertility in CD9-Deficient Mice. *Science* 287, 319–321. doi:10.1126/science.287.5451.319

Letunic, I., and Bork, P. (2021). Interactive Tree of Life (iTOL) V5: an Online Tool for Phylogenetic Tree Display and Annotation. *Nucleic Acids Res.* 49, W293–W296. doi:10.1093/nar/gkab301

Miyado, K., Yamada, G., Yamada, S., Hasuwa, H., Nakamura, Y., Ryu, F., et al. (2000). Requirement of CD9 on the Egg Plasma Membrane for Fertilization. *Science* 287, 321–324. doi:10.1126/science.287.5451.321

Nishimura, K., Han, L., Bianchi, E., Wright, G. J., de Sanctis, D., and Jovine, L. (2016). The Structure of Sperm Izumo1 Reveals Unexpected Similarities with Plasmodium Invasion Proteins. *Curr. Biol.* 26, R661–R662. doi:10.1016/j.cub.2016.06.028

Noda, T., Lu, Y., Fujihara, Y., Oura, S., Koyano, T., Kobayashi, S., et al. (2020). Sperm Proteins SOF1, TMEM95, and SPACA6 Are Required for Sperm–oocyte Fusion in Mice. *Proc. Natl. Acad. Sci. USA* 117, 11493–11502. doi:10.1073/pnas.1922650117

Noda, T., Blaha, A., Fujihara, Y., Gert, K., Emori, C., Deneke, V. E., et al. (2021). Sperm Membrane Proteins DCST1 and DCST2 Are Required for the Sperm-Egg Fusion Process in Mice and Fish. bioRxiv [Preprint]. Available at: https://www.biorxiv.org/content/10.1101/2021.04.18.440256 (Accessed October 28, 2021).

Schoch, C. L., Ciufo, S., Domrachev, M., Hotton, C. L., Kannan, S., Khovanskaya, R., et al. (2020). NCBI Taxonomy: A Comprehensive Update on Curation, Resources and Tools, *Database* 2020, 1–21. doi:10.1093/database/baaa062

Sievers, F., Wilm, A., Dineen, D., Gibson, T. J., Karplus, K., Li, W., et al. (2011). Fast, Scalable Generation of High-Quality Protein Multiple Sequence Alignments Using Clustal Omega, *Mol. Syst. Biol.* 7, 539. doi:10.1038/msb.2011.75

Stein, P., Savy, V., Williams, A. M., and Williams, C. J. (2020). Modulators of Calcium Signalling at Fertilization. *Open Biol.* 10, 200118. doi:10.1098/RSOB.200118

Waterhouse, A. M., Procter, J. B., Martin, D. M. A., Clamp, M., and Barton, G. J. (2009). Jalview Version 2--a Multiple Sequence Alignment Editor and Analysis Workbench. *Bioinformatics* 25, 1189–1191. doi:10.1093/bioinformatics/btp033

Wolenski, J. S., and Hart, N. H. (1987). Scanning Electron Microscope Studies of Sperm Incorporation into the Zebrafish (Brachydanio) Egg. *J. Exp. Zool.* 243, 259–273. doi:10.1002/jez.1402430211

Yanagimachi, R., Cherr, G., Matsubara, T., Andoh, T., Harumi, T., Vines, C., et al. (2013). Sperm Attractant in the Micropyle Region of Fish and Insect Eggs1. *Biol. Reprod.* 88, 47. doi:10.1095/biolreprod.112.105072

Conflict of Interest: The authors declare that the research was conducted in the absence of any commercial or financial relationships that could be construed as a potential conflict of interest.

Publisher's Note: All claims expressed in this article are solely those of the authors and do not necessarily represent those of their affiliated organizations, or those of the publisher, the editors and the reviewers. Any product that may be evaluated in this article, or claim that may be made by its manufacturer, is not guaranteed or endorsed by the publisher.

frontiers in Cell and Developmental Biology

REVIEW
published: 07 January 2022
doi: 10.3389/fcell.2021.807313

HAP2-Mediated Gamete Fusion: Lessons From the World of Unicellular Eukaryotes

Jennifer F. Pinello[1†] *and Theodore G. Clark*[2*†]

[1]*Department of Cell Biology and Molecular Genetics, University of Maryland, College Park, MD, United States,* [2]*Department of Microbiology and Immunology, Cornell University, Ithaca, NY, United States*

Most, if not all the cellular requirements for fertilization and sexual reproduction arose early in evolution and are retained in extant lineages of single-celled organisms including a number of important model organism species. In recent years, work in two such species, the green alga, *Chlamydomonas reinhardtii*, and the free-living ciliate, *Tetrahymena thermophila*, have lent important new insights into the role of HAP2/GCS1 as a catalyst for gamete fusion in organisms ranging from protists to flowering plants and insects. Here we summarize the current state of knowledge around how mating types from these algal and ciliate systems recognize, adhere and fuse to one another, current gaps in our understanding of HAP2-mediated gamete fusion, and opportunities for applying what we know in practical terms, especially for the control of protozoan parasites.

Keywords: *Tetrahymena thermophila*, *Chlamydomonas reinhardtii*, HAP2/GCS1, membrane fusion, fertilization

OPEN ACCESS

Edited by:
Maria Jiménez-Movilla, University of Murcia, Spain

Reviewed by:
Gavin Wright, University of York, United Kingdom
Tomoko Igawa, Chiba University, Japan

***Correspondence:**
Theodore G. Clark
tgc3@cornell.edu

†These authors have contributed equally to this work

Specialty section:
This article was submitted to Molecular and Cellular Reproduction, a section of the journal Frontiers in Cell and Developmental Biology

Received: *02 November 2021*
Accepted: *15 November 2021*
Published: *07 January 2022*

Citation:
Pinello JF and Clark TG (2022) HAP2-Mediated Gamete Fusion: Lessons From the World of Unicellular Eukaryotes. Front. Cell Dev. Biol. 9:807313. doi: 10.3389/fcell.2021.807313

1 INTRODUCTION

Sexual reproduction was almost certainly present in the last eukaryotic common ancestor (LECA) and continues to be an important if not essential part of the life cycle of organisms ranging from metazoans to single-celled protists (Goodenough and Heitman, 2014; Speijer et al., 2015; Brandeis, 2021). While sex is often cryptic in microbial eukaryotes (Dunthorn and Katz, 2010; Hofstatter and Lahr, 2019), it is readily observed and easy to manipulate in several well-studied model organism species including *Chlamydomonas reinhardtii* and *Tetrahymena thermophila*. Indeed, these simple to grow, genetically tractable systems have yielded important insights into the basic principles underlying gamete-gamete interactions culminating with membrane fusion. This is perhaps best exemplified in recent work on HAP2/GCS1, an ancient gamete fusogen that is now recognized as a catalyst for zygote formation in representative species across all of the major eukaryotic kingdoms of life (Mori et al., 2006; Steele and Dana, 2009; Mori et al., 2015; Speijer et al., 2015).

Elucidation of the role of *HAP2/GCS1* in fertilization began with independent studies in *Arabidopsis thaliana* (Johnson et al., 2004; von Besser et al., 2006), *Lilium longiflorum* (Mori et al., 2006) and *Chlamydomonas reinhardtii* (Liu et al., 2008) demonstrating the necessity of corresponding gene products for male fertility and suggesting their potential role in gamete fusion. Subsequent studies demonstrated that HAP2 is, in fact, a class II (CII) membrane fusogen whose structural features closely mimic those of envelope proteins from Dengue, Zika and related viruses, as well as cell-cell fusion proteins (AFF-1 and EFF-1) from the nematode worm, *C. elegans* which adopt a similar fold (Fédry et al., 2017; Pinello et al., 2017; Valansi et al., 2017). The presence of CII fusogens in eukaryotic cells and the viruses that infect them has interesting and important implications for the origins of sex, the evolution of class II membrane fusogens more generally, and the molecular mechanisms by which HAP2 catalyzes the formation of membrane pores between male and female

gametes (Wong and Johnson, 2010; Doms, 2017; Fédry et al., 2017; Pinello et al., 2017; Valansi et al., 2017; Clark, 2018).

The following review addresses our current understanding of gamete recognition, adherence, and fusion in *Chlamydomonas reinhardtii* and *Tetrahymena thermophila*, with an emphasis on the role of HAP2 in membrane fusion and how the HAP2/GCS1 machinery could potentially be exploited to block the transmission of parasitic protists to prevent disease.

2 *CHLAMYDOMONAS REINHARDTII* AND *TETRAHYMENA THERMOPHILA* AS MODEL ORGANISMS

Owing principally to their ease of growth and facile genetics, *Chlamydomonas reinhardtii* and *Tetrahymena thermophila* have served as key models for studies of eukaryotic cellular and molecular biology since the 1960s (Harris, 2001; Collins, 2012; Orias, 2012; Ruehle et al., 2016; Salomé and Merchant, 2019). A free-living freshwater ciliate that feeds largely on bacteria, *T. thermophila* inhabits lakes and ponds in eastern and central North America. *C. reinhardtii*, on the other hand, is a biciliated unicellular green alga, known principally as a temperate soil dweller but is also found in freshwater ecosystems across a wide geographic range (Sasso et al., 2018).

In the laboratory, *Tetrahymena* and *Chlamydomonas* grow rapidly on inexpensive media in small and large volume cultures, and clonal isolates can be preserved for long-term use (Cassidy-Hanley, 2012; Harris, 2013). More importantly, their sexual cycles can be readily induced and synchronized to generate gametes or mating types that can pair and undergo fertilization in a highly predictable manner. Indeed, gamete fusion in both systems occurs at specific, identifiable regions of mating cells allowing in-depth studies of membrane dynamics during gamete merger. Furthermore, the application of forward and reverse genetics in these systems has made possible the identification of proteins involved in gamete recognition and signaling, membrane adhesion and fusion, and revealed many of the molecular details of fertilization that apply not just to protists but metazoans as well.

Aside from work on HAP2/GCS1 and fertilization more generally, *Tetrahymena* has served as a key model for the study of genome editing (Cheng et al., 2019); stimulus-dependent secretion (Turkewitz, 2004); ciliary and microtubule-based motility (Gibbons and Rowe, 1965; Vale and Yano Toyoshima, 1988; Suryavanshi et al., 2010; Reynolds et al., 2018); ribosome structure and function (Rabl et al., 2011; Wilson and Doudna Cate, 2012); transgenerational inheritance and the role of small RNAs in chromatin dynamics (Couzin, 2002; Liu et al., 2007; Noto and Mochizuki, 2017; Neeb and Nowacki, 2018; Bastiaanssen and Joo, 2021). *Tetrahymena* has also been responsible for major discoveries in the areas of telomere structure and biosynthesis (Blackburn et al., 2006; Jiang et al., 2015); catalytic (self-splicing) RNAs (Herschlag and Cech, 1990; Hedberg and Johansen, 2013); and the role of histone modifications in gene expression (Brownell et al., 1996; Allis and Jenuwein, 2016; Wahab et al., 2020).

Similarly, *Chlamydomonas* has a rich history of important scientific contributions in the areas of photosynthesis and chloroplast structure (Levine and Goodenough, 1970; Engel et al., 2015); ciliary motility, biogenesis and intraflagellar transport (Rosenbaum and Witman, 2002); channelrhodopsins and their applications in optogenetics (Nagel et al., 2003; Zhang et al., 2006; Hegemann and Nagel, 2013); algal biofuel production (Beer et al., 2009; Gimpel et al., 2013); as well as gamete fusion (Ferris et al., 1996; Ferris and Goodenough, 1997; Kurvari et al., 1998; Wang et al., 2006; Liu et al., 2008; Fédry et al., 2017; Zhang et al., 2021).

Genetic strains and other materials including plasmids, BACs, fosmids, educational kits, protocols and other resources are available for *Tetrahymena thermophila* and *Chlamydomonas reinhardtii* through established stock centers at Cornell University, Washington University in St. Louis, and the University of Minnesota (https://tetrahymena.vet.cornell.edu/; https://www.chlamycollection.org/). Additional resources for experimental work in these systems include well maintained genomic and transcriptomic databases (Stover et al., 2012; Xiong et al., 2013; Gallaher et al., 2015, 2018; Blaby and Blaby-Haas, 2017; Sheng et al., 2020). The availability of mRNA expression data for genes that are differentially regulated in resting, lysin-treated, and activated *plus* and *minus* gametes of *C. reinhardtii* (Ning et al., 2013), as well as vegetatively growing, starved and conjugating *T. thermophila* (Miao et al., 2009; Xiong et al., 2013) are particularly relevant to fertilization research.

3 SEXUAL REPRODUCTION IN *CHLAMYDOMONAS* AND *TETRAHYMENA*: OVERVIEW

The principal stages leading up to and including gamete fusion in *Chlamydomonas* and *Tetrahymena* are shown in **Figure 1**. In the case of *C. reinhardtii*, vegetatively growing haploid cells are genetically destined to express either of two mating types, *plus* (+) or *minus* (−) when deprived of nitrogen in the presence of blue light. These conditions bring mating type-specific genes into expression, enabling *plus* and *minus* mating types to eventually pair and then fuse to form zygotes (Ferris and Goodenough, 1997; Goodenough et al., 2007). Pairing begins with interactions between cilia that then triggers cell wall release and the formation of distinct mating structures which protrude from each cell, eventually contacting each other at their distal tips (Cole et al., 2015, 2018). HAP2/GCS1 localizes to the mating structures of *minus* (−) gametes and is essential for initiating formation of a fusion pore that expands into a single contiguous membrane around both cells forming the zygote (Liu et al., 2008, 2015). Subsequent stages of the life cycle, include nuclear fusion (karyogamy) (Ning et al., 2013), zygospore development, meiosis and the formation of four haploid progeny that will divide mitotically when nitrogen is restored (Goodenough et al., 2007).

In the case of *T. thermophila*, sexual reproduction is induced by nutrient starvation, which initiates a program of new gene

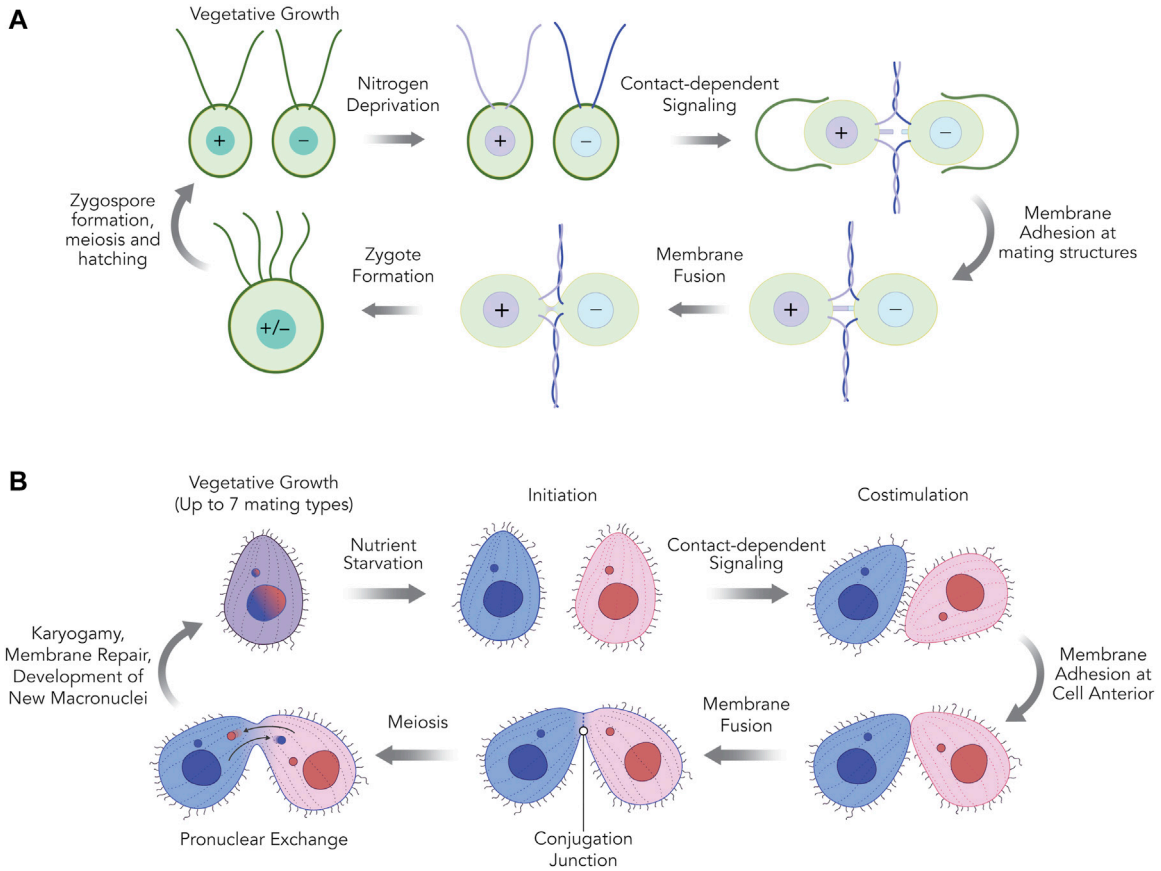

FIGURE 1 | The mating reactions of *Chlamydomonas reinhardtii* **(A)** and *Tetrahymena thermophila* **(B)** cells. **(A)** In *C. reinhardtii*, when asexually dividing haploid cells of *plus* or *minus* mating types are deprived of nitrogen, they undergo gametogenesis. After *plus* and *minus* gametes are mixed, adhesion between *plus* and *minus* cilia stimulate gamete activation; a cyclic AMP-dependent signaling pathway leading to cell wall loss, upregulation of gamete-specific genes, and the maturation of a single membranous protrusion between the two cilia called the mating structure. The tips of the *plus* and *minus* mating structure membranes adhere and fuse quickly, producing a single quadriciliated zygote (~10 min). Following ciliary resorption, zygotes develop into a resilient dormancy stage with a hard outer cell wall called the zygospore, which is maintained until environmentally favorable (nitrogen-replete) conditions return. Meiosis and hatching of the zygospore produces four haploid progeny cells (two *minus* and two *plus*) capable of vegetative growth. **(B)** In *T. thermophila,* when asexually dividing cells of any of the seven different mating types are deprived of nutrients they undergo "initiation" allowing subsequent sexual interactions. An initiated mating type can undergo conjugation with any of the other six mating types, but not their own. After initiated cells of two different mating types are mixed, physical interactions between the two cells further activate and mature the cells in a contact-dependent stage known as "costimulation," leading to the upregulation of specific genes and the maturation of a patch of membrane at the anterior end of the cell where mating cells eventually adhere. Membrane adhesion is weak at first but then becomes tight, and by ~2.5 h cell pairs are firmly joined at a crescent-shaped zone of membrane studded with hundreds of fusion pores called the conjugation junction. Between 5–6 h after mixing, haploid pronuclear products of meiosis made in each of the two partner cells are exchanged across the conjugation junction and fuse to a stationary haploid pronucleus in the partner to create a zygotic nuclear product. These zygotic nuclei undergo further differentiation within their respective cells and at about 10–11 h after mixing, the membrane fusion pores at the conjugation junction are repaired and the two cells separate from one another. Upon return to nutrient-replete conditions, the exconjugant cells immediately divide, generating four progeny "karyonide" cells capable of vegetative growth.

expression that activates the early stages of mating competence (Bruns and Brussard, 1974; Wellnitz and Bruns, 1979; Xiong et al., 2013). Transient contacts between starved cells of different mating type (referred to as "co-stimulation") then lead to the upregulation of a further set of genes including those required for adhesion and gamete fusion. Notably, this stage is also accompanied by the remodeling of a region at the anterior of cells where different mating types eventually form tight pairs known as the nuclear exchange or conjugation junction (Pagliaro and Wolfe, 1987; Cole, 2006; Cervantes et al., 2013; Xiong et al., 2013). Following these interactions, HAP2/GCS1 localizes to the junction and catalyzes the formation of a hundred or more individual membrane pores that expand over time to form a lacy curtain separating cells (Cole et al., 2014, 2015). Subsequent stages of sexual development include meiosis, the exchange of migratory haploid pronuclei across the conjugation junction, karyogamy, the development of new macronuclei, restoration of membrane integrity in mating pairs, and separation of progeny cells that will divide mitotically when nutrients are restored. Rather than being sexually dichotomous, *Tetrahymena thermophila* can express up to seven different mating types that are established randomly through genome rearrangements at the mating type (*mat*) locus following sexual conjugation. Individual mating types can be isolated as clonal lines that express

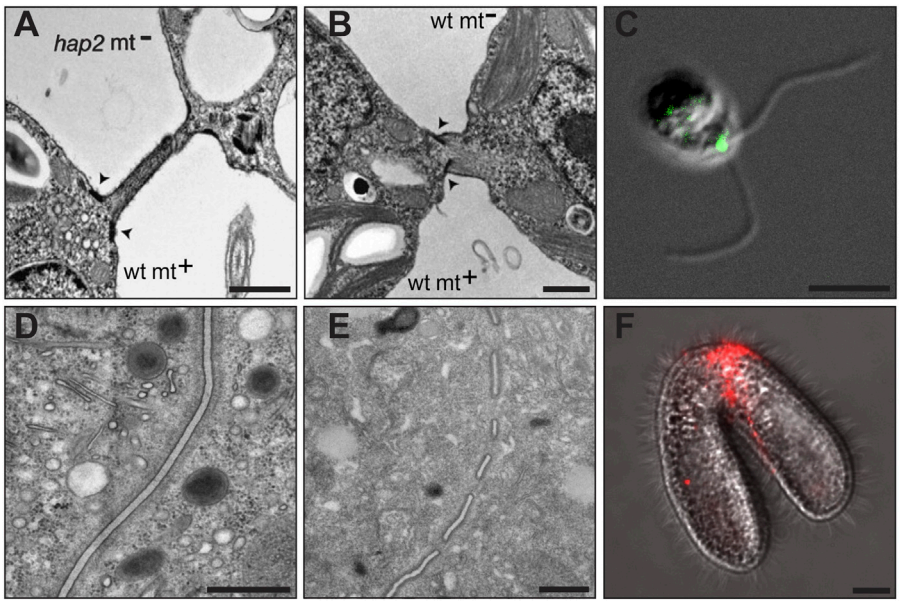

FIGURE 2 | HAP2-mediated membrane fusion in *Chlamydomonas* **(A–C)** and *Tetrahymena* **(D–F)***. **(A)** A transmission electron micrograph (TEM) of *Chlamydomonas* gametes showing the adhering mating structures between a *minus* gamete in which the *HAP2* gene was disrupted (*hap2* mt⁻) and a wild type *plus* gamete (wt mt+). Arrowheads point to the electron dense doublet regions at the base of the *plus* gamete mating structure. *Minus* gametes lacking HAP2 adhere to *plus* gametes by the tips of their mating structures but fail to fuse. **(B)** A TEM of wild type *Chlamydomonas plus* and *minus* mating structures immediately after membrane fusion occurs. The fusion pore continues to expand giving way to a single continuous membrane surrounding zygote. **(C)** An immunofluorescence image of a *Chlamydomonas minus* gamete showing a green punctum where HA-tagged HAP2 protein localizes between the two cilia, the site of the *minus* mating structure. **(D)** A TEM showing membranes at the conjugation junction of a *Tetrahymena* mating pair in which both cells have the *HAP2* gene deleted and are unable to form fusion pores. Note the continuous membranes in the center of the image extending from top to bottom. **(E)** A TEM showing multiple membrane fusion pores at the conjugation junction of a wild type mating pair of *Tetrahymena* cells. In wild type pairs, numerous pores, or interruptions are present along the length of the junctional membranes that continue to expand, but never extend beyond the junction itself and are eventually repaired at the conclusion of mating to allow cells to separate. **(F)** An immunofluorescence image of a *Tetrahymena* mating pair showing a red band of signal where HA-tagged HAP2 protein localizes to the conjugation junction between the two mating cells, the site of membrane fusion pore formation. Scale bars are 200 nM **(A–B)**, 5 μMb **(C)**, 500 nM **(D-E)**, and 10 μM **(D)**. *TEMs of interacting *Chlamydomonas* gametes, originally published by Liu et al. in Genes & Development 2008 Apr 15; 22(8):1,051-68 (DOI: 10.1101/gad.1656508) were adapted for this figure and are used here with permission from the authors under license # CC-BY-NC 4.0. TEMs and immunofluorescence image of mating *Tetrahymena* cells, originally published by Cole et al. in Current Biology 2014 Sep 22; 24(18):2,168–2,173 (DOI: 10.1016/j.cub.2014.07.064) were adapted for this figure and are used here with the permission of the journal.

a single mating type when sexual reproduction is activated (see below). A given mating type can mate with any of the other six mating types but not with itself.

3.1 Acquisition of Mating Competence: Nutrient Deprivation and Cell-Cell Signaling

Acquisition of mating competence in *C. reinhardtii* is induced by suspending vegetatively growing *plus* or *minus* cells in nitrogen-free medium for at least 6 h in the presence of light (Sager and Granick, 1954; Harris, 2009). Nitrogen starvation promotes the formation pre-gametes (Treier et al., 1989; Beck and Acker, 1992) and activates a phototropin responsible for blue light detection (Huang and Beck, 2003). Exposure to light then mediates a signaling cascade responsible for new gene expression and pre-gamete maturation (Pan et al., 1996, 1997).

At the cellular level, nitrogen depletion and gamete maturation are accompanied by a reduction in photosynthetic activity, along with degradation of chloroplasts and cellular ribosomes (Sager and Granick, 1954; Harris, 2009). Transcriptional profiling studies have identified early-, middle-, and late-expressed genes throughout the process that provide molecular markers for the various stages of gametic differentiation (Treier and Beck, 1991; Abe et al., 2004). Interestingly, like *Tetrahymena*, the differentiation of *C. reinhardtii* into mating competent gametes is a reversible process. In the case of *C. reinhardtii,* the re-introduction of nitrogen-replete media in the presence of light will cause cells to revert to a vegetative, asexually dividing state (Sager and Granick, 1954).

Until recently, pheromone-like substances capable of modulating the behavior *C. reinhardtii* gametes had not been identified. In 2019, however, a 23 amino acid amidated peptide that can attract *minus* gametes and repel *plus* gametes was described (Luxmi et al., 2019). This peptide (a short peptide fragment from the cellular protein Cre03.g204500), along with the enzymatic machinery for conversion of peptidylglycine substrates into α-amidated products, was shown to be released from cells via ciliary ectosomes during gametogenesis (Luxmi et al., 2019). While it is not yet clear if this factor is a true pheromone, it is tempting to speculate that bioactive peptides could play such a role in natural aquatic settings where dispersed gametes must find each other to mate.

Regardless of a role for putative pheromones in mating behavior, when mature *plus* and *minus* gametes of *C.*

reinhardtii are mixed, they quickly adhere through interactions between their cilia (**Figure 2**). Cultures with large numbers of equally mixed *plus* and *minus* gametes agglutinate and form aggregates. Aggregates eventually sort themselves into individual *plus* and *minus* pairs that then fuse. Ciliary adhesion is mediated by multi-pass transmembrane proteins (agglutinins) on *plus* and *minus* gametes named SAG1 and SAD1, respectively (Goodenough et al., 1978; Hwang et al., 1981; Ferris et al., 2005). Interactions between these proteins trigger protein kinase- and kinesin-2 dependent activation of a ciliary adenylyl cyclase, followed almost immediately by a near 20-fold increase in intracellular levels of cAMP (Zhang et al., 1991; Saito et al., 1993; Pan and Snell, 2002; Wang et al., 2006; Snell and Goodenough, 2009).

Elevation of intracellular cAMP is required for all subsequent morphological changes associated with gamete activation, including the enlargement of ciliary tips, cell wall loss, and the emergence of mating structures (Pasquale and Goodenough, 1987). Although SAG1 and SAD1 are detectable on cilia of naive gametes, the majority is present on plasma membranes. Interestingly, SAG1 has been shown to be recruited from the cell body to cilia in a microtubule-dependent fashion (Ranjan et al., 2019) and appears to be shed from cilia in association with ectosomes (Cao et al., 2015; Wood and Rosenbaum, 2015). Addition of purified SAG1-containing ectosomes to cultures of naive *minus* gametes causes isoagglutination and gamete activation in the absence of a mating partner. Similarly, addition of exogenous dibutyryl cAMP, together with inhibitors of cyclic nucleotide phosphodiesterase, bypasses the requirements for ciliary recognition and can alone stimulate the morphological changes that accompany gamete activation (Pijst et al., 1984; Pasquale and Goodenough, 1987).

As noted above, removal of the cell wall, a prerequisite for gamete fusion, is also triggered by elevated intracellular cAMP. Cell wall lysis is catalyzed by a secreted zinc metalloproteinase termed gametic lysin (Claes, 1971; Schlösser et al., 1976; Buchanan and Snell, 1988) that is stored in an insoluble inactive state in the periplasm (Claes, 1977; Matsuda et al., 1978; Buchanan et al., 1989). Upon agglutination and elevation of intracellular cAMP, the enzyme becomes activated through cleavage by a serine-like protease resulting in cell wall dissolution (Snell et al., 1989; Luxmi et al., 2018). Interestingly, the cell wall of *Chlamydomonas* is composed of hydroxyproline-rich glycoproteins rather than cellulose (Horne et al., 1971; Adair and Mecham, 1990; Woessner and Goodenough, 1992; Ferris et al., 2001). Likewise, many *Chlamydomonas* gamete-specific proteins involved in recognition and adhesion (*e.g.* SAG1, SAD1, and MAR1) contain hydroxyproline-rich repeats (Adair, 1985), although it is unclear whether any of these are substrates for gametic lysin.

In addition to control by cAMP, experiments using the calcium ionophore A23187 have demonstrated a role for Ca^{++}-signaling in cell wall dissolution. In these studies, A23187 by itself triggered cell wall lysis of both *plus* and *minus* mating types in isolation (Claes, 1980). Later studies showed that lidocaine (in a manner reversible by addition of Ca^{2+} and Mg^{2+}) inhibited cell wall loss without interfering with ciliary agglutination or tip activation (Snell et al., 1982). While the pharmacology of calcium channels in *C. reinhardtii* is still under scrutiny (Liang and Pan, 2013), these findings suggested that elevation of cAMP may alter channel activity in ciliary membranes allowing Ca^{++} entry, secretion of stored gametic lysin and cell wall dissolution.

Following cell wall removal, membrane protuberances known as mating structures form at the anterior of cells between the cilia. Formation of the mating structures along with subsequent membrane events associated directly with gamete fusion in *C. reinhardtii* are described below (*Membrane dynamics at sites of gamete fusion*).

In *Tetrahymena thermophila*, nutritional starvation is achieved by washing cells of different mating types into low ionic strength buffers for 70–75 min at 30°C (Wellnitz and Bruns, 1979). The period of "initiation" prior to allorecognition (that is, physical contacts between cells of different mating types) is accompanied by up-regulation of >200 genes (Xiong et al., 2013) and is inhibited by elevated buffer concentrations (Wellnitz and Bruns, 1979). Once initiation is complete, cells of different mating types can be combined into a single flask, allowing contacts between cells, effectively synchronizing the later stages of sexual development.

Transient interactions between cells (referred to as "co-stimulation") triggers a new round of RNA and protein synthesis involving up-regulation of >1,800 genes (Xiong et al., 2013), many of which, including *HAP2/GCS1,* turn on almost immediately after cells are combined (Cole et al., 2014). While the signaling pathways activated during this stage have yet to be defined, several factors come into play during co-stimulation. First, a non-mating type specific substance is continuously released from cells in response to nutritional starvation and is necessary for different mating types to advance to full mating competence during the process of co-stimulation (Adair et al., 1978; Wolfe et al., 1979). This material is relatively heat stable and non-dialyzable, although its identity and role in cell-cell signaling are unknown.

Along with this "soluble" factor, different mating types must undergo multiple direct contacts between cells over a period of at least 20 min to activate the downstream events required for tight (that is, mechanically stable) pairing, which begins approximately 1 h after starved cells are mixed (Brown et al., 1993). Interestingly, as cells become activated, they initially form weak, transient pairs that can be either homotypic (between cells of the same mating type) or heterotypic (between cells of different mating type). Only heterotypic interactions provide the signals necessary to fully activate cells. Nevertheless, the fact that weak homotypic pairing occurs in the lead-up to conjugation suggests that cells produce both (mating type) specific and non-specific adhesive molecules as they become activated (Cole, 2016).

While the signaling pathways triggered by collisions between different mating types of *T. thermophila* are still unknown, there is substantial indirect evidence that, as in the case of *C. reinhardtii*, activation is initiated through contacts between cilia (Love and Rotheim, 1984; Wolfe et al., 1993). First and foremost, deciliated cells are unable to pair (Wolfe et al., 1993). Experiments to explore whether purified cilia from one mating

type can induce mating competence in cells of a different mating type have nevertheless failed because free cilia are phagocytosed and act as a protein source, eliciting starved cells to exit the sexual cycle and begin vegetative growth (Wolfe et al., 1993).

Irrespective of the role of cilia in contact-dependent signaling, the weak homotypic interactions that occur early after starved cells are combined, eventually give way to more numerous and stable interactions between cells of different mating types. Such interactions occur primarily along the ventral surfaces of cells, anterior to the oral apparatus where mating cells eventually form "tight" pairs along a specialized region known as the conjugation junction (Cole, 2006, Cole, 2016) (**Figure 1**). The lead up to tight pairing is accompanied by major structural changes at the cell cortex where the junction eventually forms including loss of dense core secretory granules, alveolar membranes, cilia and ciliary basal bodies, along with changes in shape at the cell anterior from pointed to slightly blunt (Wolfe and Grimes, 1979). More global changes in overall cell shape (e.g., shortening along the longitudinal axis) have also been noted (Fujishima et al., 1993).

Coincident with these structural alterations, concanavalin-A (Con-A) binding receptors at the plasma membrane become concentrated at the cell anterior, a phenomenon known as Con-A "tipping" (Wolfe and Grimes, 1979; Wolfe and Feng, 1988). The addition of Con-A to live cells during "co-stimulation" blocks the formation of mating pairs suggesting that glycosylated receptors (presumably, membrane glycoproteins) play a role in adhesion. The redistribution of Con-A receptors to the nascent conjugation junction along with the changes in cell shape that accompany mating would also argue for the involvement of the cytoskeleton in the events leading up to adhesion and membrane pore formation. Coincidentally, Con-A has been shown to block the mating reaction in *Chlamydomonas* as well, although by an entirely different mechanism that involves an inhibition of cell wall dissolution (Claes, 1975), possibly through lectin binding to gametic lysin (Snell et al., 1982).

3.2 Mating Type Determination

At the genetic level, mating types of *Chlamydomonas* and *Tetrahymena* are governed by genes at specific chromosomal regions known as the mating type loci. In *C. reinhardtii*, the mating type locus encompasses a genetically complex, 0.2–0.4 Mbp region on chromosome six that is rearranged between the two mating-type haplotypes and orchestrates the expression of genes for gamete recognition, adhesion, and fusion, as well as genes involved in sporulation, mitochondrial and chloroplast inheritance (Goodenough et al., 1995; Ferris et al., 2002; De Hoff et al., 2013). Underlying control of these genes is the RWP-RK transcription factor, Minus Dominance, or *MID*, a master regulator expressed in *minus* mating type cells following cAMP-dependent activation (Ferris and Goodenough, 1997; Lin and Goodenough, 2007).

MID is only present at the mating type locus of minus cells and exerts its control by suppressing *plus* gamete-specific developmental programs and stimulating the expression of *minus* gamete-specific genes such as HAP2 and MAR1 (see below) that lie outside the locus itself (Ferris and Goodenough, 1997; Lin and Goodenough, 2007). For example, the presence of MID blocks the expression of *plus* gamete specific ciliary agglutinin SAG1, but induces the expression of the *minus* gamete-specific agglutinin SAD1 (Sekimoto, 2017). In *minus* cells, mutations of MID promote differentiation into infertile "pseudo-*plus*" gametes, while the forced expression of MID in *plus* cells leads to their differentiation into minus gametes (Ferris and Goodenough, 1997; Goodenough and Heitman, 2014). As with C. *reinhardtii*, ectopic expression of MID in female (*plus*) gametes of the related alga, V. *carteri*, leads to a pseudo-male gametic phenotype (Geng et al., 2014), and MID orthologs can be functionally substituted between different species of algae (Geng et al., 2018). These findings demonstrate a conserved role of MID in algal mating type determination, and indicate that plus/female gamete differentiation is the default state in these systems (Goodenough and Heitman, 2014; Coelho and Umen, 2021).

Interestingly, MID homologs have been identified in other protists (*Dictyostelium discoideum* and *Entamoeba histolytica*) as well as in *land plants* (Riaño-Pachón et al., 2008; Blanc-Mathieu et al., 2017; Yamazaki et al., 2017; Geng et al., 2018). In contrast with algae, however, RWP-RK transcription factors in plants specify female gamete differentiation, while Myb transcription factors (DUO1 and DUO3) control spermatogenesis and upregulation of male gamete-specific transcripts such as HAP2 (Borg et al., 2011; Higo et al., 2018; Hisanaga et al., 2019).

Finally, aside from regulation at the transcriptional level, mating type ratios in *Chlamydomonas* are maintained through differences in sequence organization at the mating type loci of *plus* and *minus* cells, which have a suppressive effect on recombination within this region of chromosome 6 (Goodenough et al., 2007; De Hoff et al., 2013). As a consequence, the zygote is always heterozygous diploid with respect to the mating type locus and gives rise to four meiotic progeny at fixed ratios (*viz*., 2:2) of *plus* and *minus* cells that can easily be separated after hatching (Goodenough et al., 2007).

In the case of *Tetrahymena*, mating types are also specified by proteins encoded at the mating type locus (*mat*) (Nanney and Caughey, 1953; Orias et al., 2017). Nevertheless, rather than being inherited in a Mendelian fashion, mating types of *T. thermophila* are determined randomly and independently in cell progeny after fertilization has occurred (Cervantes et al., 2013; Orias et al., 2017). The molecular basis of mating type determination in *Tetrahymena* was established in landmark work by investigators at the University of California, Santa Barbara and the Wuhan Academy of Hydrobiology in 2013 (Cervantes et al., 2013). Briefly, the mating type genes encode pairs of transmembrane proteins designated, MTA and MTB, that are expressed upon starvation. While sexually mature vegetatively growing cells have the potential to express only a single mating type specified by one *MTA/MTB* gene pair in somatic macronuclei, germline micronuclei of inbred *T. thermophila* strains contain several incomplete *MTA*/*MTB* gene pairs (five or six depending on the micronuclear *mat* allele), specifying different mating types and organized in a tandem array at the *mat* locus. After fertilization and karyogamy, developing macronuclei undergo a series of immunoglobulin-like genome rearrangements that give rise to one functional *MTA/MTB* gene

pair at the *mat* locus, with each of the four progeny cells (karyonides) from a given mating having the potential to generate a different functional gene pair on a random basis (Cervantes et al., 2013).

The *MTA* and *MTB* genes of *T. thermophila* are distantly related and gave rise to paralogs in different *Tetrahymena* species presumably through gene duplication and mutational drift (Orias et al., 2017; Yan et al., 2021). Nevertheless, each of the seven MTA and MTB proteins have variable N-terminal extracellular domains with two tandem cysteine-rich furin-like repeat motifs of unknown function, along with C-termini containing five membrane-spanning helices. Mating type specificity most likely resides in the predicted extracellular portion of MTA and MTB, which comprise at least two thirds of each protein. The precise details of allorecognition remain to be established, and it is not known whether the MTA and MTB proteins act in concert (that is, as heterodimers) or independently, or whether they mediate the same or different aspects of recognition and adhesion, however the deletion of the corresponding genes impairs the ability of cells to pair or form progeny (Cervantes et al., 2013).

While mating type selection is a prerequisite for sex in *T. thermophila*, there is at least one additional step necessary for cells to achieve full sexual maturity. At some point after conjugation, vegetatively growing cells reach a stage termed "adolescence" where they can mate successfully with cells that are fully sexually mature, but not with other "adolescent" cells despite their ability to express compatible mating type proteins (Rogers and Karrer, 1985). Why this is true has yet to be determined, although it may be that these adolescent cells are unable to respond to, or deliver signals to other adolescent cells during the process of "co-stimulation" (Rogers and Karrer, 1985). Apparently, adolescent cells must undergo additional cell divisions to reach full sexual maturity.

3.3 Membrane Dynamics at Sites of Gamete Fusion

Despite similarities in the mechanisms that trigger mating competence in *Chlamydomonas* and *Tetrahymena*, the membrane events associated with gamete adherence and fusion in these systems are quite different. In *Chlamydomonas*, membrane fusion is initiated at the tips of so-called, mating structures (also known as "fertilization tubules"), microvillus-shaped protrusions of the plasma membrane at the anterior ends of *plus* and *minus* gametes between the two cilia (Weiss et al., 1977) (**Figures 2A,B**). In naive *plus* gametes, the mating structures bud from an area of electron density (referred to as "doublets") just beneath the plasma membrane and extend ~3 μM from the membrane at their maximal length (Cavalier-Smith, 1975; Goodenough and Weiss, 1975; Triemer and Malcolm Brown, 1975). *Plus* mating structures are supported by actin filaments *in vivo* and can be isolated from mechanically disrupted cells by differential centrifugation through sucrose and Percoll density gradients (Detmers et al., 1985; Wilson et al., 1997). *Minus* mating structures are more diminutive (~1 μM in length), have no obvious cytoskeletal support, and bud from an electron dense patch of membrane with no underlying doublet zone (Weiss et al., 1977; Goodenough et al., 1982). The extracellular surfaces of activated *plus* and *minus* mating structures appear to be coated with a fringe of proteinaceous material visible by transmission electron microscopy (Goodenough et al., 1982).

Interactions between the cilia bring the mating structures of each cell into close contact. Once contact occurs, membranes at the tips of the mating structures adhere and fuse. The cytoplasmic bridge linking the cells then shortens rapidly and the gametes themselves transition from a face-to-face to a side-to-side orientation as they continue to fuse laterally from anterior to posterior until they are completely merged (Snell and Goodenough, 2009). In mass cultures, the reaction is highly synchronous and 1:1 mixtures of *plus* and *minus* gametes complete fusion within ~10 min.

Recently, the FUS1-MAR1 receptor pair essential for mating structure adherence was identified. FUS1 is expressed only in *plus* gametes (Misamore et al., 2003), and the mating structures of *fus1 plus* gamete mutants (whose FUS1 gene is disrupted) are incapable of adhering to those of *minus* gametes despite normal interactions between cilia (i.e., agglutination) and activation (Ferris et al., 1996; Misamore et al., 2003). Transmission electron microscopy has shown that *fus1* gametes lack the proteinaceous fringe on the surface of their activated *plus* mating structures (Goodenough et al., 1982). Consistent with this, immunofluorescence localization studies have shown that FUS1 protein redistributes along the entire surface of the *plus* gamete mating structure when cells become activated (Misamore et al., 2003). The *FUS1* gene encodes an 823 amino acid glycoprotein with a long N-terminal extracellular domain, a single transmembrane helix, and a short cytoplasmic tail (Ferris et al., 1996). The extracellular region is characterized by seven immunoglobulin-like domains and bears a strong resemblance to the modeled protein structure of the plant sperm gamete adhesion protein, GEX2 (Mori et al., 2014; Pinello et al., 2021). This structural resemblance suggests that FUS1 and GEX2 may be members a conserved family of gamete adhesion proteins shared across green organisms.

Co-immunoprecipitation studies have shown that MAR1 and FUS1 directly interact through their respective ectodomains. Furthermore, disruption of the *MAR1* gene (*mar1*) in *minus* gametes prevents the adherence of mating structures and subsequent fusion in crosses with wild type *plus* gametes but has no effect on ciliary adhesion and gamete activation.

A transgene encoding a FLAG-tagged version of MAR1 can rescue adherence of mating structures and gamete fusion when introduced into *mar1 minus* cells. Furthermore, expression of the same construct can rescue adherence of mating structures when introduced into *minus* mutants carrying disruptions in both *mar1* and *hap2*, demonstrating a key role for MAR1 in membrane adhesion *per se* (Pinello et al., 2021). Immunofluorescence localization studies indicate that MAR1 is only expressed in *minus* gametes and localizes to sites where the mating structures appear in both naive and activated cells.

The *MAR1* gene encodes a 1018-residue, single-pass transmembrane protein with a long cytoplasmic tail. Orthologs

are present in only a few closely related algal species suggesting that MAR1 is a lineage-specific adhesion protein (Pinello et al., 2021). Interestingly, the MAR1 ectodomain contains a proline-rich region with five repeating "PPSPX" motifs that are seen in other *Chlamydomonas* hydroxyproline-rich glycoproteins such as SAG1 and SAD1 (Ferris et al., 2005). Notably, aside from its interactions with FUS1, MAR1 also interacts with the gamete fusogen, HAP2. Antibody pull-down studies have demonstrated that FLAG-tagged MAR1 can associate with HAP2-HA, and MAR1 is required for proper expression and localization of HAP2 on the mating structures of *minus* gametes as shown by immunofluorescence microscopy (Pinello et al., 2021). These interactions suggest that MAR1 and other lineage-specific gamete adhesion proteins may act as gatekeepers for the gamete membrane fusion reactions in *C. reinhardtii* and other species which rely on HAP2 for fertilization.

Aside from FUS1 and MAR1, mutant studies indicate that additional proteins may be involved in gamete adherence and fusion in *C. reinhardtii*. For example, a temperature sensitive *minus* gamete mutant, *gam10*, has been shown to allow adhesion between mutant (*minus*) and wild type (*plus*) cells via their mating structures but is blocked in gamete fusion (Forest, 1983). The *gam10* mutation is not *HAP2* since the *HAP2* gene is intact and also expressed in *gam10* cells (Liu et al., 2010). However, a mutant cell line with a *minus* phenotype similar to that of *gam10* has recently been identified that is defective in a gene with putative involvement in the 5-deoxystrigol biosynthetic pathway (Aksoy et al., 2021). Further characterization of this strain will be necessary to define a possible relationship with *gam10*, along with a potential role for the 5-deoxystrigol biosynthetic pathway in gamete adherence and/or fusion. In other studies, a disruption in *MID*, the master regulator of mating type determination, has suggested a role for additional proteins in gamete adhesion and/or fusion. In this case, the *imp11 minus* cell line, which is defective in *MID*, defaults to an infertile pseudo-*plus* phenotype. These cells lack the *plus* mating type locus (along with *FUS1*) and produce mating structures that are unable to adhere or fuse to wild type *minus* gametes. Interestingly, ectopic expression of a *FUS1* transgene in the *imp11* strain rescued the ability of these cells to undergo mating structure adhesion with wild type *minus* cells (Goodenough et al., 1982; Galloway and Goodenough, 1985; Ferris et al., 1996) but gamete fusion was still impaired (rapid fusion only occurred in response to pH shock) (Ferris and Goodenough, 1997; Misamore et al., 2003). Since the wild type *minus* gametes in those crosses expressed functional versions of HAP2 and MAR1, some uncharacterized protein(s) specified by the *plus* mating type locus (which is not present in the *imp11* mutant) likely contributes to efficient gamete fusion in *Chlamydomonas*.

Finally, while the mating structures of *plus* gametes contain abundant actin filaments, *plus* cells pretreated with cytochalasin D can be activated and produce mating structures that lack F-actin when mixed with *minus* gametes. These actin-less *plus* mating structures make contact with the tips of the mating structures of *minus* cells but membrane fusion is strongly inhibited in these pairs (Mesland et al., 1980; Goodenough et al., 1982; Detmers et al., 1983). Additionally, the *ida5* strain of *C. reinhardtii*, which contains a nonsense mutation in the sole actin gene of *C. reinhardtii* resulting in a large deletion towards the actin C-terminus, also shows greatly reduced gamete fusion (Kato-Minoura et al., 1997). These findings strongly suggest that filamentous actin within the *plus* gamete mating structure facilitates *Chlamydomonas* cell-cell adhesion and/or fusion and are certainly consistent with now growing evidence for the involvement of F-actin in cell-cell fusion in metazoan cells (Kim and Chen, 2019; Chan et al., 2020).

In the case of *Tetrahymena*, different mating types adhere and fuse at a specialized region near the anterior of cells known as the conjugation junction (Cole, 2006). The junction itself lacks structures normally associated with the cell cortex and instead becomes an organizing center for membrane remodeling events including the formation of hundreds of HAP2-dependent fusion pores (Cole et al., 2015, 2018). When viewed *en face*, the boundaries of the conjugation junction take the shape of an inverted heart, or chevron roughly 8–10 μm in diameter. The apposed membranes on either side are separated at a uniform distance of ~40 nm (**Figure 2**) and appear to be supported by proteinaceous scaffolds on their cytosolic face (Wolfe, 1982; Cole et al., 2015).

Initially, junctional membranes are planar and continuous, but as pairs begin to form, out-pocketings appear on both membranes extending into the extracellular space and towards the apposed membrane on either side of the junction. These protuberances (which are roughly the diameter of the mating structures of *Chlamydomonas*, viz., ~50 nm), eventually fuse with the apposed membrane creating pores along the length of the junction that connect the two cells (Cole et al., 2015). Over time, the pores expand laterally, eventually forming a network, or curtain of membrane tubules as their advancing fronts approach each other (Wolfe, 1982; Cole, 2006). The fact that membrane protuberances which mark the sites of membrane fusion are generated from both cells of a mating pair would clearly argue that the initiation of pore formation is not restricted to a single mating type in this species. That notion is strongly supported by the observation that *HAP2/GCS1* is expressed in all seven mating types of *T. thermophila* as well (see below).

Conventional electron microscopy, freeze fracture and 3-D reconstructions of cryopreserved sections (electron tomography) have offered spectacular views of junctional membranes during pore formation and expansion, along with insights into the complex nature of these processes (Wolfe, 1982; Orias et al., 1983; Cole et al., 2015, 2018). For example, following the initiation of pore formation, small vesicles or tubules are released into the extracellular (luminal) space at sites immediately adjacent to nascent pores, only to be enveloped by membrane clefts or folds extending into the lumen from sites more distal to the pores (Cole et al., 2014, 2015). These membrane high jinks result in the formation of what appear to be multivesicular bodies that are reclaimed into the cytoplasm with the overall process contributing to, if not underlying, pore expansion (Cole et al., 2015). Adding to the complexity, an entirely separate trans-junctional membrane reticulum (presumably an extension of the smooth endoplasmic reticulum), invades the pores from either side, coming in close

proximity to their borders (Cole et al., 2015). The close associations between the trans-junctional membrane reticulum and dynamic pore structures has suggested that lipid exchange between the two membrane systems may occur in order to support pore formation and expansion (Cole et al., 2015).

In this regard, it is worth noting that mass spectrometric imaging studies of mating cells indicate that membranes at the conjugation junction are depleted in the abundant cylindrical lipid, phosphatidyl choline, and are enriched in cone-shaped lipids such as 2-aminoethylphosphonolipid compared with membranes on the cell body (Ostrowski et al., 2004). This finding is clearly consistent with the large numbers of pores at the conjugation junction and their intrinsic membrane curvature. Somewhat paradoxically however, kinetic studies also suggest that depletion of phosphatidyl choline at the junctional membranes occurs after most cells have formed pores, which would argue that alterations in membrane lipids are not a driving force in the initiation of pore formation (Kurczy et al., 2010).

Although HAP2/GCS1 is almost certainly the catalyst for cell-cell fusion during fertilization in *T. thermophila* (see below), the complexities of pore formation and expansion revealed in ultrastructural studies clearly suggest that other proteins are involved in the initiation and resolution of membrane pores in this system. To identify such proteins, a variety of innovative approaches have been employed. Ethanol fixation and mechanical disruption of mating pairs by sonication has yielded structures remarkably similar in size and shape to the conjugation junction (Cole et al., 2008). Using a proteomics-based approach, it was possible to identify as many as 15 proteins associated with these structures (Cole et al., 2008), some of which were likely contaminants, and some, bona fide constituents of the conjugation junction including "fenestrin", a 64 kDa protein that had been linked to the nuclear exchange junction in previous work (Nelsen et al., 1994), and cytoskeletal proteins (epiC; α- and β-tubulin) that had also been localized to the conjugation junction using immuno-labeling techniques (Orias et al., 1983; Williams et al., 1987; Gaertig and Fleury, 1992; Williams et al., 1995).

Another fruitful approach towards identifying proteins involved in fertilization in the *Tetrahymena* system is illustrated by studies on Zfr1, a zinc-finger protein that appears to have a role in cell-cell pairing (Xu et al., 2012). *ZFR1* was identified as a member of a network of genes that is upregulated when starved cells of different mating types are mixed. Tagging and over-expression of the corresponding protein showed that the *ZFR1* gene product localizes to the conjugation junction. Consistent with its lack of expression during vegetative growth, deletion of the *ZFR1* gene had no apparent effect on mitotically growing cells (Xu et al., 2012). By contrast, crosses between nutritionally starved *ΔZFR1* knockout strains were found to be capable of forming pairs, but failed to complete normal sexual development (Xu et al., 2012). On closer inspection, *ΔZFR1* knockout pairs came apart earlier during the sexual cycle and were more sensitive to mechanical disruption when compared to wild type pairs. This unstable pairing phenotype clearly suggests that the corresponding gene product plays some role in the adherence of mating cells, and while Zfr1 is not predicted to be a membrane protein, it does contain a hydrophobic C-terminus and may traffic through the Golgi apparatus based on localization studies (Xu et al., 2012). Of course, an indirect role for Zfr1 in pair stability through an effect on other proteins cannot be ruled out. Regardless of the precise role of Zfr1 in membrane adhesion, reverse genetic approaches involving deletion of genes that are upregulated during conjugation have proven to be extremely informative in the case of both *ZFR1* and *HAP2* and could easily be applied to identify other proteins that play a role in membrane adhesion and/or pore formation in *Tetrahymena*.

Finally, less systematic approaches have allowed the identification of a number of other proteins that localize to the conjugation junction at different time points in mating and may play important roles in fertilization in the *Tetrahymena* system. Such proteins include, Cda13p, a small membrane protein believed to have a role in membrane trafficking that also localizes to a ring associated with the junction in the period immediately before and just after pronuclear exchange (Zweifel et al., 2009); BLT1, a β-tubulin multigene family member which localizes to micronuclei and micronuclear meiotic spindles of conjugating cells that transiently decorates the nuclear exchange junction (Pucciarelli et al., 2012); and TCB25 (Tcb2), a calcium-binding protein thought to play a role in pronuclear exchange (Hanyu et al., 1995; Cole et al., 2018).

3.4 HAP2-dependent Gamete Fusion

Genetic screens for male sterility in *Arabidopsis thaliana* identified *hap2* as one of 32 haploid-disrupting (*hapless*) genotypes that define pollen grain development and/or pollen tube growth and guidance in this species (Johnson et al., 2004). In parallel studies, transcriptional profiling of mRNAs expressed at different stages of pollen development in *Lilium longiflorum*, identified a gene, designated *GCS1*, that was specifically upregulated in generative cells, the precursors of sperm (Mori et al., 2006). *HAP2* and *GCS1* were homologs, and targeted gene disruptions of *HAP2* in *Arabidopsis* established a role for the corresponding gene product in fertilization and suggested a possible function in gamete recognition/activation, sperm-egg attachment, or sperm-egg fusion (Johnson et al., 2004; von Besser et al., 2006; Mori et al., 2006). Independently, studies in *Chlamydomonas reinhardtii* and the malarial parasite *Plasmodium falciparum,* solidified the importance of HAP2/GCS1 in fertilization and extended the work in plants by demonstrating a functional role for HAP2 at a step after gamete adhesion (most likely fusion) in two widely diverged protists (Liu et al., 2008). Furthermore, the presence of *HAP2/GCS1* homologs in species outside of plants argued persuasively that its function was conserved across a broad range of taxa (Mori et al., 2006; Liu et al., 2008; Steele and Dana, 2009; Wong and Johnson, 2010).

In *Chlamydomonas*, *minus* gametes with a disruption in the *HAP2* gene (*hap2*) underwent normal ciliary adhesion, gamete activation, and mating structure adhesion when mixed with *plus* gametes but failed to complete fertilization and form quadriciliated zygotes (Liu et al., 2008). Importantly, HAP2/GCS1 localized precisely to the region of *minus* cells where

gamete fusion occurs (namely the *minus* mating structure) and ultrastructural studies demonstrated an inability of *plus* and *minus* mating structures to fuse in crosses between wild type *plus* and *hap2*-disrupted *minus* strains (Liu et al., 2008) (**Figures 2A–C**). Similar assays in *Plasmodium berghei* found that HAP2/GCS1 was expressed and localized over the entire plasma membrane of male gametes (consistent with indiscriminate sites of gamete attachment and membrane fusion in this species), while mutant cells deficient in HAP2 were able to attach but were unable to fuse with female gametes (see below). Subsequent studies in *C. reinhardtii* demonstrated that the HAP2 protein, along with the fertilization-essential membrane proteins, FUS1 and MAR1, were rapidly degraded after cell-cell fusion, showing tight regulation of the gamete membrane fusion machinery in a possible block to polygamy (Johnson, 2010; Liu et al., 2010; Pinello et al., 2021).

Following this work, studies in *Tetrahymena* reinforced the idea that HAP2 functions downstream of gamete membrane attachment, but with an interesting twist (Cole et al., 2014). *T. thermophila* has seven sexes/mating types raising an interesting question as to how a "male" gamete-specific fusion factor functions in an organism that is, for all intents and purposes, sexually ambiguous. Studies by Cole et al. demonstrated that *HAP2* was expressed in all seven mating types of *T. thermophila*, and that fertilization and membrane fusion were completely blocked only when *HAP2* was disrupted in both cells of a mating pair (Cole et al., 2014). As shown in **Figure 2**, different mating types lacking *HAP2* adhered to one another along their entire junctional interface but failed to form fusion pores (**Figure 2D**). In wild type crosses, however, characteristic fusion pores formed at regular intervals along the junctional membranes creating cytoplasmic bridges between mating cells (**Figure 2E**). Localization studies at the light (**Figure 2F**) and electron microscopic levels demonstrated that HAP2 was present at the conjugation junction, precisely where membrane fusion was taking place as was previously shown for *C. reinhardtii* and *P. berghei* (Cole et al., 2014).

Given that HAP2 is expressed in all seven mating types of *T. thermophila* and that pore formation appears to be initiated on both sides of the conjugation junction (see above, *Membrane Dynamics at Sites of Gamete Fusion*), one might predict that deletion of *HAP2* from one cell of a mating pair would have little-to-no effect on mating efficiency in the *Tetrahymena* system. Nevertheless, in crosses between genetically marked WT and *ΔHAP2* deletion strains, fertility was shown to decline by as much as 80% (Cole et al., 2014). This was consistent with subsequent findings that used flow cytometry and exchange of fluorescently-tagged cytosolic proteins between cells as a readout for pore formation in mating pairs (Pinello et al., 2017). In these latter studies, the number of pairs capable of exchanging dye was reduced by 80–90% in crosses between WT and *ΔHAP2* knockout strains (Pinello et al., 2017). Furthermore, the rate at which individual WT X *ΔHAP2* pairs formed pores was also significantly reduced, although the final level of protein exchange in the small percentage of cells that did form pores was essentially the same in WT X *ΔHAP2* and WT X WT crosses (Pinello et al., 2017). Taken together, these results suggested that successful mating between WT and *ΔHAP2* deletion strains is an all-or-none phenomenon with most pairs being unable to form pores (or, at least, a sufficient number of pores to allow measurable dye exchange). As argued below (see *Discussion*), the most plausible explanation for these findings is that cooperative interactions between the fusion machinery on both membranes of a mating pair is required for efficient pore formation to occur in *T. thermophila*.

The requirement for *HAP2/GCS1* in fertilization and its function downstream of gamete adhesion in a variety of different systems, clearly pointed to a role for HAP2 in membrane fusion. Nevertheless, until recently, large differences in primary amino acid sequence between *HAP2* orthologs of different species, together with an absence of homologies to known membrane fusogens left open questions regarding HAP2's precise function. Those questions were answered using a variety of analytical approaches. First, HAP2 orthologs were shown to assume a 3-dimensional structure closely resembling class II membrane fusogens of enveloped viruses (Fédry et al., 2017; Pinello et al., 2017; Valansi et al., 2017). Second, biophysical studies demonstrated the ability of the HAP2 ectodomain, as well as predicted HAP2 fusion peptides to interact directly with model membranes (Fédry et al., 2017; Pinello et al., 2017). And finally, under appropriate conditions, ectopic expression of *A. thaliana* HAP2 ortholog was shown to be capable of mediating cell-cell fusion in cultured mammalian cells (Valansi et al., 2017). As described in the following section on protein structure, a large part of this work focused on HAP2 molecules from unicellular eukaryotes.

3.4.1 Structural Requirements for HAP2 Function

The basic structural features of HAP2/GCS1 orthologs from *Chlamydomonas* and *Tetrahymena* are shown in **Figure 3A**. In many ways, these proteins are representative of the HAP2/GCS1 family overall. Both are single-pass transmembrane proteins. Based on their primary sequence, they vary in size (the *C. reinhardtii* protein being somewhat larger at 1,139 amino acids, compared to 742 amino acids in the case of *T. thermophila* protein). They also share weak homology overall but are identifiable as cousins through homology at the so-called HAP2/GCS1 domain (PFAM 10699), a stretch of ~50 amino acids in the extracellular domain that, with few exceptions (e.g. *Drosophila melanogaster*, is conserved across the HAP2/GCS1 family (Garcia, 2012; Fedry et al., 2018). Many orthologs, including the *Chlamydomonas* and *Tetrahymena* proteins, have a cysteine-rich, poly-basic stretch in the cytosolic region immediately following the transmembrane helix. Nevertheless, there is considerable variation in the size of HAP2/GCS1 cytosolic domains overall. For example, some species (e.g., *Chlamydomonas reinhardtii* and *Toxoplasma gondii*) have extended intracellular domains with 500 residues or more, while others have almost no cytoplasmic tail whatsoever (*Ichthyophthirius multifiliis* [a parasitic ciliate]; *Pediculus humanus corporis* [the human body louse]; and, *Trypanosoma cruzi* [the etiologic agent of Chagas disease] (Liu et al., 2015). Substitutions or deletions of the entire HAP2 cytoplasmic domain, or certain polybasic or potentially palmitoylated

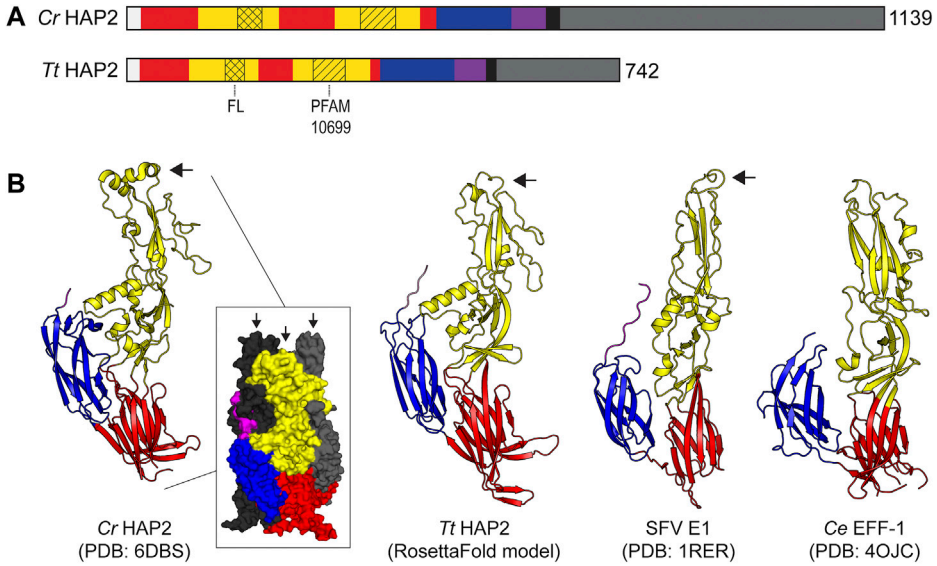

FIGURE 3 | HAP2 Protein domains and structure. **(A)** Protein domain schematic showing the organization of HAP2 monomers from N′ to C′ terminus **(left to right)** from *T. thermophila* (Tt) and *C. reinhardtii* (Cr). The signal peptide is white; domain I is red; domain II is yellow; fusion loop (FL) is indicated with crosshatch; PFAM10699 (HAP2/GCS1 domain) is indicated with diagonal lines; domain III is blue; stem is purple; transmembrane domain is black; and, the cytoplasmic domain is gray. The number of amino acids in each protein is shown on the far right at the C′ terminus. **(B)** X-ray and model ectodomain protein structures showing the homology of HAP2 and other class II fusogens from viruses and cells. From left to right: the crystal structure of the *C. reinhardtii* HAP2 post-fusion trimer with one cartoon protomer **(left)** and a surface representation of the trimer (inset) with colored domains on the front protomer and the two back protomers in black and gray, respectively (Feng et al., 2018); a RosettaFold model protein structure of a *Tetrahymena* HAP2 monomer (Baek et al., 2021); a single protomer from the trimeric crystal structure of the Semliki Forest Virus E1 class II fusion protein (Gibbons et al., 2004); a single protomer from the trimeric crystal structure of the *C. elegans* class II cell-cell fusion protein EFF-1 (Perez-Vargas et al., 2014). Black arrows point to the fusion loops. Protein databank IDs (PDB) are shown below the images.

cysteine residues within the cytosolic domains of various HAP2/GCS1 orthologs have been shown to impact protein localization and/or function but those impacts appear to be different in different species and the functional role of the cytosolic domains is still under scrutiny (Mori et al., 2010; Wong et al., 2010; Liu et al., 2015; Pinello et al., 2017).

Early efforts to make sense of HAP2/GCS1 function relied heavily on mutational studies designed to link alterations in phenotype (either loss of fertility or failure to fuse) to either single amino acids or larger regions of protein structure (Mori et al., 2010; Wong et al., 2010; Liu et al., 2015; Pinello et al., 2017). While informative in some cases (for example, domain swaps between HAP2/GCS1 orthologs of related species showed some evidence of lineage-specificity in the extracellular domains of plant proteins (Wong et al., 2010)), this overall approach involved guess work, and as often as not, changes to the protein led either to a complete loss of expression (presumably due to protein misfolding) or failure of the protein to reach its correct destination within the cell for reasons that were not always easy to interpret.

Nevertheless, a breakthrough in our understanding of HAP2/GCS1 function came with the unraveling of the protein's 3-dimensional structure using disparate approaches, namely, x-ray crystallography and structure homology modeling. In the latter case, algorithms that compare secondary structural elements in query sequences to known structures in the PDB Protein Databank (Raptor X; Phyre2; HHblits; LOMETS, etc.) were used by two laboratories to parse the structures of the HAP2/GCS1 ectodomains from *Tetrahymena* and *Arabidopsis* (Pinello et al., 2017; Valansi et al., 2017). At the same time, Felix Rey's laboratory at the Pasteur Institute in collaboration with William Snell's group at UT Southwestern Medical Center, solved the x-ray crystal structure of a recombinantly expressed version of the *C. reinhardtii* HAP2 ectodomain at 3.3Å resolution (Fédry et al., 2017). Both approaches led to the same conclusion—HAP2/GCS1 is a Class II fusion protein (CII). Improved structures of the *C. reinhardtii* protein, as well as a nearly complete and partial structure of the HAP2/GCS1 ectodomains from *Arabidopsis thaliana* and *Trypanosoma cruzi*, respectively (Fedry et al., 2018; Feng et al., 2018; Baquero et al., 2019), have validated this conclusion and shed additional light on the organization of these proteins particularly in the regions of the "fusion loops" (see below).

The striking architectural similarities between HAP2/GCS1 ectodomains from *C. reinhardtii* and *T. thermophila*, and comparable regions of the E1 glycoprotein of Semliki Forest Virus (a classic CII viral fusogen) and the Epithelial Fusion Failure protein one of *C. elegans* (a CII protein required for cell-cell fusion in nematode worms) are shown in **Figure 3B** (Gibbons et al., 2004; Perez-Vargas et al., 2014; Feng et al., 2018; Baek et al., 2021). As with other CII fusogens, the ectodomains of HAP2/GCS1 are comprised of three mostly beta-strand-containing globular regions (domains I, II and III) connected by a stem to a single transmembrane domain (**Figures 3A,B**).

Importantly, all HAP2/GCS1 structures solved to date contain hydrophobic "fusions loops" between beta-strands c and d at the apical tip of domain II (**Figure 3B**, black arrow). Hydrophobic residues in these loop structures insert into the outer leaflets of apposed target membranes and are key functional determinants for membrane fusion present in all class II viral proteins (see below, *Models of HAP2/GCS1-mediated fusion*). Finally, consistent with the known behavior of class II fusogens (see below), purified HAP2/GCS1 ectodomains form trimers when interacting with liposomes or detergent and their solved structures reflect the trimeric, post-fusion conformation of each protein with its fusion loop and transmembrane domain positioned as they would be in the fused membrane (Fédry et al., 2017; Feng et al., 2018) (**Figure 3B**, left).

Along with these similarities, interesting differences between viral class II proteins and HAP2/GCS1 orthologs have also been noted. For example, the first crystal structure of the *Chlamydomonas* HAP2 ectodomain revealed that its long (39 amino acid) fusion loop is bisected by a salt bridge connecting an arginine residue at position 185 in the loop (R185) with a glutamic acid residue at position 126 (E126) (Fédry et al., 2017). These arginine and glutamic acid residues are highly conserved within the HAP2/GCS1 family but are notably absent in class II viral proteins and the *C. elegans* FF family of cell-cell fusogens. Moreover, the R185-E126 salt bridge in the algal protein appears to play a critical role in organizing the membrane interacting regions of HAP2/GCS1 to ensure fusion (Fédry et al., 2017; Fedry et al., 2018). Functional studies in *Chlamydomonas* showed that mutating the single R185 residue in the loop region completely blocked gamete fusion without disrupting either HAP2 protein expression or localization. Furthermore, *in vitro* studies with purified HAP2 ectodomains showed that interactions of trimers with liposomes (measured by their co-floatation on sucrose gradients) was strictly dependent on the presence of the R185 residue.

In subsequent work, a higher resolution (2.6 Å) structure of the *Chlamydomonas* HAP2 ectodomain provided additional information about the location, orientation, and structural relationships of key residues within the HAP2 fusion loop, including R185 (Feng et al., 2018). This new study revealed that residue R185 is highly dynamic within a stable carbonyl cage suggesting that it may serve as a flexible pivot point for the apical end of domain II relative to the trimer axis—a flexibility that could allow for adjustments in orientation and positioning of the fusion loops during the membrane fusion reaction. Furthermore, these results presented the possibility that this carbonyl cage could be one of the drivers of HAP2/GCS1 domain II conservation across species, since three of the four residues comprising the cage fall within this domain (Feng et al., 2018).

Despite the overall conservation of the arginine-glutamic acid salt bridge, fusion loops themselves appear to have undergone significant diversification within the HAP2/GCS1 lineage. Comparative studies of x-ray crystal structures of widely diverged HAP2/GCS1 orthologs from *Arabidopsis thaliana* and *Trypanosoma* cruzi have shown that whereas the plant protein has a single fusion loop with an amphipathic helix (dubbed αF) that juts towards the membrane surface, the parasite ortholog has three small nonpolar loops (Fedry et al., 2018). By contrast, the fusion loop region of the *Chlamydomonas* ortholog is unusually large and has two loops extending a total of three fusion helices containing hydrophobic residues (Feng et al., 2018). Whether these differences in structure reflect differences in the target membrane compositions with which these different species' HAP2 proteins interact is unclear, however, the necessity of fusion loop helical domains has been demonstrated in membrane interaction studies *in vitro* as well as fertility assays *in vivo* (Feng et al., 2018; Baquero et al., 2019; Zhang et al., 2021).

3.4.2 HAP2-dependent Fusion Requires Membrane Attachment and Trimerization

Studies of viral class II fusogens have laid the groundwork for our current understanding of how HAP2/GCS1 mediates gamete fusion. Following virus attachment and uptake into host cells, the low pH environment of the of the endosome triggers a dramatic intra- and intermolecular reconfiguration of the fusion proteins that promotes merger of the virus envelope with endosomal membranes (Wahlberg and Garoff, 1992; Lescar et al., 2001; Sánchez-San Martín et al., 2009). During this reconfiguration, the fusion loop at the tip of domain II becomes exposed and inserts into the endosomal membrane, creating a protein bridge between the two membranes (Hammar et al., 2003; Liu and Kielian, 2009). Individual fusion proteins then trimerize (Wahlberg et al., 1992; Liu and Kielian, 2009) and undergo a conformational change in which domain III (blue) folds back towards domain I and the lower part of domain II, creating a dimple in the apposed membranes. As fold back continues, the transmembrane anchor in the viral-membrane is brought into contact with the fusion loop in the endosomal membrane (Kielian and Rey, 2006; Sánchez-San Martín et al., 2009). The accompanying distortions of both membranes destabilize the lipid bilayers, leading to membrane fusion.

New work in *Chlamydomonas* has shown that 1) HAP2 forms trimers *in vivo* that are essential for fusion; 2) hydrophobic residues in the fusion loop are critical for enhancing trimerization; and, 3) mating structure adhesion is essential for HAP2 trimerization (Zhang et al., 2021). Similar to viral class II proteins (Wahlberg et al., 1992; Gibbons and Kielian, 2002; de Boer et al., 2012), it was found that some proportion of HAP2 trimers remains resistant to low heat and low concentrations of reducing agent (45°C, 10 mM DTT) making it possible to detect the presence of the trimer with SDS-PAGE and immunoblotting and follow the kinetics of trimer formation *in vivo* during the course of fertilization (Zhang et al., 2021). Within 10 min of mixing wild type *C. reinhardtii plus* and *minus* gametes, HAP2 trimers were readily detected on immunoblots. Interestingly, only a portion of total cellular HAP2 formed trimers (~450 kDa), while the rest remained as two ~150 kDa monomer bands. Site-directed mutagenesis of leucine residues (L310E and L448E) designed to interfere with hydrophobic interactions present at the trimer core inhibited the trimerization of recombinant HAP2 ectodomain *in vitro* and blocked gamete merger *in vivo*, indicating that trimer formation is essential for fusion. Importantly, HAP2 trimer formation was also found to

specifically require gamete membrane adhesion. When *Chlamydomonas plus* gametes lacking the *Chlamydomonas* membrane adhesion protein FUS1 were mixed with *minus* gametes, cells underwent wild-type levels of ciliary agglutination, gamete activation, and even mechanical contacts at their mating structures, but failed to form HAP2 trimers and failed to fuse, showing that gamete membrane adhesion is required for HAP2 trimer formation *in vivo* (Zhang et al., 2021). Selective mutations of the large *Chlamydomonas* HAP2 fusion surface, including additive mutations of hydrophobic residues from one, two, or all three of the fusion helices, allowed the additional observation that after gamete membrane adhesion occurs, interactions of the *Chlamydomonas* HAP2 fusion loop with the target *plus* gamete membrane contribute to the formation of HAP2 trimers *in vivo*. These data were supported by *in vitro* studies showing that recombinant HAP2 ectodomains undergo spontaneous trimerization upon incubation with liposomes at neutral pH (Fédry et al., 2017; Baquero et al., 2019).

4 HAP2/GCS1 IN PROTOZOAN PARASITES: TARGETS FOR TRANSMISSION-BLOCKING VACCINES AND A TOOL FOR THE IDENTIFICATION OF CRYPTIC SEXUAL LIFE CYCLES

Parasitic protists are among the most important disease-causing agents of humans and animals, nevertheless vaccines targeting these agents have proven difficult to develop especially when compared their viral and bacterial counterparts (Bowman, 2014). The fact that immunity in response to natural infection often takes years to develop and may never afford complete or long-lasting protection are among the greatest challenges for the development of effective vaccines against parasitic agents. Parasites are masters of immune evasion and many of the difficulties associated with anti-parasite vaccine development can be ascribed to their complex lifecycles. For example, *Plasmodium falciparum*, an apicomplexan responsible for the most severe forms of human malaria, cycles between extracellular stages capable of expressing multiple, variant surface antigens over time as well as intracellular stages that escape antibody detection entirely. The development of effective subunit vaccines against such agents is akin to hitting a hidden, moving, and ever-changing target.

In addition to vaccines that are designed to block parasite infection and growth within the host, investigators are also focusing on transmission-blocking vaccines (TBV), which have the potential to interrupt the sexual phase of parasite's life cycle that is required for disease transmission (Vogel, 2010). Like other eukaryotes, sex is an obligate part of the life cycle of many, if not most parasitic protists. Furthermore, antigens associated with certain parasites' sexual development are often only expressed in an insect vector and can be highly conserved. Several such antigens, including HAP2, are considered promising candidates for transmission-blocking vaccine development. As discussed below, HAP2 orthologs are present in a wide range of parasitic protists where their essential function in gamete fusion is conserved. At the same time, the absence of *HAP2* genes in vertebrates lessens the potential for side-effects due to cross-reacting antibodies in immunized patients. Multiple studies investigating HAP2 as a possible vaccine antigen are now in progress and stand to benefit from structure/activity studies in model organisms designed to pinpoint regions of the protein most likely to bind neutralizing antibodies. Apart from vaccine development, studies of HAP2 expression have also begun to shed light on the cryptic sexual cycles of many parasitic protists. In either case, the preponderance of this work has been done with apicomplexans, distant relatives of ciliates and dinoflagellates, which are also among the most important parasites of humans and animals.

Coccidia comprise one of the largest subgroups of the Apicomplexa. In these organisms, sexual reproduction occurs in intestinal cells of infected animals with resultant oocysts being expelled in the feces and ingested by the next host. In the poultry industry, coccidia belonging to the genus *Eimeria* sicken birds and have a major impact on egg and meat production (Sharman et al., 2010). While vaccines for *Eimeria* are available, they often provide less than full protection against disease outbreaks. This and recently developed resistance to anti-coccidian chemotherapeutics underlines the need for improved control measures including new vaccines (Ahmad et al., 2016). One approach along these lines has been the development of CoxAbic® (Wallach et al., 2008), a crude preparation of gametocyte antigens and one of the first examples of a transmission-blocking vaccine successfully employed against a parasite model (Wallach et al., 2008). Injection of this vaccine into breeding hens just before egg laying was found to reduce oocyst shedding and generate maternal antibodies that protected chicks from infectious challenge with three different *Eimeria* species through at least 8 weeks of age.

Following the success of this approach, specific sexual stage antigens produced as recombinant proteins are now being explored as *Eimeria* vaccine candidates (Jang et al., 2010). In 2015, RNA Seq analysis of *E. tenella* identified a variety of such antigens, including HAP2, which were found to be expressed in male microgametocytes in the caeca of infected chickens and not in asexual merozoite or sporozoite stages (Walker et al., 2015). This study revealed molecular aspects of fertilization in *Eimeria* that were not previously known and opens the door to testing HAP2 as a vaccine antigen for interrupting *Eimeria* transmission.

Toxoplasma gondii, another widely distributed coccidian and one of the most successful parasites on earth (Griffin et al., 2019) is also being explored as a target for transmission-blocking vaccine development. *T. gondii* has a broad host range infecting most warm-blooded animals and birds as intermediate hosts. Cats are the definitive hosts and become infected by ingesting prey containing tissue cysts, known as bradyzoites. Sexual reproduction occurs exclusively in the intestinal epithelia of infected animals and gives rise to oocysts that are shed in the feces. As a disease agent, *Toxoplasma* has a significant economic impact in the sheep industry where it causes abortion (Innes et al., 2009) and can be highly pathogenic in

wildlife species such as sea otters (Miller et al., 2004). In humans, *T. gondii* generally causes mild-to-asymptomatic disease in healthy individuals but can have devasting effects in immunocompromised adults, as well as children infected *in utero* during pregnancy. The ability of *T. gondii* to persist for long periods both in the environment and within the host makes this agent especially difficult to control, and while veterinary vaccines have been developed that reduce the formation of tissue cysts (Innes et al., 2009; Zhang et al., 2013), a strategy to lower the prevalence of *Toxoplasma* oocysts in the environment would be highly desirable. Toward that end, recent progress has been made in understanding the expression and regulation of sexual stage antigens in *T. gondii*, including HAP2.

In 2020, Farhat et al. discovered a MORC-driven transcriptional switch that controls *T. gondii* development and sexual commitment (Farhat et al., 2020). Through the assembly of histone deacetylase, HDAC3, and HAP2-related transcription factors, MORC was found to repress the transcription of HAP2 and a broad set of other sexual stage genes in non-sexual stages of *T. gondii*. Depletion of MORC allowed the release of this transcriptional repression and the expression of *HAP2* (Farhat et al., 2020). While the HAP2 protein has yet to be detected or localized to specific stages of the *T. gondii* life cycle, consistent with previous studies in coccidian *E. tenella* (Walker et al., 2015), *HAP2* RNA transcripts were found to increase in abundance during parasite development in the intestinal tissue of infected cats (Ramakrishnan et al., 2019).

With the idea that HAP2 plays a critical role in fertilization, *T. gondii*, strains lacking the *HAP2* gene were generated and tested as potential live attenuated vaccines (Ramakrishnan et al., 2019). Following administration to cats, *HAP2* deletion strains produced only small numbers of misshapen oocysts that showed no evidence of meiosis or diploidy and failed to sporulate. This would strongly suggest that HAP2 is required for fertilization in *T. gondii* and puts to rest earlier speculation regarding the role of fertilization in the development of infectious oocysts (Ferguson, 2002). When tested as live vaccines, the *ΔHAP2* deletion strains, as might be expected, did not prevent systemic infection of immunized cats challenged with virulent wild-type parasites (Ramakrishnan et al., 2019), however, they did completely block the production of infectious oocysts in these animals providing an exciting proof-of-principle that a transmission-blocking vaccine for *T. gondii* is within reach. As an alternative to rationally attenuated vaccines (which require growth of large numbers of parasites), one could easily envisage the use of recombinant subunit or nucleic acid vaccines encoding the HAP2 protein.

In addition to studies with *Eimeria* spp. and *Toxoplasma*, HAP2 expression has been documented in several other coccidian species including *Cystoisospora suis* and *Cryptosporidium parvum* (Feix et al., 2020; Lippuner et al., 2018). In *Cystoisospora suis*, an agriculturally important pathogen of swine, cell-free culture conditions were identified that allow progression of asexual merozoites into sexual stages of the parasite through the oocyst stage *in vitro*. *HAP2* transcripts were found to be upregulated during this progression (Feix et al., 2021) leading to interest in HAP2 as a possible transmission-blocking vaccine for this species as well. By contrast, *HAP2* transcripts were found to be present at similar levels in all stages of the life cycle of *Cryptosporidium parvum* (Lippuner et al., 2018). While somewhat unexpected given the pattern of HAP2 transcription in other organisms, certain species, such as the alga *Gonium pectorale*, have been found to the control the stage-specific expression of HAP2 post-translationally (Kawai-Toyooka et al., 2014), and the levels of HAP2 protein within different stages of *C. parvum* are still not known.

In addition to the coccidians, HAP2 is being actively studied in Haemosporidia (similar to Aconoidasida), an important group of apicomplexan parasites that cycle between vertebrate and arthropod hosts. Within this group, *Babesia spp*. and *Plasmodium spp*. are hugely consequential. The genus *Babesia* is comprised of >100 species that cause tick-borne illness in humans and animals and result in significant economic losses particularly in the cattle industry (Griffin et al., 2019). Recent studies in *Babesia bovis* have shown that *HAP2* gene expression occurs within tick midgut and not in blood-stage parasites (Hussein et al., 2017). Consistent with this, deletion of the *HAP2* gene blocked morphological development of gametic stages and prevented expression of the 6-cys family member *A* and *B* genes, which are normal markers of sexual stage parasites in the tick midgut (Alzan et al., 2016; Hussein et al., 2017). In 2017, studies of *HAP2* expression in *B. bigemina* (another species responsible for bovine babesiosis) resulted in similar findings and, more importantly, showed that antibodies against conserved HAP2 peptides significantly reduced the *in vitro* formation of zygotes from sexual forms (Camacho-Nuez et al., 2017). Although multiple wildlife species can serve as reservoirs for *Babesia spp*., the development of transmission-blocking vaccines targeting HAP2 could be useful for reducing parasite prevalence in endemic areas where domesticated cattle herds routinely graze.

The genus *Plasmodium* can also infect humans and animals but is most well known in the context of human malaria, a disease responsible for ~400,000 deaths (the majority in children) and over a million cases each year primarily in sub-Saharan Africa (Griffin et al., 2019). Of the five *Plasmodium* species that infect humans, *P. falciparum* is the most important in terms of overall morbidity and mortality. Despite decades of effort, only a single vaccine targeting *P. falciparum*, viz. Mosquirix™ (GlaxoSmithKline), has been recommended by the World Health Organization for widespread use. This 3-dose recombinant subunit formulation contains the major surface antigen on infectious sporozoites, namely, CSP, and provides ~34% efficacy in preventing severe disease in children aged 5–17 months (RTS,S Clinical Trials Partnership, 2014; Laurens, 2020). A more recent, R21/Matrix-M vaccine, which also targets CSP and uses a different adjuvant, appears more promising (Datoo et al., 2021). The latter vaccine is undergoing phase three clinical trials (University of Oxford, 2021) but is not yet approved.

The expression of variant surface antigens at different stages of the parasite life cycle is among the most important reasons for the failure of vaccines targeting *P. falciparum*. Nevertheless, parasite transmission requires an obligate sexual stage in which male and female gametocytes are produced in the human and then

transferred to female Anopheles mosquitoes when they take a blood meal. Gametocytes complete development in the mosquito midgut and then undergo fertilization. Because these final steps in sexual development occur only in the insect vector, *Plasmodium* proteins expressed after ingestion by mosquitos are not subject to selective pressure from the vertebrate immune system (and therefore less subject to variation) but are nevertheless exposed to antibodies taken up with the blood meal. Indeed, there is now considerable evidence for the effectiveness of immunization with sexual stage antigens in blocking parasite transmission within closed laboratory settings demonstrating proof-of-concept for the use of this approach in the field (Blagborough et al., 2013).

The presence of *Plasmodium* HAP2 orthologs was recognized in 2006 (Mori et al., 2006), and it was not long after that *HAP2* was shown to be essential for fertilization of *P. berghei* (Liu et al., 2008). In the latter case, *HAP2* gene disruption had no effect on either exflagellation or the adherence male and female gametes, but completely blocked gamete fusion and ookinete development (Liu et al., 2008). By contrast, macrogametes lacking *HAP2* were fully capable of fertilization and ookinete development following interaction with wild type microgametes (Hirai et al., 2008; Liu et al., 2008). These findings spurred considerable interest in HAP2 as a candidate antigen for the development of transmission-blocking vaccines for *Plasmodium* (Sinden et al., 2012). In promising studies, Angrisano and co-workers have shown that immunization of mice with a short, 18-residue polypeptide encoding the *Plasmodium berghei* HAP2 fusion loop, elicited specific humoral antibody responses capable of blocking fertilization *in vitro* by up to 89.9% and transmission *in vivo* by up to 58.9% when mosquitoes were fed on immunized mice (Angrisano et al., 2017). Furthermore, a significant, dose-dependent reduction in the number of oocysts present in the mosquito midgut was seen when antibodies against the *P. falciparum* HAP2 fusion loop were mixed with infected blood from African donors and then fed to mosquitoes in standard membrane feeding assays (Angrisano et al., 2017). By combining immunogenic peptides with recombinant protein-based vaccine formulations now being tested for malaria (Datoo et al., 2021; Jelínková et al., 2021) it may be possible to reduce parasite prevalence in endemic areas through reduced transmission while at the same time protecting individuals against disease.

Lastly, HAP2 orthologs have been identified in the Kinetoplastid parasites of humans in the genera *Trypanosoma* and *Leishmania*. While it is unclear whether fertilization/sexual reproduction is obligatory for infectious transmission of these parasites, *Trypanosomes* undergo a sexual stage in tsetse fly or triatomine insect vectors as evidenced by genetic exchange (Jenni et al., 1986; Gaunt et al., 2003), cytoplasmic mixing between parasites (that is cell-cell fusion) (Gibson et al., 2008), and the expression of conserved meiosis-specific genes prior to cell-cell fusion (Peacock et al., 2011, 2014). Recent single-cell RNA-seq studies have demonstrated that *T. brucei* HAP2 is one of a cluster of gamete-specific genes upregulated in the salivary glands of infected tsetse flies (Hutchinson et al., 2021), and YFP-tagged HAP2 has been shown to be expressed in parasites isolated from tsetse fly salivary glands (Castellanos, 2018). As noted above, the crystal structure of domain II of *T. cruzi* HAP2 has also been solved and displays overall conservation of structure when compared to other the class II fusion proteins, but also has substantial differences from *Chlamydomonas* and *Arabidopsis* HAP2 in the arrangement and structure of its membrane interaction motif (Fedry et al., 2018).

A HAP2/GCS1 ortholog has also been shown to be present in *Leishmania spp*. (Hirai et al., 2008; Liu et al., 2008), and studies of its expression and function have begun to offer unique insights as well as a new tool to study the parasites' cryptic sexual cycle. *Leishmania* promastigotes experience a meiosis-like genetic exchange during their development in the Phlebotomine sandfly vector (Akopyants et al., 2009; Rougeron et al., 2010; Inbar et al., 2019), but less is known about the cellular interactions that accompany this process. Recently, however, DNA damage-induced cell stress has been shown to elicit upregulation in the expression of HAP2 and other conserved sexual transcripts, as well as an increase the efficiency of inter- and intra-specific genetic hybridization of *Leishmania* spp. *in vitro* (Louradour et al., 2021). Indeed, it is now possible to use the expression of an mNeonGreen-tagged HAP2 transgene as a marker for *L. tropica* promastigote mating competence. Separation of cells using fluorescence activated cell sorting has made it possible to examine matings between parasites that either do or do not express HAP2, and only promastigotes expressing HAP2 were found to be capable of hybridization. Reminiscent of work in *Tetrahymena*, these studies also showed that while the presence of HAP2 was required in only one of the two parental populations for genetic hybrids to form, crosses in which both parental lines expressed HAP2 showed much higher frequencies of hybrid formation (Louradour et al., 2021). Overall, this approach offers fundamentally new opportunities for dissecting the facultative sexual stage of *Leishmania* parasites.

5 DISCUSSION

Despite everything we have learned about the role of HAP2/GCS1 in gamete fusion, there are still many unanswered questions regarding the HAP2-dependent fusion machinery, its evolutionary history, and its potential application in blocking fertility in parasites or other species. Regarding the fusion machinery itself, like viral CII fusogens, HAP2 must localize to specific sites on the plasma membrane and then assemble into a trimer to ensure that fusion occurs. Elucidation of the HAP2 pre-fusion conformation and a further understanding of the mechanisms that trigger its transition to a trimeric state will require additional work. As noted here, there is abundant evidence that HAP2/GCS1 does not act alone. Beyond membrane attachment, there are likely additional factors that are important in localizing HAP2 to sites of gamete fusion as well as promoting fusion itself. These could include other proteins such as actin, or DMP8/9-like proteins which adopt a faciliatory role in gamete fusion in *Arabidopsis* (Takahashi et al., 2018; Cyprys et al., 2019), as well as specific lipids that may accommodate HAP2/GCS1 fusion loops or promote membrane curvature itself.

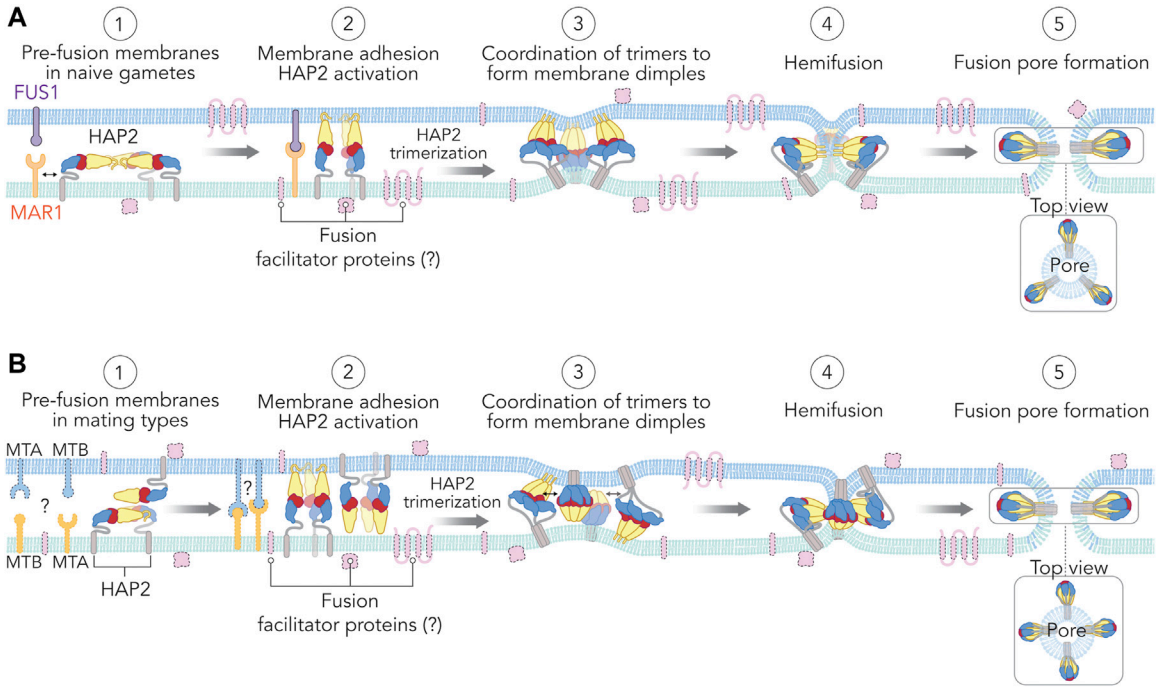

FIGURE 4 | Model molecular mechanisms for the **(A)** *Chlamydomonas* and **(B)** *Tetrahymena* gamete membrane fusion reactions. **(1)** Before fusion, HAP2 is expressed on the *Chlamydomonas minus* gamete mating structure, and membranes at the developing conjugation junction of *Tetrahymena* in an as yet unknown pre-fusion state. Both species strongly upregulate HAP2 expression after mixing of different mating types. The cytoplasmic domains of some proteins are not shown. Also, other conserved or species-specific fusion facilitator proteins (pink) that have not yet been identified may actively participate in this process. **(2)** In *Chlamydomonas,* FUS1-MAR1 mediated membrane adhesion activates HAP2 out of its pre-fusion state on naive *minus* gametes, driving HAP2 fusion loop interactions with the *plus* gamete membrane and trimer formation. In *Tetrahymena* the membrane adhesion proteins are unknown, but it is possible that MTA and MTB proteins are involved in this recognition event, and similarly activate HAP2. **(3)** During conformational changes, the fusion loops and transmembrane domains of HAP2 proteins anchored in both membranes helps pull the two lipid bilayers close together. A circular coordination of several HAP2 trimers undergoing such changes is expected to form dimples in the apposed membranes. *Chlamydomonas* HAP2 trimers bridge the two membranes with their fusion loops anchored in the target *plus* gamete membrane, whereas *Tetrahymena*, having HAP2 protein expressed and functional on the membranes of both mating types, could undergo a different coordination of HAP2 trimers that contributes to its fusion efficiency. **(4)** As HAP2 conformational changes continue to fold domain III (blue) back against the domain II (yellow) the two membranes are pulled even closer together, helping to initiate hemifusion, a lipid mixing event between the outer leaflets of the two bilayers. **(5)** Completion of HAP2 trimerization induces full mixing of both leaflets of the lipid bilayer and creates membrane fusion pore with stable post-fusion HAP2 homotrimers fastened in the fused membrane by their fusion loops and transmembrane domains. In this model, for simplicity the fusion pore is encircled by three or four trimers in a top-down view, but in reality, it is not known how many HAP2 trimers are necessary for fusion pore formation in any species.

Regardless of any hypothetical requirement for additional facilitators, a basic model for HAP2/GCS1-mediated gamete fusion emerges from work on *Chlamydomonas* (**Figure 4**). As indicated earlier, HAP2 in its pre-fusion conformation is expressed in *minus* gametes at the site of the nascent mating structure and is further upregulated during interactions with *plus* gametes. FUS1-MAR1 mediated membrane adhesion then facilitates HAP2 activation, allowing interaction of its fusion loops with membranes on *plus* gametes and driving trimerization of the protein (**Figures 4A-1,2**). Presumably, coordinated foldback of several HAP2 trimers then leads to the formation of dimples on apposed membranes where the multiple fusion loops and transmembrane domains congregate (**Figures 4A-3**). As foldback continues, the two apposed membranes are pulled even closer, helping overcome the hydration barrier between the two bilayers and initiating hemifusion, the mixing of the outer leaflets of the two bilayers (**Figures 4A-4**). As transmembrane domains and fusion loops come together, full mixing of the two leaflets occurs and creates a membrane fusion pore (**Figures 4A-5**). In *Chlamydomonas*, the pore(s) expands quickly to completely fuse the two gamete cells.

While this model is straightforward and comports with a vast body of work on viral CII proteins where fusion is driven unilaterally from one membrane, data on HAP2/GCS1-mediated gamete fusion in *Tetrahymena*, along with studies of AFF-1/EFF-1-mediated cell-cell fusion in *C. elegans* force a consideration of alternative models in instances where efficient pore formation requires that fusogens be present on apposed membranes. As described earlier, while a small percentage of *Tetrahymena* mating pairs can undergo fusion when HAP2 is expressed unilaterally on one membrane, the low efficiency of pore formation in crosses of wildtype cells with *ΔHAP2* deletion partners strongly suggests that some type of bilateral interaction occurs between mating cells that is HAP2-dependent. Although one can only speculate as to what those interactions might be, it is reasonable to infer they involve either 1) heterotypic interactions

between HAP2 and some hypothetical receptor(s) on apposed membranes that allows pores to form more readily (for example by enhancing membrane adhesion); 2) homotypic interactions between HAP2 monomers/dimer/trimers across apposed membranes that promote the initiation and/or opening of fusion pores between cells; or, 3) some combination of hetero- and homotypic interactions. Before speculating further, it is worth noting that massive overexpression of HAP2 in wild type cells (WT-OE) using a high-copy ribosomal DNA vector paired with a robust cadmium-inducible promoter, failed to increase the percent fusion observed in crosses between WT-OE and *ΔHAP2* deletion strains (Pinello et al., 2017). The inability of HAP2 overexpression to rescue or compensate for the lack of HAP2 on the apposed membrane would argue that the low fusion efficiency seen in these crosses is likely not due to in insufficient density of HAP2 on one membrane. Indeed, these data reinforce the idea that fusion pore formation is an all-or-none phenomenon since the opening of even a small number of pores in such crosses might be expected to rescue fusion efficiency of the *ΔHAP2* partner through the transfer of *HAP2* mRNA from the wildtype cell to its *ΔHAP2* partner.

Along with these observations, studies with the class II fusogens AFF-1 and EFF-1 from *C. elegans* also support the idea that CII fusogens can interact across membranes. In mosaic animals containing mixtures of cells that retained or lacked the *eff-1* gene, cell-cell fusion only occurred between cells that contained the gene (Podbilewicz et al., 2006). Furthermore, ectopically expressed AFF-1 and EFF-1 were capable of driving fusion of heterologous cells and, in some cases, could substitute for viral fusogens in pseudotyped virus infection assays, but only when the proteins were expressed in adjacent cells (in the case of cell-cell fusion) or target cells (in the case of virus fusion assays) (Podbilewicz et al., 2006; Sapir et al., 2007; Avinoam et al., 2011; Perez-Vargas et al., 2014). Given that AFF-1 and EFF-1 lack bona fide fusion loops and have no obvious way to generate motive force on apposed membranes, a requirement for bilateral (*trans*-) interactions between these proteins makes sense and various models for AFF-1/EFF-1-mediated pore formation involving monomer-dimer as well as trimer-trimer interactions have been proposed (Podbilewicz, 2014; Zeev-Ben-Mordehai et al., 2014). Similarly, studies with *Arabidopsis* HAP2 (Valansi et al., 2017) indicate that bilateral interactions are required for syncytia formation when the plant protein is expressed ectopically in mammalian cells despite the fact that it functions unilaterally during fertilization and appears to have a functional fusion loop (Johnson et al., 2004; Mori et al., 2006; Fedry et al., 2018).

There is considerable evidence that *Tetrahymena* HAP2/GCS1 also has a functional fusion loop, although substitution of an alanine residue for the highly conserved arginine expected to play a critical role in stabilizing the loop (see above, *Structural requirements for HAP2/GCS1-mediated fusion*) had no effect on fusion in crosses between wildtype and mutant (HAP2-R164A) *Tetrahymena* strains (Pinello et al., 2017). While this could be interpreted to mean that *T. thermophila* HAP2 does not have (or does not require) a fusion loop, it is entirely possible that the wildtype protein on one mating partner can rescue an otherwise defective HAP2-R164A on its mating partner through *trans*-interactions between HAP2 proteins on apposed membranes. To test that idea, it will be necessary to examine the effects of the HAP2-R164A mutation expressed in both cells of a mating *Tetrahymena* pair. Crosses between HAP2-R164A mutant cell lines would be expected to generate wildtype levels of fusion (if *T. thermophila* HAP2 can function in the absence of a fusion loop), while the same crosses would be expected to completely block fusion (if *T. thermophila* HAP2 requires a functional fusion loop in at least one mating partner). Certainly, the latter outcome would argue the importance of bilateral *trans*-interactions between HAP2 proteins on both cells of a mating pair and necessitate a model for HAP2-mediated fusion in *Tetrahymena* that accommodates both *trans*-interactions of the fusogen as well as HAP2 fusion loop interactions with the membrane. More generally, these types of studies raise the possibility that class II fusion proteins can blend different aspects of these underlying unilateral and bilateral activities depending on the context in which they are expressed. A model consistent with the idea that *Tetrahymena* HAP2 contains a functional fusion loop and can function bilaterally across membranes is shown in **Figure 4B**. Certainly, there is no *a priori* reason that the expression of HAP2, or any other gamete fusogen, should be restricted to a given mating type. Indeed, from an evolutionary perspective, the expression of HAP2/GCS1 in both mating partners in the case of *Tetrahymena* and other species may be a reflection of an ancestral isogamous state that was discarded in sexually dichotomous organisms (Mori et al., 2006; Cole et al., 2014; Kawai-Toyooka et al., 2014; Okamoto et al., 2016).

On a broader level, while the relationship between eukaryotic and viral class II fusogens is certainly intriguing and has obvious implications for the origins of eukaryotic sex, perhaps more pertinent to this review is whether HAP2/GCS1 has any role in fertilization in vertebrates. To date, database searches for HAP2/GCS1-like sequences in vertebrate genomes have come up short. Given the weak homologies between bona fide HAP2/GCS1 orthologs this may not be entirely surprising, however, it is just as likely that the corresponding gene was lost in the lineages leading to vertebrates. Given their conserved 3-dimensional organization, comparisons between known HAP2/GCS1 structures and predicted structures of protein-coding sequences within vertebrate genomes might yield useful information along these lines. Additional structural features conserved among HAP2/GCS1 orthologs might also serve as useful markers in this regard (Fedry et al., 2018).

Finally, on a more practical level, studies of parasitic protists have now made clear the utility of HAP2/GCS1 both as a vaccine target, and as marker for cryptic sexual activity in various species. Continued development of HAP2/GCS1 as an immunogen, along with further proof-of-concept that transmission-blocking vaccines (either in human or veterinary medicine) can be effective in natural settings are much anticipated. *Eimeria* and

Babesia are perhaps the best models in which to test the effectiveness of such vaccines on reducing parasite prevalence in open agricultural environments. Along with the discovery that antibodies to the *Plasmodium* HAP2 fusion loop alone can generate a transmission blocking effect in mice and humans (Angrisano et al., 2017), it will also be important to identify a range of other possible HAP2 epitopes that can elicit neutralizing antibodies in target species. Useful in this regard would be further research to identify the pre-fusion structure of HAP2/GCS1 as well as interacting partners that could themselves be targets for vaccination, along with strategies to improve vaccine potency and delivery. For example, the use mRNA-based vaccines or repeat arrays of short immunogenic peptides as were used in a recent malaria vaccine targeting the circumsporozoite protein (Jelínková et al., 2021) could potentially bypass the need to make full-length or partial versions of the HAP2/GCS1 protein which can be difficult using conventional recombinant protein expression platforms. With further success along these lines, it may soon be possible to develop new types of bivalent parasitic vaccines that include both an immunogen designed to protect the vaccinated individual from severe disease, along with a HAP2/GCS1-type immunogen to block parasite transmission and provide a broader level of protection across a community. It is possible that such a vaccine approach might allow a greater reduction in overall disease prevalence with fewer individuals needing to be vaccinated.

AUTHOR CONTRIBUTIONS

JP contributed to the writing, the design of figures and the conceptual framework of the manuscript overall. TC contributed to the writing, the design of figures and the conceptual framework of the manuscript overall.

FUNDING

Funding was provided by the National Institutes of Health, award number 5P40OD010964-17 to TC in support of the National Tetrahymena Stock Center; and award number F32-GM126735 to JP for research in *Chlamydomonas reinhardtii* on the molecular mechanisms of a gamete membrane fusion reaction during fertilization.

ACKNOWLEDGMENTS

We thank University of Maryland colleagues Drs. William J. Snell, Mayanka Awasthi, Jun Zhang, and Peeyush Ranjan; Cornell University colleagues Drs. Dwight Bowman, Donna Cassidy-Hanley; and Drs. Eric Cole (St. Olaf), Marcella Cervantes (Albion College) and Eduardo Orias (U.C. Santa Barbara) for helpful discussions; and Ms. Grace Hsu for her assistance with scientific illustrations.

REFERENCES

Abe, J., Kubo, T., Takagi, Y., Saito, T., Miura, K., Fukuzawa, H., et al. (2004). The Transcriptional Program of Synchronous Gametogenesis in *Chlamydomonas reinhardtii*. *Curr. Genet.* 46, 304–315. doi:10.1007/s00294-004-0526-4

Adair, W. S., and Mecham, R. P. (1990). *Organization and Assembly of Plant and Animal Extracellular Matrix*. San Diego: Academic Press.

Adair, W. S., Barker, R., Turner, R. S., and Wolfe, J. (1978). Demonstration of a Cell-free Factor Involved in Cell Interactions during Mating in *Tetrahymena*. *Nature* 274, 54–55. doi:10.1038/274054a0

Adair, W. S. (1985). Characterization of *Chlamydomonas* Sexual Agglutinins. *J. Cel Sci Suppl* 1985, 233–260. doi:10.1242/jcs.1985.supplement_2.13

Ahmad, T. A., El-Sayed, B. A., and El-Sayed, L. H. (2016). Development of Immunization Trials against *Eimeria* Spp. *Trials Vaccinol.* 5, 38–47. doi:10.1016/j.trivac.2016.02.001

Akopyants, N. S., Kimblin, N., Secundino, N., Patrick, R., Peters, N., Lawyer, P., et al. (2009). Demonstration of Genetic Exchange during Cyclical Development of *Leishmania* in the Sand Fly Vector. *Science* 324, 265–268. doi:10.1126/science.1169464

Aksoy, M., La, T., Lam, N., and Forest, C. (2021). A Forward Genetic Screen for Isolation of Fusion Defective Mating Type Minus Mutants in *Chlamydomonas reinhardtii*. *Hacettepe J. Biol. Chem.* 49, 321–332. doi:10.15671/hjbc.689397

Allis, C. D., and Jenuwein, T. (2016). The Molecular Hallmarks of Epigenetic Control. *Nat. Rev. Genet.* 17, 487–500. doi:10.1038/nrg.2016.59

Alzan, H. F., Lau, A. O. T., Knowles, D. P., Herndon, D. R., Ueti, M. W., Scoles, G. A., et al. (2016). Expression of 6-Cys Gene Superfamily Defines *Babesia Bovis* Sexual Stage Development within Rhipicephalus Microplus. *Plos One* 11, e0163791. doi:10.1371/journal.pone.0163791

Angrisano, F., Sala, K. A., Da, D. F., Liu, Y., Pei, J., Grishin, N. V., et al. (2017). Targeting the Conserved Fusion Loop of HAP2 Inhibits the Transmission of *Plasmodium berghei* and *falciparum*. *Cel Rep.* 21, 2868–2878. doi:10.1016/j.celrep.2017.11.024

Avinoam, O., Fridman, K., Valansi, C., Abutbul, I., Zeev-Ben-Mordehai, T., Maurer, U. E., et al. (2011). Conserved Eukaryotic Fusogens Can Fuse Viral Envelopes to Cells. *Science* 332, 589–592. doi:10.1126/science.1202333

Baek, M., DiMaio, F., Anishchenko, I., Dauparas, J., Ovchinnikov, S., Lee, G. R., et al. (2021). Accurate Prediction of Protein Structures and Interactions Using a Three-Track Neural Network. *Science* 373, 871–876. doi:10.1126/science.abj8754

Baquero, E., Fedry, J., Legrand, P., Krey, T., and Rey, F. A. (2019). Species-Specific Functional Regions of the Green Alga Gamete Fusion Protein HAP2 Revealed by Structural Studies. *Structure* 27, 113–124.e4. doi:10.1016/j.str.2018.09.014

Bastiaanssen, C., and Joo, C. (2021). Small RNA-Directed DNA Elimination: the Molecular Mechanism and its Potential for Genome Editing. *RNA Biol.* 18, 1540–1545. doi:10.1080/15476286.2021.1885208

Beck, C. F., and Acker, A. (1992). Gametic Differentiation of *Chlamydomonas reinhardtii*. *Plant Physiol.* 98, 822–826. doi:10.1104/pp.98.3.822

Beer, L. L., Boyd, E. S., Peters, J. W., and Posewitz, M. C. (2009). Engineering Algae for Biohydrogen and Biofuel Production. *Curr. Opin. Biotechnol.* 20, 264–271. doi:10.1016/j.copbio.2009.06.002

Blaby, I. K., and Blaby-Haas, C. E. (2017). "Genomics and Functional Genomics in *Chlamydomonas reinhardtii*," in *Chlamydomonas: Molecular Genetics and Physiology*. *Microbiology Monographs*. Editor M. Hippler (Cham: Springer International Publishing), 1–26. doi:10.1007/978-3-319-66365-4_1

Blackburn, E. H., Greider, C. W., and Szostak, J. W. (2006). Telomeres and Telomerase: the Path from maize, *Tetrahymena* and Yeast to Human Cancer and Aging. *Nat. Med.* 12, 1133–1138. doi:10.1038/nm1006-1133

Blagborough, A. M., Churcher, T. S., Upton, L. M., Ghani, A. C., Gething, P. W., and Sinden, R. E. (2013). Transmission-blocking Interventions Eliminate Malaria from Laboratory Populations. *Nat. Commun.* 4, 1812. doi:10.1038/ncomms2840

Blanc-Mathieu, R., Krasovec, M., Hebrard, M., Yau, S., Desgranges, E., Martin, J., et al. (2017). Population Genomics of Picophytoplankton Unveils Novel Chromosome Hypervariability. *Sci. Adv.* 3, e1700239. doi:10.1126/sciadv.1700239

Borg, M., Brownfield, L., Khatab, H., Sidorova, A., Lingaya, M., and Twell, D. (2011). The R2R3 MYB Transcription Factor DUO1 Activates a Male

Germline-Specific Regulon Essential for Sperm Cell Differentiation in *Arabidopsis*. *Plant Cel.* 23, 534–549. doi:10.1105/tpc.110.081059

Bowman, D. D. (2014). *Georgis' Parasitology for Veterinarians*. 10th edition. St. Louis, Missouri: Elsevier.

Brandeis, M. (2021). Were Eukaryotes Made by Sex? Sex Might have been Vital for Merging Endosymbiont and Host Genomes Giving Rise to Eukaryotes. *BioEssays* 43, 2000256. doi:10.1002/bies.202000256

Brown, F., Tirone, S., and Wolfe, J. (1993). Early Encounters of the Repetitive Kind: a Prelude to Cell Adhesion in Conjugating *Tetrahymena thermophila*. *Dev. Dyn.* 196, 195–204. doi:10.1002/aja.1001960306

Brownell, J. E., Zhou, J., Ranalli, T., Kobayashi, R., Edmondson, D. G., Roth, S. Y., et al. (1996). *Tetrahymena* Histone Acetyltransferase A: A Homolog to Yeast Gcn5p Linking Histone Acetylation to Gene Activation. *Cell* 84, 843–851. doi:10.1016/S0092-8674(00)81063-6

Bruns, P. J., and Brussard, T. B. (1974). Pair Formation in *Tetrahymena pyriformis*, an Inducible Developmental System. *J. Exp. Zool.* 188, 337–344. doi:10.1002/jez.1401880309

Buchanan, M. J., and Snell, W. J. (1988). Biochemical Studies on Lysin, a Cell wall Degrading Enzyme Released during Fertilization in *Chlamydomonas*. *Exp. Cel Res.* 179, 181–193. doi:10.1016/0014-4827(88)90357-6

Buchanan, M. J., Imam, S. H., Eskue, W. A., and Snell, W. J. (1989). Activation of the Cell wall Degrading Protease, Lysin, during Sexual Signalling in *Chlamydomonas*: the Enzyme Is Stored as an Inactive, Higher Relative Molecular Mass Precursor in the Periplasm. *J. Cel Biol.* 108, 199–207. doi:10.1083/jcb.108.1.199

Camacho-Nuez, M., Hernández-Silva, D. J., Castañeda-Ortiz, E. J., Paredes-Martínez, M. E., Rocha-Martínez, M. K., Alvarez-Sánchez, M. E., et al. (2017). Hap2, a Novel Gene in *Babesia bigemina* Is Expressed in Tick Stages, and Specific Antibodies Block Zygote Formation. *Parasites Vectors* 10, 568. doi:10.1186/s13071-017-2510-0

Cao, M., Ning, J., Hernandez-Lara, C. I., Belzile, O., Wang, Q., Dutcher, S. K., et al. (2015). Uni-directional Ciliary Membrane Protein Trafficking by a Cytoplasmic Retrograde IFT Motor and Ciliary Ectosome Shedding. *eLife* 4, e05242. doi:10.7554/eLife.05242

Cassidy-Hanley, D. M. (2012). "*Tetrahymena* in the Laboratory: Strain Resources, Methods for Culture, Maintenance, and Storage," in *Methods in Cell Biology* (Amsterdam, Boston, Heidelberg: Elsevier/Academic Press), 237–276. doi:10.1016/B978-0-12-385967-9.00008-6

Castellanos, F. (2018). Membrane-Mediated Cell Biological Communication Mechanisms in Reproduction. Available at: http://ora.ox.ac.uk/objects/uuid:232ec994-34bc-4903-b16b-f9c54815a481 (Accessed August 11, 2021).

Cavalier-Smith, T. (1975). Electron and Light Microscopy of Gametogenesis and Gamete Fusion inChlamydomonas Reinhardii. *Protoplasma* 86, 1–18. doi:10.1007/BF01275619

Cervantes, M. D., Hamilton, E. P., Xiong, J., Lawson, M. J., Yuan, D., Hadjithomas, M., et al. (2013). Selecting One of Several Mating Types through Gene Segment Joining and Deletion in *Tetrahymena thermophila*. *Plos Biol.* 11, e1001518. doi:10.1371/journal.pbio.1001518

Chan, K. M. C., Son, S., Schmid, E. M., and Fletcher, D. A. (2020). A Viral Fusogen Hijacks the Actin Cytoskeleton to Drive Cell-Cell Fusion. *eLife* 9, e51358. doi:10.7554/eLife.51358

Cheng, T., Wang, Y., Huang, J., Chen, X., Zhao, X., Gao, S., et al. (2019). Our Recent Progress in Epigenetic Research Using the Model Ciliate, *Tetrahymena thermophila*. *Mar. Life Sci. Technol.* 1, 4–14. doi:10.1007/s42995-019-00015-0

Claes, H. (1971). Autolyse der zellwand bei den gameten von *Chlamydomonas reinhardii*. *Archiv. Mikrobiol.* 78, 180–188. doi:10.1007/BF00424874

Claes, H. (1975). Influence of Concanavalin A on Autolysis of Gametes from *Chlamydomonas reinhardii*. *Arch. Microbiol.* 103, 225–230. doi:10.1007/BF00436354

Claes, H. (1977). Non-specific Stimulation of the Autolytic System in Gametes from *Chlamydomonas reinhardii*. *Exp. Cel Res.* 108, 221–229. doi:10.1016/S0014-4827(77)80028-1

Claes, H. (1980). Calcium Lonophore-Induced Stimulation of Secretory Activity in *Chlamydomonas reinhardii*. *Arch. Microbiol.* 124, 81–86. doi:10.1007/BF00407032

Clark, T. (2018). HAP2/GCS1: Mounting Evidence of Our True Biological EVE? *Plos Biol.* 16, e3000007. doi:10.1371/journal.pbio.3000007

Coelho, S. M., and Umen, J. (2021). Switching it Up: Algal Insights into Sexual Transitions. *Plant Reprod.* 34, 287–296. doi:10.1007/s00497-021-00417-0

Cole, E. S., Anderson, P. C., Fulton, R. B., Majerus, M. E., Rooney, M. G., Savage, J. M., et al. (2008). A Proteomics Approach to CloningFenestrinfrom the Nuclear Exchange Junction ofTetrahymena. *J. Eukaryot. Microbiol.* 55, 245–256. doi:10.1111/j.1550-7408.2008.00337.x

Cole, E. S., Cassidy-Hanley, D., Fricke Pinello, J., Zeng, H., Hsueh, M., Kolbin, D., et al. (2014). Function of the Male-gamete-specific Fusion Protein HAP2 in a Seven-Sexed Ciliate. *Curr. Biol.* 24, 2168–2173. doi:10.1016/j.cub.2014.07.064

Cole, E. S., Giddings, T. H., Ozzello, C., Winey, M., O'Toole, E., Orias, J., et al. (2015). Membrane Dynamics at the Nuclear Exchange junction during Early Mating (One to Four Hours) in the Ciliate *Tetrahymena thermophila*. *Eukaryot. Cel.* 14, 116–127. doi:10.1128/EC.00164-14

Cole, E. S., Dmytrenko, O., Chmelik, C. J., Li, M., Christensen, T. A., Macon, E. P., et al. (2018). Restoration of Cellular Integrity Following "Ballistic" Pronuclear Exchange during *Tetrahymena* Conjugation. *Dev. Biol.* 444, 33–40. doi:10.1016/j.ydbio.2018.09.019

Cole, E. S. (2006). "The *Tetrahymena* Conjugation Junction," in *Cell-Cell Channels* (New York, NY: Springer New York), 39–62. doi:10.1007/978-0-387-46957-7_3

Cole, E. S. (2016). "Cell-Cell Interactions Leading to Establishment of a Mating Junction in Tetrahymena and Paramecium, Two "Contact-Mediated" Mating Systems," in *Biocommunication of Ciliates*. Editors G. Witzany and M. Nowacki (Cham: Springer International Publishing), 195–220. doi:10.1007/978-3-319-32211-7_12

K. Collins ed. (2012). *Tetrahymena thermophila*. 1. ed. Amsterdam Boston Heidelberg: Elsevier/Academic Press.

Couzin, J. (2002). Small RNAs Make Big Splash. *Science* 298, 2296–2297. doi:10.1126/science.298.5602.2296

Cyprys, P., Lindemeier, M., and Sprunck, S. (2019). Gamete Fusion Is Facilitated by Two Sperm Cell-Expressed DUF679 Membrane Proteins. *Nat. Plants* 5, 253–257. doi:10.1038/s41477-019-0382-3

Datoo, M. S., Natama, M. H., Somé, A., Traoré, O., Rouamba, T., Bellamy, D., et al. (2021). Efficacy of a Low-Dose Candidate Malaria Vaccine, R21 in Adjuvant Matrix-M, with Seasonal Administration to Children in Burkina Faso: a Randomised Controlled Trial. *Lancet* 397, 1809–1818. doi:10.1016/S0140-6736(21)00943-0

de Boer, S. M., Kortekaas, J., Spel, L., Rottier, P. J. M., Moormann, R. J. M., and Bosch, B. J. (2012). Acid-activated Structural Reorganization of the Rift Valley Fever Virus Gc Fusion Protein. *J. Virol.* 86, 13642–13652. doi:10.1128/JVI.01973-12

De Hoff, P. L., Ferris, P., Olson, B. J. S. C., Miyagi, A., Geng, S., and Umen, J. G. (2013). Species and Population Level Molecular Profiling Reveals Cryptic Recombination and Emergent Asymmetry in the Dimorphic Mating Locus of *C. reinhardtii*. *Plos Genet.* 9, e1003724. doi:10.1371/journal.pgen.1003724

Detmers, P. A., Goodenough, U. W., and Condeelis, J. (1983). Elongation of the Fertilization Tubule in *Chlamydomonas*: New Observations on the Core Microfilaments and the Effect of Transient Intracellular Signals on Their Structural Integrity. *J. Cel Biol.* 97, 522–532. doi:10.1083/jcb.97.2.522

Detmers, P. A., Carboni, J. M., and Condeelis, J. (1985). Localization of Actin in *Chlamydomonas* Using Antiactin and NBD-Phallacidin. *Cel Motil.* 5, 415–430. doi:10.1002/cm.970050505

Doms, R. W. (2017). What Came First-The Virus or the Egg? *Cell* 168, 755–757. doi:10.1016/j.cell.2017.02.012

Dunthorn, M., and Katz, L. A. (2010). Secretive Ciliates and Putative Asexuality in Microbial Eukaryotes. *Trends Microbiol.* 18, 183–188. doi:10.1016/j.tim.2010.02.005

Engel, B. D., Schaffer, M., Kuhn Cuellar, L., Villa, E., Plitzko, J. M., and Baumeister, W. (2015). Native Architecture of the *Chlamydomonas* Chloroplast Revealed by *In Situ* Cryo-Electron Tomography. *eLife* 4, e04889. doi:10.7554/eLife.04889

Farhat, D. C., Swale, C., Dard, C., Cannella, D., Ortet, P., Barakat, M., et al. (2020). A MORC-Driven Transcriptional Switch Controls *Toxoplasma* Developmental Trajectories and Sexual Commitment. *Nat. Microbiol.* 5, 570–583. doi:10.1038/s41564-020-0674-4

Fédry, J., Liu, Y., Péhau-Arnaudet, G., Pei, J., Li, W., Tortorici, M. A., et al. (2017). The Ancient Gamete Fusogen HAP2 Is a Eukaryotic Class II Fusion Protein. *Cell* 168, 904–915.e10. doi:10.1016/j.cell.2017.01.024

Fedry, J., Forcina, J., Legrand, P., Péhau-Arnaudet, G., Haouz, A., Johnson, M., et al. (2018). Evolutionary Diversification of the HAP2 Membrane Insertion Motifs to Drive Gamete Fusion across Eukaryotes. *Plos Biol.* 16, e2006357. doi:10.1371/journal.pbio.2006357

Feix, A. S., Cruz-Bustos, T., Ruttkowski, B., and Joachim, A. (2020). Characterization of *Cystoisospora suis* sexual stages *in vitro*. *Parasit. Vectors* 13, 143. doi:10.1186/s13071-020-04014-4

Feix, A. S., Cruz-Bustos, T., Ruttkowski, B., Mötz, M., Rümenapf, T., and Joachim, A. (2021). Progression of Asexual to Sexual Stages of *Cystoisospora suis* in a Host Cell-free Environment as a Model for Coccidia. *Parasitology* 148, 1475–1481. doi:10.1017/S0031182021001074

Feng, J., Dong, X., Pinello, J., Zhang, J., Lu, C., Iacob, R. E., et al. (2018). Fusion Surface Structure, Function, and Dynamics of Gamete Fusogen HAP2. *Elife* 7, e39772. doi:10.7554/eLife.39772

Ferguson, D. J. (2002). *Toxoplasma gondii* and Sex: Essential or Optional Extra? *Trends Parasitol.* 18, 355–359. doi:10.1016/s1471-4922(02)02330-9

Ferris, P. J., and Goodenough, U. W. (1997). Mating Type in *Chlamydomonas* Is Specified by Mid, the *Minus*-Dominance Gene. *Genetics* 146, 859–869. doi:10.1093/genetics/146.3.859

Ferris, P. J., Woessner, J. P., and Goodenough, U. W. (1996). A Sex Recognition Glycoprotein Is Encoded by the Plus Mating-type Gene Fus1 of *Chlamydomonas reinhardtii*. *Mol. Biol. Cel.* 7, 1235–1248. doi:10.1091/mbc.7.8.1235

Ferris, P. J., Woessner, J. P., Waffenschmidt, S., Kilz, S., Drees, J., and Goodenough, U. W. (2001). Glycosylated Polyproline II Rods with Kinks as a Structural Motif in Plant Hydroxyproline-Rich Glycoproteins. *Biochemistry* 40, 2978–2987. doi:10.1021/bi0023605

Ferris, P. J., Armbrust, E. V., and Goodenough, U. W. (2002). Genetic Structure of the Mating-type Locus of *Chlamydomonas reinhardtii*. *Genetics* 160, 181–200. doi:10.1093/genetics/160.1.181

Ferris, P. J., Waffenschmidt, S., Umen, J. G., Lin, H., Lee, J.-H., Ishida, K., et al. (2005). Plus and Minus Sexual Agglutinins from *Chlamydomonas reinhardtii*. *Plant Cel.* 17, 597–615. doi:10.1105/tpc.104.028035

Forest, C. L. (1983). Specific Contact between Mating Structure Membranes Observed in Conditional Fusion-Defective *Chlamydomonas* Mutants. *Exp. Cel Res.* 148, 143–154. doi:10.1016/0014-4827(83)90194-5

Fujishima, M., Tsuda, M., Mikami, Y., and Shinoda, K. (1993). Costimulation-induced Rounding in *Tetrahymena thermophila*: Early Cell Shape Transformation Induced by Sexual Cell-To-Cell Collisions between Complementary Mating Types. *Dev. Biol.* 155, 198–205. doi:10.1006/dbio.1993.1018

Gaertig, J., and Fleury, A. (1992). Spatio-temporal Reorganization of Intracytoplasmic Microtubules Is Associated with Nuclear Selection and Differentiation during the Developmental Process in the ciliate *Tetrahymena thermophila*. *Protoplasma* 167, 74–87. doi:10.1007/BF01353583

Gallaher, S. D., Fitz-Gibbon, S. T., Glaesener, A. G., Pellegrini, M., and Merchant, S. S. (2015). *Chlamydomonas* Genome Resource for Laboratory Strains Reveals a Mosaic of Sequence Variation, Identifies True Strain Histories, and Enables Strain-Specific Studies. *Plant Cel.* 27, 2335–2352. doi:10.1105/tpc.15.00508

Gallaher, S. D., Fitz-Gibbon, S. T., Strenkert, D., Purvine, S. O., Pellegrini, M., and Merchant, S. S. (2018). High-throughput Sequencing of the Chloroplast and Mitochondrion of *Chlamydomonas reinhardtii* to Generate Improved De Novo Assemblies, Analyze Expression Patterns and Transcript Speciation, and Evaluate Diversity Among Laboratory Strains and Wild Isolates. *Plant J.* 93, 545–565. doi:10.1111/tpj.13788

Galloway, R. E., and Goodenough, U. W. (1985). Genetic Analysis of Mating Locus Linked Mutations in *Chlamydomonas reinhardii*. *Genetics* 111, 447–461. doi:10.1093/genetics/111.3.447

Garcia, V. E. (2012). A Generative Cell Specific 1 Ortholog in *Drosophila melanogaster*. Available at: https://digital.lib.washington.edu/researchworks/bitstream/handle/1773/20270/Garcia_washington_0250O_10191.pdf?sequence=1 (Accessed January 18, 2016).

Gaunt, M. W., Yeo, M., Frame, I. A., Stothard, J. R., Carrasco, H. J., Taylor, M. C., et al. (2003). Mechanism of Genetic Exchange in American *Trypanosomes*. *Nature* 421, 936–939. doi:10.1038/nature01438

Geng, S., De Hoff, P., and Umen, J. G. (2014). Evolution of Sexes from an Ancestral Mating-type Specification Pathway. *PLOS Biol.* 12, e1001904. doi:10.1371/journal.pbio.1001904

Geng, S., Miyagi, A., and Umen, J. G. (2018). Evolutionary Divergence of the Sex-Determining Gene MID Uncoupled from the Transition to Anisogamy in Volvocine Algae. *Development* 145, dev162537. doi:10.1242/dev.162537

Gibbons, D. L., and Kielian, M. (2002). Molecular Dissection of the Semliki Forest Virus Homotrimer Reveals Two Functionally Distinct Regions of the Fusion Protein. *J. Virol.* 76, 1194–1205. doi:10.1128/JVI.76.3.1194-1205.2002

Gibbons, I. R., and Rowe, A. J. (1965). Dynein: A Protein with Adenosine Triphosphatase Activity from Cilia. *Science* 149, 424–426. doi:10.1126/science.149.3682.424

Gibbons, D. L., Vaney, M.-C., Roussel, A., Vigouroux, A., Reilly, B., Lepault, J., et al. (2004). Conformational Change and Protein-Protein Interactions of the Fusion Protein of Semliki Forest Virus. *Nature* 427, 320–325. doi:10.1038/nature02239

Gibson, W., Peacock, L., Ferris, V., Williams, K., and Bailey, M. (2008). The Use of Yellow Fluorescent Hybrids to Indicate Mating in *Trypanosoma brucei*. *Parasites Vectors* 1, 4. doi:10.1186/1756-3305-1-4

Gimpel, J. A., Specht, E. A., Georgianna, D. R., and Mayfield, S. P. (2013). Advances in Microalgae Engineering and Synthetic Biology Applications for Biofuel Production. *Curr. Opin. Chem. Biol.* 17, 489–495. doi:10.1016/j.cbpa.2013.03.038

Goodenough, U., and Heitman, J. (2014). Origins of Eukaryotic Sexual Reproduction. *Cold Spring Harbor Perspect. Biol.* 6, a016154. doi:10.1101/cshperspect.a016154

Goodenough, U. W., and Weiss, R. L. (1975). Gametic Differentiation in *Chlamydomonas reinhardtii*. III. Cell wall Lysis and Microfilament-Associated Mating Structure Activation in Wild-type and Mutant Strains. *J. Cel Biol.* 67, 623–637. doi:10.1083/jcb.67.3.623

Goodenough, U. W., Hwang, C., and Warren, A. J. (1978). Sex-Limited Expression of Gene Loci Controlling Flagellar Membrane Agglutination in the *Chlamydomonas* Mating Reaction. *Genetics* 89, 235–243. doi:10.1093/genetics/89.2.235

Goodenough, U. W., Detmers, P. A., and Hwang, C. (1982). Activation for Cell Fusion in *Chlamydomonas*: Analysis of Wild-type Gametes and Nonfusing Mutants. *J. Cel Biol.* 92, 378–386. doi:10.1083/jcb.92.2.378

Goodenough, U. W., Armbrust, E. V., Campbell, A. M., and Ferris, P. J. (1995). Molecular Genetics of Sexuality in *Chlamydomonas*. *Annu. Rev. Plant Physiol. Plant Mol. Biol.* 46, 21–44. doi:10.1146/annurev.pp.46.060195.000321

Goodenough, U., Lin, H., and Lee, J.-H. (2007). Sex Determination in *Chlamydomonas*. *Semin. Cel Dev. Biol.* 18, 350–361. doi:10.1016/j.semcdb.2007.02.006

Griffin, D., Gwadz, R., Hotez, P., Knirsch, C., and Despommier, D. (2019). "Parasitic Diseases Seventh Edition," in *Amazon Digital Services LLC - Kdp Print Us*. Available at: https://books.google.com/books?id=20BbxQEACAAJ.

Hammar, L., Markarian, S., Haag, L., Lankinen, H., Salmi, A., and Cheng, R. H. (2003). Prefusion Rearrangements Resulting in Fusion Peptide Exposure in Semliki Forest Virus. *J. Biol. Chem.* 278, 7189–7198. doi:10.1074/jbc.M206015200

Hanyu, K., Takemasa, T., Numata, O., Takahashi, M., and Watanabe, Y. (1995). Immunofluorescence Localization of a 25-kDa *Tetrahymena* EF-Hand Ca(2+)-Binding Protein, TCBP-25, in the Cell Cortex and Possible Involvement in Conjugation. *Exp. Cel Res.* 219, 487–493. doi:10.1006/excr.1995.1256

Harris, E. H. (2001). *Chlamydomonas* as a Model Organism. *Annu. Rev. Plant Physiol. Plant Mol. Biol.* 52, 363–406. doi:10.1146/annurev.arplant.52.1.363

Harris, E. H. (2009). *The Chlamydomonas Sourcebook: Introduction to Chlamydomonas and its Laboratory Use: Volume 1*. Cambridge, United Kingdom: Academic Press.

Harris, E. H. (2013). The *Chlamydomonas* Sourcebook: A Comprehensive Guide To Biology and Laboratory Use. Cambridge, United Kingdom: Elsevier.

Hedberg, A., and Johansen, S. D. (2013). Nuclear Group I Introns in Self-Splicing and beyond. *Mobile DNA* 4, 17. doi:10.1186/1759-8753-4-17

Hegemann, P., and Nagel, G. (2013). From Channelrhodopsins to Optogenetics. *EMBO Mol. Med.* 5, 173–176. doi:10.1002/emmm.201202387

Herschlag, D., and Cech, T. R. (1990). Catalysis of RNA Cleavage by the *Tetrahymena thermophila* Ribozyme. 2. Kinetic Description of the Reaction

of an RNA Substrate that Forms a Mismatch at the Active Site. *Biochemistry* 29, 10172–10180. doi:10.1021/bi00496a004

Higo, A., Kawashima, T., Borg, M., Zhao, M., López-Vidriero, I., Sakayama, H., et al. (2018). Transcription Factor DUO1 Generated by Neo-Functionalization Is Associated with Evolution of Sperm Differentiation in Plants. *Nat. Commun.* 9, 5283. doi:10.1038/s41467-018-07728-3

Hirai, M., Arai, M., Mori, T., Miyagishima, S.-y., Kawai, S., Kita, K., et al. (2008). Male Fertility of Malaria Parasites Is Determined by GCS1, a Plant-type Reproduction Factor. *Curr. Biol.* 18, 607–613. doi:10.1016/j.cub.2008.03.045

Hisanaga, T., Yamaoka, S., Kawashima, T., Higo, A., Nakajima, K., Araki, T., et al. (2019). Building New Insights in Plant Gametogenesis from an Evolutionary Perspective. *Nat. Plants* 5, 663–669. doi:10.1038/s41477-019-0466-0

Hofstatter, P. G., and Lahr, D. J. G. (2019). All Eukaryotes Are Sexual, unless Proven Otherwise. *BioEssays* 41, 1800246. doi:10.1002/bies.201800246

Horne, R. W., Davies, D. R., Norton, K., and Gurney-Smith, M. (1971). Electron Microscope and Optical Diffraction Studies on Isolated Cell Walls from *Chlamydomonas*. *Nature* 232, 493–495. doi:10.1038/232493a0

Huang, K., and Beck, C. F. (2003). Phototropin Is the Blue-Light Receptor that Controls Multiple Steps in the Sexual Life Cycle of the green Alga *Chlamydomonas reinhardtii*. *Proc. Natl. Acad. Sci.* 100, 6269–6274. doi:10.1073/pnas.0931459100

Hussein, H. E., Bastos, R. G., Schneider, D. A., Johnson, W. C., Adham, F. K., Davis, W. C., et al. (2017). The *Babesia bovis* Hap2 Gene Is Not Required for Blood Stage Replication, but Expressed upon *In Vitro* Sexual Stage Induction. *Plos Negl. Trop. Dis.* 11, e0005965. doi:10.1371/journal.pntd.0005965

Hutchinson, S., Foulon, S., Crouzols, A., Menafra, R., Rotureau, B., Griffiths, A. D., et al. (2021). The Establishment of Variant Surface Glycoprotein Monoallelic Expression Revealed by Single-Cell RNA-Seq of *Trypanosoma brucei* in the Tsetse Fly Salivary Glands. *Plos Pathog.* 17, e1009904. doi:10.1371/journal.ppat.1009904

Hwang, C. J., Monk, B. C., and Goodenough, U. W. (1981). Linkage of Mutations Affecting Minus Flagellar Membrane Agglutinability to the Mt - Mating-type Locus of *Chlamydomonas*. *Genetics* 99, 41–47. doi:10.1093/genetics/99.1.41

Inbar, E., Shaik, J., Iantorno, S. A., Romano, A., Nzelu, C. O., Owens, K., et al. (2019). Whole Genome Sequencing of Experimental Hybrids Supports Meiosis-like Sexual Recombination in *Leishmania*. *Plos Genet.* 15, e1008042. doi:10.1371/journal.pgen.1008042

Innes, E. A., Bartley, P. M., Maley, S., Katzer, F., and Buxton, D. (2009). Veterinary Vaccines against *Toxoplasma gondii*. *Mem. Inst. Oswaldo Cruz* 104, 246–251. doi:10.1590/S0074-02762009000200018

Jang, S. I., Lillehoj, H. S., Lee, S. H., Lee, K. W., Park, M. S., Cha, S.-R., et al. (2010). *Eimeria Maxima* Recombinant Gam82 Gametocyte Antigen Vaccine Protects against Coccidiosis and Augments Humoral and Cell-Mediated Immunity. *Vaccine* 28, 2980–2985. doi:10.1016/j.vaccine.2010.02.011

Jelínková, L., Jhun, H., Eaton, A., Petrovsky, N., Zavala, F., and Chackerian, B. (2021). An Epitope-Based Malaria Vaccine Targeting the Junctional Region of Circumsporozoite Protein. *Npj Vaccin.* 6, 1–10. doi:10.1038/s41541-020-00274-4

Jenni, L., Marti, S., Schweizer, J., Betschart, B., Le Page, R. W. F., Wells, J. M., et al. (1986). Hybrid Formation between African *Trypanosomes* during Cyclical Transmission. *Nature* 322, 173–175. doi:10.1038/322173a0

Jiang, J., Chan, H., Cash, D. D., Miracco, E. J., Ogorzalek Loo, R. R., Upton, H. E., et al. (2015). Structure of *Tetrahymena* Telomerase Reveals Previously Unknown Subunits, Functions, and Interactions. *Science* 350, aab4070. doi:10.1126/science.aab4070

Johnson, M. A., von Besser, K., Zhou, Q., Smith, E., Aux, G., Patton, D., et al. (2004). *Arabidopsis* Hapless Mutations Define Essential Gametophytic Functions. *Genetics* 168, 971–982. doi:10.1534/genetics.104.029447

Johnson, M. A. (2010). Fertilization: Monogamy by Mutually Assured Destruction. *Curr. Biol.* 20, R571–R573. doi:10.1016/j.cub.2010.05.026

Kato-Minoura, T., Hirono, M., and Kamiya, R. (1997). *Chlamydomonas* Inner-Arm Dynein Mutant, ida5, Has a Mutation in an Actin-Encoding Gene. *J. Cel Biol.* 137, 649–656. doi:10.1083/jcb.137.3.649

Kawai-Toyooka, H., Mori, T., Hamaji, T., Suzuki, M., Olson, B. J. S. C., Uemura, T., et al. (2014). Sex-Specific Posttranslational Regulation of the Gamete Fusogen GCS1 in the Isogamous Volvocine Alga *Gonium pectorale*. *Eukaryot. Cel.* 13, 648–656. doi:10.1128/EC.00330-13

Kielian, M., and Rey, F. A. (2006). Virus Membrane-Fusion Proteins: More Than One Way to Make a Hairpin. *Nat. Rev. Microbiol.* 4, 67–76. doi:10.1038/nrmicro1326

Kim, J. H., and Chen, E. H. (2019). The Fusogenic Synapse at a Glance. *J. Cel Sci.* 132, jcs213124. doi:10.1242/jcs.213124

Kurczy, M. E., Piehowski, P. D., Van Bell, C. T., Heien, M. L., Winograd, N., and Ewing, A. G. (2010). Mass Spectrometry Imaging of Mating *Tetrahymena* Show that Changes in Cell Morphology Regulate Lipid Domain Formation. *Proc. Natl. Acad. Sci.* 107, 2751–2756. doi:10.1073/pnas.0908101107

Kurvari, V., Grishin, N. V., and Snell, W. J. (1998). A Gamete-specific, Sex-Limited Homeodomain Protein in *Chlamydomonas*. *J. Cel Biol.* 143, 1971–1980. doi:10.1083/jcb.143.7.1971

Laurens, M. B. (2020). RTS,S/AS01 Vaccine (Mosquirix^{TM}): an Overview. *Hum. Vaccin. Immunother.* 16, 480–489. doi:10.1080/21645515.2019.1669415

Lescar, J., Roussel, A., Wien, M. W., Navaza, J., Fuller, S. D., Wengler, G., et al. (2001). The Fusion Glycoprotein Shell of Semliki Forest Virus. *Cell* 105, 137–148. doi:10.1016/s0092-8674(01)00303-8

Levine, R. P., and Goodenough, U. W. (1970). The Genetics of Photosynthesis and of the Chloroplast in *Chlamydomonas reinhardi*. *Annu. Rev. Genet.* 4, 397–408. doi:10.1146/annurev.ge.04.120170.002145

Liang, Y., and Pan, J. (2013). Regulation of Flagellar Biogenesis by a Calcium Dependent Protein Kinase in *Chlamydomonas reinhardtii*. *Plos One* 8, e69902. doi:10.1371/journal.pone.0069902

Lin, H., and Goodenough, U. W. (2007). Gametogenesis in the *Chlamydomonas reinhardtii Minus* Mating Type Is Controlled by Two Genes, MID and MTD1. *Genetics* 176, 913–925. doi:10.1534/genetics.106.066167

Lippuner, C., Ramakrishnan, C., Basso, W. U., Schmid, M. W., Okoniewski, M., Smith, N. C., et al. (2018). RNA-Seq Analysis during the Life Cycle of *Cryptosporidium parvumi* Reveals Significant Differential Gene Expression between Proliferating Stages in the Intestine and Infectious Sporozoites. *Int. J. Parasitol.* 48, 413–422. doi:10.1016/j.ijpara.2017.10.007

Liu, C. Y., and Kielian, M. (2009). E1 Mutants Identify a Critical Region in the Trimer Interface of the Semliki forest Virus Fusion Protein. *J. Virol.* 83, 11298–11306. doi:10.1128/JVI.01147-09

Liu, Y., Taverna, S. D., Muratore, T. L., Shabanowitz, J., Hunt, D. F., and Allis, C. D. (2007). RNAi-dependent H3K27 Methylation Is Required for Heterochromatin Formation and DNA Elimination in *Tetrahymena*. *Genes Dev.* 21, 1530–1545. doi:10.1101/gad.1544207

Liu, Y., Tewari, R., Ning, J., Blagborough, A. M., Garbom, S., Pei, J., et al. (2008). The Conserved Plant Sterility Gene HAP2 Functions after Attachment of Fusogenic Membranes in *Chlamydomonas* and *Plasmodium* Gametes. *Genes Dev.* 22, 1051–1068. doi:10.1101/gad.1656508

Liu, Y., Misamore, M. J., and Snell, W. J. (2010). Membrane Fusion Triggers Rapid Degradation of Two Gamete-Specific, Fusion-Essential Proteins in a Membrane Block to Polygamy in *Chlamydomonas*. *Development* 137, 1473–1481. doi:10.1242/dev.044743

Liu, Y., Pei, J., Grishin, N., and Snell, W. J. (2015). The Cytoplasmic Domain of the Gamete Membrane Fusion Protein HAP2 Targets the Protein to the Fusion Site in *Chlamydomonas* and Regulates the Fusion Reaction. *Development* 142, 962–971. doi:10.1242/dev.118844

Louradour, I., Ferreira, T. R., Duge, E., Karunaweera, N., Paun, A., and Sacks, D. (2021). Stress Conditions Promote the Mating Competency of *Leishmania* Promastigotes *In Vitro* Marked by Expression of the Ancestral Gamete Fusogen HAP2. *Microbiology*. doi:10.1101/2021.08.31.458317

Love, B., and Rotheim, M. B. (1984). Cell Surface Interactions in Conjugation: *Tetrahymena* Ciliary Membrane Vesicles. *Mol. Cel. Biol.* 4, 681–687. doi:10.1128/mcb.4.4.681

Luxmi, R., Blaby-Haas, C., Kumar, D., Rauniyar, N., King, S. M., Mains, R. E., et al. (2018). Proteases Shape the *Chlamydomonas* Secretome: Comparison to Classical Neuropeptide Processing Machinery. *Proteomes* 6, 36. doi:10.3390/proteomes6040036

Luxmi, R., Kumar, D., Mains, R. E., King, S. M., and Eipper, B. A. (2019). Cilia-based Peptidergic Signaling. *Plos Biol.* 17, e3000566. doi:10.1371/journal.pbio.3000566

Matsuda, Y., Tamaki, S., and Tsubo, Y. (1978). Mating Type Specific Induction of Cell wall Lytic Factor by Agglutination of Gametes in *Chlamydomonas reinhardtii*. *Plant Cel Physiol.* 19, 1253–1261. doi:10.1093/oxfordjournals.pcp.a075706

Mesland, D. A., Hoffman, J. L., Caligor, E., and Goodenough, U. W. (1980). Flagellar Tip Activation Stimulated by Membrane Adhesions in *Chlamydomonas* Gametes. *J. Cel Biol.* 84, 599–617. doi:10.1083/jcb.84.3.599

Miao, W., Xiong, J., Bowen, J., Wang, W., Liu, Y., Braguinets, O., et al. (2009). Microarray Analyses of Gene Expression during the *Tetrahymena thermophila* Life Cycle. *PLOS ONE* 4, e4429. doi:10.1371/journal.pone.0004429

Miller, M. A., Grigg, M. E., Kreuder, C., James, E. R., Melli, A. C., Crosbie, P. R., et al. (2004). An Unusual Genotype of *Toxoplasma gondii* Is Common in California Sea Otters (Enhydra Lutris Nereis) and Is a Cause of Mortality. *Int. J. Parasitol.* 34, 275–284. doi:10.1016/j.ijpara.2003.12.008

Misamore, M. J., Gupta, S., and Snell, W. J. (2003). The *Chlamydomonas* Fus1 Protein Is Present on the Mating Type Plus Fusion Organelle and Required for a Critical Membrane Adhesion Event During Fusion With Minus Gametes. *MBoC* 14, 2530–2542. doi:10.1091/mbc.E02-12-0790

Mori, T., Kuroiwa, H., Higashiyama, T., and Kuroiwa, T. (2006). GENERATIVE CELL SPECIFIC 1 Is Essential for Angiosperm Fertilization. *Nat. Cel Biol.* 8, 64–71. doi:10.1038/ncb1345

Mori, T., Hirai, M., Kuroiwa, T., and Miyagishima, S.-y. (2010). The Functional Domain of GCS1-Based Gamete Fusion Resides in the Amino Terminus in Plant and Parasite Species. *PloS one* 5, e15957. doi:10.1371/journal.pone.0015957

Mori, T., Igawa, T., Tamiya, G., Miyagishima, S.-Y., and Berger, F. (2014). Gamete Attachment Requires GEX2 for Successful Fertilization in *Arabidopsis*. *Curr. Biol.* 24, 170–175. doi:10.1016/j.cub.2013.11.030

Mori, T., Kawai-Toyooka, H., Igawa, T., and Nozaki, H. (2015). Gamete Dialogs in Green Lineages. *Mol. Plant* 8, 1442–1454. doi:10.1016/j.molp.2015.06.008

Nagel, G., Szellas, T., Huhn, W., Kateriya, S., Adeishvili, N., Berthold, P., et al. (2003). Channelrhodopsin-2, a Directly Light-Gated Cation-Selective Membrane Channel. *Proc. Natl. Acad. Sci.* 100, 13940–13945. doi:10.1073/pnas.1936192100

Nanney, D. L., and Caughey, P. A. (1953). Mating Type Determination in *Tetrahymena pyriformis*. *Proc. Natl. Acad. Sci.* 39, 1057–1063. doi:10.1073/pnas.39.10.1057

Neeb, Z. T., and Nowacki, M. (2018). RNA-mediated Transgenerational Inheritance in Ciliates and Plants. *Chromosoma* 127, 19–27. doi:10.1007/s00412-017-0655-4

Nelsen, E. M., Williams, N. E., Yi, H., Knaak, J., and Frankel, J. (1994). "Fenestrin" and Conjugation in *Tetrahymena thermophila*. *J. Eukaryot. Microbiol.* 41, 483–495. doi:10.1111/j.1550-7408.1994.tb06047.x

Ning, J., Otto, T. D., Pfander, C., Schwach, F., Brochet, M., Bushell, E., et al. (2013). Comparative Genomics in *Chlamydomonas* and *Plasmodium* Identifies an Ancient Nuclear Envelope Protein Family Essential for Sexual Reproduction in Protists, Fungi, Plants, and Vertebrates. *Genes Dev.* 27, 1198–1215. doi:10.1101/gad.212746.112

Noto, T., and Mochizuki, K. (2017). Whats, Hows and Whys of Programmed DNA Elimination in *Tetrahymena*. *Open Biol.* 7, 170172. doi:10.1098/rsob.170172

Okamoto, M., Yamada, L., Fujisaki, Y., Bloomfield, G., Yoshida, K., Kuwayama, H., et al. (2016). Two HAP2-GCS1 Homologs Responsible for Gamete Interactions in the Cellular Slime Mold with Multiple Mating Types: Implication for Common Mechanisms of Sexual Reproduction Shared by Plants and Protozoa and for Male-Female Differentiation. *Dev. Biol.* 415, 6–13. doi:10.1016/j.ydbio.2016.05.018

Orias, J. D., Hamilton, E. P., and Orias, E. (1983). A Microtubule Meshwork Associated with Gametic Pronucleus Transfer across a Cell-Cell junction. *Science* 222, 181–184. doi:10.1126/science.6623070

Orias, E., Singh, D. P., and Meyer, E. (2017). Genetics and Epigenetics of Mating Type Determination in *Paramecium* and *Tetrahymena*. *Annu. Rev. Microbiol.* 71, 133–156. doi:10.1146/annurev-micro-090816-093342

Orias, E. (2012). "*Tetrahymena thermophila* Genetics: Concepts and Applications," in *Methods in Cell Biology* (Amsterdam, Boston, Heidelberg: Elsevier/Academic Press), 301–325. doi:10.1016/B978-0-12-385967-9.00010-4

Ostrowski, S. G., Van Bell, C. T., Winograd, N., and Ewing, A. G. (2004). Mass Spectrometric Imaging of Highly Curved Membranes during *Tetrahymena* Mating. *Science* 305, 71–73. doi:10.1126/science.1099791

Pagliaro, L., and Wolfe, J. (1987). Concanavalin A Binding Induces Association of Possible Mating-type Receptors with the Cytoskeleton in *Tetrahymena*. *Exp. Cel Res.* 168, 138–152. doi:10.1016/0014-4827(87)90423-X

Pan, J., and Snell, W. J. (2002). Kinesin-II Is Required for Flagellar Sensory Transduction during Fertilization in *Chlamydomonas*. *Mol. Biol. Cel.* 13, 1417–1426. doi:10.1091/mbc.01-11-0531

Pan, J. M., Haring, M. A., and Beck, C. F. (1996). Dissection of the Blue-Light-dependent Signal-Transduction Pathway Involved in Gametic Differentiation of *Chlamydomonas reinhardtii*. *Plant Physiol.* 112, 303–309. doi:10.1104/pp.112.1.303

Pan, J. M., Haring, M. A., and Beck, C. F. (1997). Characterization of Blue Light Signal Transduction Chains that Control Development and Maintenance of Sexual Competence in *Chlamydomonas reinhardtii*. *Plant Physiol.* 115, 1241–1249. doi:10.1104/pp.115.3.1241

Pasquale, S. M., and Goodenough, U. W. (1987). Cyclic AMP Functions as a Primary Sexual Signal in Gametes of *Chlamydomonas reinhardtii*. *J. Cel. Biol.* 105, 2279–2292. doi:10.1083/jcb.105.5.2279

Peacock, L., Ferris, V., Sharma, R., Sunter, J., Bailey, M., Carrington, M., et al. (2011). Identification of the Meiotic Life Cycle Stage of *Trypanosoma brucei in* the Tsetse Fly. *Proc. Natl. Acad. Sci. U.S.A.* 108, 3671–3676. doi:10.1073/pnas.1019423108

Peacock, L., Bailey, M., Carrington, M., and Gibson, W. (2014). Meiosis and Haploid Gametes in the Pathogen *Trypanosoma brucei*. *Curr. Biol.* 24, 181–186. doi:10.1016/j.cub.2013.11.044

Pérez-Vargas, J., Krey, T., Valansi, C., Avinoam, O., Haouz, A., Jamin, M., et al. (2014). Structural Basis of Eukaryotic Cell-Cell Fusion. *Cell* 157, 407–419. doi:10.1016/j.cell.2014.02.020

Pijst, H. L. A., van Driel, R., Janssens, P. M. W., Musgrave, A., and van den Ende, H. (1984). Cyclic AMP Is Involved in Sexual Reproduction of *Chlamydomonas eugametos*. *FEBS Lett.* 174, 132–136. doi:10.1016/0014-5793(84)81091-1

Pinello, J. F., Lai, A. L., Millet, J. K., Cassidy-Hanley, D., Freed, J. H., and Clark, T. G. (2017). Structure-Function Studies Link Class II Viral Fusogens with the Ancestral Gamete Fusion Protein HAP2. *Curr. Biol.* 27, 651–660. doi:10.1016/j.cub.2017.01.049

Pinello, J. F., Liu, Y., and Snell, W. J. (2021). MAR1 Links Membrane Adhesion to Membrane Merger during Cell-Cell Fusion in *Chlamydomonas*. *Dev. Cell.* doi:10.1016/j.devcel.2021.10.023

Podbilewicz, B. (2014). Virus and Cell Fusion Mechanisms. *Annu. Rev. Cel Dev. Biol.* 30, 111–139. doi:10.1146/annurev-cellbio-101512-122422

Podbilewicz, B., Leikina, E., Sapir, A., Valansi, C., Suissa, M., Shemer, G., et al. (2006). The *C. elegans* Developmental Fusogen EFF-1 Mediates Homotypic Fusion in Heterologous Cells and *In Vivo*. *Dev Cell.* 11 (4), 471–481. doi:10.1016/j.devcel.2006.09.004

Pucciarelli, S., Ballarini, P., Sparvoli, D., Barchetta, S., Yu, T., Detrich, H. W., et al. (2012). Distinct Functional Roles of β-Tubulin Isotypes in Microtubule Arrays of *Tetrahymena thermophila*, a Model Single-Celled Organism. *PLoS ONE* 7, e39694. doi:10.1371/journal.pone.0039694

Rabl, J., Leibundgut, M., Ataide, S. F., Haag, A., and Ban, N. (2011). Crystal Structure of the Eukaryotic 40 *S* Ribosomal Subunit in Complex with Initiation Factor 1. *Science* 331, 730–736. doi:10.1126/science.1198308

Ramakrishnan, C., Maier, S., Walker, R. A., Rehrauer, H., Joekel, D. E., Winiger, R. R., et al. (2019). An Experimental Genetically Attenuated Live Vaccine to Prevent Transmission of *Toxoplasma gondii* by Cats. *Sci. Rep.* 9, 1474. doi:10.1038/s41598-018-37671-8

Ranjan, P., Awasthi, M., and Snell, W. J. (2019). Transient Internalization and Microtubule-dependent Trafficking of a Ciliary Signaling Receptor from the Plasma Membrane to the Cilium. *Curr. Biol.* 29, 2942–2947.e2. doi:10.1016/j.cub.2019.07.022

Reynolds, M. J., Phetruen, T., Fisher, R. L., Chen, K., Pentecost, B. T., Gomez, G., et al. (2018). The Developmental Process of the Growing Motile Ciliary Tip Region. *Sci. Rep.* 8, 7977. doi:10.1038/s41598-018-26111-2

Rianõ-Pacho´n, D. M., Correa, L. G. G., Trejos-Espinosa, R., and Mueller-Roeber, B. (2008). Green Transcription Factors: A *Chlamydomonas* Overview. *Genetics* 179, 31–39. doi:10.1534/genetics.107.086090

Rogers, M. B., and Karrer, K. M. (1985). Adolescence in *Tetrahymena thermophila*. *Proc. Natl. Acad. Sci. U.S.A.* 82, 436–439. doi:10.1073/pnas.82.2.436

Rosenbaum, J. L., and Witman, G. B. (2002). Intraflagellar Transport. *Nat. Rev. Mol. Cel Biol.* 3, 813–825. doi:10.1038/nrm952

Rougeron, V., De Meeûs, T., Kako Ouraga, S., Hide, M., and Bañuls, A.-L. (2010). "Everything You Always Wanted to Know about Sex (But Were Afraid to Ask)" in *Leishmania* after Two Decades of Laboratory and Field Analyses. *Plos Pathog.* 6, e1001004. doi:10.1371/journal.ppat.1001004

RTS,S Clinical Trials Partnership (2014). Efficacy and Safety of the RTS,S/AS01 Malaria Vaccine during 18 Months after Vaccination: a Phase 3 Randomized, Controlled Trial in Children and Young Infants at 11 African Sites. *Plos Med.* 11, e1001685. doi:10.1371/journal.pmed.1001685

Ruehle, M. D., Orias, E., and Pearson, C. G. (2016). *Tetrahymena* as a Unicellular Model Eukaryote: Genetic and Genomic Tools. *Genetics* 203, 649–665. doi:10.1534/genetics.114.169748

Sánchez-San Martín, C., Liu, C. Y., and Kielian, M. (2009). Dealing with Low pH: Entry and Exit of Alphaviruses and Flaviviruses. *Trends Microbiol.* 17, 514–521. doi:10.1016/j.tim.2009.08.002

Sager, R., and Granick, S. (1954). Nutritional Control of Sexuality in *Chlamydomonas reinhardi*. *J. Gen. Physiol.* 37, 729–742. doi:10.1085/jgp.37.6.729

Saito, T., Small, L., and Goodenough, U. (1993). Activation of Adenylyl Cyclase in *Chlamydomonas reinhardtii* by Adhesion and by Heat. *J. Cel Biol.* 122, 137–147. doi:10.1083/jcb.122.1.137

Salomé, P. A., and Merchant, S. S. (2019). A Series of Fortunate Events: Introducing *Chlamydomonas* as a Reference Organism. *Plant Cel.* 31, 1682–1707. doi:10.1105/tpc.18.00952

Sapir, A., Choi, J., Leikina, E., Avinoam, O., Valansi, C., Chernomordik, L. V., et al. (2007). AFF-1, a FOS-1-Regulated Fusogen, Mediates Fusion of the Anchor Cell in *C. elegans*. *Dev. Cell* 12, 683–698. doi:10.1016/j.devcel.2007.03.003

Sasso, S., Stibor, H., Mittag, M., and Grossman, A. R. (2018). From Molecular Manipulation of Domesticated *Chlamydomonas reinhardtii* to Survival in Nature. *eLife* 7, e39233. doi:10.7554/eLife.39233

Schlösser, U. G., Sachs, H., and Robinson, D. G. (1976). Isolation of Protoplasts by Means of a "species-specific" Autolysine in *Chlamydomonas*. *Protoplasma* 88, 51–64. doi:10.1007/BF01280359

Sekimoto, H. (2017). Sexual Reproduction and Sex Determination in green Algae. *J. Plant Res.* 130, 423–431. doi:10.1007/s10265-017-0908-6

Sharman, P. A., Smith, N. C., Wallach, M. G., and Katrib, M. (2010). Chasing the golden Egg: Vaccination against Poultry Coccidiosis. *Parasite Immunol.* 32, 590–598. doi:10.1111/j.1365-3024.2010.01209.x

Sheng, Y., Duan, L., Cheng, T., Qiao, Y., Stover, N. A., and Gao, S. (2020). The Completed Macronuclear Genome of a Model Ciliate *Tetrahymena thermophila* and its Application in Genome Scrambling and Copy Number Analyses. *Sci. China Life Sci.* 63, 1534–1542. doi:10.1007/s11427-020-1689-4

Sinden, R. E., Carter, R., Drakeley, C., and Leroy, D. (2012). The Biology of Sexual Development of *Plasmodium*: the Design and Implementation of Transmission-Blocking Strategies. *Malar. J.* 11, 70. doi:10.1186/1475-2875-11-70

Snell, W. J., and Goodenough, U. W. (2009). "Flagellar Adhesion, Flagellar-Generated Signaling, and Gamete Fusion during Mating," in *The Chlamydomonas Sourcebook*. Editors E. H. Harris, D. B. Stern, and G. B. Witman. Second Edition (London: Academic Press), 369–394. doi:10.1016/B978-0-12-370873-1.00049-6

Snell, W. J., Buchanan, M., and Clausell, A. (1982). Lidocaine Reversibly Inhibits Fertilization in *Chlamydomonas*: a Possible Role for Calcium in Sexual Signalling. *J. Cel Biol.* 94, 607–612. doi:10.1083/jcb.94.3.607

Snell, W. J., Eskue, W. A., and Buchanan, M. J. (1989). Regulated Secretion of a Serine Protease that Activates an Extracellular Matrix-Degrading Metalloprotease during Fertilization in *Chlamydomonas*. *J. Cel Biol.* 109, 1689–1694. doi:10.1083/jcb.109.4.1689

Speijer, D., Lukeš, J., and Eliáš, M. (2015). Sex Is a Ubiquitous, Ancient, and Inherent Attribute of Eukaryotic Life. *Proc. Natl. Acad. Sci. USA* 112, 8827–8834. doi:10.1073/pnas.1501725112

Steele, R. E., and Dana, C. E. (2009). Evolutionary History of the HAP2/GCS1 Gene and Sexual Reproduction in Metazoans. *PLoS One* 4, e7680. doi:10.1371/journal.pone.0007680

Stover, N. A., Punia, R. S., Bowen, M. S., Dolins, S. B., and Clark, T. G. (2012). Tetrahymena Genome Database Wiki: a Community-Maintained Model Organism Database. *Database* 2012, bas007. doi:10.1093/database/bas007

Suryavanshi, S., Eddé, B., Fox, L. A., Guerrero, S., Hard, R., Hennessey, T., et al. (2010). Tubulin Glutamylation Regulates Ciliary Motility by Altering Inner Dynein Arm Activity. *Curr. Biol.* 20, 435–440. doi:10.1016/j.cub.2009.12.062

Takahashi, T., Mori, T., Ueda, K., Yamada, L., Nagahara, S., Higashiyama, T., et al. (2018). The Male Gamete Membrane Protein DMP9/DAU2 Is Required for Double Fertilization in Flowering Plants. *Development* 145, dev170076. doi:10.1242/dev.170076

Treier, U., and Beck, C. F. (1991). Changes in Gene Expression Patterns during the Sexual Life Cycle of *Chlamydomonas reinhardtii*. *Physiol. Plant* 83, 633–639. doi:10.1034/j.1399-3054.1991.830416.x

Treier, U., Fuchs, S., Weber, M., Wakarchuk, W. W., and Beck, C. F. (1989). Gametic Differentiation in *Chlamydomonas reinhardtii*: Light Dependence and Gene Expression Patterns. *Arch. Microbiol.* 152, 572–577. doi:10.1007/BF00425489

Triemer, R. E., and Malcolm Brown, R. (1975). Fertilization in *Chlamydomonas reinhardi*, with Special Reference to the Structure, Development, and Fate of the Choanoid Body. *Protoplasma* 85, 99–107. doi:10.1007/BF01567761

Turkewitz, A. P. (2004). Out with a Bang! *Tetrahymena* as a Model System to Study Secretory Granule Biogenesis. *Traffic* 5, 63–68. doi:10.1046/j.1600-0854.2003.00155.x

University of Oxford (2021). A Phase III Randomized Controlled Multi-centre Trial to Evaluate the Efficacy of the R21/Matrix-M Vaccine in African Children against Clinical Malaria. clinicaltrials.gov. Available at: https://clinicaltrials.gov/ct2/show/NCT04704830 (Accessed August 5, 2021).

Valansi, C., Moi, D., Leikina, E., Matveev, E., Graña, M., Chernomordik, L. V., et al. (2017). *Arabidopsis* HAP2/GCS1 Is a Gamete Fusion Protein Homologous to Somatic and Viral Fusogens. *J. Cel. Biol.* 216, 571–581. doi:10.1083/jcb.201610093

Vale, R. D., and Yano Toyoshima, Y. (1988). Rotation and Translocation of Microtubules *In Vitro* Induced by Dyneins from *Tetrahymena* Cilia. *Cell* 52, 459–469. doi:10.1016/S0092-8674(88)80038-2

Vogel, G. (2010). The 'Do Unto Others' Malaria Vaccine. *Science* 328, 847–848. doi:10.1126/science.328.5980.847

von Besser, K., Frank, A. C., Johnson, M. A., and Preuss, D. (2006). *Arabidopsis* HAP2(GCS1) Is a Sperm-Specific Gene Required for Pollen Tube Guidance and Fertilization. *Development* 133, 4761–4769. doi:10.1242/dev.02683

Wahab, S., Saettone, A., Nabeel-Shah, S., Dannah, N., and Fillingham, J. (2020). Exploring the Histone Acetylation Cycle in the Protozoan Model *Tetrahymena thermophila*. *Front. Cel Dev. Biol.* 8, 509. doi:10.3389/fcell.2020.00509

Wahlberg, J. M., and Garoff, H. (1992). Membrane Fusion Process of Semliki Forest Virus. I: Low pH-Induced Rearrangement in Spike Protein Quaternary Structure Precedes Virus Penetration into Cells. *J. Cel Biol.* 116, 339–348. doi:10.1083/jcb.116.2.339

Wahlberg, J. M., Bron, R., Wilschut, J., and Garoff, H. (1992). Membrane Fusion of Semliki Forest Virus Involves Homotrimers of the Fusion Protein. *J. Virol.* 66, 7309–7318. doi:10.1128/jvi.66.12.7309-7318.1992

Walker, R. A., Sharman, P. A., Miller, C. M., Lippuner, C., Okoniewski, M., Eichenberger, R. M., et al. (2015). RNA Seq Analysis of the *Eimeria tenellai* Gametocyte Transcriptome Reveals Clues about the Molecular Basis for Sexual Reproduction and Oocyst Biogenesis. *BMC Genomics* 16, 94. doi:10.1186/s12864-015-1298-6

Wallach, M. G., Ashash, U., Michael, A., and Smith, N. C. (2008). Field Application of a Subunit Vaccine against an Enteric Protozoan Disease. *PLoS One* 3, e3948. doi:10.1371/journal.pone.0003948

Wang, Q., Pan, J., and Snell, W. J. (2006). Intraflagellar Transport Particles Participate Directly in Cilium-Generated Signaling in *Chlamydomonas*. *Cell* 125, 549–562. doi:10.1016/j.cell.2006.02.044

Weiss, R. L., Goodenough, D. A., and Goodenough, U. W. (1977). Membrane Differentiations at Sites Specialized for Cell Fusion. *J. Cel Biol.* 72, 144–160. doi:10.1083/jcb.72.1.144

Wellnitz, W. R., and Bruns, P. J. (1979). The Pre-pairing Events in *Tetrahymena thermophila*. *Exp. Cel Res.* 119, 175–180. doi:10.1016/0014-4827(79)90346-X

Williams, N. E., Honts, J. E., and Jaeckel-Williams, R. F. (1987). Regional Differentiation of the Membrane Skeleton in *Tetrahymena*. *J. Cel Sci* 87 (Pt 3), 457–463. doi:10.1242/jcs.87.3.457

Williams, N. E., Honts, J. E., Dress, V. M., Nelsen, E. M., and Frankel, J. (1995). Monoclonal Antibodies Reveal Complex Structure in the Membrane Skeleton of *Tetrahymena*. *J. Eukaryot. Microbiol.* 42, 422–427. doi:10.1111/j.1550-7408.1995.tb01606.x

Wilson, D. N., and Doudna Cate, J. H. (2012). The Structure and Function of the Eukaryotic Ribosome. *Cold Spring Harbor Perspect. Biol.* 4, a011536. doi:10.1101/cshperspect.a011536

Wilson, N. F., Foglesong, M. J., and Snell, W. J. (1997). The *Chlamydomonas* Mating Type Plus Fertilization Tubule, a Prototypic Cell Fusion Organelle: Isolation, Characterization, and *In Vitro* Adhesion to Mating Type Minus Gametes. *J. Cel Biol.* 137, 1537–1553. doi:10.1083/jcb.137.7.1537

Woessner, J. P., and Goodenough, U. W. (1992). Zygote and Vegetative Cell wall Proteins in *Chlamydomonas reinhardtii* Share a Common Epitope, (SerPro)X. *Plant Sci.* 83, 65–76. doi:10.1016/0168-9452(92)90063-R

Wolfe, J., and Feng, S. (1988). Concanavalin A Receptor 'tipping' in *Tetrahymena* and its Relationship to Cell Adhesion during Conjugation. *Development* 102, 699–708. doi:10.1242/dev.102.4.699

Wolfe, J., and Grimes, G. W. (1979). Tip Transformation in *Tetrahymena*: A Morphogenetic Response to Interactions between Mating Types*. *The J. Protozool.* 26, 82–89. doi:10.1111/j.1550-7408.1979.tb02737.x

Wolfe, J., Turner, R., Barker, R., and Adair, W. S. (1979). The Need for an Extracellular Component for Cell Pairing in *Tetrahymena*. *Exp. Cel Res.* 121, 27–30. doi:10.1016/0014-4827(79)90440-3

Wolfe, J., Mpoke, S., and Tirone, S. F. (1993). Cilia, Ciliary Concanavalin A-Binding Proteins, and Mating Recognition in *Tetrahymena thermophila*. *Exp. Cel Res.* 209, 342–349. doi:10.1006/excr.1993.1319

Wolfe, J. (1982). The Conjugation Junction of *Tetrahymena*: Its Structure and Development. *J. Morphol.* 172, 159–178. doi:10.1002/jmor.1051720204

Wong, J. L., and Johnson, M. A. (2010). Is HAP2-GCS1 an Ancestral Gamete Fusogen? *Trends Cel Biol.* 20, 134–141. doi:10.1016/j.tcb.2009.12.007

Wong, J. L., Leydon, A. R., and Johnson, M. A. (2010). HAP2(GCS1)-dependent Gamete Fusion Requires a Positively Charged Carboxy-Terminal Domain. *Plos Genet.* 6, e1000882. doi:10.1371/journal.pgen.1000882

Wood, C. R., and Rosenbaum, J. L. (2015). Ciliary Ectosomes: Transmissions from the Cell's Antenna. *Trends Cel Biol.* 25, 276–285. doi:10.1016/j.tcb.2014.12.008

Xiong, J., Lu, Y., Feng, J., Yuan, D., Tian, M., Chang, Y., et al. (2013). *Tetrahymena* Functional Genomics Database (TetraFGD): an Integrated Resource for *Tetrahymena* Functional Genomics. *Database (Oxford)* 2013, bat008. doi:10.1093/database/bat008

Xu, J., Tian, H., Wang, W., and Liang, A. (2012). The Zinc finger Protein Zfr1p Is Localized Specifically to Conjugation junction and Required for Sexual Development in *Tetrahymena thermophila*. *PloS one* 7, e52799. doi:10.1371/journal.pone.0052799

Yamazaki, T., Ichihara, K., Suzuki, R., Oshima, K., Miyamura, S., Kuwano, K., et al. (2017). Genomic Structure and Evolution of the Mating Type Locus in the green Seaweed *Ulva partita*. *Sci. Rep.* 7, 11679. doi:10.1038/s41598-017-11677-0

Yan, G., Yang, W., Han, X., Chen, K., Xiong, J., Hamilton, E. P., et al. (2021). Evolution of the Mating Type Gene Pair and Multiple Sexes in *Tetrahymena*. *iScience* 24, 101950. doi:10.1016/j.isci.2020.101950

Zeev-Ben-Mordehai, T., Vasishtan, D., Siebert, C. A., and Grünewald, K. (2014). The Full-Length Cell-Cell Fusogen EFF-1 Is Monomeric and Upright on the Membrane. *Nat. Commun.* 5, 3912. doi:10.1038/ncomms4912

Zhang, Y. H., Ross, E. M., and Snell, W. J. (1991). ATP-dependent Regulation of Flagellar Adenylylcyclase in Gametes of *Chlamydomonas reinhardtii*. *J. Biol. Chem.* 266, 22954–22959. doi:10.1016/S0021-9258(18)54447-1

Zhang, F., Wang, L.-P., Boyden, E. S., and Deisseroth, K. (2006). Channelrhodopsin-2 and Optical Control of Excitable Cells. *Nat. Methods* 3, 785–792. doi:10.1038/nmeth936

Zhang, N.-Z., Chen, J., Wang, M., Petersen, E., and Zhu, X.-Q. (2013). Vaccines against *Toxoplasma gondii*: New Developments and Perspectives. *Expert Rev. Vaccin.* 12, 1287–1299. doi:10.1586/14760584.2013.844652

Zhang, J., Pinello, J. F., Fernández, I., Baquero, E., Fedry, J., Rey, F. A., et al. (2021). Species-specific Gamete Recognition Initiates Fusion-Driving Trimer Formation by Conserved Fusogen HAP2. *Nat. Commun.* 12, 4380. doi:10.1038/s41467-021-24613-8

Zweifel, E., Smith, J., Romero, D., Giddings, T. H., Winey, M., Honts, J., et al. (2009). Nested Genes *CDA12* and *CDA13* Encode Proteins Associated with Membrane Trafficking in the Ciliate *Tetrahymena thermophila*. *Eukaryot. Cel.* 8, 899–912. doi:10.1128/EC.00342-08

Conflict of Interest: The authors declare that the research was conducted in the absence of any commercial or financial relationships that could be construed as a potential conflict of interest.

Publisher's Note: All claims expressed in this article are solely those of the authors and do not necessarily represent those of their affiliated organizations, or those of the publisher, the editors and the reviewers. Any product that may be evaluated in this article, or claim that may be made by its manufacturer, is not guaranteed or endorsed by the publisher.

frontiers in Cell and Developmental Biology

MINI REVIEW
published: 10 January 2022
doi: 10.3389/fcell.2021.824024

Fusexins, HAP2/GCS1 and Evolution of Gamete Fusion

Nicolas G. Brukman, Xiaohui Li and Benjamin Podbilewicz**

Department of Biology, Technion- Israel Institute of Technology, Haifa, Israel

Gamete fusion is the climax of fertilization in all sexually reproductive organisms, from unicellular fungi to humans. Similarly to other cell-cell fusion events, gamete fusion is mediated by specialized proteins, named fusogens, that overcome the energetic barriers during this process. In recent years, HAPLESS 2/GENERATIVE CELL-SPECIFIC 1 (HAP2/GCS1) was identified as the fusogen mediating sperm-egg fusion in flowering plants and protists, being both essential and sufficient for the membrane merger in some species. The identification of HAP2/GCS1 in invertebrates, opens the possibility that a similar fusogen may be used in vertebrate fertilization. HAP2/GCS1 proteins share a similar structure with two distinct families of exoplasmic fusogens: the somatic Fusion Family (FF) proteins discovered in nematodes, and class II viral glycoproteins (e.g., rubella and dengue viruses). Altogether, these fusogens form the Fusexin superfamily. While some attributes are shared among fusexins, for example the overall structure and the possibility of assembly into trimers, some other characteristics seem to be specific, such as the presence or not of hydrophobic loops or helices at the distal tip of the protein. Intriguingly, HAP2/GCS1 or other fusexins have neither been identified in vertebrates nor in fungi, raising the question of whether these genes were lost during evolution and were replaced by other fusion machinery or a significant divergence makes their identification difficult. Here, we discuss the biology of HAP2/GCS1, its involvement in gamete fusion and the structural, mechanistic and evolutionary relationships with other fusexins.

Keywords: sperm, oocyte, fusexins, gamete fusion, fertilization, HAP2/GCS1, eff-1, class II viral fusion proteins

OPEN ACCESS

Edited by:
Amber R. Krauchunas, University of Delaware, United States

Reviewed by:
Jeff Lee, University of Toronto, Canada

****Correspondence:***
Nicolas G. Brukman
nbrukman@technion.ac.il
Benjamin Podbilewicz
podbilew@technion.ac.il

Specialty section:
This article was submitted to Molecular and Cellular Reproduction, a section of the journal Frontiers in Cell and Developmental Biology

Received: *28 November 2021*
Accepted: *21 December 2021*
Published: *10 January 2022*

Citation:
Brukman NG, Li X and Podbilewicz B (2022) Fusexins, HAP2/GCS1 and Evolution of Gamete Fusion. Front. Cell Dev. Biol. 9:824024. doi: 10.3389/fcell.2021.824024

INTRODUCTION

The merging of the plasma membranes of two independent cells with the subsequent formation of an individual cell containing both cytoplasmic contents mixed is known as cell-cell fusion. This biological process is mediated and finely controlled by fusion proteins, termed fusogens, which are specialized proteins capable of overcoming the energetic barriers required for the fusion to occur (Chernomordik and Kozlov, 2003) and are both necessary and sufficient to mediate membrane merging (Brukman et al., 2019). In particular, the fusion between two gametes or "gamete fusion" is one of the hallmarks of meiotic sex and its ubiquitous distribution among eukaryotes suggests an ancestral origin (Ramesh et al., 2005; Speijer et al., 2015; Radzvilavicius, 2016). The first gamete fusogen identified was HAPLESS 2/GENERATIVE CELL-SPECIFIC 1 (HAP2/GCS1) that catalyzes fertilization in flowering plants, protists and probably in some invertebrates. This protein was originally found as an essential sperm factor required for male fertility in flowering plants (Johnson et al., 2004; Mori et al., 2006; von Besser et al., 2006) being later shown that it is necessary for mating in *Chlamydomonas* and *Plasmodium* (Hirai et al., 2008; Liu et al., 2008). More recently, the *Arabidopsis* HAP2/GCS1 (*At*HAP2/GCS1) was shown to be sufficient to induce fusion of mammalian cells in culture and the infection of enveloped virus to cells (Valansi et al., 2017).

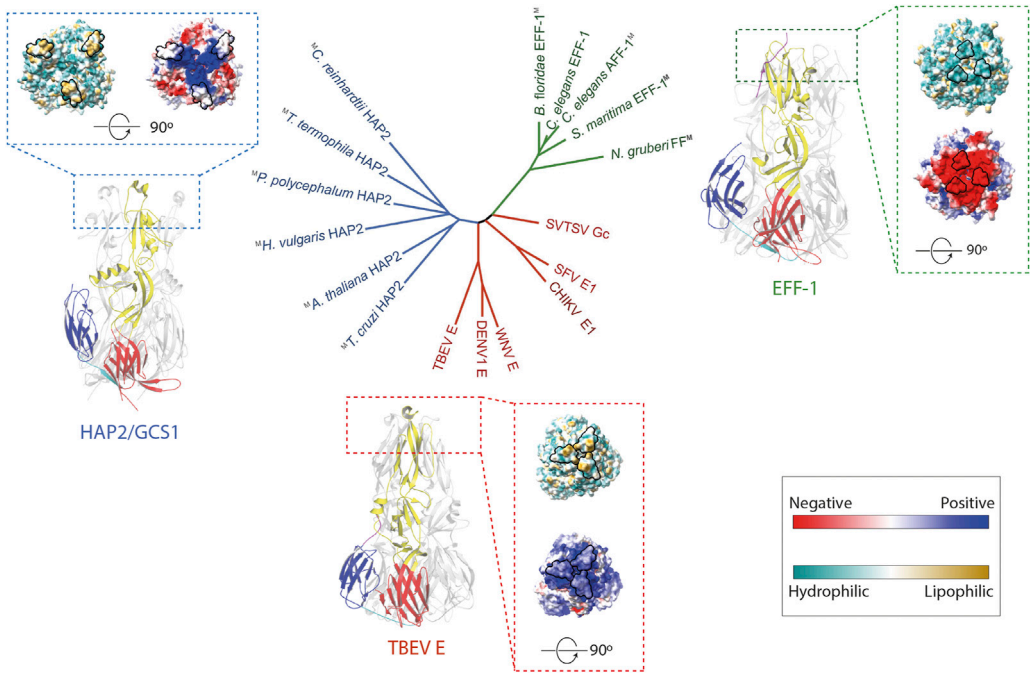

FIGURE 1 | The Fusexin superfamily. Ribbon representation of the fusion protein trimers *C. elegans* EFF-1 (PDB 4OJC; Pérez-Vargas et al., 2014), TBEV E (PDB 1URZ; Bressanelli et al., 2004), and *A. thaliana* HAP2 (PDB 5OW3; Fedry et al., 2018) with domains I, II, III colored by red, yellow, blue, respectively. Surface representation of trimers viewed from the membrane was displayed. The surface is colored according to the electrostatic potential on a scale from -5 to 5 kT/e (calculated with APBS, Jurrus et al., 2018) from red (negative) to blue (positive). Solvent-excluded surfaces of trimers are colored based on molecular lipophilicity potential maps, ranging from dark cyan (hydrophilic) to dark gold (lipophilic). Proposed fusion loops at the tip of domain II are contoured in black. In the center, an unrooted tree inferred using a distance matrix extracted from (Valansi et al., 2017). Colors are HAP2/GCS1, blue; FF proteins, green; class II viral fusogens, red. M superscript represents models.

Strikingly, HAP2/GCS1 shares an overall three-dimensional structure with the somatic Fusion Family (FF) proteins discovered in nematodes (Mohler et al., 2002; Sapir et al., 2007; Pérez-Vargas et al., 2014) and with class II viral glycoproteins (e.g., dengue, rubella and zika viruses) (Fédry et al., 2017; Pinello et al., 2017; Valansi et al., 2017). This superfamily of fusion proteins essential for sexual reproduction and exoplasmic merger of plasma membranes was named Fusexin. Even though the mechanisms of cell-cell and virus-cell fusion are diverse and may be mediated by different families of fusion proteins (Segev et al., 2018; Vance and Lee, 2020), the fusexins represent a remarkable case of ancestral fusogens present across the tree of life. Here we review the recent research on HAP2/GCS1-mediated gamete fusion and its functional and structural relationships with other fusexins. Furthermore, we compare the regulation of fusion processes driven by fusexins to the fertilization process in mammals, where the presence of distant members of the Fusexin superfamily is uncertain.

STRUCTURAL SIMILARITIES AND DIFFERENCES BETWEEN FUSEXINS

Previous studies have shown FF proteins, like *C. elegans'* EFF-1 (*Ce*EFF-1), and HAP2/GCS1 are structurally homologous to viral class II fusion proteins and display a trimeric, postfusion hairpin conformation consisting of three β-sheet-rich domains (DI, DII, DIII) (**Figure 1**) (Pérez-Vargas et al., 2014; Fédry et al., 2017; Pinello et al., 2017; Valansi et al., 2017). The first of the three domains consist of a β-barrel, followed by a mostly β-stranded elongated domain, and an Immunoglobulin (Ig)-like domain. They are anchored to the cell surface by transmembrane domains at the C terminus. Even though these proteins share very low sequence similarities, the surprising conservation in their architecture suggests that they share a common ancestor forming the Fusexin superfamily (**Figure 1**). A particular region on one end of the ectodomain has been extensively studied due to functional implications (**Figure 1**). In viral class II fusion proteins, fusion loops or α-helices located at the tip of domain II containing hydrophobic residues have been proposed to insert into the target membrane during conformational changes, like tick-borne encephalitis virus protein E (Bressanelli et al., 2004). In *Ce*EFF-1, the cd loop at the membrane-proximal side may play a similar structural role, however it is mainly composed of acidic residues forming an electronegative surface which is unlikely to interact with lipidic membranes (Pérez-Vargas et al., 2014). The fusion loops regions in HAP2/GCS1 orthologs are highly variable, with a single helix in *At*HAP2/GCS1, three short loops in *Trypanosoma cruzi* (*Tc*HAP2/GCS1) and three amphipathic helices in *Chlamydomonas reinhardtii* (*Cr*HAP2/GCS1)

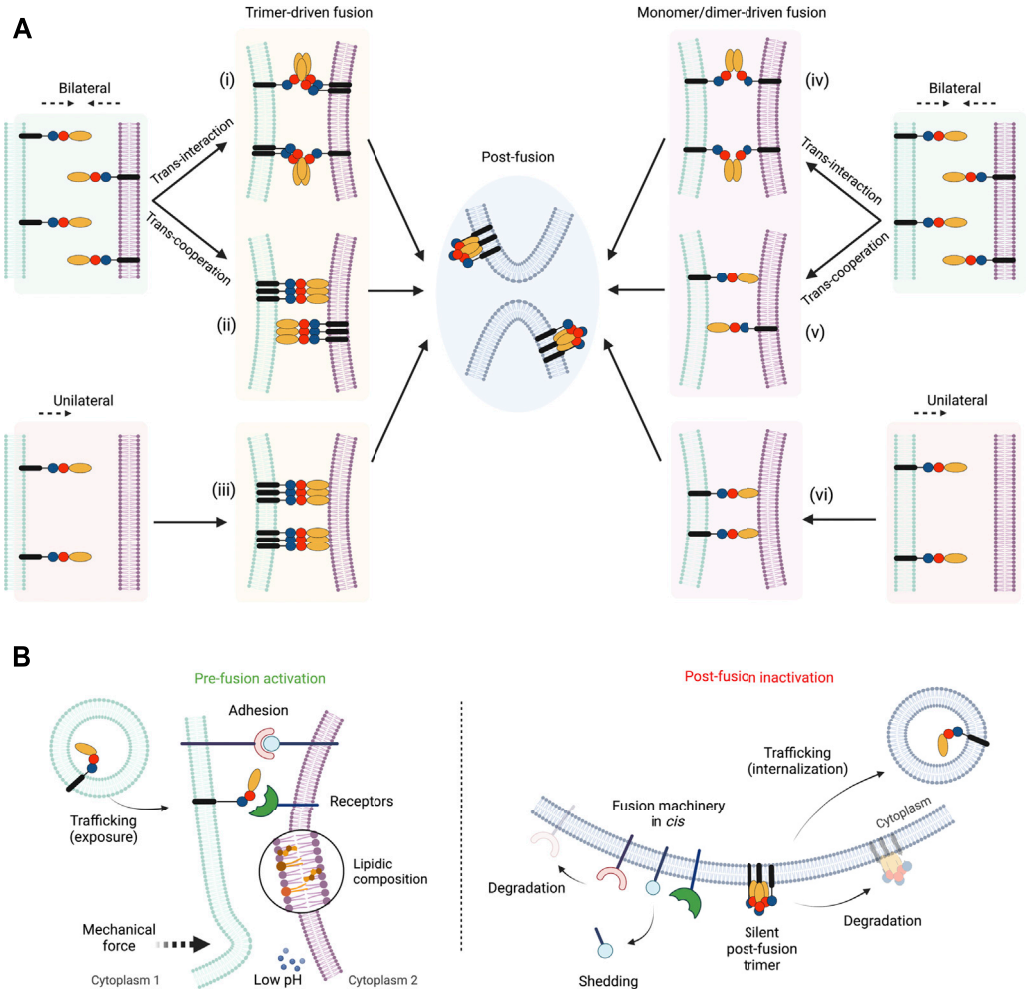

FIGURE 2 | Pathways and regulations of fusexin-mediated fusion. **(A)** Different models for the mechanism of action of fusexins. Fusion can be induced from both merging membranes ("bilateral," i, ii, iv and v) or from one of them ("unilateral," iii and vi). Within the bilateral mechanism, fusexins may interact forming dimers or trimers leading to fusion ("trans-interaction," reminiscent of trans-SNAREs, i and iv) or cooperate by binding to the opposed membrane ("trans-cooperation," ii and v). Depending on the intermediate states that mediate membrane merging the mechanisms can be divided into trimer-driven fusion (i, ii and iii) or monomer/dimer-driven fusion (iv, v and vi). Independently of the mechanism, the post-fusion conformation is hairpin-shaped trimers. **(B)** Known mechanisms of pre-fusion activation (left panel) or post-fusion inactivation (right panel) of fusexins described in this review. Created with BioRender.com.

(Baquero et al., 2019). The functional relevance of the different configuration of this region is discussed in the next section.

MECHANISMS OF ACTION OF FUSEXINS

One Way or Another

How do fusexins mediate membrane fusion? First of all, some fusogens may be required only in one of the opposing membranes, as in the case of class II viral glycoproteins (Podbilewicz, 2014), while others must be present on both sides, like the EFF-1 and AFF-1 somatic fusogens (Podbilewicz et al., 2006; Avinoam et al., 2011). These two possible mechanisms are termed unilateral and bilateral, respectively (**Figure 2**). However, in the case of HAP2/GCS1 the evidence is controversial. On one hand, the deletion of the *Athap/gcs1* gene induces male-specific sterility (Johnson et al., 2004; von Besser et al., 2006), even though some levels of expression were detected in ovules (Borges et al., 2008), suggesting a unilateral mechanism of action. In contrast, when studied in heterologous systems, *At*HAP2/GCS1 could mediate exoplasmic fusion only bilaterally (Valansi et al., 2017). Similarly to flowering plants, genetic studies in *Plasmodium* and *Chlamyodomonas*, showed that HAP2/GSC1 is absolutely required in only one of the fusing gametes (Hirai et al., 2008; Liu et al., 2008). By contrast, in the ciliated protozoan *Tetrahymena thermophila*, all seven mating types express HAP2/GCS1 and its absence in only 1 cell of the mating pair disrupts fusion (Cole et al., 2014; Pinello et al., 2017). The slime mold *Dictyostelium* represents a particular case where two

homologs of HAP2/GCS1 were identified: HgrB, which is expressed in the three sex types, and HgrA, expressed only in types I and II (Okamoto et al., 2016). Genetic studies suggest that both HgrA and HgrB are essential in both membranes in crosses between types I and II, but only in one membrane when crossed with the third gamete type (Okamoto et al., 2016; Bloomfield, 2019).

Regardless of the species, structural and biochemical studies show that the hydrophobic tip of domain II of HAP2/GCS1 (**Figure 1**) is critical for interactions with liposomes (Pinello et al., 2017; Fédry et al., 2018; Feng et al., 2018; Baquero et al., 2019). This HAP2/GCS1-membrane interaction is consistent with a unilateral pathway (**Figures 2Aiii,vi**) but also with a bilateral mechanism with trans-cooperation (**Figures 2Aii,v**), or even a hybrid system. More recently, this hydrophobic region was shown to be relevant for oligomerization in *Chlamydomonas* (Zhang et al., 2021). It was shown that the formation of a small population of SDS-resistant trimers in this species was observed even in the absence of fusion, however, the temporal and spatial resolution of these experiments is not sufficient to confirm that these trimers are responsible for membrane merging.

Which Comes First, the Fusion or the Trimer?

As mentioned before, all fusexins studied thus far can form trimers. The most studied group within the Fusexin superfamily are the viral class II fusion proteins. In mature virions of alphaviruses and flaviviruses, these proteins exist as heterodimers/trimers or homodimers, respectively, in some cases lying parallel to the membrane and forming an icosahedral lattice on its surface (Zhang et al., 2003; Voss et al., 2010). Upon internalization into the target cells, the low pH within endosomal compartments triggers the activity of class II fusogens leading to infection (White et al., 2008). It is commonly accepted that class II viral fusogens, after a transient monomeric state, trimerize before fusion and that the zippering of these trimers is the driving force for membrane merger (Baquero et al., 2013). In the post-fusion state, these proteins can be found in the already previously mentioned folded trimers of hairpins, however, the existence of the hypothetical extended trimer has not been experimentally confirmed. Therefore, the possibility that monomers rearrange into hairpins to induce fusion prior to their trimerization cannot be excluded (**Figures 2Aiv,v,vi**).

Even though *Ce*EFF-1 is suggested to be monomeric on cell-derived membrane vesicles (Zeev-Ben-Mordehai et al., 2014), its ectodomain purified and crystallized as a post-fusion trimer (Pérez-Vargas et al., 2014). The monomeric (but not trimeric) soluble protein was able to inhibit cell-cell fusion *in vitro* (Pérez-Vargas et al., 2014) and soluble EFF-1 trimers stimulate the fusion of insect cells ectopically expressing EFF-1 (Podbilewicz et al., 2006). Similarly to viral fusexins, EFF-1-mediated fusion can be blocked by adding soluble domain III (Pérez-Vargas et al., 2014). Based on the presence of an electronegative instead of a hydrophobic patch on the tip of the domain II and the bilateral requirement of EFF-1, it was proposed that trimers/dimers are formed in *trans* and that a bidirectional zippering occurs from both fusing membranes (Podbilewicz, 2014, **Figure 2Ai,iv**). However, a trans-cooperation mechanism where cis-trimers are required from both sides is still a possible model (**Figure 2Aii**). In the latter scenario, the binding to the opposite membrane might be indirect, distinctly to Class II viral fusexins that involve direct hydrophobic interactions with the membranes.

Whether fusion is mediated by monomers, dimers, trimers or even higher oligomeric states is not completely elucidated and different fusexins may utilize different strategies that should not be excluded (**Figure 2A**).

FINE-TUNING OF GAMETE FUSION

Fusion must be a tightly-regulated process. Excessive gamete fusion can lead to non-specific fertilization or to polygamy that may produce unviable polyploid zygotes. Also, the fusion of gametes to their same type or to somatic cells must be avoided. In this sense, even after cell fate determination and gamete encounter, many regulatory mechanisms are established to regulate the activity of gamete fusogens.

Attach and Fuse

Specific adhesion of the gametes seems to be a robust way of regulating fusion as fusogens require the membranes to be in close proximity (Hernández and Podbilewicz, 2017). The concept of "fertilization synapse" was introduced to describe the complex arrangement of the membranes to enable fusion (Krauchunas et al., 2016). In flowering plants, the sperm-specific protein GEX2 (Gamete EXpressed 2) contains Ig-like domains and it was shown to be essential for sperm attachment and the subsequent fertilization (Mori et al., 2014). The known *Chlamydomonas* factor for gamete adhesion is FUS1 (Ferris et al., 1996; Misamore et al., 2003), which also contains extracellular Ig-like domains that form a structure similar to the one of GEX2 (Pinello et al., 2021). In contrast to the plant counterpart, FUS1 is expressed in the plus mating type, the opposite membrane to HAP2/GCS1. However, no direct interaction between them was reported. Recently, MAR1 (Minus Adhesion Receptor 1) has been suggested to be the molecular partner of FUS1 in the minus gamete and a key regulator of HAP2/GCS1 localization to the fusion site (Pinello et al., 2021, **Figure 2B**). The only attachment couple known in mammals is the sperm-borne Izumo1 and the oocyte-specific Juno (Izumo Receptor). While the former is a type I transmembrane Ig-like protein, the latter is bound to the egg plasma membrane by a GPI anchor. The interaction between these two proteins leads to tight gamete binding that is species specific and is essential for fusion to occur (Inoue et al., 2005; Bianchi et al., 2014; Bianchi and Wright, 2015). This molecular interaction appears to be an evolutionary novelty as Juno is present only in mammals, however, Izumo1 has a broader distribution involving many lineages of vertebrates (Grayson, 2015). Interestingly, an Izumo-like gene involved in late stages of fertilization was described also in *C. elegans* (Nishimura et al., 2015; Takayama et al., 2021).

The Correct Time and Place

The localization of the fusogens plays a crucial role to regulate fusion. For example, in *C. elegans* the dynamic internalization of EFF-1 into intracellular early endosomes regulates its function (Smurova and Podbilewicz, 2017). Similarly, *At*HAP2/GCS1 localization to the plasma membrane increases upon interaction with EC1 (Egg Cell 1), a small cysteine-rich protein secreted by the female gamete, which is necessary for sperm cell plasma membrane to gain fusion competence (Sprunck et al., 2012). In mammals, the egg tetraspanin CD9 is proposed to be responsible for membrane organization and correct localization of adhesion- and fusion-related proteins, such as Juno (Inoue et al., 2020; Umeda et al., 2020). In the mammalian sperm, Izumo1 localizes into the acrosome, giant intracellular vesicle in the head. Only after undergoing capacitation, a maturation process in the female tract, the acrosomal content is released and Izumo1 relocalizes to the equatorial region of the plasma membrane where tight binding to the oocyte plasma membrane occurs (Satouh et al., 2012). The fusogens involved in mammalian gamete fusion may follow similar localization behavior to Juno and/or Izumo1.

More Than Just Lipidic Bilayers

Another factor affecting the activity of fusion is the lipidic composition of both membranes. For example, cholesterol in the target membrane promotes the fusion mediated by some viral class II fusexins (Umashankar et al., 2008; Osuna-Ramos et al., 2018; Pattnaik and Chakraborty, 2021). On the other hand, *At*HAP2/GCS1 was reported to bind better to liposomes containing a lipid that mimics the phospholipid phosphatidylserine (Fedry et al., 2018). Phosphatidylserine is a known mediator of many fusion events (Whitlock and Chernomordik, 2021), including EFF-1-mediated neuronal repair of axons in *C. elegans* (Neumann et al., 2015) and mammalian fertilization (Rival et al., 2019). Albeit lipids may affect the activity of fusion proteins, the composition of the membrane by itself is known to determine the curvature of the bilayer and, therefore, influence directly the progression of hemifusion and pore opening (reviewed in Chernomordik and Kozlov, 2008).

Mechanical Forces at Play

An additional element that could contribute to the cell-cell fusion process is the membrane tension by mechanical forces. For instance, it is proposed that during muscle formation in *Drosophila melanogaster* and in *Schizosaccharomyces pombe* mating, actin-rich protrusions from 1 cell are resisted by actomyosin contractions in the other, producing membrane stress that leads to fusion (Kim and Chen, 2019; Muriel et al., 2021). In this sense, actin polymerization was shown to improve EFF-1-driven fusion of insect cells in culture (Shilagardi et al., 2013). Furthermore, EFF-1 and F-actin colocalize during seam cell daughter-hyp7 cell fusion in the *C. elegans* larvae, however, this interaction seems to be important for the correct localization of the fusogen rather than a mechanical induction of fusion (Yang et al., 2017). The surface of mammalian oocytes is structurally complex and its cortex is enriched with F-actin (Longo, 1985, 1987). Nonetheless, the relevance of this actin network specifically for mammalian gamete fusion is unclear since contradicting results were reported [reviewed in (Sun and Schatten, 2006)]. It is possible that it is involved in membrane merging or in the later incorporation of the sperm. In addition, the actin cytoskeleton might control the position of the sperm during fusion, distancing it from the maternal chromosomes avoiding the elimination of paternal chromosomes during the formation of the second polar body (Mori et al., 2021). Cortical actin dynamics are also required for the correct trafficking of the cortical granules (Connors et al., 1998; Vogt et al., 2019), specialized vesicles of the oocyte that contribute to the block of polyspermy after fertilization.

Mechanical stress on the membranes can also be generated by the pushing and pulling movements of the sperm after attachment. Even though it was previously thought that motility was dispensable for mammalian gamete fusion (Yanagimachi, 1988), recent studies have suggested that a specific beating mode of the flagellum is required for this process (Ravaux et al., 2016) supporting older studies using human gametes (Wolf et al., 1995). It is also possible that these kinetic perturbations are only required for the accumulation of CD9 to the fusion site (Chalbi et al., 2014).

Switching the Fusexins off

After fusion occurs, a rapid functional silencing of the fusogens is often required. First of all, if the fusion proteins require trans-interactions to be activated (with receptors or to other fusogens), the post-fusion configuration by itself serves as a mechanism of preventing them since all the proteins end up in the same membrane. Alternatively, the fusogens might be removed from the membrane by internalization, as is reported for *Ce*EFF-1 (Smurova and Podbilewicz, 2016), or simply by degradation, such as *Cr*HAP2/GCS1 (Liu et al., 2010). Certainly, the adhesion molecules can suffer these changes turning the membrane into fusion incompetent. For example, *Chlamydomonas* FUS1 is also degraded after fertilization (Liu et al., 2010) and the mammalian Juno is shed in extracellular vesicles from the surface of the oocyte after fusion (Bianchi et al., 2014). Other biochemical changes in the gametes triggered by fertilization may also affect the activity of the fusogens and block further fusion events. Fast changes in electric potential occur in the plasma membrane of fertilized eggs of some organisms with external fertilization, like sea urchins and frogs, which prevents polyspermy (Jaffe, 1976; Cross and Elinson, 1980). More recently, the release of inorganic zinc from mammalian fertilized oocytes was described as "zinc sparks" which can induce changes in the sperm or in the membrane of the oocyte itself (Kim et al., 2011; Duncan et al., 2016). These changes may induce conformational changes in the fusogens, in the same way that low pH induces structural rearrangements in the viral fusexins, but into an inactivating form. Finally, there is biochemical evidence for EFF-1 and viral Class II proteins that trimerization is irreversible (Bressanelli et al., 2004; Modis et al., 2004; Liao and Kielian, 2005; Nayak et al., 2009; Pérez-Vargas et al., 2014), which would mean that whenever the post-fusion conformation is reached the protein remains locked. This represents a regulatory mechanism that prevents additional fusion events from occurring. Likely this irreversibility of the trimerization is also true for HAP2/GCS1, however, these studies are still missing.

PERSPECTIVES

Even though the overall fusexin architecture is strikingly conserved, their distribution among extremely distant organisms possibly has arisen into a diversity of mechanisms of action that might be similar or not (**Figure 2**). The differences in sequence, local structural features, molecular environments and interactions highlight the necessity of studying the individual biology of fusexins while avoiding overgeneralization.

On the other hand, mammals and other HAP2/GCS1-lacking organisms present an ongoing mystery. While several genes were found to be required for gamete fusion to occur (Brukman et al., 2019; Bianchi and Wright, 2020), the identity of the proteins that are both essential and sufficient for membrane merging is still unknown in fungi and vertebrates. New artificial intelligence-based tools that predict the folding of proteins (Jumper et al., 2021) may be the key to find other families of fusogens that may have replaced HAP2/GCS1, or else uncover those proteins that diverged significantly during evolution but kept the essential structure of fusexins or other families of fusogens that may have replaced HAP2/GCS1.

AUTHOR CONTRIBUTIONS

NB and BP conceived and drafted the manuscript. NB and XL prepared the figures. NB, XL, and BP wrote the manuscript, discussed its content, and revised the work. All authors approved the final submitted version.

FUNDING

Work in our lab is funded by the Israel Science Foundation (ISF grants 257/17, 2462/18, 2327/19 and 178/20). This project has received funding from the European Union's Horizon 2020 research and innovation programme under the Marie Skłodowska-Curie grant agreement No 844807.

ACKNOWLEDGMENTS

The authors would like to thank Debora J. Cohen, Natalia Pascuali, Yael Iosilevskii, Clari Valansi and the members of Podbilewicz lab for the insightful discussions and comments on this review.

REFERENCES

Avinoam, O., Fridman, K., Valansi, C., Abutbul, I., Zeev-Ben-Mordehai, T., Maurer, U. E., et al. (2011). Conserved Eukaryotic Fusogens Can Fuse Viral Envelopes to Cells. *Science* 332, 589–592. doi:10.1126/science.1202333

Baquero, E., Albertini, A. A., Vachette, P., Lepault, J., Bressanelli, S., and Gaudin, Y. (2013). Intermediate Conformations during Viral Fusion Glycoprotein Structural Transition. *Curr. Opin. Virol.* 3, 143–150. doi:10.1016/j.coviro.2013.03.006

Baquero, E., Fédry, J., Legrand, P., Krey, T., and Rey, F. A. (2019). Species-Specific Functional Regions of the Green Alga Gamete Fusion Protein HAP2 Revealed by Structural Studies. *Structure* 27, 113–124. doi:10.1016/j.str.2018.09.014

Bianchi, E., Doe, B., Goulding, D., and Wright, G. J. (2014). Juno Is the Egg Izumo Receptor and Is Essential for Mammalian Fertilization. *Nature* 508, 483–487. doi:10.1038/nature13203

Bianchi, E., and Wright, G. J. (2015). Cross-species Fertilization: The Hamster Egg Receptor, Juno, Binds the Human Sperm Ligand, Izumo1. *Phil. Trans. R. Soc. B* 370 (1661), 20140101. doi:10.1098/rstb.2014.0101

Bianchi, E., and Wright, G. J. (2020). Find and Fuse: Unsolved Mysteries in Sperm-Egg Recognition. *Plos Biol.* 18, e3000953. doi:10.1371/journal.pbio.3000953

Bloomfield, G. (2019). Sex and Macrocyst Formation in Dictyostelium. *Int. J. Dev. Biol.* 63, 439–446. doi:10.1387/ijdb.190183gb

Borges, F., Gomes, G., Gardner, R., Moreno, N., McCormick, S., Feijo´, J. A., et al. (2008). Comparative Transcriptomics of Arabidopsis Sperm Cells. *Plant Physiol.* 148, 1168–1181. doi:10.1104/pp.108.125229

Bressanelli, S., Stiasny, K., Allison, S. L., Stura, E. A., Duquerroy, S., Lescar, J., et al. (2004). Structure of a Flavivirus Envelope Glycoprotein in its Low-pH-Induced Membrane Fusion Conformation. *EMBO J.* 23, 728–738. doi:10.1038/sj.emboj.7600064

Brukman, N. G., Uygur, B., Podbilewicz, B., and Chernomordik, L. V. (2019). How Cells Fuse. *J. Cel Biol.* 218, 1436–1451. doi:10.1083/jcb.201901017

Chalbi, M., Barraud-Lange, V., Ravaux, B., Howan, K., Rodriguez, N., Soule, P., et al. (2014). Binding of Sperm Protein Izumo1 and its Egg Receptor Juno Drives Cd9 Accumulation in the Intercellular Contact Area Prior to Fusion during Mammalian Fertilization. *Development* 141, 3732–3739. doi:10.1242/dev.111534

Chernomordik, L. V., and Kozlov, M. M. (2003). Protein-Lipid Interplay in Fusion and Fission of Biological Membranes, 175–207. doi:10.1146/annurev.biochem.72.121801.16150472

Cole, E. S., Cassidy-Hanley, D., Fricke Pinello, J., Zeng, H., Hsueh, M., Kolbin, D., et al. (2014). Function of the Male-gamete-specific Fusion Protein HAP2 in a Seven-Sexed Ciliate. *Curr. Biol.* 24, 2168–2173. doi:10.1016/j.cub.2014.07.064

Connors, S. A., Kanatsu-Shinohara, M., Schultz, R. M., and Kopf, G. S. (1998). Involvement of the Cytoskeleton in the Movement of Cortical Granules during Oocyte Maturation, and Cortical Granule Anchoring in Mouse Eggs. *Develop. Biol.* 200, 103–115. doi:10.1006/dbio.1998.8945

Cross, N. L., and Elinson, R. P. (1980). A Fast Block to Polyspermy in Frogs Mediated by Changes in the Membrane Potential. *Develop. Biol.* 75, 187–198. doi:10.1016/0012-1606(80)90154-2

Duncan, F. E., Que, E. L., Zhang, N., Feinberg, E. C., O'Halloran, T. V., and Woodruff, T. K. (2016). The Zinc Spark Is an Inorganic Signature of Human Egg Activation. *Sci. Rep.* 6 (16), 24737–24738. doi:10.1038/srep24737

Fédry, J., Forcina, J., Legrand, P., Péhau-Arnaudet, G., Haouz, A., Johnson, M., et al. (2018). Evolutionary Diversification of the HAP2 Membrane Insertion Motifs to Drive Gamete Fusion across Eukaryotes. *Plos Biol.* 16, e2006357. doi:10.1371/JOURNAL.PBIO.2006357

Fédry, J., Liu, Y., Péhau-Arnaudet, G., Pei, J., Li, W., Tortorici, M. A., et al. (2017). The Ancient Gamete Fusogen HAP2 Is a Eukaryotic Class II Fusion Protein. *Cell* 168, 904–915. doi:10.1016/j.cell.2017.01.024

Feng, J., Dong, X., Pinello, J., Zhang, J., Lu, C., Iacob, R. E., et al. (2018). Fusion Surface Structure, Function, and Dynamics of Gamete Fusogen HAP2. *Elife* 7, e39772. doi:10.7554/eLife.39772

Ferris, P. J., Woessner, J. P., and Goodenough, U. W. (1996). A Sex Recognition Glycoprotein Is Encoded by the Plus Mating-type Gene Fus1 of Chlamydomonas Reinhardtii. *MBoC* 7, 1235–1248. doi:10.1091/mbc.7.8.1235

Grayson, P. (2015). Izumo1 and Juno: the Evolutionary Origins and Coevolution of Essential Sperm-Egg Binding Partners. *R. Soc. Open Sci.* 2, 150296. doi:10.1098/RSOS.150296

Hernández, J. M., and Podbilewicz, B. (2017). The Hallmarks of Cell-Cell Fusion. *Development* 144, 4481–4495. doi:10.1242/dev.155523

Hirai, M., Arai, M., Mori, T., Miyagishima, S.-y., Kawai, S., Kita, K., et al. (2008). Male Fertility of Malaria Parasites Is Determined by GCS1, a Plant-type Reproduction Factor. *Curr. Biol.* 18, 607–613. doi:10.1016/j.cub.2008.03.045

Inoue, N., Ikawa, M., Isotani, A., and Okabe, M. (2005). The Immunoglobulin Superfamily Protein Izumo Is Required for Sperm to Fuse with Eggs. *Nature* 434, 234–238. doi:10.1038/nature03362

Inoue, N., Saito, T., and Wada, I. (2020). Unveiling a Novel Function of CD9 in Surface Compartmentalization of Oocytes. *Development* 147, dev189985. doi:10.1242/DEV.189985

Jaffe, L. A. (1976). Fast Block to Polyspermy in Sea Urchin Eggs Is Electrically Mediated. *Nature* 261, 68–71. doi:10.1038/261068a0

Johnson, M. A., von Besser, K., Zhou, Q., Smith, E., Aux, G., Patton, D., et al. (2004). Arabidopsis Hapless Mutations Define Essential Gametophytic Functions. *Genetics* 168, 971–982. doi:10.1534/genetics.104.029447

Jumper, J., Evans, R., Pritzel, A., Green, T., Figurnov, M., Ronneberger, O., et al. (2021). Highly Accurate Protein Structure Prediction with AlphaFold. *Nature* 596, 583–589. doi:10.1038/s41586-021-03819-2

Jurrus, E., Engel, D., Star, K., Monson, K., Brandi, J., Felberg, L. E., et al. (2018). Improvements to the APBS Biomolecular Solvation Software Suite. *Protein Sci.* 27, 112–128. doi:10.1002/pro.3280

Kim, A. M., Bernhardt, M. L., Kong, B. Y., Ahn, R. W., Vogt, S., Woodruff, T. K., et al. (2011). Zinc Sparks Are Triggered by Fertilization and Facilitate Cell Cycle Resumption in Mammalian Eggs. *ACS Chem. Biol.* 6, 716–723. doi:10.1021/cb200084y

Kim, J. H., and Chen, E. H. (2019). The Fusogenic Synapse at a Glance. *J. Cel Sci.* 132, jcs213124. doi:10.1242/JCS.213124

Krauchunas, A. R., Marcello, M. R., and Singson, A. (2016). The Molecular Complexity of Fertilization: Introducing the Concept of a Fertilization Synapse. *Mol. Reprod. Dev.* 83, 376–386. doi:10.1002/mrd.22634

Liao, M., and Kielian, M. (2005). Domain III from Class II Fusion Proteins Functions as a Dominant-Negative Inhibitor of Virus Membrane Fusion. *J. Cel Biol.* 171, 111–120. doi:10.1083/jcb.200507075

Liu, Y., Misamore, M. J., and Snell, W. J. (2010). Membrane Fusion Triggers Rapid Degradation of Two Gamete-specific, Fusion-Essential Proteins in a Membrane Block to Polygamy inChlamydomonas. *Development* 137, 1473–1481. doi:10.1242/dev.044743

Liu, Y., Tewari, R., Ning, J., Blagborough, A. M., Garbom, S., Pei, J., et al. (2008). The Conserved Plant Sterility Gene HAP2 Functions after Attachment of Fusogenic Membranes in Chlamydomonas and Plasmodium Gametes. *Genes Dev.* 22, 1051–1068. doi:10.1101/gad.1656508

Longo, F. J. (1987). Actin-plasma Membrane Associations in Mouse Eggs and Oocytes. *J. Exp. Zool.* 243, 299–309. doi:10.1002/jez.1402430215

Longo, F. J. (1985). Fine Structure of the Mammalian Egg Cortex. *Am. J. Anat.* 174, 303–315. doi:10.1002/aja.1001740310

Misamore, M. J., Gupta, S., and Snell, W. J. (2003). TheChlamydomonasFus1 Protein Is Present on the Mating TypeplusFusion Organelle and Required for a Critical Membrane Adhesion Event during Fusion withminusGametes. *MBoC* 14, 2530–2542. doi:10.1091/mbc.e02-12-0790

Modis, Y., Ogata, S., Clements, D., and Harrison, S. C. (2004). Structure of the Dengue Virus Envelope Protein after Membrane Fusion. *Nature* 427, 313–319. doi:10.1038/nature02165

Mohler, W. A., Shemer, G., del Campo, J. J., Valansi, C., Opoku-Serebuoh, E., Scranton, V., et al. (2002). The Type I Membrane Protein EFF-1 Is Essential for Developmental Cell Fusion. *Develop. Cel.* 2, 355–362. doi:10.1016/s1534-5807(02)00129-6

Mori, M., Yao, T., Mishina, T., Endoh, H., Tanaka, M., Yonezawa, N., et al. (2021). RanGTP and the Actin Cytoskeleton Keep Paternal and Maternal Chromosomes Apart during Fertilization. *J. Cel Biol.* 220, e202012001. doi:10.1083/jcb.202012001

Mori, T., Igawa, T., Tamiya, G., Miyagishima, S.-y., and Berger, F. (2014). Gamete Attachment Requires GEX2 for Successful Fertilization in Arabidopsis. *Curr. Biol.* 24, 170–175. doi:10.1016/j.cub.2013.11.030

Mori, T., Kuroiwa, H., Higashiyama, T., and Kuroiwa, T. (2006). Generative Cell Specific 1 Is Essential for Angiosperm Fertilization. *Nat. Cel Biol.* 8, 64–71. doi:10.1038/ncb1345

Muriel, O., Michon, L., Kukulski, W., and Martin, S. G. (2021). Ultrastructural Plasma Membrane Asymmetries in Tension and Curvature Promote Yeast Cell Fusion. *J. Cel Biol.* 220, e202103142. doi:10.1083/jcb.202103142

Nayak, V., Dessau, M., Kucera, K., Anthony, K., Ledizet, M., and Modis, Y. (2009). Crystal Structure of Dengue Virus Type 1 Envelope Protein in the Postfusion Conformation and its Implications for Membrane Fusion. *J. Virol.* 83, 4338–4344. doi:10.1128/jvi.02574-08

Neumann, B., Coakley, S., Giordano-Santini, R., Linton, C., Lee, E. S., Nakagawa, A., et al. (2015). EFF-1-mediated Regenerative Axonal Fusion Requires Components of the Apoptotic Pathway. *Nature* 517, 219–222. doi:10.1038/nature14102

Nishimura, H., Tajima, T., Comstra, H. S., Gleason, E. J., and L'Hernault, S. W. (2015). The Immunoglobulin-like Gene Spe-45 Acts during Fertilization in *Caenorhabditis elegans* like the Mouse Izumo1 Gene. *Curr. Biol.* 25, 3225–3231. doi:10.1016/j.cub.2015.10.056

Okamoto, M., Yamada, L., Fujisaki, Y., Bloomfield, G., Yoshida, K., Kuwayama, H., et al. (2016). Two HAP2-GCS1 Homologs Responsible for Gamete Interactions in the Cellular Slime Mold with Multiple Mating Types: Implication for Common Mechanisms of Sexual Reproduction Shared by Plants and Protozoa and for Male-Female Differentiation. *Develop. Biol.* 415, 6–13. doi:10.1016/j.ydbio.2016.05.018

Osuna-Ramos, J. F., Reyes-Ruiz, J. M., and del Ángel, R. M. (2018). The Role of Host Cholesterol during Flavivirus Infection. *Front. Cel. Infect. Microbiol.* 8, 388. doi:10.3389/fcimb.2018.00388

Pattnaik, G. P., and Chakraborty, H. (2021). Cholesterol: A Key Player in Membrane Fusion that Modulates the Efficacy of Fusion Inhibitor Peptides. *Vitam. Horm.* 117, 133–155. doi:10.1016/bs.vh.2021.06.003

Pérez-Vargas, J., Krey, T., Valansi, C., Avinoam, O., Haouz, A., Jamin, M., et al. (2014). Structural Basis of Eukaryotic Cell-Cell Fusion. *Cell* 157, 407–419. doi:10.1016/j.cell.2014.02.020

Pinello, J. F., Lai, A. L., Millet, J. K., Cassidy-Hanley, D., Freed, J. H., and Clark, T. G. (2017). Structure-function Studies Link Class II Viral Fusogens with the Ancestral Gamete Fusion Protein HAP2. *Curr. Biol.* 27, 651–660. doi:10.1016/j.cub.2017.01.049

Pinello, J. F., Liu, Y., and Snell, W. J. (2021). MAR1 Links Membrane Adhesion to Membrane Merger during Cell-Cell Fusion in Chlamydomonas. *Develop. Cel.* 56, 3380–3392. doi:10.1016/j.devcel.2021.10.023

Podbilewicz, B., Leikina, E., Sapir, A., Valansi, C., Suissa, M., Shemer, G., et al. (2006). The *C. elegans* Developmental Fusogen EFF-1 Mediates Homotypic Fusion in Heterologous Cells and *In Vivo*. *Develop. Cel.* 11, 471–481. doi:10.1016/j.devcel.2006.09.004

Podbilewicz, B. (2014). Virus and Cell Fusion Mechanisms. *Annu. Rev. Cel Dev. Biol.* 30, 111–139. doi:10.1146/annurev-cellbio-101512-122422

Radzvilavicius, A. L. (2016). Evolutionary Dynamics of Cytoplasmic Segregation and Fusion: Mitochondrial Mixing Facilitated the Evolution of Sex at the Origin of Eukaryotes. *J. Theor. Biol.* 404, 160–168. doi:10.1016/j.jtbi.2016.05.037

Ramesh, M., Malik, S., and Logsdon, J. (2005). A Phylogenomic Inventory of Meiotic GenesEvidence for Sex in Giardia and an Early Eukaryotic Origin of Meiosis. *Curr. Biol.* 15, 185–191. doi:10.1016/s0960-9822(05)00028-x

Ravaux, B., Garroum, N., Perez, E., Willaime, H., and Gourier, C. (2016). A Specific Flagellum Beating Mode for Inducing Fusion in Mammalian Fertilization and Kinetics of Sperm Internalization. *Sci. Rep.* 6 (1 6), 31886–31913. doi:10.1038/srep31886

Rival, C. M., Xu, W., Shankman, L. S., Morioka, S., Arandjelovic, S., Lee, C. S., et al. (2019). Phosphatidylserine on Viable Sperm and Phagocytic Machinery in Oocytes Regulate Mammalian Fertilization. *Nat. Commun.* 10, 4456. doi:10.1038/S41467-019-12406-Z

Sapir, A., Choi, J., Leikina, E., Avinoam, O., Valansi, C., Chernomordik, L. V., et al. (2007). AFF-1, a FOS-1-Regulated Fusogen, Mediates Fusion of the Anchor Cell in *C. elegans*. *Develop. Cel.* 12, 683–698. doi:10.1016/j.devcel.2007.03.003

Satouh, Y., Inoue, N., Ikawa, M., and Okabe, M. (2012). Visualization of the Moment of Mouse Sperm-Egg Fusion and Dynamic Localization of IZUMO1. *J. Cel Sci.* 125, 4985–4990. doi:10.1242/jcs.100867

Segev, N., Avinoam, O., and Podbilewicz, B. (2018). Fusogens. *Curr. Biol.* 28, R378–R380. doi:10.1016/j.cub.2018.01.024

Shilagardi, K., Li, S., Luo, F., Marikar, F., Duan, R., Jin, P., et al. (2013). Actin-propelled Invasive Membrane Protrusions Promote Fusogenic Protein Engagement during Cell-Cell Fusion. *Science* 340, 359–363. doi:10.1126/science.1234781

Smurova, K., and Podbilewicz, B. (2017). Endocytosis Regulates Membrane Localization and Function of the Fusogen EFF-1. *Small GTPases* 8, 177–180. doi:10.1080/21541248.2016.1211399

Smurova, K., and Podbilewicz, B. (2016). RAB-5- and DYNAMIN-1-Mediated Endocytosis of EFF-1 Fusogen Controls Cell-Cell Fusion. *Cel Rep.* 14, 1517–1527. doi:10.1016/j.celrep.2016.01.027

Speijer, D., Lukeš, J., and Eliáš, M. (2015). Sex Is a Ubiquitous, Ancient, and Inherent Attribute of Eukaryotic Life. *Proc. Natl. Acad. Sci. USA* 112, 8827–8834. doi:10.1073/pnas.1501725112

Sprunck, S., Rademacher, S., Vogler, F., Gheyselinck, J., Grossniklaus, U., and Dresselhaus, T. (2012). Egg Cell-Secreted EC1 Triggers Sperm Cell Activation during Double Fertilization. *Science* 338, 1093–1097. doi:10.1126/science.1223944

Sun, Q.-Y., and Schatten, H. (2006). Regulation of Dynamic Events by Microfilaments during Oocyte Maturation and Fertilization. *Reproduction* 131, 193–205. doi:10.1530/rep.1.00847

Takayama, J., Tajima, T., Onami, S., and Nishimura, H. (2021). *C. elegans* Spermatozoa Lacking Spe-45 Are Incapable of Fusing with the Oocyte Plasma Membrane. *microPublication Biol.* doi:10.17912/micropub.biology.000372

Umashankar, M., Sa´nchez-San Marti´n, C., Liao, M., Reilly, B., Guo, A., Taylor, G., et al. (2008). Differential Cholesterol Binding by Class II Fusion Proteins Determines Membrane Fusion Properties. *J. Virol.* 82, 9245–9253. doi:10.1128/jvi.00975-08

Umeda, R., Satouh, Y., Takemoto, M., Nakada-Nakura, Y., Liu, K., Yokoyama, T., et al. (2020). Structural Insights into Tetraspanin CD9 Function. *Nat. Commun.* 11 (1 11), 1606–1611. doi:10.1038/s41467-020-15459-7

Valansi, C., Moi, D., Leikina, E., Matveev, E., Graña, M., Chernomordik, L. V., et al. (2017). Arabidopsis HAP2/GCS1 Is a Gamete Fusion Protein Homologous to Somatic and Viral Fusogens. *J. Cel Biol.* 216, 571–581. doi:10.1083/jcb.201610093

Vance, T. D. R., and Lee, J. E. (2020). Virus and Eukaryote Fusogen Superfamilies. *Curr. Biol.* 30, R750–R754. doi:10.1016/j.cub.2020.05.029

Vogt, E.-J., Tokuhiro, K., Guo, M., Dale, R., Yang, G., Shin, S.-W., et al. (2019). Anchoring Cortical Granules in the Cortex Ensures Trafficking to the Plasma Membrane for post-fertilization Exocytosis. *Nat. Commun.* 10, 2271. doi:10.1038/s41467-019-10171-7

von Besser, K., Frank, A. C., Johnson, M. A., and Preuss, D. (2006). Arabidopsis HAP2(GCS1) Is a Sperm-specific Gene Required for Pollen Tube Guidance and Fertilization. *Development* 133, 4761–4769. doi:10.1242/dev.02683

Voss, J. E., Vaney, M.-C., Duquerroy, S., Vonrhein, C., Girard-Blanc, C., Crublet, E., et al. (2010). Glycoprotein Organization of Chikungunya Virus Particles Revealed by X-ray Crystallography. *Nature* 468, 709–712. doi:10.1038/nature09555

White, J. M., Delos, S. E., Brecher, M., and Schornberg, K. (2008). Structures and Mechanisms of Viral Membrane Fusion Proteins: Multiple Variations on a Common Theme, 189–219. doi:10.1080/1040923080205832043

Whitlock, J. M., and Chernomordik, L. V. (2021). Flagging Fusion: Phosphatidylserine Signaling in Cell-Cell Fusion. *J. Biol. Chem.* 296, 100411. doi:10.1016/j.jbc.2021.100411

Wolf, J. P., Feneux, D., Ducot, B., Rodrigues, D., and Jouannet, P. (1995). Influence of Sperm Movement Parameters on Human Sperm-Oolemma Fusion. *Reproduction* 105, 185–192. doi:10.1530/jrf.0.1050185

Yanagimachi, R. (1988). "Chapter 1 Sperm-Egg Fusion," in *Current Topics In Membranes And Transport*. Editor F. Bronner (San Diego, CA: Academic Press), 3–43. doi:10.1016/s0070-2161(08)60129-x

Yang, Y., Zhang, Y., Li, W.-J., Jiang, Y., Zhu, Z., Hu, H., et al. (2017). Spectraplakin Induces Positive Feedback between Fusogens and the Actin Cytoskeleton to Promote Cell-Cell Fusion. *Develop. Cel* 41, 107–120. doi:10.1016/j.devcel.2017.03.006

Zeev-Ben-Mordehai, T., Vasishtan, D., Siebert, C. A., and Grünewald, K. (2014). The Full-Length Cell-Cell Fusogen EFF-1 Is Monomeric and Upright on the Membrane. *Nat. Commun.* 5 (1 5), 3912–3919. doi:10.1038/ncomms4912

Zhang, J., Pinello, J. F., Fernández, I., Baquero, E., Fedry, J., Rey, F. A., et al. (2021). Species-specific Gamete Recognition Initiates Fusion-Driving Trimer Formation by Conserved Fusogen HAP2. *Nat. Commun.* 12 (1 12), 1–12. doi:10.1038/s41467-021-24613-8

Zhang, W., Chipman, P. R., Corver, J., Johnson, P. R., Zhang, Y., Mukhopadhyay, S., et al. (2003). Visualization of Membrane Protein Domains by Cryo-Electron Microscopy of Dengue Virus. *Nat. Struct. Mol. Biol.* 10, 907–912. doi:10.1038/nsb990

Conflict of Interest: The authors declare that the research was conducted in the absence of any commercial or financial relationships that could be construed as a potential conflict of interest.

Publisher's Note: All claims expressed in this article are solely those of the authors and do not necessarily represent those of their affiliated organizations, or those of the publisher, the editors and the reviewers. Any product that may be evaluated in this article, or claim that may be made by its manufacturer, is not guaranteed or endorsed by the publisher.

frontiers in Cell and Developmental Biology

ORIGINAL RESEARCH
published: 12 January 2022
doi: 10.3389/fcell.2021.810118

Sperm IZUMO1 Is Required for Binding Preceding Fusion With Oolemma in Mice and Rats

Takafumi Matsumura[1,2†], *Taichi Noda*[1,3,4], *Yuhkoh Satouh*[1†], *Akane Morohoshi*[1,5], *Shunsuke Yuri*[6], *Masaki Ogawa*[1,2], *Yonggang Lu*[1,7], *Ayako Isotani*[1,6,7] and *Masahito Ikawa*[1,2,5,7,8*]

[1]Department of Experimental Genome Research, Research Institute for Microbial Diseases, Osaka University, Suita, Japan, [2]Graduate School of Pharmaceutical Sciences, Osaka University, Suita, Japan, [3]Division of Reproductive Biology, Institute of Resource Development and Analysis, Kumamoto University, Kumamoto, Japan, [4]Priority Organization for Innovation and Excellence, Kumamoto University, Kumamoto, Japan, [5]Graduate School of Medicine, Osaka University, Suita, Japan, [6]Graduate School of Science and Technology, Nara Institute of Science and Technology, Ikoma, Japan, [7]Immunology Frontier Research Center, Osaka University, Suita, Japan, [8]Laboratory of Reproductive Systems Biology, Institute of Medical Science, The University of Tokyo, Tokyo, Japan

OPEN ACCESS

Edited by:
Amber R. Krauchunas, University of Delaware, United States

Reviewed by:
Bart Gadella, Utrecht University, Netherlands
Pablo Bermejo-Álvarez, Instituto Nacional de Investigación y Tecnología Agraria y Alimentaria (INIA), Spain

***Correspondence:**
Masahito Ikawa
ikawa@biken.osaka-u.ac.jp

†Present address:
Takafumi Matsumura, Department of Regenerative Medicine, Yokohama City University Graduate School of Medicine, Yokohama, Japan
Yuhkoh Satouh, Laboratory of Molecular Traffic, Institute for Molecular and Cellular Regulation, Gunma University, Maebashi, Japan

Specialty section:
This article was submitted to Molecular and Cellular Reproduction, a section of the journal Frontiers in Cell and Developmental Biology

Received: 06 November 2021
Accepted: 21 December 2021
Published: 12 January 2022

Citation:
Matsumura T, Noda T, Satouh Y, Morohoshi A, Yuri S, Ogawa M, Lu Y, Isotani A and Ikawa M (2022) Sperm IZUMO1 Is Required for Binding Preceding Fusion With Oolemma in Mice and Rats. Front. Cell Dev. Biol. 9:810118. doi: 10.3389/fcell.2021.810118

Fertilization occurs as the culmination of multi-step complex processes. First, mammalian spermatozoa undergo the acrosome reaction to become fusion-competent. Then, the acrosome-reacted spermatozoa penetrate the zona pellucida and adhere to and finally fuse with the egg plasma membrane. IZUMO1 is the first sperm protein proven to be essential for sperm-egg fusion in mammals, as *Izumo1* knockout mouse spermatozoa adhere to but fail to fuse with the oolemma. However, the IZUMO1 function in other species remains largely unknown. Here, we generated *Izumo1* knockout rats by CRISPR/Cas9 and found the male rats were infertile. Unlike in mice, *Izumo1* knockout rat spermatozoa failed to bind to the oolemma. Further investigation revealed that the acrosome-intact sperm binding conceals a decreased number of the acrosome-reacted sperm bound to the oolemma in *Izumo1* knockout mice. Of note, we could not see any apparent defects in the binding of the acrosome-reacted sperm to the oolemma in the mice lacking recently found fusion-indispensable genes, *Fimp*, *Sof1*, *Spaca6*, or *Tmem95*. Collectively, our data suggest that IZUMO1 is required for the sperm-oolemma binding prior to fusion at least in rat.

Keywords: fertilization, sperm-oolemma adhesion, gamete fusion, FOLR4, knockout, Juno

INTRODUCTION

In sexual reproduction, the binding and fusion between the plasma membranes of spermatozoa and eggs are fundamental prerequisites for successful fertilization. In mammals, the spermatozoa ejaculated into the female reproductive tract undergo physiological, biochemical, and morphological changes (i.e., capacitation and acrosome reaction) to gain fertilization competency. The capacitated and acrosome-reacted sperm pass through the oocyte cumulus cell layer and the zona pellucida (ZP) and eventually bind to and fuse with the egg plasma membrane (Okabe, 2013). In the early days, several candidate sperm proteins involved in sperm-egg fusion have been identified using enzyme inhibitors and antibodies that block the *in vitro* fertilization (IVF) (Okabe, 2018). However, when their functions were challenged using the gene knockout (KO) mice,

only IZUMO1 was found indispensable for the sperm-egg fusion (Okabe, 2018; Fujihara et al., 2020; Lamas-Toranzo et al., 2020; Noda et al., 2020).

IZUMO1 is an immunoglobulin (Ig)-like type I membrane protein that localizes to the acrosomal membrane and translocates to the sperm plasma membrane during the acrosome reaction (Satouh et al., 2012; Isotani et al., 2017). *Izumo1* KO spermatozoa can penetrate the ZP but cannot fuse with the egg plasma membrane, resulting in male sterility (Inoue et al., 2005). Through an Avidity-based Extracellular Interaction Screen (AVEXIS) assay, IZUMO1 was found to interact with a glycosylphosphatidylinositol (GPI)-anchored protein, JUNO (also called FOLR4 or IZUMO1R), expressed on the oolemma (Bushell et al., 2008; Bianchi et al., 2014). The tertiary structures of IZUMO1, JUNO, and their complex have been intensively studied by X-ray crystallography (Aydin et al., 2016; Han et al., 2016; Kato et al., 2016; Nishimura et al., 2016; Ohto et al., 2016). The IZUMO1-JUNO, ligand-receptor interaction exists in mice and humans in a species-specific manner, implying that the two molecules might govern the gamete incompatibility among species (Bianchi and Wright, 2015).

Nevertheless, unlike other eukaryotic fusion proteins (e.g., HAP2/GCS1), neither of the two molecules possesses a fusogenic peptide or enables the cell-cell fusion *in vitro* by transient expression (Bianchi et al., 2014; Aydin et al., 2016). In addition, the cultured cells, such as HEK293T and COS-7 cells, transiently expressing mouse IZUMO1 can tightly bind to but not fuse with the ZP-free mouse eggs, suggesting the IZUMO1-JUNO interaction alone is insufficient for membrane fusion (Inoue et al., 2013; Ohto et al., 2016). Given these findings, researchers speculate that IZUMO1 and JUNO are implicated in sperm-egg binding rather than fusion. However, the number of *Izumo1* KO mouse spermatozoa bound to the oolemma of the ZP-free eggs is comparable to the wild-type group (Inoue et al., 2005), rendering the detailed role of IZUMO1 during the sperm-egg fusion unclear.

In this study, we deleted *Izumo1* in rats using the CRISPR/Cas9 system and analyzed the IZUMO1 function during rat fertilization. Combined with a reanalysis of the *Izumo1* KO mice, our data indicate that IZUMO1 is required for binding the acrosome-reacted spermatozoa to oolemma prior to fusion.

MATERIALS AND METHODS

Animals

All mice and rats were maintained under specific-pathogen-free conditions with *ad libitum* feeding. B6D2F1 mice were purchased from Japan SLC, Inc. B6D2-Tg(CAG/Su9-DsRed2,Acr3-EGFP) RBGS002Osb mice and STOCK Izumo1<tm1Osb> (*Izumo1* KO or *Izumo*$^{-/-}$) mice that are generated and maintained in our laboratory are used for generating *Izumo1*$^{-/-}$; RBGS mice. B6D2-4930451I11Rik<em1Osb> (*Fimp* KO) mice, STOCK Llcfc1<em2Osb> (*Sof1* KO) mice, B6D2-Spaca6<em2Osb> (*Spaca6* KO) mice, and B6D2-Tmem95<em1Osb> (*Tmem95* KO) mice are generated and maintained in our laboratory. WIAR rats were purchased from Institute for Animal Reproduction. Wistar rats were purchased from Charles River Laboratories Japan, Inc.

Protein Sequence Alignment and Prediction of Domain Structure

IZUMO1 sequences used for alignment are retrieved from the National Center for Biotechnology Information (NCBI) database: *Homo sapiens* (Human), NP_872381.2; *Mus musculus* (Mouse), NP_001018013.1; *Rattus norvegicus* (Rat), NP_001017514.1; *Bos taurus* (Cattle), XP_024835010.1; *Strigops habroptila* (Kakapo), XP_030366609.1; *Terrapene carolina triunguis* (Turtle), XP_026513927.1; and *Danio rerio* (Zebrafish), NP_001314727.1. The domain structure of IZUMO1 was derived from the NCBI database or was predicted by the Simple Modular Architecture Research Tool (SMART). Sequence alignment of IZUMO1 homologs was conducted and visualized using the Clustal Omega program (https://www.ebi.ac.uk/Tools/msa/clustalo/).

Generation of *Izumo1*-Deficient Rat

We generated a pX330 (#42230, Addgene, Cambridge, MA, USA) plasmid encoding a single-guide RNA (sgRNA) and the Cas9 protein to target the second exon of *Izumo1* (target sequence: 5′-GGTGGCTGCAATAAAGACTT-3′). The DNA cleavage activity of this plasmid was validated as described previously (Mashiko et al., 2013). Superovulated WIAR (3–4 weeks old) females were mated with the mature males, and the two-pronuclear zygotes were collected from the oviduct. The circular pX330 plasmid was injected into one pronucleus of each zygote at concentrations of 5 ng/μl, 10 ng/μl, or 20 ng/μl (Mashiko et al., 2013). The following primer set was used for genotyping PCR of rat *Izumo1* (Forward: 5′-TGTTTAGCACCCTCCTCCCTGC-3′, Reverse: 5′-AGAGAGTATGTATCTCTGCCTGTCCTGG-3′).

RT-PCR

The total RNA was collected from the adult rat testes, purified using NucleoSpin RNA Plus (Takara, Kyoto, Japan), and reverse-transcribed into cDNA using SuperScript IV VILO Master Mix (Thermo Fisher Scientific, Waltham, MA, USA). PCR was performed using KOD DNA polymerase (Toyobo, Osaka, Japan); the PCR conditions for detecting rat *Izumo1* were as follows: initial denaturing at 98°C for 30 s, followed by denaturing at 98°C for 15 s, annealing at 55°C for 5 s, and elongation 68°C for 5 s for 33 cycles. The PCR conditions for detecting rat *Actb* were as follows: initial denaturing at 98°C for 30 s, followed by denaturing at 98°C for 15 s, annealing at 58°C for 5 s, and elongation at 68°C for 5 s for 30 cycles. The PCR primers for rat *Izumo1* were: Forward; 5′-ATGGGGCTACATTTTACACTC-3′ and Reverse; 5′-TTAGTTATCTGCTTCCTCAACC-3’. The PCR primers for rat *Actb* were: Forward; 5′-GTCCACCCGCGAGTACAAC-3′ and Reverse; 5′-GGATGCCTCTCTTGCTCTGG-3′.

Antibodies

The mouse monoclonal antibody against rat CD46 [MM1] (ab180652) was purchased from Abcam (Cambridge, UK). The

rat monoclonal antibody against IZUMO1 (KS-64 125) (Ikawa et al., 2011) and rabbit polyclonal antibody against human IZUMO1 (Inoue et al., 2005) are generated in our laboratory as previously described. The goat anti-rat IgG Alexa Fluor 488-conjugated antibody (A11006), goat anti-mouse IgG antibody labeled with Alexa Fluor 568 (A11004), and goat anti-rabbit IgG Alexa Fluor Plus 488-conjugated antibody (A11034) were purchased from Thermo Fisher Scientific.

Testis Histological Analysis

Testes were fixed in 4% paraformaldehyde in PBS and were processed for plastic embedding using Technovit® 8100 (Mitsui Chemicals, Tokyo, Japan) as described previously (Matsumura et al., 2019). Sections were made at a thickness of 5 μm and treated with 1% periodic acid (Wako, Osaka, Japan) for 10 min, followed by treatment with the Schiff's reagent (Muto Pure Chemicals Co., Ltd., Tokyo, Japan) for 15 min. The sections were further stained with Mayer's hematoxylin solution (Wako) and observed under a light microscope.

Sperm Analysis

For detecting IZUMO1 in sperm cells, the frozen rat testes were disaggregated in PBS using BioMasher II (Nippi, Tokyo, Japan), and the germ cells were smeared on glass slides. The cells were air-dried on microscope slides, washed with PBS, and permeabilized with methanol. After treatment with image-iT FX Signal enhancer (Thermo Fisher Scientific) for 30 min at room temperature, the cells were incubated with the rabbit anti-human IZUMO1 polyclonal antibody (1:100) diluted by Can Get Signal A (Toyobo) at 4°C for overnight. After incubation with goat anti-rabbit IgG Alexa Fluor Plus 488 (1:200) and Lectin PNA Alexa Fluor 568 conjugate (Thermo Fisher Scientific) (1:200) for 1 h at room temperature, the spermatozoa were stained with Hoechst 33342 to visualize the nuclei (Dojindo, Kumamoto, Japan) and were mounted in Prolong Diamond (Thermo Fisher Scientific). For sperm morphological analysis, the cauda epididymal spermatozoa of male rats were incubated in the Human Tubal Fluid (HTF) medium (Aoto et al., 2011) for 10 min and observed under a BX50F phase-contrast microscope (Olympus, Tokyo, Japan).

Mating Test

Each male rat was caged with two Wistar females for 2 months. The number of delivered pups was counted. Copulation was confirmed by the formation of vaginal plugs or the presence of spermatozoa in the vaginal smears. Alternatively, superovulated Wistar females (3–4 weeks old) were mated with the male rats (3–6 months old). The eggs were collected from the oviducts of the superovulated females about 22 h after the hCG injection and mating. The eggs were observed under an inverted microscope (Olympus IX71), and the fertilization rate was recorded.

Rat Sperm-Oolemma Fusion Assay

The HTF medium was prepared as described previously (Aoto et al., 2011). The cauda epididymal spermatozoa from male rats (3–6 months old) were preincubated for an hour in the HTF medium. The final sperm concentration was adjusted to 1×10^5 spermatozoa/mL in 100 μl HTF medium drops for insemination. The cumulus-oocyte complexes were collected from the oviductal ampulla of the superovulated females (3–4 weeks old), and the cumulus cells were removed by 0.03% hyaluronidase. The cumulus-free eggs were subsequently treated with 1 mg/ml collagenase to remove the ZP. To assess the sperm-egg fusion, the ZP-free eggs were fixed with 2% paraformaldehyde and stained by Hoechst 33342 after insemination for 5 h. Swollen sperm nuclei could be observed in the ooplasm when fusion occurred. The sperm-oolemma adhesion was assessed under a microscope at 0, 0.5, 2, and 5 h after insemination. To examine the acrosome status, spermatozoa were probed with anti-CD46 antibody (MM1) (1:200) and goat anti-mouse IgG Alexa Fluor 568-conjugated secondary antibody (1:200) in the HTF medium. An hour after insemination, the eggs were stained by Hoechst 33342, and the Z-stack images were captured using a BZ-X710 microscope (Keyence, Osaka, Japan). The total number of bound spermatozoa was counted. The spermatozoa in the HTF medium were smeared on microscope slides and observed under a fluorescence microscope.

Mouse Sperm-Oolemma Fusion Assay

The Toyoda-Yokoyama-Hosi (TYH) medium was prepared as described previously (Toyoda et al., 1971) and used for sperm preincubation, egg preparation, and insemination. The cauda epididymal spermatozoa from adult male mice (3–6 months) were preincubated for 2 h. The final concentration of spermatozoa was adjusted to 1×10^5 spermatozoa/mL in 100 μl TYH medium drops for insemination. Twenty minutes after insemination, the ZP-free eggs were moved to fresh medium drops, fixed with 0.8% paraformaldehyde, and stained by Hoechst 33342. The eggs were transferred to glass-bottomed chambers to observe *Acr*-EGFP fluorescence using a spinning-disk confocal microscope (Olympus). The cauda epididymal spermatozoa obtained from *Fimp*, *Sof1*, *Tmem95*, and *Spaca6* KO male mice were preincubated at a concentration of $1–2 \times 10^5$ spermatozoa/mL for 2.5 h followed by probing with the monoclonal antibody against IZUMO1 (KS-64 125) (1:100) and goat anti-rat IgG Alexa Fluor 488-conjugated antibody (1:200) for another 30 min. The sperm concentration was adjusted to 1×10^5 spermatozoa/mL in 100 μl fresh medium drops and incubated with the ZP-free eggs for 30 min. The eggs were gently washed in fresh medium drops three times and fixed with 0.2% paraformaldehyde. The spermatozoa from B6D2F1 or $Sof1^{+/-}$(*Sof1* Het) male mice were used as control. The eggs were observed using a BZ-X710 microscope (Keyence). For calculating the total number of spermatozoa bound to the oolemma, the sperm tails were counted using a bright field microscope. The spermatozoa with and without green fluorescence in the acrosome were recognized as acrosome-intact and acrosome-reacted, respectively.

Statistical Analysis

Statistical analyses were performed using a two-tailed student's t-test ($n \geqq 3$). Differences were considered significant at $p < 0.05$. Data represent the means ± standard deviation (SD), and error bars indicate SD.

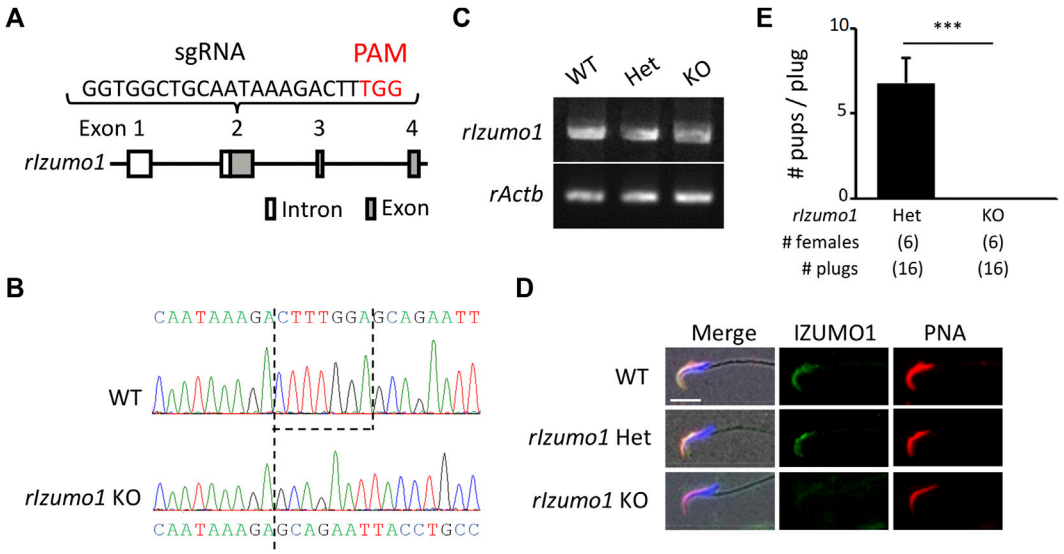

FIGURE 1 | Generation of *Izumo1*-deficient rats using CRISPR/Cas9. **(A)** Design of sgRNA for disrupting *Izumo1* in rats. White and gray boxes represent the untranslated and coding regions, respectively. **(B)** Genomic *Izumo1* sequences of WT and mutant (*Izumo1*$^{-7/-7}$) alleles. **(C)** Detection of rat *Izumo1* mRNA in testis by RT-PCR. **(D)** Immunostaining of IZUMO1 in the testicular sperm from WT or mutant rats. The acrosomal caps and the nuclei were stained by the fluorophore-conjugated Lectin PNA and Hoechst 33342, respectively. Scale bar = 10 μm. **(E)** The average number of pups per copulatory plug. Three males each were tested for the *Izumo1* Het and *Izumo1* KO groups. ***$p < 0.001$.

Biological Resources Availability Statement

The *Izumo1* KO rat strain was deposited under the name W; WIAR-*Izumo1*<em1Osb>, which will be available through the National BioResource Project for the Rat in Japan (NBRP; Kyoto, Japan). The B6D2-Tg(CAG/Su9-DsRed2, Acr3-EGFP) RBGS002Osb mice, STOCK Izumo1<tm1Osb> (*Izumo1* KO or *Izumo1*$^{-/-}$) mice, B6D2-4930451I11Rik<em1Osb> (*Fimp* KO), STOCK Llcfc1<em2Osb> (*Sof1* KO), B6D2-Spaca6<em2Osb> (*Spaca6* KO), and B6D2-Tmem95<em1Osb> (*Tmem95* KO) mouse lines used in this study are available through either the Riken BioResource Center (Riken BRC; Tsukuba, Japan) or the Center for Animal Resources and Development, Kumamoto University (CARD; Kumamoto, Japan).

RESULTS

Izumo1 KO Male Rats Are Infertile due to Fertilization Defects

The amino acid sequences of IZUMO1 are conserved in mammals, birds, reptiles, and fish (**Supplementary Figure S1**). To knockout rat *Izumo1* with the CRISPR/Cas9-mediated gene disruption, we designed a single-guide RNA (sgRNA) targeting the second exon of *Izumo1* (**Figure 1A**). By injecting the sgRNA/Cas9 expressing plasmid (pX330) into the pronuclei of 215 zygotes, we obtained a male and a female mutant rat (2/13 pups, 15.3%) (**Supplementary Figures S2A,B**). As the mutant male rat (*Izumo1*$^{-8/-29}$) showed sterility (Supplementary Figure 2C), we established a mutant line harboring 7-bp deletion by pairing the mutant female with a wild-type (WT) male (**Figure 1B**). We confirmed that *Izumo1*$^{-7/-7}$ (KO) rats that *Izumo1* mRNA derived from the mutant allele were transcribed in the testis (**Figure 1C**). But the translation of IZUMO1 is expected to be interrupted by a premature termination codon introduced by the frameshift (**Supplementary Figure S2D**). Indeed, the loss of IZUMO1 protein in the sperm acrosome was confirmed by immunostaining (**Figure 1D**). When *Izumo1*$^{wt/-7}$ (Het) or *Izumo1* KO male rats were individually caged with WT females for 2 months, all *Izumo1* Het males sired pups (pups/plug: 6.79 ± 1.45), whereas *Izumo1* KO males did not produce any pups despite the normal mating behavior indicated by formation of the copulation plugs (**Figure 1E**).

Izumo1 KO Rat Spermatozoa Show Impaired Adhesion to the Oolemma

Periodic acid-Schiff (PAS) staining of testis sections showed no sign of defects in the spermatogenesis of *Izumo1* KO rats (**Supplementary Figure S3A**). In addition, there were no apparent abnormalities in the morphology of *Izumo1* KO spermatozoa collected from the cauda epididymis (**Supplementary Figure S3B**). To determine the fertilizing ability of *Izumo1* KO spermatozoa *in vivo*, we collected eggs from the oviduct of wild-type females 22 h after pairing with the KO males. Though *Izumo1* KO spermatozoa penetrated the ZP at a comparable rate as the Het spermatozoa, no fertilized eggs were observed (**Figures 2A,B**).

We next performed *in vitro* fertilization using the enzymatically ZP-removed eggs. While the WT and Het spermatozoa successfully adhered to and fused with the eggs after an hour of insemination (oolemma-bound and fused spermatozoa: 3.77 ± 0.94 and 1.36 ± 0.33 spermatozoa/egg, respectively), none of the *Izumo1* KO spermatozoa adhered to

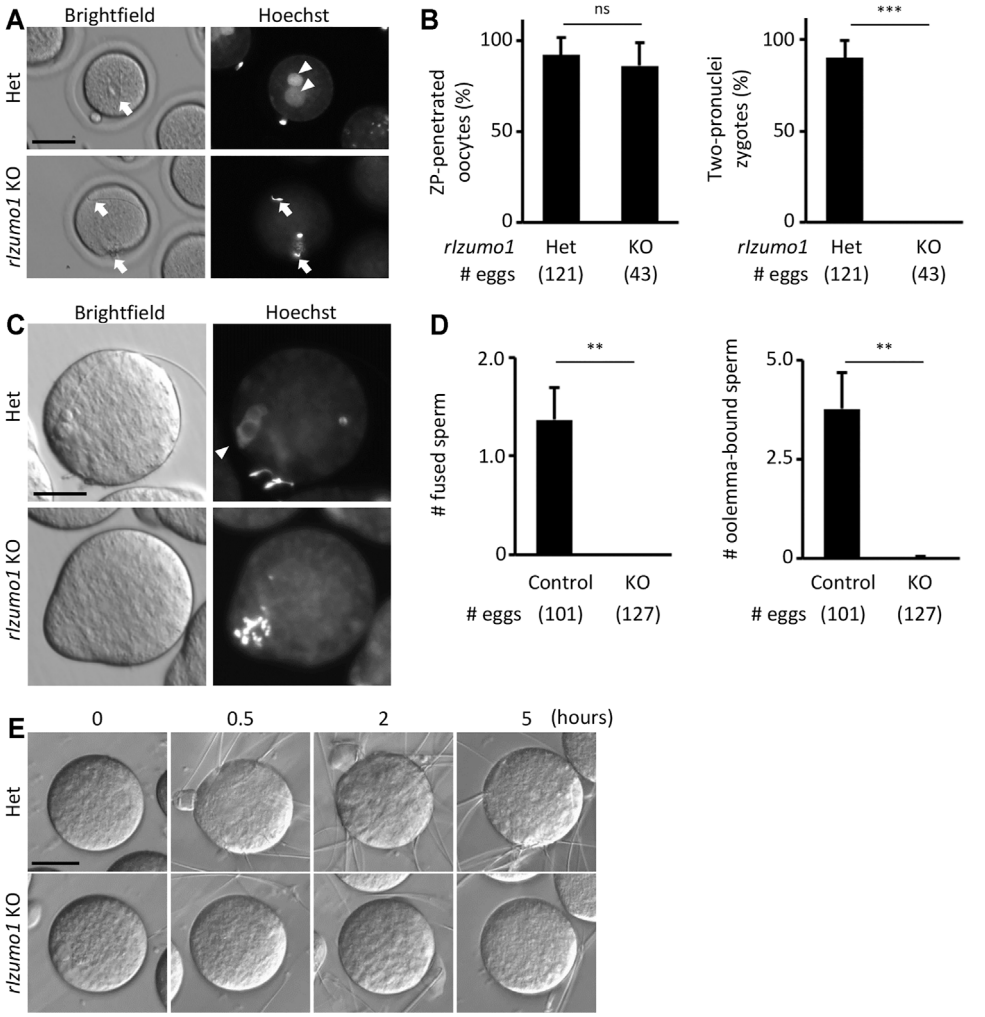

FIGURE 2 | Impaired ability to bind to the oolemma in *Izumo1* KO rat sperm. **(A)** The eggs recovered from the ampulla of the superovulated females mated with *Izumo1* Het or *Izumo1* KO male. The nuclei were stained by Hoechst 33342. Scale bar = 100 μm. **(B)** The average ratio of the ZP-penetrated eggs (left) or two-pronuclear zygotes (right) to the total recovered eggs. ns represents no statistical difference. ***$p < 0.001$. **(C)** The sperm-egg fusion was assessed by staining the nuclei with Hoechst 33342. Fused sperm are indicated by the fluorescence signals of the swollen sperm nuclei. Scale bar = 50 μm. **(D)** The average numbers of the fused spermatozoa (left) and oolemma-bound spermatozoa (right). *Izumo1* WT and Het rat sperm were used as control. **$p < 0.01$ **(E)** The sperm-egg adhesion was captured at 0, 0.5, 2, and 5 h after insemination. Scale bar = 50 μm.

or fused with the eggs (oolemma-bound and fused spermatozoa: 0.02 ± 0.03 and 0 ± 0 spermatozoa/egg, respectively) (**Figures 2C,D**). Even when we extended the insemination period up to 5 h, adhesion of the *Izumo1* KO spermatozoa to the oolemma was not observed (**Figure 2E**, **Supplementary Movies S1, S2**). These findings suggest the sterility of *Izumo1* KO rats is attributed to the inability of KO spermatozoa to bind to the oolemma.

Rat Spermatozoa Acquire Egg Binding Ability After Acrosome Reaction

In mice and hamsters, it is known that both the acrosome-intact and reacted spermatozoa can stick to the surface of the ZP-free eggs (Phillips and Yanagimachi, 1982; Calarco, 1991; Yanagimachi, 1994; Satouh et al., 2012). Since IZUMO1 is exposed to the sperm surface during the acrosome reaction (Satouh et al., 2012; Isotani et al., 2017), the attachment of the acrosome-intact spermatozoa to the oolemma does not involve the IZUMO1-JUNO interaction and does not lead to subsequent fusion between the two plasma membranes. Thus, in the following text, the acrosome-intact or reacted spermatozoa attachment to the oolemma is referred to as the fusion-incompetent or fusion-competent sperm adhesion, respectively. To rule out the fusion-incompetent sperm adhesion, we assessed the acrosome status of the live spermatozoa by immunostaining of CD46 (**Supplementary Figure S4A**). Like IZUMO1, CD46 is localized to the inner acrosomal membrane and is translocated to the sperm plasma membrane during the acrosome reaction (Mizuno et al., 2004). Since CD46 is inaccessible to the antibody before being exposed to the sperm surface, no fluorescence signals should be seen in the live acrosome-intact spermatozoa. As a result, 82.6 ± 12.4% of the spermatozoa

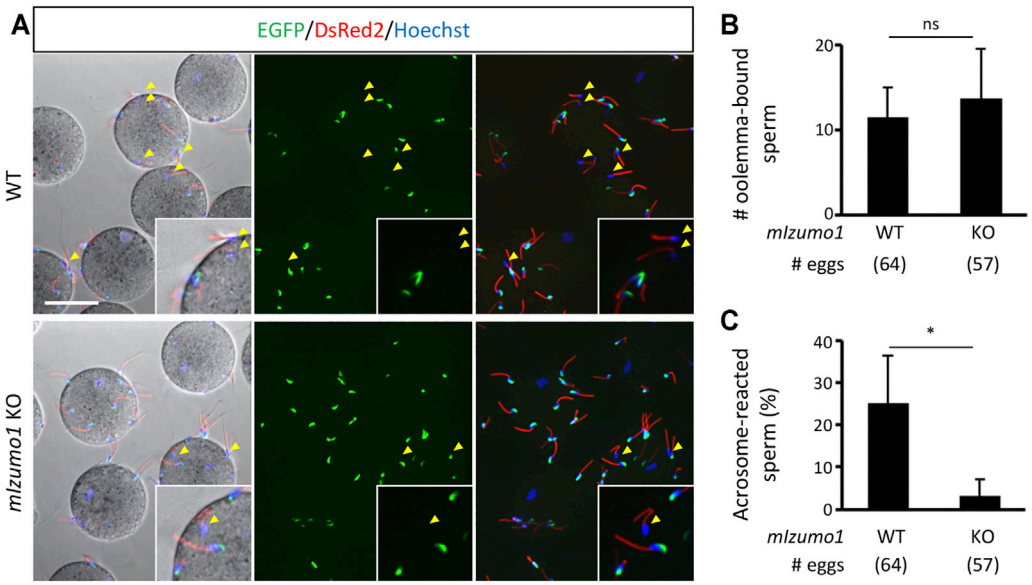

FIGURE 3 | Reduced binding of the acrosome-reacted *Izumo1* KO mouse sperm to the oolemma. **(A)** A representative image of mouse sperm adhered to egg membrane. Spermatozoa with the EGFP signals are acrosome-intact, whereas the ones without EGFP are acrosome-reacted (yellow arrowhead). DsRed2 is expressed in the sperm midpiece. The sperm nuclei were stained by Hoechst 33342. Scale bar = 50 μm **(B)** The total numbers of oolemma-bound spermatozoa. ns represents no statistical difference. **(C)** The ratios of the acrosome-reacted sperm to the total number of oolemma-bound sperm. *$p < 0.05$.

adhered to the oolemma were acrosome-reacted, whereas 24.5 ± 11.2% of the spermatozoa in the medium were acrosome-reacted (**Supplementary Figures S4B,C**), indicating that the acrosome-intact spermatozoa are less prone to adhering to the oolemma compared with the acrosome-reacted spermatozoa in rats.

IZUMO1 Plays a Critical Role in Acrosome Reacted Sperm Binding to Oolemma in Mice

The lack of adhesion ability of the *Izumo1* KO rat spermatozoa to the oolemma is distinct from our previous study, in which we could not see apparent defects in the adhesion of *Izumo1* KO mouse spermatozoa to the oolemma (Inoue et al., 2005). Of note, it was reported that the acrosome-reacted spermatozoa hardly bind to the *JUNO* KO eggs in mice (Bianchi et al., 2014). Thus, we speculated that an excessive number of the acrosome-intact spermatozoa adhered to the oolemma might conceal a lack of fusion-competent adhesion by the acrosome-reacted spermatozoa. To address this concern, we generated *Izumo1* KO mice carrying the RBGS (Red Body Green Spermatozoa) transgene that encodes EGFP in the acrosome and DsRed2 in the mitochondria to re-evaluate the sperm acrosome status during fertilization. The mouse spermatozoa were preincubated for 2 h and incubated with the ZP-free eggs for 20 min in the TYH medium. We did not see any differences in the average rates of the acrosome reaction in WT and *Izumo1* KO spermatozoa (WT: 20.8 ± 15.8%; KO: 21.7 ± 11.0%). While the total numbers of the spermatozoa bound to the oolemma were comparable between the WT and KO groups (**Figures 3A,B**), the percentage of the oolemma-bound acrosome-reacted spermatozoa was drastically decreased in the *Izumo1* KO mice (WT: 25.3 ± 11.3%; KO: 3.28 ± 3.78%, **Figure 3C**).

Mouse Spermatozoa Lacking Other Fusion-Related Genes Are Not Defective in Binding to the Oolemma

Recent studies uncovered novel sperm proteins necessary for sperm-egg fusion in addition to IZUMO1 (Lorenzetti et al., 2014; Fujihara et al., 2020; Lamas-Toranzo et al., 2020; Noda et al., 2020; Inoue et al., 2021; Noda et al., 2021), yet whether these molecules are involved in the gamete adhesion or fusion remains unclear. Hence, we performed the sperm-egg fusion assays using the *Fimp*, *Sof1*, *Spaca6*, and *Tmem95* mutant mouse spermatozoa with the sperm acrosome status being unraveled using an anti-IZUMO1 antibody. As a result, we could not see apparent differences in both the total numbers of bound spermatozoa and the ratios of the acrosome-reacted spermatozoa to the total bound spermatozoa between the WT and KO groups (**Figures 4A–C**).

DISCUSSION

The cell-cell membrane adhesion and fusion processes are considered independent biological events, each of which requires its suites of molecules. For instance, the gamete adhesion is potentiated by FUS1, whereas HAP2 regulates the gamete fusion in *Chlamydomonas reinhardtii* (Misamore et al.,

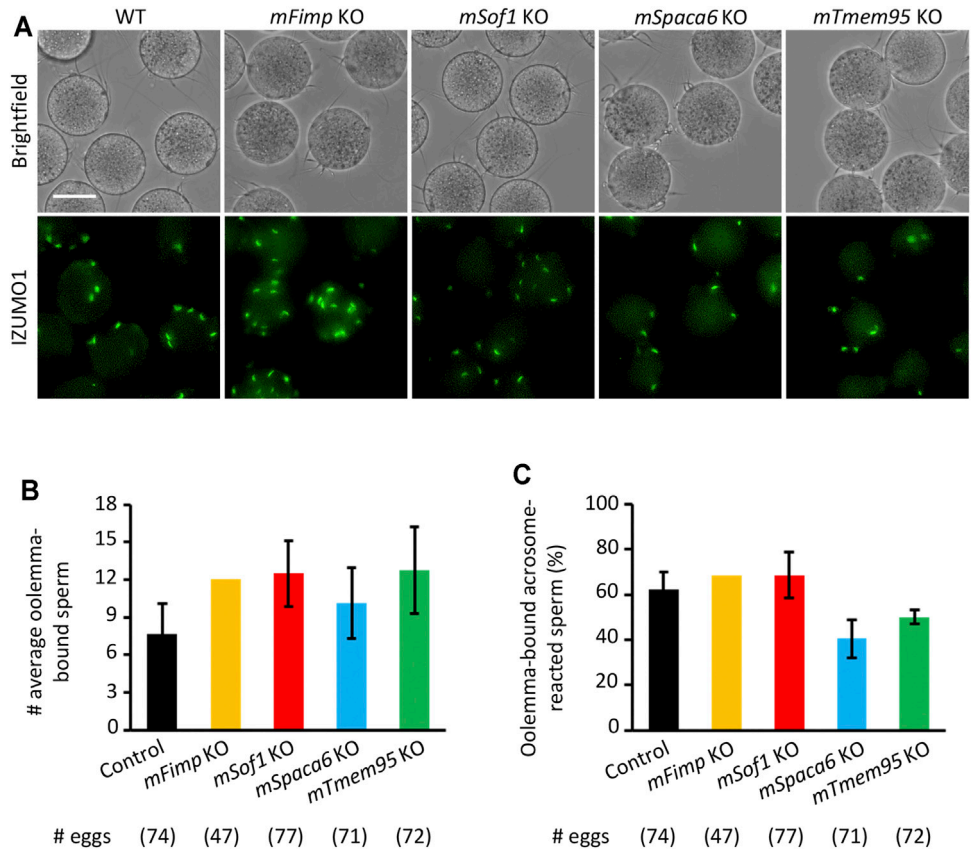

FIGURE 4 | Mutant sperm lacking the novel fusion-related genes bind to the oolemma after the acrosome reaction. **(A)** Observation of the binding between WT eggs and WT or *Fimp*, *Sof1*, *Tmem95*, and *Spaca6* KO spermatozoa. The acrosome-reacted sperm on the oolemma are indicated by the fluorescence signals of IZUMO1. Scale bar = 50 μm. **(B)** The numbers of total oolemma-bound spermatozoa. WT and *Sof1* Het mouse sperm were used as control. **(C)** The ratio of the acrosome-reacted sperm to the total oolemma-bound sperm. WT and *Sof1* Het mouse sperm were used as control.

2003; Liu et al., 2008; Aguilar et al., 2013; Hernandez and Podbilewicz, 2017). In mammal syngamy, studies using the cultured cell lines strongly suggest that IZUMO1 and JUNO are responsible for the sperm-egg adhesion instead of fusion per se – the HEK293T, COS-7, and K562 cells expressing IZUMO1 (Inoue et al., 2013; Chalbi et al., 2014; Ohto et al., 2016) or JUNO (Bianchi et al., 2014; Chalbi et al., 2014; Kato et al., 2016) attach to the ZP-free eggs or sperm, respectively, but never fused with them. To better understand the functions of IZUMO1 and JUNO, the plasma membrane fusion needs to be directly investigated using sperm and eggs. However, the ZP-intact eggs are not ideal for studying gamete fusion *in vitro*. With the presence of the ZP, sperm penetration and fusion timing is not controllable. In addition, the cortical reaction is triggered after incorporating the initial spermatozoon with the oolemma, thereby preventing additional spermatozoa from penetrating the ZP and approaching the oolemma. Therefore, the ZP should be removed mechanically by a piezo-driven micromanipulator or chemically by collagenase or acidic Tyrode before the fusion analysis (Yamagata et al., 2002; Inoue et al., 2005; Yamatoya et al., 2011; Nozawa et al., 2018). Nevertheless, the acrosomal-intact sperm, which cannot pass through the ZP or fuse with the oolemma, non-specifically bind to the egg membrane in a fusion-incompetent way in mice and hamsters (Phillips and Yanagimachi, 1982; Calarco, 1991; Yanagimachi, 1994).

Like mice and hamsters, rats have been used as a popular rodent model for spermatogenesis and reproductive toxicology (Russell et al., 1993; OECD, 2016). However, they have not been used intensively in the fertilization field due to a delay in developing a highly efficient and convenient *in vitro* fertilization system (Honda et al., 2019). Distinct to the previous findings using mice or hamsters, we discovered that the acrosome-intact sperm in rats are less likely to adhere to the oolemma than the acrosome-reacted sperm. Such uniqueness in the rats enables us to explicitly quantify the fusion-competent binding between the acrosome-reacted sperm and oolemma. In a previous study, the acrosome-intact human sperm adhered to the mouse egg plasma membrane but not to the human egg surface (Liu and Baker, 1994). Thus, it is tempting to speculate that the fusion-incompetent sperm adhesion in mice and hamsters might be attributed to the molecular architecture of the egg plasma membrane.

In combination with a transgene encoding Acrosin-GFP, the sperm acrosome status can be readily examined by the presence or absence of the green fluorescence signals (Nakanishi et al., 1999; Hasuwa et al., 2010). In 2014, Bianchi et al. reported the adhesion rate of the acrosome-reacted *Acr*-GFP spermatozoa to the JUNO-deficient egg membrane is significantly reduced compared to that of the wild-type group. Here, using a similar approach, we discovered that the IZUMO1-deficient mouse spermatozoa hardly adhere to the egg membrane after the acrosome reaction. However, a small population of the acrosome-reacted *Izumo1* KO mouse spermatozoa can still adhere to the oolemma, which might be attributed to the existence of other sperm-oolemma adhesion machinery on top of the IZUMO1-JUNO interaction in mice.

Interestingly, a more recent study indicates that SPACA6 is absent in the *Izumo1* KO mouse spermatozoa (Inoue et al., 2021). Therefore, it remains possible that the complete loss of the oolemma binding ability in the *Izumo1* KO rat spermatozoa might be attributed to not only the loss of the IZUMO1-JUNO interaction but also the collaterally disrupted interactions between SPACA6 or other sperm surface proteins with their receptors on the egg surface. Therefore, to further investigate the complex functions of those newly identified fusion-related molecules, the fusion-competent adhesion between the Juno KO eggs and the *Fimp*, *Sof1*, *Spaca6*, or *Tmem95* KO spermatozoa that retain IZUMO1 should also be analyzed. It should be noted that, while we are preparing this manuscript, *Dcst1/2* KO spermatozoa were also added to the list (Inoue et al., 2021; Noda et al., 2021).

In conclusion, our data suggest that IZUMO1 is critical for the sperm-egg adhesion preceding the plasma membrane fusion in mice and rats. Rats have been demonstrated as a suitable model for the study of mammalian fertilization because the acrosome-intact spermatozoa are less likely to adhere to the ZP-free egg surface non-specifically. Furthermore, the CRISPR/Cas9 system simplifies genome editing in rats, thereby making the genetically modified rats more accessible for researchers. Collectively, this study highlights that the rat model could be intensively employed for efficient screening of molecules involved in the sperm-egg adhesion and fusion by either genetic approaches or inhibition analyses using recombinant proteins or antibodies.

DATA AVAILABILITY STATEMENT

The original contributions presented in the study are included in the article/**Supplementary Material**, further inquiries can be directed to the corresponding author.

ETHICS STATEMENT

The animal study was reviewed and approved by the Animal Care and Use Committee of the Research Institute for Microbial Diseases, Osaka University, Japan (#Biken-AP-R03-01-0).

AUTHOR CONTRIBUTIONS

TM, AI, and MI designed the research. TM, TN, YS, AM, MO, and AI performed research. TN, AI, MO, and SY produced the mutant strains. TM, TN, YS, AI, and MI analyzed data. TM, YL, and MI wrote the paper. All authors reviewed and commented on the manuscript.

FUNDING

This work was supported by the Ministry of Education, Culture, Sports, Science, and Technology (MEXT)/Japan Society for the Promotion of Science (JSPS) KAKENHI grants (JP19J01276 to TM, JP18K14612 and JP20H03172 to TN, JP19K06686 to YS, JP19J12450 to AM, JP18K16735 to YL, JP21K19267 to AI, JP19H05750, JP21H05033, JPJSBP120208403 to MI); JST, PRESTO Grant JPMJPR2148 to TN; and Takeda Science Foundation grants to TN and MI; The Nakajima Foundation to TN; and the Eunice Kennedy Shriver National Institute of Child Health and Human Development (P01HD087157 and R01HD088412 to MI); and the Bill and Melinda Gates Foundation (INV-001902 to MI). The funders had no role in study design, data collection, analysis, decision to publish, or manuscript preparation. Drs. TM and AM were JSPS research fellows. Open access charges were funded by the Bill and Melinda Gates Foundation (INV-001902 to MI).

ACKNOWLEDGMENTS

We would like to thank the members of the Department of Experimental Genome Research, and NPO for Biotechnology Research and Development for experimental assistance and discussion.

SUPPLEMENTARY MATERIAL

The Supplementary Material for this article can be found online at: https://www.frontiersin.org/articles/10.3389/fcell.2021.810118/full#supplementary-material

REFERENCES

Aguilar, P. S., Baylies, M. K., Fleissner, A., Helming, L., Inoue, N., Podbilewicz, B., et al. (2013). Genetic Basis of Cell-Cell Fusion Mechanisms. *Trends Genet.* 29 (7), 427–437. doi:10.1016/j.tig.2013.01.011

Aoto, T., Takahashi, R.-I., and Ueda, M. (2011). A Protocol for Rat *In Vitro* Fertilization during Conventional Laboratory Working Hours. *Transgenic Res.* 20 (6), 1245–1252. doi:10.1007/s11248-011-9492-z

Aydin, H., Sultana, A., Li, S., Thavalingam, A., and Lee, J. E. (2016). Molecular Architecture of the Human Sperm IZUMO1 and Egg JUNO Fertilization Complex. *Nature* 534 (7608), 562–565. doi:10.1038/nature18595

Bianchi, E., Doe, B., Goulding, D., and Wright, G. J. (2014). Juno Is the Egg Izumo Receptor and Is Essential for Mammalian Fertilization. *Nature* 508 (7497), 483–487. doi:10.1038/nature13203

Bianchi, E., and Wright, G. J. (2015). Cross-species Fertilization: the Hamster Egg Receptor, Juno, Binds the Human Sperm Ligand, Izumo1. *Phil. Trans. R. Soc. B* 370 (1661), 20140101. doi:10.1098/rstb.2014.0101

Bushell, K. M., Söllner, C., Schuster-Boeckler, B., Bateman, A., and Wright, G. J. (2008). Large-scale Screening for Novel Low-Affinity Extracellular Protein Interactions. *Genome Res.* 18 (4), 622–630. doi:10.1101/gr.7187808

Calarco, P. G. (1991). Fertilization of the Mouse Oocyte. *J. Elec. Microsc. Tech.* 17 (4), 401–411. doi:10.1002/jemt.1060170404

Chalbi, M., Barraud-Lange, V., Ravaux, B., Howan, K., Rodriguez, N., Soule, P., et al. (2014). Binding of Sperm Protein Izumo1 and its Egg Receptor Juno Drives Cd9 Accumulation in the Intercellular Contact Area Prior to Fusion during Mammalian Fertilization. *Development* 141 (19), 3732–3739. doi:10.1242/dev.111534

Fujihara, Y., Lu, Y., Noda, T., Oji, A., Larasati, T., Kojima-Kita, K., et al. (2020). Spermatozoa Lacking Fertilization Influencing Membrane Protein (FIMP) Fail to Fuse with Oocytes in Mice. *Proc. Natl. Acad. Sci. USA* 117 (17), 9393–9400. doi:10.1073/pnas.1917060117

Han, L., Nishimura, K., Sadat Al Hosseini, H., Bianchi, E., Wright, G. J., and Jovine, L. (2016). Divergent Evolution of Vitamin B9 Binding Underlies Juno-Mediated Adhesion of Mammalian Gametes. *Curr. Biol.* 26 (3), R100–R101. doi:10.1016/j.cub.2015.12.034

Hasuwa, H., Muro, Y., Ikawa, M., Kato, N., Tsujimoto, Y., and Okabe, M. (2010). Transgenic Mouse Sperm that Have green Acrosome and Red Mitochondria Allow Visualization of Sperm and Their Acrosome Reaction *In Vivo*. *Exp. Anim.* 59 (1), 105–107. doi:10.1538/expanim.59.105

Hernández, J. M., and Podbilewicz, B. (2017). The Hallmarks of Cell-Cell Fusion. *Development* 144 (24), 4481–4495. doi:10.1242/dev.155523

Honda, A., Tachibana, R., Hamada, K., Morita, K., Mizuno, N., Morita, K., et al. (2019). Efficient Derivation of Knock-Out and Knock-In Rats Using Embryos Obtained by *In Vitro* Fertilization. *Sci. Rep.* 9 (1), 11571. doi:10.1038/s41598-019-47964-1

Ikawa, M., Tokuhiro, K., Yamaguchi, R., Benham, A. M., Tamura, T., Wada, I., et al. (2011). Calsperin Is a Testis-specific Chaperone Required for Sperm Fertility. *J. Biol. Chem.* 286 (7), 5639–5646. doi:10.1074/jbc.M110.140152

Inoue, N., Hagihara, Y., and Wada, I. (2021). Evolutionarily Conserved Sperm Factors, DCST1 and DCST2, Are Required for Gamete Fusion. *eLife* 10, e66313. doi:10.7554/eLife.66313

Inoue, N., Hamada, D., Kamikubo, H., Hirata, K., Kataoka, M., Yamamoto, M., et al. (2013). Molecular Dissection of IZUMO1, a Sperm Protein Essential for Sperm-Egg Fusion. *Development* 140 (15), 3221–3229. doi:10.1242/dev.094854

Inoue, N., Ikawa, M., Isotani, A., and Okabe, M. (2005). The Immunoglobulin Superfamily Protein Izumo Is Required for Sperm to Fuse with Eggs. *Nature* 434 (7030), 234–238. doi:10.1038/nature03362

Isotani, A., Matsumura, T., Ogawa, M., Tanaka, T., Yamagata, K., Ikawa, M., et al. (2017). A Delayed Sperm Penetration of Cumulus Layers by Disruption of Acrosin Gene in Rats†. *Biol. Reprod.* 97 (1), 61–68. doi:10.1093/biolre/iox066

Kato, K., Satouh, Y., Nishimasu, H., Kurabayashi, A., Morita, J., Fujihara, Y., et al. (2016). Structural and Functional Insights into IZUMO1 Recognition by JUNO in Mammalian Fertilization. *Nat. Commun.* 7, 12198. doi:10.1038/ncomms12198

Lamas-Toranzo, I., Hamze, J. G., Bianchi, E., Fernández-Fuertes, B., Pérez-Cerezales, S., Laguna-Barraza, R., et al. (2020). TMEM95 Is a Sperm Membrane Protein Essential for Mammalian Fertilization. *Elife* 9, e53913. doi:10.7554/eLife.53913

Liu, D. Y., and Baker, H. W. G. (1994). Acrosome Status and Morphology of Human Spermatozoa Bound to the Zona Pellucida and Oolemma Determined Using Oocytes that Failed to Fertilize *In Vitro*. *Hum. Reprod.* 9 (4), 673–679. doi:10.1093/oxfordjournals.humrep.a138570

Liu, Y., Tewari, R., Ning, J., Blagborough, A. M., Garbom, S., Pei, J., et al. (2008). The Conserved Plant Sterility Gene HAP2 Functions after Attachment of Fusogenic Membranes in Chlamydomonas and Plasmodium Gametes. *Genes Dev.* 22 (8), 1051–1068. doi:10.1101/gad.1656508

Lorenzetti, D., Poirier, C., Zhao, M., Overbeek, P. A., Harrison, W., and Bishop, C. E. (2014). A Transgenic Insertion on Mouse Chromosome 17 Inactivates a Novel Immunoglobulin Superfamily Gene Potentially Involved in Sperm-Egg Fusion. *Mamm. Genome* 25 (3-4), 141–148. doi:10.1007/s00335-013-9491-x

Mashiko, D., Fujihara, Y., Satouh, Y., Miyata, H., Isotani, A., and Ikawa, M. (2013). Generation of Mutant Mice by Pronuclear Injection of Circular Plasmid Expressing Cas9 and Single Guided RNA. *Sci. Rep.* 3, 3355. doi:10.1038/srep03355

Matsumura, T., Endo, T., Isotani, A., Ogawa, M., and Ikawa, M. (2019). An Azoospermic Factor Gene, Ddx3y and its Paralog, Ddx3x Are Dispensable in Germ Cells for Male Fertility. *J. Reprod. Develop.* 65 (2), 121–128. doi:10.1262/jrd.2018-145

Misamore, M. J., Gupta, S., and Snell, W. J. (2003). TheChlamydomonasFus1 Protein Is Present on the Mating TypeplusFusion Organelle and Required for a Critical Membrane Adhesion Event during Fusion withminusGametes. *MBoC* 14 (6), 2530–2542. doi:10.1091/mbc.e02-12-0790

Mizuno, M., Harris, C. L., Johnson, P. M., and Morgan, B. P. (2004). Rat Membrane Cofactor Protein (MCP; CD46) Is Expressed Only in the Acrosome of Developing and Mature Spermatozoa and Mediates Binding to Immobilized Activated C31. *Biol. Reprod.* 71 (4), 1374–1383. doi:10.1095/biolreprod.104.030114

Nakanishi, T., Ikawa, M., Yamada, S., Parvinen, M., Baba, T., Nishimune, Y., et al. (1999). Real-time Observation of Acrosomal Dispersal from Mouse Sperm Using GFP as a Marker Protein. *FEBS Lett.* 449 (2-3), 277–283. doi:10.1016/s0014-5793(99)00433-0

Nishimura, K., Han, L., Bianchi, E., Wright, G. J., de Sanctis, D., and Jovine, L. (2016). The Structure of Sperm Izumo1 Reveals Unexpected Similarities with Plasmodium Invasion Proteins. *Curr. Biol.* 26 (14), R661–R662. doi:10.1016/j.cub.2016.06.028

Noda, T., Blaha, A., Fujihara, Y., Gert, K. R., Emori, C., Deneke, V. E., et al. (2021). Sperm Membrane Proteins DCST1 and DCST2 Are Required for the Sperm-Egg Fusion Process in Mice and Fish. *bioRxiv* 2004, 440256. doi:10.1101/2021.04.18.440256

Noda, T., Lu, Y., Fujihara, Y., Oura, S., Koyano, T., Kobayashi, S., et al. (2020). Sperm Proteins SOF1, TMEM95, and SPACA6 Are Required for Sperm–oocyte Fusion in Mice. *Proc. Natl. Acad. Sci. USA* 117 (21), 11493–11502. doi:10.1073/pnas.1922650117

Nozawa, K., Satouh, Y., Fujimoto, T., Oji, A., and Ikawa, M. (2018). Sperm-borne Phospholipase C Zeta-1 Ensures Monospermic Fertilization in Mice. *Sci. Rep.* 8 (1), 1315. doi:10.1038/s41598-018-19497-6

OECD (2016). *Test No. 421: Reproduction/Developmental Toxicity Screening Test*. Paris: OECD Publishing.

Ohto, U., Ishida, H., Krayukhina, E., Uchiyama, S., Inoue, N., and Shimizu, T. (2016). Structure of IZUMO1-JUNO Reveals Sperm-Oocyte Recognition during Mammalian Fertilization. *Nature* 534 (7608), 566–569. doi:10.1038/nature18596

Okabe, M. (2018). Sperm-egg Interaction and Fertilization: Past, Present, and Future. *Biol. Reprod.* 99 (1), 134–146. doi:10.1093/biolre/ioy028

Okabe, M. (2013). The Cell Biology of Mammalian Fertilization. *Development* 140 (22), 4471–4479. doi:10.1242/dev.090613

Phillips, D. M., and Yanagimachi, R. (1982). Difference in the Manner of Association of Acrosome-Intact and Acrosome-Reacted Hamster Spermatozoa with Egg Microvilli as Revealed by Scanning Electron Microscopy. (Hamster/sperm-egg Association/scanning Electron Microscopy). *Dev. Growth Differ.* 24 (6), 543–551. doi:10.1111/j.1440-169x.1982.00543.x

Russell, L. D., Ettlin, R. A., Hikim, A. P. S., and Clegg, E. D. (1993). Histological and Histopathological Evaluation of the Testis. *Int. J. Androl.* 16 (1), 83. doi:10.1111/j.1365-2605.1993.tb01156.x

Satouh, Y., Inoue, N., Ikawa, M., and Okabe, M. (2012). Visualization of the Moment of Mouse Sperm-Egg Fusion and Dynamic Localization of IZUMO1. *J. Cel Sci* 125 (Pt 21), 4985–4990. doi:10.1242/jcs.100867

Toyoda, Y., Yokoyama, M., and Hosi, T. (1971). Studies on the Fertilization of Mouse Eggs *In Vitro*. *Jpn. J. Anim. Reprod.* 16 (4), 152–157. doi:10.1262/jrd1955.16.152

Yamagata, K., Nakanishi, T., Ikawa, M., Yamaguchi, R., Moss, S. B., and Okabe, M. (2002). Sperm from the Calmegin-Deficient Mouse Have normal Abilities for

Binding and Fusion to the Egg Plasma Membrane. *Develop. Biol.* 250 (2), 348–357. doi:10.1006/dbio.2002.0803

Yamatoya, K., Ito, C., Araki, M., Furuse, R., and Toshimori, K. (2011). One-step Collagenase Method for Zona Pellucida Removal in Unfertilized Eggs: Easy and Gentle Method for Large-Scale Preparation. *Reprod. Med. Biol.* 10 (2), 97–103. doi:10.1007/s12522-011-0075-8

Yanagimachi, R. (1994). "Mammalian Fertilization," in *The Physiology of Reproduction*. Editor E. Knobil (Houston, Texas, United States: Gulf Professional Publishing).

Conflict of Interest: The authors declare that the research was conducted in the absence of any commercial or financial relationships that could be construed as a potential conflict of interest.

Publisher's Note: All claims expressed in this article are solely those of the authors and do not necessarily represent those of their affiliated organizations, or those of the publisher, the editors and the reviewers. Any product that may be evaluated in this article, or claim that may be made by its manufacturer, is not guaranteed or endorsed by the publisher.

frontiers in Cell and Developmental Biology

MINI REVIEW
published: 21 January 2022
doi: 10.3389/fcell.2021.827214

Fertilization of Ascidians: Gamete Interaction, Self/Nonself Recognition and Sperm Penetration of Egg Coat

Takako Saito[1] *and Hitoshi Sawada*[2,3]*

[1]Faculty of Agriculture Department of Applied Life Sciences, Shizuoka University, Shizuoka, Japan, [2]Depatment of Food and Nutritional Environment, College of Human Life and Environment, Kinjo Gakuin University, Nagoya, Japan, [3]Graduate School of Science, Nagoya University, Nagoya, Japan

Fertilization is one of the most important events in living organisms to generate a new life with a mixed genetic background. To achieve successful fertilization, sperm and eggs must undergo complex processes in a sequential order. Fertilization of marine invertebrate *Ciona intestinalis* type *A (Ciona robusta)* has been studied for more than a hundred years. Ascidian sperm are attracted by chemoattractants from eggs and bind to the vitelline coat. Subsequently, sperm penetrate through the vitelline coat proteolytically and finally fuse with the egg plasma membrane. Here, we summarize the fertilization mechanisms of ascidians, particularly from sperm-egg interactions to sperm penetration of the egg coat. Since ascidians are hermaphrodites, inbreeding depression is a serious problem. To avoid self-fertilization, ascidians possess a self-incompatibility system. In this review, we also describe the molecular mechanisms of the self-incompatibility system in *C. intestinalis* type A governed by three allelic gene pairs of *s-Themis* and *v-Themis*.

Keywords: ascidian, sperm, egg, self-sterility, self-incompatibility, lysin, proteasome

OPEN ACCESS

Edited by:
Enrica Bianchi,
University of York, United Kingdom

Reviewed by:
Alessandra Gallo,
Stazione Zoologica Anton Dohrn Napoli, Italy
Shin Matsubara,
Suntory Foundation for Life Sciences, Japan

***Correspondence:**
Hitoshi Sawada
sawada@kinjo-u.ac.jp

Specialty section:
This article was submitted to Molecular and Cellular Reproduction, a section of the journal Frontiers in Cell and Developmental Biology

Received: *01 December 2021*
Accepted: *30 December 2021*
Published: *21 January 2022*

Citation:
Saito T and Sawada H (2022) Fertilization of Ascidians: Gamete Interaction, Self/Nonself Recognition and Sperm Penetration of Egg Coat. Front. Cell Dev. Biol. 9:827214. doi: 10.3389/fcell.2021.827214

INTRODUCTION

Fertilization of marine invertebrates has been extensively studied in classical research. This is not only because a large quantity of gametes can be obtained but also because *in vitro* fertilization experiments are easier in marine invertebrates than in mammals. Studying marine invertebrates led to the discovery of fundamental biological processes, including the fertilization process. The marine invertebrate *Ciona intestinalis* type A [another name: *Ciona robusta* (Brunetti et al., 2015)] is one of the model animals used to study many fields of biology, including reproductive biology (Sawada et al., 2001). The availability of draft genome sequences, transcriptomic and proteomics data and gene knockdown and gene editing techniques has supported the progress of *C. intestinalis* (type A) studies (Satou et al., 2001; Dehal et al., 2002; Shoguchi et al., 2006; Endo et al., 2011; Sasaki et al., 2014; Sasakura et al., 2017; Pickett and Zeller, 2018). Since ascidians are hermaphrodites, self-fertilization can occur. To avoid self-fertilization, many ascidians acquire a self-incompatibility (SI) system. After self/nonself-recognition, only nonself sperm can penetrate through the proteinaceous egg coat called the vitelline coat (VC) or chorion.

Ascidian fertilization consists of five major steps: 1) sperm chemotaxis, 2) sperm binding to the VC, 3) self/nonself-recognition, 4) sperm penetration through the VC, 5) gamete fusion (**Figure 1**), similar to the fertilization processes as previously reviewed (Vacquier and Swanson, 2011; Gallo and Costantini, 2012). In *C. intestinalis* (type A), spermatozoa are attracted toward the eggs by sperm attractant SAAF, a sulfated steroid 3,4,7,26-tetrahydroxycholestane-3,26-disulfate (Yoshida et al., 2002). Transient intracellular Ca^{2+} increase is induced by SAAF gradient (Shiba et al., 2008), which is

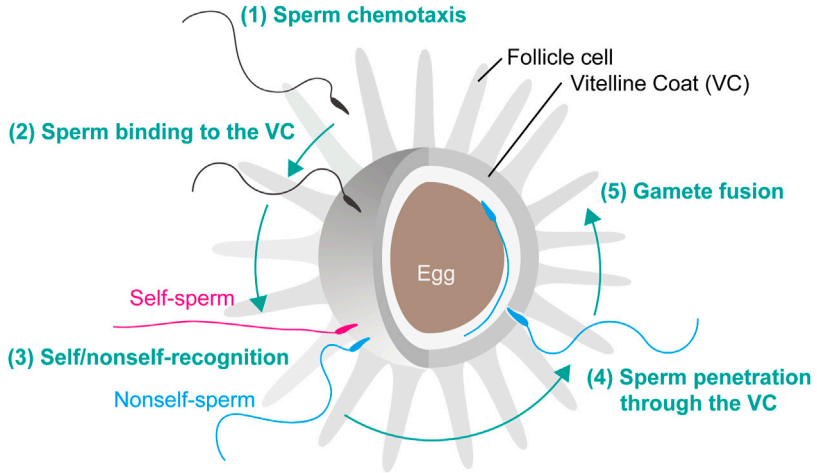

FIGURE 1 | Fertilization steps of *C. intestinalis*. Fertilization is initiated by the following steps. (1) Sperm chemotaxis. (2) Binding of spermatozoa to the VC. (3) Interaction of self/nonself-recognition proteins that induce the signal transduction cascade leading to the SI response. (4) Penetration of nonself-recognized sperm through the VC. (5) Fusion of the egg and sperm plasma membranes resulting in fertilization and subsequent activation of zygote development.

mediated by store-operated calcium channel (Yoshida et al., 2003) and sperm-membrane SAAF-binding protein, Ca-ATPase (Yoshida et al., 2018). After sperm chemotaxis, spermatozoa bind to the VC and undergo "sperm reaction", which is characterized by vigorous movement on the VC and mitochondrial sliding and eventual shedding (Lambert and Epel, 1979; Lambert and Koch, 1988). Most animal spermatozoon besides teleosts has an acrosome at the tip of sperm head and undergoes acrosome reaction, an exocytosis of the acrosomal vesicle, upon sperm binding to the carbohydrate or proteinaceous egg coat. However, the acrosome of ascidian sperm is very tiny and it is still unclear whether the acrosome reaction takes place before (De Santis et al., 1980) or after (Fukumoto, 1988) sperm penetration of the VC. In this minireview, we describe our current understanding and future perspectives on ascidian fertilization, particularly in steps 2) to 4). After sperm penetration of the egg coat, gamete fusion takes place, which is mediated by sperm IZUMO1 and egg JUNO and CD9 in mice (see review: Okabe, 2018). However, the molecular basis of gamete fusion is poorly understood in ascidians. Recently, GCS1/Hap2 is reported to play a pivotal role in gamete fusion in plants and animals (see review: Mori et al., 2015), but the homologous genes and their functions are not known in ascidians or vertebrates.

GAMETE INTERACTION

Sperm-Egg Interaction

After sperm attraction to the egg, gamete interaction takes place between the egg coat and sperm head (**Figure 1**). The egg coat is an extracellular matrix called the zona pellucida (ZP) in mammals and the vitelline envelope (VE) or VC in other animals. Structurally and evolutionally conserved egg coat proteins and ZP domain proteins are the major components of ZP, VE and VC (Aagaard et al., 2006; Goudet et al., 2008; Yamada et al., 2009). In mouse, the highly glycosylated proteins ZP1, ZP2 and ZP3, all of which contain a ZP domain at the C termini, are the building blocks of a filamentous network generated by polymerization of ZP domains (Bork and Sander, 1992; Jovine et al., 2002; Stsiapanava et al., 2020). Current studies have revealed that the N-terminal region of mouse and human ZP2 and the marine mollusk abalone VE receptor for lysin (VERL) crucially regulate gamete interactions (Gahlay et al., 2010; Avella et al., 2014; Raj et al., 2017). Similarly, the VC of ascidian eggs is constructed by ZP domain proteins (Sawada et al., 2002a; Kürn et al., 2007a; Yamada et al., 2009). In *C. intestinalis*, 11 ZP domain proteins have been identified by proteomic analysis of VC, and CiVC57 constitutes the most abundant ZP domain protein in VC. CiVC57 consists of a von Willebrand factor domain, 24 EGF-like repeats, a ZP domain, and a C-terminal transmembrane domain (Yamada et al., 2009). CiUrabin is an abundant protein on the surface of sperm, and in the lipid-raft-membrane fraction, it can bind to CiVC57, suggesting that CiVC57 and CiUrabin play a key role in gamete interaction (Yamaguchi et al., 2011; Nakazawa et al., 2015). CiUrabin belongs to a cysteine-rich secretory protein (CRISP) family containing a pathogenesis-related (PR) domain and a glycosylphosphatidylinositol (GPI)-anchor attachment site (Yamaguchi et al., 2011). Sperm CRISP family proteins participate in several steps in mammalian fertilization (Gonzalez et al., 2021). In particular, the PR domain of CRISP-1 is evolutionarily conserved and involved in sperm-egg binding (Ellerman et al., 2006). In addition, sperm-egg binding in another ascidian *Halocynthia roretzi* is mediated by the CRISP family protein HrUrabin (Urayama et al., 2008). Most likely, the interaction between CiVC57 and CiUrabin participates in the primary binding between sperm and VC in *C. intestinalis* (Yamaguchi et al., 2011; Saito et al., 2012).

It is also worth noting that *C. intestinalis* sperm α-L-fucosidase and L-fucosyl residues of glycoproteins on the VC play a key role

in sperm binding to the VC for the following reasons (Hoshi et al., 1983; Hoshi et al., 1985). Sperm binding to the VC of glycerin-treated (glycerinated) eggs, whose VC sperm can bind to but not penetrate, was inhibited by L-fucose but not by D-fucose (Rosati and De Santis, 1980). In addition, α-L-fucosidase substrates (aryl α-L-fucoside) and competitive inhibitors (aryl β-L-fucoside) but not stereoisomer (aryl α-D-fucoside) blocked sperm binding to VC (Hoshi et al., 1983; Hoshi, 1985; Hoshi, 1986). α-L-fucosidase is located at the tip and the surface of the sperm head, as revealed by immunocytochemistry using several monoclonal antibodies raised against the purified enzyme. Whereas *C. intestinalis* sperm α-L-fucosidase showed an optimum pH for activity of approximately 3.9, it showed 2% or less of maximum activity in normal seawater (Hoshi et al., 1985). Sperm bound to VC in normal seawater detached within 7 min at 20°C but not at 0°C after decreasing the pH near the optimum pH of the enzyme (Hoshi et al., 1985; Hoshi, 1986). These results led to the conclusion that α-L-fucosidase at the tip of the sperm head is responsible for the primary binding of sperm to the fucosyl glycoprotein(s) on the VC in *C. intestinalis* (De Santis et al., 1983).

Self/Nonself-Recognition Molecules

Shortly after sperm binding to the VC, a self/nonself-recognition process takes place on the VC (Morgan, 1939; Rosati and De Santis, 1978; Kawamura et al., 1987; **Figure 1**, **Figure 2A**). Identification of self/nonself-recognition molecules was attempted by several groups, and candidate molecules have been proposed (Kawamura et al., 1991; Pinto et al., 1995; Marino et al., 1998; Kürn et al., 2007a; Kürn et al., 2007b; Harada et al., 2008). Marino et al. proposed that autologous peptide-associating hsp70 on the surface of folliele cells participates in self/nonself-recognition during oogenesis, by analogy to antigenic peptide-presenting MHC (Marino et al., 1998). However, the peptides trapped by hsp70 have not been identified. Kawamura et al. found several factors in the acid-extract involved in allorecogniton, i.e., a non-allorecognizing glucose-enriched inhibitor of the gamete interaction and Glu/Gln-enriched peptide modulators, which function as cofactors in allorecognition of sperm receptors (Kawamura et al., 1991; **Figure 2A**). Khalturin and his colleague identified several genes expressed in oocytes and follicle cells that are highly polymorphic among individuals. They suggested that these highly polymorphic ZP domain proteins and sushi domain-containing protein vCRL1 may be the molecular basis for fertilization and allorecognition in *C. intestinalis* type B (Khalturin et al., 2005; Kürn et al., 2007a; Kürn et al., 2007b). However, their segregation and gene-knockdown analyses of *vCRL1* indicated that vCRL is important for the establishment and maintenance of the blood system, not in self/nonself-recognition (Sommer et al., 2012).

Self-sterility in *C. intestinalis* was first reported by Thomas Hunt Morgan, the founder of modern genetics, more than a hundred years ago (Morgan, 1910). Murabe and Hoshi (2002) and Harada et al. (2008) repeated Morgan's experiments to determine whether crossing between sperm and eggs from selfed F1 siblings resulted in fertile or sterile offspring (Morgan, 1942; 1942), and they confirmed Morgan's observation that one-way cross-sterility occurs between selfed F1 siblings, and this scarcely occurs under natural conditions (Murabe and Hoshi, 2002; Harada et al., 2008). Morgan concluded that the SI system is genetically controlled and hypothesized that this explains one-way cross sterility (Morgan, 1942). Morgan assumed that the "male" SI genes are expressed in haploids, while the "female" SI genes are expressed in diploids. This is called the "haploid sperm hypothesis". Heterozygous individuals (A/a) release A-sperm and a-sperm, either of which can fertilize a homozygous individual's eggs (a/a-eggs or A/A-eggs). On the other hand, homozygous individuals (A/A or a/a) release A-sperm or a-sperm alone, respectively, which cannot fertilize a heterozygous individual's eggs (A/a-eggs), because both the A-sperm receptor and a-sperm receptor reside in the VC. Based on these criteria, Harada et al. carried out fertilization experiments between selfed F1 siblings and searched for a one-way cross-sterile combination. Seventy marker genes on 14 chromosomes were examined by PCR to determine whether they were homozygous or heterozygous (Harada et al., 2008). According to these strategies, two loci (locus A on chromosome 2q and locus B on chromosome 7q) were identified as loci responsible for SI. Among the approximately 20 genes in locus A, only one gene product (fibrinogen-like protein) was identified in the VC by proteome analysis (Yamada et al., 2009), and a polymorphic gene expressed in the testis was identified as a candidate sperm-side SI factor. These gene pairs were designated *v-Themis-A* and *s-Themis-A,* and two similar gene pairs were identified in locus B and named *s/v-Themis-B* and *s/v-Themis-B2* (Harada et al., 2008; Sawada et al., 2020). Taken together, there are three multiallelic pairs of SI candidate genes: egg-side genes (*v-Themis-A*, *v-Themis-B* and *v-Themis-B2*) and sperm-side genes (*s-Themis-A*, *s-Themis-B* and *s-Themis-B2*) (Harada et al., 2008; Yamada et al., 2009; Sawada et al., 2020). Interestingly, these are highly polymorphic genes and are tightly linked: *v-Themis* genes are encoded in the first intron of *s-Themis* genes in the opposite direction (Harada et al., 2008; Sawada et al., 2020). The sperm-side SI genes *s-Themis-A*, *B*, and *B2* show homology to mammalian *PKD1* or *PKDREJ*, which both contain a hypervariable region (HVR), receptor for egg jelly (REJ), G protein-coupled receptor proteolysis site (GPS), lipoxygenase homology 2 (LH2) domain, and 5 (in case of *s-Themis-A*) or 11 (in case of s-*Themis-B* and *s-Themis-B2*) pass transmembrane (TM) domain. Notably, *s-Themis-B* and *s-Themis-B2* possess a cation channel [polycystic kidney disease (PKD) channel] domain in their C-terminal regions (Harada et al., 2008; Sawada et al., 2020). When three allelic gene pairs were matched (in the case of the same haplotypes), even nonself-fertilization was strongly blocked (Sawada et al., 2020). In addition, by gene editing experiments, *s/v-Themis-A* genes and *s/v-Themis-B/B2* genes were found to be indispensable for self-sterility (Sawada et al., 2020). After sperm recognize the VC as self, drastic and acute Ca^{2+} influx occurs in spermatozoa,

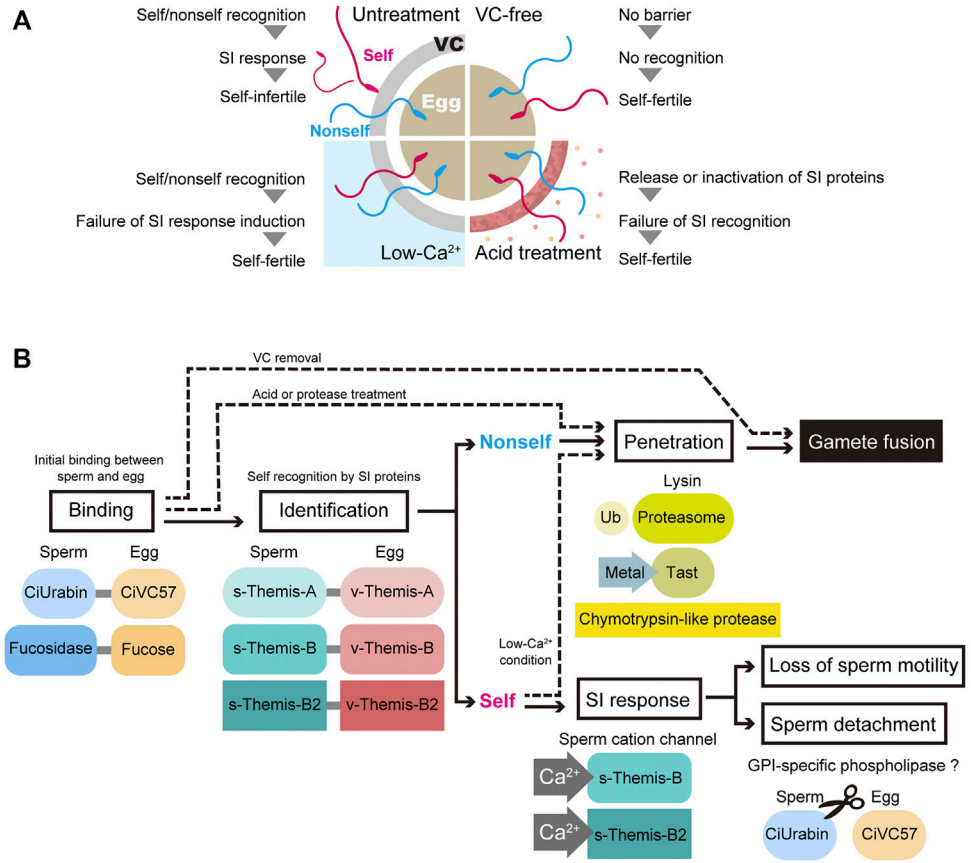

FIGURE 2 | Current status of fertilization and self-incompatibility system. **(A)** Schematic representation of artificial self/nonself-fertilization in *C. intestinalis*. There are several ways to achieve artificial self-fertilization. Removing the VC and treating the VC with acidic seawater or proteases relieves the self-fertilization block. In addition, the inhibition of Ca^{2+} influx in spermatozoa, which is controlled by the external Ca^{2+} concentration, is sufficient to block the self-fertilization signal. **(B)** Gamete proteins involved in each step of fertilization are illustrated. Ub, ubiquitin; Tast, tunicate astacin-like metalloprotease with thrombospondin-type-1 repeat.

referred to as the SI response (Saito et al., 2012). This dramatic SI response causes sperm detachment from the VC and loss of sperm motility, because intracellular Ca^{2+} concentration regulates sperm behavior and flagellar beating. Although the SI response abolishes the fertility of self-recognized sperm, low-Ca^{2+} seawater enables self-fertilization (Hashimoto et al., submitted; **Figures 2A,B**). These results indicate that the increase in intracellular Ca^{2+} concentration triggers the SI response in spermatozoa.

Since the SI system is abolished by acid treatment of the VC, putative SI proteins might be released (Kawamura et al., 1991). Therefore, acid extracts of the VC were investigated by LC/MS, and Ci-v-Themis-like protein was identified as a new SI candidate protein (Otsuka et al., 2013). As the name indicates, Ci-v-Themis-like protein has a fibrinogen-like domain, similar to v-Themis-A, -B and -B2. However, Ci-v-Themis-like protein is not polymorphic among individuals. Although this protein is unlikely to participate in the SI system, it is probably involved in gamete binding or the assembly of v-Themis proteins on the VC (Otsuka et al., 2013).

Taken together, spermatozoa are equally attracted to self and nonself eggs and are capable of binding to the VC before recognizing the eggs as self or nonself. The interaction between sperm fucosidase and the VC fucose moiety must be maintained even after recognition as nonself, since nonself sperm binding to the VC is inhibited by fucose and fucose glycosides (Hoshi et al., 1983; Hoshi et al., 1985). Sperm fucosidase-fucose interactions may be involved in the interaction between s-Themis and v-Themis. On the other hand, the CiUrabin-CiVC57 interaction may be broken after sperm recognize the VC as self, since most self-sperm detach from the VC (Kawamura et al., 1987; Saito et al., 2012). In this process, GPI-specific phospholipase might be activated after sperm recognize the VC as self. Shortly after sperm binding to the VC, gametes undergo a judgment of self- or nonself-gametes using three allelic protein pairs of s-Themis and v-Themis, and only self-recognized sperm are rejected because self-recognition triggers the SI response (**Figure 2B**). s/v-Themis homologous genes were also identified in self-sterile species, such as *H. roretzi* and *C. savignyi*. However, participation of these proteins in SI is not known, since crossing experiments and genetic analysis have not been done. Since human sperm PKDREJ shows significant polymorphism (Hamm et al., 2007), it is an intriguing issue to clarify whether these variations are related to fertilization efficiency.

SPERM VITELLINE-COAT LYSINS

Sperm utilize the lytic agent "lysin", which enables sperm to penetrate through the proteinaceous egg coat (**Figure 1**). In ascidians, nonself-sperm lysin must be activated after self/nonself-recognition on the VC, which allows sperm to penetrate the VC. Generally, deuterostome spermatozoa appear to utilize enzymatic lysins, since protease inhibitors can inhibit fertilization, particularly sperm penetration of the ZP, VE or VC. In mammals, sperm acrosin, an acrosomal trypsin-like protease, is thought to be a zona-lysin (Hoshi, 1985). However, acrosin was found to be a nonessential gene for sperm penetration of the ZP and fertilization in mouse, as revealed by studies of *acrosin* knockout (KO) mice (Baba et al., 1994). In fact, acrosomal protease(s) other than acrosin are responsible for the sperm penetration process in mice (Yamagata et al., 1998). On the other hand, it was recently reported that *acrosin* is essential for hamster fertilization, more precisely sperm penetration of the ZP, by studying an *acrosin*-KO hamster model (Hirose et al., 2020). Therefore, whether acrosin is a zona-lysin depends on the species.

Hoshi et al. explored sperm proteases functioning as lysins using *Halocynthia roretzi*. Trypsin inhibitor (leupeptin) and chymotrypsin inhibitor (chymostatin) blocked the fertilization of intact eggs but not of VC-free eggs. Therefore, sperm trypsin-like and chymotrypsin-like proteases appear to participate in the sperm penetration of the VC, most likely as lysins (Hoshi et al., 1981). Sawada and his colleagues purified two trypsin-like proteases, ascidian acrosin and spermosin, from *H. roretzi* sperm extract (Sawada et al., 1984a). The involvement of both enzymes in fertilization was confirmed by comparing the abilities of various leupeptin analogs in inhibition of fertilization with their purified enzymatic activities (Sawada et al., 1984b). However, these enzymes showed no appreciable VC-degrading activity. Then, chymotrypsin-like protease was purified using Suc-Leu-Leu-Val-Tyr-MCA, the strongest inhibitor of fertilization among the chymotrypsin substrates tested, and the purified enzyme was identified as the proteasome (Sawada et al., 2002a). The purified proteasome from sperm can degrade the main component of the VC, HrVC70, after ubiquitination. Furthermore, anti-proteasome and anti-multiubiquitin antibodies and proteasome inhibitors inhibited fertilization. Lys-234 of HrVC70 appears to be ubiquitinated during fertilization, followed by degradation by the proteasome secreted upon sperm activation (sperm reaction) (Saitoh et al., 1993; Sawada et al., 2002a; Sakai et al., 2003). These results indicate that the sperm ubiquitin–proteasome system plays a pivotal role in fertilization, functioning as a VC lysin (Sawada et al., 2002b; Sawada, 2002). Notably, spermatozoa of mammals (Sutovsky et al., 2004), quail (Sasanami et al., 2012) and sea urchins (Yokota and Sawada, 2007) also utilize the sperm proteasome as egg-coat lysin.

In *C. intestinalis*, the effects of leupeptin and chymostatin on fertilization were examined (Hoshi, 1985). In this species, fertilization was inhibited by chymostatin but not by leupeptin, suggesting that *C. intestinalis* (Phlebobranch) and *H. roretzi* (Stolidobranch) utilize a different lysin system. A 24-kDa chymotrypsin-like protease was purified from *C. intestinalis* sperm, and the purified enzyme affected the outer layer of the VC, as revealed by electron microscopy (Marino et al., 1992). Analogous to *H. roretzi*, the participation of the sperm proteasome in fertilization was investigated in *C. intestinalis*. The proteasome inhibitors MG115 and MG132 inhibited the fertilization of intact eggs but not VC-free eggs (Sawada et al., 1998). In addition, these inhibitors showed no appreciable inhibition of sperm binding to the VC of glycerinated eggs. These results suggest that the proteasome plays a key role in sperm penetration through the VC but not in sperm binding to the VC (**Figure 2B**). Further studies are needed to clarify the target VC protein(s) of these proteases.

To investigate whether these proteases are exposed to the plasma membrane of the sperm head, proteomic analysis of sperm surface proteins from *C. intestinalis* was performed (Nakazawa et al., 2015). Unexpectedly, chymotrypsin-like protease or proteasome subunits were not identified under the conditions tested. Instead, several metalloproteases, which are referred to as "Tast (tunicate astacin-like metalloprotease with thrombospondin type 1 repeat)", were identified as the major proteases (Nakazawa et al., 2019). The involvement of metalloproteases in fertilization was tested by the metalloprotease inhibitor GM6001. GM6001 strongly inhibited the fertilization of intact eggs but not VC-free eggs, and GM6001 did not inhibit sperm binding to the VC of glycerinated eggs. Furthermore, when isolated VC was incubated with intact sperm, several VC proteins, including CiVC57, were degraded and inhibited by GM6001. Therefore, Tasts are promising candidates for VC lysin, although we cannot exclude the possibility that the 24-kDa chymotrypsin-like protease and the proteasome are also involved in sperm penetration of the VC. Generally, metalloproteases, such as matrix metalloproteases, or the proteasome are very powerful tools to degrade insoluble proteins. It is interesting to note that several egg coat-targeting proteases, such as mouse egg ovastacin (Burkart et al., 2012) and medaka hatching enzymes (Yasumasu et al., 1992), belong to astacin-like metalloproteases. Further detailed studies on the molecular mechanisms of degradation of VC proteins by sperm proteases functioning as lysins remain to be elucidated.

CONCLUDING REMARKS

We summarized the current working hypothesis of the mechanisms of fertilization in *C. intestinalis,* particularly from the sperm binding to the VC to the sperm penetration through the VC (**Figure 2B**). Shortly after sperm binding to the VC, which is mediated by interactions between CiUrabin and CiVC57, self/nonself-recognition molecules may be recruited to the binding site. When three allelic pairs (haplotypes), i.e., s/v-Themis-A, s/v-Themis-B, and s/v-Themis-B2, are matched (self-recognition), drastic Ca^{2+} influx occurs in spermatozoa, and the self-recognized sperm detaches from the VC or quits moving on the VC. Recognizing autologous proteins rather than an enormous number of allogeneic proteins is much easier and more reasonable. Genome editing experiments clearly demonstrated that s/v-Themis-A and s/v-Themis-B/B2 are indispensable for self/nonself-recognition. In addition,

s-Themis-B and -B2 were more crucial than s-Themis-A in the SI system (Sawada et al., 2020). This is not at variance with the fact that both s-Themis-B and s-Themis-B2 contain a cation channel at their C-termini that is probably involved in Ca^{2+} influx. Similar to the SI system in Papaveraceae, Ca^{2+} influx in spermatozoa may induce sperm cell apoptosis. Further studies are necessary to demonstrate the protein–protein interaction between s-Themis and v-Themis. Intracellular signal transduction after the SI response is also an intriguing issue to be investigated. In the lysin system, we revealed the importance of a novel astacin-like metalloprotease (Tast) in sperm passage of the VC. Elucidating the physiological substrates of sperm Tasts and proteasomes are also important issues that remain to be clarified.

AUTHOR CONTRIBUTIONS

TS and HS summarized the current investigation of fertilization in ascidian *C. intestinalis*. TS and HS wrote the manuscript, which was edited by HS.

FUNDING

This work was supported by JSPS KAKENHI Grant Number JP17K15128 (to TS) and JP17H03672, JP20K06621 (to HS), as well as by a research grant from the Fujiwara Natural History Foundation (to TS).

REFERENCES

Aagaard, J. E., Yi, X., Maccoss, M. J., and Swanson, W. J. (2006). Rapidly Evolving Zona Pellucida Domain Proteins Are a Major Component of the Vitelline Envelope of Abalone Eggs. *Proc. Natl. Acad. Sci.* 103, 17302–17307. doi:10.1073/pnas.0603125103

Avella, M. A., Baibakov, B., and Dean, J. (2014). A Single Domain of the ZP2 Zona Pellucida Protein Mediates Gamete Recognition in Mice and Humans. *J. Cell Biol* 205, 801–809. doi:10.1083/jcb.201404025

Baba, T., Azuma, S., Kashiwabara, S., and Toyoda, Y. (1994). Sperm from Mice Carrying a Targeted Mutation of the Acrosin Gene Can Penetrate the Oocyte Zona Pellucida and Effect Fertilization. *J. Biol. Chem.* 269, 31845–31849. doi:10.1016/s0021-9258(18)31772-1

Bork, P., and Sander, C. (1992). A Large Domain Common to Sperm Receptors (Zp2 and Zp3) and TGF-β Type III Receptor. *FEBS Lett.* 300, 237–240. doi:10.1016/0014-5793(92)80853-9

Brunetti, R., Gissi, C., Pennati, R., Caicci, F., Gasparini, F., and Manni, L. (2015). Morphological Evidence that the Molecularly Determined *Ciona intestinalis* Type A and Type B Are Different Species: *Ciona Robusta* and *Ciona intestinalis*. *J. Zoolog. Syst. Evol. Res.* 53, 186–193. doi:10.1111/jzs.12101

Burkart, A. D., Xiong, B., Baibakov, B., Jiménez-Movilla, M., and Dean, J. (2012). Ovastacin, a Cortical Granule Protease, Cleaves ZP2 in the Zona Pellucida to Prevent Polyspermy. *J. Cell Biol* 197, 37–44. doi:10.1083/jcb.201112094

De Santis, R., Jamunno, G., and Rosati, F. (1980). A Study of the Chorion and the Follicle Cells in Relation to the Sperm-Egg Interaction in the Ascidian, *Ciona intestinalis*. *Dev. Biol.* 74, 490–499. doi:10.1016/0012-1606(80)90449-2

De Santis, R., Pinto, M. R., Cotelli, F., Rosati, F., Monroy, A., and D'alessio, G. (1983). A Fucosyl Glycoprotein Component with Sperm Receptor and Sperm-Activating Activities from the Vitelline Coat of *Ciona intestinalis* Eggs. *Exp. Cell Res.* 148, 508–513. doi:10.1016/0014-4827(83)90172-6

Dehal, P., Satou, Y., Campbell, R. K., Chapman, J., Degnan, B., De Tomaso, A., et al. (2002). The Draft Genome of *Ciona intestinalis* : Insights into Chordate and Vertebrate Origins. *Science* 298, 2157–2167. doi:10.1126/science.1080049

Ellerman, D. A., Cohen, D. J., Da Ros, V. G., Morgenfeld, M. M., Busso, D., and Cuasnicú, P. S. (2006). Sperm Protein "DE" Mediates Gamete Fusion through an Evolutionarily Conserved Site of the CRISP Family. *Dev. Biol.* 297, 228–237. doi:10.1016/j.ydbio.2006.05.013

Endo, T., Ueno, K., Yonezawa, K., Mineta, K., Hotta, K., Satou, Y., et al. (2011). CIPRO 2.5: *Ciona intestinalis* Protein Database, a Unique Integrated Repository of Large-Scale Omics Data, Bioinformatic Analyses and Curated Annotation, with User Rating and Reviewing Functionality. *Nucleic Acids Res.* 39, D807–D814. doi:10.1093/nar/gkq1144

Fukumoto, M. (1988). Fertilization in Ascidians: Apical Processes and Gamete Fusion in *Ciona intestinalis* Spermatozoa. *J. Cell Sci.* 89, 189–196. doi:10.1242/jcs.89.2.189

Gahlay, G., Gauthier, L., Baibakov, B., Epifano, O., and Dean, J. (2010). Gamete Recognition in Mice Depends on the Cleavage Status of an Egg's Zona Pellucida Protein. *Science* 329, 216–219. doi:10.1126/science.1188178

Gallo, A., and Costantini, M. (2012). Glycobiology of Reproductive Processes in Marine Animals: the State of the Art. *Mar. Drugs* 10, 2861–2892. doi:10.3390/md10122861

Gonzalez, S. N., Sulzyk, V., Weigel Muñoz, M., and Cuasnicu, P. S. (2021). Cysteine-Rich Secretory Proteins (CRISP) Are Key Players in Mammalian Fertilization and Fertility. *Front. Cell Dev. Biol.* 9. doi:10.3389/fcell.2021.800351

Goudet, G., Mugnier, S., Callebaut, I., and Monget, P. (2008). Phylogenetic Analysis and Identification of Pseudogenes Reveal a Progressive Loss of Zona Pellucida Genes during Evolution of Vertebrates. *Biol. Reprod.* 78, 796–806. doi:10.1095/biolreprod.107.064568

Hamm, D., Mautz, B. S., Wolfner, M. F., Aquadro, C. F., and Swanson, W. J. (2007). Evidence of Amino Acid Diversity-Enhancing Selection within Humans and Among Primates at the Candidate Sperm-Receptor Gene PKDREJ. *Am. J. Hum. Genet.* 81, 44–52. doi:10.1086/518695

Harada, Y., Takagaki, Y., Sunagawa, M., Saito, T., Yamada, L., Taniguchi, H., et al. (2008). Mechanism of Self-Sterility in a Hermaphroditic Chordate. *Science* 320, 548–550. doi:10.1126/science.1152488

Hirose, M., Honda, A., Fulka, H., Tamura-Nakano, M., Matoba, S., Tomishima, T., et al. (2020). Acrosin Is Essential for Sperm Penetration through the Zona Pellucida in Hamsters. *Proc. Natl. Acad. Sci. USA* 117, 2513–2518. doi:10.1073/pnas.1917595117

Hoshi, M., De Santis, R., Pinto, M. R., Cotelli, F., and Rosati, F. (1985). Sperm Glycosidases as Mediators of Sperm-Egg Bindig in the Ascidians. *Zoolog. Sci.* 2, 65–69.

Hoshi, M., De Santis, R., Pinto, M. R., Cotelli, F., and Rosata, F. (1983). Is Sperm α-L-Fucosidase Responsible for Sperm-Egg Binding in Ciona Intestinalis. *The Sperm Cell.*, Editor J. André (The Hauge: Martinus Nijhoff Publishers), 107–110. doi:10.1007/978-94-009-7675-7_20

Hoshi, M. (1985). "Lysins," in *Biology of Fertilization*. Editors C. B. Metz and A. Monroy (New York: Academic Press), 431–462. doi:10.1016/b978-0-12-492602-8.50020-6

Hoshi, M., Numakunai, T., and Sawada, H. (1981). Evidence for Participation of Sperm Proteinases in Fertilization of the Solitary Ascidian, *Halocynthia Roretzi*: Effects of Protease Inhibitors. *Dev. Biol.* 86, 117–121. doi:10.1016/0012-1606(81)90322-5

Hoshi, M. (1986). Sperm Glycosidase as a Plausible Mediator of Sperm Binding to the Vitelline Envelope in Ascidians. *Adv. Exp. Med. Biol.* 207, 251–260. doi:10.1007/978-1-4613-2255-9_15

Jovine, L., Qi, H., Williams, Z., Litscher, E., and Wassarman, P. M. (2002). The ZP Domain Is a Conserved Module for Polymerization of Extracellular Proteins. *Nat. Cell Biol* 4, 457–461. doi:10.1038/ncb802

Kawamura, K., Fujita, H., and Nakauchi, M. (1987). Cytological Characterization of Self Incompatibility in Gametes of the Ascidian, *Ciona intestinalis*. *Dev. Growth Differ.* 29, 627–642. doi:10.1111/j.1440-169X.1987.00627.x

Kawamura, K., Nomura, M., Kameda, T., Shimamoto, H., and Nakauchi, M. (1991). Self-Nonself Recognition Activity Extracted from Self-Sterile Eggs of the Ascidian, *Ciona intestinalis*. *Dev. Growth Differ.* 33, 139–148. doi:10.1111/j.1440-169X.1991.00139.x

Khalturin, K., Kurn, U., Pinnow, N., and Bosch, T. C. (2005). Towards a Molecular Code for Individuality in the Absence of MHC: Screening for Individually Variable Genes in the Urochordate. *Dev. Comp. Immunol.* 29, 759–773. doi:10.1016/j.dci.2005.01.006

Kürn, U., Sommer, F., Bosch, T. C. G., and Khalturin, K. (2007a). In the Urochordate *Ciona intestinalis* Zona Pellucida Domain Proteins Vary Among Individuals. *Dev. Comp. Immunol.* 31, 1242–1254. doi:10.1016/j.dci.2007.03.011

Kürn, U., Sommer, F., Hemmrich, G., Bosch, T. C. G., and Khalturin, K. (2007b). Allorecognition in Urochordates: Identification of a Highly Variable Complement Receptor-like Protein Expressed in Follicle Cells of Ciona. *Dev. Comp. Immunol.* 31, 360–371. doi:10.1016/j.dci.2006.06.008

Lambert, C. C., and Epel, D. (1979). Calcium-mediated Mitochondrial Movement in Ascidian Sperm during Fertilization. *Dev. Biol.* 69, 296–304. doi:10.1016/0012-1606(79)90293-8

Lambert, C. C., and Koch, R. A. (1988). Sperm Binding and Penetration during Ascidian Fertilization. *Dev. Growth Differ.* 30, 325–336. doi:10.1111/j.1440-169x.1988.00325.x

Marino, R., De Santis, R., Hirohashi, N., Hoshi, M., Pinto, M. R., and Usui, N. (1992). Purification and Characterization of a Vitelline Coat Lysin from *Ciona Intestinalis* Spermatozoa. *Mol. Reprod. Dev.* 32, 383–388. doi:10.1002/mrd.1080320412

Marino, R., Pinto, M. R., Cotelli, F., Lamia, C. L., and De Santis, R. (1998). The Hsp70 Protein Is Involved in the Acquisition of Gamete Self-Sterility in the Ascidian *Ciona intestinalis*. *Development* 125, 899–907. doi:10.1242/dev.125.5.899

Morgan, T. H. (1910). Cross- and Self-Fertilization in Ciona Intestinalis. *Archiv für Entwicklungsmechanik der Organismen* 30, 206–235. doi:10.1007/BF02263809

Morgan, T. H. (1939). The Genetic and the Physiological Problems of Self-Sterility in Ciona. III. Induced Self-Fertilization. *J. Exp. Zool.* 80, 19–54. doi:10.1002/jez.1400800103

Morgan, T. H. (1942). The Genetic and the Physiological Problems of Self-Sterility in Ciona. VI. Theoretical Discussion of Genetic Data. *J. Exp. Zool.* 95, 37–59. doi:10.1002/jez.1400950105

Morgan, T. H. (1942). The Genetic and the Physiological Problems of Self-Sterility in Ciona. V. The Genetic Problem. *J. Exp. Zool.* 90, 199–228. doi:10.1002/jez.1400900205

Mori, T., Kawai-Toyooka, H., Igawa, T., and Nozaki, H. (2015). Gamete Dialogs in Green Lineages. *Mol. Plant* 8, 1442–1454. doi:10.1016/j.molp.2015.06.008

Murabe, N., and Hoshi, M. (2002). Re-examination of Sibling Cross-Sterility in the Ascidian, *Ciona intestinalis*: Genetic Background of the Self-Sterility. *Zoolog. Sci.* 19, 527–538. doi:10.2108/zsj.19.527

Nakazawa, S., Shirae-Kurabayashi, M., Otsuka, K., and Sawada, H. (2015). Proteomics of Ionomycin-Induced Ascidian Sperm Reaction: Released and Exposed Sperm Proteins in the Ascidian *Ciona intestinalis*. *Proteomics* 15, 4064–4079. doi:10.1002/pmic.201500162

Nakazawa, S., Shirae-Kurabayashi, M., and Sawada, H. (2019). The Role of Metalloproteases in Fertilisation in the Ascidian Ciona Robusta. *Sci. Rep.* 9, 1009. doi:10.1038/s41598-018-37721-1

Okabe, M. (2018). Sperm-egg Interaction and Fertilization: Past, Present, and Future. *Biol. Reprod.* 99, 134–146. doi:10.1093/biolre/ioy028

Otsuka, K., Yamada, L., and Sawada, H. (2013). cDNA Cloning, Localization, and Candidate Binding Partners of Acid-Extractable Vitelline-Coat Protein Ci-v-themis-like in the Ascidian *Ciona intestinalis*. *Mol. Reprod. Dev.* 80, 840–848. doi:10.1002/mrd.22213

Pickett, C. J., and Zeller, R. W. (2018). Efficient Genome Editing Using CRISPR-Cas-Mediated Homology Directed Repair in the Ascidian *Ciona Robusta*. *Genesis* 56, e23260. doi:10.1002/dvg.23260

Pinto, M. R., De Santis, R., and Usui, N. (1995). Specific Induction of Self-Discrimination by Follicle Cells in *Ciona intestinalis* Oocytes. *Dev. Growth Differ.* 37, 287–291. doi:10.1046/j.1440-169X.1995.t01-2-00006.x

Raj, I., Sadat Al Hosseini, H., Dioguardi, E., Nishimura, K., Han, L., Villa, A., et al. (2017). Structural Basis of Egg Coat-Sperm Recognition at Fertilization. *Cell* 169, 1315–1326. doi:10.1016/j.cell.2017.05.033

Rosati, F., and De Santis, R. (1978). Studies on Fertilization in the Ascidans. *Exp. Cell Res.* 112, 111–119. doi:10.1016/0014-4827(78)90531-1

Rosati, F., and Santis, R. D. (1980). Role of the Surface Carbohydrates in Sperm-Egg Interaction in *Ciona intestinalis*. *Nature* 283, 762–764. doi:10.1038/283762a0

Saito, T., Shiba, K., Inaba, K., Yamada, L., and Sawada, H. (2012). Self-incompatibility Response Induced by Calcium Increase in Sperm of the Ascidian *Ciona intestinalis*. *Proc. Natl. Acad. Sci.* 109, 4158–4162. doi:10.1073/pnas.1115086109

Saitoh, Y., Sawada, H., and Yokosawa, H. (1993). High-molecular-weight Protease Complexes (Proteasomes) of Sperm of the Ascidian, *Halocynthia Roretzi*: Isolation, Characterization, and Physiological Roles in Fertilization. *Dev. Biol.* 158, 238–244. doi:10.1006/dbio.1993.1182

Sakai, N., Sawada, H., and Yokosawa, H. (2003). Extracellular Ubiquitin System Implicated in Fertilization of the Ascidian, Halocynthia Roretzi: Isolation and Characterization. *Dev. Biol.* 264, 299–307. doi:10.1016/j.ydbio.2003.07.016

Sasaki, H., Yoshida, K., Hozumi, A., and Sasakura, Y. (2014). CRISPR/Cas9-mediated Gene Knockout in the Ascidian *Ciona Intestinalis*. *Dev. Growth Differ.* 56, 499–510. doi:10.1111/dgd.12149

Sasakura, Y., Yoshida, K., and Treen, N. (2017). Genome Editing of the Ascidian *Ciona intestinalis* with TALE Nuclease. *Methods Mol. Biol.* 1630, 235–245. doi:10.1007/978-1-4939-7128-2_19

Sasanami, T., Sugiura, K., Tokumoto, T., Yoshizaki, N., Dohra, H., Nishio, S., et al. (2012). Sperm Proteasome Degrades Egg Envelope Glycoprotein ZP1 during Fertilization of Japanese Quail (*Coturnix japonica*). *Reproduction* 144, 423–431. doi:10.1530/rep-12-0165

Satou, Y., Imai, K. S., and Satoh, N. (2001). Action of Morpholinos in Ciona Embryos. *Genesis* 30, 103–106. doi:10.1002/gene.1040

Sawada, H. (2002). Ascidian Sperm Lysin System. *Zoolog. Sci.* 19, 139–151. doi:10.2108/zsj.19.139

Sawada, H., Pinto, M. R., and De Santis, R. (1998). Participation of Sperm Proteasome in Fertilization of the Phlebobranch ascidian *Ciona Intestinalis*. *Mol. Reprod. Dev.* 50, 493–498. doi:10.1002/(sici)1098-2795(199808)50:4<493:aid-mrd13>3.0.co;2-3

Sawada, H., Sakai, N., Abe, Y., Tanaka, E., Takahashi, Y., Fujino, J., et al. (2002a). Extracellular Ubiquitination and Proteasome-Mediated Degradation of the Ascidian Sperm Receptor. *Proc. Natl. Acad. Sci.* 99, 1223–1228. doi:10.1073/pnas.032389499

Sawada, H., Takahashi, Y., Fujino, J., Flores, S. Y., and Yokosawa, H. (2002b). Localization and Roles in Fertilization of Sperm Proteasomes in the ascidianHalocynthia Roretzi. *Mol. Reprod. Dev.* 62, 271–276. doi:10.1002/mrd.10089

Sawada, H., Yamamoto, K., Yamaguchi, A., Yamada, L., Higuchi, A., Nukaya, H., et al. (2020). Three Multi-Allelic Gene Pairs Are Responsible for Self-Sterility in the Ascidian *Ciona intestinalis*. *Sci. Rep.* 10, 2514. doi:10.1038/s41598-020-59147-4

Sawada, H., Yokosawa, H., and Ishii, S. (1984a). Purification and Characterization of Two Types of Trypsin-like Enzymes from Sperm of the Ascidian (Prochordata) Halocynthia Roretzi. Evidence for the Presence of Spermosin, a Novel Acrosin-like Enzyme. *J. Biol. Chem.* 259, 2900–2904. doi:10.1016/S0021-9258(17)43233-9

Sawada, H., Yokosawa, H., and Lambert, C. C. (2001). *The Biology of Ascidians*. Tokyo: Springer. doi:10.1007/978-4-431-66982-1

Sawada, H., Yokosawa, H., Someno, T., Saino, T., and Ishii, S. (1984b). Evidence for the Participation of Two Sperm Proteases, Spermosin and Acrosin, in Fertilization of the Ascidian, *Halocynthia Roretzi*: Inhibitory Effects of Leupeptin Analogs on Enzyme Activities and Fertilization. *Dev. Biol.* 105, 246–249. doi:10.1016/0012-1606(84)90281-1

Shiba, K., Baba, S. A., Inoue, T., and Yoshida, M. (2008). Ca^{2+} Bursts Occur Around a Local Minimal Concentration of Attractant and Trigger Sperm Chemotactic Response. *Proc. Natl. Acad. Sci.* 105, 19312–19317. doi:10.1073/pnas.0808580105

Shoguchi, E., Kawashima, T., Satou, Y., Hamaguchi, M., Sin-I, T., Kohara, Y., et al. (2006). Chromosomal Mapping of 170 BAC Clones in the Ascidian *Ciona intestinalis*. *Genome Res.* 16, 297–303. doi:10.1101/gr.4156606

Sommer, F., Awazu, S., Anton-Erxleben, F., Jiang, D., Klimovich, A. V., Klimovich, B. V., et al. (2012). Blood System Formation in the Urochordate *Ciona intestinalis* Requires the Variable Receptor vCRL1. *Mol. Biol. Evol.* 29, 3081–3093. doi:10.1093/molbev/mss120

Stsiapanava, A., Xu, C., Brunati, M., Zamora-Caballero, S., Schaeffer, C., Bokhove, M., et al. (2020). Cryo-EM Structure of Native Human Uromodulin, a Zona Pellucida Module Polymer. *EMBO J.* 39, e106807. doi:10.15252/embj.2020106807

Sutovsky, P., Manandhar, G., Mccauley, T. C., Caamaño, J. N., Sutovsky, M., Thompson, W. E., et al. (2004). Proteasomal Interference Prevents Zona Pellucida Penetration and Fertilization in Mammals. *Biol. Reprod.* 71, 1625–1637. doi:10.1095/biolreprod.104.032532

Urayama, S., Harada, Y., Nakagawa, Y., Ban, S., Akasaka, M., Kawasaki, N., et al. (2008). Ascidian Sperm Glycosylphosphatidylinositol-Anchored CRISP-like Protein as a Binding Partner for an Allorecognizable Sperm Receptor on the Vitelline Coat. *J. Biol. Chem.* 283, 21725–21733. doi:10.1074/jbc.M802631200

Vacquier, V. D., and Swanson, W. J. (2011). Selection in the Rapid Evolution of Gamete Recognition Proteins in Marine Invertebrates. *Cold Spring Harbor Perspect. Biol.* 3, a002931. doi:10.1101/cshperspect.a002931

Yamada, L., Saito, T., Taniguchi, H., Sawada, H., and Harada, Y. (2009). Comprehensive Egg Coat Proteome of the Ascidian *Ciona intestinalis* Reveals Gamete Recognition Molecules Involved in Self-Sterility. *J. Biol. Chem.* 284, 9402–9410. doi:10.1074/jbc.M809672200

Yamagata, K., Murayama, K., Kohno, N., Kashiwabara, S.-i., and Baba, T. (1998). p-Aminobenzamidine-sensitive Acrosomal Protease(s) Other Than Acrosin Serve the Sperm Penetration of the Egg Zona Pellucida in Mouse. *Zygote* 6, 311–319. doi:10.1017/S0967199498000264

Yamaguchi, A., Saito, T., Yamada, L., Taniguchi, H., Harada, Y., and Sawada, H. (2011). Identification and Localization of the Sperm CRISP Family Protein CiUrabin Involved in Gamete Interaction in the Ascidian *Ciona intestinalis*. *Mol. Reprod. Dev.* 78, 488–497. doi:10.1002/mrd.21329

Yasumasu, S., Yamada, K., Akasaka, K., Mitsunaga, K., Iuchi, I., Shimada, H., et al. (1992). Isolation of cDNAs for LCE and HCE, Two Constituent Proteases of the Hatching Enzyme of *Oryzias latipes*, and Concurrent Expression of Their mRNAs during Development. *Dev. Biol.* 153, 250–258. doi:10.1016/0012-1606(92)90110-3

Yokota, N., and Sawada, H. (2007). Sperm Proteasomes are Responsible for the Acrosome Reaction and Sperm Penetration of the Vitelline Envelope During Fertilization of the Sea Urchin Pseudocentrotus Depressus.. *Dev. Biol.* 308, 222–231. doi:10.1016/j.ydbio.2007.05.025

Yoshida, K., Shiba, K., Sakamoto, A., Ikenaga, J., Matsunaga, S., Inaba, K., et al. (2018). Ca^{2+} Efflux via Plasma Membrane Ca2+-ATPase Mediates Chemotaxis in Ascidian Sperm. *Sci. Rep.* 8, 16622. doi:10.1038/s41598-018-35013-2

Yoshida, M., Ishikawa, M., Izumi, H., De Santis, R., and Morisawa, M. (2003). Store-operated Calcium Channel Regulates the Chemotactic Behavior of Ascidian Sperm. *Proc. Natl. Acad. Sci.* 100, 149–154. doi:10.1073/pnas.0135565100

Yoshida, M., Murata, M., Inaba, K., and Morisawa, M. (2002). A Chemoattractant for Ascidian Spermatozoa Is a Sulfated Steroid. *Proc. Natl. Acad. Sci.* 99, 14831–14836. doi:10.1073/pnas.242470599

Conflict of Interest: The authors declare that the research was conducted in the absence of any commercial or financial relationships that could be construed as a potential conflict of interest.

Publisher's Note: All claims expressed in this article are solely those of the authors and do not necessarily represent those of their affiliated organizations, or those of the publisher, the editors and the reviewers. Any product that may be evaluated in this article, or claim that may be made by its manufacturer, is not guaranteed or endorsed by the publisher.

frontiers in Cell and Developmental Biology

REVIEW
published: 27 January 2022
doi: 10.3389/fcell.2022.827454

The Importance of Gene Duplication and Domain Repeat Expansion for the Function and Evolution of Fertilization Proteins

Alberto M. Rivera and Willie J. Swanson*

Department of Genome Sciences, University of Washington, Seattle, WA, United States

The process of gene duplication followed by gene loss or evolution of new functions has been studied extensively, yet the role gene duplication plays in the function and evolution of fertilization proteins is underappreciated. Gene duplication is observed in many fertilization protein families including Izumo, DCST, ZP, and the TFP superfamily. Molecules mediating fertilization are part of larger gene families expressed in a variety of tissues, but gene duplication followed by structural modifications has often facilitated their cooption into a fertilization function. Repeat expansions of functional domains within a gene also provide opportunities for the evolution of novel fertilization protein. ZP proteins with domain repeat expansions are linked to species-specificity in fertilization and TFP proteins that experienced domain duplications were coopted into a novel sperm function. This review outlines the importance of gene duplications and repeat domain expansions in the evolution of fertilization proteins.

Keywords: gene duplication, fertilization, subfunctionalization, neofunctionalization, sperm, egg, reproduction

OPEN ACCESS

Edited by:
Enrica Bianchi,
University of York, United Kingdom

Reviewed by:
Shunsuke Nishio,
Karolinska Institutet (KI), Sweden
Esther Betran,
University of Texas at Arlington, United States

****Correspondence:***
Alberto M. Rivera
albertomarcosrivera@gmail.com
amrivera@uw.edu

Specialty section:
This article was submitted to Molecular and Cellular Reproduction, a section of the journal Frontiers in Cell and Developmental Biology

Received: *02 December 2021*
Accepted: *12 January 2022*
Published: *27 January 2022*

Citation:
Rivera AM and Swanson WJ (2022) The Importance of Gene Duplication and Domain Repeat Expansion for the Function and Evolution of Fertilization Proteins. Front. Cell Dev. Biol. 10:827454. doi: 10.3389/fcell.2022.827454

INTRODUCTION

The fertilization of oocytes by sperm is an essential function in sexual reproduction, and multiple stages of the fertilization cascade have been described (Vacquier, 1998). First the sperm is drawn to the egg through chemotaxis (Ramírez-Gómez et al., 2019), and it then binds to the egg and releases proteins stored in the acrosome. The sperm then passes through the glycoproteinaceous egg coat (Monne et al., 2008; Wilburn and Swanson, 2016) (named Zona Pellucida in mammals), and proceeds to the oocyte cell membrane to initiate fusion (Siu et al., 2021). Understanding fertilization requires knowledge of both these broad steps of the fertilization cascade and the molecular mechanism underlying them. Research into the evolution and function of gametic proteins has implications for the development of novel contraception or treatments for unexplained human infertility (Gelbaya et al., 2014).

Many fertilization proteins are members of gene families that result from whole gene duplication events, which is a common mechanism for gene birth (Hughes, 1994). There has been extensive research into the relationship between gene duplication and other aspects of reproductive biology, including the neuroendocrine control of reproduction (Dufour et al., 2020), protease activity in the female reproductive tract (Kelleher et al., 2007; Kelleher and Markow, 2009), the resolution of sexual conflict (Gallach et al., 2010, 2011; Connallon and Clark, 2011; Gallach and Betrán, 2011), and hybridization barriers (Ting et al., 2004). This review specifically focuses on our growing knowledge of duplicated protein families implicated in fertilization. These proteins include the Izumo1 and Juno

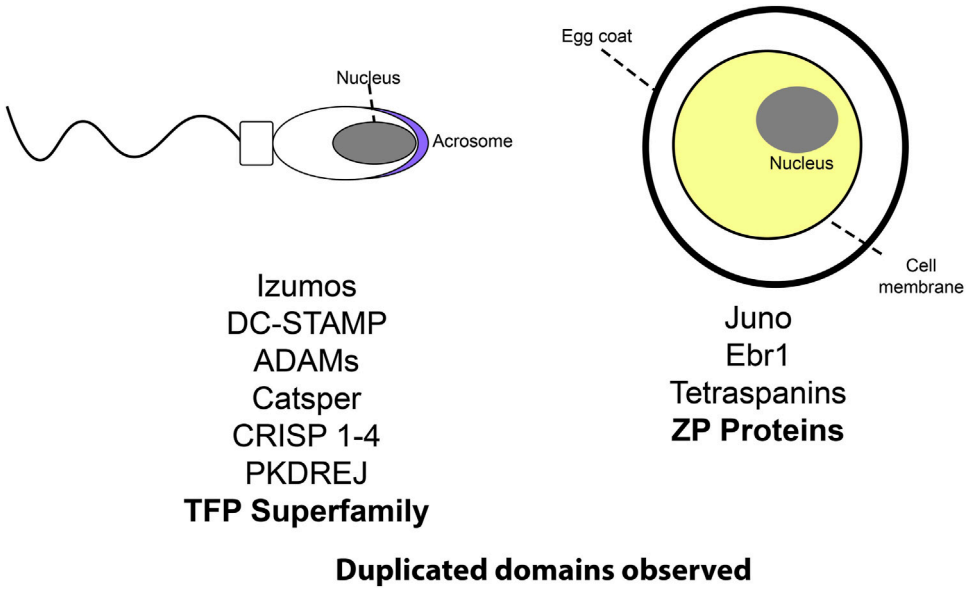

FIGURE 1 | A cartoon schematic listing several protein families involved in reproduction. Those with notable repeat expansions are bolded.

pair of interacting proteins, which each arose from independent gene duplication events and are essential to gamete membrane fusion function in mammals (Bianchi et al., 2014). DCST1 and DCST2 are paralogous proteins expressed in the sperm membrane of some bilateral animals, that are essential for fertilization (Inoue et al., 2021a, 1). Other duplicated proteins that act in fertilization include ADAMs (Primakoff and Myles, 2000; Civetta, 2003; Finn and Civetta, 2010), CRISPs (Busso et al., 2007; Da Ros et al., 2008; Gibbs et al., 2011; Maldera et al., 2014), Catspers (Clapham and Garbers, 2005; Navarro et al., 2008; Speer et al., 2021), and PKDREJ on the male side (Sutton et al., 2008), and tetraspanins (CD9,CD81) (Le Naour et al., 2000, 9; Miyado et al., 2000; Frolikova et al., 2018) and EBR1 on the female side (Kamei and Glabe, 2003; Hart, 2013). Genomic resources suggests that most of these families (ADAMs, tetraspanins, EBR, PKRDEJ, Catsper) have orthologs in other bilateral animals, while CRISP has orthologs in animals and in yeast (Howe et al., 2021).

Duplicated genes can experience further structural diversification, such as the duplication of individual functional protein domains. Proteins containing tandemly duplicated domains constitute a small, but significant portion of the genome (Han et al., 2007; Nacher et al., 2010). Independent tandem duplications of individual functional domains is also a recurrent trend in some protein families (TFP,ZP) (Galindo et al., 2002; Aagaard et al., 2010; Doty et al., 2016). There are several families of reproductive proteins on both the sperm and egg that show a history of being coopted from non-reproductive functions (**Figure 1**). Three finger proteins (TFPs) have been frequently coopted for fertilization including SPACA4 in tetrapods, Bouncer in fish, and multiple classes of sperm proteins in plethodontid salamanders (PMF, SPFs) (Doty et al., 2016; Fujihara et al., 2021). Salamander SPFs have a duplicated three finger protein domain, and have evolved structural modifications to those domains (Doty et al., 2016). Similarly, the family of ZP proteins (named after the Zona Pellucida), essential components of egg coats across vertebrates and invertebrates (Wilburn and Swanson, 2016), show evidence of independent expansions of ZP-N domains in different lineages (Liang and Dean, 1993; Galindo et al., 2002). These highlight the role of gene duplication and repeat domain expansions in fertilization. An observed trend is rapid sequence evolution in reproductive proteins (Swanson and Vacquier, 2002), and newly duplicated domains can provide novel substrates for evolving new functions at multiple stages of the fertilization cascade.

The role of duplications in genome evolution is well documented across the tree of life. (Kondrashov et al., 2002; Conant and Wolfe, 2008). Gene duplication (Ponting, 2008) is an important source for new genetic material that facilitates biological innovation. The duplication and differentiation of genomic regions has been linked to the evolution of modularity in organisms (Wagner et al., 2007). Modularity is an abstract concept in which part of an organism (such as a network of protein interactions) functions largely autonomously relative to other aspects of the organisms' biology (Wagner and Altenberg, 1996; West-Eberhard, 2005). Duplicated genes can participate in existing modular protein interaction networks, which facilitates increasing biological complexity of these networks (Wagner et al., 2007). Such increases in modular network complexity through gene duplication has been linked to adaptations in humans (Perry et al., 2007). Duplicated functional domains can similarly contribute to the evolution of biological complexity. This review will discuss both whole gene duplications and within gene domain duplications, and their role in the evolution of reproductive functions.

When genes duplicate they experience one of three possible fates: pseudogenization, subfunctionalization, and neofunctionalization

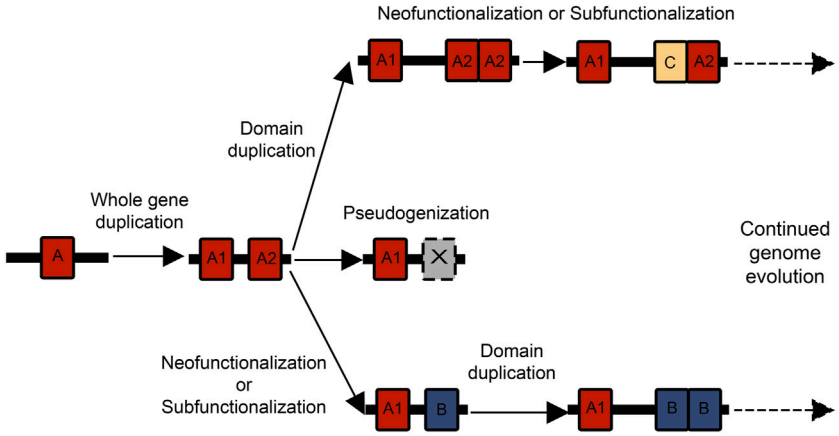

FIGURE 2 | There are multiple possible combinations of whole gene and domain duplications that can birth new genes and functional domains. Often a whole gene duplication begins the process, and then one of the gene duplicates experiences a domain expansion. These genes can then act as substrates for further duplication and neofunctionalization or subfunctionalization events.

(Walsh, 2003; Innan, 2009). Due to redundancies in function, the duplicated gene may no longer experience conservation and accumulate silencing mutations, resulting in a non-coding "pseudogene" (**Figure 2**). New mutations are frequently deleterious, so pseudogenization is hypothesized to be the most common fate of duplicated genes (Lynch and Conery, 2000). However, the other two fates of duplicated genes (subfunctionalization and neofunctionalization) are common mechanisms for biological innovation. Under neofunctionalization, one gene copy maintains its original function while the other experiences positive selection and evolves a novel function. While under subfunctionalization, both copies parse the original function, and neither gene is sufficient (Walsh, 2003; Innan, 2009).

Tandem duplications of individual protein domains within a gene can add greater complexity to the duplication process. Paralogous genes experiencing relaxed selection can have greater freedom for tandem domain duplications. There is strong research interest in the mechanisms underlying domain repeat expansions and how they affect the evolution of protein families (Björklund et al., 2005, 2006; Vogel et al., 2005; Weiner et al., 2006; Moore et al., 2008; Buljan and Bateman, 2009). Repeats can experience concerted evolution where they maintain a high degree of sequence identity (Elder and Turner, 1995; Liao, 1999), through unequal recombination and gene conversion (Schimenti, 1999). Under this scenario, the repeat expansion of highly identical domains is itself an innovation that could allow proteins to evolve novel functions. A repeat domain expansion could also affect dosage or protein interaction networks. Repeated domains could similarly differentiate in amino acid sequence, leading to neofunctionalization or subfunctionalization with the original domain. There are many possible orders and combinations of whole gene duplications and domain duplications that can contribute to the expansion of gene families (**Figure 2**). The process by which duplicate genes are maintained and experience subfunctionalization or neofunctionalization has been characterized under the duplication-degeneration-complementation model (DDC) (Force et al., 1999). While most classical population genetics models (Walsh, 2003; Innan, 2009) primarily discuss the effect of silencing or beneficial mutations on coding regions, the DDC model focuses on the effect of mutations on regulatory regions and subfunctionalization. Essentially, mutations that can silence certain regulatory regions in a duplicate gene can lead to the two genes partitioning expression and eventually function (Force et al., 1999). Other models have suggested subfunctionalization is primarily important as a transition phase to neofunctionalization (Rastogi and Liberles, 2005). The mechanisms of subfunctionalization and neofunctionalization remain a subject of rich debate, and concepts like the DDC model could have ramifications for protein evolution.

Subfunctionalization and neofunctionalization are foundational to the evolution of increased complexity in genomes and protein networks, and it is worth examining their particular importance in fertilization. Fertilization proteins are some of the most rapidly evolving proteins in genomes, as evidenced by high amino divergence (Swanson and Vacquier, 2002). Their rapid evolution is likely driven by factors such as sexual conflict and molecular arms race dynamics between gametes, which can also contribute to the maintenance of fertilization barriers between species (Gavrilets and Waxman, 2002; Gavrilets, 2014). The general trend of rapid evolution in reproductive proteins could facilitate the subfunctionalization or neofunctionalization of domains.

IZUMO/JUNO

The fusion of sperm and egg is necessary for fertilization, but there are only a few known pairs of interacting gametic proteins identified at this stage (Wilburn and Swanson, 2016). After years of research the interacting pair Izumo1 and Juno were identified in mammals (Bianchi et al., 2014). Izumo1 is the sperm expressed protein that mediates fusion (Inoue et al., 2005), and it interacts with the egg surface bound folate receptor 4 (known as Juno) (Bianchi and Wright, 2014). Izumo1 and Juno are each part of

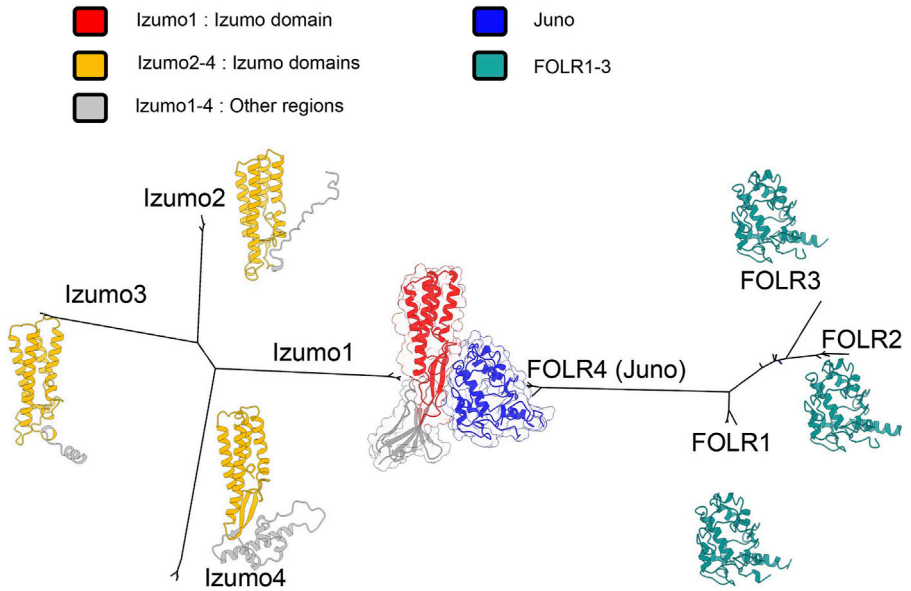

FIGURE 3 | Unrooted maximum likelihood phylogenies for *Izumo* and *FOLR* gene families in a subset of primates, based on multiple sequence alignments (Katoh and Standley, 2013; Kozlov et al., 2019). Both gene families independently duplicated, but *FOLR4* was coopted to bind *Izumo1*. Crystal structures have been obtained for the Izumo1-Juno complex (Aydin et al., 2016). For other proteins, alphafold predicted structures were used (Jumper et al., 2021). Using predictions of signal peptides and transmembrane domains, and secondary structural alignments, we identified shared izumo domains (Sonnhammer et al., 1998; Krogh et al., 2001; Almagro Armenteros et al., 2019).

protein families with multiple paralogues, but only the Izumo1/Juno pair is capable of interacting (Bianchi et al., 2014). There are four members of both the Izumo (Ellerman et al., 2009) and folate receptor families (FOLR) in mammals (Elwood, 1989; Shen et al., 1994; Spiegelstein et al., 2000; Petronella and Drouin, 2014). Despite being part of the folate receptor family, Juno does not actually bind folate, exemplifying how a single member of this gene family has been coopted for a novel reproductive function (Bianchi et al., 2014).

While Juno represents a clear cooption into fertilization, the evolution of the Izumo gene family could also present an interesting example of neofunctionalization. Izumo1-4 all have a highly structurally conserved Izumo domain, but Izumo1 and Izumo4 have a shared pair of β-strands extending from this domain. Izumo1 experienced further structural modifications, as its β-strand extensions act as a hinge between the Izumo domain and a coopted immunoglobulin-like domain (Aydin et al., 2016; Ohto et al., 2016). Such substantial structural changes could be important for the protein's ability to bind Juno. Research into other Izumo proteins suggests their involvement in fertilization. Izumo1-3 are transmembrane testis expressed proteins (Ellerman et al., 2009), while Izumo4 lacks a transmembrane domain and is expressed in the acrosome (Guasti et al., 2020). Izumo3 shows evidence of positive selection (Grayson and Civetta, 2012), and is necessary for sperm acrosome formation (Inoue et al., 2021b). The parallel histories of structural modifications in Izumo1 and Juno allowed for this essential interaction to evolve.

The relationship between Izumo1, Juno and their paralogs is highlighted by our phylogeny (**Figure 3**), which contains a long branch leading to Juno (FOLR4). This could reflect the rapid accumulation of mutations in the Juno branch as it was coopted to bind Izumo1 during gametic membrane fusion. Crystal structures confirm that 1:1 binding complexes form between Izumo1 and Juno (Aydin et al., 2016; Ohto et al., 2016). The adhesion of Izumo1 and Juno is conserved in mammals, and after the adhesion event Juno is released from the egg's surface in vesicles and may act to bind and neutralize acrosome reacted sperm (Bianchi et al., 2014). In mammals, this interaction functions as a block against polyspermy (Bianchi and Wright, 2014). Blocks to polyspermy are essential, because eggs that fuse with multiple sperm are not viable and mammalian blocks to polyspermy exist at both the cell membrane (Evans, 2020) and egg coat (Fahrenkamp et al., 2020).

Mutations to residues conserved in mammals greatly reduce binding, highlighting that particular changes to amino acid sequence and protein structure facilitated the neofunctionalization of Juno (Aydin et al., 2016). The more variable structural features (Ohto et al., 2016) in Juno may be important for the species-specificity of its binding to Izumo1 (Bianchi et al., 2014; Bianchi and Wright, 2015; Han et al., 2016). Comparative genetic analyses identify positive selection in a subset of mammals (Laurasiatheria) (Grayson and Civetta, 2012), and that Juno is likely rapidly coevolving with Izumo1, which contributes to the specificity of their interactions (Grayson, 2015). This specific binding is essential to both Juno's function in initiating membrane fusion, and the post-fusion neutralization of acrosome-reacted sperm (Wright and Bianchi, 2016).

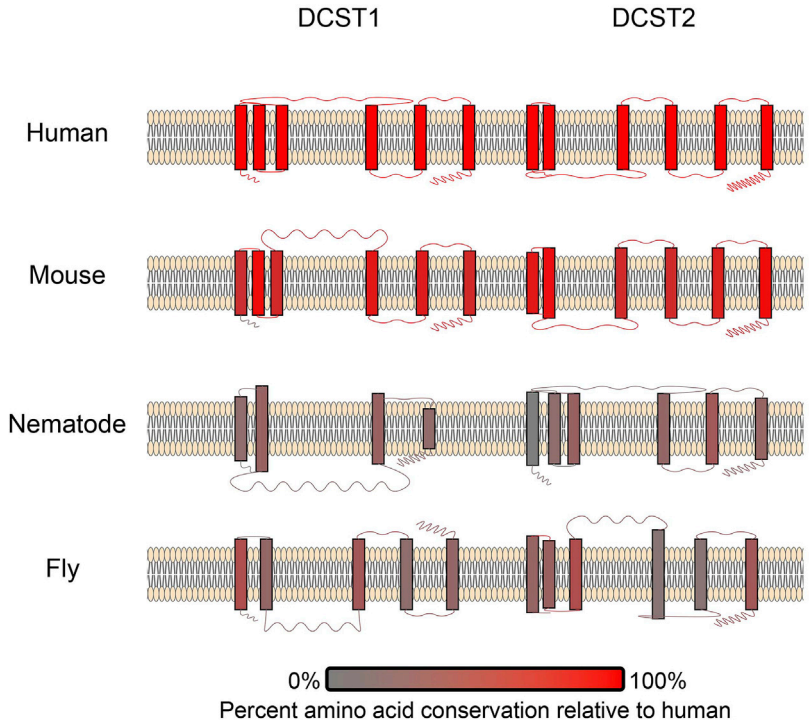

FIGURE 4 | A schematic of DCST1/2 proteins in multiple species. The number of transmembrane domains and loop lengths differ across species. Transmembrane domains and loops are colored based on conservation (Pei et al., 2008), where red coloration signifies amino acid conservation relative to humans. Therefore, the human examples are all red.

DCST

While Izumo1 and Juno are thought to initiate the complex molecular process of gametic membrane fusion in mammals, recent transgenic experiments and complementation studies have demonstrated that DCST1 and DCST2 are also essential (Inoue et al., 2021a). The DCST1/2 proteins are expressed on the sperm surface, and contain variable (4–6) transmembrane helical domains (DC-STAMP) (Inoue et al., 2021a, 1). DC-STAMP (dendritic cell specific transmembrane protein) refers to both the name of the domain and one of the proteins that contains this domain (Hartgers et al., 2000). The originally identified DC-STAMP protein has four transmembrane domains (Hartgers et al., 2001), and it is highly expressed in myeloid dendrocytes (Hartgers et al., 2000, 2001; Eleveld-Trancikova et al., 2005, 2008). The expression of DC-STAMP has been induced in macrophages (Staege et al., 2001) and osteoclasts (Nomiyama et al., 2005). This broad array of functions has motivated much research into the molecular mechanisms of DC-STAMP interactions, which has supported a role in osteoclast fusion (Kukita et al., 2004; Yagi et al., 2005; Jansen et al., 2009). There is also evidence of DC-STAMP related signaling in immune response (Nair et al., 2016). Along with these other diverse functions, it seem that DC-STAMP domains have been coopted into an essential role in sperm-egg membrane fusion.

DCST1/2 are the first known essential fertilization factors that are conserved in both vertebrates and invertebrates (Inoue et al., 2021a). DCST1/2 orthologues have been identified in both *Caenorhabditis* and *Drosophila* (Kroft et al., 2005; Wilson et al., 2006, 2018), which is the first known example sperm related factors being conserved this broadly across vertebrates and invertebrates (Inoue et al., 2021a, 1). However, there has been extensive structural diversification of these DCST1/2 across animals (**Figure 4**), especially between invertebrates and vertebrates. The low sequence identity of DCST1/2 proteins across animals, makes the conservation of reproductive function all the more remarkable. The ubiquitin ligase activity of DCST1 (Nair et al., 2016) raises questions about the function of DCST1/2 in sperm. There is intense research interest into the signal activity of long non-coding RNA produced by DCST1 and its effect on cancer cell progression (Hu et al., 2020; Ai et al., 2021, 1; Wang et al., 2021). More investigation is necessary to understand the function of DC-STAMP domains in a broad range of signaling networks, and how they were neofunctionalized in sperm DCST1/2.

ZP DOMAINS

ZP proteins are an essential class of egg coat proteins. An important feature of ZP proteins is the ZP module that

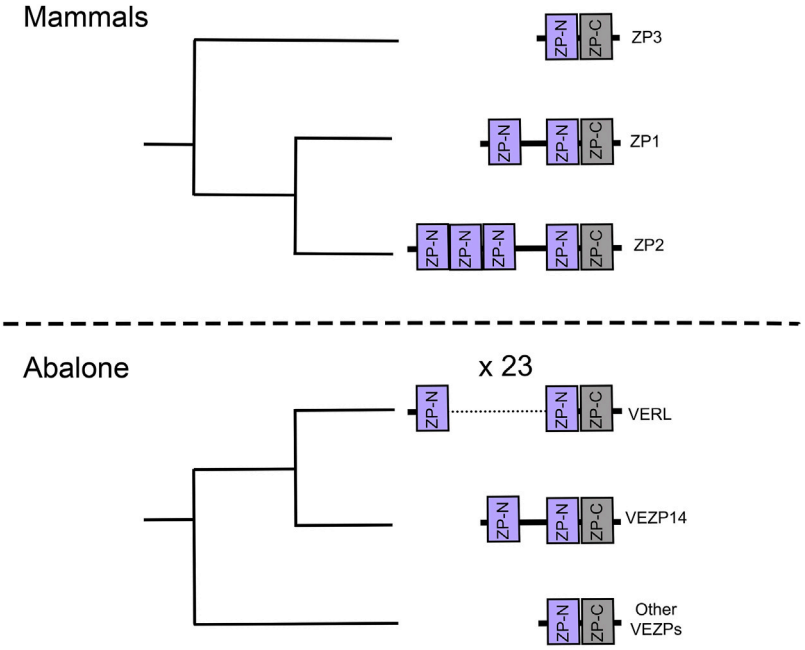

FIGURE 5 | Cladograms of ZP-N proteins are based on phylogenies from the literature (Aagaard et al., 2010; Claw and Swanson, 2012). These suggest independent repeat expansion of the ZP-N domain in both abalone and human egg coat genes.

consists of two domains, ZP-N and ZP-C, named after their relative N-terminal and C-terminal positioning. ZP-N and ZP-C domain are immunoglobular domains with characteristic patterns of disulfide bonding and β-sheets (Bokhove and Jovine, 2018), and likely resulted from an ancestral domain duplication. The variability in amino acid sequence, disulfide placement, and loop structures between ZP-N and ZP-C (Lin et al., 2011) suggests differences in their biological function and evolutionary history.

ZP-N domains are of particular interest, because they form asymmetric dimers with their β-sandwich edges which are believed to promote polymerization between ZP modules (Jovine et al., 2002; Wilburn and Swanson, 2017; Bokhove and Jovine, 2018). There are several ZP proteins identified in vertebrates (ZP1-4, ZPAX and ZPD), and there appears to be a history of lineage specific gain and loss of ZP proteins among vertebrates (Galindo et al., 2002; Conner et al., 2005; Goudet et al., 2008; Claw and Swanson, 2012; Meslin et al., 2012; Shu et al., 2015; Killingbeck and Swanson, 2018). Like other families discussed in this review, there also multiple ZP proteins with non-reproductive functions (e.g., uromodulin and tectorin-alpha) (Legan et al., 1997; Brunati et al., 2015; Bokhove et al., 2016). This may be another example of domains being coopted into a reproductive function, and ZP-N polymerization domains may be important for egg coat assembly and structure.

Not only has gene duplication produced an assortment of ZP proteins, there are also examples of independent repeat expansions of ZP-N in both vertebrates and invertebrate egg coat proteins (**Figure 5**). Some have only one additional ZP-N domain, but there are more dramatic repeat expansion like mammalian ZP2 (4 ZP-Ns) and abalone VERL (23 ZP-Ns) (Galindo et al., 2002). This process of domain duplications helped contribute to the diversity of ZP proteins. Given the ability of ZP-N domains to dimerize (Jovine et al., 2002; Bokhove and Jovine, 2018; Litscher and Wassarman, 2020), their duplications could create opportunities to evolve novel binding functions. Proteins with duplicated ZP-N domains, such as mammalian ZP2 and abalone VERL, are thought to be essential for species-specific in fertilization (Avella et al., 2013, 2014; Raj et al., 2017). Species-specificity in abalone is associated with the coevolution between VERL and the sperm protein lysin (Galindo et al., 2003; Clark et al., 2009), suggesting a cooption of ZP-Ns in sperm-egg interactions during egg coat dissolution.

Neofunctionalization of ZP-N domains can also drive new interactions between ZP proteins, such as the evolution of essential intermolecular crosslinks (Nishimura et al., 2019), which affect the physical assemblage of proteins in the supramolecular structure of the egg coat. Indeed, mouse research has suggested the importance of egg coat supramolecular structure in fertilization (Rankin et al., 2003; Avella et al., 2013). The structure of the egg coat is also important for the oocyte's ability to block polyspermy. Protein cleavage of ZP2 is thought to initiate other egg coat structural modifications, which "harden" the egg coat and prevent sperm binding (Bleil et al., 1981; Gahlay et al., 2010; Fahrenkamp et al., 2020). Gene and domain duplications has produced a family of ZP proteins that contribute to the egg coat supramolecular structure, and are involved in both sperm recognition and polyspermy avoidance.

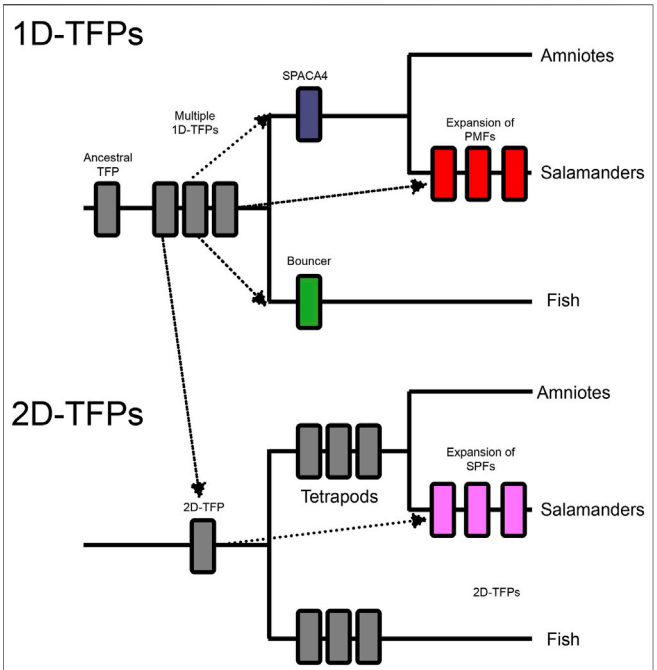

FIGURE 6 | These two cladograms outline the whole gene and domain duplications within the three finger protein superfamilty (TFPs) and their expansions into reproductive systems. An ancestral single domain TFP (1D-TFP), duplicated into multiple vertebrate 1D-TFPs, and also had a domain level duplication which created a lineage of two TFP domain proteins (2D-TFPs). The 1D-TFPs produced tetrapod SPACA4, fish Bouncer, and multiple salamander PMFs. The 2D-TFPs also duplicated throughout vertebrates including salamander SPFs. Both salamander PMF and SPF protein families include both sperm and pheromone expressed members (Wilburn et al., 2022).

TFP SUPERFAMILY

Three finger proteins are defined by their TFP domains, which have a characteristic disulfide bonding pattern and fold (Galat, 2008; Galat et al., 2008). The broader TFP protein superfamily also includes proteins with structurally modified TFP-like domains (Galat, 2015). While TFPs were originally identified in snake toxins (Low et al., 1976; Tsernoglou and Petsko, 1977), members of the TFP superfamily have been to coopted for reproductive functions into sperm (SPACA4, PMFs, and SPFs), egg (Bouncer), and pheromones (PMFs, and SPFs) (Doty et al., 2016; Fujihara et al., 2021; Wilburn et al., 2022) (**Figure 6**). Bouncer plays a role in species-specific sperm-egg fusion in teleost fish (Herberg et al., 2018), which raises questions about how other TFPs may function in fertilization. The TFP superfamily includes both soluble and membrane bound proteins, and has great functional diversity across many tissues and taxa (Alape-Girón et al., 1999; Tsetlin, 1999; Kini, 2002; Nirthanan et al., 2003; Kessler et al., 2017). Similar to ZP proteins, we observe a history of gene duplication, repeat expansion of domains, and functional diversification of TFP containing proteins.

An ancestral TFP protein experienced gene duplication to produce an assortment of single TFP-like domain proteins (1D-TFPs). One of these TFP genes experienced a tandem domain expansion to produce the ancestor of proteins with two TFP-like domains (2D-TFPs). Three independent cooption events have produced TFPs in gametes (**Figure 6**). A cooption of 1D-TFPs occurred in the ancestor of tetrapods and produced both Bouncer in fish, and SPACA4 in amniotes (**Figure 6**). Despite their protein homology, Bouncer is egg expressed while SPACA4 is sperm expressed and it is implicated in interactions between the sperm and egg coat (Fujihara et al., 2021), highlighting the functional diversification of TFPs. Another independent cooption of 1D-TFPs resulted in the sperm expressed plethodontid modulating factor (PMFs) salamanders, which extensively duplicated producing a diverse family of reproductive molecules (Wilburn et al., 2012, 2014, 2017; Doty et al., 2016). Salamander PMFs are hypervariable proteins expressed in multiple tissues, and while they are structurally similar to other TFPs, they differ in loop length and disulfide bridge patterning, and show evidence of persistent diversification and positive selection (Palmer et al., 2010; Wilburn et al., 2012, 2014).

Among 2D-TFPs there was independent cooption into the sodefrin precursor-like factors (SPFs) of salamander sperm. SPFs then experienced their own history of gene duplications and radiation (Palmer et al., 2007). Both PMFs and SPFs experienced disulfide bond reshuffling relative to the canonical 1D-TFP and 2D-TFP binding patterns, and these changes reflect the neofunctionalization of these molecules (Doty et al., 2016). These striking examples of independent gene duplications and neofunctionalization for reproductive functions raises questions as to whether there a more additional unknown cooptions of TFPs, and whether some protein domains are more susceptible to cooption in diverse biological contexts.

Both PMFs and SPFs are highly duplicated protein families, with some members being coopted into pheromone function and others for sperm expression (Doty et al., 2016; Wilburn et al., 2022). As the sperm paralogs of PMFs and SPFs have only recently been discovered, functional studies have not yet been conducted. Male salamanders produce large number of PMFS and SPFs within their mental glands which promote ritual courtship behavior in females (Doty et al., 2016). Duplications of secreted male-expressed sperm proteins could have provided an evolutionary substrate to evolve new pheromones (Wilburn et al., 2022). Structural changes in PMFs and SPFs, such as disulfide shuffling, may contribute to new functions in both sperm and pheromones. The TFP's superfamily's history of gene duplication, domain duplication, and neofunctionalization provides a unique model for the evolution of large gene families involved in fertilization.

DISCUSSION AND CONCLUSION

Within this review we discussed examples of duplicated gene families with roles in fertilization. Gene duplication and neofunctionalization is an essential process for the evolution of greater genomic and functional complexity in organisms.

Duplicated paralogous genes have been coopted into both sperm (Izumo1, DCST1/2) and egg (Juno) proteins involved in gamete membrane fusion (Bianchi et al., 2014; Inoue et al., 2021a, 1). Domain duplications within paralogs is also observed in the TFP superfamily and ZPs and has allowed both groups of genes to adopt novel functions at multiple stages of fertilization. As seen with TFPs, duplication events are often followed by notable protein structural changes (Doty et al., 2016) which may be tied to their cooption for novel fertilization functions. It is intriguing to consider hypotheses that account for these patterns of gene family expansion and diversification common in reproductive molecules.

Duplication events can facilitate the rapid evolution and neofunctionalization observed in many families of fertilization proteins. This rapid evolution can also be influenced by multiple factors such as sexual conflict, polyspermy avoidance, or genetic drift (Vacquier et al., 1997). The necessity of pathogen avoidance or blocks to polyspermy can drive oocytes to evolve reduced sperm binding ability. The sperm would then coevolutionarily "chase" the egg, which can contribute to the rapid sequence evolution of gametic proteins, and to the species-specificity of these protein interactions (Gavrilets and Waxman, 2002; Gavrilets, 2014). The rapid evolution of reproductive proteins is explored in terms of amino acid mutations, but the repeat expansion of domains could also be part of this trend. Proteins with repeated domains could experience drift resulting in ever-changing molecular target, that interacting proteins must coevolutionarily chase (Vacquier et al., 1997).

Duplications of reproductive proteins can also contribute to the phenomenon of functional redundancy, in which two duplicated genes have partially overlapping functions and can compensate for each other's loss (Kafri et al., 2009). Functional redundancy has been observed in the CRISP family of reproductive proteins (Curci et al., 2020), and this property could emerge in other large protein families. While functional redundancy seems like it would be temporary as duplicated genes subfunctionalized or neofunctionalized, it can be a surprisingly evolutionarily stable property. Functional redundancy could confer fitness advantages by maintaining the robusticity of protein interaction networks in spite of stochasticity of expression between cells (Kafri et al., 2009). The rapid evolution of other reproductive proteins in these networks could place even greater value on robustness and stability of essential functions. Robusticity in these protein networks is believed to reduce the fitness cost of new mutations, which would increase the "evolvability" of these proteins and facilitate functional innovation (Kirschner and Gerhart, 2008). The concepts of functional redundancy and robusticity of function may also apply to domain repeat expansions like the ZP-N domains of VERL. The processes of gene duplication, repeat domain expansion, structural modification, and neofunctionalization have been fundamental to the evolution of reproductive molecules across life.

AUTHOR CONTRIBUTIONS

Both authors were involved in the conception of this review. AR principally conducted the literature review, and the writing of the manuscript. WS provided substantial literature suggestions and editorial feedback.

FUNDING

The lab is funded by the NIH grant HD105025 awarded to WS.

ACKNOWLEDGMENTS

We thank Damien B. Wilburn for sharing his code for visualizing transmembrane proteins, and fellow lab members Jolie Carlisle and Jan Aagaard for engaging in discussions.

REFERENCES

Aagaard, J. E., Vacquier, V. D., MacCoss, M. J., and Swanson, W. J. (2010). ZP Domain Proteins in the Abalone Egg Coat Include a Paralog of VERL under Positive Selection that Binds Lysin and 18-kDa Sperm Proteins. *Mol. Biol. Evol.* 27, 193–203. doi:10.1093/molbev/msp221

Ai, Y., Liu, S., Luo, H., Wu, S., Wei, H., Tang, Z., et al. (2021). lncRNA DCST1-AS1 Facilitates Oral Squamous Cell Carcinoma by Promoting M2 Macrophage Polarization through Activating NF-κB Signaling. *J. Immunol. Res.* 2021, 1–9. doi:10.1155/2021/5524231

Alape-Girón, A., Persson, B., Cederlund, E., Flores-Díaz, M., Gutiérrez, J. M., Thelestam, M., et al. (1999). Elapid Venom Toxins: Multiple Recruitments of Ancient Scaffolds. *Eur. J. Biochem.* 259, 225–234. doi:10.1046/j.1432-1327.1999.00021.x

Almagro Armenteros, J. J., Tsirigos, K. D., Sønderby, C. K., Petersen, T. N., Winther, O., Brunak, S., et al. (2019). SignalP 5.0 Improves Signal Peptide Predictions Using Deep Neural Networks. *Nat. Biotechnol.* 37, 420–423. doi:10.1038/s41587-019-0036-z

Avella, M. A., Xiong, B., and Dean, J. (2013). The Molecular Basis of Gamete Recognition in Mice and Humans. *Mol. Hum. Reprod* 19, 279–289. doi:10.1093/molehr/gat004

Avella, M. A., Baibakov, B., and Dean, J. (2014). A Single Domain of the ZP2 Zona Pellucida Protein Mediates Gamete Recognition in Mice and Humans. *J. Cell. Biol.* 205, 801–809. doi:10.1083/jcb.201404025

Aydin, H., Sultana, A., Li, S., Thavalingam, A., and Lee, J. E. (2016). Molecular Architecture of the Human Sperm IZUMO1 and Egg JUNO Fertilization Complex. *Nature* 534, 562–565. doi:10.1038/nature18595

Bianchi, E., and Wright, G. J. (2014). Izumo Meets Juno. *Cell Cycle* 13, 2019–2020. doi:10.4161/cc.29461

Bianchi, E., and Wright, G. J. (2015). Cross-species Fertilization: the Hamster Egg Receptor, Juno, Binds the Human Sperm Ligand, Izumo1. *Phil. Trans. R. Soc. B* 370, 20140101. doi:10.1098/rstb.2014.0101

Bianchi, E., Doe, B., Goulding, D., and Wright, G. J. (2014). Juno Is the Egg Izumo Receptor and Is Essential for Mammalian Fertilization. *Nature* 508, 483–487. doi:10.1038/nature13203

Björklund, Å. K., Ekman, D., Light, S., Frey-Skött, J., and Elofsson, A. (2005). Domain Rearrangements in Protein Evolution. *J. Mol. Biol.* 353, 911–923. doi:10.1016/j.jmb.2005.08.067

Björklund, Å. K., Ekman, D., and Elofsson, A. (2006). Expansion of Protein Domain Repeats. *Plos Comput. Biol.* 2, e114. doi:10.1371/journal.pcbi.0020114

Bleil, J. D., Beall, C. F., and Wassarman, P. M. (1981). Mammalian Sperm-Egg Interaction: Fertilization of Mouse Eggs Triggers Modification of the Major

Zona Pellucida Glycoprotein, ZP2. *Dev. Biol.* 86, 189–197. doi:10.1016/0012-1606(81)90329-8

Bokhove, M., and Jovine, L. (2018). Structure of Zona Pellucida Module Proteins. *Curr. Topic Dev. Biol.* 130, 413–442. doi:10.1016/bs.ctdb.2018.02.007

Bokhove, M., Nishimura, K., Brunati, M., Han, L., de Sanctis, D., Rampoldi, L., et al. (2016). A Structured Interdomain Linker Directs Self-Polymerization of Human Uromodulin. *Proc. Natl. Acad. Sci. USA* 113, 1552–1557. doi:10.1073/pnas.1519803113

Brunati, M., Perucca, S., Han, L., Cattaneo, A., Consolato, F., Andolfo, A., et al. (2015). The Serine Protease Hepsin Mediates Urinary Secretion and Polymerisation of Zona Pellucida Domain Protein Uromodulin. *Elife* 4, e08887. doi:10.7554/eLife.08887

Buljan, M., and Bateman, A. (2009). The Evolution of Protein Domain Families. *Biochem. Soc. Trans.* 37, 751–755. doi:10.1042/BST0370751

Busso, D., Goldweic, N. M., Hayashi, M., Kasahara, M., and Cuasnicú, P. S. (2007). Evidence for the Involvement of Testicular Protein CRISP2 in Mouse Sperm-Egg Fusion1. *Biol. Reprod.* 76, 701–708. doi:10.1095/biolreprod.106.056770

Civetta, A. (2003). Positive Selection within Sperm-Egg Adhesion Domains of Fertilin: An ADAM Gene with a Potential Role in Fertilization. *Mol. Biol. Evol.* 20, 21–29. doi:10.1093/molbev/msg002

Clapham, D. E., and Garbers, D. L. (2005). International Union of Pharmacology. L. Nomenclature and Structure-Function Relationships of CatSper and Two-Pore Channels. *Pharmacol. Rev.* 57, 451–454. doi:10.1124/pr.57.4.7

Clark, N. L., Gasper, J., Sekino, M., Springer, S. A., Aquadro, C. F., and Swanson, W. J. (2009). Coevolution of Interacting Fertilization Proteins. *Plos Genet.* 5, e1000570. doi:10.1371/journal.pgen.1000570

Claw, K. G., and Swanson, W. J. (2012). Evolution of the Egg: New Findings and Challenges. *Annu. Rev. Genom. Hum. Genet.* 13, 109–125. doi:10.1146/annurev-genom-090711-163745

Conant, G. C., and Wolfe, K. H. (2008). Turning a Hobby into a Job: How Duplicated Genes Find New Functions. *Nat. Rev. Genet.* 9, 938–950. doi:10.1038/nrg2482

Connallon, T., and Clark, A. G. (2011). The Resolution of Sexual Antagonism by Gene Duplication. *Genetics* 187, 919–937. doi:10.1534/genetics.110.123729

Conner, S. J., Lefièvre, L., Hughes, D. C., and Barratt, C. L. R. (2005). Cracking the Egg: Increased Complexity in the Zona Pellucida. *Human Reprod.* 20, 1148–1152. doi:10.1093/humrep/deh835

Curci, L., Brukman, N. G., Weigel Muñoz, M., Rojo, D., Carvajal, G., Sulzyk, V., et al. (2020). Functional Redundancy and Compensation: Deletion of Multiple Murine Crisp Genes Reveals Their Essential Role for Male Fertility. *FASEB j.* 34, 15718–15733. doi:10.1096/fj.202001406R

Da Ros, V. G., Maldera, J. A., Willis, W. D., Cohen, D. J., Goulding, E. H., Gelman, D. M., et al. (2008). Impaired Sperm Fertilizing Ability in Mice Lacking Cysteine-RIch Secretory Protein 1 (CRISP1). *Dev. Biol.* 320, 12–18. doi:10.1016/j.ydbio.2008.03.015

Doty, K. A., Wilburn, D. B., Bowen, K. E., Feldhoff, P. W., and Feldhoff, R. C. (2016). Co-option and Evolution of Non-olfactory Proteinaceous Pheromones in a Terrestrial Lungless Salamander. *J. Proteomics* 135, 101–111. doi:10.1016/j.jprot.2015.09.019

Dufour, S., Quérat, B., Tostivint, H., Pasqualini, C., Vaudry, H., and Rousseau, K. (2020). Origin and Evolution of the Neuroendocrine Control of Reproduction in Vertebrates, with Special Focus on Genome and Gene Duplications. *Physiol. Rev.* 100, 869–943. doi:10.1152/physrev.00009.2019

Elder, J. F., and Turner, B. J. (1995). Concerted Evolution of Repetitive DNA Sequences in Eukaryotes. *Q. Rev. Biol.* 70, 297–320. doi:10.1086/419073

Eleveld-Trancikova, D., Triantis, V., Moulin, V., Looman, M. W. G., Wijers, M., Fransen, J. A. M., et al. (2005). The Dendritic Cell-Derived Protein DC-STAMP Is Highly Conserved and Localizes to the Endoplasmic Reticulum. *J. Leukoc. Biol.* 77, 337–343. doi:10.1189/jlb.0804441

Eleveld-Trancikova, D., Janssen, R. A. J., Hendriks, I. A. M., Looman, M. W. G., Moulin, V., Jansen, B. J. H., et al. (2008). The DC-Derived Protein DC-STAMP Influences Differentiation of Myeloid Cells. *Leukemia* 22, 455–459. doi:10.1038/sj.leu.2404910

Ellerman, D. A., Pei, J., Gupta, S., Snell, W. J., Myles, D., and Primakoff, P. (2009). Izumo Is Part of a Multiprotein Family Whose Members Form Large Complexes on Mammalian Sperm. *Mol. Reprod. Dev.* 76, 1188–1199. doi:10.1002/mrd.21092

Elwood, P. C. (1989). Molecular Cloning and Characterization of the Human Folate-Binding Protein cDNA from Placenta and Malignant Tissue Culture (KB) Cells. *J. Biol. Chem.* 264, 14893–14901. doi:10.1016/S0021-9258(18)63786-X

Evans, J. P. (2020). Preventing Polyspermy in Mammalian Eggs-Contributions of the Membrane Block and Other Mechanisms. *Mol. Reprod. Dev.* 87, 341–349. doi:10.1002/mrd.23331

Fahrenkamp, E., Algarra, B., and Jovine, L. (2020). Mammalian Egg Coat Modifications and the Block to Polyspermy. *Mol. Reprod. Dev.* 87, 326–340. doi:10.1002/mrd.23320

Finn, S., and Civetta, A. (2010). Sexual Selection and the Molecular Evolution of ADAM Proteins. *J. Mol. Evol.* 71, 231–240. doi:10.1007/s00239-010-9382-7

Force, A., Lynch, M., Pickett, F. B., Amores, A., Yan, Y.-l., and Postlethwait, J. (1999). Preservation of Duplicate Genes by Complementary, Degenerative Mutations. *Genetics* 151, 1531–1545. doi:10.1093/genetics/151.4.1531

Frolikova, M., Manaskova-Postlerova, P., Cerny, J., Jankovicova, J., Simonik, O., Pohlova, A., et al. (2018). CD9 and CD81 Interactions and Their Structural Modelling in Sperm Prior to Fertilization. *Ijms* 19, 1236. doi:10.3390/ijms19041236

Fujihara, Y., Herberg, S., Blaha, A., Panser, K., Kobayashi, K., Larasati, T., et al. (2021). The Conserved Fertility Factor SPACA4/Bouncer Has Divergent Modes of Action in Vertebrate Fertilization. *Proc. Natl. Acad. Sci. USA* 118, e2108777118. doi:10.1073/pnas.2108777118

Gahlay, G., Gauthier, L., Baibakov, B., Epifano, O., and Dean, J. (2010). Gamete Recognition in Mice Depends on the Cleavage Status of an Egg's Zona Pellucida Protein. *Science* 329, 216–219. doi:10.1126/science.1188178

Galat, A., Gross, G., Drevet, P., Sato, A., and Ménez, A. (2008). Conserved Structural Determinants in Three-Fingered Protein Domains. *FEBS J.* 275, 3207–3225. doi:10.1111/j.1742-4658.2008.06473.x

Galat, A. (2008). The Three-Fingered Protein Domain of the Human Genome. *Cell. Mol. Life Sci.* 65, 3481–3493. doi:10.1007/s00018-008-8473-8

Galat, A. (2015). Multidimensional Drift of Sequence Attributes and Functional Profiles in the Superfamily of the Three-Finger Proteins and Their Structural Homologues. *J. Chem. Inf. Model.* 55, 2026–2041. doi:10.1021/acs.jcim.5b00322

Galindo, B. E., Moy, G. W., Swanson, W. J., and Vacquier, V. D. (2002). Full-Length Sequence of VERL, the Egg Vitelline Envelope Receptor for Abalone Sperm Lysin. *Gene* 288, 111–117. doi:10.1016/s0378-1119(02)00459-6

Galindo, B. E., Vacquier, V. D., and Swanson, W. J. (2003). Positive Selection in the Egg Receptor for Abalone Sperm Lysin. *Proc. Natl. Acad. Sci.* 100, 4639–4643. doi:10.1073/pnas.0830022100

Gallach, M., and Betrán, E. (2011). Intralocus Sexual Conflict Resolved through Gene Duplication. *Trends Ecol. Evol.* 26, 222–228. doi:10.1016/j.tree.2011.02.004

Gallach, M., Chandrasekaran, C., and Betrán, E. (2010). Analyses of Nuclearly Encoded Mitochondrial Genes Suggest Gene Duplication as a Mechanism for Resolving Intralocus Sexually Antagonistic Conflict in Drosophila. *Genome Biol. Evol.* 2, 835–850. doi:10.1093/gbe/evq069

Gallach, M., Domingues, S., and Betrán, E. (2011). Gene Duplication and the Genome Distribution of Sex-Biased Genes. *Int. J. Evol. Biol.* 2011, 1–20. doi:10.4061/2011/989438

Gavrilets, S., and Waxman, D. (2002). Sympatric Speciation by Sexual Conflict. *Proc. Natl. Acad. Sci.* 99, 10533–10538. doi:10.1073/pnas.152011499

Gavrilets, S. (2014). Is Sexual Conflict an "Engine of Speciation". *Cold Spring Harbor Perspect. Biol.* 6, a017723. doi:10.1101/cshperspect.a017723

Gelbaya, T. A., Potdar, N., Jeve, Y. B., and Nardo, L. G. (2014). Definition and Epidemiology of Unexplained Infertility. *Obstet. Gynecol. Surv.* 69(2), 109–115. doi:10.1097/OGX.0000000000000043

Gibbs, G. M., Orta, G., Reddy, T., Koppers, A. J., Martinez-Lopez, P., Luis de la Vega-Beltran, J., et al. (2011). Cysteine-rich Secretory Protein 4 Is an Inhibitor of Transient Receptor Potential M8 with a Role in Establishing Sperm Function. *Proc. Natl. Acad. Sci.* 108, 7034–7039. doi:10.1073/pnas.1015935108

Goudet, G., Mugnier, S., Callebaut, I., and Monget, P. (2008). Phylogenetic Analysis and Identification of Pseudogenes Reveal a Progressive Loss of Zona Pellucida Genes during Evolution of Vertebrates1. *Biol. Reprod.* 78, 796–806. doi:10.1095/biolreprod.107.064568

Grayson, P., and Civetta, A. (2012). Positive Selection and the Evolution of Izumo Genes in Mammals. *Int. J. Evol. Biol.* 2012, 1–7. doi:10.1155/2012/958164

Grayson, P. (2015). Izumo1 and Juno: the Evolutionary Origins and Coevolution of Essential Sperm-Egg Binding Partners. *R. Soc. Open Sci.* 2, 150296. doi:10.1098/rsos.150296

Guasti, P. N., Souza, F. F., Scott, C., Papa, P. M., Camargo, L. S., Schmith, R. A., et al. (2020). Equine Seminal Plasma and Sperm Membrane: Functional Proteomic Assessment. *Theriogenology* 156, 70–81. doi:10.1016/j.theriogenology.2020.06.014

Han, J.-H., Batey, S., Nickson, A. A., Teichmann, S. A., and Clarke, J. (2007). The Folding and Evolution of Multidomain Proteins. *Nat. Rev. Mol. Cel. Biol.* 8, 319–330. doi:10.1038/nrm2144

Han, L., Nishimura, K., Sadat Al Hosseini, H., Bianchi, E., Wright, G. J., and Jovine, L. (2016). Divergent Evolution of Vitamin B9 Binding Underlies Juno-Mediated Adhesion of Mammalian Gametes. *Curr. Biol.* 26, R100–R101. doi:10.1016/j.cub.2015.12.034

Hart, M. W. (2013). Structure and Evolution of the Sea star Egg Receptor for Sperm Bindin. *Mol. Ecol.* 22, 2143–2156. doi:10.1111/mec.12251

Hartgers, F. C., Vissers, J. L. M., Looman, M. W. G., Zoelen, C. v., Huffine, C., Figdor, C. G., et al. (2000). DC-STAMP, a Novel Multimembrane-Spanning Molecule Preferentially Expressed by Dendritic Cells. *Eur. J. Immunol.* 30, 3585–3590. doi:10.1002/1521-4141(200012)30:12<3585:aid-immu3585>3.0.co;2-y

Hartgers, F. C., Looman, M. W. G., van der Woning, B., Merkx, G. F. M., Figdor, C. G., and Adema, G. J. (2001). Genomic Organization, Chromosomal Localization, and 5′ Upstream Region of the Human DC-STAMP Gene. *Immunogenetics* 53, 145–149. doi:10.1007/s002510100302

Herberg, S., Gert, K. R., Schleiffer, A., and Pauli, A. (2018). The Ly6/uPAR Protein Bouncer Is Necessary and Sufficient for Species-specific Fertilization. *Science* 361, 1029–1033. doi:10.1126/science.aat7113

Howe, K. L., Achuthan, P., Allen, J., Allen, J., Alvarez-Jarreta, J., Amode, M. R., et al. (2021). Ensembl 2021. *Nucleic Acids Res.* 49, D884–D891. doi:10.1093/nar/gkaa942

Hu, S., Yao, Y., Hu, X., and Zhu, Y. (2020). LncRNA DCST1-AS1 Downregulates miR-29b through Methylation in Glioblastoma (GBM) to Promote Cancer Cell Proliferation. *Clin. Transl. Oncol.* 22, 2230–2235. doi:10.1007/s12094-020-02363-1

Hughes, A. L. (1994). The Evolution of Functionally Novel Proteins after Gene Duplication. *Proc. R. Soc. Lond. B* 256, 119–124. doi:10.1098/rspb.1994.0058

Innan, H. (2009). Population Genetic Models of Duplicated Genes. *Genetica* 137, 19–37. doi:10.1007/s10709-009-9355-1

Inoue, N., Ikawa, M., Isotani, A., and Okabe, M. (2005). The Immunoglobulin Superfamily Protein Izumo Is Required for Sperm to Fuse with Eggs. *Nature* 434, 234–238. doi:10.1038/nature03362

Inoue, N., Hagihara, Y., and Wada, I. (2021a). Evolutionarily Conserved Sperm Factors, DCST1 and DCST2, Are Required for Gamete Fusion. *Elife* 10, e66313. doi:10.7554/eLife.66313

Inoue, N., Satouh, Y., and Wada, I. (2021b). IZUMO Family Member 3, IZUMO3, Is Involved in Male Fertility through the Acrosome Formation. *Mol. Reprod. Dev.* 88, 479–481. doi:10.1002/mrd.23520

Jansen, B. J. H., Eleveld-Trancikova, D., Sanecka, A., van Hout-Kuijer, M., Hendriks, I. A. M., Looman, M. G. W., et al. (2009). OS9 Interacts with DC-STAMP and Modulates its Intracellular Localization in Response to TLR Ligation. *Mol. Immunol.* 46, 505–515. doi:10.1016/j.molimm.2008.06.032

Jovine, L., Qi, H., Williams, Z., Litscher, E., and Wassarman, P. M. (2002). The ZP Domain Is a Conserved Module for Polymerization of Extracellular Proteins. *Nat. Cell Biol.* 4, 457–461. doi:10.1038/ncb802

Jumper, J., Evans, R., Pritzel, A., Green, T., Figurnov, M., Ronneberger, O., et al. (2021). Highly Accurate Protein Structure Prediction with AlphaFold. *Nature* 596, 583–589. doi:10.1038/s41586-021-03819-2

Kafri, R., Springer, M., and Pilpel, Y. (2009). Genetic Redundancy: New Tricks for Old Genes. *Cell* 136, 389–392. doi:10.1016/j.cell.2009.01.027

Kamei, N., and Glabe, C. G. (2003). The Species-specific Egg Receptor for Sea Urchin Sperm Adhesion Is EBR1,a Novel ADAMTS Protein. *Genes Dev.* 17, 2502–2507. doi:10.1101/gad.1133003

Katoh, K., and Standley, D. M. (2013). MAFFT Multiple Sequence Alignment Software Version 7: Improvements in Performance and Usability. *Mol. Biol. Evol.* 30, 772–780. doi:10.1093/molbev/mst010

Kelleher, E. S., and Markow, T. A. (2009). Duplication, Selection and Gene Conversion in a Drosophila mojavensis Female Reproductive Protein Family. *Genetics* 181, 1451–1465. doi:10.1534/genetics.108.099044

Kelleher, E. S., Swanson, W. J., and Markow, T. A. (2007). Gene Duplication and Adaptive Evolution of Digestive Proteases in Drosophila Arizonae Female Reproductive Tracts. *Plos Genet.* 3, e148. doi:10.1371/journal.pgen.0030148

Kessler, P., Marchot, P., Silva, M., and Servent, D. (2017). The Three-finger Toxin Fold: a Multifunctional Structural Scaffold Able to Modulate Cholinergic Functions. *J. Neurochem.* 142, 7–18. doi:10.1111/jnc.13975

Killingbeck, E. E., and Swanson, W. J. (2018). Egg Coat Proteins Across Metazoan Evolution. *Curr. Top. Dev. Biol.* 130, 443–488. doi:10.1016/bs.ctdb.2018.03.005

Kini, R. M. (2002). Molecular Moulds with Multiple Missions: Functional Sites in Three-finger Toxins. *Clin. Exp. Pharmacol. Physiol.* 29, 815–822. doi:10.1046/j.1440-1681.2002.03725.x

Kirschner, M. W., and Gerhart, J. C. (2008). *The Plausibility of Life: Resolving Darwin's Dilemma*. New Haven: Yale University Press. doi:10.12987/9780300128673

Kondrashov, F. A., Rogozin, I. B., Wolf, Y. I., and Koonin, E. V. (2002). Selection in the Evolution of Gene Duplications. *Genome Biol.* 3, research0008. doi:10.1186/gb-2002-3-2-research0008

Kozlov, A. M., Darriba, D., Flouri, T., Morel, B., and Stamatakis, A. (2019). RAxML-NG: a Fast, Scalable and User-Friendly Tool for Maximum Likelihood Phylogenetic Inference. *Bioinformatics* 35, 4453–4455. doi:10.1093/bioinformatics/btz305

Kroft, T. L., Gleason, E. J., and L'Hernault, S. W. (2005). The Spe-42 Gene Is Required for Sperm-Egg Interactions during C. elegans Fertilization and Encodes a Sperm-specific Transmembrane Protein. *Dev. Biol.* 286, 169–181. doi:10.1016/j.ydbio.2005.07.020

Krogh, A., Larsson, B., von Heijne, G., and Sonnhammer, E. L. L. (2001). Predicting Transmembrane Protein Topology with a Hidden Markov Model: Application to Complete genomes11Edited by F. Cohen. *J. Mol. Biol.* 305, 567–580. doi:10.1006/jmbi.2000.4315

Kukita, T., Wada, N., Kukita, A., Kakimoto, T., Sandra, F., Toh, K., et al. (2004). RANKL-induced DC-STAMP Is Essential for Osteoclastogenesis. *J. Exp. Med.* 200, 941–946. doi:10.1084/jem.20040518

Le Naour, F., Rubinstein, E., Jasmin, C., Prenant, M., and Boucheix, C. (2000). Severely Reduced Female Fertility in CD9-Deficient Mice. *Science* 287, 319–321. doi:10.1126/science.287.5451.319

Legan, P. K., Rau, A., Keen, J. N., and Richardson, G. P. (1997). The Mouse Tectorins: Modular Matrix Proteins of the Inner Ear Homologous To Components of the Sperm-Egg Adhesion System. *J. Biol. Chem.* 272, 8791–8801. doi:10.1074/jbc.272.13.8791

Liang, L. F., and Dean, J. (1993). Conservation of Mammalian Secondary Sperm Receptor Genes Enables the Promoter of the Human Gene to Function in Mouse Oocytes. *Dev. Biol.* 156, 399–408. doi:10.1006/dbio.1993.1087

Liao, D. (1999). Concerted Evolution: Molecular Mechanism and Biological Implications. *Am. J. Hum. Genet.* 64, 24–30. doi:10.1086/302221

Lin, S. J., Hu, Y., Zhu, J., Woodruff, T. K., and Jardetzky, T. S. (2011). Structure of Betaglycan Zona Pellucida (ZP)-C Domain Provides Insights into ZP-Mediated Protein Polymerization and TGF- Binding. *Proc. Natl. Acad. Sci.* 108, 5232–5236. doi:10.1073/pnas.1010689108

Litscher, E. S., and Wassarman, P. M. (2020). Zona Pellucida Proteins, Fibrils, and Matrix. *Annu. Rev. Biochem.* 89, 695–715. doi:10.1146/annurev-biochem-011520-105310

Low, B. W., Preston, H. S., Sato, A., Rosen, L. S., Searl, J. E., Rudko, A. D., et al. (1976). Three Dimensional Structure of Erabutoxin B Neurotoxic Protein: Inhibitor of Acetylcholine Receptor. *Proc. Natl. Acad. Sci.* 73, 2991–2994. doi:10.1073/pnas.73.9.2991

Lynch, M., and Conery, J. S. (2000). The Evolutionary Fate and Consequences of Duplicate Genes. *Science* 290, 1151–1155. doi:10.1126/science.290.5494.1151

Maldera, J. A., Weigel Munoz, M., Chirinos, M., Busso, D., Ge Raffo, F., Battistone, M. A., et al. (2014). Human Fertilization: Epididymal hCRISP$_1$ Mediates Sperm-Zona Pellucida Binding through its Interaction with ZP$_3$. *Mol. Hum. Reprod.* 20, 341–349. doi:10.1093/molehr/gat092

Meslin, C., Mugnier, S., Callebaut, I., Laurin, M., Pascal, G., Poupon, A., et al. (2012). Evolution of Genes Involved in Gamete Interaction: Evidence for Positive Selection, Duplications and Losses in Vertebrates. *PLOS ONE* 7, e44548. doi:10.1371/journal.pone.0044548

Miyado, K., Yamada, G., Yamada, S., Hasuwa, H., Nakamura, Y., Ryu, F., et al. (2000). Requirement of CD9 on the Egg Plasma Membrane for Fertilization. *Science* 287, 321–324. doi:10.1126/science.287.5451.321

Monné, M., Han, L., Schwend, T., Burendahl, S., and Jovine, L. (2008). Crystal Structure of the ZP-N Domain of ZP3 Reveals the Core Fold of Animal Egg coats. *Nature* 456, 653–657. doi:10.1038/nature07599

Moore, A. D., Björklund, Å. K., Ekman, D., Bornberg-Bauer, E., and Elofsson, A. (2008). Arrangements in the Modular Evolution of Proteins. *Trends Biochem. Sci.* 33, 444–451. doi:10.1016/j.tibs.2008.05.008

Nacher, J. C., Hayashida, M., and Akutsu, T. (2010). The Role of Internal Duplication in the Evolution of Multi-Domain Proteins. *Biosystems* 101, 127–135. doi:10.1016/j.biosystems.2010.05.005

Nair, S., Bist, P., Dikshit, N., and Krishnan, M. N. (2016). Global Functional Profiling of Human Ubiquitome Identifies E3 Ubiquitin Ligase DCST1 as a Novel Negative Regulator of Type-I Interferon Signaling. *Sci. Rep.* 6, 36179. doi:10.1038/srep36179

Navarro, B., Kirichok, Y., Chung, J. J., and Clapham, D. E. (2008). Ion Channels that Control Fertility in Mammalian Spermatozoa. *Int. J. Dev. Biol.* 52, 607–613. doi:10.1387/ijdb.072554bn

Nirthanan, S., Gopalakrishnakone, P., Gwee, M. C. E., Khoo, H. E., and Kini, R. M. (2003). Non-conventional Toxins from Elapid Venoms. *Toxicon* 41, 397–407. doi:10.1016/S0041-0101(02)00388-4

Nishimura, K., Dioguardi, E., Nishio, S., Villa, A., Han, L., Matsuda, T., et al. (2019). Molecular Basis of Egg Coat Cross-Linking Sheds Light on ZP1-Associated Female Infertility. *Nat. Commun.* 10, 3086. doi:10.1038/s41467-019-10931-5

Nomiyama, H., Egami, K., Wada, N., Tou, K., Horiuchi, M., Matsusaki, H., et al. (2005). Short Communication: Identification of Genes Differentially Expressed in Osteoclast-like Cells. *J. Interferon Cytokine Res.* 25, 227–231. doi:10.1089/jir.2005.25.227

Ohto, U., Ishida, H., Krayukhina, E., Uchiyama, S., Inoue, N., and Shimizu, T. (2016). Structure of IZUMO1-JUNO Reveals Sperm-Oocyte Recognition during Mammalian Fertilization. *Nature* 534, 566–569. doi:10.1038/nature18596

Palmer, C. A., Watts, R. A., Houck, L. D., Picard, A. L., and Arnold, S. J. (2007). Evolutionary Replacement of Components in a Salamander Pheromone Signaling Complex: More Evidence for Phenotypic-Molecular Decoupling. *Evolution* 61, 202–215. doi:10.1111/j.1558-5646.2007.00017.x

Palmer, C. A., Watts, R. A., Hastings, A. P., Houck, L. D., and Arnold, S. J. (2010). Rapid Evolution of Plethodontid Modulating Factor, a Hypervariable Salamander Courtship Pheromone, Is Driven by Positive Selection. *J. Mol. Evol.* 70, 427–440. doi:10.1007/s00239-010-9342-2

Pei, J., Kim, B. H., and Grishin, N. V. (2008). PROMALS3D: a Tool for Multiple Protein Sequence and Structure Alignments. *Nucleic Acids Res.* 36, 2295–2300. doi:10.1093/nar/gkn072

Perry, G. H., Dominy, N. J., Claw, K. G., Lee, A. S., Fiegler, H., Redon, R., et al. (2007). Diet and the Evolution of Human Amylase Gene Copy Number Variation. *Nat. Genet.* 39, 1256–1260. doi:10.1038/ng2123

Petronella, N., and Drouin, G. (2014). Purifying Selection against Gene Conversions in the Folate Receptor Genes of Primates. *Genomics* 103, 40–47. doi:10.1016/j.ygeno.2013.10.004

Ponting, C. P. (2008). The Functional Repertoires of Metazoan Genomes. *Nat. Rev. Genet.* 9, 689–698. doi:10.1038/nrg2413

Primakoff, P., and Myles, D. G. (2000). The ADAM Gene Family: Surface Proteins with Adhesion and Protease Activity. *Trends Genet.* 16, 83–87. doi:10.1016/S0168-9525(99)01926-5

Raj, I., Sadat Al Hosseini, H., Dioguardi, E., Nishimura, K., Han, L., Villa, A., et al. (2017). Structural Basis of Egg Coat-Sperm Recognition at Fertilization. *Cell* 169, 1315–1326.e17. doi:10.1016/j.cell.2017.05.033

Ramírez-Gómez, H. V., Tuval, I., Guerrero, A., and Darszon, A. (2019). Analysis of Sperm Chemotaxis. *Methods Cell Biol.* 151, 473–486. doi:10.1016/bs.mcb.2018.12.002

Rankin, T. L., Coleman, J. S., Epifano, O., Hoodbhoy, T., Turner, S. G., Castle, P. E., et al. (2003). Fertility and Taxon-Specific Sperm Binding Persist after Replacement of Mouse Sperm Receptors with Human Homologs. *Dev. Cel.* 5, 33–43. doi:10.1016/s1534-5807(03)00195-3

Rastogi, S., and Liberles, D. A. (2005). Subfunctionalization of Duplicated Genes as a Transition State to Neofunctionalization. *BMC Evol. Biol.* 5, 28. doi:10.1186/1471-2148-5-28

Schimenti, J. C. (1999). Mice and the Role of Unequal Recombination in Gene-Family Evolution. *Am. J. Hum. Genet.* 64, 40–45. doi:10.1086/302220

Shen, F., Ross, J. F., Wang, X., and Ratnam, M. (1994). Identification of a Novel Folate Receptor, a Truncated Receptor, and Receptor Type .Beta. In Hematopoietic Cells: cDNA Cloning, Expression, Immunoreactivity, and Tissue Specificity. *Biochemistry* 33, 1209–1215. doi:10.1021/bi00171a021

Shu, L., Suter, M. J.-F., and Räsänen, K. (2015). Evolution of Egg coats: Linking Molecular Biology and Ecology. *Mol. Ecol.* 24, 4052–4073. doi:10.1111/mec.13283

Siu, K. K., Serrão, V. H. B., Ziyyat, A., and Lee, J. E. (2021). The Cell Biology of Fertilization: Gamete Attachment and Fusion. *J. Cell Biol.* 220, e202102146. doi:10.1083/jcb.202102146

Sonnhammer, E. L., von Heijne, G., and Krogh, A. (1998). A Hidden Markov Model for Predicting Transmembrane Helices in Protein Sequences. *Proc. Int. Conf. Intell. Syst. Mol. Biol.* 6, 175–182.

Speer, K. F., Allen-Waller, L., Novikov, D. R., and Barott, K. L. (2021). Molecular Mechanisms of Sperm Motility Are Conserved in an Early-Branching Metazoan. *Proc. Natl. Acad. Sci. USA* 118, e2109993118. doi:10.1073/pnas.2109993118

Spiegelstein, O., Eudy, J. D., and Finnell, R. H. (2000). Identification of Two Putative Novel Folate Receptor Genes in Humans and Mouse. *Gene* 258, 117–125. doi:10.1016/S0378-1119(00)00418-2

Staege, H., Brauchlin, A., Schoedon, G., and Schaffner, A. (2001). Two Novel Genes FIND and LIND Differentially Expressed in Deactivated and Listeria -infected Human Macrophages. *Immunogenetics* 53, 105–113. doi:10.1007/s002510100306

Sutton, K. A., Jungnickel, M. K., and Florman, H. M. (2008). A Polycystin-1 Controls Postcopulatory Reproductive Selection in Mice. *Proc. Natl. Acad. Sci.* 105, 8661–8666. doi:10.1073/pnas.0800603105

Swanson, W. J., and Vacquier, V. D. (2002). The Rapid Evolution of Reproductive Proteins. *Nat. Rev. Genet.* 3, 137–144. doi:10.1038/nrg733

Ting, C. T., Tsaur, S.-C., Sun, S., Browne, W. E., Chen, Y.-C., Patel, N. H., et al. (2004). Gene Duplication and Speciation in Drosophila: Evidence from the Odysseus Locus. *Proc. Natl. Acad. Sci.* 101, 12232–12235. doi:10.1073/pnas.0401975101

Tsernoglou, D., and Petsko, G. A. (1977). Three-dimensional Structure of Neurotoxin a from Venom of the Philippines Sea Snake. *Proc. Natl. Acad. Sci.* 74, 971–974. doi:10.1073/pnas.74.3.971

Tsetlin, V. (1999). Snake Venom Alpha-Neurotoxins and Other 'three-finger' Proteins. *Eur. J. Biochem.* 264, 281–286. doi:10.1046/j.1432-1327.1999.00623.x

Vacquier, V. D., Swanson, W. J., and Lee, Y.-H. (1997). Positive Darwinian Selection on Two Homologous Fertilization Proteins: what Is the Selective Pressure Driving Their Divergence. *J. Mol. Evol.* 44, S15–S22. doi:10.1007/PL00000049

Vacquier, V. D. (1998). Evolution of Gamete Recognition Proteins. *Science* 281, 1995–1998. doi:10.1126/science.281.5385.1995

Vogel, C., Teichmann, S. A., and Pereira-Leal, J. (2005). The Relationship between Domain Duplication and Recombination. *J. Mol. Biol.* 346, 355–365. doi:10.1016/j.jmb.2004.11.050

Wagner, G. P., and Altenberg, L. (1996). Perspective: Complex Adaptations and the Evolution of Evolvability. *Evolution* 50, 967–976. doi:10.1111/j.1558-5646.1996.tb02339.x

Wagner, G. P., Pavlicev, M., and Cheverud, J. M. (2007). The Road to Modularity. *Nat. Rev. Genet.* 8, 921–931. doi:10.1038/nrg2267

Walsh, B. (2003). Population-Genetic Models of the Fates of Duplicate Genes. *Genetica* 118, 279–294. doi:10.1007/978-94-010-0229-5_16

Wang, J., Lei, C., Shi, P., Teng, H., Lu, L., Guo, H., et al. (2021). LncRNA DCST1-AS1 Promotes Endometrial Cancer Progression by Modulating the MiR-665/HOXB5 and MiR-873-5p/CADM1 Pathways. *Front. Oncol.* 11, 3112. doi:10.3389/fonc.2021.714652

Weiner, J., 3rd, Beaussart, F., and Bornberg-Bauer, E. (2006). Domain Deletions and Substitutions in the Modular Protein Evolution. *FEBS J.* 273, 2037–2047. doi:10.1111/j.1742-4658.2006.05220.x

West-Eberhard, M. J. (2005). Developmental Plasticity and the Origin of Species Differences. *Proc. Natl. Acad. Sci.* 102, 6543–6549. doi:10.1073/pnas.0501844102

Wilburn, D. B., and Swanson, W. J. (2016). From Molecules to Mating: Rapid Evolution and Biochemical Studies of Reproductive Proteins. *J. Proteomics* 135, 12–25. doi:10.1016/j.jprot.2015.06.007

Wilburn, D. B., and Swanson, W. J. (2017). The "ZP Domain" Is Not One, but Likely Two Independent Domains. *Mol. Reprod. Dev.* 84, 284–285. doi:10.1002/mrd.22781

Wilburn, D. B., Bowen, K. E., Gregg, R. G., Cai, J., Feldhoff, P. W., Houck, L. D., et al. (2012). Proteomic and UTR Analyses of a Rapidly Evolving Hypervariable Family of Vertebrate Pheromones. *Evolution* 66, 2227–2239. doi:10.1111/j.1558-5646.2011.01572.x

Wilburn, D. B., Bowen, K. E., Doty, K. A., Arumugam, S., Lane, A. N., Feldhoff, P. W., et al. (2014). Structural Insights into the Evolution of a Sexy Protein: Novel Topology and Restricted Backbone Flexibility in a Hypervariable Pheromone from the Red-Legged Salamander, Plethodon shermani. *PLOS ONE* 9, e96975. doi:10.1371/journal.pone.0096975

Wilburn, D. B., Arnold, S. J., Houck, L. D., Feldhoff, P. W., and Feldhoff, R. C. (2017). Gene Duplication, Co-option, Structural Evolution, and Phenotypic Tango in the Courtship Pheromones of Plethodontid Salamanders. *Herpetologica* 73, 206–219. doi:10.1655/Herpetologica-D-16-00082.1

Wilburn, D. B., Kunkel, C. L., Feldhoff, R. C., Feldhoff, P. W., and Searle, B. C. (2022). Recurrent Co-option and Recombination of Cytokine and Three finger Proteins in Multiple Reproductive Tissues throughout Salamander Evolution. *bioRxiv*. doi:10.1101/2022.01.04.475003

Wilson, K. L., Fitch, K. R., Bafus, B. T., and Wakimoto, B. T. (2006). Sperm Plasma Membrane Breakdown during Drosophila Fertilization Requires Sneaky, an Acrosomal Membrane Protein. *Development* 133, 4871–4879. doi:10.1242/dev.02671

Wilson, L. D., Obakpolor, O. A., Jones, A. M., Richie, A. L., Mieczkowski, B. D., Fall, G. T., et al. (2018). The Caenorhabditis elegans Spe-49 Gene Is Required for Fertilization and Encodes a Sperm-specific Transmembrane Protein Homologous to SPE-42. *Mol. Reprod. Dev.* 85, 563–578. doi:10.1002/mrd.22992

Wright, G. J., and Bianchi, E. (2016). The Challenges Involved in Elucidating the Molecular Basis of Sperm-Egg Recognition in Mammals and Approaches to Overcome Them. *Cell Tissue Res.* 363, 227–235. doi:10.1007/s00441-015-2243-3

Yagi, M., Miyamoto, T., Sawatani, Y., Iwamoto, K., Hosogane, N., Fujita, N., et al. (2005). DC-STAMP Is Essential for Cell-Cell Fusion in Osteoclasts and Foreign Body Giant Cells. *J. Exp. Med.* 202, 345–351. doi:10.1084/jem.20050645

Conflict of Interest: The authors declare that the research was conducted in the absence of any commercial or financial relationships that could be construed as a potential conflict of interest.

frontiers in Cell and Developmental Biology

ORIGINAL RESEARCH
published: 23 February 2022
doi: 10.3389/fcell.2022.828947

Recurrent Co-Option and Recombination of Cytokine and Three Finger Proteins in Multiple Reproductive Tissues Throughout Salamander Evolution

Damien B. Wilburn[1]*, *Christy L. Kunkel*[2], *Richard C. Feldhoff*[3], *Pamela W. Feldhoff*[3] and *Brian C. Searle*[1]

[1]Department of Biomedical Informatics, The Ohio State University, Columbus, OH, United States, [2]Department of Biology, John Carroll University, Cleveland Heights, OH, United States, [3]Department of Biochemistry and Molecular Genetics, University of Louisville, Louisville, KY, United States

OPEN ACCESS

Edited by:
Amber R Krauchunas,
University of Delaware, United States

Reviewed by:
Lena Arévalo,
University Hospital Bonn, Germany
Ronald Michael Bonett,
University of Tulsa, United States

***Correspondence:**
Damien B. Wilburn
Damien.Wilburn@osumc.edu

Specialty section:
This article was submitted to Molecular and Cellular Reproduction, a section of the journal Frontiers in Cell and Developmental Biology

Received: 04 December 2021
Accepted: 01 February 2022
Published: 23 February 2022

Citation:
Wilburn DB, Kunkel CL, Feldhoff RC, Feldhoff PW and Searle BC (2022) Recurrent Co-Option and Recombination of Cytokine and Three Finger Proteins in Multiple Reproductive Tissues Throughout Salamander Evolution. Front. Cell Dev. Biol. 10:828947. doi: 10.3389/fcell.2022.828947

Reproductive proteins evolve at unparalleled rates, resulting in tremendous diversity of both molecular composition and biochemical function between gametes of different taxonomic clades. To date, the proteomic composition of amphibian gametes is largely a molecular mystery, particularly for Urodeles (salamanders and newts) for which few genomic-scale resources exist. In this study, we provide the first detailed molecular characterization of gametes from two salamander species (*Plethodon shermani* and *Desmognathus ocoee*) that are models of reproductive behavior. Long-read PacBio transcriptome sequencing of testis and ovary of both species revealed sex-specific expression of many genes common to vertebrate gametes, including a similar expression profile to the egg coat genes of *Xenopus* oocytes. In contrast to broad conservation of oocyte genes, major testis transcripts included paralogs of salamander-specific courtship pheromones (PRF, PMF, and SPF) that were confirmed as major sperm proteins by mass spectrometry proteomics. Sperm-specific paralogs of PMF and SPF are likely the most abundant secreted proteins in *P. shermani* and *D. ocoee*, respectively. In contrast, sperm PRF lacks a signal peptide and may be expressed in cytoplasm. PRF pheromone genes evolved independently multiple times by repeated gene duplication of sperm PRF genes with signal peptides recovered through recombination with PMF genes. Phylogenetic analysis of courtship pheromones and their sperm paralogs support that each protein family evolved for these two reproductive contexts at distinct evolutionary time points between 17 and 360 million years ago. Our combined phylogenetic, transcriptomic and proteomic analyses of plethodontid reproductive tissues support that the recurrent co-option and recombination of TFPs and cytokine-like proteins have been a novel driving force throughout salamander evolution and reproduction.

Keywords: salamander, fertilization, proteomics, sperm, pheromone

INTRODUCTION

Sexual reproduction is a hallmark of most animal life cycles and is the process by which progeny are generated from the recombination of two genomes, usually from individuals of the same species. Numerous types of reproductive barriers exist to restrict such recombination – including physical boundaries, niche utilization, asynchronous mating cycles, and genetic incompatibilities – and the formation of new barriers is what ultimately transforms interbreeding populations into discrete species (Rundle and Nosil, 2005). While ecological and genetic forces have been well investigated as drivers of speciation, the role of molecular prezygotic barriers such as gamete recognition on speciation has been a topic of increasing relevance in diverse eukaryotic taxa, including fungi (Jones and Bennett, 2011), plants (Pease et al., 2016), insects (Swanson et al., 2001; Noh and Marshall, 2016), mollusks (Wilburn et al., 2018), fish (Herberg et al., 2018), and mammals (Monne et al., 2008; Avella et al., 2014). In nearly all eukaryotic species, the genes associated with reproduction are among the fastest evolving in their respective genomes, rivaling or exceeding the rate of immune gene evolution (Swanson and Vacquier, 2002; Wilburn and Swanson, 2016). In contrast to genes associated with somatic phenotypes, reproduction-related genes can evolve through a runaway sexual selection process that can yield unparalleled rates of molecular evolution and are hypothesized to contribute to speciation (Arnold and Houck, 2016; Wilburn and Swanson, 2016; Wilburn et al., 2017). However, explicitly testing such hypotheses has been hampered by our limited understanding of the biochemical mechanisms underlying sexual reproduction, including sperm-egg interactions in animals (Wilburn and Swanson, 2016). Recently published structural and biochemical studies have begun to provide insight into the molecular basis of egg-sperm recognition in marine invertebrates, fishes, birds, and mammals (Ichikawa et al., 2016; Raj et al., 2017; Herberg et al., 2018; Wilburn et al., 2018), but among vertebrates substantially less attention has been given to reptiles and amphibians. This is especially true for salamanders, where to date there have been no studies characterizing the molecular composition of salamander gametes. This is consistent with a general lack of molecular resources for salamanders, whose genomes are ~5–30X larger than humans (depending on the species) and have been immensely difficult to assemble using short-read sequencing technologies (Nowoshilow et al., 2018; Sessions and Wake, 2021). In this study, we present the first molecular characterization of salamander gametes for two species that are established models of reproduction and prezygotic mating barriers.

Lungless salamanders (family Plethodontidae) are the most speciose family of salamanders (496 out of 766 species) with expansive radiations throughout the North and Central American coasts, and are classic models of mating behavior and pheromone communication (Houck and Arnold, 2003; Shen et al., 2015; AmphibiaWeb, 2021). Male and female salamanders engage in a stereotyped courtship whose precise details vary by species, but a common feature to all plethodontid salamanders is the inclusion of a "tail straddling walk." During this period, the female salamander will straddle the tail of the male while the pair walk in unison for up to an hour, and this prepares the female to receive a spermatophore that the male will deposit on the substrate (Houck and Arnold, 2003). The male salamanders of most plethodontid species deliver non-volatile protein pheromones to females during the tail straddling walk via a chin gland (referred to as the mental gland) that can alter her mating behavior, such as reducing the length of the walk (Wilburn et al., 2017). The males of most species transdermally deliver pheromones by abrading the female dorsum with skin protrusions called "premaxillary teeth" (Houck and Arnold, 2003). However, in a single clade of *Plethodon* species restricted to eastern North America, males possess a large pad-like mental gland that is "slapped" against the female snout, delivering pheromones to the olfactory system, activating neurons that project to the brain, and directly alter female neurophysiology and mating behavior (Rollmann et al., 1999; Wirsig-Wiechmann et al., 2002; Laberge et al., 2008; Wilburn and Feldhoff, 2019). The slapping and scratching pheromone delivery systems have been most thoroughly examined in the red-legged salamander (*Plethodon shermani*) and the Ocoee salamander (*Desmognathus ocoee*), respectively. From these two species, three major pheromone families have been chemically purified and experimentally demonstrated to alter female mating behavior: Sodefrin Precursor-like Factor (SPF), Plethodontid Modulating Factor (PMF), and Plethodontid Receptivity Factor (PRF) (Rollmann et al., 1999; Houck et al., 2007; Wilburn et al., 2015).

All three major pheromone families (SPF, PMF, and PRF) are rapidly evolving within Plethodontidae and have been co-opted for pheromone function at different evolutionary times (Watts et al., 2004; Palmer et al., 2007; Palmer et al., 2010). SPF is the oldest known pheromone family in vertebrates, with homologs shared between salamanders and anurans (frogs and toads) that have been separated by ~360 million years (Bossuyt et al., 2019). PMF is also an ancient pheromone likely found in the last common ancestor of all plethodontid salamanders (~66 million years ago) and is homologous to the three-fingered protein (TFP) superfamily (Wilburn et al., 2012; Shen et al., 2015). Despite this homology, PMF is not a classical TFP as changes in the disulfide bonding pattern have resulted in a unique topology that increases structural flexibility in rapidly evolving regions of the molecule (Wilburn et al., 2014a). SPF is also related to the TFP superfamily, but with two TFP-like domains that have even more distinct disulfide bonding patterns (Doty et al., 2016). The structural consequences of this altered disulfide pattern are unknown as a structure of SPF has not yet been characterized. In contrast, PRF is a relatively new pheromone that is only found in *Plethodon* species of eastern North America (~17 million years old) and is related to IL-6 cytokines (Rollmann et al., 1999; Shen et al., 2015). In the models for slapping (*P. shermani*) and scratching (*D. ocoee*) delivery, PRF and PMF are the major pheromones in *P. shermani* versus SPF being dominant in *D. ocoee*. All three families are highly paralogous, and each species usually has multiple expressed protein variants of each pheromone (Wilburn et al., 2012; Chouinard et al., 2013; Doty et al., 2016; Wilburn et al., 2017). Beyond gene duplication, all

three pheromone families have experienced rapid evolutionary change via positive selection. This accelerated evolution is hypothesized to be a product of coevolution with female receptors and may function to restrict mating between closely related species that share overlapping habitat ranges (Watts et al., 2004; Palmer et al., 2005; Palmer et al., 2007; Palmer et al., 2010; Wilburn et al., 2012).

While pre-mating reproductive barriers of plethodontid salamanders have been well studied, post-mating pre-zygotic barriers such as gametic recognition between egg and sperm have not yet been investigated. Little is known about the molecular composition of amphibian gametes beyond studies of a single frog genus (*Xenopus spp*.), and it is unknown if salamanders possess homologs of many common gamete-associated genes. Salamander genomes are extraordinarily large (~5–30X the human genome) which has challenged their sequencing and assembly (Nowoshilow et al., 2018). Consequently, salamanders have historically been excluded from comparative genomic analyses that would identify such genes. In this study, we provide the first detailed molecular description of salamander gametes based on long-read transcriptomic analyses of plethodontid ovary and testis, paired with proteomic analysis of plethodontid sperm from the model species *P. shermani* and *D. ocoee*. A surprising discovery was that sperm express high levels of paralogs to all three pheromone families. Through molecular phylogenetic analysis, we find that each family was independently co-opted at different times throughout plethodontid and amphibian evolution. Careful examination of the pheromone families, their sperm paralogs, and homologous vertebrate proteins revealed a complex evolutionary pattern where two protein families have been repeatedly co-opted for reproductive functions through recurrent gene duplications, rapid evolution, and recombination.

MATERIALS AND METHODS

Animal Care and Biological Sample Collection

Plethodontid salamanders were collected during their breeding season in early August, with *P. shermani* collected at Wayah Bald (Macon County, North Carolina; 35°10′48″ N, 83°33′38″ W) and *D. ocoee* collected at Deep Gap (Clay County, North Carolina; 35°02′20″ N, 83°33′08″ W). Salamanders were sexed based on large ova visible through the ventral body wall in females, the presence of a large mental gland in male *P. shermani*, and premaxillary teeth in male *D. ocoee*. Animals were temporarily maintained at Highlands Biological Station where they were individually housed in clean plastic boxes (17 × 9 × 13 cm) lined with a damp paper towel and a second damp crumpled paper towel as a refuge, with temperature and humidity maintained at 15–18°C and ~70% humidity, respectively. Animals were transferred weekly to clean boxes with fresh substrate and fed two waxworms (*Galleria mellonella*). Testis and ovary samples were collected from two male and female specimens of each species by briefly anesthetizing animals in 7% diethyl ether in water, euthanizing them by rapid decapitation, quickly dissecting reproductive tissue from the body cavity, and preserving tissue samples in RNAlater (Ambion). For sperm sample collection, staged mating trials were performed as adapted from Wilburn et al. (2015). Briefly, a single male and female salamander from the same species were paired in a clean plastic box lined with a damp paper towel under limited red light. Pairs of salamanders were visually monitored for courtship behavior, and if a pair successfully performed a tail straddling walk and a spermatophore was deposited on the substrate, the courtship was disrupted to prevent insemination, and the spermatophore collected using sterile forceps. Spermatophores were gently triturated in 100 µl amphibian Ringer's solution for 15 min to release sperm and soluble components from the spermatophore casing, insoluble components (including sperm cells) collected by centrifugation at 10,000 × g for 10 min, and then stored in RNAlater. All animals were collected with appropriate permits from the North Carolina Wildlife Resources Commission and animal care protocols were reviewed and approved under the Highlands Biological Station Institutional Animal Care and Use Committee (Protocol #15-07).

RNA Isolation and Gonad Transcriptome Sequencing

RNA was isolated from individual testis and ovary samples of both *P. shermani* and *D. ocoee* using a combination of Trizol extraction and silica column purification. First, tissue samples were homogenized in 1 ml Trizol (Thermo Fisher), insoluble material removed by brief centrifugation, the sample incubated for 3 min at room temperature following addition of 0.2 ml chloroform and vortexing, centrifuged at 14,000 × g for 15 min at 4°C, and the supernatant was collected. Second, the supernatant was mixed with 0.35 ml ethanol, applied to a RNeasy column (Qiagen) with centrifugation 10,000 × g for 20 s, and serially washed with 0.2 ml Buffer RW1 and twice with 0.5 ml Buffer RPE with matching centrifugation steps of 10,000 × g for 20 s. The collection tube was replaced after the Buffer RW1 and following the final RPE wash, residual ethanol was removed by a final centrifugation step at 10,000 × g for 3 min. RNA was eluted into 50 µl RNase-free water and concentration estimated based on 260 nm absorbance. To prepare RNA for PacBio Iso-Seq analysis, single-stranded cDNA was generated from RNA using the SMARTer cDNA synthesis kit (Clontech, Palo Alto, CA) with tagged oligo-dT primers that include one of eight 15-bp barcodes to distinguish individual samples (2 species × 2 tissues × 2 biological replicates). Double stranded cDNA was amplified using Accuprime High-Fidelity Taq polymerase (Thermo Fisher) with PCR cycles of 95°C for 15 s, 65°C for 30 s, and 68°C for 6 min, preceded by a single initial melting phase of 95°C for 2 min. Cycle number was optimized for each sample to avoid overamplification. The cDNA was purified using AmpureXP beads (Pacific Biosciences) at final concentrations of both 1.0X beads to isolate all cDNA molecules and 0.4X to enrich for higher molecular weight. DNA concentration was accurately measured using Quant-iT Picogreen (Thermo Fisher) and each sample was pooled in a mass ratio of 4:1 favoring high molecular weight

cDNA. All barcoded samples were pooled in nearly equal amounts to produce a single library prepared using the SMRTbell Template Prep Kit 1.0-SPv3 (Pacific Biosciences, Menlo Park, CA) according to the manufacturer's protocol. The library was supplied to the University of Washington PacBio sequencing facility and analyzed using a PacBio Sequel system with a SMRT Cell 8M recorded for 30 h. Raw movies were decoded to full length non-concatenated cDNA sequences with circular consensus averaging using the IsoSeq3 software pipeline. Data were deposited to the NCBI Sequence Read Archive (BioProject ID PRJNA785352).

Bioinformatic Analysis of Transcriptomic Data

Pacbio Iso-Seq reads were greedily clustered using isONclust (Sahlin and Medvedev, 2020) and transcript abundance estimated as the read count per cluster and normalized to the total number of reads per sample, reported as transcripts per million (TPM). For each read, all possible coding sequences from an initiator Met to stop codon that coded for at least 30 amino acids were identified from the three forward reading frames (Iso-Seq reads are stranded), and then filtered to retain only the set of longest possible non-overlapping coding sequences per read. Potential coding sequences and their protein translations were aggregated from all reads. Protein translations supported by at least 2 reads were included in a search database for proteomic analysis. This putative protein data was also analyzed by protein BLAST to Uniref90 (accessed 28 August 2020) (Camacho et al., 2009) and leader signal peptide sequences identified by signalp (Armenteros et al., 2019). For each gene cluster, the sex ratio of each species was computed as the $\log_{10}$ ratio of average testis abundance in TPM to average ovary abundance in TPM, adjusted with a pseudocount of 1.0 TPM for numerical stability.

Proteomics Sample Preparation and Liquid Chromatography Mass Spectrometry

Plethodontid spermatophores stored in RNAlater were centrifuged at 10,000 × g for 10 min, RNAlater removed, the pellet resuspended in 50 µl 10% (w/v) SDS/50 mM TEAB/20 mM DTT, and incubated at 65°C for 30 min. The samples were briefly chilled on ice and disulfide bonds alkylated by addition of 4.6 µl 0.5M iodoacetamide with incubation in the dark at room temperature for 30 min. Samples were acidified by addition of 5.6 µl 12% phosphoric acid, mixed with 0.35 ml 90% methanol/100 mM TEAB before the entire solution was applied to a suspension trap (S-Traps; Protifi LLC) by centrifugation at 4,000 × g for 30 s, and three washes of 0.4 ml 90% methanol/100 mM TEAB were applied using the same centrifugation conditions. S-Traps were loaded with 125 µl trypsin solution (50 ng/µl in 50 mM TEAB; Promega) and incubated at 47°C for 2 h. Peptides were extracted from S-Traps by serial application of 50 mM TEAB, 0.2% formic acid, and 50% acetonitrile/0.2% formic acid in 80 µl volumes followed by centrifugation at 1,000 × g for 1 min. Resulting peptides were dried with vacuum centrifugation and resuspended in 0.1% formic acid at concentrations of ~1 µg per 3 µl immediately prior to mass spectrometry acquisition. Four biological peptide samples from each species were pooled for mass spectrometry analysis.

Tryptic peptides were separated with a Thermo Easy nLC 1200 and emitted into a Thermo Exploris 480 using a 75 µm inner diameter fused silica capillary with an in-house pulled tip. The column was packed with 3 µm ReproSil-Pur C18 beads (Dr. Maisch) to 28 cm. A Kasil fritted trap column was created from 150 µm inner diameter capillary packed to 1.5 cm with the same C18 beads. Peptide separation was performed over a 90-minute linear gradient using 250 nL/min flow with solvent A as 0.1% formic acid in water and solvent B as 0.1% formic acid in 80% acetonitrile. For each injection, 3 µl (400–900 m/z injections) or 5 µl (900–1,000 m/z injections) was loaded. Following the approach described in (Pino et al., 2020), six gas-phase fractionated data independent acquisition (GPF-DIA) experiments were acquired of each sample (120,000 precursor resolution, 30,000 fragment resolution, fragment AGC target of 1,000%, max IIT of 55 ms, NCE of 27, +3H assumed charge state) using 4 m/z precursor isolation windows in a staggered window pattern with optimized window placements (i.e., 398.4–502.5 m/z, 498.5–602.5 m/z, 598.5–702.6 m/z, 698.6–802.6 m/z, 798.6–902.7 m/z, and 898.7–1,002.7 m/z).

Mass Spectrometry Data Processing

Putative proteins sequenced by at least 2 reads in the combined plethodontid gonad transcriptome (300,472 total sequences) were digested *in silico* to create all possible +2H and +3H peptides between 7 and 30 amino acids with precursor m/z within 396.43 and 1,002.70, assuming up to one missed tryptic cleavage. Peptide fragmentation and retention time predictions for these peptides were made with the Prosit webserver (2020 HCD model, 2019 iRT model) (Gessulat et al., 2019) and collected in a spectrum library using the approach presented in Searle et al. (Searle et al., 2020). DIA data was demultiplexed (Amodei et al., 2019) with 10 ppm accuracy after peak picking in ProteoWizard (version 3.0.18113) (Chambers et al., 2012). Library searches were performed using EncyclopeDIA (version 1.2.2) (Searle et al., 2018), which was set to search with 10 ppm precursor, fragment, and library tolerances, considering both B and Y ions and assuming trypsin digestion. Detected peptides were filtered to a 1% peptide and protein-level false discovery rate. Mass spectrometry data have been deposited on the ProteomeXchange Consortium via the PRIDE (Perez-Riverol et al., 2019) partner repository with the dataset identifier PXD030143. Peptides were organized into protein groups based on parsimonious analysis of sequence clusters (i.e., "genes") from the gonad transcriptome, with multiple clusters consolidated into an individual protein group if at least two identified peptides were shared between clusters. If at least three peptides were

TABLE 1 | Summary statistics of plethodontid gonad transcriptome.

Property	Quantity
Total number of reads	3,096,431
P. shermani testis reads	719,087
D. ocoee testis reads	722,082
P. shermani ovary reads	831,814
D. ocoee ovary reads	823,448
Mean length of full-length, non-concatamer reads	2,321
Number of sequence clusters	166,909
Mean number of reads per cluster	18.6
Number of non-singleton clusters	60,007
Mean number of reads per non-singleton cluster	49.8
Number of non-singleton clusters with *P. shermani* reads	39,655
Number of non-singleton clusters with *D. ocoee* reads	36,858
Number of clusters with testis-biased expression (>10-fold) in *P. shermani* (without singletons)	3,152 (7.9%)
Number of clusters with ovary-biased expression (>10-fold) in *P. shermani* (without singletons)	2,405 (6.1%)
Number of clusters with testis-biased expression (>10-fold) in *D. ocoee* (without singletons)	3,083 (8.4%)
Number of clusters with ovary-biased expression (>10-fold) in *D. ocoee* (without singletons)	3,298 (9.0%)

detected for a protein group, protein abundance was estimated as the mean ion intensity of the three most intense peptides (Silva et al., 2006).

Molecular Evolutionary Analysis of Courtship Pheromones and Sperm Paralogs

Homologs of pheromone proteins were identified in the gonad proteomics database by protein BLAST using sequences of PRF, PMF, and SPF for which there is proteomic evidence in plethodontid mental glands (Wilburn et al., 2012; Wilburn et al., 2014b; Doty et al., 2016). Given the high sequence divergence between TFP homolog families, additional TFP-like sequences were identified in the gonad proteomics database by searching with the regular expression ".{2}C.{5,30}C.{2,20}C.{5,30}C.{2,20}C.{5,30}CC.{4}CN" using a custom Python script. PMF and all TFP-like sequences in the sperm proteomes were compared to other TFP families using sequences from representative vertebrate species if the TFP family was amphibian-specific (Amplexin, Prod1), detected by protein BLAST with the sperm paralog of PMF regardless of e-value CD59, Ly6E, SLURP1, Prostate Stem Cell Antigen) or is associated with fertilization (SPACA4, Bouncer). Homologs of SPF were similarly curated based on homologs identified to protein BLAST to sequences of representative vertebrate species with a bias towards amphibian SPF-like sequences from the references (Van Bocxlaer et al., 2015; Maex et al., 2016; Bossuyt et al., 2019). PRF phylogenetics focused only on sequences identified in the gonad proteomics database. Protein groups were aligned using MAFFT (v7.475) with E-INS-I (Katoh and Standley, 2013), and maximum likelihood trees were estimated using raxml-ng (v.0.9.0) (Kozlov et al., 2019) with 100 starting trees (50 random, 50 parsimony) using the LG amino acid substitution matrix and gamma distributed rate heterogeneity. Branch support was computed as the transfer bootstrap effect (TBE) (Lemoine et al., 2018) from 200 bootstrap trees.

RESULTS

Transcriptomic Analysis of Plethodontid Testis and Ovary

Transcriptomic analysis of RNA isolated from testis and ovary of *P. shermani* and *D. ocoee* was performed using PacBio Iso-Seq to enumerate potential proteins within plethodontid gametes. While short-read sequencing technologies require that reads be assembled (either *de novo* or by genomic alignment) to reconstruct protein coding sequences, PacBio Iso-Seq utilizes long read single molecule sequencing with circular adapters and consensus averaging to produce high-quality, full-length transcript sequences without assembly (Gonzalez-Garay, 2016). Using RNA isolated from testis and ovary samples of both species in biological duplicate ($n = 8$), molecularly barcoded cDNA was synthesized, pooled, and sequenced using a single PacBio SMRT cell to generate a total of ~3 million reads with similar proportions for each sample (**Table 1**). Reads were clustered based on sequence similarity by the greedy algorithm isONclust into putative gene groups, and for simplicity we will refer to each read cluster as a gene. In both *P. shermani* and *D. ocoee*, comparison of relative gene expression between testis and ovary revealed dramatically different expression patterns between the gonads. Both testis and ovary express several thousand sex-biased genes (defined as >10-fold difference between the tissues), but gene expression patterns in testis were more extreme by multiple metrics. First, the mostly highly expressed genes in testis were found at ~5–10X higher levels compared to the most abundant transcripts in ovary. Second, highly abundant transcripts in testis were almost always sex-biased, while this is less common in ovary (**Figure 1**; **Table 2**; **Supplementary Table S1**). Third, testis expresses many more thousands of genes compared to ovary,

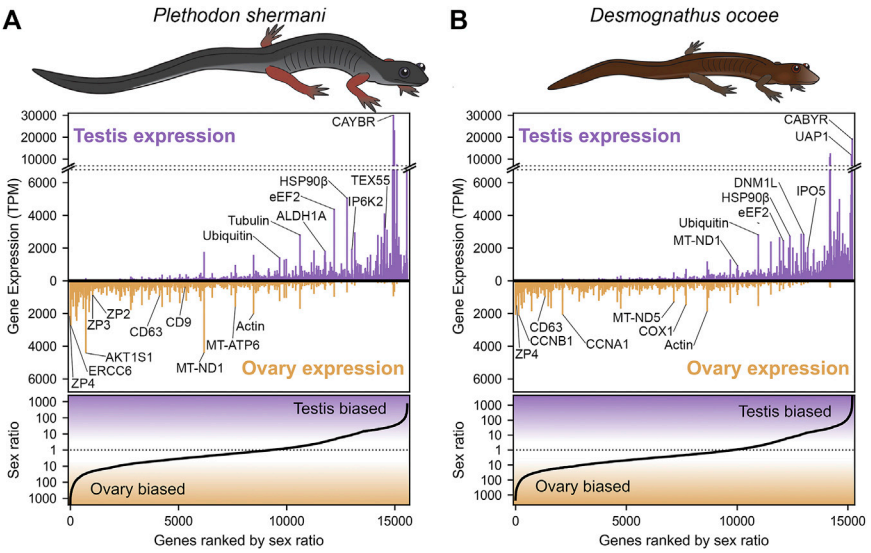

FIGURE 1 | Abundance and sex bias of gene expression in plethodontid gonads. Comparison of the relative gene expression (measured as transcripts per million, TPM) between testis and ovary for major genes (supported by at least 10 reads) identified in the plethodontid gonad transcriptome for **(A)** *P. shermani* and **(B)** *D. ocoee*. For each species, genes are ranked in order from most ovary-biased to most testis-biased with genes of interest annotated in the upper panel.

TABLE 2 | Transcriptome abundance of major sex-biased genes.

Gene	*P. shermani*				*D. ocoee*				Protein % identity
	Testis (TPM)	Ovary (TPM)	Log_{10} sex ratio	Sex ratio rank	Testis (TPM)	Ovary (TPM)	Log_{10} sex ratio	Sex ratio rank	
ZP4	0	2,166	−3.34	1	0	1,569	−3.20	3	87.6
ERCC6	3	2,734	−2.86	16	0	344	−2.54	64	90.3
SMYD3	3	2,341	−2.79	23	0	480	−2.68	36	85.7
CCNA1	26	2,203	−1.91	263	134	2,078	−1.19	2,120	94.4
Perilipin	34	2,463	−1.85	294	14	1,493	−2.00	256	83.9
CCNB1	24	1,325	−1.73	396	11	2,130	−2.25	145	93.2
ZP3	31	978	−1.49	690	2	579	−2.24	148	57.5
AKT1S1	148	4,414	−1.47	717	39	440	−1.05	2,830	96.7
ZP2	34	919	−1.42	794	0	353	−2.55	60	84.2
CD63	199	930	−0.67	4,130	38	905	−1.37	1,300	80.6
CD9	31	98	−0.50	5,362	34	211	−0.78	4,363	89.5
ALDH1a	1,844	565	0.51	11,776	1,272	49	1.41	14,056	100
eEF2	4,403	975	0.65	12,203	2,472	507	0.69	12,092	100
HSP90β	5,097	709	0.86	12,788	2,757	414	0.82	12,389	98.5
IP6K2	1,950	226	0.93	13,018	2,869	270	1.02	12,896	99.1
IPO5	1,563	83	1.27	14,179	2044	142	1.15	13,194	97.4
DNM1l	1,077	47	1.35	14,472	2,840	231	1.09	13,012	99.7
TEX55	3,245	138	1.37	14,541	2,112	66	1.50	14,273	99.4
ODF2	2,085	83	1.39	14,644	5,882	2	3.23	15,197	50.4
UPP	7,370	239	1.49	14,899	3,882	0	3.59	15,203	78.3
CABYR	30,134	949	1.50	14,935	19,530	7	3.37	15,199	86.5
spPRF	1,872	52	1.55	15,040	223	0	2.35	15,100	40.8
UAP1	3,519	93	1.57	15,072	12,158	27	2.64	15,162	100
AKAP4	7,655	200	1.58	15,096	4,214	98	1.63	14,535	100
spSPF	2,139	54	1.59	15,114	460	0	2.66	15,165	76.2

most of which are at very low abundance (i.e., singleton reads) (**Supplementary Figure S1**). This observation is consistent with genome wide transcription within testis as is common in other vertebrates and may enhance genomic fidelity through increased proofreading (Xia et al., 2020). Fourth, both within and between species, there is greater variability in the expression profiles of testis samples compared to ovary (**Supplementary Figure S2**). Such transcriptional variation in testis may relate to the percent of

testicular RNA derived from sperm versus other cell types, as well as the proportion of sperm at different stages of spermatogenesis. Both variables are known to seasonally vary from May through September (Woodley, 1994), with all samples in this study collected in August.

Examination of ovary-biased genes identified a few major functional categories common to vertebrate oocytes. The most evident example was zona pellucida (ZP) associated proteins: a family of secreted glycoproteins common to all animal oocytes that polymerize to form an extracellular egg coat that restricts sperm access to the egg plasma membrane. This egg coat is termed the zona pellucida (ZP) in mammals and the vitelline membrane (VM) in amphibians (Wassarman, 1999; Wilburn and Swanson, 2018). In both plethodontid species, homologs of the ZP genes *zp4*, *zp3*, and *zp2* were identified in the same gene expression rank order, with *zp4* being the first and third most ovary-biased genes in *P. shermani* and *D. ocoee*, respectively. This expression pattern more closely resembles the relative ZP protein abundances in the VM of *Xenopus spp*., where there is similar stoichiometry of ZP3 and ZP4 with lower levels of ZP2 (Lindsay et al., 2002) compared to the mammalian ZP where ZP3 and ZP2 are the major components with substantially less ZP4 and/or its close paralog ZP1. No other ZP genes were identified in the plethodontid transcriptome, including *zpax* and *zpd* that are minor components of the Xenopus VM, indicating that the plethodontid VM (and possibly the VM of other salamanders) may be similar but less complex than its anuran counterparts. Comparison of the *P. shermani* and *D. ocoee* sequences suggest that *zp3* may be evolving more rapidly with only 57.5% shared protein identity between the species, compared to ~85% identity for both *zp4* and *zp2*. Another interesting set of ovary biased genes were *cd9* and *cd63* that code for tetraspanin proteins associated with vesicular and cell fusion. In mammals, CD9 is highly expressed by oocytes and is considered a major candidate that facilitates sperm-egg fusion, while CD63 is more associated with exosomes found in follicular fluid produced by granulosa cells that surround oocytes and serve a different role in oogenesis (Jankovičová et al., 2015). The increased expression of *cd63* relative to *cd9* in the ovaries of both *P. shermani* and *D. ocoee* may support that salamander oocytes express both proteins, consistent with plethodontid ovaries having few if any supporting cells around developing eggs (D.B. Wilburn and P.W. Feldhoff, personal observations). Additional highly expressed ovary-biased genes common to vertebrate oocytes include *perilipin* which regulates lipid acquisition and lipid droplet formation during mammalian oogenesis (Yang et al., 2010; Zhang et al., 2014), and *smyd3* which codes for a histone methyltransferase which regulates expression of transcription factors critical for mammalian oocyte maturation and early embryonic development (Bai et al., 2016). Furthermore, one of the most abundant transcripts in *P. shermani* ovaries was a homolog of *ercc6* which in humans codes for a DNA binding protein involved in transcription-coupled DNA damage repair, and may play a role in preserving genomic fidelity in the salamander germline (Troelstra et al., 1992).

Proteomic Analysis of Mature Plethodontid Sperm

Following meiosis and compaction of the nuclear genome, vertebrate sperm and egg are usually transcriptionally silent. Gametes differentiate via a complex cellular program that selectively translates transcripts using RNA binding proteins and waves of cytoplasmic polyadenylation (Belloc et al., 2008; Brook et al., 2009). Consequently, transcriptomic profiling of gonads primarily samples RNA from immature gametes (as well as other cell types in the tissue) that may not well represent their mature, fully differentiated forms. During plethodontid courtship, sperm is transferred by the male depositing a spermatophore on the substrate which the female will accept via her cloaca. By mating salamanders in the laboratory but interrupting courtship between spermatophore deposition and insemination, we exploited this system of external sperm transfer to collect spermatophores from *P. shermani* and *D. ocoee* and performed proteomic analysis of mature sperm. For each species, tryptic peptides were prepared from four spermatophores (each from a separate male salamander) and pooled in approximately equimolar amounts (based on total ion current) for proteomic analysis by mass spectrometry. Using the gonad transcriptome supplemented with mental gland cDNA sequences as a search database, we identified a total of 7,287 peptides for 1,648 protein groups in *P. shermani* sperm and 5,308 peptides for 1,157 protein groups in *D. ocoee* sperm. Protein groups, which are defined based on shared peptides identified in the sperm proteome (see methods), typically contain multiple genes from the transcriptome analysis as sequence variation in either the coding or noncoding regions may have led to the formation of multiple read clusters that contain similar predicted proteins.

For protein groups with at least three detected peptides, protein abundance was estimated using the mean ion intensity of the three most intense ions (Silva et al., 2006; **Figure 2**). In both species, the most abundant protein was derived from genes with low transcript abundance and no significant BLAST hits. These small (~6.5 kDa), highly abundant proteins with ~50% of residues being arginine most likely function similarly to sperm protamines which replace nuclear histones following meiosis. The plethodontid protamine-like sequences are ~2–3X smaller than protamines of either mammals or *Xenopus spp*., and are devoid of cysteine residues that form intermolecular disulfide bonds and stabilize the mammalian sperm genome (Hutchison et al., 2017). Present at high levels in both the testis transcriptome and sperm proteome of both species were homologs of enzymes associated with uracil metabolism: uridine phosphorylase (UPP) and UDP-N-acetylhexosamine pyrophosphorylase (UAP1). UPP can reversibly interconvert uracil and ribose-1-phosphate into uridine and phosphate, while UAP1 converts uracil triphosphate (UTP) into UDP-N-acetylglucosamine or UDP-N-acetylgalactosamine that are substrates of protein glycosylation. In studies of human prostate cancer cell lines (Itkonen et al., 2013; Itkonen et al., 2015), activation of the

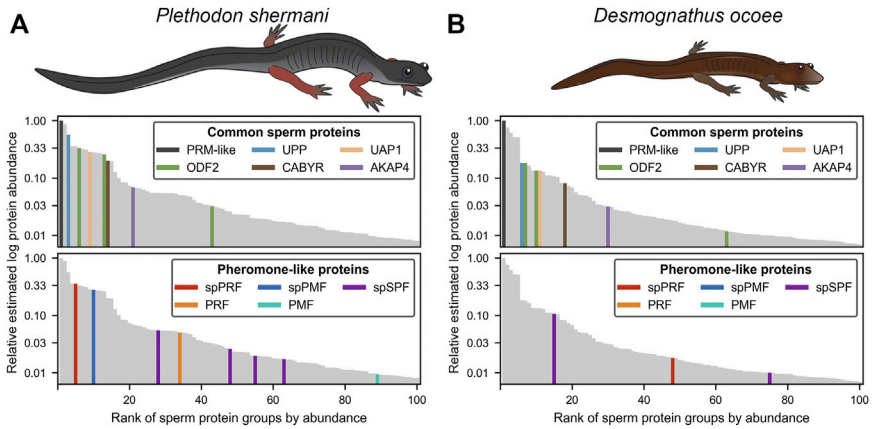

FIGURE 2 | Relative abundance of major proteins in the plethodontid sperm proteome. Comparison of the estimated protein abundance (measured as the mean intensity of the three most intense peptides per protein group) for the top 100 proteins identified in the sperm of **(A)** *P. shermani* and **(B)** *D. ocoee*. For each species, estimated protein abundances were normalized to the most abundant identified protein (which was a novel protamine-like protein in both *P. shermani* and *D. ocoee*). Proteins are ranked according to their relative abundance. Common sperm proteins and pheromone-like proteins are separately highlighted relative to the protein abundance distribution for each species.

androgen receptor (AR) increases expression of UAP1 such that similar regulatory machinery may be driving its high expression in plethodontid sperm. Also found at high levels in both the testis transcriptome and sperm proteome of both species were major proteins associated with the sperm flagellum, including multiple homologs of ODF2 that form outer dense fibers surrounding the flagellar axoneme (Zhao et al., 2018), which are further surrounded by a fibrous sheath largely comprised of AKAP4 and CABYR (Naaby-Hansen et al., 2002; Li et al., 2010). Notably, homologs of major mammalian sperm proteins associated with oocyte ZP or sperm-egg plasma membrane fusion, such as acrosin, SPACA4, or Izumo1 (Bianchi et al., 2014; Hirose et al., 2020; Fujihara et al., 2021) were observed at very low abundance in the testis transcriptome. Acrosin is the only example of these proteins that was observed in the *P. shermani* sperm proteome as the 483rd most abundant protein, and none were observed in *D. ocoee* sperm.

Beyond major structural and metabolic proteins, some of the most abundant proteins in the sperm proteomes of both *P. shermani* and *D. ocoee* were paralogs of the major mental gland pheromones SPF, PMF, and PRF. Based on signal peptide prediction, the sperm paralogs of PMF (spPMF) and SPF (spSPF) were estimated to be the most abundant secreted proteins in *P. shermani* and *D. ocoee*, respectively, while the sperm paralogs of PRF (spPRF) were surprisingly lacking signal peptides. The sperm expression patterns of these pheromone paralogs also mirror their mental gland expression within each species, with spPRF and spPMF being more abundant in *P. shermani* compared to spSPF which was more abundant in *D. ocoee*. Also surprising was the detection of the pheromone proteins themselves in the sperm proteome, but at much lower levels than their sperm-specific paralogs (*P. shermani*: [spPRF]/[PRF] ≈ 7, [spPMF]/[PMF] ≈ 30; *D. ocoee*: [spSPF]/[SPF] ≈ 27). Given the magnitude of these expression differences and known functions for the pheromones in regulating female courtship behavior (Rollmann et al., 1999; Houck et al., 2007; Wilburn et al., 2015), we hypothesize that pheromone expression in sperm is the result of leaky gene expression. As both pheromone transcript and protein levels are correlated with seasonal elevation in plasma androgen levels (Woodley, 1994; Wilburn et al., 2019), the sperm paralogs likely rely on similar regulatory machinery. High levels of *spPRF* and *spSPF* in testis of both *P. shermani* and *D. ocoee* was consistent with their elevated protein expression, while *spPMF* was much less abundant than expected with only seven transcript reads acquired from all samples. This suggests that *spPMF* may be transcribed and/or translated at a different stage of sperm development relative to the other pheromone paralogs. Interestingly, no pheromone sequences were identified in the transcriptome.

Molecular Evolutionary Analysis of Plethodontid Courtship Pheromones and Their Sperm Paralogs

To investigate the evolutionary dynamics between courtship pheromones and their sperm paralogs, detailed phylogenetic molecular evolutionary analyses were performed on each of the three pheromone families: PMF, SPF, and PRF. PMF is a family of small ~7 kDa proteins with homology to the TFP superfamily, a highly diverse family of vertebrate proteins whose functions include examples such as neurotoxins and cytotoxins within snake venoms (Fry, 2005), spatial signaling during amphibian limb regeneration (Garza-Garcia et al., 2009), membrane receptors in mammalian tissue reorganization (Blasi and Carmeliet, 2002), and regulation of the complement system (Davies et al., 1989). Despite this extraordinary array of functions, TFPs are defined by their namesake "three finger" topology that includes a 2- and 3-stranded β-sandwich stabilized by a core of eight cysteine residues that adopt an invariant disulfide bonding pattern. Some TFPs include an extra pair of cysteines that form an

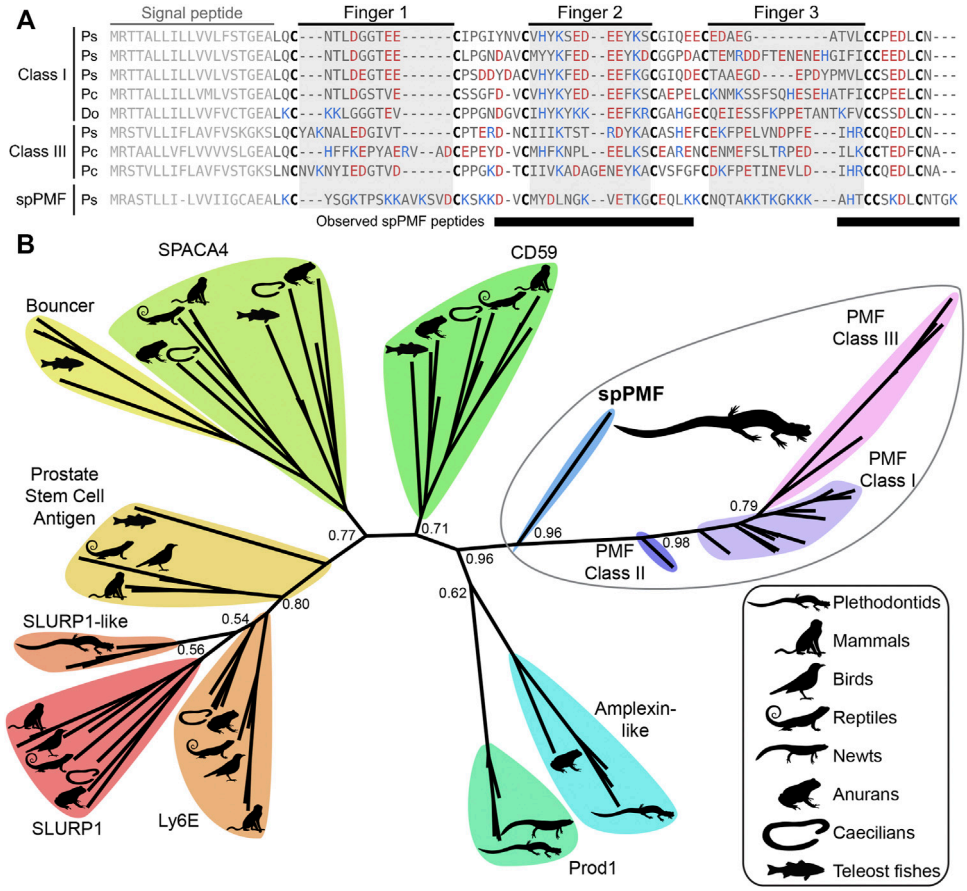

FIGURE 3 | Comparison of sperm PMF (spPMF) to pheromone PMF and other TFP proteins. **(A)** Alignment of spPMF with major class I and III PMF proteins found in the mental gland proteomes of *P. shermani* (Ps), *P. cinereus* (Pc), and *D. ocoee* (Do). Bars beneath the alignment denote sequence coverage of tryptic peptides identified in the *P. shermani* sperm proteome. Cysteine residues that define the relative spacing of the three fingers in TFPs are denoted in bold, with basic and acidic residues colored in blue and red, respectively. The signal peptide that is not part of the mature protein sequence is greyed out. **(B)** Maximum likelihood tree of spPMF and related TFP proteins in vertebrates, with branch support reported for major nodes between TFP paralogs. The three classes of PMF pheromones form a single, plethodontid-specific clade with spPMF, suggesting that a common ancestral gene gave rise to both the mental gland and sperm proteins independent of other major TFP families.

extra disulfide bond within the first finger that does not affect the arrangement of the 8-cysteine core, and we will refer to these extra disulfide containing proteins as 10C-TFPs compared to 8C-TFPs. While both the lengths of the β-strand and the exact spacing of the first 5 (or 7) cysteines can vary between homologs, the only strictly conserved sequence motif in the TFP domain is the last eight residues being CCXXXXCN, with the terminal asparagine participating in two critical H-bonds that stabilize the β-sandwich structure (Galat et al., 2008). While PMF is homologous to and possesses the sequence characteristics of 8C-TFPs, the solution structure for the most abundant PMF in the *P. shermani* mental gland revealed a novel protein topology with an altered disulfide bonding pattern (Wilburn et al., 2014a). This major PMF is only one out of more than 30 proteins in the *P. shermani* mental gland that are highly polymorphic with only ~30% average identity between amino acid sequences. The PMF coding sequence evolves extremely rapidly while the flanking untranslated regions (UTRs) within PMF mRNAs are unusually conserved with ~98% nucleotide identity in both the 5′ and 3′ UTR sequences. Analysis of the PMF UTR sequences identified three paralogous classes of PMF genes (Class I, II, and III) that were likely present in the last common ancestor of all plethodontid salamanders (Wilburn et al., 2012). Most *P. shermani* PMFs are of Class I or III (~50% total pheromone by mass) while the *D. ocoee* mental gland expresses only a single Class I PMF at low levels (<5% total pheromone) (Chouinard et al., 2013; Doty et al., 2016).

The sequence of spPMF possesses several notable characteristics when compared to the major pheromone PMFs of *P. shermani*, *D. ocoee*, and an intermediate species *Plethodon cinereus* (**Figure 3A**). While most PMFs are highly negatively charged, spPMF has an estimated net charge of +14 at physiological pH with 20 out of the 71 residues being lysine and none are arginine. The density of these positive charges is especially high in finger 3, which also possesses a potential N-glycosylation site following Cys 5. Despite the large number

of lysine residues, spPMF lacks a lysine at position 30 that normally would form a salt bridge with E35 to stabilize finger 2. The C-terminus of spPMF also contains a unique three residue extension (TGK) past the conserved asparagine, with peptide coverage from the proteomics data confirming that these additional residues are present in the mature protein. There was no detectable sequence similarity between the spPMF UTRs to those of Class I, II, or III. Protein BLAST searches of spPMF returned PMF as the top hit but with only modest confidence (e-value ~ 1e-5), and given the extreme sequence differences, it was unclear if spPMF might be more closely related to another 8C-TFP family. Phylogenetic analysis was performed with a diverse panel of TFP sequences that included all characterized PMFs, all TFP sequences in the sperm proteomes (including spPMF), as well as representatives of other amphibian-specific TFPs (Amplexin, Prod1), families detected by BLAST searches of plethodontid gonad-associated TFPs regardless of e-value (CD59, Ly6E, SLURP1, Prostate Stem Cell Antigen), and TFPs with known reproductive functions (SPACA4, Bouncer). Based on the estimated maximum likelihood tree, spPMF was found on a relatively long branch adjacent to the pheromone PMFs, supporting that they share a more recent common ancestor compared to all other analyzed TFPs (**Figure 3B**). Since the gene duplications that gave rise to the three PMF classes likely occurred in the last common ancestor of plethodontid salamanders, this topology suggests that the duplication event separating PMF and spPMF is similarly ancient. Sister to PMF/spPMF are the other amphibian specific families Prod1 and Amplexin-like proteins, both of which are present in plethodontid salamanders, supporting that a single gene duplication of an ancestral amphibian TFP may have given rise to the ancestor of PMF and spPMF. As presence of a mental gland are considered the ancestral condition of plethodontid salamanders (Sever et al., 2016), it is unclear in which tissue such a PMF-like ancestor may have originated, but likely evolved to function as both a pheromone and a sperm protein at similar evolutionary points.

SPF is an incredibly ancient pheromone family with homologs that influence female mating behavior in both caudates (salamanders and newts) and anurans (frogs and toads), implying that SPF has played a critical role in amphibian reproduction for ~360 million years (Bossuyt et al., 2019). An ancient gene duplication of SPF produced two families, SPFα and SPFβ, that were both present in the last common ancestor of amphibians, with subsequent duplications giving rise to multiple paralogs within all examined taxa (Janssenswillen et al., 2014). The mental gland pheromones of plethodontid salamanders are derived from SPFα while most characterized pheromones in other caudates and frogs are descended from SPFβ (Maex et al., 2016). Recent transcriptomic analysis supports that plethodontid salamanders may express SPFβ pheromones in other courtship glands (Herrboldt et al., 2021). Like PMF, SPF is also homologous to the TFP superfamily as a distantly related subfamily that arose from a tandem duplication of 10C-TFPs and has two TFP-like domains. In the major SPF of *D. ocoee*, both TFP-like domains have highly altered disulfide bonding patterns that likely produce distinct topologies and are not classical TFPs (Doty et al., 2016). To characterize the relationship between SPF and spSPF, a maximum likelihood tree was generated based on SPF homologs identified by BLAST for all major vertebrate clades where SPFs from salamanders and newts were overrepresented to improve resolution around plethodontid sequences (**Figure 4A**). Manual examination of these sequences identified five variations of cysteine spacings that ranged in complexity from two stereotypical 10C-TFP patterns to the highly altered arrangement determined for the major *D. ocoee* SPF (**Figure 4B**). Teleost fish exclusively had predicted proteins with two canonical 10C-TFP patterns – the likely ancestral condition of these SPF-like proteins – and the maximum likelihood tree was rooted on the branch of fish homologs with true two domain TFPs (2D-TFPs). All spSPF sequences shared the same cysteine spacing where the first TFP-like domain had a normal 10C-TFP pattern and the second domain was missing the conserved C-terminal CCXXXXCN motif critical for stabilizing the β-sandwich structure. While the plethodontid pheromone SPFs formed a single clade nested among other SPFα sequences, spSPF sequences identified in the gonad transcriptome localized to five well supported clades (>90% bootstrap support): 3 in SPFβ and 2 in SPFα. The most abundant spSPF proteins in both *P. shermani* and *D. ocoee* sperm was localized to one of the SPFβ clades with close homology to SPF12 and SPF13 from the Mexican axolotl (*Ambystoma mexicanum*). Maex et al. (2016) identified multiple new SPF proteins in male axolotl salamanders with transcriptomic analysis suggesting that most paralogs were expressed by male cloacal glands. However, SPF12/13 were unusual compared to other paralogs with ~100–5,000x lower transcript abundance in cloacal glands despite strong proteomic evidence of the proteins in water that was inhabited by male salamanders during mating. The close phylogenetic relationship of axolotl SPF12/13 with spSPF of both *P. shermani* and *D. ocoee* suggests that these axolotl proteins may instead be sperm proteins rather than pheromones, and would place the origin of spSPF at the base of modern salamanders (~160 million years ago) (Shen et al., 2015). In contrast to PMF where a single plethodontid gene likely gave rise to both the pheromone and sperm paralogs, the role of SPF in these two reproductive contexts arose independently from ancient paralogs that appears to have duplicated ~360 million years ago in the last common ancestor of amphibians.

While SPF and PMF are ancestral to all plethodontid salamanders (~66 million years ago), PRF is a relatively young pheromone family related to α-helical cytokines and only present in the mental gland of *Plethodon* spp. from eastern North America that evolved ~17 million years ago (Shen et al., 2015). Detection of spPRF in both the transcriptome and proteome of *D. ocoee* (separated from *P. shermani* by ~43 million years) implies that spPRF is much older than the pheromone paralogs and likely originated as a sperm protein. BLAST searches of both spPRF and PRF to annotated vertebrate genomes identified cardiotrophins as the most similar homologs by sequence. Cardiotrophin-like sequences were identified with low but testis-biased expression in the gonad transcriptomes of both *P. shermani* and *D. ocoee*, supporting the hypothesis that the

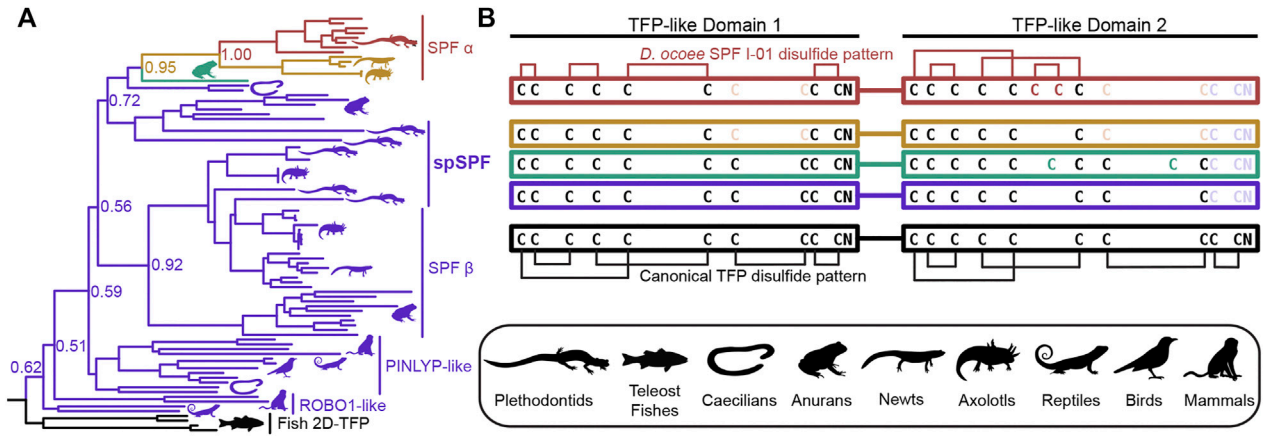

FIGURE 4 | Evolution of SPF protein evolution relative to 2D-TFPs. **(A)** A maximum likelihood tree of SPF-like protein sequences from representative vertebrates with overrepresentation of salamanders and newts, where numbers denote branch support of major nodes. Tree branches are colored according to the arrangement of cysteine residues in the underlying sequence alignment as denoted in **(B)**. Black denotes the ancestral condition of two tandem 10C-TFP sequences that likely adopt the canonical disulfide pattern, and additional colors denoting sequential cysteine loss (light color text) and gain (dark color text), with the empirically determined disulfide pattern of *D. ocoee* SPF-I01 shown in red (Doty et al., 2016). The three is rooted on the branch of teleost fish proteins that are the only available sequences with the ancestral 2D-TFP cysteine spacing. Plethodontid mental gland pheromone SPF sequences are exclusively found within the red SPFα clade, with different spSPF paralogs being found in both the upper SPFα and lower SPFβ clades that share the purple cysteine pattern. The phylogenetic separation of the plethodontid pheromones from spSPF supports that each protein family was independently derived from gene duplications present in the last common ancestor of amphibians ~360 million years ago.

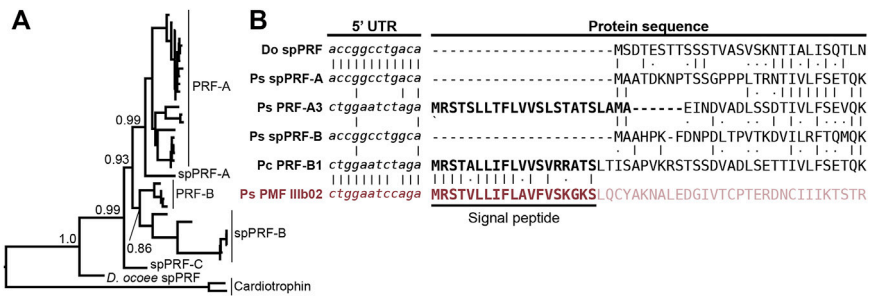

FIGURE 5 | Multiple independent origins of pheromone PRF and recombination with PMF. **(A)** A maximum likelihood-based phylogeny of PRF and spPRF with numbers denoting branch support of major nodes and rooting based on cardiotrophin-like sequences from *P. shermani* and *D. ocoee*. The topology supports that an ancestral spPRF gene repeatedly duplicated into at least three families in *Plethodon*, and subsequent gene duplications of spPRF-A and B independently gave rise to PRF-A and B pheromone families. **(B)** Alignment of select PRF and PMF sequences around the translation start site of each protein. Despite high similarity in 5′ UTR and N-terminal protein sequence of spPRF from *D. ocoee* (Do) and *P. shermani* (Ps), representative PRF-A and B sequences from *P. shermani* and *P. cinereus* (Pc), respectively, have a distinct 5′ UTR sequence in addition to a signal peptide. This new PRF leader sequence is highly similar to that of PMF class III, such that it was likely acquired via recombination following the independent duplications of spPRF-A and B that gave rise to PRF-A and B, respectively.

common ancestor of these proteins may have also had male-biased expression that facilitated the co-option of spPRF from cardiotrophins for sperm function. A maximum likelihood tree was estimated from all cardiotrophin and spPRF sequences identified in the gonad transcriptome in addition to representative PRF pheromone sequences from each major clade of eastern *Plethodon* spp. The cardiotrophin-like sequences from *P. shermani* and *D. ocoee* testis were found on a single long branch that was used to root the phylogeny (**Figure 5A**). The first branch in the PRF/spPRF clade separated all *Plethodon* sequences from *D. ocoee* spPRF, consistent with a sperm origin for PRF-like proteins. Within *Plethodon*, spPRF sequences were found in three separate clades and named according to homology with pheromone PRF types. Prior molecular evolutionary analysis identified two families of pheromone PRF: PRF-A which is common to all eastern *Plethodon spp.* and PRF-B which is only found in species closely related to *P. cinereus* with transdermal pheromone delivery (Wilburn et al., 2014b). As expression of PRF-B was only found in species with the more ancestral delivery system, it was hypothesized to be older than PRF-A (Watts et al., 2004). Instead, the updated phylogeny with spPRF sequences strongly supports that PRF-A and PRF-B arose independently from different spPRF paralogs termed spPRF-A and spPRF-B,

respectively (**Figure 5A**). We were unable to distinguish the relative abundance of spPRF-A and spPRF-B in the *P. shermani* sperm proteome as most of the high intensity spPRF peptides are common to both paralogs. The third clade of spPRF termed spPRF-C is likely ancestral to spPRF-A/spPRF-B but at much lower abundance, as few reads were identified in the testis transcriptome and no peptides unique to spPRF-C were detected in the sperm proteome. Compared to the unique histories of SPF/spSPF evolving independently and PMF/spPMF likely sharing a single origin, a third pattern is observed for PRF/spPRF where a family of sperm proteins was independently co-opted multiple times for pheromone activity.

In contrast to the pheromones and their sperm paralogs discussed so far, all spPRF sequences lack a signal peptide that would normally target it for secretion indicating that spPRF may be an intracellular protein. Peptides that include the initiator methionine of both spPRF-A and spPRF-B were observed in the *P. shermani* sperm proteome confirming that there is not a cryptic N-terminal signal peptide. To the best of our knowledge, spPRF is the first cytokine-like protein identified without a signal peptide. Presence of signal peptides in the testis-biased cardiotrophin-like sequences supports that spPRF lost its signal peptide following duplication from a cardiotrophin-like ancestor. While PMF and SPF require the oxidizing environment of the endoplasmic reticulum for proper disulfide bond formation, PRF adopts a predominantly α-helical fold without disulfides that could fold independently in cytoplasm (Houck et al., 2008). Secondary structure prediction of spPRF supports that it forms a similar α-helical topology and has no additional cysteine residues. Interestingly, while spPRF may be intracellular, both PRF-A and PRF-B have signal peptides despite independently arising from spPRFs lacking them. It was noticed that the PRF signal peptides were similar in amino acid sequence to those of PMF. Based on unpublished partial genomic sequences, the gene structure of PMF includes three coding exons homologous to other TFP genes where ~90% of the signal peptide is coded by the first exon. Based on the shared sequence similarity and the high co-expression of PRF and PMF in *Plethodon* mental glands, we hypothesized that the PRF signal peptide may have been co-opted from a PMF gene. Manual alignment of the signal peptides between PRF-A/B and PMF classes I-III found the highest similarity between PRF-B and PMF Class III. Expansion of the alignment into the 5′ UTR immediately upstream revealed almost identical sequences between PRF-A, PRF-B, and PMF Class III that was distinct from spPRFs of both *P. shermani* and *D. ocoee* (**Figure 5B**). As the UTRs are ~98% identical between PMF paralogs of the same class, this high level of conservation in the PRF and PMF class III 5′ UTR strongly supports that an ancestral spPRF gene duplicated and recombined with a class III-like PMF to ultimately become PRF expressed by the mental gland. Given the independent origins of PRF-A and PRF-B, and the sequences of their 5′ UTR and signal peptides relative to PMF class III, our hypothesis as to the order of events is that spPRF-B duplicated and recombined with PMF class III to yield PRF-B, followed by spPRF-A duplicating and recombining with PRF-B to produce PRF-A.

DISCUSSION

Gametic fusion is an essential biological process for the reproduction of most animal species, yet despite more than a century of research, it largely remains a molecular enigma as to *how* these highly specialized cells mechanistically accomplish this feat with species-specificity. The earliest studies of fertilization were in external fertilizing marine invertebrates where large numbers of gametes could be easily isolated for biochemical fractionation, and research continues for classic models such as sea urchins and abalone where the molecular interactions of sperm and egg proteins are best characterized (Wilburn et al., 2019; Wessel et al., 2021). Advances in gene editing technologies have elevated genetic knockouts as one of the primary tools to identify gamete recognition proteins, especially in mammals, but high rates of gene duplication and functional redundancy in gametic proteins can confound such studies (Baba et al., 1994; Isotani et al., 2017; Hirose et al., 2020). Due to these many challenges, there are currently only four *bona fide* pairs of interacting sperm-egg proteins identified in any animal species (Wilburn and Swanson, 2016). The extraordinarily fast evolution of reproductive proteins also facilitates the birth and death of new fertilization genes, resulting in gametic proteins often being shared by only closely related taxa and limiting the inferences that can be made about more distantly related species. As such, there is a need within reproductive biology to expand the taxonomic breadth of model systems and more attention paid to clades that have been historically understudied. As a prime example of this myopia, amphibians are a major class of vertebrates with more than 6,000 species that have evolved over ~360 million years, and yet molecular characterization of amphibian gametes has been limited to a single genus of frogs (*Xenopus spp.*). In this study, we have provided the first detailed transcriptomic and proteomic analysis of gametes for one of the other major amphibian types: salamanders.

One of the most unusual qualities of plethodontid salamanders is the enormous size of their genomes: compared to the ~3 billion base pair haploid genome of humans, the sizes of the *P. shermani* and *D. ocoee* haploid genomes are ~27 billion and ~17 billion base pairs, respectively (Herrick and Sclavi, 2014). Plethodontid genomes contain high levels of long retrotransposons in intronic and intergenic regions (Sun et al., 2012), and this enormous genome likely creates unique challenges during gametogenesis such as proper meiotic chromosome segregation, maintenance of genome fidelity, as well as regulation of transcription and splicing of sex-specific genes with very large introns. Two of the most abundant ovary-biased transcripts code for the DNA repair protein ERCC6 and the histone methyltransferase SMYD3 which aid in these processes. The most abundant sperm protein of both species is an extremely positively charged ~6.5 kDa protein that resembles protamines of other vertebrates and likely functions in replacement of histones as scaffolding for the nuclear genome. These protamine-like proteins are smaller and more arginine rich than their likely mammalian and *Xenopus* analogs, making them likely intrinsically disordered absent DNA. DNA packaged with poly-Arg is more dense than when packaged with poly-Lys

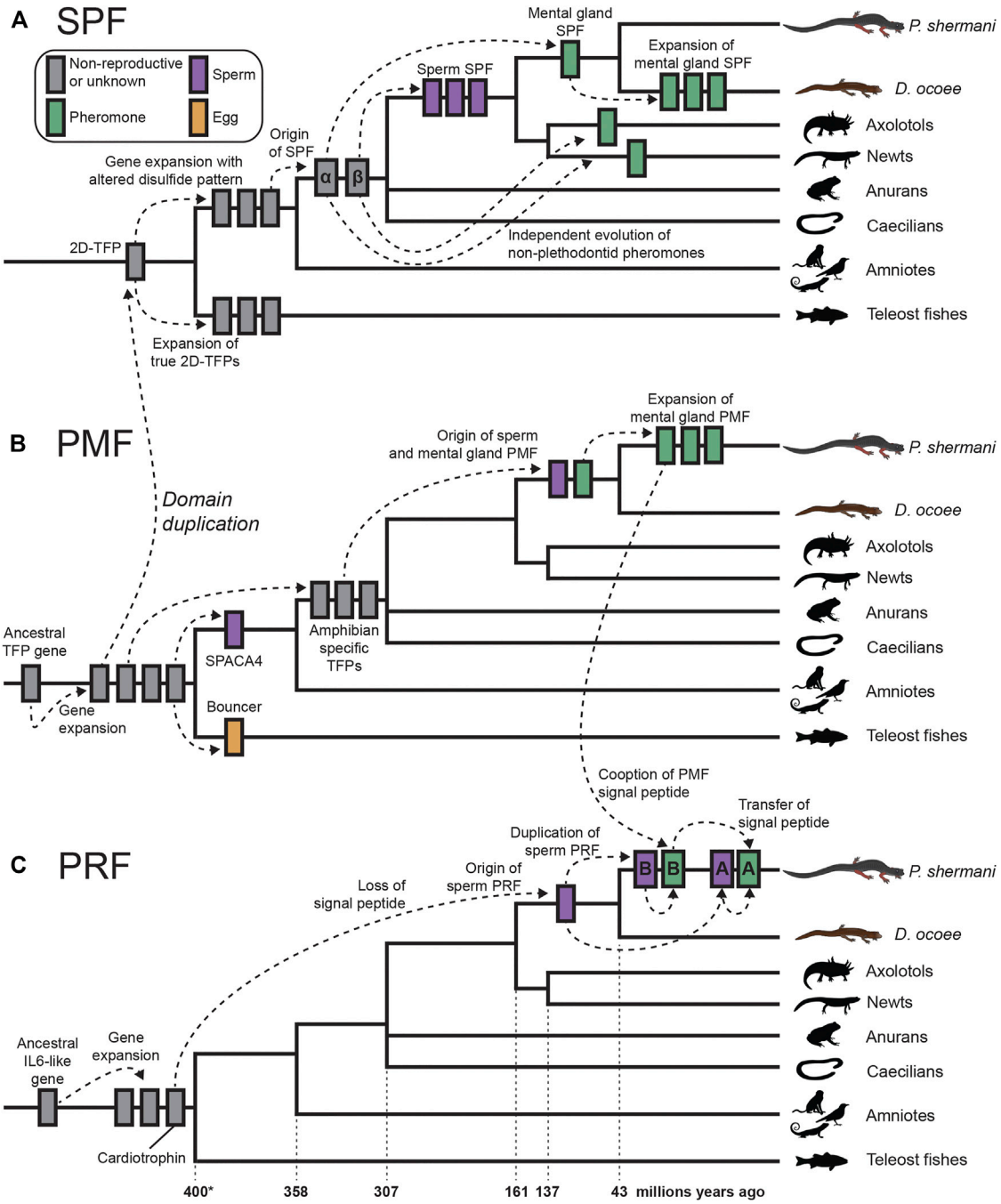

FIGURE 6 | Proposed model of cytokine and TFP evolution generating both plethodontid pheromones and sperm proteins. **(A)** An ancestral tandem duplication of a 10C-TFP protein produced the first 2D-TFP that subsequently expanded into independent families, with teleost fish having 2D-TFPs that retained the canonical disulfide patterns, and tetrapods having a separate family with a different disulfide pattern (purple in **Figure 4**). Further duplication of these tetrapod proteins resulted in the SPFα and SPFβ families within amphibians that independently gave rise to multiple descendants, including plethodontid pheromones from SPFα and spSPF from SPFβ. Within plethodontids, further expansion of pheromone SPFs occurred in *D. ocoee* relative to *P. shermani*. **(B)** A progenitor 8C-TFP gene expanded at the base of vertebrates giving rise to several families, including the 10C-TFP from which SPF is originally derived. Another 10C-TFP led to the evolution of SPACA4 in tetrapod sperm and Bouncer in fish oocytes. Continued evolution of an 8C-TFP family led to the evolution of PMF in plethodontid salamanders, likely through an amphibian-specific intermediate, with sperm and mental gland paralogs evolving nearly simultaneously. Following transition from transdermal to olfactory delivery, there was a large expansion of PMF genes in *P. shermani* relative to *D. ocoee*. **(C)** PRF is distantly related to IL-6 cytokines and expanded into several related genes early in vertebrate evolution, including a cardiotrophin-like gene. Within plethodontid salamanders, a descendent of the cardiotrophins duplicated and lost its signal peptide to yield spPRF. Continued expansion of spPRF genes in *Plethodon* spp. resulted in spPRF-A and B that independently duplicated into PRF-A and B, respectively. PRF-A and B seemingly reacquired extracellular expression through recombination with a PMF gene. Based on the sequence alignment, we propose that PRF-B first co-opted the PMF signal peptide (and partial 5′ UTR sequence), with PRF-A acquiring its signal peptide by recombination with PRF-B.

(DeRouchey et al., 2013), and there may be a high premium on more tightly condensing the nuclear genome in the relatively small sperm cell. A more efficient system of nuclear packaging may also more effectively inhibit transcription in developing sperm, and if so, this may help explain the discrepancy in transcript and protein abundance in testis versus mature sperm, respectively.

For both plethodontid species, most genes with ovary biased expression coded for structural and metabolic proteins common to animal oocytes and we found no clear examples of salamander-specific innovations. Among the structural proteins, we were particularly interested in ZP genes that code for proteins in the VM, the extracellular egg coat that functions as a molecular gate to restrict both the number and species of sperm that may fertilize an oocyte. The plethodontid VM is likely similar in composition to the *Xenopus* VM with ZP4 and ZP3 being the major glycoproteins with smaller amounts of ZP2. Compared to other vertebrate clades, the amphibian VM is most biochemically similar to the mammalian ZP, and mouse ZP proteins are even able to integrate into the *Xenopus laevis* VM when synthetic mRNAs are microinjected into developing oocytes (Doren et al., 1999). While the molecular mechanisms of both mammalian ZP and *Xenopus* VM dissolution are poorly characterized, a few sperm proteins that physically interact with the mammalian ZP have been identified (Mori et al., 1993), although we found no homologs of these proteins in either the gonad transcriptome or sperm proteomes. Recently, a membrane-bound 10C-TFP called SPACA4 was implicated in mammalian ZP dissolution when sperm from *spaca4*-null mice could only fertilize oocytes without a ZP (Fujihara et al., 2021). While the precise function of SPACA4 remains unknown, the possible role of a TFP in ZP dissolution is intriguing given that spPMF and spPRF are likely the most abundant secreted sperm proteins in *P. shermani* and *D. ocoee*. The extreme positive charge of spPMF is also comparable to highly positively charged fertilization proteins in the marine mollusk abalone that mediate both egg coat dissolution and egg-sperm plasma membrane fusion (Wilburn et al., 2019). SPACA4 was present in the gonad transcriptome at very low levels and no peptides were detected in the sperm proteome of either species.

The evolutionary dynamics of the plethodontid courtship pheromones and their sperm paralogs spotlights the tremendous diversity of reproductive functions possible from only two protein families that are repeatedly subjected to gene duplication and sexual selection (summarized in **Figure 6**). SPF is the oldest known family of protein pheromones that evolved ~360 million years ago, derived from the ancestral tandem duplication of a 10C-TFP into the 2D-TFPs. Many paralogs of SPF are common in amphibian secretory glands which may be delivered by an array of courtship behaviors. For example, male palmate newts with aquatic reproduction release SPF into the water column from their cloaca and use their tails to propel these pheromones posteriorly to create a concentration gradient for chemotaxis (Van Bocxlaer et al., 2015). This passive broadcast of SPF pheromones contrasts with private transfer of SPF proteins when a male *D. ocoee* abrades the dorsum to a single female with his premaxillary teeth where pheromones are presumably diffused into the female bloodstream rather than stimulate the olfactory system (Houck et al., 2007). Recently, an extremely similar system was discovered in *Plectrohyla* frogs where males scratch the female dorsum with their teeth delivering SPF expressed by glands in the upper lip (Schulte et al., 2021). Despite the similarity in delivery system, the SPF pheromones of plethodontid salamanders and *Plectrohyla* frogs are independently derived from the SPFα and SPFβ families, respectively, that arose by gene duplication in a common ancestor of amphibians. As the highly abundant spSPF proteins in plethodontid sperm are also part of the SPFβ family, the original duplication that gave rise to these two distinctive plethodontid proteins also occurred at the base of amphibian evolution ~360 million years ago. The major spSPF proteins are only ~76% identical between *P. shermani* and *D. ocoee* such that sexual selection from coevolving female oocyte receptors may be driving rapid evolution, although both functional studies and sequencing of spSPF in additional plethodontid species are necessary to test this hypothesis. The evolution of spSPF is one example of at least three independent recruitments of TFP-like proteins into vertebrate gametes. Another TFP recruitment of TFPs for reproduction is SPACA4 in tetrapod sperm and its close teleost fish homolog Bouncer which regulates species-specific egg-sperm fusion (Herberg et al., 2018). It is intriguing that closely related TFP proteins are expressed in both male and female gametes of different vertebrate clades but it remains unknown if egg Bouncer represents an ancestral condition of these proteins or if Bouncer/SPACA4 are independent paralogs that happen to share a more recent common ancestor than other TFPs. The third TFP recruitment is PMF, a plethodontid-specific TFP-like family that seemingly evolved from an amphibian-specific TFP ancestor as both a sperm protein and courtship pheromone ~43 million years ago (Shen et al., 2015). Following the innovation of olfactory pheromone delivery in *Plethodon spp*., the number and diversity of PMF genes rapidly expanded with the mental gland expressing >30 rapidly evolving proteins (Wilburn et al., 2012). Given the extraordinary molecular sensitivity and specificity of ligand binding to olfactory receptors (Leinders-Zufall et al., 2009), we hypothesized that transition from transdermal to olfactory delivery reduced the minimum concentration of PMF necessary to stimulate female receptors and expressing more PMF proteins maximizes the chances of male reproductive success (Wilburn et al., 2014b). By contrast, the expression of a single highly abundant spPMF by *P. shermani* sperm may be indicative of stoichiometric binding to an abundant egg receptor.

Of the three major pheromone families, PRF has perhaps the most convolved evolutionary history: a secreted cardiotrophin-like ancestor lost its signal peptide to become a likely cytoplasmic sperm protein, followed by a gene duplication of this spPRF recombining with PMF to reacquire secretion as a pheromone. It is especially remarkable that this signal peptide reacquisition for pheromone PRF occurred twice, with PRF-A and PRF-B arising independently from spPRF-A and spPRF-B, respectively. Based on 5′ UTR and signal peptide sequences, we hypothesize this occurred through a two-step duplication process where PRF-B acquired its signal peptide from PMF class III, and then PRF-A acquired its

signal peptide from PRF-B. While PMF and other TFPs are highly prone to gene duplication, it is conspicuous that the PRF signal peptide arose from a highly expressed gene in the same tissue and may suggest an important role of transcriptionally active genes being more prone to gene duplication because of chromatin structure. This would be especially relevant for highly expressed gametic genes where duplications could fix in the germline and be more exposed to natural or sexual selection. Abundant expression of all three pheromones in the plethodontid sperm proteome (although at lower levels than the sperm paralogs) may indicate leaky expression of androgen responsive genes during sperm maturation, which could expose these pheromone loci to similar modes of gene evolution as their sperm-specific paralogs. This complex interplay between genes expressed by male secondary sex characteristics can likely help explain both the extraordinary number and the rapid evolution of plethodontid pheromone proteins. In summary, our transcriptomic and proteomic analyses of plethodontid gametic proteins highlight the novelty of reproductive proteins present in poorly characterized species, such as salamanders, and how new fertilization proteins may evolve to facilitate species-specific fertilization in vertebrates.

DATA AVAILABILITY STATEMENT

The datasets presented in this study can be found in online repositories. The names of the repository/repositories and accession number(s) can be found below: https://www.ncbi.nlm.nih.gov/PRJNA785352; http://www.proteomexchange.org/ PXD030143.

ETHICS STATEMENT

The animal study was reviewed and approved by Highlands Biological Station Institutional Animal Care and Use Committee.

AUTHOR CONTRIBUTIONS

DW, RF, and PF contributed to the conception and design of the study. DW, CK, RF, and PF performed field collections, animal care, staged courtship trials, and dissection for tissue collection. DW prepared transcriptomic libraries and proteomic samples. BS performed all mass spectrometry experiments. DW and BS analyzed the data. DW drafted the manuscript with revisions from BS and RF. All authors read and approved the submitted version.

FUNDING

This work was supported in part by National Institutes of Health grants K99-HD090201 to DW. and R01-GM133981 to BS., as well as Highlands Biological Statin Grant-in-Aid to DW.

SUPPLEMENTARY MATERIAL

The Supplementary Material for this article can be found online at: https://www.frontiersin.org/articles/10.3389/fcell.2022.828947/full#supplementary-material

REFERENCES

Almagro Armenteros, J. J., Tsirigos, K. D., Sønderby, C. K., Petersen, T. N., Winther, O., Brunak, S., et al. (2019). SignalP 5.0 Improves Signal Peptide Predictions Using Deep Neural Networks. *Nat. Biotechnol.* 37, 420–423. doi:10.1038/s41587-019-0036-z

Amodei, D., Egertson, J., Maclean, B. X., Johnson, R., Merrihew, G. E., Keller, A., et al. (2019). Improving Precursor Selectivity in Data-independent Acquisition Using Overlapping Windows. *J. Am. Soc. Mass. Spectrom.* 30, 669–684. doi:10.1007/s13361-018-2122-8

Amphibiaweb (2021). *Information on Amphiban Biology and Conservation [web Application] [Online]*. Berkeley, California: AmphibiaWeb. Available at: http://amphibiaweb.org (Accessed December 2, 2021).

Arnold, S. J., and Houck, L. D. (2016). Can the Fisher-Lande Process Account for Birds of Paradise and Other Sexual Radiations? *The Am. Naturalist* 187, 717–735. doi:10.1086/686258

Avella, M. A., Baibakov, B., and Dean, J. (2014). A Single Domain of the ZP2 Zona Pellucida Protein Mediates Gamete Recognition in Mice and Humans. *J. Cel. Biol.* 205, 801–809. doi:10.1083/jcb.201404025

Baba, T., Azuma, S., Kashiwabara, S., and Toyoda, Y. (1994). Sperm from Mice Carrying a Targeted Mutation of the Acrosin Gene Can Penetrate the Oocyte Zona Pellucida and Effect Fertilization. *J. Biol. Chem.* 269, 31845–31849. doi:10.1016/s0021-9258(18)31772-1

Bai, H., Li, Y., Gao, H., Dong, Y., Han, P., and Yu, H. (2016). Histone Methyltransferase SMYD3 Regulates the Expression of Transcriptional Factors during Bovine Oocyte Maturation and Early Embryonic Development. *Cytotechnology* 68, 849–859. doi:10.1007/s10616-014-9838-5

Belloc, E., Piqué, M., and Méndez, R. (2008). Sequential Waves of Polyadenylation and Deadenylation Define a Translation Circuit that Drives Meiotic Progression. *Biochem. Soc. Trans.* 36, 665–670. doi:10.1042/bst0360665

Bianchi, E., Doe, B., Goulding, D., and Wright, G. J. (2014). Juno Is the Egg Izumo Receptor and Is Essential for Mammalian Fertilization. *Nature* 508, 483–487. doi:10.1038/nature13203

Blasi, F., and Carmeliet, P. (2002). uPAR: a Versatile Signalling Orchestrator. *Nat. Rev. Mol. Cel Biol* 3, 932–943. doi:10.1038/nrm977

Bossuyt, F., Schulte, L. M., Maex, M., Janssenswillen, S., Novikova, P. Y., Biju, S. D., et al. (2019). Multiple Independent Recruitment of Sodefrin Precursor-like Factors in Anuran Sexually Dimorphic Glands. *Mol. Biol. Evol.* 36, 1921–1930. doi:10.1093/molbev/msz115

Brook, M., Smith, J. W. S., and Gray, N. K. (2009). The DAZL and PABP Families: RNA-Binding Proteins with Interrelated Roles in Translational Control in Oocytes. *Reproduction* 137, 595–617. doi:10.1530/rep-08-0524

Camacho, C., Coulouris, G., Avagyan, V., Ma, N., Papadopoulos, J., Bealer, K., et al. (2009). BLAST+: Architecture and Applications. *BMC Bioinformatics* 10, 421. doi:10.1186/1471-2105-10-421

Chambers, M. C., Maclean, B., Burke, R., Amodei, D., Ruderman, D. L., Neumann, S., et al. (2012). A Cross-Platform Toolkit for Mass Spectrometry and Proteomics. *Nat. Biotechnol.* 30, 918–920. doi:10.1038/nbt.2377

Chouinard, A. J., Wilburn, D. B., Houck, L. D., and Feldhoff, R. C. (2013). "Individual Variation in Pheromone Isoform Ratios of the Red-Legged Salamander, *Plethodon shermani*," in *Chemical Signals in Vertebrates 12*. Editors M. L. East and M. Dehnhard (New York: Springer), 99–115. doi:10.1007/978-1-4614-5927-9_8:

Davies, A., Simmons, D. L., Hale, G., Harrison, R. A., Tighe, H., Lachmann, P. J., et al. (1989). CD59, an LY-6-like Protein Expressed in Human Lymphoid Cells, Regulates the Action of the Complement Membrane Attack Complex on Homologous Cells. *J. Exp. Med.* 170, 637–654. doi:10.1084/jem.170.3.637

Derouchey, J., Hoover, B., and Rau, D. C. (2013). A Comparison of DNA Compaction by Arginine and Lysine Peptides: a Physical Basis for Arginine Rich Protamines. *Biochemistry* 52, 3000–3009. doi:10.1021/bi4001408

Doren, S., Landsberger, N., Dwyer, N., Gold, L., Blanchette-Mackie, J., and Dean, J. (1999). Incorporation of Mouse Zona Pellucida Proteins into the Envelope of *Xenopus laevis* Oocytes. *Develop. Genes Evol.* 209, 330–339. doi:10.1007/s004270050261

Doty, K. A., Wilburn, D. B., Bowen, K. E., Feldhoff, P. W., and Feldhoff, R. C. (2016). Co-option and Evolution of Non-olfactory Proteinaceous Pheromones in a Terrestrial Lungless Salamander. *J. Proteomics* 135, 101–111. doi:10.1016/j.jprot.2015.09.019

Fry, B. G. (2005). From Genome to "venome": Molecular Origin and Evolution of the Snake Venom Proteome Inferred from Phylogenetic Analysis of Toxin Sequences and Related Body Proteins. *Genome Res.* 15, 403–420. doi:10.1101/gr.3228405

Fujihara, Y., Herberg, S., Blaha, A., Panser, K., Kobayashi, K., Larasati, T., et al. (2021). The Conserved Fertility Factor SPACA4/Bouncer Has Divergent Modes of Action in Vertebrate Fertilization. *Proc. Natl. Acad. Sci.* 7118, 4. doi:10.1073/pnas.2108777118

Galat, A., Gross, G., Drevet, P., Sato, A., and Ménez, A. (2008). Conserved Structural Determinants in Three-Fingered Protein Domains. *FEBS J.* 275, 3207–3225. doi:10.1111/j.1742-4658.2008.06473.x

Garza-Garcia, A., Harris, R., Esposito, D., Gates, P. B., and Driscoll, P. C. (2009). Solution Structure and Phylogenetics of Prod1, a Member of the Three-finger Protein Superfamily Implicated in Salamander Limb Regeneration. *PLOS ONE* 4, e7123. doi:10.1371/journal.pone.0007123

Gessulat, S., Schmidt, T., Zolg, D. P., Samaras, P., Schnatbaum, K., Zerweck, J., et al. (2019). Prosit: Proteome-wide Prediction of Peptide Tandem Mass Spectra by Deep Learning. *Nat. Methods* 16, 509–518. doi:10.1038/s41592-019-0426-7

Gonzalez-Garay, M. L. (2016). *Introduction to Isoform Sequencing Using pacific Biosciences Technology (Iso-Seq)*. Dordrecht: Springer, 141–160. doi:10.1007/978-94-017-7450-5_6

Herberg, S., Gert, K. R., Schleiffer, A., and Pauli, A. (2018). The Ly6/uPAR Protein Bouncer Is Necessary and Sufficient for Species-specific Fertilization. *Science* 361, 1029–1033. doi:10.1126/science.aat7113

Herrboldt, M. A., Steffen, M. A., McGouran, C. N., and Bonett, R. M. (2021). Pheromone Gene Diversification and the Evolution of Courtship Glands in Plethodontid Salamanders. *J. Mol. Evol.* 89, 576–587. doi:10.1007/s00239-021-10026-0

Herrick, J., and Sclavi, B. (2014). A New Look at Genome Size, Evolutionary Duration and Genetic Variation in Salamanders. *Comptes Rendus Palevol* 13, 611–621. doi:10.1016/j.crpv.2014.06.002

Hirose, M., Honda, A., Fulka, H., Tamura-Nakano, M., Matoba, S., Tomishima, T., et al. (2020). Acrosin Is Essential for Sperm Penetration through the Zona Pellucida in Hamsters. *Proc. Natl. Acad. Sci. USA* 117, 2513–2518. doi:10.1073/pnas.1917595117

Houck, L. D., and Arnold, S. J. (2003). "Courtship and Mating Behavior," in *Phylogeny and Reproductive Biology of Urodela (Amphibia)*. Editor D. M. Sever (Enfield, New Hampshire: Science Publishers), 383–424.

Houck, L. D., Mead, L. S., Watts, R. A., Arnold, S. J., Feldhoff, P. W., and Feldhoff, R. C. (2007). "A Candidate Vertebrate Pheromone, SPF, Increases Female Receptivity in a Salamander," in *Chemical Signals in Vertebrates 11*. Editors J. Hurst, R. Beynon, and D. Muller-Schwarze (New York: Springer), 213–221.:

Houck, L. D., Watts, R. A., Arnold, S. J., Bowen, K. E., Kiemnec, K. M., Godwin, H. A., et al. (2008). A Recombinant Courtship Pheromone Affects Sexual Receptivity in a Plethodontid Salamander. *Chem. Senses* 33, 623–631. doi:10.1093/chemse/bjn027

Hutchison, J. M., Rau, D. C., and Derouchey, J. E. (2017). Role of Disulfide Bonds on DNA Packaging Forces in Bull Sperm Chromatin. *Biophysical J.* 113, 1925–1933. doi:10.1016/j.bpj.2017.08.050

Ichikawa, Y., Matsuzaki, M., Hiyama, G., Mizushima, S., and Sasanami, T. (2016). Sperm-egg Interaction during Fertilization in Birds. *J. Poult. Sci.* 53, 173–180. doi:10.2141/jpsa.0150183

Isotani, A., Matsumura, T., Ogawa, M., Tanaka, T., Yamagata, K., Ikawa, M., et al. (2017). A Delayed Sperm Penetration of Cumulus Layers by Disruption of Acrosin Gene in Rats†. *Biol. Reprod.* 97, 61–68. doi:10.1093/biolre/iox066

Itkonen, H. M., Engedal, N., Babaie, E., Luhr, M., Guldvik, I. J., Minner, S., et al. (2015). UAP1 Is Overexpressed in Prostate Cancer and Is Protective against Inhibitors of N-Linked Glycosylation. *Oncogene* 34, 3744–3750. doi:10.1038/onc.2014.307

Itkonen, H. M., Minner, S., Guldvik, I. J., Sandmann, M. J., Tsourlakis, M. C., Berge, V., et al. (2013). O-GlcNAc Transferase Integrates Metabolic Pathways to Regulate the Stability of C-MYC in Human Prostate Cancer Cells. *Cancer Res.* 73, 5277–5287. doi:10.1158/0008-5472.can-13-0549

Jankovičová, J., Simon, M., Antalíková, J., Cupperová, P., and Michalková, K. (2015). Role of Tetraspanin CD9 Molecule in Fertilization of Mammals. *Physiol. Res.* 64, 279. doi:10.33549/physiolres.932876

Janssenswillen, S., Vandebergh, W., Treer, D., Willaert, B., Maex, M., Van Bocxlaer, I., et al. (2014). Origin and Diversification of a Salamander Sex Pheromone System. *Mol. Biol. Evol.* 32, 472–480. doi:10.1093/molbev/msu316

Jones, S. K., and Bennett, R. J. (2011). Fungal Mating Pheromones: Choreographing the Dating Game. *Fungal Genet. Biol.* 48, 668–676. doi:10.1016/j.fgb.2011.04.001

Katoh, K., and Standley, D. M. (2013). MAFFT Multiple Sequence Alignment Software Version 7: Improvements in Performance and Usability. *Mol. Biol. Evol.* 30, 772–780. doi:10.1093/molbev/mst010

Kozlov, A. M., Darriba, D., Flouri, T., Morel, B., and Stamatakis, A. (2019). RAxML-NG: a Fast, Scalable and User-Friendly Tool for Maximum Likelihood Phylogenetic Inference. *Bioinformatics* 35, 4453–4455. doi:10.1093/bioinformatics/btz305

Laberge, F., Feldhoff, R. C., Feldhoff, P. W., and Houck, L. D. (2008). Courtship Pheromone-Induced C-fos-like Immunolabeling in the Female Salamander Brain. *Neuroscience* 151, 329–339. doi:10.1016/j.neuroscience.2007.11.006

Leinders-Zufall, T., Ishii, T., Mombaerts, P., Zufall, F., and Boehm, T. (2009). Structural Requirements for the Activation of Vomeronasal Sensory Neurons by MHC Peptides. *Nat. Neurosci.* 12, 1551–1558. doi:10.1038/nn.2452

Lemoine, F., Domelevo Entfellner, J.-B., Wilkinson, E., Correia, D., Dávila Felipe, M., De Oliveira, T., et al. (2018). Renewing Felsenstein's Phylogenetic Bootstrap in the Era of Big Data. *Nature* 556, 452–456. doi:10.1038/s41586-018-0043-0

Li, Y. F., He, W., Kim, Y. H., Mandal, A., Digilio, L., Klotz, K., et al. (2010). CABYR Isoforms Expressed in Late Steps of Spermiogenesis Bind with AKAPs and Ropporin in Mouse Sperm Fibrous Sheath. *Reprod. Biol. Endocrinol.* 8, 101–119. doi:10.1186/1477-7827-8-101

Lindsay, L. L., Yang, J. C., and Hedrick, J. L. (2002). Identification and Characterization of a Unique *Xenopus laevis* Egg Envelope Component, ZPD. *Dev. Growth Differ.* 44, 205–212. doi:10.1046/j.1440-169x.2002.00635.x

Maex, M., Van Bocxlaer, I., Mortier, A., Proost, P., and Bossuyt, F. (2016). Courtship Pheromone Use in a Model Urodele, the Mexican Axolotl (*Ambystoma mexicanum*). *Sci. Rep.* 6, 20184. doi:10.1038/srep20184

Monné, M., Han, L., Schwend, T., Burendahl, S., and Jovine, L. (2008). Crystal Structure of the ZP-N Domain of ZP3 Reveals the Core Fold of Animal Egg coats. *Nature* 456, 653–657. doi:10.1038/nature07599

Mori, E., Baba, T., Iwamatsu, A., and Mori, T. (1993). Purification and Characterization of a 38-kDa Protein, Sp38, with Zona Pellucida-Binding Property from Porcine Epididymal Sperm. *Biochem. Biophysical Res. Commun.* 196, 196–202. doi:10.1006/bbrc.1993.2234

Naaby-Hansen, S., Mandal, A., Wolkowicz, M. J., Sen, B., Westbrook, V. A., Shetty, J., et al. (2002). CABYR, a Novel Calcium-Binding Tyrosine Phosphorylation-Regulated Fibrous Sheath Protein Involved in Capacitation. *Develop. Biol.* 242, 236–254. doi:10.1006/dbio.2001.0527

Noh, S., and Marshall, J. L. (2016). Sorted Gene Genealogies and Species-specific Nonsynonymous Substitutions point to Putative Postmating Prezygotic Isolation Genes inAllonemobiuscrickets. *PeerJ* 4, e1678. doi:10.7717/peerj.1678

Nowoshilow, S., Schloissnig, S., Fei, J.-F., Dahl, A., Pang, A. W. C., Pippel, M., et al. (2018). The Axolotl Genome and the Evolution of Key Tissue Formation Regulators. *Nature* 554, 50–55. doi:10.1038/nature25458

Palmer, C. A., Watts, R. A., Gregg, R. G., Mccall, M. A., Houck, L. D., Highton, R., et al. (2005). Lineage-specific Differences in Evolutionary Mode in a Salamander Courtship Pheromone. *Mol. Biol. Evol.* 22, 2243–2256. doi:10.1093/molbev/msi219

Palmer, C. A., Watts, R. A., Hastings, A. P., Houck, L. D., and Arnold, S. J. (2010). Rapid Evolution of Plethodontid Modulating Factor, a Hypervariable Salamander Courtship Pheromone, Is Driven by Positive Selection. *J. Mol. Evol.* 70, 427–440. doi:10.1007/s00239-010-9342-2

Palmer, C. A., Watts, R. A., Houck, L. D., Picard, A. L., and Arnold, S. J. (2007). Evolutionary Replacement of Components in a Salamander Pheromone Signaling Complex: More Evidence for Phenotypic-Molecular Decoupling. *Evolution* 61, 202–215. doi:10.1111/j.1558-5646.2007.00017.x

Pease, J. B., Guerrero, R. F., Sherman, N. A., Hahn, M. W., and Moyle, L. C. (2016). Molecular Mechanisms of Postmating Prezygotic Reproductive Isolation Uncovered by Transcriptome Analysis. *Mol. Ecol.* 25, 2592–2608. doi:10.1111/mec.13679

Perez-Riverol, Y., Csordas, A., Bai, J., Bernal-Llinares, M., Hewapathirana, S., Kundu, D. J., et al. (2019). The PRIDE Database and Related Tools and Resources in 2019: Improving Support for Quantification Data. *Nucleic Acids Res.* 47, D442–D450. doi:10.1093/nar/gky1106

Pino, L. K., Just, S. C., Maccoss, M. J., and Searle, B. C. (2020). Acquiring and Analyzing Data Independent Acquisition Proteomics Experiments without Spectrum Libraries. *Mol. Cell Proteomics* 19, 1088–1103. doi:10.1074/mcp.p119.001913

Raj, I., Sadat Al Hosseini, H., Dioguardi, E., Nishimura, K., Han, L., Villa, A., et al. (2017). Structural Basis of Egg Coat-Sperm Recognition at Fertilization. *Cell* 169, 1315–1326. e1317. doi:10.1016/j.cell.2017.05.033

Rollmann, S. M., Houck, L. D., and Feldhoff, R. C. (1999). Proteinaceous Pheromone Affecting Female Receptivity in a Terrestrial Salamander. *Science* 285, 1907–1909. doi:10.1126/science.285.5435.1907

Rundle, H. D., and Nosil, P. (2005). Ecological Speciation. *Ecol. Lett.* 8, 336–352. doi:10.1111/j.1461-0248.2004.00715.x

Sahlin, K., and Medvedev, P. (2020). *De Novo* clustering of Long-Read Transcriptome Data Using a Greedy, Quality Value-Based Algorithm. *J. Comput. Biol.* 27, 472–484. doi:10.1089/cmb.2019.0299

Schulte, L. M., Martel, A., Cruz-Elizalde, R., Ramírez-Bautista, A., and Bossuyt, F. (2021). Love Bites: Male Frogs (Plectrohyla, Hylidae) Use Teeth Scratching to Deliver Sodefrin Precursor-like Factors to Females during Amplexus. *Front. Zool* 18, 59–14. doi:10.1186/s12983-021-00445-6

Searle, B. C., Pino, L. K., Egertson, J. D., Ting, Y. S., Lawrence, R. T., Maclean, B. X., et al. (2018). Chromatogram Libraries Improve Peptide Detection and Quantification by Data Independent Acquisition Mass Spectrometry. *Nat. Commun.* 9, 5128. doi:10.1038/s41467-018-07454-w

Searle, B. C., Swearingen, K. E., Barnes, C. A., Schmidt, T., Gessulat, S., Küster, B., et al. (2020). Generating High Quality Libraries for DIA MS with Empirically Corrected Peptide Predictions. *Nat. Commun.* 11, 1548. doi:10.1038/s41467-020-15346-1

Sessions, S. K., and Wake, D. B. (2021). Forever Young: Linking Regeneration and Genome Size in Salamanders. *Develop. Dyn.* 250, 768–778. doi:10.1002/dvdy.279

Sever, D. M., Siegel, D. S., Taylor, M. S., and Beachy, C. K. (2016). Phylogeny of Mental Glands, Revisited. *Copeia* 104, 83–93. doi:10.1643/ch-14-210

Shen, X.-X., Liang, D., Chen, M.-Y., Mao, R.-L., Wake, D. B., and Zhang, P. (2015). Enlarged Multilocus Data Set Provides Surprisingly Younger Time of Origin for the Plethodontidae, the Largest Family of Salamanders. *Syst. Biol.* 65, 66–81. doi:10.1093/sysbio/syv061

Silva, J. C., Gorenstein, M. V., Li, G.-Z., Vissers, J. P. C., and Geromanos, S. J. (2006). Absolute Quantification of Proteins by LCMSE. *Mol. Cell Proteomics* 5, 144–156. doi:10.1074/mcp.m500230-mcp200

Sun, C., Shepard, D. B., Chong, R. A., López Arriaza, J., Hall, K., Castoe, T. A., et al. (2012). LTR Retrotransposons Contribute to Genomic Gigantism in Plethodontid Salamanders. *Genome Biol. Evol.* 4, 168–183. doi:10.1093/gbe/evr139

Swanson, W. J., Clark, A. G., Waldrip-Dail, H. M., Wolfner, M. F., and Aquadro, C. F. (2001). Evolutionary EST Analysis Identifies Rapidly Evolving Male Reproductive Proteins in Drosophila. *Proc. Natl. Acad. Sci.* 98, 7375–7379. doi:10.1073/pnas.131568198

Swanson, W. J., and Vacquier, V. D. (2002). The Rapid Evolution of Reproductive Proteins. *Nat. Rev. Genet.* 3, 137–144. doi:10.1038/nrg733

Troelstra, C., Van Gool, A., De Wit, J., Vermeulen, W., Bootsma, D., and Hoeijmakers, J. H. J. (1992). ERCC6, a Member of a Subfamily of Putative Helicases, Is Involved in Cockayne's Syndrome and Preferential Repair of Active Genes. *Cell* 71, 939–953. doi:10.1016/0092-8674(92)90390-x

Van Bocxlaer, I., Treer, D., Maex, M., Vandebergh, W., Janssenswillen, S., Stegen, G., et al. (2015). Side-by-side Secretion of Late Palaeozoic Diverged Courtship Pheromones in an Aquatic Salamander. *Proc. R. Soc. B: Biol. Sci.* 282, 2960. doi:10.1098/rspb.2014.2960

Wassarman, P. M. (1999). Mammalian Fertilization. *Cell* 96, 175–183. doi:10.1016/s0092-8674(00)80558-9

Watts, R. A., Palmer, C. A., Feldhoff, R. C., Feldhoff, P. W., Houck, L. D., Jones, A. G., et al. (2004). Stabilizing Selection on Behavior and Morphology Masks Positive Selection on the Signal in a Salamander Pheromone Signaling Complex. *Mol. Biol. Evol.* 21, 1032–1041. doi:10.1093/molbev/msh093

Wessel, G. M., Wada, Y., Yajima, M., and Kiyomoto, M. (2021). Bindin Is Essential for Fertilization in the Sea Urchin. *Proc. Natl. Acad. Sci.* 118, 6118. doi:10.1073/pnas.2109636118

Wilburn, D. B., Tuttle, L. M., Klevit, R. E., and Swanson, W. J. (2019). Indirect Sexual Selection Drives Rapid Sperm Protein Evolution in Abalone. *eLife* 8, e52628. doi:10.7554/eLife.52628

Wilburn, D. B., Arnold, S. J., Houck, L. D., Feldhoff, P. W., and Feldhoff, R. C. (2017). Gene Duplication, Co-option, Structural Evolution, and Phenotypic Tango in the Courtship Pheromones of Plethodontid Salamanders. *Herpetologica* 73, 206–219. doi:10.1655/herpetologica-d-16-00082.1

Wilburn, D. B., Bowen, K. E., Doty, K. A., Arumugam, S., Lane, A. N., Feldhoff, P. W., et al. (2014a). Structural Insights into the Evolution of a Sexy Protein: Novel Topology and Restricted Backbone Flexibility in a Hypervariable Pheromone from the Red-Legged Salamander, *Plethodon shermani*. *PLOS ONE* 9, e96975. doi:10.1371/journal.pone.0096975

Wilburn, D. B., Bowen, K. E., Feldhoff, P. W., and Feldhoff, R. C. (2014b). Proteomic Analyses of Courtship Pheromones in the Redback Salamander, *Plethodon cinereus*. *J. Chem. Ecol.* 40, 928–939. doi:10.1007/s10886-014-0489-y

Wilburn, D. B., Bowen, K. E., Gregg, R. G., Cai, J., Feldhoff, P. W., Houck, L. D., et al. (2012). Proteomic and Utr Analyses of a Rapidly Evolving Hypervariable Family of Vertebrate Pheromones. *Evolution* 66, 2227–2239. doi:10.1111/j.1558-5646.2011.01572.x

Wilburn, D. B., Eddy, S. L., Chouinard, A. J., Arnold, S. J., Feldhoff, R. C., and Houck, L. D. (2015). Pheromone Isoform Composition Differentially Affects Female Behaviour in the Red-Legged Salamander, *Plethodon shermani*. *Anim. Behav.* 100, 1–7. doi:10.1016/j.anbehav.2014.10.019

Wilburn, D. B., and Feldhoff, R. C. (2019). An Annual Cycle of Gene Regulation in the Red-Legged Salamander Mental Gland: from Hypertrophy to Expression of Rapidly Evolving Pheromones. *BMC Dev. Biol.* 19, 10. doi:10.1186/s12861-019-0190-z

Wilburn, D. B., and Swanson, W. J. (2018). "Egg, Comparative Vertebrate," in *Encylopedia of Reproduction*. Editor M. A. Skinner. 2nd ed (Cambridge, MA, USA: Academic Press). In press.

Wilburn, D. B., and Swanson, W. J. (2016). From Molecules to Mating: Rapid Evolution and Biochemical Studies of Reproductive Proteins. *J. Proteomics* 135, 12–25. doi:10.1016/j.jprot.2015.06.007

Wilburn, D. B., Tuttle, L. M., Klevit, R. E., and Swanson, W. J. (2018). Solution Structure of Sperm Lysin Yields Novel Insights into Molecular Dynamics of Rapid Protein Evolution. *Proc. Natl. Acad. Sci. USA* 115, 1310–1315. doi:10.1073/pnas.1709061115

Wirsig-Wiechmann, C. R., Houck, L. D., Feldhoff, P. W., and Feldhoff, R. C. (2002). Pheromonal Activation of Vomeronasal Neurons in Plethodontid Salamanders. *Brain Res.* 952, 335–344. doi:10.1016/s0006-8993(02)03369-3

Woodley, S. K. (1994). Plasma Androgen Levels, Spermatogenesis, and Secondary Sexual Characteristics in Two Species of Plethodontid Salamanders with Dissociated Reproductive Patterns. *Gen. Comp. Endocrinol.* 96, 206–214. doi:10.1006/gcen.1994.1175

Xia, B., Yan, Y., Baron, M., Wagner, F., Barkley, D., Chiodin, M., et al. (2020). Widespread Transcriptional Scanning in the Testis Modulates Gene Evolution Rates. *Cell* 180, 248–262. e221. doi:10.1016/j.cell.2019.12.015

Yang, X., Dunning, K. R., Wu, L. L.-Y., Hickey, T. E., Norman, R. J., Russell, D. L., et al. (2010). Identification of Perilipin-2 as a Lipid Droplet Protein Regulated in

Oocytes during Maturation. *Reprod. Fertil. Dev.* 22, 1262–1271. doi:10.1071/rd10091

Zhang, R., Fu, X., Jia, B., Liu, C., Cheng, K., and Zhu, S. (2014). Expression of Perilipin 2 (PLIN2) in Porcine Oocytes during Maturation. *Reprod. Dom Anim.* 49, 875–880. doi:10.1111/rda.12386

Zhao, W., Li, Z., Ping, P., Wang, G., Yuan, X., and Sun, F. (2018). Outer Dense Fibers Stabilize the Axoneme to Maintain Sperm Motility. *J. Cel. Mol. Med.* 22, 1755–1768. doi:10.1111/jcmm.13457

Conflict of Interest: The authors declare that the research was conducted in the absence of any commercial or financial relationships that could be construed as a potential conflict of interest.

Publisher's Note: All claims expressed in this article are solely those of the authors and do not necessarily represent those of their affiliated organizations or those of the publisher, the editors, and the reviewers. Any product that may be evaluated in this article, or claim that may be made by its manufacturer, is not guaranteed or endorsed by the publisher.

frontiers in Cell and Developmental Biology

ORIGINAL RESEARCH
published: 24 February 2022
doi: 10.3389/fcell.2022.810961

Toll-like Receptor 2 is Involved in Calcium Influx and Acrosome Reaction to Facilitate Sperm Penetration to Oocytes During *in vitro* Fertilization in Cattle

Dongxue Ma[1], *Mohamed Ali Marey*[1,2], *Masayuki Shimada*[3] *and Akio Miyamoto*[1]*

[1]Global Agromedicine Research Center (GAMRC), Obihiro University of Agriculture and Veterinary Medicine, Obihiro, Japan, [2]Department of Theriogenology, Faculty of Veterinary Medicine, Damanhur University, Behera, Egypt, [3]Graduate School of Integrated Sciences for Life, Hiroshima University, Higashi-Hiroshima, Japan

OPEN ACCESS

Edited by:
Maria Jiménez-Movilla, University of Murcia, Spain

Reviewed by:
Claudia Lydia Treviño, National Autonomous University of Mexico, Mexico
Manuel Alvarez Rodriguez, Linköping University, Sweden

***Correspondence:**
Akio Miyamoto
akiomiya@obihiro.ac.jp

Specialty section:
This article was submitted to Molecular and Cellular Reproduction, a section of the journal Frontiers in Cell and Developmental Biology

Received: *08 November 2021*
Accepted: *04 January 2022*
Published: *24 February 2022*

Citation:
Ma D, Marey MA, Shimada M and Miyamoto A (2022) Toll-like Receptor 2 is Involved in Calcium Influx and Acrosome Reaction to Facilitate Sperm Penetration to Oocytes During in vitro Fertilization in Cattle. Front. Cell Dev. Biol. 10:810961. doi: 10.3389/fcell.2022.810961

Cumulus cells of ovulated cumulus-oocyte complexes (COCs) express Toll-like receptor 2 (TLR2), pathogen recognition receptors, to recognize and react to sperm signals during fertilization. Sperm also express TLR2, but its contribution to the sperm-oocytes crosstalk is still unclear. Here, we adapted the *in vitro* fertilization (IVF) model to characterize the potential relevance of sperm TLR2 in sperm-oocytes interactions during fertilization in bovine. The IVF results showed that the ligation of sperm TLR2 with its specific antagonist/agonist resulted in down/up-regulation of the cleavage and blastocyst rates either in COCs or cumulus-free oocytes, but not in zona pellucida (ZP)-free oocytes. The computer-assisted sperm analysis (CASA) system revealed that sperm motility parameters were not affected in TLR2 antagonist/agonist-treated sperm. However, fluorescence imaging of sperm-ZP interactions revealed that the blockage or activation of the TLR2 system in sperm reduced or enhanced both binding and penetration abilities of sperm to ZP compared to control, respectively. Flow cytometrical analysis of acrosome reaction (AR) demonstrated that the TLR2 system adjusted the occurrence of AR in ZP-attached sperm, suggesting that sperm TLR2 plays physiological impacts on the sperm-oocyte crosstalk *via* regulating ZP-triggered AR in sperm. Given that calcium (Ca^{2+}) influx is a pre-requisite step for the induction of AR, we investigated the impact of the TLR2 system on the ionophore A23187-induced Ca^{2+} influx into sperm. Notably, the exposure of sperm to TLR2 antagonist/agonist reduced/increased the intracellular Ca^{2+} level in sperm. Together, these findings shed new light that the TLR2 system is involved in sperm AR induction which enables sperm to penetrate and fertilize oocytes during the fertilization, at least *in vitro*, in cows. This suggests that sperm possibly developed a quite flexible sensing mechanism simultaneously against pathogens as well as COCs toward fertilization with the same TLR2 of the innate immune system.

Keywords: sperm, toll-like receptor 2, *in vitro* fertilization, acrosome reaction, intracellular Ca^{2+} influx, bovine

INTRODUCTION

Fertilization failure is one of the main reasons for infertility which has been attributed to either sperm or oocyte factors (Kashir et al., 2010). Male factors represent approximately 40% of all infertility cases in humans (Kumar and Singh., 2015), such as abnormal sperm parameters which are usually associated with virus/bacterial infection and inflammation. In mammals, sperm are not capable of fertilizing oocytes immediately after ejaculation, but they must first undergo a period of preparation including capacitation and acrosome reaction (AR) (Liu et al., 2012).

Sperm capacitation is a prerequisite step to successful fertilization (Austin, 1951; Chang, 1951) that involves a series of biochemical transformations, including changes in sperm metabolism, intracellular pH, intracellular cyclic adenosine monophosphate (cAMP), and intracellular calcium concentration, all of which prepare sperm to undergo AR to penetrate the zona pellucida (ZP) and fertilize oocytes (Breitbart et al., 2005; Kwon et al., 2013). Despite investigations, it is not completely understood whether fertilizing spermatozoon initiates its AR during its voyage through the cumulus cells or when it binds to the ZP (Gadella, 2012). However, fertilizing spermatozoon must undergo AR to penetrate the ZP, in which the outer acrosomal membrane fuses with the overlying plasma membrane (Yanagimachi, 1994; Honda et al., 2002; Mao and Yang, 2013). Therefore, only the acrosome-reacted sperm are existent in the perivitelline space and can fuse with the plasma membrane of the oocyte to effect fertilization (Austin, 1975; Saling et al., 1979; Toshimori, 1982; Inoue et al., 2005; Avella and Dean., 2011).

The regulation of calcium (Ca^{2+}) influx plays a key role in many physiological cell functions, such as cell growth, apoptosis, exocytosis, muscle contraction, and gene transcription (Chun and Prince, 2006). In sperm, it is well known that Ca^{2+} release and influx are essential for the acquisition of sperm fertilizing competence through the induction of capacitation and AR. The *in vitro* capacitation of bovine sperm with heparin is accomplished by the extracellular Ca^{2+} uptake by the sperm through Ca^{2+} channels which ultimately increase the intracellular Ca^{2+} levels in the sperm head leading to activation of adenylyl cyclase to form cAMP, which further activates protein kinase A (PKA) to phosphorylate protein tyrosine (Parrish et al., 1999; Marquez and Suarez 2004; Ijiri et al., 2012). Although the specific sequence of events that trigger the AR after capacitation is not fully understood, there is evidence that it involves elevations of intracellular pH, cytosolic Ca^{2+}, membrane hyperpolarization, acrosomal alkalization, and acrosomal Ca^{2+} release (Darszon et al., 2011; Nishigaki et al., 2014; Stival et al., 2016; Chávez et al., 2017). These events promote acrosome swelling, deformation of the outer acrosomal membrane (OAM), interaction and docking with the overlying plasma membrane (PM), and finally, the fusion between OAM and PM that promotes acrosomal exocytosis and release of hydrolytic enzymes, principally, the trypsin-like acrosin to penetrate the ZP and fertilize the oocyte (Mayorga et al., 2007; Sosa et al., 2014; Aldana et al., 2021).

Toll-like receptors (TLRs) are innate immune cell receptors that specifically recognize pathogenic microorganisms and mount an early immune response, resulting in the production of pro-inflammatory mediators (Akira et al., 2001). Moreover, TLRs are involved in several reproductive functions including ovulation, fertilization, gestation, and parturition (Kannaki et al., 2011). In males, TLRs play a role in steroidogenesis and spermatogenesis (Saeidi et al., 2014). Among TLRs family members, TLR2 and TLR4 are expressed in cumulus cells of cumulus-oocyte complexes (COCs) and play immuno-protective functions critical for cell survival during ovulation and fertilization (Shimada et al., 2006; Liu et al., 2008).

Specifically, it has been shown that co-culturing of sperm and COCs during *in vitro* fertilization (IVF) induces activation of cumulus cells TLR2/4 signaling pathway in mice (Shimada et al., 2008). In that model, the release of hyaluronidase from sperm degrades the hyaluronan-rich matrix of the COCs releasing hyaluronan fragments which subsequently act as endogenous ligands for cumulus cells TLR2/4. This binding could activate the production of certain cytokines/chemokines essential for sperm capacitation, thus enhance fertilization. The findings suggest a physiological role of the TLR2/4 pathway as a regulatory loop between sperm and COCs during fertilization (Stern et al., 2006; Shimada et al., 2008). Of note, human sperm express TLR2, which is functional for the recognition of bacterial endotoxins during infection (Fujita et al., 2011), but their role in sperm interactions with oocytes during fertilization is still unknown. Most recently, we demonstrated that TLR2 is localized in the posterior segment of the bull sperm head (Akthar et al., 2020). Therefore, we adapted the IVF model to clarify the potential relevance of sperm TLR2 in sperm-oocytes interactions during fertilization in bovine. Our initial observations prompted us to hypothesize that bull sperm TLR2 is functional in sperm-oocyte interactions during fertilization. To examine this hypothesis, sperm TLR2 was ligated by their specific antagonist/agonist before being co-cultured with oocytes. Then, we investigated the embryo cleavage and developmental competence, sperm-ZP binding and penetration rates, and ZP or ionophore A23187-induced AR. Further, the direct impact of sperm TLR2 blockage/activation on sperm motility kinetics, AR, and intracellular Ca^{2+} influx was analyzed.

MATERIALS AND METHODS

Ethical Approval

Animal experiments described in this article were conducted following the Guiding Principles for the Care and Use of Research Animals Promulgated by Obihiro University of Agriculture and Veterinary Medicine, Japan. The protocol was approved by the Committee on the Ethics of Animal Experiments of the Obihiro University of Agriculture and Veterinary Medicine (Permit number 19–111).

Experimental Design

The design and framework of multiple investigations performed in the present study was illustrated in **Figure 1**. Initially, to

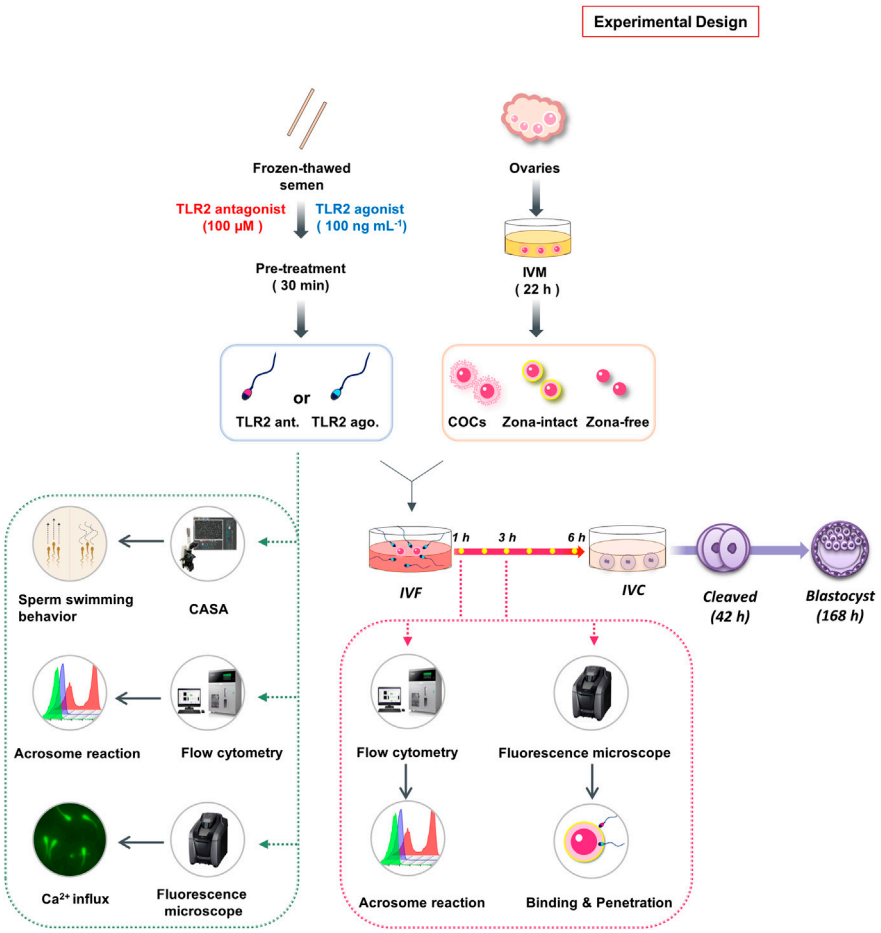

FIGURE 1 | Schematic representation of the study experimental design. Initially, to investigate the potential contribution of sperm TLR2 in sperm-oocyte interaction during *in vitro* fertilization, TLR2 antagonist (CU-CPT22; 100 μM) or TLR2 agonist (Pam3Cys; 100 ng ml^{-1}) was used for the blockage or activation of TLR2 in frozen-thawed bull sperm for 30 min, respectively. Sperm were then washed, adjusted to a concentration of 0.5 × 10^6 sperm ml^{-1}, and co-cultured with matured intact COCs, cumulus-free (zona intact), or zona-free oocytes for 6 h. Cleavage rate and blastocyst rate were evaluated at 42 and 168 h post-insemination respectively. Moreover, the ability of TLR2 antagonist/agonist treated sperm to bind or penetrate ZP and the subsequent induction of AR was evaluated after 1 and 3 h of the co-culture using fluorescence microscopy and flow cytometry, respectively. Based on the results, more focus was given to the direct impact of blockage/activation of sperm TLR2 on sperm motility parameters, AR, and intracellular Ca^{2+} influx using CASA analysis, flow cytometry, and fluorescence microscopy, respectively.

investigate the potential contribution of sperm TLR2 in sperm-oocyte interaction during *in vitro* fertilization, a specific TLR2 antagonist (CU-CPT22) or TLR2 agonist (Pam3Cys) was used for the blockage or activation of sperm TLR2, respectively. It was shown that cumulus cells of COCs also express TLR2 and their activation or blockage modulates the fertilization ratio (Shimada et al., 2008). To investigate the impact of "sperm TLR2" on fertilization, the sperm were basically pre-exposed to TLR2 antagonist or agonist before their co-culture with oocytes under IVF conditions. Washed frozen-thawed bull sperm were pre-exposed either to TLR2 antagonist (100 μM) or TLR2 agonist (100 ng ml^{-1}) for 30 min, washed, adjusted to a concentration of 0.5×10^6 sperm ml^{-1}, and co-cultured with matured COCs for 6 h. Then, cleavage rate and blastocyst rate were evaluated at 42 and 168 h post-insemination, respectively. Our initial observations showed that the blockage/activation of sperm TLR2 inhibited/stimulated the oocyte fertilization and embryo developmental competence. To understand the underlying mechanisms, we assessed the impact of sperm TLR2 on the sperm-cumulus cells interaction or sperm-ZP fusion *via* co-culturing of TLR2 antagonist/agonist treated sperm with matured cumulus-free (zona-intact) or zona-free oocytes for 6 h, respectively and the cleavage rate was determined at 42 h post-insemination. Moreover, the ability of TLR2 antagonist/agonist treated sperm to bind and/or penetrate ZP and the subsequent induction of AR was evaluated after 1 and 3 h of the co-culture using fluorescence microscopy and flow cytometry, respectively. Based on the results, more focus was given to the direct impact of TLR2 on sperm motility parameters, AR, and intracellular Ca^{2+} influx using CASA analysis, flow cytometry, and fluorescence microscopy, respectively.

Cumulus-Oocyte Complexes (COCs) Collection and *in vitro* Maturation (IVM)

Bovine ovaries were collected from the local slaughterhouse (Obihiro, Hokkaido, Japan), kept in saline supplemented with 1% penicillin-streptomycin (Gibco, Grand Island, United States) at approximately 35°C, and immediately transported to the laboratory within 1–2 h. COCs collection and IVM were performed as previously described (Ideta et al., 2013) with minor modifications. Briefly, COCs were aspirated from individual visible antral follicles of 2–6 mm in diameter using a 10 ml syringe attached to an 18 G needle. Then, oocytes were washed 3 times in oocyte collection medium (OCM; Research Institute for the Functional Peptides Co., Ltd.) supplemented with 10% fetal bovine serum (FBS, Biowest). Each 40–50 oocytes with a homogenous cytoplasm and surrounded by at least three layers of compact cumulus cells were matured *in vitro* using 500 µl of high performance-modified 199 medium (HP-M199; Research Institute for the Functional Peptides Co., Ltd.) supplemented with 10 ng ml^{-1} epidermal growth factor (EGF, Sigma) and 10% FBS for 22 h at 38.5°C in 5% CO_2 with humidified air.

Blockage and Activation of TLR2 Pathway in Sperm

A synthetic TLR2 antagonist (CU-CPT22, Calbiochem) (Cheng et al., 2012; Grabowski, et al., 2020) or Pam3Cys, a synthetic TLR2 ligand (ab142085, Abcam) (Reitermann et al., 1989) was used to specifically and selectively block or activate the sperm TLR2, respectively. Initially, preliminary dose-dependent and time-dependent experiments were conducted to identify cytotoxic or detrimental effects of TLR2 antagonist and agonist on sperm motility and viability as analyzed by CASA and flow cytometry (**Supplementary Table S1** and **Supplementary Figure S1**). Next, based on our previous investigations (Ezz et al., 2019; Akthar et al., 2019; Morillo, et al., 2020; Elesh et al., 2021) and our initial trials, the pre-treatment of sperm by TLR2 antagonist (100 µM) or agonist (100 ng ml^{-1}) for 30 min was designated as an effective model to test our hypothesis without generating any cytotoxic or detrimental effects on sperm motility and viability.

Frozen semen straws were obtained from three highly fertile Holstein bulls from the Genetics Hokkaido Association (Hokkaido, Japan). Semen straws were thawed at 37 °C for 30 s, pooled together, and washed twice using a modified sperm-tyrode's albumin lactate pyruvate (SP-TALP) (Parrish et al., 1988; Marquez and Suarez, 2007) at 300 g for 5 min at room temperature. After washing, sperm were treated either by TLR2 antagonist (100 µM) or agonist (100 ng ml^{-1}) for 30 min, respectively. TLR2 antagonist (Stock solution: 100 mM) was dissolved in DMSO and used at a concentration of 100 µM (100 µM = 36.24 µg ml^{-1}) while TLR2 agonist (Stock solution: 100 µg ml^{-1}) was dissolved in 50% ethanol and used at a concentration of 100 ng ml^{-1}. Similarly, the sperm group with 0.1% DMSO or 0.05% ethanol was kept as a control group for TLR2 antagonist- or TLR2-agonist treated sperm, respectively. Sperm were then washed twice at 300 g for 5 min in SP-TALP and resuspended in fertilization medium IVF100 (Research Institute for the Functional Peptides, Yamagata, Japan).

In vitro Fertilization (IVF)

After maturation, COCs were collected and either kept intact, or cumulus cells and/or zona pellucida were removed. Cumulus cells were removed by gentle repeated pipetting with 300 µg ml^{-1} hyaluronidase (Sigma-Aldrich, Steinheim, Germany). The preparation of zona-free oocytes was performed as previously described (Takahashi et al., 2013) with slight modifications. Briefly, the zona pellucida of denuded oocytes were dissolved with 5 mg ml^{-1} pronase (protease from *Streptomyces* griseus, Sigma-Aldrich, Steinheim, Germany) for 1 min under visual monitoring. The thin residual layers were physically removed using a narrow bore glass pipette. Zona-free oocytes were rapidly washed 5 times with 0.1% bovine serum albumin (BSA) in PBS and kept at 38.5°C under 5% CO_2 in humidified air for 1 h recovery. IVF was achieved by co-culturing of TLR2 antagonist/agonist-treated sperm (0.5 ×10^6 sperm ml^{-1}) either with intact COCs, cumulus-free oocytes, or zona-free oocytes (10–15 oocytes) in 100 µL droplets of IVF100 medium under mineral oil for 6 h at 38.5 °C in 5% CO_2 in humidified air.

In vitro Culture (IVC)

After IVF, cumulus cells were removed by repeated pipetting with 300 µg ml^{-1} hyaluronidase. Presumptive zygotes (n = 30–35) were transferred to 400 µL BO-IVC medium (IVF-bioscience, Poland, Sokolow Podlaski) in 4-well plates under mineral oil at 38.5°C in a humidified atmosphere of 5% O_2, 5% CO_2, and 90% N_2. Cleavage rate and blastocyst development were assessed at 42 and 168 h (Day 7) post-insemination, respectively (Day 0 = day of fertilization).

Sperm-ZP Binding and Penetration Assay

For investigating the sperm-ZP binding and penetration, TLR2 antagonist/agonist-treated sperm (0.5×10^6 sperm ml^{-1}) were co-incubated with cumulus-free oocytes (n = 15–20) in each 100 µL fertilization droplets at 38.5°C in 5% CO_2 in humidified air for 1 and 3 h. At 1 h and 3 h of co-incubation, sperm-oocyte complexes were washed 10 times in PBS containing 1 mg ml^{-1} polyvinyl alcohol (PVA-PBS) to remove ZP-loosely attached sperm while only ZP-strongly attached sperm were counted as a sperm-ZP binding ratio (Takahashi et al., 2013). For assessment of sperm-ZP penetration, sperm-oocyte complexes were repeatedly aspirated with a pipette of an inner diameter slightly smaller than the size of the oocyte to remove all attached sperm and only those with heads embedded in the ZP or perivitelline space were counted as sperm-ZP penetration ratio (Liu et al., 2004). Next, oocytes were fixed in 5% glutaraldehyde solution (072-02262, Fujifilm) in PBS for 30 min at room temperature then, washed with PVA-PBS before being incubated with 5 µg ml^{-1} Hoechst 33342 (Sigma-Aldrich, B2261) for 15 min in the dark (Grullón et al., 2013). Finally, oocytes were placed in droplets of glycerol, mounted on the slide, and covered with a cover slide. The number of sperms bound or penetrated the ZP of each oocyte was counted independently by 2 observers using a fluorescence microscope (Keyence, BZ-X800, Osaka, Japan).

Assessment of Sperm Kinematics

The impact of pre-treatment of sperm by TLR2 antagonist/agonist on sperm motility parameters was analyzed using the

computer-assisted sperm analysis system (CASA) (SMAS; Kaga Electronics, Tokyo, Japan). Sperm were incubated in SP-TALP medium supplemented either by TLR2 antagonist (100 μM) or TLR2 agonist (100 ng ml^{-1}), for 30 min, washed twice, resuspended in SP-TALP at a concentration 5–10×10^{6} sperm ml^{-1}, and cultured for further 1 or 3 h. Sperm motility parameters (Total motility (%), progressive motility (%), average path velocity (VAP, μm/s), straight-line velocity (VSL, μm/s), curvilinear velocity (VCL, μm/s), amplitude of lateral head displacement (ALH, μm), beat cross frequency (BCF, Hz), straightness (STR, %), and linearity (LIN, %)), were assessed at different time points (0, 1, and 3 h) using CASA system. CASA was performed based on a previous method with minor modifications (Kanno et al., 2017). Briefly, a 3 μl of the sperm sample was pipetted and loaded into a pre-warmed (37°C) standard count four chamber Leja slide (SC 20-01-04-B). To analyze sperm motility parameters, a minimum of 200 sperm at three different fields were examined in each group.

Assessment of Acrosome Reaction (AR)

Sperm AR can be induced either by ZP, as a physiological stimulus, during sperm-ZP binding or by calcium ionophore as a chemical stimulus (Yanagimachi, 1994; Strünker et al., 2011). To investigate the impact of pre-treatment of sperm by TLR2 antagonist/agonist on the ZP-inducted AR, TLR2 antagonist/agonist pre-treated sperm were co-cultured with cumulus-free oocytes for 1 h or 3 h under IVF conditions. Then, ZP-bound sperm were collected, as mentioned above, and incubated with 25 μg ml^{-1} fluorescein peanut agglutinin FITC-conjugate (PNA-FITC; Vector Laboratories, FL-1071) for 8 min at 38.5°C in dark. The percent of acrosome-reacted sperm was analyzed by flow cytometry (Sony SH800 Cell Sorter, Tokyo, Japan). For chemical induction of AR by calcium ionophore, motile sperm were prepared using a modified swim-up method (Parrish et al., 1988) and treated by TLR2 antagonist/agonist as previously described. Then, sperm were stimulated with or without calcium ionophore A23187 (1 μM, C7522, Sigma) for 60 min at 38.5°C in the dark. After incubation, sperm were washed twice and double-stained with 1 μl of 1 mg ml^{-1} propidium iodide (cell viability test *via* detection of plasma membrane damage (PMD)) (PI; P4170, Sigma) and 1 μl of 5 mg ml^{-1} PNA-FITC mixed with 200 μl sperm dilution and incubated for 8 min at 38.5°C in dark. The percentage of PI-negative and PNA-FITC-positive (live and acrosome reacted) sperm were determined immediately by flow cytometry. Additionally, stained sperm samples were smeared, fixed, and examined under fluorescence microscope.

Single-Cell Imaging Measurement of Intracellular Calcium Influx

Assessment of intracellular calcium influx was recorded during the A23817-induced AR assay as previously described (Marquez and Suarez, 2007) with minor modifications. Immediately before the addition of A23817 to induce AR as above-mentioned, each sample was loaded with 5 μM Fluo-4 AM (F311, Dojindo, Japan) for 40 min at 38.5°C in the dark and washed twice to remove free Fluo-4 AM. Then, Fluo-4 AM-loaded sperm were incubated for another 20 min with a fresh medium before adding calcium ionophore A23187 (1 μM as a final concentration). The sperm fluorescence was measured by the fluorescence microscope. Images were captured every 5 min for a total of 1 h, with A23187 added after the initial five readings (every 1 min). The images were analyzed using BZ-X800 Analyzer and each sperm head was selected as the region of interest. Data were normalized using the following equation (F/F0)-1. where F0 is the average of the first five readings before the addition of A23187 and F is the fluorescence intensity obtained at each time point.

Statistical Analysis

Data are presented as the mean ± S.E.M of 3–5 independent experiments. Statistical analyses were performed using GraphPad Prism five software (GraphPad Software, La Jolla, CA, United States). One-way analysis of variance (ANOVA) followed by Bonferroni's post-comparison test (>two groups) or two sample *t*-test (two groups) was used to compare the mean differences among the groups. Data were considered to be statistically significant at (*$p < 0.05$, **$p < 0.01$, ***$p < 0.001$, or ****$p < 0.0001$).

RESULTS

Blockage/Activation of Sperm TLR2 Suppressed/Enhanced the Cleavage and Blastocyst Rates in COCs

To investigate the potential role of sperm TLR2 in sperm-oocyte interaction, sperm were pre-treated by TLR2 antagonist/agonist for 30 min, washed, and further co-cultured with intact COCs for 6 h under IVF conditions. The results showed that the blockage of sperm with TLR2 antagonist induced a substantial decline in the cleavage and blastocyst rates (**Figure 2A**). Meanwhile, the activation of sperm with TLR2 agonist enhanced cleavage and blastocyst rates (**Figure 2B**).

Blockage/Activation of Sperm TLR2 Suppressed/Enhanced the Cleavage Rate in Cumulus-free Oocytes, but Not in Zona-free Oocytes

To further explore the impact of sperm TLR2 on sperm crosstalk with cumulus cells and/or ZP, TLR2 antagonist/agonist treated sperm were co-cultured with matured cumulus-free or zona-free oocytes for 6 h, and cleavage rate was analyzed. Likewise, results revealed that the blockage/activation of sperm TLR2 suppressed/increased the cleavage rate in cumulus-free oocytes, but not with zona-free oocytes, compared to control (**Figures 3A,B**). These findings could imply that sperm TLR2 plays a pivotal role in sperm-ZP interactions.

TLR2 Pathway Mediates Sperm-ZP Binding and Sperm-ZP Penetration Abilities

Based on the above-mentioned results, we hypothesized that the activation of sperm TLR2 is a pre-requisite step for enabling

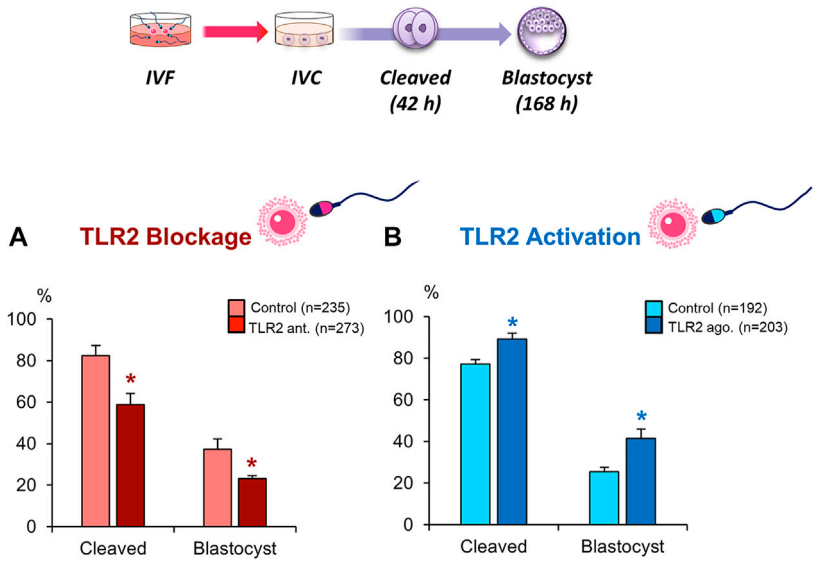

FIGURE 2 | Blockage/activation of sperm TLR2 suppressed/enhanced the cleavage and blastocyst rates in COCs. Sperm were pre-treated by **(A)** TLR2 antagonist (100 μM) or **(B)** TLR2 agonist (100 ng ml^{-1}) for 30 min, washed, and co-cultured with cumulus-free(zona-intact) and zona-free oocytes. Percentage of fertilized oocytes observed after 42 h post insemination and blastocyst on Day 7 (Day 0 = day of fertilization). Data reported as means ± S.E.M. Different superscript asterisks denote a significant difference ($p < 0.05$). The number of presumptive zygotes for each treatment group (from three independent experiments) is specified above each Figure.

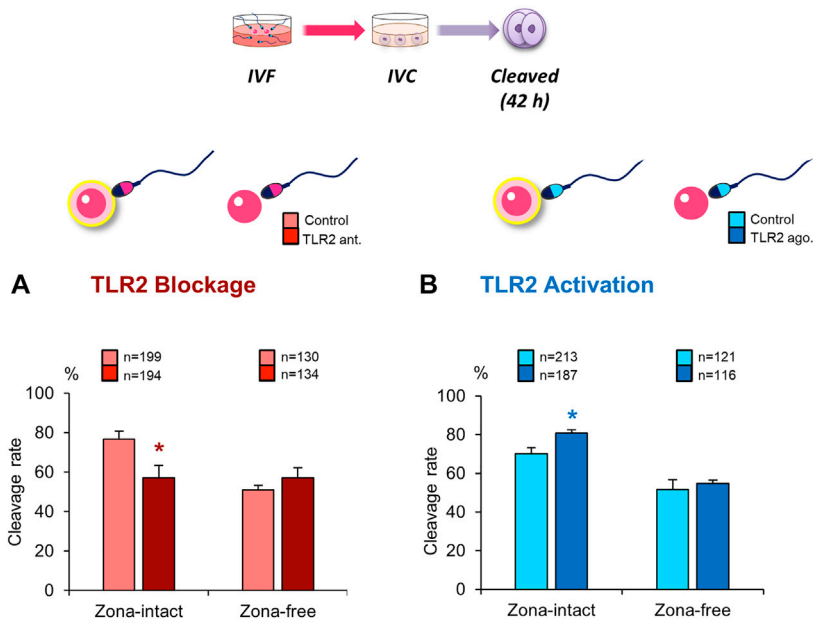

FIGURE 3 | Blockage/activation of sperm TLR2 suppressed/enhanced the cleavage rate in cumulus-free oocytes, but not in zona-free oocytes. Sperm were pre-treated by **(A)** TLR2 antagonist (100 μM) or **(B)** TLR2 agonist (100 ng ml^{-1}) for 30 min, washed, and co-cultured with cumulus-free (zona-intact) and zona-free oocytes. Percentage of fertilized oocytes observed after 42 h post insemination. Data reported as means ± S.E.M. Different superscript asterisks denote a significant difference ($p < 0.05$). The number of presumptive zygotes for each treatment group (from three independent experiments) is specified above each Figure.

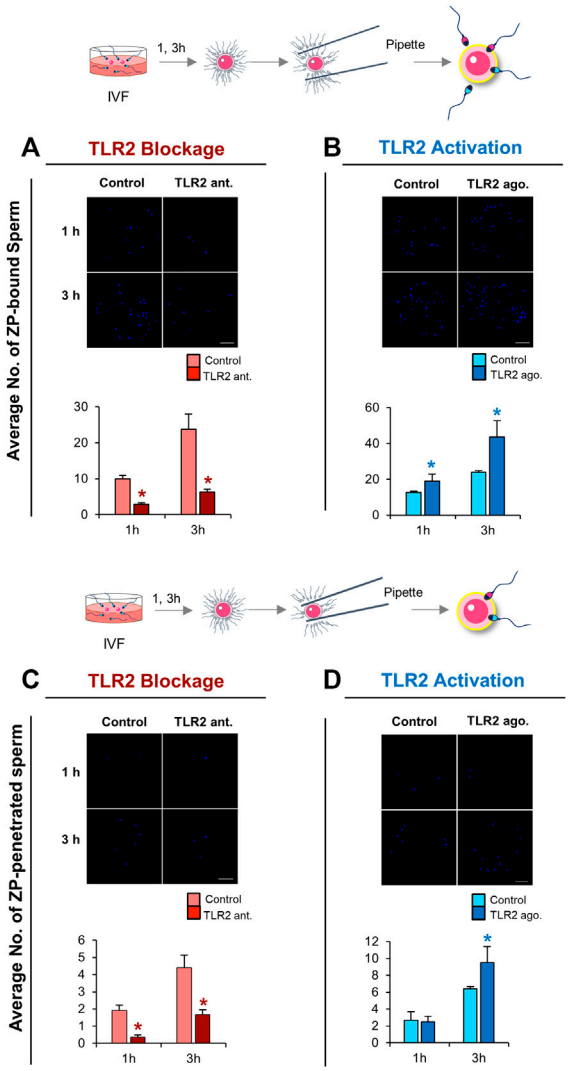

FIGURE 4 | TLR2 pathway mediates sperm-ZP binding and sperm-ZP penetration abilities. Sperm were pre-treated by TLR2 antagonist (100 μM) or TLR2 agonist (100 ng ml^{-1}) for 30 min, washed, and co-cultured with cumulus-free oocytes (n = 15–20) for 1 and 3 h. Sperm-oocyte complexes were washed to remove ZP-loosely attached sperm while only ZP-strongly attached sperm were counted as sperm-ZP binding ratio after staining with Hoechst 33342 and observed at ×200 magnification. Sperm with heads embedded in the ZP or perivitelline space were counted as sperm-ZP penetration ratio **(A)** Representative image of zona-binding observed in control and TLR2 antagonist treated group and the average number of sperm bound to the ZP at 1 and 3 h was counted **(B)** Representative image of zona-binding observed in control and TLR2 agonist treated group and the average number of sperm bound to the ZP at 1 and 3 h was counted **(C)** Representative image of zona-penetration observed in control and TLR2 antagonist treated group and the average number of sperm penetrated to the ZP at 1 and 3 h was counted **(D)** Representative image of zona-penetration observed in control and TLR2 agonist treated group and the average number of sperm penetration to the ZP at 1 and 3 h was counted. Data reported as means ± S.E.M of three independent experiments. Different superscript asterisks denote a significant difference ($p < 0.05$). Scale bar = 50 μm.

sperm to bind and/or penetrate ZP. To test this hypothesis, the ability of TLR2 antagonist/agonist treated sperm to bind and/or penetrate ZP was tested at 1 and 3 h of co-incubation with cumulus-free oocytes. The results showed that the blockage/activation of sperm TLR2 suppressed/increased the number of ZP-bound sperm at 1 and 3 h of co-culture (**Figures 4A,B**). Likewise, pre-treatment of sperm with TLR2 antagonist suppressed the average number of ZP-penetrated sperm compared to the control group at 1 and 3 h ($p < 0.05$) (**Figure 4C**). Conversely, pre-treatment of sperm with TLR2 agonist increased the average number of ZP-penetrated sperm compared to the control group at 3 h ($p < 0.05$) (**Figure 4D**).

Pre-treatment of Sperm With TLR2 Antagonist/Agonist did Not Disturb Sperm Motility Parameters

To determine whether the impact of sperm TLR2 on sperm-oocyte communication was attributed to their direct effect on sperm motility parameters, we analyzed different motility parameters of TLR2 antagonist/agonist pre-treated sperm at different time points (0, 1, and 3 h) of the next culture using CASA system. The results showed that the pre-treatment of sperm with TLR2 antagonist/agonist did not affect all sperm motility parameters, related to their fertilizing competence (Total motility (%), progressive motility (%), average path velocity (VAP, μm/s), straight-line velocity (VSL, μm/s), curvilinear velocity (VCL, μm/s), the amplitude of lateral head displacement (ALH, μm), beat cross frequency (BCF, Hz), straightness (STR, %), and linearity (LIN, %)), at all tested time points (**Supplementary Table S2A,B).** These findings prompted us to hypothesize that TLR2 regulates sperm interactions with oocytes without interfering with sperm motility parameters.

TLR2 System Impacts the ZP-Induced Acrosome Reaction in Sperm Under IVF Conditions

Induction of AR is an essential step for mammalian sperm to penetrate the ZP and fertilize oocytes (Breitbart et al., 2005; Kwon et al., 2013). The results of flow cytometry revealed that the blockage of sperm TLR2 suppressed the induction of AR in ZP-bound sperm at 1 and 3 h under IVF conditions compared to control (**Figure 5A**). While the activation of sperm TLR2 increased the induction of AR in ZP-bound sperm at 3 h under IVF conditions (**Figure 5B**). These results may account for the ability of sperm TLR2 to regulate sperm-ZP binding and penetration and thereby fertilizing oocytes *via* the induction of AR.

TLR2 System Impacts A23187-Triggered Acrosome Reaction in Sperm

To further confirm our hypothesis, we evaluated the impact of sperm TLR2 on the chemical induction of AR by calcium ionophore A23187. Initially, flow cytometry results showed that the addition of 1 μM of A23187 induced AR in sperm compared to control (38.33 ± 2.05% vs 0.28 ± 0.06%).

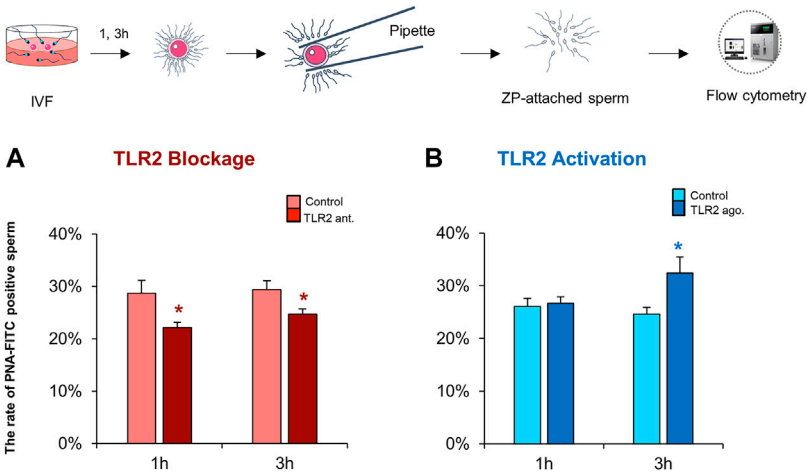

FIGURE 5 | TLR2 system impacts the ZP-induced acrosome reaction in sperm under IVF conditions. Sperm were pre-treated by TLR2 antagonist (100 μM) or TLR2 agonist (100 ng ml^{-1}) for 30 min, washed, and co-cultured with cumulus-free oocytes for 1 and 3 h. Then, ZP-attached sperm were collected and incubated with 25 μg ml^{-1} fluorescein peanut agglutinin FITC-conjugate (PNA-FITC) for 8 min at 38.5°C in dark. The percent of acrosome-reacted sperm was analyzed by flow cytometry **(A)** TLR2 antagonist reduces the ZP-induced acrosome reaction in sperm under IVF conditions **(B)** TLR2 agonist increases the ZP-induced acrosome reaction in sperm under IVF conditions. Data reported as means ± S.E.M of five independent experiments. Different superscript asterisks denote a significant difference ($p < 0.05$).

However, the blockage of TLR2 did not independently interfere with sperm AR, but it suppressed A23187-triggered AR (**Figure 6A,C,E**). On the other hand, the activation of TLR2 interfered with sperm AR neither alone nor in combination with A23187 compared to the control or A23187-triggered AR group, respectively (**Figure 6B,D,F**). These findings further confirm a pivotal connection between sperm TLR2 system and their interaction with oocytes, possibly through the regulation of AR induction.

TLR2 System Manipulates the Intracellular Calcium (Ca^{2+}) Uptake in A23187-Triggered Sperm

TLR2 pathway regulates calcium (Ca^{2+}) mobilization through the cell (Yu et al., 2014; Conejeros et al., 2015), which is essential for the acquisition of sperm fertilizing competence through induction of capacitation and AR (Florman and First, 1988a; Florman and First, 1988b; Parrish et al., 1999). Therefore, this experiment was conducted to identify the impact of TLR2 pathway on the intracellular Ca^{2+} uptake by bull sperm using single-cell imaging. The results showed that the exposure of sperm to TLR2 antagonist/agonist alone did not induce detectable changes in sperm Ca^{2+} influx (data not shown). Once A23187 was added, individual sperm immediately experienced the fluorescence intensity in all tested groups. In the control group, fluorescence intensity elevated sharply once A23187 was added, then showed a sustained and sluggish elevation, and finally kept stable for individual sperm. However, TLR2 antagonist (**Supplementary video 2**) treated sperm showed lower levels of fluorescence compared to control (**Supplementary video 1**). TLR2 agonist (**Supplementary video 4**) treated sperm showed higher levels of fluorescence compared to control (**Supplementary video 3**) (**Figures 7A–D**).

DISCUSSION

Accumulating evidence is building that different TLRs, as innate immune receptors, have been implicated in the regulation of several physiological functions of female reproduction including ovulation, fertilization, gestation, and parturition (Shimada et al., 2006; Liu et al., 2008; Kannaki et al., 2011). The current study sheds new light on the functional relevance of the TLR2 system in the acquisition of sperm fertilizing competence at the sperm-oocyte interface during the fertilization in bovine. Here, we adapted IVF models to investigate the impact of sperm TLR2 on sperm-oocyte interactions. Specifically, the results showed that the TLR2 system partly relates to the AR induction to penetrate ZP and fertilize oocytes, that is possibly mediated by Ca^{2+} transmembrane influx.

It was evident that stimulation of TLR2 pathway in cumulus cells of ovulated COCs indirectly stimulates sperm capacitation to enhance fertilization (Shimada et al., 2008). Also, sperm express TLR2 (Fujita et al., 2011; Akthar et al., 2020). These facts prompted us to hypothesize that the TLR2 system is directly involved in sperm interactions with oocytes for preparing sperm to fertilize the oocyte. The current results showed that the ligation of sperm TLR2 with its specific antagonist/agonist before being co-cultured with COCs down/up-regulated cleavage and blastocyst rates. Similar responses were obtained when higher (5×10^6 ml^{-1}) or lower (0.1×10^6 ml^{-1}) concentrations of sperm were used during IVF (**Supplementary Figure S2**). Importantly, testing our hypothesis using a wide range of sperm concentrations enabled us to exclude the possibility of biased results due to abnormal fertilization by polyspermy that might

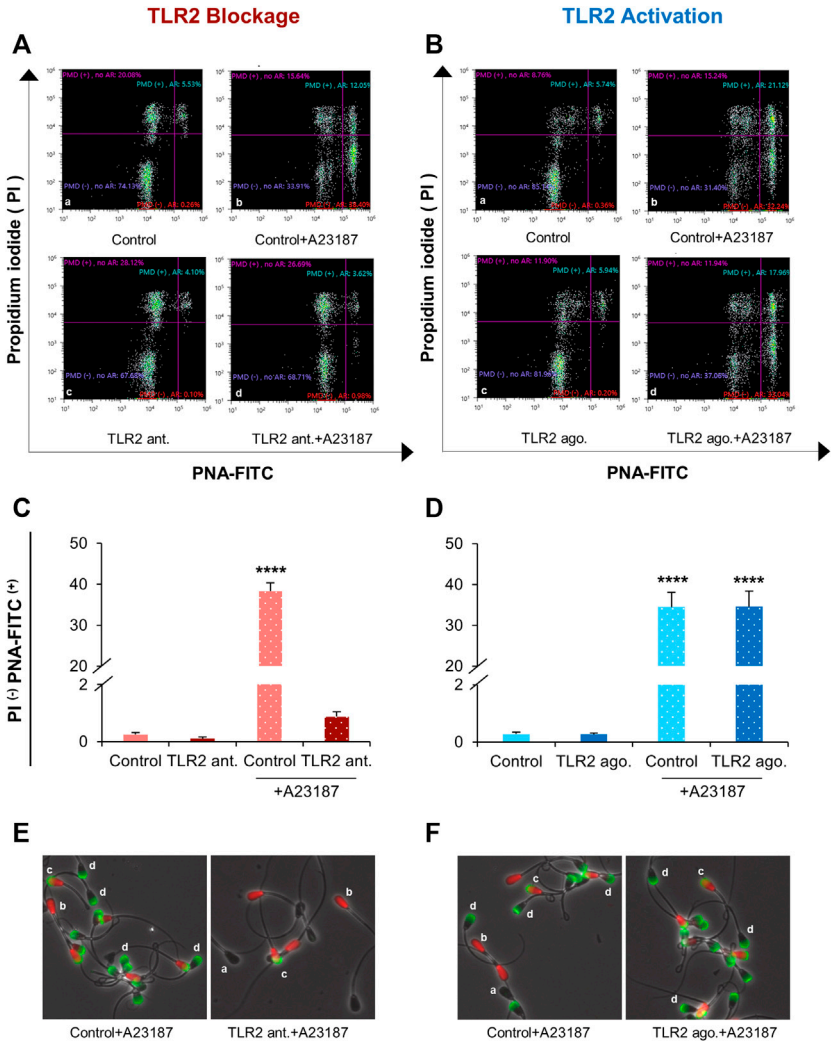

FIGURE 6 | Effect of TLR2 antagonist and agonist treatment on sperm acrosome reaction (AR) triggered by A23187**.** Swim-up sperm were pre-treated by TLR2 antagonist (100 μM) or TLR2 agonist (100 ng ml^{-1}) for 30 min, washed, and triggered with or without 1 μM A23187 for 60 min. Then sperm were incubated with fluorescein peanut agglutinin FITC-conjugate (PNA-FITC; for detection of induction of acrosome reaction (AR)) and propidium iodide (PI; for detection of plasma membrane damage (PMD)) for 8 min at 38.5°C in dark. The percent of live and acrosome-reacted sperm was analyzed by fluorescence microscopy and flow cytometry. Untreated sperm were kept as a negative control **(A)** Representative dot plot diagram; a: Control; c: 100 μM TLR2 antagonist; b: Control +1 μM A23187; d: 100 μM TLR2 antagonist +1 μM A23187 and **(C)** Analysis of PNA-FITC and PI staining of bovine sperm in different treatment groups by flow cytometry **(B)** Representative dot plot diagram; a: Control; c: 100 ng ml^{-1} TLR2 agonist; b: Control +1 μM A23187; d: 100 ng ml^{-1} TLR2 agonist +1 μM A23187 and **(D)** Analysis of PNA-FITC and PI staining of bovine sperm in different treatment groups by flow cytometry **(E)** Representative images of TLR2 antagonist-treated sperm or **(F)** TLR2 agonist-treated sperm stained with FITC-PNA and PI viewed with fluorescence microscope (200×). a: live intact acrosome, b: dead intact acrosome, c: dead reacted acrosome, d: live reacted acrosome. Data reported as means ± S.E.M of five independent experiments. Asterisks denote a significant variance **** ($p < 0.0001$) between the different groups compared to control.

develop by using a high sperm number during IVF (Li et al., 2003; Snook et al., 2011). Therefore, we suggest that such responses were partially independent of the number of sperm assigned to fertilize oocytes but probably related to the fertilizing competence of individual sperm. Additionally, the results showed that the degree of stimulative effect by TLR2 agonist on the cleavage and blastocyst rates was relatively lower than that of suppressing effect by TLR2 antagoinst especially with high sperm concentrations (5×10^6 sperm ml^{-1}) in IVF (**Supplementary Figure S2**). This might account for the presence of endogenous ligands for the TLR2 pathway such as low molecular weight hyaluronan, obtained from the degradation of the hyaluronan-rich matrix of ovulated COCs by hyaluronidase released from sperm (Shimada et al., 2008).

Cellular mechanisms of sperm-COCs interactions for the induction of fertilization comprise three consequential levels including invasion of cumulus cell layers followed by penetration of ZP and finally, the fusion with oocytes cell membrane for transmission of the paternal genetic message encoded in the DNA (Cox et al., 1993; Anifandis et al., 2014). To identify the functional role of sperm TLR2 in the process of

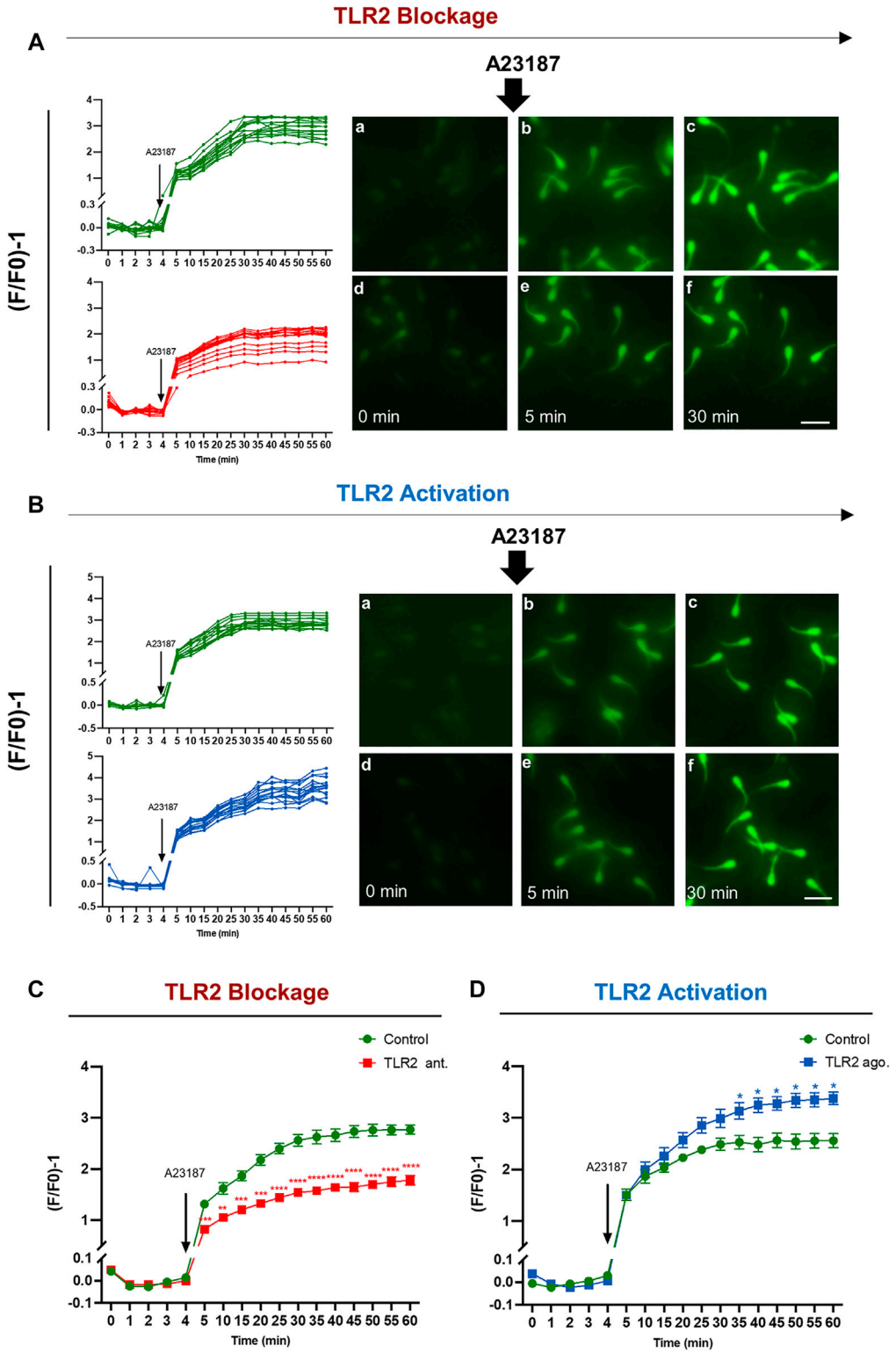

FIGURE 7 | TLR2 system manipulates the intracellular calcium uptake by bovine sperm. Swim-up sperm were pre-treated by TLR2 antagonist (100 μM) or TLR2 agonist (100 ng ml^{-1}) for 30 min, washed, and loaded with 5 μM Fluo-4 AM for 40 min at 38.5°C in the dark before adding calcium ionophore A23187 (1 μM as a final concentration). The sperm fluorescence was measured by the fluorescence microscope. Images were captured every 5 min for a total of 1 h, with A23187 added after the initial five readings (every 1 min). The images were analyzed using BZ-X800 Analyzer and each sperm head was selected as the region of interest. Data were normalized using the following equation (F/F0)-1. where F0 is the average of the first five readings before the addition of

(*Continued*)

FIGURE 7 | A23187 and F is the fluorescence intensity obtained at each time point **(A)** Single-cell imaging of Fluo-4 fluorescence in bovine sperm in response to treatment: Control (a–c) and 100 μM TLR2 antagonist (d–f) **(B)** Single-cell imaging of Fluo-4 fluorescence in bovine sperm in response to treatment: Control (a–c) and 100 ng ml^{-1} TLR2 agonist (d–f). Photos were taken before treatment (a, d), at 5 min (b, e), and 30 min (c, f) (Left) Measurement for individual sperm in each treatment for 60 min incubation. Original magnification ×200(a–f). Scale bar = 20 μm **(C)** TLR2 antagonist decreases the average intracellular calcium uptake by bovine sperm in response to treatment with A23187 **(D)** TLR2 agonist increases the average intracellular calcium uptake by bovine sperm in response to treatment with A23187. Data reported as means ± S.E.M of five independent experiments. Asterisks denote a significant variance * ($p < 0.05$); ** ($p < 0.01$); *** ($p < 0.001$); **** ($p < 0.0001$) between the treatment group compared to control.

sperm-COCs interaction, the sperm pre-treated with TLR2 antagonist/agonist were co-cultured with cumulus-free oocytes or zona-free oocytes, and the cleavage rate was evaluated. Our data showed that the blockage or activation of the TLR2 pathway selectively manipulated the cleavage rate in cumulus-free oocytes but not in zona-free oocytes, signifying that the TLR2 pathway is involved mainly in sperm-ZP interactions, rather than the sperm-oocyte fusion. Likewise, the average numbers of ZP-bound and/or ZP-penetrated sperm were down/up-regulated by the blockage/activation of the TLR2 pathway in sperm. Sperm-ZP binding and penetration are crucial steps during fertilization (Oehninger et al., 1997) since ZP is the last barrier for the sperm before fertilizing the oocyte (Coutinho daSilva et al., 2012). Previous studies have demonstrated that lower sperm binding and penetration ratios are major causes of infertility in humans (Liu and Baker, 2000), mice (Dai et al., 2017), and bovine (Hamze et al., 2020). Therefore, it seems that the TLR2 system in bull sperm takes part in the dynamic interactions of sperm with ZP during oocyte fertilization.

Cumulus cells attract, trap, and select active sperm during the process of fertilization (Cox et al., 1993). One could argue that the current findings might be due to the direct impact of TLR2 antagonist/agonist on sperm viability and motility parameters. Especially, during pathological conditions, the drastic activation of the TLR2 pathway (using a relatively high concentration of TLR2 agonist, peptidoglycan; 1 μg ml^{-1} or Pam3Cys; 10 μg ml^{-1} for long incubation time; 6 h) reduced sperm total and progressive motility through decreasing the level of ATP production in mice (Zhu et al., 2016). In our model, the CASA analysis revealed that the pre-treatment of sperm with TLR2 antagonist or agonist for 30 min did not affect the sperm motility parameters at different time points in the subsequent culture. This suggests that the TLR2 pathway regulates sperm-ZP binding and penetration and subsequent sperm fertilizing ability without disrupting their motility and viability.

Clearly, the fertilizing spermatozoon must undergo AR to penetrate the ZP, in which the outer acrosomal membrane fuses with the overlying plasma membrane (Yanagimachi, 1994; Mao and Yang, 2013), Our results showed that the blockage/activation of the TLR2 pathway reduced/increased the AR in ZP-attached sperm. Additionally, the results showed that the blockage of TLR2 strongly reduced AR in A23187-triggered sperm. In contrast, the activation of the TLR2 pathway did not affect the high level of AR induction in A23187-triggered sperm. Also, our preliminary observation showed that increasing the concentrations of A23187 and/or TLR2 agonist did not induce a further increase in AR induction in A23187-triggered sperm (data not shown), suggesting that A23187 evoked the maximum threshold plateau of induction of AR *in vitro* which cannot be further enhanced by using any other stimulus. Together, these results suggest that the TLR2 pathway mediates sperm AR in response to ZP attachment.

TLR2 is a transmembrane receptor and its binding with a specific agonist induces the phosphorylation of several intracellular signaling adaptor proteins through the MyD88-dependent signaling pathway (Akira et al., 2001). Our recent observations showed that the treatment of sperm by TLR2 agonist or antagonist did not affect TLR2 localization and expression in sperm (Akthar et al., 2020). In mice, phosphatidylinositol 3-kinase (PI3K), as one of TLR2 signal transduction proteins (Zhu et al., 2016), is involved in the process of AR induction by ZP (Jungnickel et al., 2007). In support of this, the phosphorylation levels of PI3K were increased during the capacitation of bovine sperm (Rotman et al., 2010). Therefore, we suggest that PI3K could be the candidate to act as a commonly-shared signaling protein of the TLR2 pathway for the regulation of ZP-induced AR. Further investigations are needed to explore the downstream adaptor proteins of the TLR2 signaling pathway which are involved in regulating the process of ZP-triggered AR in bovine.

Increasing the intracellular Ca^{2+} triggers multiple physiological events in spermatozoa, such as hyperactivation, chemotaxis, capacitation, and acrosomal reaction in several mammalian species (Darszon et al., 2011; Correia et al., 2015). Acrosome serves as a store of Ca^{2+} which has been entered during capacitation and mobilized into the cytoplasm during AR (Watson and Plummer, 1986; Chiu et al., 2010). It has been demonstrated that the TLR2 pathway regulates Ca^{2+} mobilization through the cell; TLR2 agonist, Pam3Cys, stimulates Ca^{2+} influx in neutrophils (Conejeros et al., 2015), human mast cells (Yu et al., 2014), and airway epithelial cells *via* TLR2-dependent signaling and modulates proinflammatory response to bacterial infection (Chun and Prince, 2006). Therefore, we hypothesized that the TLR2 pathway regulates AR *via* mediating Ca^{2+} transmembrane transport. In support of this hypothesis, we observed that the exposure of sperm to TLR2 antagonist/agonist reduced/increased the Ca^{2+} influx into sperm during the process of AR induction using A23187. Inappropriately, we could not quantify the intracellular Ca^{2+} level of individual attached-ZP sperm because of the very limited number of those sperm mechanically detached from ZP especially after loading with Fluo-4 AM. Our observation suggests that TLR2 is involved in regulating Ca^{2+} transmembrane influx during the induction of AR, at least, in A23187-triggered sperm. However, the underlying molecular signaling of the TLR2-triggered Ca^{2+} entry mechanism and its possible link and relation

with Ca^{2+} channels maily CatSper channels remains to be unclear and requires further investigations.

Overall, our findings suggest that the TLR2 system regulates sperm fertilizing competence and interactions of oocytes during the fertilization, at least *in vitro*, in cattle. The proposed mechanisms involve controlling Ca^{2+} transmembrane uptake for the induction of AR and subsequent penetration to ZP of oocytes to induce fertilization. Therefore, it seems that the sperm possibly developed a quite flexible sensing mechanism simultaneously against pathogens as well as COCs toward fertilization with the same TLR2 of the innate immune system. To the best of our knowledge, such physiological impact of sperm TLR2 on oocyte fertilization has not been described, and thus understanding its underlying mechanisms could have important translational implications in the context of assisted reproductive technology towards the improvement of fertility.

DATA AVAILABILITY STATEMENT

The original contributions presented in the study are included in the article/**Supplementary Material**, further inquiries can be directed to the corresponding author.

ETHICS STATEMENT

The animal study was reviewed and approved by the Committee on the Ethics of Animal Experiments of the Obihiro University of Agriculture and Veterinary Medicine (Permit number 19–111).

AUTHOR CONTRIBUTIONS

DM conceived the study. AM initiated the study design, DM and MM helped with implementation and provided statistical analysis. DM and MM described the manuscript. AM and MS revised the manuscript. All authors contributed to refinement of the study protocol and approved the final manuscript.

FUNDING

This work was supported by a Grant-in-Aid for Scientific Research (20H03122) from the Japan Society for the Promotion of Science (JSPS) and Livestock Promotional Funds of the Japan Racing Association (JRA).

ACKNOWLEDGMENTS

The authors would like to thank Chihiro Kanno, Kitasato University, Japan, for his technical support for using the CASA system, and Genetics Hokkaido for their generous supply of the semen straws used in all the experiments.

SUPPLEMENTARY MATERIAL

The Supplementary Material for this article can be found online at: https://www.frontiersin.org/articles/10.3389/fcell.2022.810961/full#supplementary-material

Supplementary Videos | Representative videos for single-cell imaging of intracellular calcium uptake by bovine sperm. Swim-up sperm were pre-treated by TLR2 antagonist (0.1 % DMSO, as a control, or 100 μM) or TLR2 agonist (0.05 % ethanol, as a control, or 100 ng ml^{-1}) for 30 min, washed, and loaded with 5 μM Fluo-4 AM for 40 min at 38.5°C in the dark before adding calcium ionophore A23187 (1 μM as a final concentration). The sperm fluorescence was detected by the fluorescence microscope. Images were captured every 5 min for a total of 1 h, with A23187 added after the initial 5 readings (every 1 min). Videos show time-lapse representative single-cell imaging of Fluo-4 fluorescence in bovine sperm in response to treatment: (Video 1) Control (0.1 % DMSO), (Video 2) 100 μM TLR2 antagonist; (Video 3) Control (0.05% ethanol), and (Video 4) 100 ng ml^{-1} TLR2 agonist.

REFERENCES

Akira, S., Takeda, K., and Kaisho, T. (2001). Toll-like Receptors: Critical Proteins Linking Innate and Acquired Immunity. *Nat. Immunol.* 2, 675–680. doi:10.1038/90609

Akthar, I., Suarez, S., Morillo, V. A., Sasaki, M., Ezz, M. A., Takahashi, K. I., et al. (2019). Sperm Enter Glands of Preovulatory Bovine Endometrial Explants and Initiate Inflammation. *Reproduction* 159, 181–192. doi:10.1530/REP-19-0414

Akthar, I., Kim, Y., Kanno, C., Horiguchi, S., Sasaki, M., Marey, M. A., et al. (2020). *Toll-like receptor 2 of bull sperm and uterus co-regulates sperm sensing by uterine gland to trigger the innate immune responses*. The 113th Society of Reproduction and Development Meeting, Sendai, Japan. doi:10.14882/jrds.113.0_P-27

Aldana, A., Carneiro, J., Martínez-Mekler, G., and Darszon, A. (2021). Discrete Dynamic Model of the Mammalian Sperm Acrosome Reaction: The Influence of Acrosomal pH and Physiological Heterogeneity. *Front. Physiol.* 12, 682790. doi:10.3389/fphys.2021.682790

Anifandis, G., Messini, C., Dafopoulos, K., Sotiriou, S., and Messinis, I. (2014). Molecular and Cellular Mechanisms of Sperm-Oocyte Interactions Opinions Relative to *In Vitro* Fertilization (IVF). *Ijms* 15, 12972–12997. doi:10.3390/ijms150712972

Austin, C. (1951). Observations on the Penetration of the Sperm into the Mammalian Egg. *Aust. Jnl. Bio. Sci.* 4, 581–596. doi:10.1071/bi9510581

Austin, C. R. (1975). Membrane Fusion Events in Fertilization. *Reproduction* 44, 155–166. doi:10.1530/jrf.0.0440155

Avella, M. A., and Dean, J. (2011). Fertilization with Acrosome-Reacted Mouse Sperm: Implications for the Site of Exocytosis. *Proc. Natl. Acad. Sci.* 108 (50), 19843–19844. doi:10.1073/pnas.1118234109

Breitbart, H., Cohen, G., and Rubinstein, S. (2005). Role of Actin Cytoskeleton in Mammalian Sperm Capacitation and the Acrosome Reaction. *Reproduction* 129, 263–268. doi:10.1530/rep.1.00269

Chang, M. C. (1951). Fertilizing Capacity of Spermatozoa Deposited into the Fallopian Tubes. *Nature* 168, 697–698. doi:10.1038/168697b0

Chávez, J. C., De la Vega-Beltrán, J. L., José, O., Torres, P., Nishigaki, T., Treviño, C. L., et al. (2018). Acrosomal Alkalization Triggers Ca2+ Release and Acrosome Reaction in Mammalian Spermatozoa. *J. Cel. Physiol.* 233, 4735–4747. doi:10.1002/jcp.26262

Cheng, K., Wang, X., Zhang, S., and Yin, H. (2012). Discovery of Small-Molecule Inhibitors of the TLR1/TLR2 Complex. *Angew. Chem. Int. Ed.* 51, 12246–12249. doi:10.1002/anie.201204910

Chiu, P. C. N., Wong, B. S. T., Lee, C.-L., Lam, K. K. W., Chung, M.-K., Lee, K.-F., et al. (2010). Zona Pellucida-Induced Acrosome Reaction in Human Spermatozoa Is Potentiated by Glycodelin-A via Down-Regulation of Extracellular Signal-Regulated Kinases and Up-Regulation of Zona

Pellucida-Induced Calcium Influx. *Hum. Reprod.* 25 (11), 2721–2733. doi:10.1093/humrep/deq243

Chun, J., and Prince, A. (2006). Activation of Ca2+-dependent Signaling by TLR2. *J. Immunol.* 177, 1330–1337. doi:10.4049/jimmunol.177.2.1330

Conejeros, I., Gibson, A. J., Werling, D., Muñoz-Caro, T., Hermosilla, C., Taubert, A., et al. (2015). Effect of the Synthetic Toll-like Receptor Ligands LPS, Pam3CSK4, HKLM and FSL-1 in the Function of Bovine Polymorphonuclear Neutrophils. *Developmental Comp. Immunol.* 52, 215–225. doi:10.1016/j.dci.2015.05.012

Correia, J., Michelangeli, F., and Publicover, S. (2015). Regulation and Roles of Ca2+ Stores in Human Sperm. *Reproduction* 150, R65–R76. doi:10.1530/REP-15-0102

Coutinho da Silva, M. A., Seidel, G. E., Jr, Squires, E. L., Graham, J. K., and Carnevale, E. M. (2012). Effects of Components of Semen Extenders on the Binding of Stallion Spermatozoa to Bovine or Equine Zonae Pellucidae. *Reproduction* 143, 577–585. doi:10.1530/REP-11-0099

Cox, J. F., Hormazábal, J., and Santa María, A. (1993). Effect of the Cumulus on *In Vitro* Fertilization of Bovine Matured Oocytes. *Theriogenology* 40, 1259–1267. doi:10.1016/0093-691X(93)90296-H

Dai, X., Lu, Y., Zhang, M., Miao, Y., Zhou, C., Cui, Z., et al. (2017). Melatonin Improves the Fertilization Ability of post-ovulatory Aged Mouse Oocytes by Stabilizing Ovastacin and Juno to Promote Sperm Binding and Fusion. *Hum. Reprod.* 32, 598–606. doi:10.1093/humrep/dew362

Darszon, A., Nishigaki, T., Beltran, C., and Treviño, C. L. (2011). Calcium Channels in the Development, Maturation, and Function of Spermatozoa. *Physiol. Rev.* 91, 1305–1355. doi:10.1152/physrev.00028.2010

Elesh, I. F., Marey, M. A., Zinnah, M. A., Akthar, I., Kawai, T., Naim, F., et al. (2021). Peptidoglycan Switches off the TLR2-Mediated Sperm Recognition and Triggers Sperm Localization in the Bovine Endometrium. *Front. Immunol.* 11, 619408. doi:10.3389/fimmu.2020.619408

Ezz, M. A., Marey, M. A., Elweza, A. E., Kawai, T., Heppelmann, M., Pfarrer, C., et al. (2019). TLR2/4 Signaling Pathway Mediates Sperm-Induced Inflammation in Bovine Endometrial Epithelial Cells *In Vitro*. *PloS one* 14, e0214516. doi:10.1371/journal.pone.0214516

Florman, H. M., and First, N. L. (1988b). Regulation of Acrosomal Exocytosis. *Developmental Biol.* 128, 464–473. doi:10.1016/0012-1606(88)90308-9

Florman, H. M., and First, N. L. (1988a). The Regulation of Acrosomal Exocytosis. *Developmental Biol.* 128, 453–463. doi:10.1016/0012-1606(88)90307-7

Fujita, Y., Mihara, T., Okazaki, T., Shitanaka, M., Kushino, R., Ikeda, C., et al. (2011). Toll-like Receptors (TLR) 2 and 4 on Human Sperm Recognize Bacterial Endotoxins and Mediate Apoptosis. *Hum. Reprod.* 26, 2799–2806. doi:10.1093/humrep/der234

Gadella, B. M. (2013). Dynamic Regulation of Sperm Interactions with the Zona Pellucida Prior to and after Fertilisation. *Reprod. Fertil. Dev.* 25, 26–37. doi:10.1071/RD12277

Grabowski, M., Bermudez, M., Rudolf, T., Šribar, D., Varga, P., Murgueitio, M. S., et al. (2020). Identification and Validation of a Novel Dual Small-Molecule TLR2/8 Antagonist. *Biochem. Pharmacol.* 177, 113957. doi:10.1016/j.bcp.2020.113957

Grullón, L. A., Gadea, J., Mondéjar, I., Matás, C., Romar, R., and Coy, P. (2013). How Is Plasminogen/plasmin System Contributing to Regulate Sperm Entry into the Oocyte? *Reprod. Sci.* 20, 1075–1082. doi:10.1177/1933719112473657

Hamze, J. G., Sánchez, J. M., O'Callaghan, E., McDonald, M., Bermejo-Álvarez, P., Romar, R., et al. (2020). JUNO Protein Coated Beads: A Potential Tool to Predict Bovine Sperm Fertilizing Ability. *Theriogenology* 155, 168–175. doi:10.1016/j.theriogenology.2020.05.025

Honda, A., Siruntawineti, J., and Baba, T. (2002). Role of Acrosomal Matrix Proteases in Sperm-Zona Pellucida Interactions. *Hum. Reprod. Update* 8, 405–412. doi:10.1093/humupd/8.5.405

Ideta, A., Aoyagi, Y., Tsuchiya, K., Kamijima, T., Nishimiya, Y., and Tsuda, S. (2013). A Simple Medium Enables Bovine Embryos to Be Held for Seven Days at 4°C. *Sci. Rep.* 3, 1173. doi:10.1038/srep01173

Ijiri, T. W., Mahbub Hasan, A. K. M., and Sato, K.-i. (2012). Protein-tyrosine Kinase Signaling in the Biological Functions Associated with Sperm. *J. Signal Transduction* 2012, 1–18. doi:10.1155/2012/181560

Inoue, N., Ikawa, M., Isotani, A., and Okabe, M. (2005). The Immunoglobulin Superfamily Protein Izumo Is Required for Sperm to Fuse with Eggs. *Nature* 434, 234–238. doi:10.1038/nature03362

Jungnickel, M. K., Sutton, K. A., Wang, Y., and Florman, H. M. (2007). Phosphoinositide-dependent Pathways in Mouse Sperm Are Regulated by Egg ZP3 and Drive the Acrosome Reaction. *Developmental Biol.* 304, 116–126. doi:10.1016/j.ydbio.2006.12.023

Kannaki, T. R., Shanmugam, M., and Verma, P. C. (2011). Toll-like Receptors and Their Role in Animal Reproduction. *Anim. Reprod. Sci.* 125, 1–12. doi:10.1016/j.anireprosci.2011.03.008

Kanno, C., Sakamoto, K. Q., Yanagawa, Y., Takahashi, Y., Katagiri, S., and Nagano, M. (2017). Comparison of Sperm Subpopulation Structures in First and Second Ejaculated Semen from Japanese Black Bulls by a Cluster Analysis of Sperm Motility Evaluated by a CASA System. *J. Vet. Med. Sci.* 79, 1359–1365. doi:10.1292/jvms.17-0012

Kashir, J., Heindryckx, B., Jones, C., De Sutter, P., Parrington, J., and Coward, K. (2010). Oocyte Activation, Phospholipase C Zeta and Human Infertility. *Hum. Reprod. Update* 16, 690–703. doi:10.1093/humupd/dmq018

Kumar, N., and Singh, A. (2015). Trends of Male Factor Infertility, an Important Cause of Infertility: a Review of Literature. *J. Hum. Reprod. Sci.* 8, 191–196. doi:10.4103/0974-1208.170370

Kwon, W.-S., Park, Y.-J., Mohamed, E.-S. A., and Pang, M.-G. (2013). Voltage-dependent Anion Channels Are a Key Factor of Male Fertility. *Fertil. Sterility* 99, 354–361. doi:10.1016/j.fertnstert.2012.09.021

Li, Y.-H., Ma, W., Li, M., Hou, Y., Jiao, L.-H., and Wang, W.-H. (2003). Reduced Polyspermic Penetration in Porcine Oocytes Inseminated in a New *In Vitro* Fertilization (IVF) System: Straw IVF1. *Biol.Reprod.* 69, 1580–1585. doi:10.1095/biolreprod.103.018937

Liu, D. Y., and Baker, H. W. G. (2000). Defective Sperm-Zona Pellucida Interaction: a Major Cause of Failure of Fertilization in Clinical *In-Vitro* Fertilization. *Hum. Reprod.* 15, 702–708. doi:10.1093/humrep/15.3.702

Liu, D. Y., Garrett, C., and Baker, H. W. G. (2004). Clinical Application of Sperm-Oocyte Interaction Tests in *In Vitro* Fertilization-Embryo Transfer and Intracytoplasmic Sperm Injection Programs. *Fertil. Sterility* 82, 1251–1263. doi:10.1016/j.fertnstert.2003.10.057

Liu, Y., Wang, D.-K., and Chen, L.-M. (2012). The Physiology of Bicarbonate Transporters in Mammalian Reproduction1. *Biol. Reprod.* 86, 33–37. doi:10.1095/biolreprod.111.096826

Liu, Z., Shimada, M., and Richards, J. S. (2008). The Involvement of the Toll-like Receptor Family in Ovulation. *J. Assist. Reprod. Genet.* 25, 223–228. doi:10.1007/s10815-008-9219-0

Mao, H.-T., and Yang, W.-X. (2013). Modes of Acrosin Functioning during Fertilization. *Gene* 526, 75–79. doi:10.1016/j.gene.2013.05.058

Marquez, B., and Suarez, S. S. (2007). Bovine Sperm Hyperactivation Is Promoted by Alkaline-Stimulated Ca2+ Influx1. *Biol. Reprod.* 76, 660–665. doi:10.1095/biolreprod.106.055038

Marquez, B., and Suarez, S. S. (2004). Different Signaling Pathways in Bovine Sperm Regulate Capacitation and Hyperactivation1. *Biol. Reprod.* 70, 1626–1633. doi:10.1095/biolreprod.103.026476

Mayorga, L. S., Tomes, C. N., and Belmonte, S. A. (2007). Acrosomal Exocytosis, a Special Type of Regulated Secretion. *Tbmb* 59, 286–292. doi:10.1080/15216540701222872

Morillo, V. A., Akthar, I., Fiorenza, M. F., Takahashi, K. I., Sasaki, M., Marey, M. A., et al. (2020). Toll-like Receptor 2 Mediates the Immune Response of the Bovine Oviductal Ampulla to Sperm Binding. *Mol. Reprod. Dev.* 87 (10), 1059–1069. doi:10.1002/mrd.23422

Nishigaki, T., José, O., González-Cota, A. L., Romero, F., Treviño, C. L., and Darszon, A. (2014). Intracellular pH in Sperm Physiology. *Biochem. Biophysical Res. Commun.* 450, 1149–1158. doi:10.1016/j.bbrc.2014.05.100

Oehninger, S., Mahony, M., Özgür, K., Kolm, P., Kruger, T., and Franken, D. (1997). Clinical Significance of Human Sperm-Zona Pellucida Binding. *Fertil. Sterility* 67, 1121–1127. doi:10.1016/s0015-0282(97)81449-5

Parrish, J. J., Susko-Parrish, J. L., and Graham, J. K. (1999). *In Vitro* capacitation of Bovine Spermatozoa: Role of Intracellular Calcium. *Theriogenology* 51, 461–472. doi:10.1016/S0093-691X(98)00240-4

Parrish, J. J., Susko-Parrish, J., Winer, M. A., and First, N. L. (1988). Capacitation of Bovine Sperm by Heparin1. *Biol. Reprod.* 38, 1171–1180. doi:10.1095/biolreprod38.5.1171

Reitermann, A., Metzger, J., Wiesmüller, K.-H., Jung, G., and Bessler, W. G. (1989). Lipopeptide Derivatives of Bacterial Lipoprotein Constitute Potent Immune

Adjuvants Combined with or Covalently Coupled to Antigen or Hapten. *Biol. Chem. Hoppe-Seyler* 370 (4), 343–352. doi:10.1515/bchm3.1989.370.1.343

Rotman, T., Etkovitz, N., Spiegel, A., Rubinstein, S., and Breitbart, H. (2010). Protein Kinase A and Protein Kinase Cα/PPP1CC2 Play Opposing Roles in the Regulation of Phosphatidylinositol 3-kinase Activation in Bovine Sperm. *Reproduction* 140, 43–56. doi:10.1530/REP-09-0314

Saeidi, S., Shapouri, F., Amirchaghmaghi, E., Hoseinifar, H., Sabbaghian, M., Sadighi Gilani, M. A., et al. (2014). Sperm protection in the Male Reproductive Tract by Toll-like Receptors. *Andrologia* 46, 784–790. doi:10.1111/and.12149

Saling, P. M., Sowinski, J., and Storey, B. T. (1979). An Ultrastructural Study of Epididymal Mouse Spermatozoa Binding to Zonae Pellucidae *In Vitro*: Sequential Relationship to the Acrosome Reaction. *J. Exp. Zool.* 209, 229–238. doi:10.1002/jez.1402090205

Shimada, M., Hernandez-Gonzalez, I., Gonzalez-Robanya, I., and Richards, J. S. (2006). Induced Expression of Pattern Recognition Receptors in Cumulus-Oocyte Complexes: Novel Evidence for Innate Immune-like Functions during Ovulation. *Mol. Endocrinol.* 20, 3228–3239. doi:10.1210/me.2006-0194

Shimada, M., Yanai, Y., Okazaki, T., Noma, N., Kawashima, I., Mori, T., et al. (2008). Hyaluronan Fragments Generated by Sperm-Secreted Hyaluronidase Stimulate Cytokine/chemokine Production via the TLR2 and TLR4 Pathway in Cumulus Cells of Ovulated COCs, Which May Enhance Fertilization. *Development* 135, 2001–2011. doi:10.1242/dev.020461

Snook, R. R., Hosken, D. J., and Karr, T. L. (2011). The Biology and Evolution of Polyspermy: Insights from Cellular and Functional Studies of Sperm and Centrosomal Behavior in the Fertilized Egg. *Reproduction* 142, 779–792. doi:10.1530/REP-11-0255

Sosa, C. M., Pavarotti, M. A., Zanetti, M. N., Zoppino, F. C. M., De Blas, G. A., and Mayorga, L. S. (2014). Kinetics of Human Sperm Acrosomal Exocytosis. *Mol. Hum. Reprod.* 21, 244–254. doi:10.1093/molehr/gau110

Stern, R., Asari, A. A., and Sugahara, K. N. (2006). Hyaluronan Fragments: an Information-Rich System. *Eur. J. Cel Biol.* 85, 699–715. doi:10.1016/j.ejcb.2006.05.009

Stival, C., Puga Molina, L. D. C., Paudel, B., Buffone, M. G., Visconti, P. E., and Krapf, D. (2016). Sperm Capacitation and Acrosome Reaction in Mammalian Sperm. *Adv. Anat. Embryol. Cel Biol.* 220, 93–106. doi:10.1007/978-3-319-30567-7_5

Strünker, T., Goodwin, N., Brenker, C., Kashikar, N. D., Weyand, I., Seifert, R., et al. (2011). The CatSper Channel Mediates Progesterone-Induced Ca2+ Influx in Human Sperm. *Nature* 471, 382–386. doi:10.1038/nature09769

Takahashi, K., Kikuchi, K., Uchida, Y., Kanai-Kitayama, S., Suzuki, R., Sato, R., et al. (2013). Binding of Sperm to the Zona Pellucida Mediated by Sperm Carbohydrate-Binding Proteins Is Not Species-specific *In Vitro* between Pigs and Cattle. *Biomolecules* 3, 85–107. doi:10.3390/biom3010085

Toshimori, K. (1982). Penetration of the Mouse Sperm Head through the Zona Pellucida *In Vivo*: An Electromicroscope Study at 200KV. *Biol. Reprod.* 26, 475–481. doi:10.1095/biolreprod26.3.475

Watson, P. F., and Plummer, J. M. (1986). Relationship between Calcium Binding Sites and Membrane Fusion during the Acrosome Reaction Induced by Lonophore in Ram Spermatozoa. *J. Exp. Zool.* 238, 113–118. doi:10.1002/jez.1402380114

Yanagimachi, R. (1994). "Mammalian Fertilization,". *The Physiology of Reproduction*. Editors E. Knobil and J. D. Neill (New York, NY, USA: Raven Press), 1, 189–317.

Yu, Y., Yip, K. H., Tam, I. Y. S., Sam, S. W., Ng, C. W., Zhang, W., et al. (2014). Differential Effects of the Toll-like Receptor 2 Agonists, PGN and Pam3CSK4 on Anti-IgE Induced Human Mast Cell Activation. *PLoS One* 9, e112989. doi:10.1371/journal.pone.0112989

Zhu, X., Shi, D., Li, X., Gong, W., Wu, F., Guo, X., et al. (2016). TLR Signalling Affects Sperm Mitochondrial Function and Motility via Phosphatidylinositol 3-kinase and Glycogen Synthase Kinase-3α. *Cell Signal.* 28, 148–156. doi:10.1016/j.cellsig.2015.12.002

Conflict of Interest: The authors declare that the research was conducted in the absence of any commercial or financial relationships that could be construed as a potential conflict of interest.

Publisher's Note: All claims expressed in this article are solely those of the authors and do not necessarily represent those of their affiliated organizations, or those of the publisher, the editors and the reviewers. Any product that may be evaluated in this article, or claim that may be made by its manufacturer, is not guaranteed or endorsed by the publisher.

frontiers | Frontiers in Cell and Developmental Biology

ORIGINAL RESEARCH
published: 05 April 2022
doi: 10.3389/fcell.2022.824629

In silico Docking Analysis for Blocking JUNO-IZUMO1 Interaction Identifies Two Small Molecules that Block *in vitro* Fertilization

Nataliia Stepanenko[1†], Omri Wolk[2†], Enrica Bianchi[3], Gavin James Wright[3], Natali Schachter-Safrai[4], Kiril Makedonski[1], Alberto Ouro[1], Assaf Ben-Meir[4], Yosef Buganim[1] and Amiram Goldblum[2]*

[1]Department of Developmental Biology and Cancer Research, Faculty of Medicine, The Institute for Medical Research Israel-Canada, Hebrew University of Jerusalem, Jerusalem, Israel, [2]Laboratory of Molecular Modeling and Drug Discovery, Faculty of Medicine, School of Pharmacy, The Institute for Drug Research, Hebrew University of Jerusalem, Jerusalem, Israel, [3]Department of Biology, Hull York Medical School, York Biomedical Research Institute, University of York, York, United Kingdom, [4]Infertility and IVF Unit, Department of Obstetrics and Gynecology, Hadassah Ein-Kerem Medical Center and Faculty of Medicine, Hebrew University of Jerusalem, Jerusalem, Israel

OPEN ACCESS

Edited by:
Khaled Machaca,
Weill Cornell Medicine- Qatar, Qatar

Reviewed by:
Masahito Ikawa,
Osaka University, Japan
Gabor Laszlo Kovacs,
University of Pécs, Hungary
Soledad Natalia Gonzalez,
CONICET Instituto de Biología y Medicina Experimental (IBYME), Argentina

***Correspondence:**
Amiram Goldblum
amiramg@ekmd.huji.ac.il

[†]These authors have contributed equally to this work

Specialty section:
This article was submitted to Molecular and Cellular Reproduction, a section of the journal Frontiers in Cell and Developmental Biology

Received: 29 November 2021
Accepted: 28 February 2022
Published: 05 April 2022

Citation:
Stepanenko N, Wolk O, Bianchi E, Wright GJ, Schachter-Safrai N, Makedonski K, Ouro A, Ben-Meir A, Buganim Y and Goldblum A (2022) In silico Docking Analysis for Blocking JUNO-IZUMO1 Interaction Identifies Two Small Molecules that Block in vitro Fertilization. Front. Cell Dev. Biol. 10:824629. doi: 10.3389/fcell.2022.824629

Combined hormone drugs are the basis for orally administered contraception. However, they are associated with severe side effects that are even more impactful for women in developing countries, where resources are limited. The risk of side effects may be reduced by non-hormonal small molecules which specifically target proteins involved in fertilization. In this study, we present a virtual docking experiment directed to discover molecules that target the crucial fertilization interactions of JUNO (oocyte) and IZUMO1 (sperm). We docked 913,000 molecules to two crystal structures of JUNO and ranked them on the basis of energy-related criteria. Of the 32 tested candidates, two molecules (i.e., Z786028994 and Z1290281203) demonstrated fertilization inhibitory effect in both an *in vitro* fertilization (IVF) assay in mice and an *in vitro* penetration of human sperm into hamster oocytes. Despite this clear effect on fertilization, these two molecules did not show JUNO–IZUMO1 interaction blocking activity as assessed by AVidity-based EXtracellular Interaction Screening (AVEXIS). Therefore, further research is required to determine the mechanism of action of these two fertilization inhibitors.

Keywords: non-hormonal contraceptives, docking, *in vitro* fertilization, JUNO–IZUMO1 interaction, human sperm penetration assay

INTRODUCTION

During the 20th century, prevention of unwanted pregnancies became a major concern for both individual women and society as a whole, resulting in the development of the first hormonal contraceptive that went into market in 1960. Since then, all orally administered contraceptives are composed of combinations of steroid hormones from the progestogen and estrogen families, which inhibit follicular development and prevent ovulation and endometrial receptivity. However, these combined hormone drugs have a serious toll on the health of many women with numerous side effects (Sabatini and Cagiano, 2006; O'Connell et al., 2007) even at lower doses (Rosenberg et al., 1999). Progestin-only contraceptives ("Mini-pills") reduce many of these risks but are still associated with a high level of discontinuation (McCann and Potter, 1994). There are many reports of the

difficulties that women encounter in developing countries to use hormonal contraceptives due to several limitations (Townsend et al., 2011).

Substantial research was, therefore, dedicated to developing non-hormonal contraceptives that could reduce or eliminate side effects. To achieve this purpose, it is vital to identify proteins involved in the process of fertilization, apart from the steroid hormone receptors, so they can be targeted by non-hormonal candidates. Many such proteins were identified over the years, mostly by knock-out experiments or by blocking with antibodies (Gupta et al., 2015). Of those, two emerge as the most crucial ones for initial interaction between gametes: IZUMO1 on sperm, discovered by Inoue et al. (2005) and its oocyte partner, JUNO, discovered by Bianchi et al. (2014). Structures of the JUNO–IZUMO1 complex were published back to back in Nature on 23 June 2016 (Aydin et al., 2016; Ohto et al., 2016). However, more than 5 years later, there has been yet no report of blocking that crucial sperm–egg interaction by small molecules. These structures are the starting points and the only basis for the research presented in this study.

In the present study, we describe a combined effort to discover the blockers of the IZUMO1–JUNO interactions, and beginning with computational predictions of candidate inhibitors of JUNO and testing top candidates by *in vitro* fertilization (IVF) experiments in mice as well as in human sperm–hamster oocytes penetration assay, we found two effective inhibitors of *in vitro* fertilization.

RESULTS

JUNO–IZUMO1 Complexes: Most Hot Spots are Common to Both Crystal Structures

The interface residues of the two JUNO structures, 5JKC and 5F4E, underwent sequential virtual alanine screening by the Bioluminate software (Beard et al., 2013) and the loss of binding energy (delta affinity) was calculated for each virtually mutated residue. The results are listed in **Supplementary Table S1** (for 5JKC) and **Supplementary Table S2** (for 5F4E). While there are some differences between the two complexes, hot spots (i.e., residues with delta affinity ≥ 4 kcal/mol) were mostly common to both structures. **Figure 1** presents the spatial arrangement of hot spots for the JUNO structures.

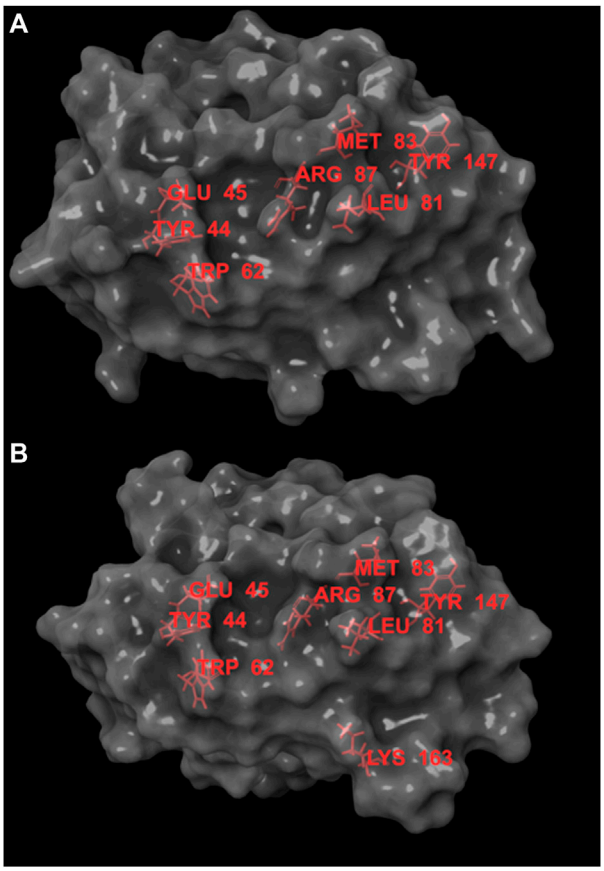

FIGURE 1 | Hot spots for JUNO structures 5JKC **(A)** and 5F4E **(B)**, the hot spots are marked in red. Hot spots are concentrated in an area narrow enough to be covered by molecules with MW ≥ 350. This area contains small grooves that can act as anchor points for ligands and provide partial protection from solvent.

TABLE 1 | Criteria for the filtering of the docked 913,000 molecules from the Enamine HTS collection.

Interaction type	Interacting residue
HBOND	ARG87
Attractive VDW interactions	TYR44, GLU45, MET83, LEU81, TYR147

Docking Produced Molecules that Interact with Most of the Hot Spots

Following the identification of hot spots, we set the docking site so that it includes most of them and docked 913,000 molecules from the Enamine HTS collection (Enamine Ltd., Ukraine). The molecules were limited to molecular weight greater than 350 g/mol, with the thought that larger molecules have better chances to encompass the full docking site and interact with most of the hot spots. The docked poses were filtered according to the criteria listed in **Table 1**. These criteria were selected to ensure that the ligands span the entire docking site and interact with most of the hot spots. However, Lys163 and Trp62 were not part of these criteria, Lys163 was excluded as it is too distant from the other hot spots, and Trp62 was excluded as we found that including it resulted in rejection of most molecules from being successfully docked.

Docked Molecules were Selected for the *in vitro* Test by Three Properties

Docked poses that met the aforementioned demands were examined according to the three main criteria: 1) docking score-the main energy parameter used in GLIDE (Friesner et al., 2004), 2) Attractive VDW contacts-number of Van der

Waals contacts favorable for ligand affinity, and 3) BSA (buried surface area)- a rough measure of a favorable hydrophobic contribution to the entropy.

We used these three properties to rank the molecules and to select several molecules for *in vitro* test. These molecules are listed in **Table 2**. Ideally, ligands should meet the geometric criteria in full and have better docking score and maximal VDW contacts and BSA. However, in some instances compromises were made to accommodate for molecules we deemed promising by viewing. For example, the molecule Z1172207733 produced a mediocre docking score, but had a large BSA that may result in a gain of entropy sufficient to cause the ligand to effectively bind to JUNO. On the other hand, the molecule Z49734016 only partially met the geometric criteria as it did not interact with TYR44 or TYR147. However, it had a very negative docking score, and a large number of VDW contacts, and so it was also picked for testing. Most of the molecules that were sent for experimental validations are from docking to 5JKC, apart from Z66693270 that was docked to 5F4E. Two of these molecules, Z786028994 and Z1290281203, were found to block *in vitro* fertilization in mice (described below), and their poses and interaction patterns with the JUNO residues are shown in **Figure 2**. Both inhibitors have VDW interactions with all of the hot spots, as well as a hydrogen bond with ARG87. In addition, Z1290281203 has a hydrogen

TABLE 2 | Top scored molecules sent for the *in vitro* test.

Molecule ID	Docking score (Kcal/mole)	Number of attractive VDW contacts	BSA (Å^2)
Z49720304	−4	292	843
Z18823321	−3.8	233	883
Z1290281203	−3.4	272	848
Z1033235866	−3.4	220	751
Z131775002	−4.4	211	748
Z56788505	−5.4	316	1,039
Z786028994	−4.3	241	832
Z1172207733	−2.4	293	986
Z49734016	−7	453	779
Z66693270	−3.3	210	818

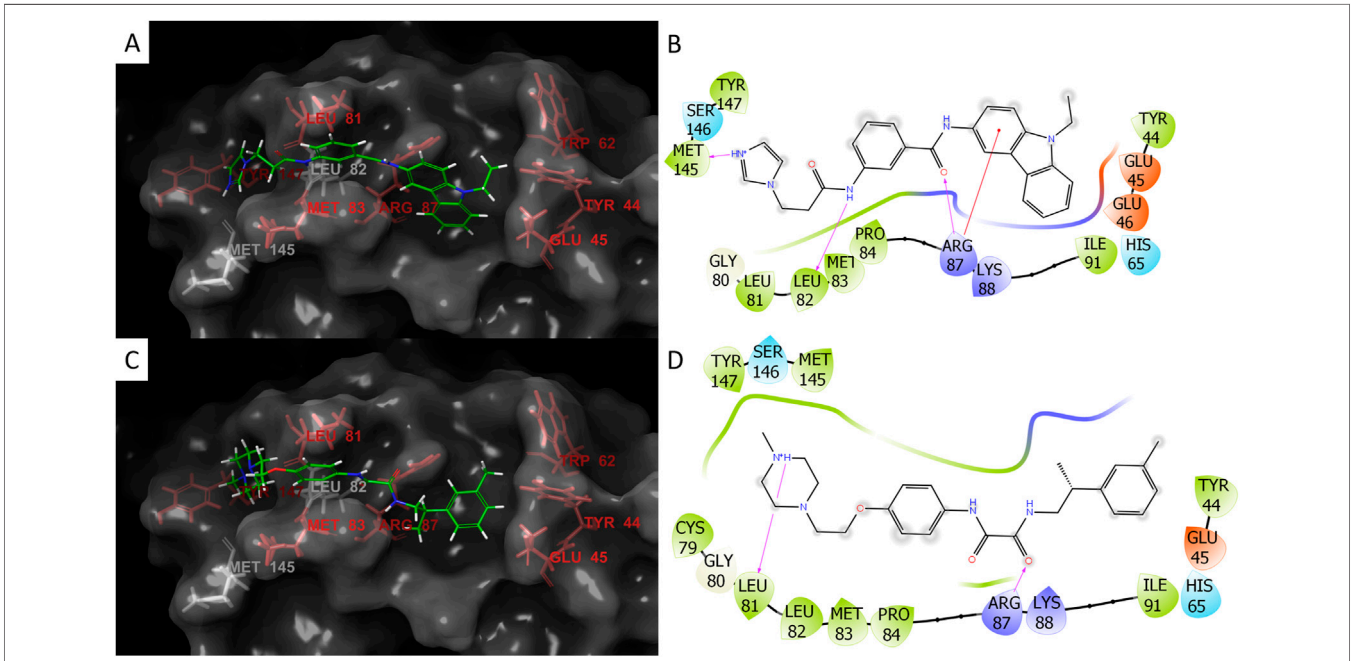

FIGURE 2 | Docking poses and interactions of the two inhibitors Z786028994 **(A,B)** and Z1290281203 **(C,D)**. For the 3D images of the poses: hot spots- red, non-hot spot residues- white, and ligand- green. For the 2D interaction plots: negative charge- red, positive charge- blue, hydrophobic residues- green, hydrogen bonds- purple arrows (the direction is donor to acceptor), and red line to the aromatic ring represents Pi-cation interaction. Both molecules span the length of the docking site and the small grooves in the protein provide partial protection from solvent **(A,C)**. Z786028994 has hydrogen bonds with ARG87, LEU82, and MET145 **(B)** and Z1290281203 has hydrogen bonds with two hot spots, ARG87 and LEU82 **(D)**.

bond with LEU81, and Z786028994 has hydrogen bonds with LEU82 and MET145.

ISE Model can Differentiate Between the "Best" and "Worst" Docked Molecules

In order to expand the pool of candidate molecules, a classification model was constructed using the Iterative Stochastic Elimination (ISE) algorithm (Stern and Goldblum, 2014) and was based on the docking results to the 5JKC JUNO structure: Docked molecules that met the geometric criteria were divided into 68 "Best" molecules (top quartile) and 69 "Worst" molecules (bottom quartile) according to the criteria listed in **Table 3**. The two sets were combined into a learning set, for which 206 molecular descriptors were calculated by MOE2018.0101 [Molecular Operating Environment (MOE) and Chemical Computing Group ULC, 2018]. The learning set was randomly divided into five parts or "folds", each containing 20% of the "Best" and 20% of the "Worst" molecules. Each four folds in turn were combined into a training set, to which the ISE algorithm was applied and produced a set of filters, and the remaining fold (i.e., the test set) was screened through those filters and its molecules were scored. Due to the iterations of different folds, all molecules were evaluated as part of a test set in one of the five different runs of modeling which were combined to produce a single, final model. .The final model consisted of 919 filters with good statistical criteria, mainly the Matthews Correlation Coefficient [MCC, (Stern and Goldblum, 2014)] values ranging from 0.86 to 0.77 for the top and bottom filter, respectively. Screening of the molecules in the test sets produced molecular indexes between −1 and 1, indicating a success or failure to pass the filters. The numbers of "Best" and "Worst" molecules at or above each index are shown in **Figure 3**. As the index increased so did the ratio of true to false positives (TP/FP), from one at an index of −1 up to 16.5 at an index of 0.75. That index was chosen to be the cutoff for candidate selection from the entire dataset, in order to minimize the number of false positives. The Enamine HTS collection of ~1.8 million molecules (Enamine Ltd., Ukraine) and a dataset of ~20 million molecules from the ZINC database (Sterling and Irwin, 2015) were screened through the model, out of which 31,555 molecules scored at or surpassed that cutoff index of 0.75. These molecules were subsequently docked to 5JKC and 5F4E using the SP method of Schrodinger's Glide (Friesner et al., 2004).

TABLE 3 | Criteria for best and worst docked molecules.

Criteria	Best	Worst
Docking score	< −3	≥ −1
BSA	≥750	≤600
Number of VDW contacts	≥250	≤150

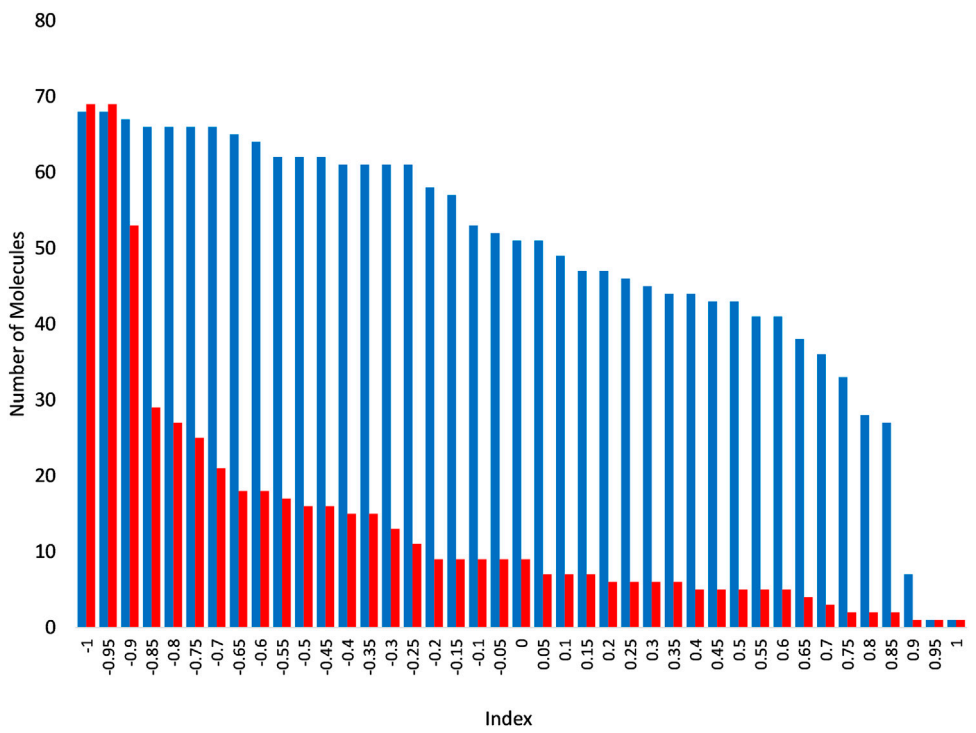

FIGURE 3 | Numbers of "Best" (blue) and "Worst" (red) above each index following screening through the ISE model. As the index increases, the number of molecules decreases in both the "Best" and "Worst" molecular sets, but at a much slower rate for the former than the latter, and so the remaining set is increasingly enriched with "Best" molecules.

We wished to examine whether interaction with only a part of the hot spots may be sufficient for blocking the JUNO–IZUMO1 interaction, and so, in addition to candidate molecules that span across the entire site (as detailed in **Table 3**), we divided the docking site into two sub-sites as listed in **Table 4**, and included molecules that interact with the hot spots on either one of those sub-sites. Here, we could include TRP62 in the criteria for successful docking to the sub-site B, as molecules docked to that site were sufficiently close to it. LYS163, on the other hand, remains too distant for most molecules to interact with. The 331 molecules that passed the filter were ranked by the three properties mentioned above, and 22 top scored molecules were sent for *in vitro* test.

Z786028994 and Z1290281203 are Potent Fertilization Inhibitors

Our *in silico* analyses identified 32 small molecule candidates (**Figure 4A**) that were predicted to bind to JUNO and could block its interaction with the sperm receptor IZUMO1. One stringent test to assess fertilization blockage is *in vitro* fertilization (IVF) assay (**Figure 4B**). Thus, we next employed IVF to test the inhibitory effect of the 32 (10 from structure based docking, 22 from ISE ligand based modeling) small molecule candidates on fertilization. To that end, we extracted oocytes from superovulated female mice and placed them in a dish containing 100 μM of either DMSO control or small molecule candidates. Immediately after, activated sperm were added to the plate and the formation of 2-cell stage embryos and blastocysts was scored after one and 4 days post sperm addition. The results of all experiments performed are detailed in **Supplementary Table S3** and shown in **Figure 4**. The vast majority of the tested molecules did not show any significant fertilization inhibition neither at the 2-cell stage nor on blastocyst formation (**Figure 4C**). Remarkably however, two small molecules namely, Z786028994 and Z1290281203 (#2 and #14, marked by black rectangle), showed no formation of either 2-cell stage embryos or blastocysts, and the small molecule Z751761886 (#28) demonstrated very few 2-cell stage embryos (**Figure 4C**). Importantly however, in contrast to Z751761886, the blockage seen with Z786028994 and Z1290281203 was not due to a toxic effect as the oocytes remained healthy even after 4 days of culturing (**Figure 4D**). Moreover, the accumulation of sperm cells in the perivitelline space of eggs treated with molecules Z786028994 and Z1290281203 strongly suggests that the fertilization failure seen by these two molecules is a result of inhibition of sperm–egg fusion (**Supplementary Figure S1**). We then moved on and tested those two molecules using lower concentrations. While a concentration of 50 μM still exhibited a strong inhibitory effect, yielding only few 2-cell stage embryos with zero blastocyst formation after 4 days of culturing, at lower concentrations of 10 and 1 μM no significant inhibitory effect was seen with these two molecules (**Figures 4E,F**). Taken together, these results indicate that Z786028994 and Z1290281203 are potent fertilization inhibitors at a concentration of 100 and 50 μM and suggest that further exploration of these small molecules is required to identify derivatives that might be able to block fertilization even at lower concentrations.

Z786028994 had the Largest Inhibition Effect on Human Sperm Fertilization in Hamster Penetration Assay

We picked the two most effective inhibitors for the hamster penetration assay from the mice experiment (Z786028994 and Z1290281203). In addition, we chose Z18823321 as being a less effective inhibitor (**Figure 4**). Following co-incubation with sperm, Z786028994 had an inhibitory effect on sperm and oocytes fusion, with a statistically significant difference in the number of penetrated sperm when compared either to the DMSO or to the control (**Figure 5**). The two other molecules (Z1290281203 and Z18823321) displayed a somewhat less inhibitory effect while having a statistically significant effect compared to DMSO. As motile sperm were observed after incubation with the molecules, the inhibition was not ascribed to a molecular toxic character. We further excluded an effect of the DMSO on sperm penetration by demonstrating no statistically significant difference in the number of penetrated sperm when incubated sperm with the DMSO alone was compared to the control.

The Small-Molecule Candidates Fail to Demonstrate JUNO–IZUMO1 Binding Interference using AVEXIS

To assess whether the small molecules could prevent the binding of JUNO and IZUMO1, we used an *in vitro* assay specifically developed to detect the interaction of receptor ectodomains named AVidity-based Extracellular Interaction Screening (AVEXIS) (Bushell et al., 2008). The ectodomain of JUNO was expressed as a soluble recombinant bait, captured on a solid surface and probed for its ability to bind the soluble pentameric ectodomain of IZUMO1. The candidate molecules or DMSO were incubated with both JUNO and IZUMO1 for 30 min, and then maintained in the media throughout the assay. Murine and human proteins were tested separately due to the species-specific characteristics of the binding (Bianchi and Wright, 2015). None of the molecules significantly affected the binding of JUNO and IZUMO1 (**Figure 6**).

TABLE 4 | Criteria for the filtering of the docked 31,555 molecules from the ISE model.

Interaction type	Sub-site A	Sub-site B
HBOND	ARG87	ARG87
Attractive VDW interactions	MET83, LEU81, TYR147	TYR44, GLU45, TRP62

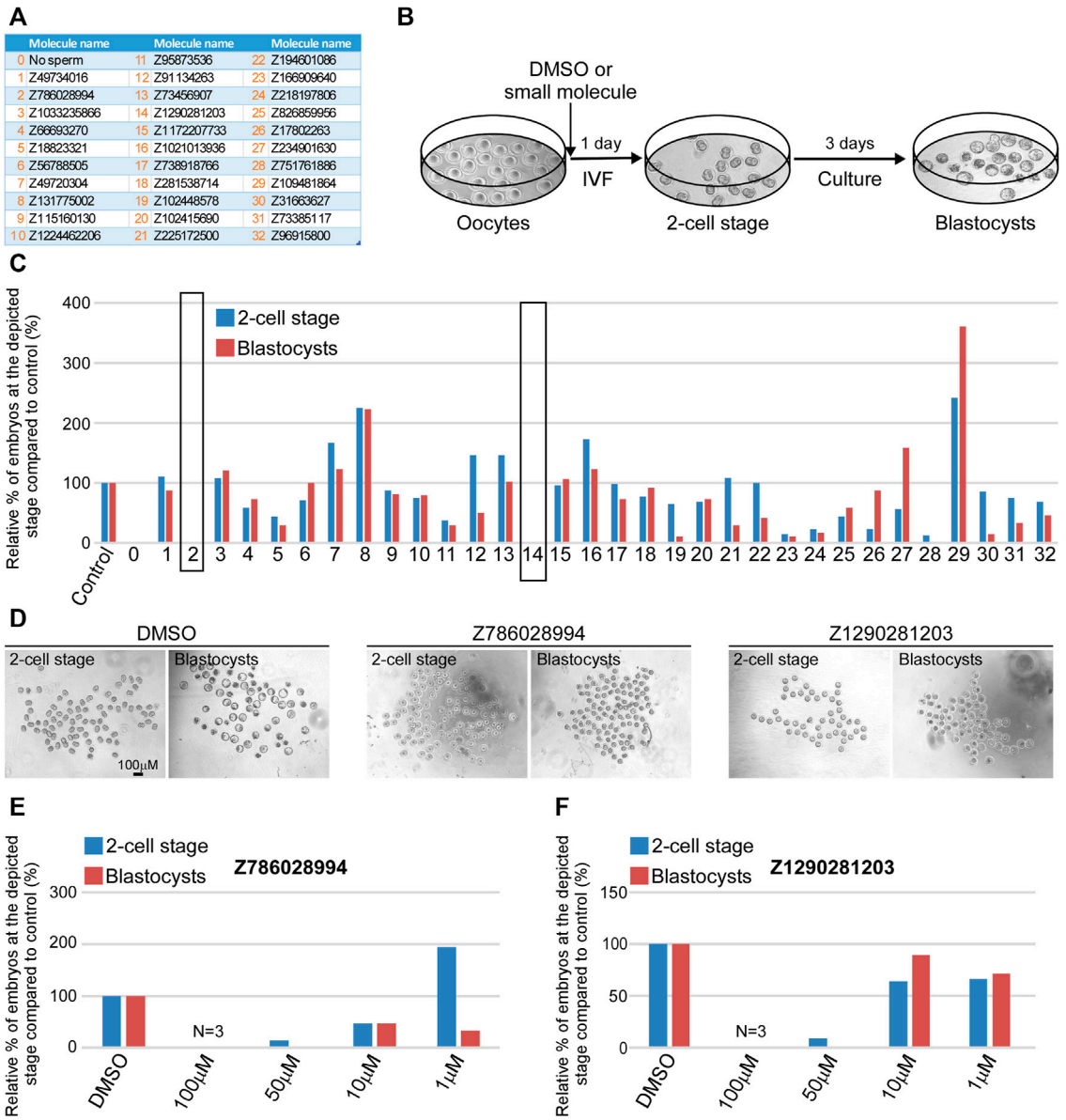

FIGURE 4 | Z786028994 and Z1290281203 demonstrate fertilization blockage at a concentration of 100 and 50 µM. **(A)** A table depicting a list of small molecules that were predicted to block JUNO–IZUMO1 interaction and were tested using IVF. **(B)** An illustration of the IVF experimental setup scheme showing the progression of embryo development after IVF. At day 1, the fertilized eggs developed into 2-cell stage embryos following by blastocysts formation at day 4 of fertilization. **(C)** Relative percentage of live embryos at day 1 (2-cell stage) and 4 (blastocyst stage) compared to positive (DMSO) and negative (no sperm) controls. All molecules presented in the graph were tested at a concentration of 100 µM. Small molecules Z786028994 and Z1290281203 (marked by black rectangle) demonstrated a complete blockage of fertilization, showing only unfertilized oocytes at day 4. **(D)** Representative bright field images of the developing embryos at day 1 (2-cell stage) and 4 (blastocyst stage) post IVF treatment in control (DMSO) and when the two small molecules were added to the extracted oocytes prior to sperm addition. **(E)** Relative percentage of the embryos at the depicted stages in the presence of different concentrations of the molecule Z786028994 compared to the DMSO control. **(F)** Relative percentage of the embryos at the depicted stages in the presence of different concentrations of the molecule Z1290281203 compared to the DMSO control.

DISCUSSION

The structure of the JUNO–IZUMO1 complex was elucidated by X-ray crystallography more than 5 years ago and published back to back in Nature, by two different groups. Ohto et al. wrote that "IZUMO1 and JUNO are ideal targets for contraceptive agents because of their crucial involvement in fertilization". Aydin et al. suggested "promising benefits for the rational development of non-hormonal contraceptives and fertility treatments for humans and other mammals". It should therefore be extremely surprising to learn that these possibilities did not produce any published echo in the research community. Until today, there are no public reports on finding of any novel inhibitor of fertilization by blocking the JUNO–IZUMO1 interaction.

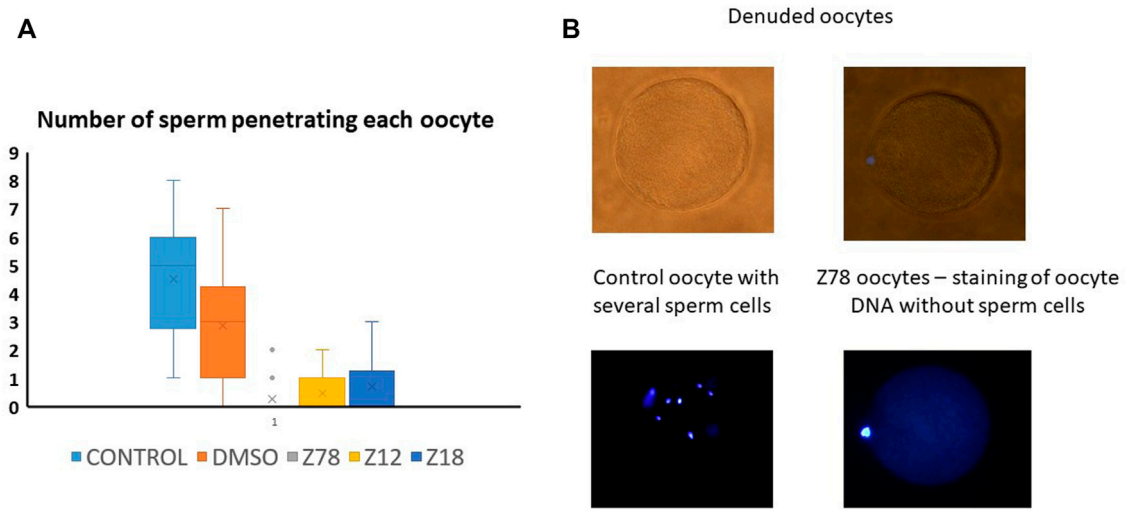

FIGURE 5 | Z786028994, Z1290281203, and Z1290281203 (marked Z78, Z12, and Z18) demonstrated penetration blockage at a concentration of 100 μM. **(A)** Number of penetrated human sperm cells into denuded hamster oocyte compared to control and DMSO. All molecules presented in the graph were tested at a concentration of 100 μM. The three tested molecules demonstrated inhibition of penetration, with the most potent inhibition by Z786028994 molecule. **(B)** Representative bright field and DAPI images of oocytes after penetration assay. Several sperm cells demonstrated inside the oocytes in the control group compared to no sperm cells penetrating the oocytes when incubated with Z786028994 molecule (just staining of the polar body).

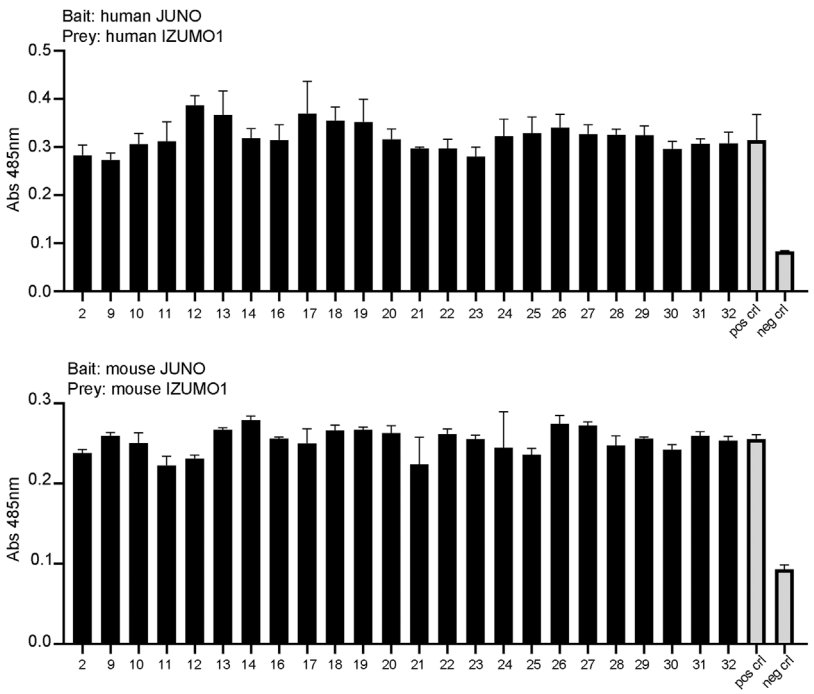

FIGURE 6 | The small molecules tested by AVEXIS did not show the ability to interfere with JUNO–IZUMO1 binding. The soluble ectodomains of JUNO and IZUMO1 were expressed as biotinylated bait and pentameric preys, respectively. Biotinylated JUNO was immobilized on a streptavidin-coated plate and probed for the ability to bind the beta-lactamase-tagged prey IZUMO1. The candidate molecules were incubated with the baits and with the preys at a concentration of 100 μM while DMSO was added to positive and negative controls. The same concentration was maintained in all steps of the assay. The binding of baits and preys was detected by the enzymatic turnover of a colorimetric substrate and quantified by absorbance readings. None of the small molecules significantly affected the binding of JUNO and IZUMO as shown by the AVEXIS performed with human **(upper panel)** and mouse **(lower panel)** proteins.

In the absence of known inhibitor structure, it is natural to use the known complexes in order to try to mimic one partner's interactions with the other partner. There are only two alternatives: either block JUNO or block IZUMO1. We decided on JUNO due to several advantages such as location (on the Egg's surface), surface structure (druggability due to surface crevices), relative conformational rigidity (compared to the large change in IZUMO1's conformation between free and bound states), and a somewhat smaller size of JUNO.

We used the structure of the JUNO–IZUMO1 complex in order to locate the most crucial (hot spots) JUNO residues for binding IZUMO1. By using virtual alanine scan—replacing each residue of JUNO that interacts directly with IZUMO1, we found seven such potential hot spots that occupy a large region on the surface of JUNO. The interaction energy difference due to mutations of these residues to alanine may be different in computations than by *in vitro* alanine scan. *In vitro*, the protein can change conformation due to replacing a side chain by the CH3 of alanine (except for Gly) and that change has an energy component. In the computations, we modify only a specific side chain but do not allow any conformational change (which may be achieved by minimizations or by Molecular Dynamics). The idea behind that restriction is that we wish to replace the interactions of IZUMO1 with JUNO in exactly the same structure that is reported in the Protein Data Bank. We do not allow rotations around the Cb-Ca bond of alanine, assuming that it has only a minor effect on enthalpy and entropy of the side chain replacement.

We Docked 913,000 molecules to the hot spot regions of 5F4E and 5JKC. We then filtered the docked poses and included those that interact with most of the hot spots, and ranked them by their docking scores, VDW contacts, and BSA. Buried surface area was considered for its contribution to the translational and rotational entropy due to the release of water molecules from the binding site to the bulk solution, a factor which is lacking in docking score calculations. Ten candidates from the top ranked molecules were sent for IVF experiments. Two molecules Z786028994 and Z1290281203 were found to fully inhibit *in vitro* fertilization in mice with concentrations of 50 and 100 μM, while some of them had a partial effect (like Z18823321). Z786028994 also completely blocked human sperm penetration to the hamster oocytes, while Z1290281203 and Z18823321 blocked it partially. Following a reviewer's comment that sperm swelling is a standard indicator of sperm penetration, we consider our results to be indicative at least of sperm oolema adhesion, being totally different for Z786028994, Z1290281203, and Z18823321 than for the DMSO or control. That is also corroborated by the fact that all samples were similarly treated by washing.

The docked poses of full inhibitors in mice, Z786028994 and Z1290281203, indicate that they interact with all the hot spots via VDW interactions. In addition, Z1290281203 has hydrogen bonds with two hot spots, ARG87 and LEU82, and Z786028994 has hydrogen bonds with ARG87, LEU82, and MET145 (**Figure 2**). The two latter residues are not hot spots, however, those hydrogen bonds may help stabilize the molecule in the specific pose. If confirmed by structural studies in crystals, the interactions of these two inhibitors can support pharmacophore-based virtual screening that would help in finding additional blockers of IVF.

Discovering two inhibitors out of ten candidates from docking less than a million molecules could suggest that docking a much larger number of molecules could find additional ones. We have only recently added nearly 200 million molecules to our "arsenal" of molecules, with about 20 million molecules from ZINC (Sterling and Irwin, 2015) and about 160 million molecules from a recently published ultra-large docking library (Lyu et al., 2019). With such proportion of success, we could envisage many more successful candidates out of that large set of candidates for docking.

Docking of databases containing millions of molecules is extremely time consuming. To allow us to exploit such large databases, we attempted to use the results of docking of the Enamine database described previously for ligand-based classification modeling. The two classes we used are the set of top third scored and bottom third scored molecules. Those were defined as "Best" and "Worst" classes to produce an ISE model that successfully discriminated between them. Screening of ~22 million molecules by that model found a large number of candidates with high scores that were docked, filtered, and ranked as mentioned above, and 22 top ranked molecules were sent for IVF tests. Unfortunately, none of these predicted molecules blocked IVF. While ISE has an excellent track record of finding novel molecules with a desired activity or property, including low micromolar hits and nanomolar leads (Cern et al., 2017; El-Atawneh and Goldblum, 2017; Da'adoosh et al., 2019; El-Atawneh et al., 2019; Da'adoosh et al., 2020), in the present case it has failed to do so. The successful ISE models were trained using published experimental data, in which the number of false positives is expected to be small. In the present case, in contrast, we used computed docking results to replace the non-existing experiments. Out of ten molecules found by docking, only two were confirmed hits. Assuming this proportion is representative for all our docking results, that means that 80% of the "Best" set are probably false positives of the docking method. Thus, it is likely that this set cannot be used to train models to identify IVF blockers.

Two separate IVF experiments were used to confirm the inhibitory activity: mouse sperm–mouse oocytes and human sperm–hamster oocytes, combined with the results of computational docking, suggest that our compounds indeed block JUNO on the oocytes of both species. However, all attempts to discover such inhibition by the AVEXIS technique developed by Bianchi and Wright did not produce evidence for direct inhibition. The direct interaction experiments were performed with HEK293 cells rather than oocytes, and it is possible that there are factors in oocytes' membrane environment (such as other membrane proteins) that interact with JUNO and stabilize it in a

conformation susceptible to the binding of the inhibitors prior to contact with the sperm, and so they are in place to disrupt the interaction with IZUMO1 and block subsequent fertilization. It should also be noted that the AVEXIS assay is specifically designed to detect the interactions between ectodomains, and it is possible that the inhibitors may disrupt some other essential function of IZUMO1 or JUNO other than its extracellular binding activity such as JUNO shedding (Bianchi et al., 2014) or structural rearrangements of IZUMO1 upon JUNO binding to bind other but as yet unidentified egg receptors (Inoue et al., 2015). However, until further research is performed, the mechanism of action of these IVF inhibitors remains unclear.

METHODS

Prediction of Hot Spots

Two crystal structures of a JUNO–IZUMO1 complex are our basis for searching to discover non-hormonal contraceptives (PDB codes 5JKC and 5F4E) (Aydin et al., 2016; Ohto et al., 2016). Both structures were prepared for docking using mostly the default settings of the protein preparation wizard of the Schrödinger software 2018-4 release (Schrödinger, 2021), with the exception of the minimization stage which was performed only on the computationally added protons. The JUNO interface residues involved in the binding of IZUMO1 were extracted from the PDBsum website (Laskowski et al., 2018). Each of these residues was virtually mutated to alanine in its turn using Schrödinger's Bioluminate software 2018-4 release (Beard et al., 2013). Following each mutation, the loss of binding energy was calculated. Mutated residues with an energy loss of 4 kcal/mol or more were considered to be hot spots.

Docking and Pose Filtering

The docking sites were set by GLIDE's (Friesner et al., 2004) grid generation to encompass the hot spots of the JUNO structure. Molecules were prepared using the default settings of the Ligprep panel in the Schrödinger software 2018-4 release, and docked to the JUNO structures using Glide's fast High Throughput Virtual Screening (HTVS) method. The resulting poses were then filtered by a set of geometric criteria that use the JUNO hot spots in order to maximize the competitive nature of potential inhibitors versus JUNO–IZUMO1 interactions. Molecules that met these criteria were re-docked using the slower standard precision (SP) method and rechecked for matching the geometric criteria. The molecules were then ranked according to three properties: docking score, number of attractive Van der Waals contacts with JUNO, and the buried surface area (BSA) created by the ligand–JUNO interaction. Top ranked molecules were sent for *in vitro* test.

Construction of the ISE Models

The Iterative Stochastic Elimination (ISE) algorithm had been previously described in detail (Stern and Goldblum, 2014). It has been successfully used by us to discover novel active molecules, based on an initial set of known activities of a set of molecules. Models were built by distinguishing between properties of these actives (usually >50 molecules) and properties of a large group (diluting the actives by 100 fold or more) of randomly picked "decoys" that represent "chemical space". A tougher case for successful classification is to distinguish among the actives, between highly active and less active molecules, usually separated by one or two orders of activity values and having a comparable set size. Once a model is achieved and is justified by statistics, we screen millions of molecules by that model and score each of them, subsequently picking the top ones which may be docked to their target if its structure has been elucidated. The problem with JUNO was and still is, 7 years after its discovery (Bianchi et al., 2014) that there are no known small molecule inhibitors of JUNO. We have thus decided to use the results of docking as if they were experimentally validated.

Docking results were thus divided into two sets of molecules "Best" and "Worst", according to the criteria based on the three properties mentioned above. For both these sets, 206 molecular descriptors were calculated by MOE2018.0101 (Molecular Operating Environment (MOE) and Chemical Computing Group ULC, 2018) and were then unified into a single learning set. All further steps in applying the ISE algorithm to results of docking are similar to any application of ISE as reviewed in Stern and Goldblum (2014).

Preparation of IVF Medium and Fertilization Drops

All powders listed in **Supplementary Table S4** were weighted as indicated and diluted in water for embryo transfer (Sigma, W1503). The medium was filtered through 0.22 μm filter and stored at 4°C for up to 3 months. At the morning of the IVF experiments, 30.7 mg of reduced glutathione (GSH) was added to 1 ml of HTF and mixed. 50 μL from this solution was added to the 5 ml of fresh HTF medium, filtered and used to prepare fertilization dishes. 90 μL drops of HTF medium with GSH were placed on the bottom of 35 mm Petri dishes (Falcon 351008), covered with mineral oil and incubated at 37°C, 5% CO_2 for 20 min.

Preparation of TYH + MBCD Sperm Pre-Incubation Medium

All powders listed in **Supplementary Table S5** were weighted and diluted in water for embryo transfer (Sigma, W1503). The medium was filtered through a 0.22 μm filter and stored at 4°C for up to 3 months. At the morning of IVF experiments, 180 μL drop of pre-incubation medium was placed on the bottom of 35 mm Petri dishes (Falcon 351008) and covered with mineral oil.

Preparation of Small Molecules

Inhibitors were purchased from Enamine (Enamine Ltd, Ukrain), diluted in DMSO to a stock concentration of 10 mM and stored at

−80°C. Each diluted inhibitor (100 μM or as indicated) was added to the HTF medium with GSH prior to sperm addition. The fertilization drops with each molecule was carefully marked, placed in humidity incubator at 37°C, 5% CO_2 for 30 min, and used for IVF.

Superovulation of the Female Mice

For each independent experiment four female mice, 3 weeks old, strain CB6/F1 were injected intraperitoneally (IP) with PMSG hormone (ProSpec, hor-272-a), and 48 h later with hCG (ProSpec, hor-007) hormone, 5IU per animal of average weight of 20 g.

Preparation of Capacitated Sperm

A male mouse of reproductive age was placed in an individual cage for 3 days before IVF experiments. On the morning of the IVF, the cauda, a structure located below the testis, was extracted and placed into a drop of TYM medium + MBCD. Few excisions were made to allow the sperm migrate out of the cauda to the medium. The plates were placed in humidity incubator at 37°C, 5% CO_2 for 1 h and stirred gently every 15 min. Following this incubation, activated sperm (sperm along the edges of the drop) were used for IVF.

In vitro Fertilization

The oviducts of superovulated mice were extracted 13.5 h after hCG injection and placed into a pre-warm M2 medium. The ampulla was tore with a needle and the oocytes were transferred into fertilization drops containing HTF medium with GSH and 100 μM of inhibitor candidate. Drops containing DMSO were used as control for all inhibitors. Activated mouse sperm were immediately added to the fertilization drops and incubated at 37°C, 5% CO_2. Following 3–4 h of incubation the eggs from each group (control and experiment) were washed with few drops of fresh HTF medium without GSH to remove cell debris, degenerating oocytes, and dead sperm. The next morning the dishes were screened under the microscope and the percentage of 2-cell stage embryos was assessed in the control and in the experimental groups. The counting was repeated at day 4 to assess the percentage of developed blastocysts.

Hamster Oocyte Retrieval

Mature female golden hamsters 8–12 weeks old were injected with 30 IU of pregnant mare serum gonadotropin (PMSG, ProSpec-Tany TechnoGene Ltd., Ness-Ziona, Israel) intraperitoneally, followed by an injection of 37 IU of human chorionic gonadotropin (hCG, ProSpec-Tany TechnoGene Ltd., Ness-Ziona, Israel) 56 h later. The hamsters were euthanized using a CO_2 chamber 17 h after administration of hCG injection. The oviducts were excised and placed in culture dishes containing saline. The ampule was tore and cumuli-oocyte complexes were collected and treated with hyaluronidase (SAGE, Trumbull, United States) for 1–2 min of incubation at 37°C. The remained cumulus cells were mechanically denuded with stripped pipette in 10% HEPES (SAGE, Trumbull, United States).

Hamster Penetration Assay

Human donor sperm were accepted from the sperm bank at the Hadassah Medical Center. The donors signed in advance with consent to use the sperm for donation or for research (approved by the local IRB). The frozen sperm dissolved on room temperature, loaded on gradient centrifuge, and washed with Multipurpose Handling Medium-Complete (Fujifilm Irvine Scientific Inc., Santa Ana, CA, United States). Dissolution of the zona pellucida was performed by placing the oocytes in 0.5 mg/ml trypsin (Biological industries, Israel) for 8 min. The oocytes were evenly divided and were incubated in 10% fertilization medium (SAGE, Trumbull, United States) with either Z786028994 (100 μM), Z1290281203 (100 μM), Z18823321 (100 μM), DMSO or no addition as control for 1 h at 37°c and 5% CO_2. The oocytes were then transferred into 100 μL drops with 250,000 motile human sperm with the same concentration of the inhibitory molecules (as mentioned above) and incubated at 37°C for 3 h. Finally, the oocytes were rinsed from extra sperm cells, fixed with formaldehyde, and stained with DAPI. The slides were examined under a fluorescence microscope at a 400 × magnification. The number of penetrated sperm in each oocyte was recorded.

Protein Expression and Interaction Screening by AVEXIS

All proteins were produced by transient transfection using an HEK293-6E expression system, and the cells were transfected with 1 μg/ml of plasmid DNA. The cells were incubated for 5 days in a shaking incubator at 37°C before supernatants were harvested, the cells were removed by centrifugation at 3220 g for 20 min, and the cell debris was removed by filtration.

Bait and prey proteins were normalized to activities that have been shown to detect transient interactions and screened using the ELISA-based AVEXIS methodology essentially as described (Kerr and Wright, 2012). 100 μL of biotinylated baits were immobilized on streptavidin-coated 96-well microtitre plates (Greiner) and washed with HBS 0.1%Tween. After washing 100 μL of normalized β-lactamase-tagged preys were added and incubated for 1 hour at room temperature. The wells were washed with HBS 0.1%Tween and finally 125 μg/ml of the β-lactamase substrate (Nitrocefin) was added. Absorbance values were measured at 485 nm on a Spark (Tecan) plate reader. The assays were repeated three times using independent protein preparations.

Biotinylated JUNO proteins were used as baits, while pentameric IZUMO1 proteins were used as preys. The small molecules were dissolved in DMSO at a concentration of 10 mM and diluted 100 times into the protein supernatants 30 min before they were added to the plates. JUNO and IZUMO with 1% DMSO were used as the positive control; the biotinylated extracellular fragment d3d4 of the rat CD4 was incubated with pentameric IZUMO1 and used as the negative control.

DATA AVAILABILITY STATEMENT

The original contributions presented in the study are included in the article/**Supplementary Material**, further inquiries can be directed to the corresponding author.

ETHICS STATEMENT

The studies involving human participants were reviewed and approved by the IRB. The ethics committee waived the requirement of written informed consent for participation. The animal study was reviewed and approved by the ethics committee (IACUC) of the Hebrew University for animal welfare (IACUC# MD-19-15843-3). The Hebrew University is an AAALAC international accredited institute.

AUTHOR CONTRIBUTIONS

OW and AG designed and performed the computational study. YB and NS designed and NS conducted the mice IVF experiments. A-BM and N-SS designed and performed the human sperm-hamster oocyte penetration tests. OW, AG, NS, YB, A-BM, and EB wrote part of the manuscript and prepared the figures. EB performed the AVEXIS assay and analyzed the data with the supervision of GJ-W.

FUNDING

AG, YB, and A-BM were funded by the Bill and Melinda Gates Foundation (investment ID OPP 1178114). EB and GJ-W were funded by the Biotechnology and Biological Sciences Research Council, United Kingdom (Grant BB/T006390/1).

ACKNOWLEDGMENTS

The authors thank Alexander Safanyaev for his contributions to the computational analysis.

SUPPLEMENTARY MATERIAL

The Supplementary Material for this article can be found online at: https://www.frontiersin.org/articles/10.3389/fcell.2022.824629/full#supplementary-material

REFERENCES

Aydin, H., Sultana, A., Li, S., Thavalingam, A., and Lee, J. E. (2016). Molecular Architecture of the Human Sperm IZUMO1 and Egg JUNO Fertilization Complex. *Nature* 534 (7608), 562–565. doi:10.1038/nature18595

Beard, H., Cholleti, A., Pearlman, D., Sherman, W., and Loving, K. A. (2013). Applying Physics-Based Scoring to Calculate Free Energies of Binding for Single Amino Acid Mutations in Protein-Protein Complexes. *PLoS One* 8 (12), e82849. doi:10.1371/journal.pone.0082849

Bianchi, E., and Wright, G. J. (2015). Cross-species Fertilization: the Hamster Egg Receptor, Juno, Binds the Human Sperm Ligand, Izumo1. *Phil. Trans. R. Soc. B* 370 (1661), 20140101. doi:10.1098/rstb.2014.0101

Bianchi, E., Doe, B., Goulding, D., and Wright, G. J. (2014). Juno Is the Egg Izumo Receptor and Is Essential for Mammalian Fertilization. *Nature* 508 (7497), 483–487. doi:10.1038/nature13203

Bushell, K. M., Söllner, C., Schuster-Boeckler, B., Bateman, A., and Wright, G. J. (2008). Large-scale Screening for Novel Low-Affinity Extracellular Protein Interactions. *Genome Res.* 18 (4), 622–630. doi:10.1101/gr.7187808

Cern, A., Marcus, D., Tropsha, A., Barenholz, Y., and Goldblum, A. (2017). New Drug Candidates for Liposomal Delivery Identified by Computer Modeling of Liposomes' Remote Loading and Leakage. *J. Controlled Release* 252, 18–27. doi:10.1016/j.jconrel.2017.02.015

Da'adoosh, B., Marcus, D., Rayan, A., King, F., Che, J., and Goldblum, A. (2019). Discovering Highly Selective and Diverse PPAR-delta Agonists by Ligand Based Machine Learning and Structural Modeling. *Sci. Rep.* 9, 1106. doi:10.1038/s41598-019-38508-8

Da'adoosh, B., Kaito, K., Miyashita, K., Sakaguchi, M., and Goldblum, A. (2020). Computational Design of Substrate Selective Inhibition. *Plos Comput. Biol.* 16 (3), e1007713. doi:10.1371/journal.pcbi.1007713

El-Atawneh, S., and Goldblum, A. (2017). Iterative Stochastic Elimination for Discovering Hits and Leads. *Chim. Oggi-Chemistry Today* 35 (5), 41–46.

El-Atawneh, S., Hirsch, S., Hadar, R., Tam, J., and Goldblum, A. (2019). Prediction and Experimental Confirmation of Novel Peripheral Cannabinoid-1 Receptor Antagonists. *J. Chem. Inf. Model.* 59 (9), 3996–4006. doi:10.1021/acs.jcim.9b00577

Enamine (Ukraine). Enamine LTD, 78 Chervonotkatska St. 02094. Kyiv, Ukraine.

Friesner, R. A., Banks, J. L., Murphy, R. B., Halgren, T. A., Klicic, J. J., Mainz, D. T., et al. (2004). Glide: a New Approach for Rapid, Accurate Docking and Scoring. 1. Method and Assessment of Docking Accuracy. *J. Med. Chem.* 47 (7), 1739–1749. doi:10.1021/jm0306430

Gupta, S. K., Malik, A., and Arukha, A. P. (2015). Ovarian and Oocyte Targets for Development of Female Contraceptives. *Expert Opin. Ther. Targets* 19 (11), 1433–1446. doi:10.1517/14728222.2015.1051305

Inoue, N., Ikawa, M., Isotani, A., and Okabe, M. (2005). The Immunoglobulin Superfamily Protein Izumo Is Required for Sperm to Fuse with Eggs. *Nature* 434 (7030), 234–238. doi:10.1038/nature03362

Inoue, N., Hagihara, Y., Wright, D., Suzuki, T., and Wada, I. (2015). Oocyte-triggered Dimerization of Sperm IZUMO1 Promotes Sperm-Egg Fusion in Mice. *Nat. Commun.* 6, 8858. doi:10.1038/ncomms9858

Kerr, J. S., and Wright, G. J. (2012). Avidity-based Extracellular Interaction Screening (AVEXIS) for the Scalable Detection of Low-Affinity Extracellular Receptor-Ligand Interactions. *J. Vis. Exp.* (61), e3881. doi:10.3791/3881

Laskowski, R. A., Jabłońska, J., Pravda, L., Vařeková, R. S., and Thornton, T. M. (2018). PDBsum: Structural Summaries of PDB Entries. *Protein Sci.* 27 (1), 129–134. doi:10.1002/pro.3289

Lyu, J., Wang, S., Balius, T. E., Singh, I., Levit, A., Moroz, Y. S., et al. (2019). Ultra-large Library Docking for Discovering New Chemotypes. *Nature* 566 (7743), 224–229. doi:10.1038/s41586-019-0917-9

McCann, M. F., and Potter, L. S. (1994). Progestin-only Oral Contraception: a Comprehensive Review. *Contraception* 50 (6 Suppl. 1), S1–S195. doi:10.1016/0010-7824(94)90115-5

Molecular Operating Environment (MOE), Chemical Computing Group ULC (2018). Molecular Operating Environment (MOE), Chemical Computing Group ULC. 1010 Sherbrooke St. West, Suite #910. Montreal, QC, Canada. H3A 2R7.

O'Connell, K., Davis, A. R., and Kerns, J. (2007). Oral Contraceptives: Side Effects and Depression in Adolescent Girls. *Contraception* 75 (4), 299–304. doi:10.1016/j.contraception.2006.09.008

Ohto, U., Ishida, H., Krayukhina, E., Uchiyama, S., Inoue, N., and Shimizu, T. (2016). Structure of IZUMO1-JUNO Reveals Sperm-Oocyte Recognition during Mammalian Fertilization. *Nature* 534 (7608), 566–569. doi:10.1038/nature18596

Rosenberg, M. J., Meyers, A., and Roy, V. (1999). Efficacy, Cycle Control, and Side Effects of Low- and Lower-Dose Oral Contraceptives: a Randomized Trial of 20 μg and 35 μg Estrogen Preparations. *Contraception* 60 (6), 321–329. doi:10.1016/s0010-7824(99)00109-2

Sabatini, R., and Cagiano, R. (2006). Comparison Profiles of Cycle Control, Side Effects and Sexual Satisfaction of Three Hormonal Contraceptives. *Contraception* 74 (3), 220–223. doi:10.1016/j.contraception.2006.03.022

Schrödinger (2021). *Schrödinger Release 2018-4*. New York, NY: Maestro, Schrödinger, LLC.

Sterling, T., and Irwin, J. J. (2015). ZINC 15 - Ligand Discovery for Everyone. *J. Chem. Inf. Model.* 55 (11), 2324–2337. doi:10.1021/acs.jcim.5b00559

Stern, N., and Goldblum, A. (2014). Iterative Stochastic Elimination for Solving Complex Combinatorial Problems in Drug Discovery. *Isr. J. Chem.* 54 (8-9), 1338–1357. doi:10.1002/ijch.201400072

Townsend, J. W., Sitruk-Ware, R., Williams, K., Askew, I., and Brill, K. (2011). New Strategies for Providing Hormonal Contraception in Developing Countries. *Contraception* 83 (5), 405–409. doi:10.1016/j.contraception.2010.08.015

Conflict of Interest: The authors declare that the research was conducted in the absence of any commercial or financial relationships that could be construed as a potential conflict of interest.

Publisher's Note: All claims expressed in this article are solely those of the authors and do not necessarily represent those of their affiliated organizations, or those of the publisher, the editors, and the reviewers. Any product that may be evaluated in this article, or claim that may be made by its manufacturer, is not guaranteed or endorsed by the publisher.

frontiers | Frontiers in Cell and Developmental Biology

ORIGINAL RESEARCH
published: 07 April 2022
doi: 10.3389/fcell.2022.795273

Recurrent Duplication and Diversification of Acrosomal Fertilization Proteins in Abalone

J. A. Carlisle[1]*, *M. A. Glenski*[2] *and W. J. Swanson*[1]

[1]Genome Sciences Department, University of Washington Medical School, Seattle, WA, United States, [2]Department of Biology, Gonzaga University, Spokane, WA, United States

Reproductive proteins mediating fertilization commonly exhibit rapid sequence diversification driven by positive selection. This pattern has been observed among nearly all taxonomic groups, including mammals, invertebrates, and plants, and is remarkable given the essential nature of the molecular interactions mediating fertilization. Gene duplication is another important mechanism that facilitates the generation of molecular novelty through functional divergence. Following duplication, paralogs may partition ancestral gene function (subfunctionalization) or acquire new roles (neofunctionalization). However, the contributions of duplication followed by sequence diversification to the molecular diversity of gamete recognition genes has been understudied in many models of fertilization. The marine gastropod mollusk abalone is a classic model for fertilization. Its two acrosomal proteins (lysin and sp18) are ancient gene duplicates with unique gamete recognition functions. Through detailed genomic and bioinformatic analyses we show how duplication events followed by sequence diversification has played an ongoing role in the evolution of abalone acrosomal proteins. The common ancestor of abalone had four members of its acrosomal protein family in a tandem gene array that repeatedly experienced positive selection. We find that both sp18 paralogs contain positively selected sites located in different regions of the paralogs, suggestive of functional divergence where selection acted upon distinct binding interfaces in each paralog. Further, a more recent species-specific duplication of both lysin and sp18 in the European abalone *H. tuberculata* is described. Despite clade-specific acrosomal protein paralogs, there are no concomitant duplications of egg coat proteins in *H. tuberculata*, indicating that duplication of egg proteins *per se* is not responsible for retention of duplicated acrosomal proteins. We hypothesize that, in a manner analogous to host/pathogen evolution, sperm proteins are selected for increased diversity through extensive sequence divergence and recurrent duplication driven by conflict mechanisms.

Keywords: fertilization, duplication, paralogs, molecular evolution, genome evolution, testes and epididymis, reproduction, sperm

OPEN ACCESS

Edited by:
Enrica Bianchi,
University of York, United Kingdom

Reviewed by:
Cameron Weadick,
University of Exeter, United Kingdom
Pablo Aguilar,
National University of General San Martín, Argentina

***Correspondence:**
J. A. Carlisle
jcarlisl@uw.edu

Specialty section:
This article was submitted to Molecular and Cellular Reproduction, a section of the journal Frontiers in Cell and Developmental Biology

Received: *14 October 2021*
Accepted: *21 February 2022*
Published: *07 April 2022*

Citation:
Carlisle JA, Glenski MA and Swanson WJ (2022) Recurrent Duplication and Diversification of Acrosomal Fertilization Proteins in Abalone. Front. Cell Dev. Biol. 10:795273. doi: 10.3389/fcell.2022.795273

INTRODUCTION

Despite their essential role in many organisms, genes functioning in fertilization or sexual reproduction are often rapidly diverging between closely related species including mammals, birds, fish, and invertebrates (Swanson and Vacquier, 2002; Swanson et al., 2003; Carlisle and Swanson, 2020). Some pairs of interacting sperm and egg gamete recognition proteins have been shown to be rapidly co-evolving, pointing to sexual conflict or sexual selection driving the rapid evolution of fertilization genes (Kamei and Glabe, 2003; Clark et al., 2009; Bianchi et al., 2014; Grayson, 2015). This rapid diversification of sperm and egg gamete recognition proteins at a sequence level can result in species-specific fertilization function (Zigler et al., 2005; Avella et al., 2014; Raj et al., 2017). Investigations into the evolution of reproductive genes paired with characterization of species-specific function can provide unique insights into infertility and reproductive isolation (Lehmann, 2018).

In addition to sequence evolution, gene duplication can also contribute to the molecular diversification of reproductive protein families. *Drosophila* seminal fluid proteins often undergo duplication and diversification, with many of these duplications being species-specific (Wagstaff and Begun, 2005; Findlay et al., 2008; Almeida and Desalle, 2009; Sirot et al., 2014; Doty et al., 2016; Wilburn et al., 2017). In mammals many well-studied reproductive proteins belong to paralogous gene families that show interesting patterns of duplication and diversification (Cai and Clapham, 2008; Aagaard et al., 2010; Grayson and Civetta, 2012; Cooper and Phadnis, 2017). The paralogous members of the mammalian CatSper gene family show recurrent patterns of positive selection (Cai and Clapham, 2008; Cooper and Phadnis, 2017). The Izumo protein family contains four paralogs associated with various reproductive functions (including the sperm fertilization gene Izumo1) and these paralogs are undergoing positive selection in differing phylogenetic groups (Grayson and Civetta, 2012). ZP2 and ZP3 are paralogous mammalian egg coat glycoproteins with differing functions in sperm-recognition and both genes have been shown to undergo positive selection in some lineages (Carlisle and Swanson, 2020). Together these examples in mammals and *Drosophila* point to a recurring pattern of duplication paired with clade-specific sequence divergence of reproductive proteins across animals. This process likely leads to functional diversification of reproductive protein paralogs. Post-duplication, functions may be partitioned between paralogs in a process called subfunctionalization or a paralog may acquire a new function *via* neofunctionalization (Rastogi and Liberles, 2005). Here, we investigate how both sequence diversification and duplication together contribute to the molecular diversification of fertilization proteins in abalone.

The marine gastropod abalone (Genus *Haliotis*) is a classic model system for studying the function of gamete recognition proteins and their evolution. Abalone sperm have an extremely large acrosome containing two gamete recognition proteins, lysin and sp18 (Lewis et al., 1980). Lysin is the sperm mediator of the dissolution of the egg's vitelline envelope (VE), and sp18 is thought to mediate sperm-egg plasma membrane fusion (Swanson and Vacquier, 1995a; Wilburn et al., 2018; Carlisle and Swanson, 2020). The abalone egg VE is an elevated glycoproteinaceous layer homologous to the mammalian egg zona pellucida (ZP) (Carlisle and Swanson, 2020). The abalone VE and mammalian ZP are biochemically and structurally similar (Mozingo et al., 1995) and both contain proteins with ZP-N domains (Swanson et al., 2011; Avella et al., 2014; Raj et al., 2017; Carlisle and Swanson, 2020). Binding between lysin and the ZP-N domains of the vitelline envelope receptor for lysin (VERL) leads to the non-enzymatic dissolution of the VE (Swanson and Vacquier, 1997; Aagaard et al., 2013; Raj et al., 2017). Three-dimensional structures of lysin, VERL and their complex have been investigated using crystallography and NMR (Kresge et al., 2000, 2001; Aagaard et al., 2013; Raj et al., 2017; Wilburn et al., 2018). The highly fusogenic protein sp18 is the putative mediator of sperm-egg plasma membrane fusion in abalone (Swanson and Vacquier, 1995a; Kresge et al., 2001). The structure of sp18 has been determined via crystallography, but no binding receptor or fertilization mechanism has been identified (Kresge et al., 2001).

Investigations into the evolution of abalone reproductive proteins have provided valuable insights within the field of reproductive biology. Lysin, sp18 and VERL have each been shown to evolve under positive selection by analysis of the ratio of rates of nonsynonymous substitutions to rates of synonymous substitutions ($d_N/d_S > 1$) (Lee et al., 1995; Swanson and Vacquier, 1995a; Galindo et al., 2003). Further, population genetic analysis indicate that lysin and its binding partner VERL are coevolving with each other (Clark et al., 2009). Previous studies of abalone egg and sperm gamete recognition proteins hint at the importance of duplication events for their evolution. Despite their divergent functions in reproduction and low sequence similarity, sp18 and lysin are paralogs with similar three-dimensional protein structures (Kresge et al., 2001). While a protein with amino acid sequence similarity and functional similarity to lysin has been identified in Tegula marine snails, a homolog to sp18 has not, potentially indicating the duplication event leading to the creation of sp18 and lysin is ancestral to abalone (Hellberg and Vacquier, 1999). The common ancestor of abalone lysin and sp18 is hypothesized to have mediated both VE dissolution and sperm egg fusion, post-duplication these ancestral functions were partitioned to lysin and sp18, respectively.

Additional evidence suggests that duplication may be contributing to the evolution of abalone sperm fertilization proteins on a more recent timescale. The European abalone *H. tuberculata* has a species-specific duplication of lysin (Clark et al., 2007). On the egg side there is also evidence of extensive gene duplication. In addition to VERL, abalone VEs contain ~30 homologous VEZP proteins containing ZP-N domains (Aagaard et al., 2006; Aagaard et al., 2010). Many of these VEZPs may be structural components of the VE that play no role in gamete recognition (Killingbeck and Swanson, 2018). However, one protein (VEZP-14) is a close paralog of VERL that has undergone positive selection and is capable of binding lysin (Aagaard et al., 2013). Abalone VEZPs have only been described in two species (*H. rufescens*, and *H. fulgens*) from the North American clade. It is unknown whether there is variation

in gene content across more distantly related abalone species (Aagaard et al., 2006).

In this study we investigated the contributions of duplication and sequence diversification to the evolution of proteins mediating fertilization across the genus *Haliotis*. Using new testes and ovary transcriptomic data and published genome assemblies we discovered novel duplications of the acrosomal proteins lysin and sp18. Some of these paralogs are ancestral to abalone and others are clade-specific. Further we discover signatures of positive selection in many of the paralogs and identify differences in distributions of positively selected sites between paralogs that suggest selection for diversification in function (subfunctionalization or neofunctionalization). Our detailed evolutionary genomic analysis reveals how recurrent patterns of duplication paired with diversification led to the evolution of abalone gamete recognition proteins and their variation between species. Repeated duplications within the protein family containing lysin and sp18 parallels the duplication and diversification of other reproductive protein families, such as mammalian Izumo and CatSper families.

MATERIALS AND METHODS

PacBio Library Preparation and Sequencing

To identify potential transcripts present in abalone gonadal tissue, methods were adapted from the PacBio Iso-seq protocolto create cDNA libraries. Ovary and testes transcriptome libraries were prepared for PacBio sequencing. RNA was extracted from *H. tuberculat*a ovary and testes samples by cesium chloride density gradient centrifugation (MacDonald et al., 1987). RNA samples were enriched for mRNA by using the Oligotext mRNA Mini Kit from Qiagen. Purified mRNA was used as the template for single stranded cDNA synthesis using the Clontech SMARTer cDNA Synthesis Kit. The cDNA was amplified by PCR using the AccuPrime High-Fidelity *Taq* system (Invitrogen, Carlsbad, CA, United States). Double stranded synthesis conditions were optimized with the following PCR program: ˚C for 2 min, followed by 20 cycles of 94˚C for 30˚s, 55˚C for 30˚s, and 68˚C for 10 min. We used unique identifying barcoded PCR primers to amplify testes (barcode: CTGCGTGCTCTACGAC) and ovary (barcode: TCAGACGATGCGTCAT) cDNA. Because of size bias during PacBio sequencing, double stranded cDNA was fractionated using Ampure XP Beads (Beckman Coulter Life Sciences) into two fractions (Ratio of 4:1 of 0.45×: 0.6× size selection). Testis and ovary cDNA were sequenced using the PacBio RSII and was performed by the Washington State University Genomics Core.

Identification of Acrosomal Protein Paralogs

We conducted phylogenetic and molecular evolutionary analysis using a combination of pre-existing Genbank sequences, sequences identified from published genomes or transcriptomes, sequences identified from newly generated ovary and testes PacBio transcriptomes. The process for identifying sequences from pre-existing or newly generated datasets is explained below, a summary of the datasets used can be found in **Supplementary Table S1**. The list of sequences included in our phylogentic analysis of lysin, sp18, and their paralogs and their sources is included in **Supplementary Table S2**.

Sequences of sp18 and lysin from the genus *Haliotis* were retrieved from NCBI Genbank sequence repository (accession numbers for lysin: L26270-79, L26281, L35180-81, L36589, M34388-89, M59968-71, M98874-75, HM582239; accession numbers for sp18: L36552-54, L36589-90, MN102340-42). These sp18 and lysin sequences were used as the initial query sequences when identifying paralogs in abalone transcriptomes and genomes. Queries of the *H. rufescens* Illumina-based testis transcriptome (Palmer et al., 2013) and the *H. tuberculata* PacBio testes transcriptome were conducted with tblastn with an e-value cutoff of 1e-10. Significant matches from the testes transcriptomes were searched against the NCBI sequence repository (July 2020) using tblastn in order to confirm homology to lysin or sp18 (McGinnis and Madden, 2004). New sequences were uploaded to Genbank under accession numbers OK491874-OK491877.

Regions of publicly available abalone genomes containing novel acrosomal protein duplications of sp18 and lysin were identified by using tblastn with a *e*-value cutoff of 1e-10 (Nam et al., 2017; Botwright et al., 2019; Gan et al., 2019; Masonbrink et al., 2019). Samtools faidx was used to extract the region of scaffolds containing the tblastn hits and 20,000 base pairs upstream and downstream of the hit. We predicted the exonic sequences of the sp18 and lysin paralogs from these extracted regions using the Protein2 Genome command of the program Exonerate version 2.2.0 (Slater and Birney, 2005). The top scoring prediction from Exonerate was used to define the paralog's exons. We used the same lysin and sp18 sequences from the tblastn search as query sequences. For all full-length sequences, the SignalP-5.0 prediction server was used to predict presence of functional signal peptides (Almagro Armenteros et al., 2019). Presence of signal peptides were predicted with probabilities >0.9; the signal peptide cleavage site was predicted with a probability >0.5.

Phylogenetic Analysis

The phylogenetic inference tool RAxML-NG was used to construct all phylogenetic trees with the LG substitution matrix (Le and Gascuel, 2008; Kozlov et al., 2019). RaxML-NG conducts maximum likelihood based phylogenetic inference and provides branch support using non-parametric bootstrapping (Kozlov et al., 2019). The best scoring topology of 20 starting trees (10 random and 10 parsimony-based) was chosen. RaxML-NG was used to perform non-parametric bootstrapping with 1,000 re-samplings that were used to re-infer a tree for each bootstrap replicate MSA. Finally, we mapped the bootstrap scores on the best-scoring starting tree. The Transfer Bootstrap Expectation (TBE) was used as a branch support metric (Lemoine et al., 2018).

DNA multiple sequence alignments (MSA) for phylogenies of lysin and sp18 and their respective paralogs were constructed.

First the protein sequences of the genes were aligned using PROMALS3D (Pei et al., 2008a; Pei et al., 2008b). PROMALS3D may use protein three-dimensional protein structures to inform protein alignments. The representative PDB 5UTG was used for lysin and lysin paralogs and the PDB 1GAK was used for sp18 and sp18-dup sequences (Kresge et al., 2000; Wilburn et al., 2018). For alignments of VEZP sequences, no structure PDB was used. The protein MSAs were used to create DNA alignments of the same genes using the Pal2Nal sever (Suyama et al., 2006). Gaps were not removed from the alignments for our analysis. After paralog identification, new MSAs of orthologous sequences were constructed for positive selection analysis using the method described above. For phylogenetic analysis of *H. rufescens* and *H. tuberculata* VEZP sequences, the protein sequences of the C-terminal ZP modules of each of the proteins were aligned using PROMALS3D (Pei et al., 2008b).

Syntenic Comparison Between *Haliotis rufescens* and *H. Rubra*

The published genome of *Haliotis rufescens* is annotated with ORFs identified *via* transcriptomic sequencing (Masonbrink et al., 2019). We collected the sequences of 2-3 large annotated ORFs surrounding lysin, sp18, and their newly described paralogs within the *H. rufescens* genome. We used these sequences as BLAST queries against the *H. rubra* genome (Gan et al., 2019). The top hits for the *H. rufescens* ORFs were annotated onto the *H. rubra* genome and used to establish synteny *between H. rubr*a scaffold 62 and the *H. rufescens* scaffolds 48 and 101. A reciprocal blast of the regions identified as orthologous ORFs in *H. rubra* were queried against the *H. rufescens* genome to verify orthology. *H. rufescens* and *H. rubra* were chosen as representative genomes from North American and Australian abalone, respectively. The genome assemblies of the North American abalone species *H. sorenseni* and *H. fulgens* are based on the *H, rufescens* assembly. The genome assembly of the North American abalone *H. discus* contains shorter scaffolds than the other published genomes, thereby preventing synteny analysis of this genomic region. The Australian abalone genomes of *H. laevigata* and *H. rubra* are similar, *H. rubra* was arbitrarily chosen to compare to *H. rufescens*, however *H. laevigata* shows the same syntenic relationship between sp18 and lysin paralogs.

Detecting Selection and Positively Selected Sites

Values of d_N/d_S for genes were estimated using the codeml program of PAML 4.8 (Yang, 2007). We compared models of selection using a likelihood ratio test (LRT) between neutral models and models with positive selection. Specifically, we compared M1a v. M2a, M7 v. M8, and M8a v. M8 using the codon frequency model F3X4. Likelihood ratio tests were performed where the likelihood ratio (LRT) statistic was twice the negative difference in likelihoods between nested models. For M1a v M2a or M7 v Model 8 the LRT was compared to the χ^2 distribution with 2 degrees of freedom (Yang, 2007). For the M8a v. M8 comparison, twice the negative difference in likelihoods between the nested models being compared, the LRT statistic, is approximated by the 50-50 mixture distribution of 0 and χ^2 with degree of freedom 1 (Swanson et al., 2003). Convergence was checked by running the analysis from multiple initial omega values. To identify specific sites in proteins evolving under positive selection, we used a Bayes Empirical Bayes threshold of [Pr (omega > 1) = 0.75].The threshold of 0.75 was chosen since it gave a sufficient number of positively selected sites in each paralog in order to perform our analysis while still reliably identifying positively selected sites. According to simulations run in Yang et al., 2005, the false positive rate of detecting positively selected sites using the BEB method is lower than 1—(Pr (omega > 1), with a threshold value of [Pr (omega > 1) = 0.7] leading to a false positive rate of 0.03 (Yang et al., 2005).

Testing for Divergence in Regions Undergoing Positive Selection in Duplicate Sperm Proteins

We designed three unbiased tests to determine if sites under positive selection in either sp18 or sp18-dup are differentially clustered between paralogs. First, we created a parametric test based on the Wald-Wolfowitz runs test (Magel and Wibowo, 1997) to determine whether positively selected sites in the paralogs sp18 and sp18-dup were non-randomly distributed in a protein alignment of both paralogs. The Wald-Wolfowitz runs test determines the randomness of a two-category data string by examining changes between categories by counting "runs." We designed a parametric version of the test to allow the inclusion of three categories. The categories were sites under positive selection in sp18, sites under selection in sp18-dup, and sites under selection in both. The order in which these sites under selection in the categories appeared in an alignment of *H. fulgens* sp18 and *H. sorenseni* sp18-dup became our data string. For the data string generated from our paralog alignment we counted how many times the identity of sites in the string changed plus one. A visualization of the pipeline for preparing this data string and counting "runs" is shown in **Supplementary Figure S1A**.

To make a parametric version of this runs test, we generated 1,000 simulated data strings *via* bootstrapping based on the proportion of sites shown to be under positive selection in either paralog. Each simulated data string was created by sampling from two strings 142 times each (142 is the length of the protein alignment between paralogs). Each string simulates the chance of a site randomly being positively selected in either paralog or not based on the proportions of the observed data string. If a site is simulated as undergoing positive selection in both paralogs it is marked in the simulated data string as such. For each of these simulated data strings we also calculated the number of runs. The number of data strings with a count of "runs" less than or equal to the count of "runs" found in the data string derived from the paralog protein alignment divided by the total number of simulated data strings gives the parametric probability that by random chance categories of sites would be more or

equally clustered compared to the true clustering observed. We also performed a version of the test where sites under selection in both paralogs were eliminated from the analysis. When these sites were eliminated the parametric runs test retained statistical significance (p-value <0.001).

For our second test we evaluated whether sites under positive selection in sp18 vs. sp18-dup were distributed throughout the sp18 crystal structure (1GAK) in a significantly different way. In MATLAB Online version 9.9, we identified the plane of best fit between the c-alpha carbons (the first carbon attached to the functional group of an amino acid) of the sp18 crystal structure using linear regression (**Supplementary Figure S2A**, **Supplementary File S1**). This plane divided the sp18 crystal structure into two sides that we arbitrarily designated "left" and "right" (**Supplementary Figure S2B**). We mapped the 62 sites in sp18 and the 30 sites in sp18-dup that are under positive selection onto the sp18 crystal structure. Given the number of amino acids sites in each side of the crystal structure, we estimated the expected number of positively selected sites from each paralog that would be expected to be located on either side as the number of amino acid sites on a side divided by the total number of amino acid sites in the molecule and multiplied by the number of positively selected sites in a sp18 paralog. We used a chi-square test to examine whether the real distribution of sites between categories rejected the null expectation. This test determined whether the distribution of sites under selection in either paralog was not distributed similarly between the sides of the protein. We also created a plane perpendicular to the plane of best fit to divide the sp18 crystal structure into the categories "top" and "bottom" (**Supplementary Figure S2C**). We repeated an analysis for this new pair of categories that is identical to what was described previously. This analysis gave us a sense if sites under selection in either paralog were clustered nonrandomly throughout the crystal structure in different ways.

For our last clustering test we determined whether sites under positive selection in a paralog were more likely to be close in proximity in three-dimensional space to another site under positive selection in the same paralog rather than a site under positive selection in the other paralog. For each site that was under selection in a paralog, we identified the closest positively selected site in three-dimensional space that belonged to either paralog. We then calculated the expected number of times by chance the closest adjacent site for each site under positive selection would belong to the same gene rather than the other paralog. We used a chi-square test to determine whether observed sites under selection in one paralog were statistically more likely to be close to positively selected sites belonging to the same paralog than what would be expected by chance. This test has four categories of sites (for each paralog the nearest site could belong to the same paralog or not), and therefore three degrees of freedom were used to determine the p-value. Sites that were under selection in both paralogs were counted twice in this analysis since these sites were undergoing positive selection independently in both paralogs. When the closest adjacent site to a positively selected site in one paralog was undergoing positive selection in both paralogs, the adjacent site was treated as belonging to the same paralog.

We also examine the sequence divergence of species-specific duplications of lysin and sp18 in H. tuberculata (**Figure 3**). In **Figure 3A**, sites that diverge between sp18 and lysin H. tuberculata paralogs are mapped onto the sp18 crystal structure (1GAK) and the lowest energy NMR ensemble of lysin (5UTG) (Kresge et al., 2001; Wilburn et al., 2018). Since lysin has been shown not to crystallize in its native formation (Wilburn et al., 2018), the NMR structure was chosen to better examine the clustering of sites that are diverging between H. tuberculata lysin paralogs at lysin's VERL binding interface.

Identification of Sp18 Peptides

H. tuberculata testis tissue was homogenized in 1% sodium dodecyl sulfate with BME at 70°C for 30 min. Testis samples were separated by SDS-PAGE using a Tris-Tricine buffering system with discontinuous 4% resolving/15% separating acrylamide gels. Samples were electrophoresed at 50 V for 15 min followed by 100 V for 90 min. The gel was run with the BioRad Broad Range Ladder and stained with Coomassie Blue R-250 for 15 min. Using the ladder as reference, the lysin and sp18-containing region (~14–22 kDa) of the polyacrylamide gel was excised using a clean scalpel, with multiple rounds of perfusion with an ammonium bicarbonate solution followed by acetonitrile to extract detergents and salts. Trypsin proteolysis of immobilized proteins was by perfusion of a Trypsin solution (40 μg/ml stock Trypsin 1:10 in 50 mM ammonium bicarbonate) and incubation at 37°C overnight. The supernatant from the digest was collected along with the supernatant from two rounds of hydration with ammonium bicarbonate and extraction with 50% acetonitrile. The collected supernatant containing the liberated peptides was concentrated to a dry pellet using a vacuum centrifuge then reconstituted in 0.1% FA for liquid chromatography tandem mass spectrometry (LC/MS-MS). Unique peptides for sp18 copy #1 were identified in the sample using the Crux toolkit comet command (Park et al., 2008). The protein sequence database was composed of a six-frame translation of the *H. tuberculata* testis transcriptome.

Identification of ZP Proteins

An exhaustive BLAST search of the *H. tuberculata* ovary transcriptome identified all cDNA sequences with homology to *H. rufescens* VEZPs. A previous study used a similar approach to originally identify known VEZPs in *H. rufescens* indicating that this approach should be sufficient to identify novel VEZPs (Aagaard et al., 2010). All cDNA sequences that matched VEZPs were filtered for duplicates using CD-HIT-EST with a threshold of 0.9 sequence identity (Huang et al., 2010). The longest sequence from each cluster created by CD-HIT-EST was chosen as the cluster's representative sequence. All *H. tuberculata* sequences from this filtering process were translated and the C-terminal ZP modules were identified by identifying conserved cysteine residues. The ZP module protein sequences from both *H. tuberculata* and *H. rufescens* were aligned using PROMALS3D (Pei et al., 2008b). The MSA of these ZP modules from were used to construct a VEZP homolog protein phylogeny using the same RAXML-NG protocol described above for lysin and sp18 paralog phylogenies. New sequences were

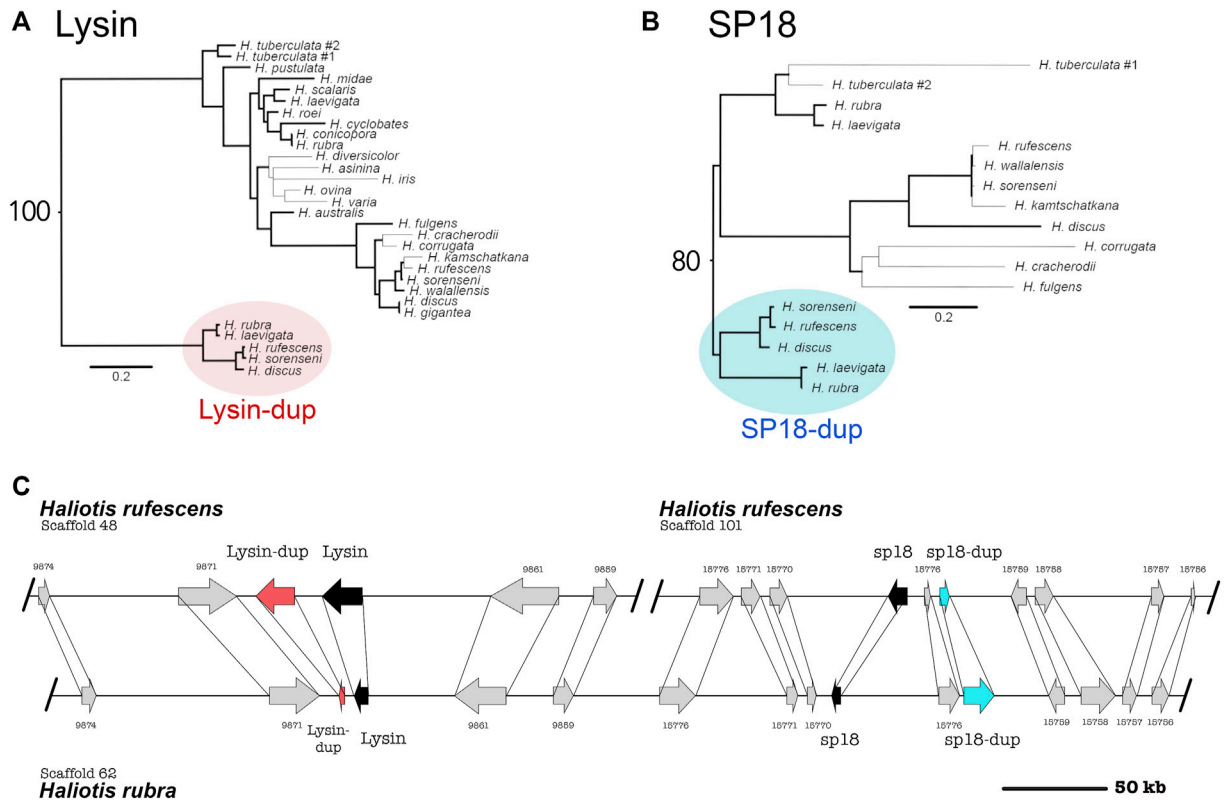

FIGURE 1 | Syntenic and phylogenetic analysis indicate that four tandem acrosomal proteins are ancestral to all abalone. **(A)** Ancestral duplication led to the paralogs lysin and lysin-dup (Red). Bold lines indicate greater than or equal to 80% bootstrap branch support. Bootstrap support for the node connecting lysin and lysin-dup sequences is 100. **(B)** Ancestral duplication led to the paralogs sp18 and sp18-dup (blue). A clade specific duplication of sp18 is present in the *H. tuberculata* testes transcriptome. Bold lines indicate greater than or equal to 80% bootstrap branch support. Bootstrap support for the node connecting sp18 and sp18-dup sequences is 80. **(C)** Lysin (black), sp18 (black) and their paralogs lysin-dup (red) and sp18-dup (blue) are found in the genomes of North American and Australian abalone. Syntenic analysis indicates that paralogs are located near each other in the abalone genome, although all four paralogs are only genetically linked in Australian abalone genome assemblies. In the North American abalone H. rufescens genome assembly, lysin and sp18 are found on separate scaffolds linked with their paralogs. The scaffolds extend beyond the breakpoint shown in the **(C)**.

uploaded to Genbank under accession numbers OK491878-OK491909.

RESULTS

Genomic Analysis Reveals Tandem Duplications of Ancestral Abalone Acrosomal Proteins

By pairing phylogenetic and genomic analysis of abalone species belonging to the North American clade (*H. rufescens*, *H. sorenseni*, *H. discus*) and the Australian clade (*H. rubra*, *H. laevigata*), we identifed ancestral duplications of both sp18 and lysin (**Figure 1**; sp18-dup and lysin-dup, respectively). We calculated maximum likelihood DNA phylogenies independently for lysin and sp18 with their paralogs and rooted the phylogenies by orthology (**Figures 1A,B**). Predicted intron/exon boundaries of the novel acrosomal protein paralogs were shared with lysin and sp18 (Metz et al., 1998). No mutations causing pseudogenization were detected within the predicted CDS of either paralog. For the abalone species with published genomes, only one (*H. rufescens*) has a published testes transcriptome (Palmer et al., 2013). Full-length sequences of lysin, sp18, and sp18-dup are expressed in the testes transcriptome of *H. rufescens*; however, lysin-dup was not detected.

Sequence analysis is consistent with the sp18-dup gene encoding a functional reproductive protein ancestral to *Haliotis*. Sp18-dup is predicted to have a signal peptide sequence and maintains a pair of cysteine residues involved in forming a structurally important disulfide-bond in sp18 (Kresge et al., 2000, 2001). Sp18-dup has not been identified in previous analysis due to the high divergence between it and sp18 (27.5% sequence identity between *H. rufescens* sp18 paralogs) obscuring homology.

Lysin-dup was identified in all abalone genomes investigated but was not detected in the testes illumina transcriptome of *H. rufescens* (Palmer et al., 2013). The absence of lysin-dup in the testes transcriptome could indicate insufficient read depth, differences in tissue-expression, or potentially pseudogenization. Since the full-length sequence of lysin-dup

TABLE 1 | Acrosomal protein paralogs are evolving under positive selection.

Gene	Model	−2Δl	d_N/d_S	% Positively Selected Sites
Sp18	M1a vs. M2a	84.2**	4.4	48
	M7 vs. M8	95.3**	4.2	48
	M8a vs. M8	84.3**	4.2	48
Sp18-dup	M1a vs. M2a	4.1	—	—
	M7 vs. M8	4.1	—	—
	M8a v M8	4.1*	1.8	49
Lysin-dup	M1a vs. M2a	1.3	—	—
	M7 vs. M8	1.5	—	—
	M8a vs. M8	1.3	—	—
Lysin	M1a vs. M2a	156.1**	1.2	21
	M7 vs. M8	156.7**	1.1	22
	M8a vs. M8	141.1**	1.1	22

*Codon substitution models were used to analyze sequences of sp18, sp18-dup, lysin-dup, and lysin. Site models allowing for several neutral models (M1a, M7, and M8a) or selection models (M2a, M8, and M8a) allowing for variation among sites, were fit to the data using PAML. Sites undergoing positive selection were detected in sp18 and lysin for all model comparisons. A more powerful test (M8a vs. M8) detected positive selection in sp18-dup as well as sp18 and lysin. Estimates of the likelihood ratio statistic (−2Δl), dN/dS, and the percentage of sites that are under positive selection are given. Significant tests are highlighted in yellow. (*Significant at p < 0.05; **Significant at p < 0.005).*

was not identified within the *H. rufescens* testis transcriptome, lysin sequences were used instead to identify lysin-dup exons within abalone genomes. However, divergence between lysin and lysin-dup likely prevented the identification of full-length coding sequence from abalone genomes. Only exons 2-4 could be identified (79% of query sequence) within *H. rufescens* and *H.rubra*. The missing exons 1 and 5 contain the signal peptide and the N- and C-termini of the molecule. In lysin, the N- and C-terminus are under strong positive selection promoting extensive divergence that reduces the ability to identify these exons using homology-based approaches (Lee et al., 1995; Lyon and Vacquier, 1999).

In the Australian abalone genomes lysin, lysin-dup, sp18, and sp18-dup are all found within a single contig with 233 kb separating the paralog pair of lysin and lysin-dup from the paralog pair of sp18 and sp18-dup. But in the genome of the North American abalone species *H. rufescens*, the paralog pair of lysin and lysin-dup are on a separate scaffold from the paralog pair of sp18 and sp18-dup. We compared the Australian contig containing the four acrosomal protein paralogs with the two *H. rufescens* contigs containing the lysin and sp18 paralog pairs respectively (**Figure 1C**). We found several ORFs surrounding each paralog pair in *H. rufescens* that were found in the same order between in *H. rubra,* indicating synteny between scaffolds. All four acrosomal proteins being located near each other in the same scaffold in the *H. rubra* genome suggests that tandem duplication led to recurrent duplications of this protein family (Reams and Roth, 2015). The sp18 ORF codes in a different direction than the other paralogs, suggesting that transposition and inversion may have also contributed to duplications within this protein family (Reams and Roth, 2015). In *H, rufescens*, the sp18 paralog pair and lysin paralog pair are found in separate scaffolds. *H. rufescens* scaffolds 48 and 101 extend beyond the breaking point shown in **Figure 1**. Therefore, the paralogs being found in separate scaffolds cannot be attributed to a fragmented genome assembly. Rather, we hypothesize that recombination led to the separation of the paralogs within *H. rufescens*.

Patterns of Divergence of Ancestral Acrosomal Protein Paralogs

Lysin, sp18, and sp18-dup all contained sites detected to be subjected to positive selection. (**Table 1**). Lysin-dup did not show signatures of positive selection, though this could be due to having insufficient sequences to provide the statistical power to conduct the test (**Table 1**) (Anisimova et al., 2001). Clustering and distribution of amino acid sites undergoing positive selection can identify regions important to the function of rapidly evolving genes (Anisimova et al., 2001). For example, many of the sites in lysin that are undergoing positive selection (11/23) are in a region of the molecule that binds its egg receptor VERL (Wilburn et al., 2018). We investigated the distribution of sites undergoing positive selection in sp18 and sp18-dup. Similar regions of the molecule undergoing positive selection in both paralogs would suggest a shared biochemical mechanism while differences in distributions of positively selected sites would indicate divergence in biochemical mechanism.

By mapping sites under positive selection onto a protein alignment of sp18 and sp18-dup, we determined that sites under positive selection in either paralog are non-randomly distributed across the protein alignment and differentially clustered. We analyzed the selected sites in the primary sequence alignment with a parametric adaptation of the runs test (Wald-Wolfowitz test) (**Figure 2A**) (Magel and Wibowo, 1997). This analysis showed that there were significant runs of sites undergoing positive selection in either paralog (p-value = 0.0331), consistent with different regions evolving under positive selection among paralogs. Positive selection acting on different regions of the protein alignment is consistent with functional divergence of paralogs.

We investigated clustering of positively selected sites in three-dimensional space. By mapping sp18 and sp18-dup positively selected sites onto the sp18 structure, it is visually apparent that there are distinct clusters of sites under selection between paralogs (**Figure 2B**). Using the plane of best fit through the crystal structure we divided the molecule into "left" and "right" sides agnostic to the location of positively selected sites. To define the "top" and "bottom" of the molecule we used a plane perpendicular to the plane of best fit. Sites under positive selection in sp18-dup were statistically more likely to be on the "right" side than on the "left" (p-value <0.05), however, sp18-dup positively selected sites were not statistically significantly enriched at either the "top" or "bottom" of the molecule (**Supplementary Figure S2**). Sp18 sites, using the same tests, showed no statistically significant difference from the null distribution. These tests show that sites under selection in sp18 and sp18-dup are distributed differently across their three-dimensional structures.

We also developed a test to examine whether sites under selection in sp18 and sp18-dup were statistically more likely to be adjacent to a site under selection from the same paralog. Such a pattern of clustering would indicate a spatial relationship between

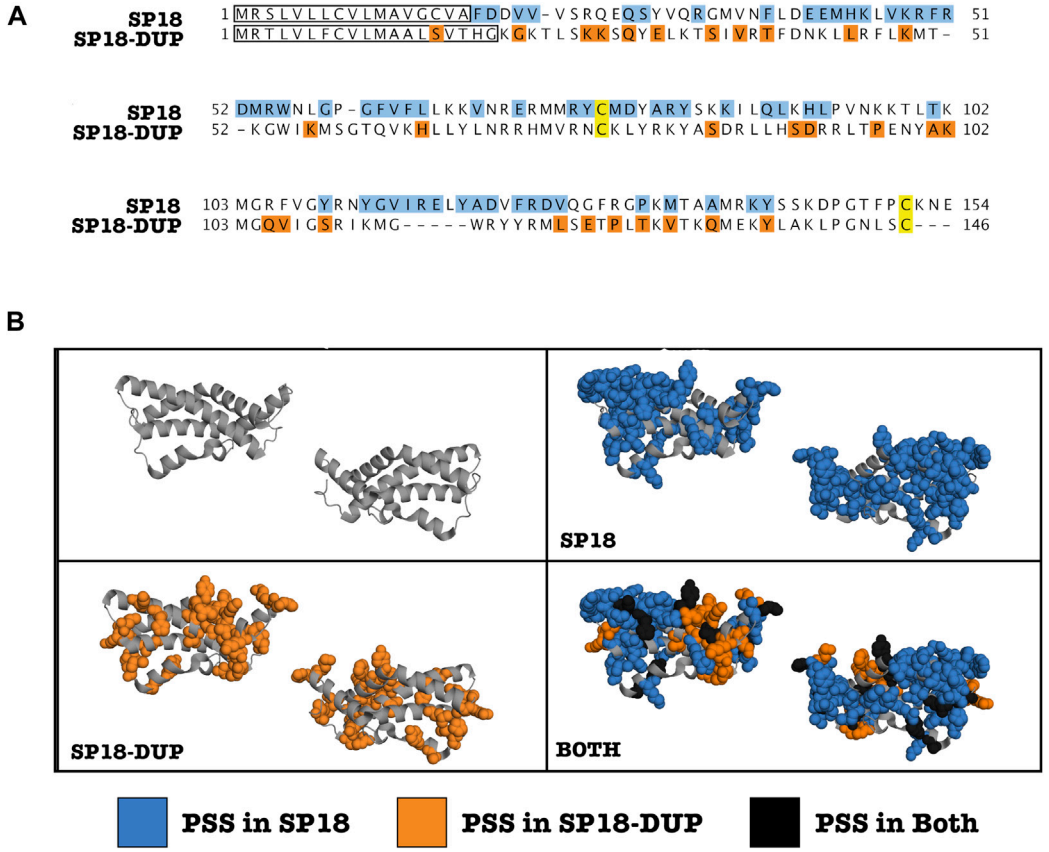

FIGURE 2 | Clustering of positively selected sites differs between SP18 and SP18-dup. **(A)** Alignment of *H. fulgens* sp18 and *H. sorenseni* sp18-dup mature protein sequences. Sites under positive selection are highlighted. Blue (Sp18), Orange (Sp18-dup), and Black (both). A modified parametric runs test was used to determine that there were statistically significant runs in linear sequence space of sites under positive selection in sp18 or sp18-dup (p-value—0.0331). Yellow sites indicate conserved cysteines shown to be involved in forming a disulfide bond in SP18. **(B)** Sites under positive selection in sp18 or sp18-dup were mapped onto the crystal structure of sp18 from *H. fulgens* and appear clustered in 3-D space.

positively selected sites belonging to a particular paralog. For each site under positive selection in sp18 or sp18-dup, we identified whether the closest positively selected site in three-dimensional space was significantly more likely to belong to the same paralog. We found that sites under selection in both paralogs were more likely to have the closest positively selected site belong to the same paralog rather than the other paralog according to a chi-squared test (p-value <0.01). Together, the runs test analysis and three-dimensional analyses point to diversifying selection post-duplication of these proteins to promote functional diversification. However, it should be noted that there is some uncertainty in the prediction of positively selected sites which is unaccounted for in our clustering analyses.

Because Lysin-dup was not detected to be under positive selection, we did not test for differences in sites under selection between lysin paralogs. However, we did evaluate how the lysin-dup sequence diverged from lysin. Many of the sites shown to be undergoing positive selection in lysin differ in sequence from lysin-dup (13/14) when comparing the *H. rufescens* sequences (**Figure 3B**). Although this comparison is not significant (p = 0.088), this suggests similar sites driving the diversification in sequence of lysin between species and between lysin and its paralog lysin-dup.

H. tuberculata sp18 and Lysin Duplications are Species-Specific

Previous work described a lysin duplication unique to *H. tuberculata* (Clark et al., 2007). The lysin paralogs were shown to be evolving under positive selection and to be maintained in the testis proteome (Clark et al., 2007). Sites that vary between European lysin paralogs are largely located on the face of the molecules interacting with lysin receptor VERL (**Figure 3A**). To investigate the presence of additional sp18 and lysin paralogs in *H. tuberculata*, we constructed a long-read PacBio testis transcriptome. Performing tBLASTN searches of the *H. tuberculata* transcriptome for lysin and sp18 revealed the previously described species-specific duplication of lysin (*H. tuberculata* lysin copy #1 and copy #2) and a novel duplication of sp18 (*H. tuberculata* sp18 copy #1 and copy #2).

Phylogenetic analysis indicates the *H. tuberculata* sp18 paralogs are the result of a recent duplication and not

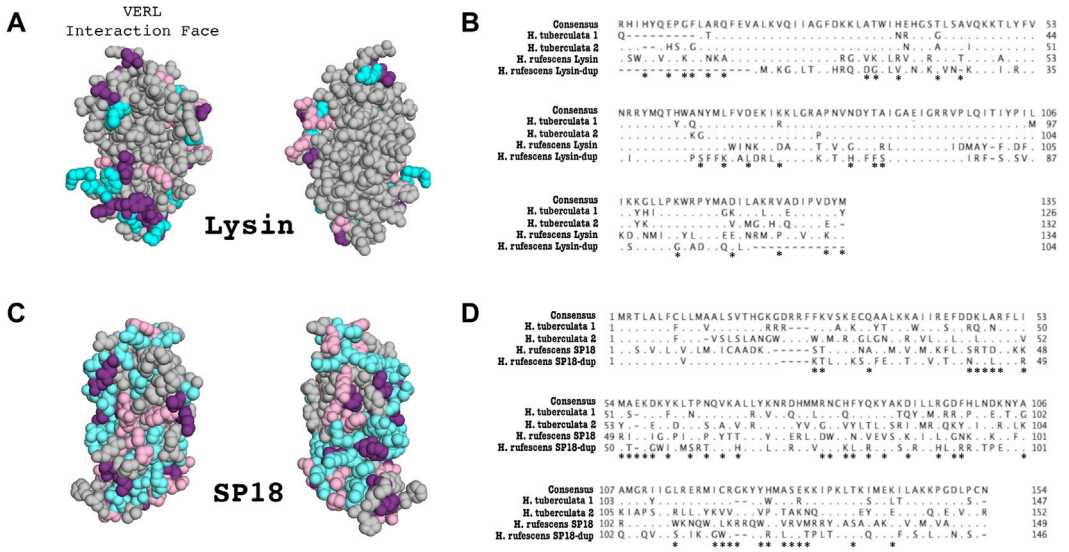

FIGURE 3 | Duplication and divergence of lysin and sp18 paralogs in *H. tuberculata*. **(A)** Sites that differentiate *H. tuberculata* lysin paralogs from *H. rufescens* lysin are mapped onto the *H. rufescens* NMR structure (PDB 5UTG). Blue–Sites that differ between *H. rufescens* lysin and *H. tuberculata* Copy #1, Pink–Sites that differ between *H. rufescens* lysin and *H. tuberculata* Copy #2, Purple–Sites that differ between *H. rufescens* lysin and both *H. tuberculata* lysin paralogs. Notably the face of the lysin molecule that interacts with VERL harbors most substitutions between *H. tuberculata* paralogs, suggestive of a shared interaction face for both *H. tuberculata* lysin paralogs. **(B)** Alignment of Lysin paralogs in *H. rufescens* and *H. tuberculata*. Both sets of paralogs arose from independent duplication events. Asterisks indicate sites that are shown to be under positive selection in *H. rufescens* lysin. **(C)** Sites that differ between *H. tuberculata* sp18 paralogs are mapped onto the crystal structure of sp18 *from H. fulgens* (PDB 1GAK). Blue–Sites that differ between *H. rufescens* sp18 and *H. tuberculata* Copy #1, Pink–Sites that differ between *H. rufescens* sp18 and H. tuberculata Copy #2, Purple–Sites that differ between *H. rufescens* sp18 and both H. tuberculata sp18 paralogs. **(D)** Alignment of sp18 paralogs in *H. rufescens* and *H. tuberculata*. Both sets of paralogs arose from independent duplication events. Asterisks indicate sites that are shown to be under positive selection in *H. rufescens* sp18.

ancestral to *Haliotis*. Sequence information from other abalone species is needed to determine whether this duplication is species-specific to *H. tuberculata*; it appears to be specific to the abalone clade containing the European species. The signal sequences of the *H. tuberculata* sp18 paralogs are more similar to each other than to signal sequences from other species' sp18 paralogs. Signal sequences are not part of the mature protein and not subjected to the same evolutionary pressures driving rapid divergence, therefore these sequences show more conservation between closely related paralogs. This similarity in signal sequence between *H. tuberculata* sp18 paralogs (15/19 sites are identical) further supports that these paralogs are the result of a non-ancestral duplication. Despite being a more recent duplication of sp18, the paralogs have a low sequence identity (39%), lower than that of the *H. tuberculata* lysin paralogs (83%). This is consistent with sp18 having a higher d_N/d_S and evolving more rapidly than lysin (**Table 1**). *H. tuberculata* sp18 paralogs maintain a pair of structurally important cysteine residues involved in forming a disulfide bond. Rapid sequence divergence, no premature stop codons, and both genes being expressed in the testis transcriptome are all indicators that both sp18 paralogs (referred to here as *H. tuberculata* copy #1 and copy #2) are likely to be functional.

The *H. tuberculata* sp18 copy #1 is the more divergent to the ancestral sequence than copy #2, as indicated by its long branch in the sp18 phylogeny (**Figure 1B**). When comparing the sequence identity of *H. tuberculata* sp18 paralogs to *H. rubra* sp18 (an outgroup sequence), copy #1 shows a lower sequence identity (41%) than copy #2 (69%). This rapid sequence divergence of copy #1 without accruing mutations causing pseudogenization suggests strong positive selection. However pairwise d_N/d_S between *H. tuberculata* sp18 paralogs could not be reliably estimated due to extensive divergence resulting in saturation (multiple substitutions per site) (Swanson and Vacquier, 1995a). Maintenance of both paralogs in the testis proteome despite the observed sequence divergence would indicate that both paralogs are being selected for functions, presumably related to fertilization. We used data dependent acquisition mass spectrometry to identify peptides belonging to either paralog in the *H. tuberculata* testes proteome. Diagnostic peptides were detected for copy #1 but not copy #2. Despite being the more divergent sp18 sequence, copy #1 is maintained in the proteome. This result indicates that copy #1 is likely important for fulfilling sp18's membrane fusion function in *H. tuberculata*.

Lack of Recent Duplications of Egg Coat Proteins

We generated an ovary PacBio transcriptome for *H. tuberculata* to identify VEZP proteins. Using the 33 VEZP and ZP-domain sequences from the *H. rufescens* ovary transcriptome as the initial query sequences, exhaustive tBlastn searches of the ovary transcriptome were used to identify all cDNA sequences with sequence similarity to any *H. rufescens* VEZP. ZP module protein

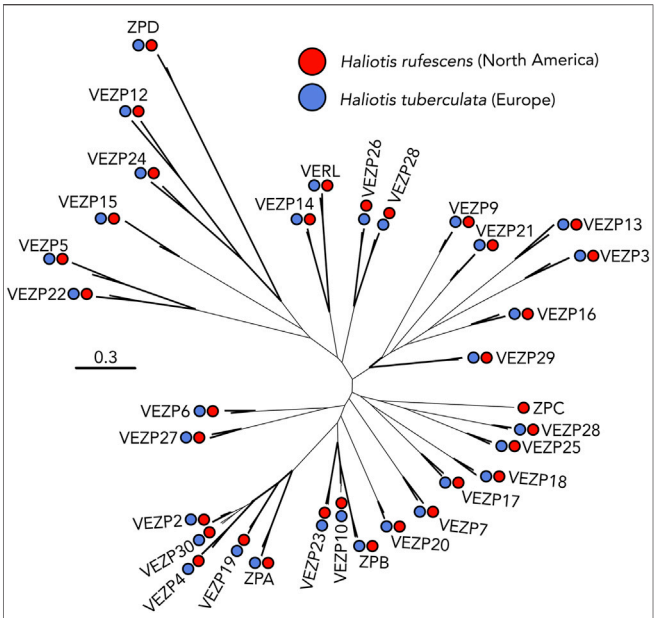

FIGURE 4 | VEZP proteins are conserved across abalone species. The distantly related abalone species *H. rufescens* (Red) and *H. tuberculata* (Blue) share the same vitelline envelope zona pellucida (VEZP) proteins within their ovary transcriptomes. Although there are species-specific duplications of lysin and sp18 *in H. tuberculata*, there is no evidence of species-specific duplications of VERL or other VEZP proteins. Bold lines indicate greater than or equal to 80% bootstrap branch support.

sequences were extracted from our *H. tuberculata* cDNA hits and the 33 *H. rufescens* VEZPs and then were aligned to construct a phylogeny (**Figure 4**). Clustering of *H. tuberculata* and *H. rufescens* ZP module sequences indicate that these distantly related abalone species have the same complement of ZP-proteins in their transcriptomes. In *H. tuberc*ulata's ovary transcriptome, orthologs of 32 of the 33 *H. rufescens* ovary ZP-domain proteins were identified. No VEZPs, including VERL and its most closely related paralogs VEZP14 and VEZP9 were duplicated. The only missing sequence belonged to ZPC, a gene whose cDNA sequence contains a premature stop codon in *H. rufescens* and for which no peptides were detected in the *H. rufescens* VE proteome (Aagaard et al., 2010). Therefore, ZPC is likely pseudogenized in *H. rufescens* and its expression its expression is no longer maintained in European abalone. Remarkably, no new ZP-module-containing proteins were identified in *H. tuberculata* despite the species having multiple clade-specific duplications of acrosomal proteins. These results suggest that the clade-specific maintenance of duplicated sperm acrosomal proteins found in the European abalone *H. tuberculata* are unlikely to be the result of duplicated egg proteins.

DISCUSSION

Despite decades of research examining the evolution of abalone fertilization genes, only recently have genomic resources been available that enable a broad investigation into the evolution of the protein families to which lysin and VERL belong. Here, we explore the contributions of duplication and sequence divergence to the evolution of abalone fertilization genes across the genus *Haliotis*. For our investigation we generated ovary and testes transcriptomes from the European abalone *H. tuberculata* and utilized recently published North American and Australian abalone genomes and a North American abalone testes transcriptome (Palmer et al., 2013; Nam et al., 2017; Botwright et al., 2019; Gan et al., 2019; Masonbrink et al., 2019). We discovered novel duplications of both lysin and sp18 ancestral to abalone, indicating that abalone lysin and sp18 are members of an ancestral abalone protein family with four members. The newly discovered sp18 paralog (sp18-dup) was shown to be undergoing positive selection, like lysin and sp18, and expressed in the testes of North American abalone. Further, differences in clustering of positively selected sites in sp18-dup compared to sp18 is potentially consistent with a model of subfunctionalization where a distinct binding interface is undergoing positive selection in sp18-dup but not sp18. However, it is also possible that this pattern of sequence divergence could be explained by neofunctionalization and sp18-dup is acquiring a different reproductive function. We investigated whether there are clade-specific duplications of abalone VEZPs or acrosomal proteins. In addition to a species-specific lysin duplication described in a previous publication (Clark et al., 2007), the *H. tuberculata* testes transcriptome contains a clade-specific duplication of sp18 not found in Australian or North American abalone species. However, no duplications of VERL or other VEZPs were observed between North American or European abalone, indicating that VEZP gene content is conserved across the genus *Haliotis*. Together, this data demonstrates that recurrent duplication and diversification driven by positive selection drives the evolution of an acrosomal protein family involved in fertilization in *Haliotis*.

Recurrent Duplication and Positive Selection of Acrosomal Proteins in Abalone

In the *H. rubra* abalone genome, the paralogs lysin, lysin-dup, sp18, and sp18-dup are found on a single scaffold. This clustering within the genome indicates that ancestral tandem duplication events occurred leading to the creation of this acrosomal protein family (Reams and Roth, 2015). Further, three of the four ancestral paralogs were shown to be maintained in the testis transcriptome and to be evolving under positive selection, a common characteristic of reproductive proteins.

This evolutionary pattern of duplication paired with sequence diversification found in the abalone acrosomal protein family can be compared to protein families in other taxa which contain sperm proteins mediating fertilization. Notably, the mammalian Izumo gene family contains four ancestral paralogs whose members all show testes-specific tissue expression in humans (Grayson and Civetta, 2012). Izumo1 is an essential gene for sperm-egg plasma membrane fusion in mammals that functions by binding the egg plasma membrane protein JUNO (Bianchi et al., 2014). There is evidence that the other three Izumo paralogs

may also possess important, although potentially varied, functions in fertility (Ellerman et al., 2009). All four paralogs have been shown to be undergoing rapid sequence evolution in at least one mammalian lineage, for Izumo1, 2, and 3 this is driven by positive selection and for Izumo4 this appears to be driven by relaxed selection (Grayson and Civetta, 2012; Grayson, 2015). Given that both the abalone acrosomal protein family and the mammalian Izumo family both contain multiple paralogs showing testis-specific function, subfunctionalization may be a common driver of the evolution of fertilization and reproductive genes across taxa. Understanding how fertilization proteins emerge and evolve can be important for identifying and understanding mechanisms of fertilization across diverse taxa.

Recurrent Functional Divergence of Abalone Acrosomal Proteins

Differences in optimal mating rates for sperm and eggs can drive antagonistic coevolution of reproductive proteins. Under this sexual conflict scenario, evolution of egg coat proteins interacting with sperm acrosomal proteins could lead to constrained evolution on the sperm side (Gavrilets and Waxman, 2002). Duplication followed by diversification of sperm fertilization proteins can be an important means of sperm escaping evolutionary constraints imposed by egg protein evolution. For two duplication events within the abalone acrosomal protein family there is evidence of functional divergence from either functional experiments [lysin vs. sp18, (Swanson and Vacquier, 1995a, b, 1997; Kresge et al., 2001; Aagaard et al., 2010)] or site-clustering analysis (sp18 vs. sp18-dup, current manuscript).

Plasma membrane fusion in fertilization or other contexts is traditionally thought to consist of two steps, binding and fusion (Bianchi and Wright, 2020). In sea urchins, both steps are mediated by different regions of the same protein, su-bindin (Vacquier and Moy, 1977; Ulrich et al., 1998; Vacquier and Swanson, 2011). However, in abalone these steps may have been partitioned between sp18 and sp18-dup *via* subfunctionalization. Abalone eggs have a thin layer directly overlaying the surface of the plasma membrane which morphologically resembles a duplication of the elevated VE (Mozingo et al., 1995). Just as lysin binds the VE protein VERL, sp18 may bind a VEZP protein found within the thin layer overlaying the abalone egg plasma membrane. Indeed, in addition, to having a strong fusagenic function, sp18 has been demonstrated to bind to VEZP proteins, an unsurprising trait for a lysin paralog (Swanson and Vacquier, 1995a; Aagaard et al., 2010). One possibility is that the subfunctionalization of sp18 and sp18-dup may have been driven by the separation of the steps of plasma membrane binding and fusion between paralogs. Additional functional characterization of each paralog's fusagenic function and ability to bind VEZPs is necessary to examine this hypothesis.

While the paralogs lysin-dup and lysin do show high sequence divergence, we were only able to detect evidence of positive selection in lysin. Therefore, the observed sequence divergence is likely driven by lysin's evolution post-duplication. Unlike the other acrosomal protein family paralogs discussed in this paper, lysin-dup is not detected in the testis transcriptome. However, there is an appealing hypothesis as to its potential function. In abalone egg coats there are two VEZP proteins capable of binding lysin, VERL the major binding partner of lysin and VEZP-14 the most recent paralog of VERL (Aagaard et al., 2013). It is possible that lysin-dup may be the binding partner of VEZP-14 and if true this could explain why lysin shows correlated evolution with VERL but not VEZP-14 (Aagaard et al., 2013). Currently there is insufficient data to test for correlated rates of evolution between lysin-dup and VEZP-14. However, further molecular and biochemical characterization through binding kinetic analysis could test the hypothesis that lysin-dup and VEZP-14 interact.

Species-Specific Duplications of Acrosomal Proteins in Abalone

Previous work described a lysin duplication unique to *H. tuberculata* and maintained in the testis proteome (Clark et al., 2007). In this study a clade-specific duplication of sp18 was discovered within the *H. tuberculata* transcriptome. Despite having two acrosomal protein duplications, European abalone's ovary transcriptome did not reveal any novel VEZP protein sequences indicative of a duplication event. While gene duplications are an ongoing contributor to the evolution of sperm fertilization genes in abalone, this may not be true for egg fertilization genes. Our data suggests that it is not duplications on the egg side driving the duplication of abalone acrosomal proteins in *H. tuberculata*. This could be explained by different selective pressures on the sperm and the egg, such as sperm competition and polyspermy risk (Carlisle and Swanson, 2020). Further, it does not seem that a process of gene birth and loss explains the evolution of abalone's acrosomal protein family since all paralogs are maintained in the transcriptome and have accrued no pseudogenizing mutations. A hypothesis for the duplication and diversification of acrosomal protein paralogs in *H. tuberculata* is that paralogs are specialized for different binding sites of their egg receptor or different allelic variants of their receptor. For example, *H. rufescens* VERL has 22 tandem ZP-N domains with three unique amino acid sequences, *H. tuberculata* VERL may show similar differences in ZP-N sequences and *H. tuberculata* lysin paralogs may be optimized for binding different ZP-N sequences (Galindo et al., 2002). In addition, the abalone *H. tuberculata* VERL may be polymorphic, as seen for *H. corrugata* VERL, and lysin paralogs are optimized for VERL allelic variants (Clark et al., 2009). This study observed that sites that vary between *H. tuberculata* lysin paralogs are largely located on the face of the molecules interacting with lysin receptor VERL (**Figure 3A**). Unlike the distribution of positively selected sites between sp18 and sp18-dup where sites are differentially clustered on the protein structure. This pattern of diversification may be suggestive of specialization of function, such as interacting with different VERL allelic variants or VERL ZP-N domains. Further characterization of VERL in *H. tuberculata* and population-level variation is necessary to explore these hypotheses.

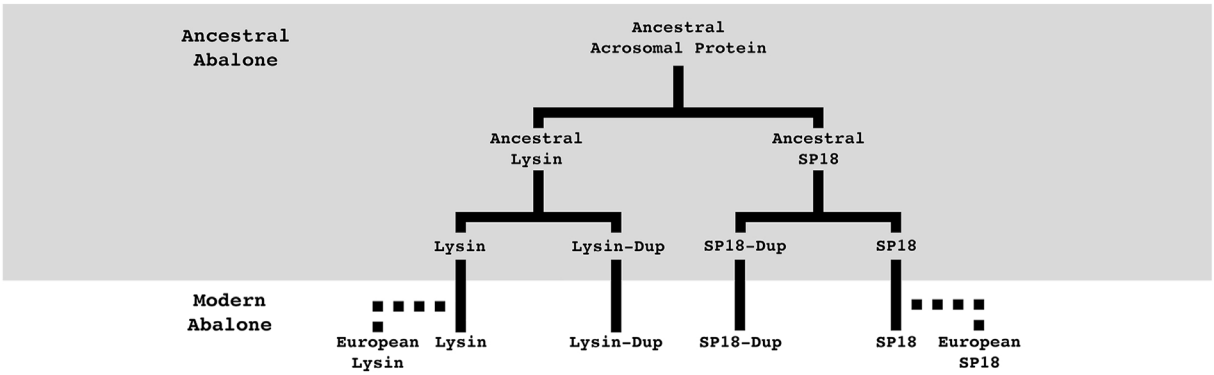

FIGURE 5 | Summary of abalone acrosomal duplications. Abalone acrosomal proteins have duplicated multiple times over the course of abalone evolution. Five duplication events can describe the currently identified protein family. Most duplications are ancestral to all abalone, but species-specific duplications in European abalone point to duplication paired with positive selection still playing an important role in the evolution of abalone fertilization pathways. Solid lines indicate orthologs present in all abalone, dotted lines indicate species-specific paralogs.

CONCLUSION

This study characterizes duplication events of a sperm acrosomal protein family with functions directly associated with fertilization. Although lysin was one of the first fertilization proteins discovered and the first for which an egg binding partner was defined, its evolutionary origins are unknown. By placing duplication events of lysin and sp18 within their genomic context and identifying clade-specific duplication events, this study has revealed the importance of duplication for the evolution of this protein family that has previously been unknown. We describe six acrosomal protein paralogs arising from both ancestral and clade-specific duplication events (**Figure 5**). Recurrent duplication events of sperm acrosomal proteins have occurred throughout the evolutionary history of abalone. For the two abalone species with transcriptomic data both have paralogs maintained in the testis transcriptome. Remarkably none of these genes have been pseudogenized and many are undergoing strong positive selection consistent with maintenance of their function in abalone reproduction. Further inquiry is required to investigate why these proteins are undergoing duplication, the functional consequences of these duplication events, and whether other fertilization proteins in other species (as also seen for the mammalian Izumo family) are undergoing recurrent duplication events.

DATA AVAILABILITY STATEMENT

The datasets presented in this study can be found in online repositories. The names of the repository/repositories and accession number(s) can be found below: https://www.ncbi.nlm.nih.gov/genbank/, OK491874-OK491909.

AUTHOR CONTRIBUTIONS

JC and WS designed the research. JC and MG performed the research. JC and WS analyzed the data. JC wrote the paper.

FUNDING

This study was supported by NIH Grant HD076862 to WS and a National Science Foundation Graduate Research Fellowship to JC (2140004). MG was supported by University of Washington School of Medicine-Gonzaga University Regional Health Partnership.

ACKNOWLEDGMENTS

Thank you to France Haliotis for help acquiring *H. tuberculata* samples, to Evan Cox, Dr. Daniel Promislow, Dr. Josh Schraiber, and Dr. Damien Wilburn for help with data analysis, and to Alberto Rivera, Dr. Jan Aagaard, and Dr. Bryce Taylor for useful discussions and comments. All research was performed on the traditional lands of the Duwamish Tribe. To learn more about the Duwamish Tribe and their continuing legacy, please visit https://www.duwamishtribe.org/.

SUPPLEMENTARY MATERIAL

The Supplementary Material for this article can be found online at: https://www.frontiersin.org/articles/10.3389/fcell.2022.795273/full#supplementary-material

REFERENCES

Aagaard, J. E., Springer, S. A., Soelberg, S. D., and Swanson, W. J. (2013). Duplicate Abalone Egg Coat Proteins Bind Sperm Lysin Similarly, but Evolve Oppositely, Consistent with Molecular Mimicry at Fertilization. *Plos Genet.* 9, e1003287. doi:10.1371/journal.pgen.1003287

Aagaard, J. E., Vacquier, V. D., MacCoss, M. J., and Swanson, W. J. (2010). ZP Domain Proteins in the Abalone Egg Coat Include a Paralog of VERL under Positive Selection that Binds Lysin and 18-kDa Sperm Proteins. *Mol. Biol. Evol.* 27, 193–203. doi:10.1093/molbev/msp221

Aagaard, J. E., Yi, X., MacCoss, M. J., and Swanson, W. J. (2006). Rapidly Evolving Zona Pellucida Domain Proteins Are a Major Component of the Vitelline Envelope of Abalone Eggs. *Proc. Natl. Acad. Sci.* 103, 17302–17307. doi:10.1073/pnas.0603125103

Almagro Armenteros, J. J., Tsirigos, K. D., Sønderby, C. K., Petersen, T. N., Winther, O., Brunak, S., et al. (2019). SignalP 5.0 Improves Signal Peptide Predictions Using Deep Neural Networks. *Nat. Biotechnol.* 37, 420–423. doi:10.1038/s41587-019-0036-z

Almeida, F. C., and Desalle, R. (2009). Orthology, Function and Evolution of Accessory Gland Proteins in the *Drosophila repleta* Group. *Genetics* 181, 235–245. doi:10.1534/genetics.108.096263

Anisimova, M., Bielawski, J. P., and Yang, Z. (2001). Accuracy and Power of the Likelihood Ratio Test in Detecting Adaptive Molecular Evolution. *Mol. Biol. Evol.* 18, 1585–1592. doi:10.1093/oxfordjournals.molbev.a003945

Avella, M. A., Baibakov, B., and Dean, J. (2014). A Single Domain of the ZP2 Zona Pellucida Protein Mediates Gamete Recognition in Mice and Humans. *J. Cell Biol* 205, 801–809. doi:10.1083/jcb.201404025

Bianchi, E., Doe, B., Goulding, D., and Wright, G. J. (2014). Juno Is the Egg Izumo Receptor and Is Essential for Mammalian Fertilization. *Nature* 508, 483–487. doi:10.1038/nature13203

Bianchi, E., and Wright, G. J. (2020). Find and Fuse: Unsolved Mysteries in Sperm-Egg Recognition. *Plos Biol.* 18, e3000953. doi:10.1371/journal.pbio.3000953

Botwright, N. A., Zhao, M., Wang, T., McWilliam, S., Colgrave, M. L., Hlinka, O., et al. (2019). Greenlip Abalone (Haliotis Laevigata) Genome and Protein Analysis Provides Insights into Maturation and Spawning. *G3 (Bethesda)* 9, 3067–3078. doi:10.1534/g3.119.400388

Cai, X., and Clapham, D. E. (2008). Evolutionary Genomics Reveals Lineage-specific Gene Loss and Rapid Evolution of a Sperm-specific Ion Channel Complex: CatSpers and CatSperβ. *PLoS One* 3, e3569. doi:10.1371/journal.pone.0003569

Carlisle, J. A., and Swanson, W. J. (2020). Molecular Mechanisms and Evolution of Fertilization Proteins. *J. Exp. Zool B Mol. Dev. Evol.* 336 (8), 652–665. doi:10.1002/jez.b.23004

Clark, N. L., Findlay, G. D., Yi, X., MacCoss, M. J., and Swanson, W. J. (2007). Duplication and Selection on Abalone Sperm Lysin in an Allopatric Population. *Mol. Biol. Evol.* 24, 2081–2090. doi:10.1093/molbev/msm137

Clark, N. L., Gasper, J., Sekino, M., Springer, S. A., Aquadro, C. F., and Swanson, W. J. (2009). Coevolution of Interacting Fertilization Proteins. *Plos Genet.* 5, e1000570. doi:10.1371/journal.pgen.1000570

Cooper, J. C., and Phadnis, N. (2017). Parallel Evolution of Sperm Hyper-Activation Ca2+ Channels. *Genome Biol. Evol.* 9, 1938–1949. doi:10.1093/gbe/evx131

Doty, K. A., Wilburn, D. B., Bowen, K. E., Feldhoff, P. W., and Feldhoff, R. C. (2016). Co-option and Evolution of Non-olfactory Proteinaceous Pheromones in a Terrestrial Lungless Salamander. *J. Proteomics* 135, 101–111. doi:10.1016/j.jprot.2015.09.019

Ellerman, D. A., Pei, J., Gupta, S., Snell, W. J., Myles, D., and Primakoff, P. (2009). Izumo Is Part of a Multiprotein Family Whose Members Form Large Complexes on Mammalian Sperm. *Mol. Reprod. Dev.* 76, 1188–1199. doi:10.1002/mrd.21092

Findlay, G. D., Yi, X., Maccoss, M. J., and Swanson, W. J. (2008). Proteomics Reveals Novel Drosophila Seminal Fluid Proteins Transferred at Mating. *Plos Biol.* 6, e178. doi:10.1371/journal.pbio.0060178

Galindo, B. E., Moy, G. W., Swanson, W. J., and Vacquier, V. D. (2002). Full-length Sequence of VERL, the Egg Vitelline Envelope Receptor for Abalone Sperm Lysin. *Gene* 288, 111–117. doi:10.1016/s0378-1119(02)00459-6

Galindo, B. E., Vacquier, V. D., and Swanson, W. J. (2003). Positive Selection in the Egg Receptor for Abalone Sperm Lysin. *Proc. Natl. Acad. Sci.* 100, 4639–4643. doi:10.1073/pnas.0830022100

Gan, H. M., Tan, M. H., Austin, C. M., Sherman, C. D. H., Wong, Y. T., Strugnell, J., et al. (2019). Best Foot Forward: Nanopore Long Reads, Hybrid Meta-Assembly, and Haplotig Purging Optimizes the First Genome Assembly for the Southern Hemisphere Blacklip Abalone (Haliotis Rubra). *Front. Genet.* 10, 889. doi:10.3389/fgene.2019.00889

Gavrilets, S., and Waxman, D. (2002). Sympatric Speciation by Sexual Conflict. *Proc. Natl. Acad. Sci.* 99, 10533–10538. doi:10.1073/pnas.152011499

Grayson, P., and Civetta, A. (2012). Positive Selection and the Evolution of Izumo Genes in Mammals. *Int. J. Evol. Biol.* 2012, 958164. doi:10.1155/2012/958164

Grayson, P. (2015). Izumo1 and Juno: the Evolutionary Origins and Coevolution of Essential Sperm-Egg Binding Partners. *R. Soc. Open Sci.* 2, 150296. doi:10.1098/rsos.150296

Hellberg, M. E., and Vacquier, V. D. (1999). Rapid Evolution of Fertilization Selectivity and Lysin cDNA Sequences in Teguline Gastropods. *Mol. Biol. Evol.* 16, 839–848. doi:10.1093/oxfordjournals.molbev.a026168

Huang, Y., Niu, B., Gao, Y., Fu, L., and Li, W. (2010). CD-HIT Suite: a Web Server for Clustering and Comparing Biological Sequences. *Bioinformatics* 26, 680–682. doi:10.1093/bioinformatics/btq003

Kamei, N., and Glabe, C. G. (2003). The Species-specific Egg Receptor for Sea Urchin Sperm Adhesion Is EBR1,a Novel ADAMTS Protein. *Genes Dev.* 17, 2502–2507. doi:10.1101/gad.1133003

Killingbeck, E. E., and Swanson, W. J. (2018). Egg Coat Proteins across Metazoan Evolution. *Curr. Top. Dev. Biol.* 130, 443–488. doi:10.1016/bs.ctdb.2018.03.005

Kozlov, A. M., Darriba, D., Flouri, T., Morel, B., and Stamatakis, A. (2019). RAxML-NG: a Fast, Scalable and User-Friendly Tool for Maximum Likelihood Phylogenetic Inference. *Bioinformatics* 35, 4453–4455. doi:10.1093/bioinformatics/btz305

Kresge, N., Vacquier, V. D., and Stout, C. D. (2001). The Crystal Structure of a Fusagenic Sperm Protein Reveals Extreme Surface Properties,. *Biochemistry* 40, 5407–5413. doi:10.1021/bi002779v

Kresge, N., Vacquier, V. D., and Stout, C. D. (2000). The High Resolution crystal Structure of green Abalone Sperm Lysin: Implications for Species-specific Binding of the Egg Receptor 1 1Edited by R. Huber. *J. Mol. Biol.* 296, 1225–1234. doi:10.1006/jmbi.2000.3533

Le, S. Q., and Gascuel, O. (2008). An Improved General Amino Acid Replacement Matrix. *Mol. Biol. Evol.* 25, 1307–1320. doi:10.1093/molbev/msn067

Lee, Y. H., Ota, T., and Vacquier, V. D. (1995). Positive Selection Is a General Phenomenon in the Evolution of Abalone Sperm Lysin. *Mol. Biol. Evol.* 12, 231–238. doi:10.1093/oxfordjournals.molbev.a040200

Lehmann, R. (2018). Matchmaking Molecule for Egg and Sperm. *Science* 361, 974–975. doi:10.1126/science.aau8356

Lemoine, F., Domelevo Entfellner, J.-B., Wilkinson, E., Correia, D., Dávila Felipe, M., De Oliveira, T., et al. (2018). Renewing Felsenstein's Phylogenetic Bootstrap in the Era of Big Data. *Nature* 556, 452–456. doi:10.1038/s41586-018-0043-0

Lewis, C. A., Leighton, D. L., and Vacquier, V. D. (1980). Morphology of Abalone Spermatozoa before and after the Acrosome Reaction. *J. Ultrastruct. Res.* 72, 39–46. doi:10.1016/s0022-5320(80)90133-1

Lyon, J. D., and Vacquier, V. D. (1999). Interspecies Chimeric Sperm Lysins Identify Regions Mediating Species-specific Recognition of the Abalone Egg Vitelline Envelope. *Dev. Biol.* 214, 151–159. doi:10.1006/dbio.1999.9411

MacDonald, R. J., Swift, G. H., Przybyla, A. E., and Chirgwin, J. M. (1987). [20] Isolation of RNA Using Guanidinium Salts. *Methods Enzymol.* 152, 219–227. doi:10.1016/0076-6879(87)52023-7

Magel, R. C., and Wibowo, S. H. (1997). Comparing the Powers of the Wald-Wolfowitz and Kolmogorov-Smirnov Tests. *Biom. J.* 39, 665–675. doi:10.1002/bimj.4710390605

Masonbrink, R. E., Purcell, C. M., Boles, S. E., Whitehead, A., Hyde, J. R., Seetharam, A. S., et al. (2019). An Annotated Genome for *Haliotis rufescens* (Red Abalone) and Resequenced Green, Pink, Pinto, Black, and White Abalone Species. *Genome Biol. Evol.* 11, 431–438. doi:10.1093/gbe/evz006

McGinnis, S., and Madden, T. L. (2004). BLAST: at the Core of a Powerful and Diverse Set of Sequence Analysis Tools. *Nucleic Acids Res.* 32, W20–W25. doi:10.1093/nar/gkh435

Metz, E. C., Robles-Sikisaka, R., and Vacquier, V. D. (1998). Nonsynonymous Substitution in Abalone Sperm Fertilization Genes Exceeds Substitution in Introns and Mitochondrial DNA. *Proc. Natl. Acad. Sci.* 95, 10676–10681. doi:10.1073/pnas.95.18.10676

Mozingo, N. M., Vacquier, V. D., and Chandler, D. E. (1995). Structural Features of the Abalone Egg Extracellular Matrix and its Role in Gamete Interaction during Fertilization. *Mol. Reprod. Dev.* 41, 493–502. doi:10.1002/mrd.1080410412

Nam, B. H., Kwak, W., Kim, Y. O., Kim, D. G., Kong, H. J., Kim, W. J., et al. (2017). Genome Sequence of pacific Abalone (Haliotis Discus Hannai): the First Draft Genome in Family Haliotidae. *Gigascience* 6, 1–8. doi:10.1093/gigascience/gix014

Palmer, M. R., McDowall, M. H., Stewart, L., Ouaddi, A., MacCoss, M. J., and Swanson, W. J. (2013). Mass Spectrometry and Next-Generation Sequencing Reveal an Abundant and Rapidly Evolving Abalone Sperm Protein. *Mol. Reprod. Dev.* 80, 460–465. doi:10.1002/mrd.22182

Park, C. Y., Klammer, A. A., Käll, L., MacCoss, M. J., and Noble, W. S. (2008). Rapid and Accurate Peptide Identification from Tandem Mass Spectra. *J. Proteome Res.* 7, 3022–3027. doi:10.1021/pr800127y

Pei, J., Kim, B.-H., and Grishin, N. V. (2008a). PROMALS3D: a Tool for Multiple Protein Sequence and Structure Alignments. *Nucleic Acids Res.* 36, 2295–2300. doi:10.1093/nar/gkn072

Pei, J., Tang, M., and Grishin, N. V. (2008b). PROMALS3D Web Server for Accurate Multiple Protein Sequence and Structure Alignments. *Nucleic Acids Res.* 36, W30–W34. doi:10.1093/nar/gkn322

Raj, I., Sadat Al Hosseini, H., Dioguardi, E., Nishimura, K., Han, L., Villa, A., et al. (2017). Structural Basis of Egg Coat-Sperm Recognition at Fertilization. *Cell* 169, 1315–1326. doi:10.1016/j.cell.2017.05.033

Rastogi, S., and Liberles, D. A. (2005). Subfunctionalization of Duplicated Genes as a Transition State to Neofunctionalization. *BMC Evol. Biol.* 5, 28. doi:10.1186/1471-2148-5-28

Reams, A. B., and Roth, J. R. (2015). Mechanisms of Gene Duplication and Amplification. *Cold Spring Harb Perspect. Biol.* 7, a016592. doi:10.1101/cshperspect.a016592

Sirot, L. K., Findlay, G. D., Sitnik, J. L., Frasheri, D., Avila, F. W., and Wolfner, M. F. (2014). Molecular Characterization and Evolution of a Gene Family Encoding Both Female- and Male-specific Reproductive Proteins in Drosophila. *Mol. Biol. Evol.* 31, 1554–1567. doi:10.1093/molbev/msu114

Slater, G., and Birney, E. (2005). Automated Generation of Heuristics for Biological Sequence Comparison. *BMC Bioinformatics* 6, 31. doi:10.1186/1471-2105-6-31

Suyama, M., Torrents, D., and Bork, P. (2006). PAL2NAL: Robust Conversion of Protein Sequence Alignments into the Corresponding Codon Alignments. *Nucleic Acids Res.* 34, W609–W612. doi:10.1093/nar/gkl315

Swanson, W. J., Aagaard, J. E., Vacquier, V. D., Monné, M., Sadat Al Hosseini, H., and Jovine, L. (2011). The Molecular Basis of Sex: Linking Yeast to Human. *Mol. Biol. Evol.* 28, 1963–1966. doi:10.1093/molbev/msr026

Swanson, W. J., Nielsen, R., and Yang, Q. (2003). Pervasive Adaptive Evolution in Mammalian Fertilization Proteins. *Mol. Biol. Evol.* 20, 18–20. doi:10.1093/oxfordjournals.molbev.a004233

Swanson, W. J., and Vacquier, V. D. (1995a). Extraordinary Divergence and Positive Darwinian Selection in a Fusagenic Protein Coating the Acrosomal Process of Abalone Spermatozoa. *Proc. Natl. Acad. Sci.* 92, 4957–4961. doi:10.1073/pnas.92.11.4957

Swanson, W. J., and Vacquier, V. D. (1995b). Liposome Fusion Induced by a Mr 18 000 Protein Localized to the Acrosomal Region of Acrosome-Reacted Abalone Spermatozoa. *Biochemistry* 34, 14202–14208. doi:10.1021/bi00043a026

Swanson, W. J., and Vacquier, V. D. (1997). The Abalone Egg Vitelline Envelope Receptor for Sperm Lysin Is a Giant Multivalent Molecule. *Proc. Natl. Acad. Sci.* 94, 6724–6729. doi:10.1073/pnas.94.13.6724

Swanson, W. J., and Vacquier, V. D. (2002). The Rapid Evolution of Reproductive Proteins. *Nat. Rev. Genet.* 3, 137–144. doi:10.1038/nrg733

Ulrich, A. S., Otter, M., Glabe, C. G., and Hoekstra, D. (1998). Membrane Fusion Is Induced by a Distinct Peptide Sequence of the Sea Urchin Fertilization Protein Bindin. *J. Biol. Chem.* 273, 16748–16755. doi:10.1074/jbc.273.27.16748

Vacquier, V. D., and Moy, G. W. (1977). Isolation of Bindin: the Protein Responsible for Adhesion of Sperm to Sea Urchin Eggs. *Proc. Natl. Acad. Sci.* 74, 2456–2460. doi:10.1073/pnas.74.6.2456

Vacquier, V. D., and Swanson, W. J. (2011). Selection in the Rapid Evolution of Gamete Recognition Proteins in marine Invertebrates. *Cold Spring Harbor Perspect. Biol.* 3, a002931. doi:10.1101/cshperspect.a002931

Wagstaff, B. J., and Begun, D. J. (2005). Comparative Genomics of Accessory Gland Protein Genes in *Drosophila melanogaster* and *D. pseudoobscura*. *Mol. Biol. Evol.* 22, 818–832. doi:10.1093/molbev/msi067

Wilburn, D. B., Arnold, S. J., Houck, L. D., Feldhoff, P. W., and Feldhoff, R. C. (2017). Gene Duplication, Co-option, Structural Evolution, and Phenotypic Tango in the Courtship Pheromones of Plethodontid Salamanders. *Herpetologica* 73, 206–219. doi:10.1655/herpetologica-d-16-00082.1

Wilburn, D. B., Tuttle, L. M., Klevit, R. E., and Swanson, W. J. (2018). Solution Structure of Sperm Lysin Yields Novel Insights into Molecular Dynamics of Rapid Protein Evolution. *Proc. Natl. Acad. Sci. USA* 115, 1310–1315. doi:10.1073/pnas.1709061115

Yang, Z. (2007). PAML 4: Phylogenetic Analysis by Maximum Likelihood. *Mol. Biol. Evol.* 24, 1586–1591. doi:10.1093/molbev/msm088

Yang, Z., Wong, W. S., and Nielsen, R. (2005). Bayes Empirical Bayes Inference of Amino Acid Sites under Positive Selection. *Mol. Biol. Evol.* 22, 1107–1118. doi:10.1093/molbev/msi097

Zigler, K. S., McCartney, M. A., Levitan, D. R., and Lessios, H. A. (2005). Sea Urchin Bindin Divergence Predicts Gamete Compatibility. *Evolution* 59, 2399–2404. doi:10.1111/j.0014-3820.2005.tb00949.x

Conflict of Interest: The authors declare that the research was conducted in the absence of any commercial or financial relationships that could be construed as a potential conflict of interest.

frontiers | Frontiers in Cell and Developmental Biology

ORIGINAL RESEARCH
published: 03 June 2022
doi: 10.3389/fcell.2022.854115

The Sperm Olfactory Receptor OLFR601 is Dispensable for Mouse Fertilization

González-Brusi L[1†], Hamzé JG[1,2†], Lamas-Toranzo I[1], Jiménez-Movilla M[2] and Bermejo-Álvarez P[1*]*

[1]Animal Reproduction Department, INIA-CSIC, Madrid, Spain, [2]Department of Cell Biology and Histology, Medical School, IMIB, University of Murcia, Murcia, Spain

Fertilization involves the fusion of two gametes by means of yet unknown membrane binding and fusion events. Over the last years, many sperm proteins have been uncovered to play essential roles in sperm-egg fusion in mammals, but their precise role in fertilization remains unknown, being unclear how these proteins interact with each other or with other yet unknown sperm proteins. The aim of this study has been to identify possible sperm proteins interacting with TMEM95, a protein essential for fertilization located in the sperm membrane. A list of 41 sperm proteins that were pulled down with TMEM95 and identified by mass spectrometry did not include other sperm proteins known to play a role in fertilization, suggesting an independent role of TMEM95 in fertilization. Between these lists, OLFR601 is allocated to the acrosomal region and may mediate affinity for an odorant involved in fertilization. However, *Olfr601* disruption did not impair the sperm fertilization ability, suggesting that its function may be redundant with that of other sperm proteins.

Keywords: fertilization, sperm, TMEM95, olfactory receptor, odorant

OPEN ACCESS

Edited by:
Benjamin Podbilewicz, Technion-Israel Institute of Technology, Israel

Reviewed by:
Pablo Aguilar, National University of General San Martín, Argentina
Vanina Gabriela Da Ros, CONICET Instituto de Biología y Medicina Experimental (IBYME), Argentina

***Correspondence:**
Jiménez-Movilla M
mariajm@um.es
Bermejo-Álvarez P
bermejo.pablo@inia.csic.es

[†]These authors have contributed equally to this work and share first authorship

Specialty section:
This article was submitted to Molecular and Cellular Reproduction, a section of the journal Frontiers in Cell and Developmental Biology

Received: *13 January 2022*
Accepted: *28 April 2022*
Published: *03 June 2022*

Citation:
L G-B, JG H, I L-T, M J-M and P B-Á (2022) The Sperm Olfactory Receptor OLFR601 is Dispensable for Mouse Fertilization. Front. Cell Dev. Biol. 10:854115. doi: 10.3389/fcell.2022.854115

1 INTRODUCTION

Sexual reproduction requires the binding and fusion of two gametes during fertilization. Despite being arguably the most relevant cell fusion event in a mammal's life, until very recently, only three proteins were proven to be essential for this process: two sperm membrane proteins [IZUMO1 (Inoue et al., 2005) and SPACA6 (Lorenzetti et al., 2014)] and JUNO, a protein located on the oolemma (i.e., oocyte membrane) (Bianchi et al., 2014). The ablation of CD9, another oolemma-located protein, significantly impairs fertilization and it has been suggested to play a structural role (Kaji et al., 2000; Le Naour et al., 2000; Miyado et al., 2000). The list of known proteins required for this process has grown considerably on the sperm side with the addition of other sperm proteins including TMEM95, FIMP, SOF1, and DCST1/2. TMEM95 ablation was reported to cause severe infertility (Pausch et al., 2014) and *in vitro* fertilization defects in bulls (Fernandez-Fuertes et al., 2017), and complete fertilization failure in mice (Lamas-Toranzo et al., 2020; Noda et al., 2020). In mice, FIMP ablation significantly reduces fertilization rates (Fujihara et al., 2020) and, similar to TMEM95, SOF1, DCST1, or DCST2 ablation prevents fertilization (Noda et al., 2020; Inoue et al., 2021). The specific role of these sperm proteins on gamete fusion is evidenced by the remarkably similar reproductive phenotype of their corresponding KOs: sperms lacking any of these proteins are morphologically and kinetically normal, being able to reach the perivitelline space while failing to ultimately fuse their membrane with that of the oocyte.

Despite the exciting momentum, it remains unknown how these newly discovered sperm proteins interact to mediate gamete fusion and whether other proteins are required. Any cell fusion event, including fertilization, requires the first step of membrane binding before membrane fusion. IZUMO1-JUNO binding remains the only known protein-to-protein interaction between the sperm membrane and the oolemma (Bianchi et al., 2014), and IZUMO1 is still the only sperm protein described to be involved in the binding step, as sperms lacking any of the other six sperm proteins (SPACA6, TMEM95, SOF1, FIMP, DCST1, and DCST2) show binding to the oolemma of zona-devoid oocytes to a similar degree as the WT counterparts (Fujihara et al., 2020; Lamas-Toranzo et al., 2020; Noda et al., 2020; Inoue et al., 2021). Although sperm binding assays may not be fully conclusive in mice because of unspecific sperm binding, the lack of known interactions between any of the other six sperm proteins and JUNO or any other oocyte protein further suggests that they may be involved in post-binding events ultimately leading to gamete fusion. In this perspective, uncovering the interactions between these and other sperm proteins may help solve the fertilization puzzle.

The shared localization of some of the proteins involved in fertilization within the sperm allows protein-to-protein interactions. IZUMO1 and TMEM95 are localized to the acrosomal region in acrosome intact sperms and relocate to the head, including the equatorial segment, after an acrosome reaction (Satouh et al., 2012; Lamas-Toranzo et al., 2020). Similar localization patterns in acrosome-intact and acrosome-reacted sperms were observed for SPACA6 in human sperm, although their localization could not be confirmed in mice (Barbaux et al., 2020). In partial contrast to IZUMO1, TMEM95, and SPACA6, FIMP localizes to the sperm head, including the equatorial segment before an acrosome reaction, being faintly detected in that region in ~60% of the acrosome-reacted sperm (Fujihara et al., 2020). Finally, the localization of SOF1, DCST1, and DCST2 is unknown, although a membrane localization is unlikely for SOF1 because it lacks a transmembrane domain. Interestingly, IZUMO1 localization is not affected by the ablation of any of the other sperm proteins involved in fertilization (Barbaux et al., 2020; Fujihara et al., 2020; Lamas-Toranzo et al., 2020; Noda et al., 2020; Inoue et al., 2021), suggesting that they play IZUMO1-independent roles in fertilization. However, SPACA6 is absent in sperms lacking DCST1, DCST2, or IZUMO1, evidencing possible interactions or relations between these four proteins (Inoue et al., 2021). The aim of this study has been to explore sperm proteins interacting with TMEM95 and to characterize the fertilization ability of sperms lacking one of these proteins: OLFR601.

2 MATERIALS AND METHODS

2.1 Production of Recombinant TMEM95 Protein

Two recombinant TMEM95 proteins were produced, one containing the transmembrane domain (TMD, 147-167 aa, Uniprot P0DJF3) and another lacking that domain (TMEM95ΔTm). The lack of a transmembrane domain facilitates its secretion and recovery, so TMEM95ΔTm was used to perform the pull-down assay. Expression plasmids [pcDNA3.1 (+)] were designed and constructed to encode mouse TMEM95 protein (UniProt P0DJF3) (GeneArt). A histidine tag (HHHHHH) was added to the C-terminus of TMEM95 and TMEM95ΔTm. In addition, a FLAG-tag (DYKDDDDK) was added in position 27-34 aa to both constructs. After verification by Sanger sequencing, Tmem95 and Tmem95ΔTm expression plasmids were amplified using Library Efficiency DH5αTM Competent cells (Thermo Fisher Scientific) and purified with a GenEluted Plasmid Kit. Chinese Hamster Ovary cells (CHO cells, the European Collection of Authenticated Cell Cultures (ECACC)) were grown (37°C, 5% CO_2, and 95% humidity) for 48–72 h to 80–90% confluence using an F-12 medium (Biowest) supplemented with 10% fetal bovine serum (Biowest) and 100 U/mL penicillin–streptomycin (Gibco). Transient transfections were performed with Lipotransfectina (Solmeglas), adding 4 µL of the reagent to a final volume of 200 µL Opti-MEM reduced-serum medium (Gibco) containing plasmids and incubated for 15 min at room temperature (RT). The complex was diluted by adding 2 ml Opti-MEM and overlaid on growing cells (37°C, 5% CO_2, and 95% humidity). The medium containing the secreted proteins was collected after 48 h, centrifuged at 4,000 g for 5 min at 4°C to remove cell debris, and concentrated in Vivaspin® Turbo 4 of 10,000 Da (Sartorius). A final volume of 200–300 µL of concentrated proteins was obtained in 20 mM sodium phosphate buffer, pH 7.4 with a protease inhibitor (EDTA-free EASYpack, Roche). A cell-growing medium containing concentrated proteins was separated by SDS-PAGE and transferred to PVDF membranes which were probed with the primary antibodies anti-Flag (Sigma F7425) and anti-TMEM95 (MyBioSource MBS7004333), both at 1:1,000 v/v in TBST 1X, 1% BSA, before visualization by chemiluminescence (Pierce ECL-Plus, Thermo Fisher Scientific).

2.1.1 Conjugation of Recombinant TMEM95ΔTm to Magnetic Beads

Magnetic Sepharose® beads (His Mag Sepharose Excel™; GE Healthcare) were homogenously resuspended and 20 µL of bead slurry was pipetted into a micro-centrifuge tube containing 500 µL of 20 mM sodium phosphate buffer, pH 7.4. The beads were washed with 500 µL of washing buffer (20 mM sodium phosphate, 0.5 M NaCl, 10 mM imidazole, pH 7.4) and finally in 500 µL of binding buffer (20 mM sodium phosphate, 0.5 M NaCl, 0.1% Tween-20, pH 7.4). Concentrated recombinant TMEM95ΔTm was incubated with washed magnetic beads (1: 1 v/v) overnight at 4°C with orbital agitation. After incubation, the beads coated with protein ($B_{TMEM95\Delta Tm}$) were washed twice with 20 mM sodium phosphate buffer (pH 7.4) to remove non-conjugated proteins. Then, they were resuspended in 20 mM sodium phosphate buffer pH 7.4 and solubilized under reducing conditions in 4X SDS sample buffer (Millipore, United States). After 10 min at 100°C, the supernatant was separated by SDS-PAGE, transferred to PVDF membranes, and probed with the anti-TMEM95 (MyBioSource, United States) as mentioned previously.

2.1.2 Pull-Down Assay

WT sperms were collected from cauda epididymis in PBS and centrifuged at 3,000 g for 7 min. Pellets were snap-frozen in liquid nitrogen and kept at −80°C until analysis. The sperm pellets were suspended in 400 µL of solubilization buffer (50 mM Tris-HCl pH 7.5, 1 mM EDTA, 1% Igepal, 0.1 mM PMSF, 10 mM iodoacetamide, 10 mM N-ethylmaleimide, phosphatase inhibitor, and protease inhibitor). The sample was centrifuged at 15,000 g for 30 min and the supernatant was co-incubated with unconjugated Sepharose® beads (B) or Sepharose® beads conjugated with TMEM95 recombinant protein as described previously ($B_{TMEM95\Delta Tm}$) at 4°C with orbital agitation overnight. After incubation, unconjugated or conjugated Sepharose® beads (B and $B_{TMEM95\Delta Tm}$) were recovered and non-specific proteins bound to B (B + sperm) or TMEM95-interacting proteins bound to $B_{TMEM95\Delta Tm}$ ($B_{TMEM95\Delta Tm+sperm}$) were eluted adding 50 µL of elution buffer (20 mM sodium phosphate, 0.5 M NaCl, 500 mM imidazole, pH 7.4) and incubated in agitation at 4°C for 1 h. This procedure was repeated three times obtaining a final volume of 150 µL. A control for bead conjugation was also included by eluting $B_{TMEM95\Delta Tm}$ beads, not incubated in the presence of sperm lysates ($B_{TMEM95\Delta Tm}$).

The eluted fractions (B + sperm, $B_{TMEM95\Delta Tm+sperm}$, and $B_{TMEM95\Delta Tm}$) were processed for proteomic analysis at a molecular biology service (SACE, University of Murcia, Spain). The protein identity was determined by mass spectrometry, carried out by using an HPLC/MS system composed of an Agilent 1290 Infinity II Series HPLC (Agilent Technologies) equipped with an automated multi-sampler module and a high speed binary pump, and connected to an Agilent 6550 Q-TOF Mass Spectrometer (Agilent Technologies, Santa Clara, CA, United States) using an Agilent Jet Stream Dual electrospray (AJS-Dual ESI) interface. Experimental parameters for HPLC and Q-TOF were set in MassHunter Workstation Data Acquisition software (Agilent Technologies, Rev. B.08.00). Data processing and analysis were performed using a Spectrum Mill MS Proteomics Workbench (Rev B.06.00.201, Agilent Technologies).

Proteins identified by mass spectrometry were listed for B, $B_{TMEM95\Delta Tm+sperm}$, and $B_{TMEM95\Delta Tm}$. A Venn diagram was used to detect sperm proteins that specifically interacted with recombinant TMEM95ΔTm (http://bioinformatics.psb.ugent.be/webtools/Venn). This list was curated to detect potential proteins involved in fertilization by applying two selection criteria: 1) absence of a fertile KO reported, based on the information of http://www.informatics.jax.org and 2) membrane localization, based on gene ontology information available in UniProt (cellular component).

2.1.3 Generation of *Olfr601* KO

All experimental procedures were approved by the INIA ACUC committee and Madrid Region Authorities (PROEX 040/17) in agreement with European legislation. sgRNA was designed against a sequence (ACAGAGCATGCGTGGCAATG) at the beginning of the coding region of *Olfr601* (NM_146314.2) using bioinformatics tools to minimize the chances of an off-target genome edition (https://crispr.mit.edu). sgRNA was synthesized and purified using a Guide-it sgRNA *In Vitro* Transcription Kit® (Takara). Capped polyadenylated Cas9 mRNA was generated by *in vitro* transcription (mMESSAGE mMACHINE T7 ULTRA kit®, Life Technologies) using as a template the plasmid pMJ920 (Addgene 42234) linearized with BbsI (NEB). mRNA was purified using a MEGAClear kit (Life Technologies).

C57CBAF1 female mice 7–8 weeks old were super-ovulated by intraperitoneal injections of 5 IU of pregnant mare serum gonadotropin (PMSG, Folligon®, MSD Animal Health) and an equivalent dose of human chorionic gonadotropin (hCG, Sigma) at a 48-h interval. The super-ovulated female mice were mated with C57CBAF1 stud males and zygotes were recovered from oviducts. Microinjections were performed with a micromanipulation system (Eppendorf TransferMan 4r and Femptojet 4i) equipped with a Leica DMi8 inverted microscope. A mixture of 150 ng/µL of Cas9 mRNA and 50 ng/µL of sgRNA was delivered into the cytoplasm of the zygotes (3–5 pL) using a filament needle (Bermejo-Álvarez et al., 2015).

After microinjection, the embryos were cultured in EmbryoMax® KSOM Mouse Embryo Media (Millipore) at 37°C under 5% CO_2 for 4 days until they reached the blastocyst stage and were transferred to a pseudo-pregnant Swiss recipient 2.5 days post-coitum (dpc). Genotyping was performed using primers spanning the target sequence (F: 5′-CACGAGCCCATGTTCCTCTT-3′, R: 5′-CACAGATGGCCA CATAGCGA-3′, 217 bp product in WT) under the following conditions: 95°C for 2 min; 35 × (94°C for 20 s, 60°C for 30 s, and 72°C for 30 s); 72°C for 5 min; hold at 8°C. The PCR products from F0 mice were purified using a FavorPrep™ PCR Purification Kit (Favorgen), cloned into pMD20 T-vectors (Takara) using Blunt TA ligase (NEB), and transformed into *Escherichia coli* DH5-α competent cells. A total of 10 positive plasmid clones from each transformation were purified (Favorgen) and Sanger-sequenced (Stabvida) to uncover the alleles generated after the CRISPR-mediated edition harbored by each individual. Following genotyping, a founder female carrying two KO alleles composed of 1 and 10 bp deletions was crossed with C57BL/6 WT males to obtain heterozygous mutants. Heterozygous F1 individuals carrying the 10 bp deletion were intercrossed to produce WT, Hz, or KO individuals used for the experiments (**Figure 2C**). Subsequent generations were genotyped by a quantitative PCR high-resolution melting (qPCR-HRM) curve analysis that allowed the detection of WT, Hz, and KO individuals. qPCRs were performed on a Mic qPCR cycler (BioMolecular Systems) with primers flanking the target sequence (F 5′-TGACCTGGTCCT CTCCACAT-3′, R 5′-AAGGCATGCGTCGAAGGTAA-3′, 88 bp product in WT, 78 bp on the KO allele). Reaction conditions were as follows: 40 × (94°C for 15 s, 56°C for 30 s, and 72°C for 20 s). Melting curves were visualized using Mic qPCR hardware (BioMolecular Systems) and contrasted with those obtained from known WT, Hz, and KO samples confirmed by Sanger sequencing.

2.1.4 RNA Analysis

Transcriptional analysis was performed as previously described. Briefly, total RNA was collected from testis, seminal vesicle, prostate, and epididymis samples (three samples/tissue) obtained from WT males using Trizol (Invitrogen). After DNAse treatment (Promega), RNA was retro-transcribed (qScript Quantabio) to cDNA. *Olfr601* and *Gapdh* transcripts were detected on cDNA by PCR using the amplification cycle described in genotyping. Primers to detect *Olfr601* were the same as those used for HRM-based genotyping (217 bp product). Primers used for *Gapdh* were F 5′-ACCCAGAAGACTGTG GATGG-3′ and R 5′-ATGCCTGCTTCACCACCTTC-3′ (247 bp). Primers used to detect the expression of other OLFRs are listed in **Supplementary Table S1**. DNAse-treated non-retro-transcribed RNA obtained from the testis served as a negative control for DNAse treatment and PCR.

2.1.5 Sperm Immunocytochemistry

Sperms from WT or KO individuals were recovered from the cauda epididymis in the HTF medium and incubated for 1 h at 37°C in a 5% CO2 water-saturated atmosphere. Following incubation, the sperms were centrifuged (3,000 g for 7 min), washed with PBS, fixed in 4% paraformaldehyde in PBS for 5 min, and washed twice in PBS. The samples were then permeabilized with 0.1% Triton X-100 in PBS and blocked with 5% FCS in PBS for 45 min at 4°C. Next, the samples were incubated with primary antibodies overnight at 4°C. The primary antibodies used were anti-OLFR601 (rabbit polyclonal custom-made, CliniSciences, 1:100), anti-TMEM95 antibody (rabbit polyclonal, MyBioSource, 1:100), and anti-IZUMO1 (mouse monoclonal KS139-34, a gift from Dr. Ikawa). After washing, the samples were incubated with secondary antibodies for 2 h at RT. The secondary antibodies used were donkey anti-rat IgG Alexa Fluor 647 and donkey anti-rabbit IgG Alexa Fluor 488 (1:500, Invitrogen). Finally, the samples were incubated for 5 min with 1 µg/ml lectin-PNA Alexa Fluor 568 (Invitrogen) and 1 µg/ml Hoechst 33342 (Sigma). They were then mounted and subsequently observed under an epifluorescence inverted microscope (Zeiss Axio Observer) equipped with structured illumination (Zeiss Apotome).

2.1.6 OLFR601 Immunoblotting

WT and KO sperms were collected from the cauda epididymis in PBS supplemented with 0.1% PVP and centrifuged at 3,000 g for 7 min. Pellets were snap-frozen in liquid nitrogen and kept at −80°C until analysis. The frozen pellets were re-suspended in Laemmli buffer (4X) and boiled for 10 min (lysis protocol #1) in a lysis buffer composed of 50 mM Tris HCl (pH8), 10 mM DTT, and 2% SDS boiled for 10 min with vigorous agitation (lysis protocol #2), in M-PERTM Mammalian Protein Extraction Reagent supplemented with HaltTM Protease Inhibitor Cocktail (100X) (Thermo Fisher Scientific) for 1 h at 4°C with vigorous agitation (lysis protocol #3) or RIPA buffer supplemented with HaltTM Protease Inhibitor Cocktail (100X) for 1 h at 4°C with vigorous agitation (lysis protocol #4). After incubation, the samples were centrifuged at 8,200 g for 10 min to discard cell debris. The supernatant containing sperm proteins was separated by SDS-PAGE and transferred to PVDF membranes which were probed with two custom polyclonal rabbit antibodies (anti-OLFR601-1 and anti-OLFR601-2, 1:1000 v/v in TBST 1X 1% BSA) before visualization by chemiluminescence (Pierce ECL-Plus, Thermo Fisher Scientific).

2.2 Fertility Tests

2.2.1 *In vivo* Fertilization Analysis

Initial fertility tests were performed on three males per genotype (WT, Hz, and KO) that were co-caged with WT 7–8 weeks old C57CBAF1 females (1:1 ratio). Mating was assessed by the presence of a copulatory plug and each male was allowed to mate twice. Twenty-one days after mating, the pups were counted to annotate the litter size. Statistical differences were analyzed by ANOVA–taking all six data/group and by performing a Wilcoxon rank-sum exact test–taking the average litter size of each male when data were not normal (Shapiro–Wilk test) or homoscedastic (Levene test) (SigmaStat package) and the level of significance was set at $p < 0.05$.

In vivo fertilization analysis was performed using WT and KO males and 7–8 week-old C57CBAF1 females. Female mice were super-ovulated as described previously and mated with WT or KO males (three individuals/group, two females/male tested). Embryos were recovered from the oviduct on 1.5 dpc and the cleavage rate was assessed upon recovery. Statistical differences were analyzed by ANOVA–taking all six data/group and by Wilcoxon rank-sum exact test–taking the average litter size of each male when data were not normal (Shapiro–Wilk test) or homoscedastic (Levene test) (SigmaStat package) and the level of significance was set at $p < 0.05$.

In vitro fertilization analysis was performed using WT and KO males and 7–8 week-old C57CBAF1 females**.** Sperms from WT or KO individuals (three individuals/group) were recovered from the cauda epididymis in an HTF medium and placed in the bottom of a previously equilibrated 300 µL drop of HTF covered with mineral oil for 2 h before IVF. After pre-incubation time, the upper 150 µL of the drop was collected and the spermatozoa concentration was analyzed. Cumulus-oocyte complexes (COCs) were recovered from the oviduct of super-ovulated female mice 14 h after hCG injection and placed in a 4-well dish with 400 µL of human tubal fluid (HTF) medium in groups of ~40 COCs per well. Previously prepared spermatozoa were immediately added to the well containing COCs at a final concentration of 10^6 spermatozoa/ml. After 4 h of co-incubation, presumptive zygotes were sequentially washed in an M2 and KSOM medium and cultured as described previously. A fusion assay was performed on the COCs collected as described (14 h after hCG injection) and the cumulus cells were removed by incubation in 300 µg/ml hyaluronidase solution in an M2 medium. Zona pellucida was removed by brief incubation in an acidic Tyrode's medium and zona-free mouse oocytes were pre-incubated in HTF with Hoechst 33342 1 µg/ml for 10 min and washed before sperm addition. After 30 min of gamete co-incubation (as mentioned previously), the oocytes were fixed in a 0.25% glutaraldehyde solution in PVS and observed under fluorescence microscopy. Statistical differences were analyzed

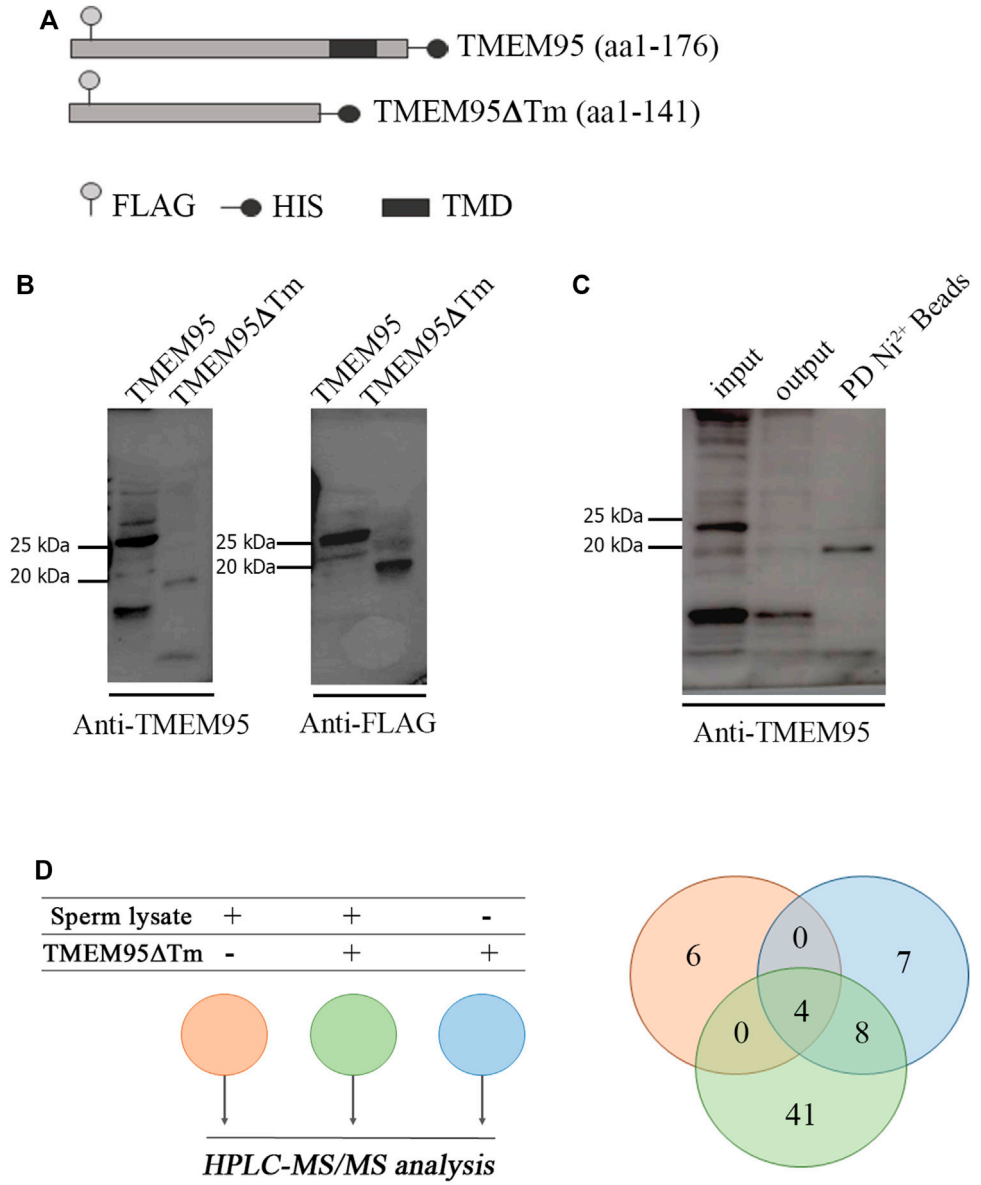

FIGURE 1 | Expression of recombinant TMEM95 and pull-down. **(A)** Schematic representation of recombinant TMEM95 proteins. FLAG sequence (), histidine tail (), and transmembrane domain () indicated. **(B)** Proteins were expressed in CHO cells, separated by SDS-PAGE and analyzed by Western blot. TMEM95 and TMEM95ΔTm were probed with anti-TMEM95 and anti-FLAG antibodies. **(C)** SDS-PAGE and Western blot of BTMEM95ΔTm. Input: medium with secreted TMEM95ΔTm before conjugation. Output: media after conjugation. IP:Ni+2 Beads: eluted fraction containing TMEM95ΔTm. **(D)** Venn diagram from the listed sperm proteins identified by HPLC-MS/MS analysis. Proteins from the sperm lysate that bind non-specifically to Sepharose® beads (pink), proteins eluted from BTMEM95ΔTm (blue), and specifically bound to TMEM95ΔTm (i.e., sperm proteins interacting with TMEM95, green, **Supplementary Table S1**).

by a Wilcoxon rank-sum exact test (SigmaStat package) and the level of significance was set at $p < 0.05$.

3 RESULTS

A pull-down assay performed on sperm lysates with beads conjugated with recombinant TMEM95 was used to uncover sperm proteins potentially interacting with TMEM95. Expression plasmids encoding TMEM95 and TMEM95ΔTm proteins (**Figure 1A**) were expressed in Chinese hamster ovary (CHO) cells and secreted proteins were successfully isolated. Each protein had the expected molecular mass. TMEM95-recombinant proteins showed a molecular weight of 25 kDa and TMEM95ΔTm (lacking the transmembrane domain) was 20 kDa on immunoblots probed with anti-Flag and anti-TMEM95 antibodies (**Figure 1B**). After incubation of beads with a medium containing secretions from transfected CHO cells, recombinant TMEM95ΔTm protein was successfully conjugated to beads (**Figure 1C**).

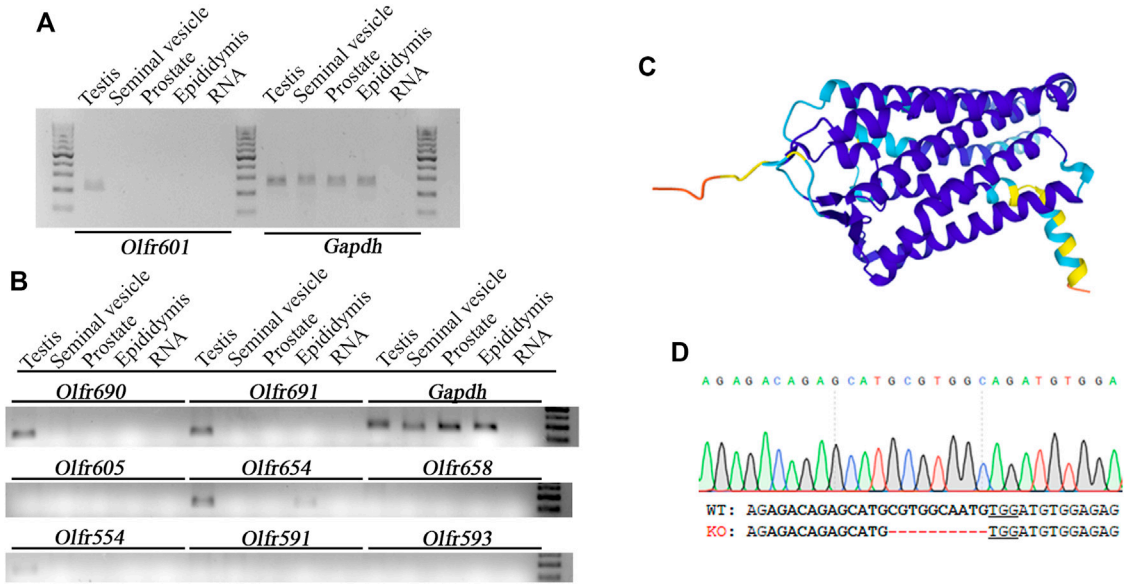

FIGURE 2 | Expression pattern, structure, and ablation details of OLFR601. **(A)** *Olfr601* mRNA is expressed exclusively in the testis (T), being undetectable in the seminal vesicles (s.v.), prostate (Pr), or epididymis (Ep). **(B)** mRNA expression of different olfactory receptors showing ~50–90 sequence identity with *Olfr601*. **(C)** OLFR601 shows a typical 3D structure of an olfactory receptor, being composed of seven helix and three unconnected beta strands according to the Alphafold model Uniprot (A2RS33). **(D)** Details of the deletion of 10 bp generated by CRISPR, selected as KO alleles to generate the mouse line. Lower letters indicate the DNA sequence for WT and KO alleles. Bold letters indicate the CRISPR target site and the PAM sequence is underlined.

The pull-down assay revealed a list of 41 sperm proteins identified by mass spectrometry (see Materials and Methods) seemingly interacting with TMEM95 (**Figure 1D**, **Supplementary Table S2**). These proteins cannot be deemed as *bona fide* TMEM95 interactors, as the pull-down assay is not completely reliable to identify interactors and requires further validation. The sperm proteins known to play relevant roles during fertilization (IZUMO1, SPACA6, SOF1, DCST1, and DCST2) were not present on that list. Nine of the proteins on the list were located on the membrane according to gene ontology information available in UniProt (Cellular Component): TRIP10, LIFR, IGHV5-16, GAPDH, OLFR601, CALCR, NID1, LRGUK, and EEF1A1. From this reduced list of nine proteins, two (CALCR and LRGUK) were reported to be localized to the acrosomal vesicle. Previous publications on KO models for these two proteins observed that *Calcr* ablation did not affect male reproductive function (Davey et al., 2008), whereas *Lrguk* ablation causes male infertility, as the protein is a major determinant of the microtubule structure within the male germline (Liu et al., 2015). TRIP10 (also known as CIP4) constitutes another interesting candidate involved in gamete fusion, as it is a Cdc-42 interacting protein involved in actin dynamics and podosome formation (Linder et al., 2000), and podosome-like structures have been involved in myoblast fusion (Sens et al., 2010). Unfortunately, *Trip10* ablation does not cause infertility in mice (Feng et al., 2010; Koduru et al., 2010) so its putative role in fertilization is unclear and could be masked by the redundant function of other genes. In this sense, after curation based on available KO models, only two of the membrane-localized sperm proteins potentially interacting with TMEM95 (IGHV5-16 and OLFR601) were not explored by gene ablation experiments before. IGHV5-16 belongs to a family of immunoglobulin heavy variables located in mouse chromosome 12 accounting for 216 genes plus other pseudogenes and 239 alleles, which makes its deletion technically challenging. In contrast, OLFR601 is a single copy gene encoding for an olfactory receptor with an unknown function. The gene does not have a direct human ortholog but shares a ~55% identity with human OR52M1, a similar percentage of identity to other proteins involved in fertilization such as IZUMO1 (**Supplementary Table S3**). Unfortunately, attempts to prove TMEM95-OLFR601 interaction by co-immunoprecipitation were unsuccessful because of the lack of a suitable antibody against OLFR601 for WB analysis (**Supplementary Figure S1**).

Olfr601 mRNA was present specifically in the testes, being absent in other male reproductive tissues such as the seminal vesicles, prostate, or epididymis (**Figure 2A**). The mRNA expression of other eight olfactory receptors displaying ~50–90% sequence identity with OLFR601 (**Supplementary Table S1**) was also assessed, showing that three of them (*Olfr690*, *Olfr691,* and *Olfr554*) were also exclusively expressed in the testis, whereas another (*Olfr654*) was expressed in the testis and epididymis (**Figure 2B**). The predicted tri-dimensional structure of OLFR601, obtained by AlphaFold (Varadi et al., 2021) was composed of seven transmembrane helices and three unconnected beta strands (**Figure 2C**), a typical structure from olfactory receptors displaying an affinity for diverse types of molecules. As such structures may drive OLFR601 affinity for an odorant, not necessarily a protein, present in the sperm or in

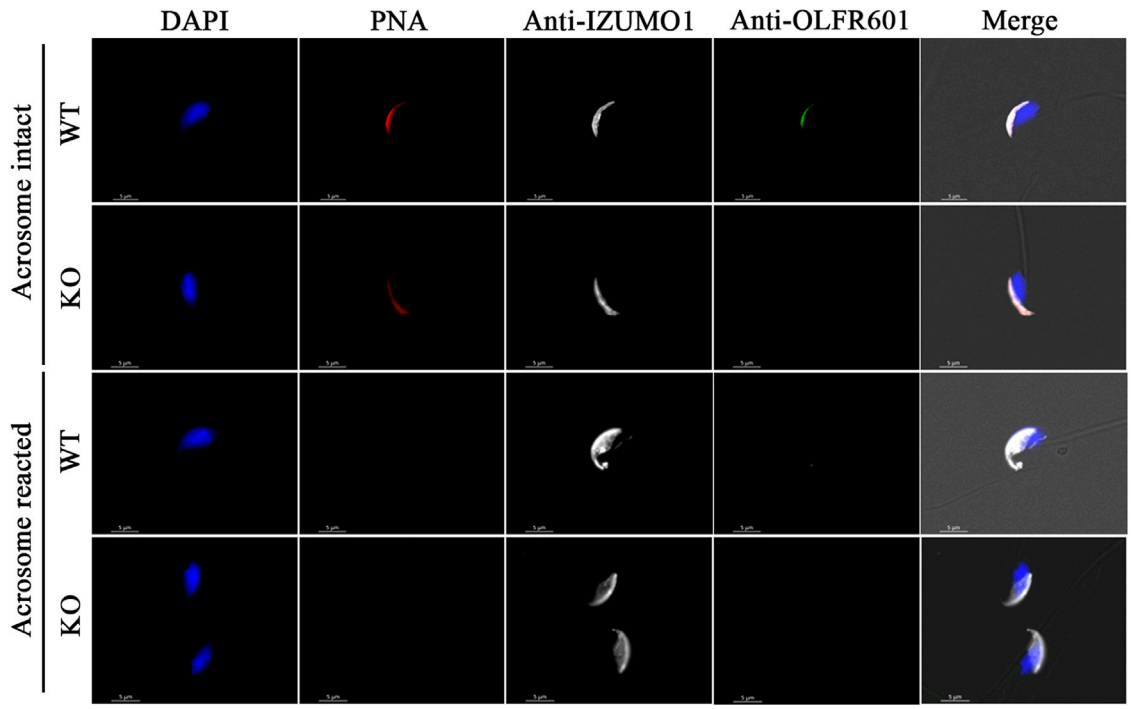

FIGURE 3 | Localization of OLFR601 and IZUMO1 in acrosome-intact or acrosome-reacted WT or *Olf601* KO sperm. Sperm nuclei were stained with DAPI (blue) and acrosomes by PNA staining (red). IZUMO1 (white) localization was not affected by *Olfr601* ablation. OLFR601 (green) localizes to the acrosomal region in acrosome-intact sperm, being undetectable in acrosome-reacted sperm. No OLFR601 protein was detected on KO sperms.

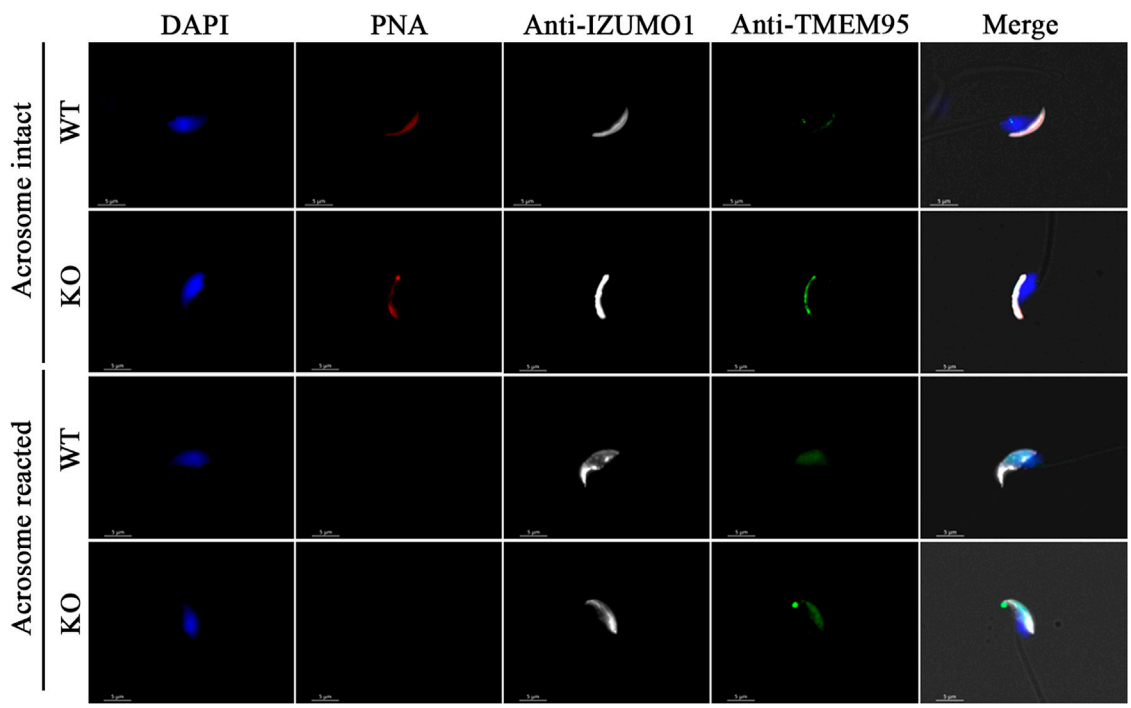

FIGURE 4 | Localization of IZUMO1 and TMEM95 in acrosome-intact or acrosome-reacted WT or *Olfr601* KO sperms. Sperm nuclei were stained with DAPI (blue) and acrosomes by PNA staining (red). The localization of IZUMO1 (white) and TMEM95 (green) was not affected by *Olfr601* ablation.

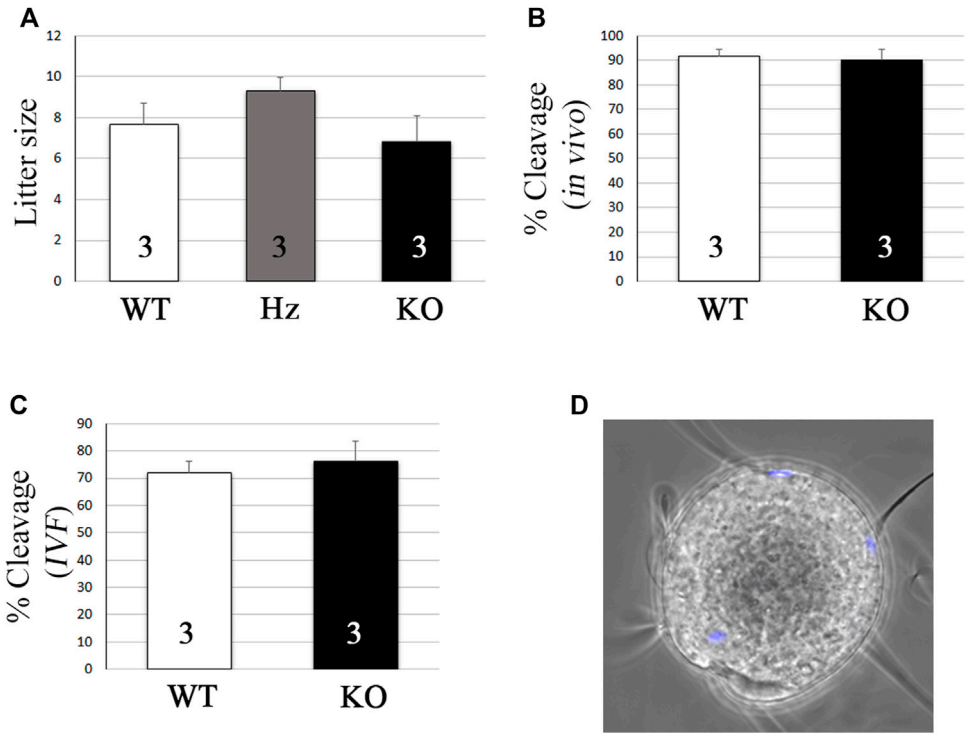

FIGURE 5 | *Olfr601* KO sperms are able to fertilize eggs. **(A)** Litter size after mating of WT or *Olfr601* KO males with WT females. Columns display mean ± s.e.m. Numbers within each column indicate the number of males tested. ANOVA $p > 0.05$. **(B)** *In vivo* fertilization rates after mating of WT or *Olfr601* KO males with super-ovulated WT females. Columns display mean ± s.e.m. Numbers within each column indicate the number of males tested. ANOVA $p > 0.05$. **(C)** *In vitro* fertilization rates following co-incubation of WT or *Olfr601* KO sperms and WT oocytes. Columns display mean ± s.e.m. Numbers within each column indicate the number of males tested. ANOVA $p > 0.05$. **(D)** Sperm-egg fusion assay. Sperm lacking OLFR601 fused with Hoechst pre-loaded zona-free eggs, which transferred the stain to them upon membrane fusion.

the oolemma, we sought to determine the role of this protein in fertilization by loss-of-function experiments.

Breeding of a mouse line harboring a KO allele composed of a 10 bp deletion that results in a 79-amino-acid-truncated peptide (**Figure 2D**) revealed no deviation from the Mendelian inheritance pattern, evidencing that OLFR601 plays no essential role during development. Protein ablation was confirmed by immunocytochemistry. OLFR601 was present in the acrosomal region of almost all (98/100) acrosome-intact WT sperms, becoming undetectable after the acrosome reaction (**Figure 3** and **Supplementary Figure S2**). As expected, no OLFR601 was detected in acrosome-intact or acrosome-reacted KO sperm. The disruption of OLFR601 did not alter IZUMO1 localization to the acrosomal region in acrosome-intact WT or KO sperm and to the head, including the equatorial segment, in acrosome-reacted WT or KO sperm. Similarly, sperms lacking OLFR601 did not show altered TMEM95 localization patterns, which localizes to the acrosomal region in acrosome-intact sperm and translocates to the head, including the equatorial segment, after the acrosome reaction in WT or KO sperms (**Figure 4**). The OLFR601 localization pattern was not affected in sperms lacking TMEM95 (Lamas-Toranzo et al., 2020) (**Supplementary Figure S3**).

KO individuals were overtly normal and KO males showed normal mating behavior and were able to father litters of a comparable size to their Hz or WT siblings (**Figure 5A**, 7.7 ± 1 vs. 9.3 ± 0.6 vs. 6.8 ± 1.3 pups, mean ± s.e.m. for WT, Hz, and KO, respectively). As expected, KO females were also fertile (data not shown). To further test if fertilization was impaired, *in vivo* and *in vitro* fertilization tests were performed to compare WT and KO sperms. *In vivo* fertilization rates using super-ovulated females were similar after mating with WT or KO males (**Figure 5B**, 91.6 ± 2.9 vs. 90.2 ± 4.2% cleavage, mean ± s.e.m. for WT and KO, respectively). Similarly, *in vitro* fertilization rates did not vary using WT or KO sperms (**Figure 5C**, 78 ± 13.3 vs. 71.8 ± 7% cleavage, mean ± s.e.m. for WT and KO, respectively). Finally, as expected based on the unaltered *in vivo* and *in vitro* fertility, OLFR601 KO sperms were able to fuse with zona-free eggs (**Figure 5D**).

4 DISCUSSION

Despite the recently enlarged list of known sperm proteins essential for fertilization, the understanding of the binding and fusion processes behind fertilization has not advanced

significantly since the discovery of JUNO (Bianchi et al., 2014), as IZUMO1:JUNO protein interaction remains the only known protein-to-protein interaction proven to be involved in mammalian fertilization. Given that IZUMO1 is involved in gamete binding through its interaction with JUNO (Bianchi et al., 2014) and that none of the other sperm proteins seems to play an essential role in gamete binding (Fujihara et al., 2020; Lamas-Toranzo et al., 2020; Noda et al., 2020; Inoue et al., 2021), the specific roles in fertilization of the other sperm proteins seemingly take place on post-binding events. However, cell fusion assays combining TMEM95, SPACA6, SOF1, IZUMO1, and JUNO found that they are not sufficient to induce cell fusion (Lamas-Toranzo et al., 2020; Noda et al., 2020), suggesting that other unknown proteins or molecules are required for membrane fusion. In this perspective, exploring the relations between these and other sperm proteins could uncover protein complexes directly or indirectly required for gamete fusion. The list of sperm proteins potentially interacting with TMEM95 based on the pull-down assay did not include IZUMO1, SPACA6, FIMP, SOF1, DCST1, or DCST2, that is, the sperm proteins known to be involved in fertilization. While the location of some of these proteins remains unknown, IZUMO1 and SPACA6 are present in similar sperm regions to TMEM95 before and after the acrosome reaction, and also share a similar predicted structure, thereby allowing possible interactions that may have not been detected by the pull-down assay. However, IZUMO1 localization is not affected by *Tmem95* ablation (Lamas-Toranzo et al., 2020), whereas, although *Spaca6* ablation does not alter IZUMO1 localization either (Noda et al., 2020), no SPACA6 protein can be detected after *Izumo1*, *Dcst1,* or *Dcst2* ablation (Inoue et al., 2021). These findings suggest that while SPACA6, IZUMO1, DCST1, and DCST2 roles are seemingly related, TMEM95 may play a role not directly related to the other sperm proteins known to be required for fertilization.

Although the list of sperm proteins pulled down with TMEM95 included diverse cytosolic and nuclear proteins, probably resulting from non-specific binding due to the low salt conditions (see Material and Methods), two of the proteins potentially interacting with TMEM95 -CALCR and LRGUK- were previously known to localize to the acrosomal region, a localization pattern compatible with a role in fertilization. The ablation of CALCR did not affect male fertility (Davey et al., 2008), proving that it does not play an essential role in fertilization. In contrast, LRGUK plays an essential role in the basal body and manchette function during spermatogenesis (Liu et al., 2015). As LRGUK is involved in sperm morphology re-modeling, it may play a role in re-modeling events occurring after gamete binding, however, exploring such a possibility would require dedicated investigation, as the altered morphology of *Lrguk* KO sperms prevents fertilization before membrane binding. Other than these two acrosomal proteins, OLFR601 was the most promising candidate to be involved in fertilization as, although the protein was not detected after the acrosome reaction, its acrosomal localization in acrosome-intact sperm coincides with TMEM95, IZUMO1, SPACA6, and FIMP.

OLFR601 displays a typical structure of an olfactory receptor, often associated with an affinity for specific molecules (odorant), not necessarily proteins. The possible involvement of odorants in fertilization may open a novel interesting perspective to uncover unknown molecules required for the process. Given that OLFR601 is lost after the acrosome reaction, its putative intervention and that of its interacting odorant during gamete fusion can only be indirect, maybe mediating the formation of complexes of proteins required for gamete fusion. However, as OLFR601 disruption does not affect any step of fertilization, it may either or not play any role in the process or play a redundant function with other receptors. In agreement with the latter possibility, the other three olfactory receptors sharing ~50% sequence identity with OLFR601 were also exclusively expressed in the testis. Olfactory receptors are known to be expressed in organs and tissues outside the olfactory epithelium, including the testes (Parmentier et al., 1992), which are the richest olfactory receptor-expressing tissues excluding the olfactory epithelium (Massberg and Hatt, 2018). Up to 91 olfactory receptors have been reported to be expressed in human and mouce sperm (Flegel et al., 2015) and several have been found to play roles in chemotaxis. In human sperm, the olfactory receptor OR1D2 localizes to the mid-piece and plays a role in sperm chemotaxis (Spehr et al., 2003). Mouse OR267-12 (OLFR16) has also been suggested to play a role in sperm chemotaxis (Fukuda et al., 2004) and OR7A5 and OR4D1 have been suggested to influence sperm motility (Veitinger et al., 2011). In any case, although the absence of an infertility phenotype following *Olfr601* ablation proves that it is not essential for fertilization, it does not exclude that the ablation may have caused some subtle alterations in the sperm that could be detected by a deeper functional analysis.

In conclusion, the ablation of the olfactory receptor OLFR601 does not disrupt fertilization, suggesting that it either does not play a role in fertilization or it plays an indirect role in gamete fusion which may be redundant with that of other proteins.

DATA AVAILABILITY STATEMENT

The original contributions presented in the study are included in the article/**Supplementary Material**; further inquiries can be directed to the corresponding authors.

ETHICS STATEMENT

All experimental procedures were approved by the Animal Care and Use Committee "Comité de experimentación Animal" from the Spanish National Institute of Agriculture Research (INIA) and Madrid Region authorities under the reference PROEX 040/17.

AUTHOR CONTRIBUTIONS

B-AP and J-MM conceived the project. HJ and J-MM designed and expressed recombinant TMEM95 proteins. HJ, J-MM, L-TI,

and B-AP were involved in pull-down experiments. G-BL and HJ performed the protein structure analysis and WB. L-TI and B-AP performed the RNA analysis. B-AP generated *Olfr601* KO. G-BL and B-AP performed the fertility tests.

FUNDING

This work was supported by the projects AGL 2017-84908-R and PID 2020-117501RB-I00 to B-AP and PID 2020-114109GB-I00 to J-MM, funded by the Spanish Ministry of Science and Innovation and FEDER funds from the European Union.

ACKNOWLEDGMENTS

The authors thank Alejandro Torrecillas Sánchez from the Molecular Biology Service (ACTI, University of Murcia, Spain) for his technical assistance and advice.

SUPPLEMENTARY MATERIAL

The Supplementary Material for this article can be found online at: https://www.frontiersin.org/articles/10.3389/fcell.2022.854115/full#supplementary-material

Supplementary Figure S1 | Attempts to detect the OLFR601 protein on the SDS-page were unsuccessful after different lysis protocols using two custom-made antibodies. OLFR601-1 is the antibody showing specific staining in ICC (**Figure 3** and **Supplementary Figure S2**).

Supplementary Figure S2 | Representative pictures of multiple acrosome-intact (PNA+) WT sperm showing consistent acrosome localization of both IZUMO1 and OLFR601. PNA-sperm loss OLFR601 while maintaining IZUMO1.

Supplementary Figure S3 | Representative pictures of acrosome-intact (PNA+) or acrosome-reacted (PNA-) *Tmem95* KO sperm. Sperms lacking TMEM95 show normal localization of OLFR601. OLFR601 localizes to the acrosomal region before the acrosome reaction and it is not detected after acrosome reaction.

Supplementary Table S1 | Details for primers used to amplify transcripts from olfactory receptors showing ~50–90 protein identity with OLFR601.

Supplementary Table S2 | Sperm proteins potentially interacting with TMEM95 according to the pull-down assay.

REFERENCES

Barbaux, S., Ialy-Radio, C., Chalbi, M., Dybal, E., Homps-Legrand, M., Do Cruzeiro, M., et al. (2020). Sperm SPACA6 Protein Is Required for Mammalian Sperm-Egg Adhesion/Fusion. *Sci. Rep.* 10 (1), 5335. Epub 2020/03/27Cited in: Pubmed; PMID 32210282. doi:10.1038/s41598-020-62091-y

Bermejo-Álvarez, P., Ramos-Ibeas, P., Park, K. E., Powell, A. P., Vansandt, L., Derek, B., et al. (2015). Tet-mediated Imprinting Erasure in H19 Locus Following Reprogramming of Spermatogonial Stem Cells to Induced Pluripotent Stem Cells. *Sci. Rep.* 5, 13691. Epub 2015/09/04[pii]. Cited in: Pubmed; PMID 26328763. doi:10.1038/srep13691srep13691

Bianchi, E., Doe, B., Goulding, D., and Wright, G. J. (2014). Juno Is the Egg Izumo Receptor and Is Essential for Mammalian Fertilization. *Nature* 508 (7497), 483–487. eng. Epub 2014/04/18[pii]. Cited in: Pubmed; PMID 24739963. doi:10.1038/nature13203nature13203

Davey, R. A., Turner, A. G., McManus, J. F., Chiu, W. M., Tjahyono, F., Moore, A. J., et al. (2008). Calcitonin Receptor Plays a Physiological Role to Protect against Hypercalcemia in Mice. *J. Bone Min. Res.* 23 (8), 1182–1193. Epub 2008/07/17. doi:10.1359/jbmr.080310

Feng, Y., Hartig, S. M., Bechill, J. E., Blanchard, E. G., Caudell, E., and Corey, S. J. (2010). The Cdc42-Interacting Protein-4 (CIP4) Gene Knock-Out Mouse Reveals Delayed and Decreased Endocytosis. *J. Biol. Chem.* 285 (7), 4348–4354. Cited in: Pubmed; PMID WOS:000275274800011. doi:10.1074/jbc.M109.041038

Fernandez-Fuertes, B., Laguna-Barraza, R., Fernandez-Gonzalez, R., Gutierrez-Adan, A., Blanco-Fernandez, A., O'Doherty, A. M., et al. (2017). Subfertility in Bulls Carrying a Nonsense Mutation in Transmembrane Protein 95 Is Due to Failure to Interact with the Oocyte Vestments†. *Biol. Reproduction* 97 (1), 50–60. eng. Epub 2017/09/02[pii]. Cited in: Pubmed; PMID 28859280. doi:10.1093/biolre/iox0653903015

Flegel, C., Vogel, F., Hofreuter, A., Schreiner, B. S. P., Osthold, S., Veitinger, S., et al. (2015). Characterization of the Olfactory Receptors Expressed in Human Spermatozoa. *Front. Mol. Biosci.* 2, 73. Epub 2016/01/19. doi:10.3389/fmolb.2015.00073

Fujihara, Y., Lu, Y., Noda, T., Oji, A., Larasati, T., Kojima-Kita, K., et al. (2020). Spermatozoa Lacking Fertilization Influencing Membrane Protein (FIMP) Fail to Fuse with Oocytes in Mice. *Proc. Natl. Acad. Sci. U.S.A.* 117 (17), 9393–9400. Epub 2020/04/17. doi:10.1073/pnas.1917060117

Fukuda, N., Yomogida, K., Okabe, M., and Touhara, K. (2004). Functional Characterization of a Mouse Testicular Olfactory Receptor and its Role in Chemosensing and in Regulation of Sperm Motility. *J. Cell Sci.* 117 (Pt 24), 5835–5845. Epub 2004/11/04. doi:10.1242/jcs.01507

Inoue, N., Hagihara, Y., and Wada, I. (2021). Evolutionarily Conserved Sperm Factors, DCST1 and DCST2, Are Required for Gamete Fusion. *Elife* 10, 10. Epub 2021/04/20. doi:10.7554/eLife.66313

Inoue, N., Ikawa, M., Isotani, A., and Okabe, M. (2005). The Immunoglobulin Superfamily Protein Izumo Is Required for Sperm to Fuse with Eggs. *Nature* 434 (7030), 234–238. eng. Epub 2005/03/11ature03362 [pii] 10.1038/nature03362. Cited in: Pubmed; PMID 15759005. doi:10.1038/nature03362

Kaji, K., Oda, S., Shikano, T., Ohnuki, T., Uematsu, Y., Sakagami, J., et al. (2000). The Gamete Fusion Process Is Defective in Eggs of Cd9-Deficient Mice. *Nat. Genet.* 24 (3), 279–282. eng. Epub 2000/03/04. doi:10.1038/73502

Koduru, S., Kumar, L., Massaad, M. J., Ramesh, N., Le Bras, S., Ozcan, E., et al. (2010). Cdc42 Interacting Protein 4 (CIP4) Is Essential for Integrin-dependent T-Cell Trafficking. *Proc. Natl. Acad. Sci. U.S.A.* 107 (37), 16252–16256. Cited in: Pubmed; PMID WOS:000281799000051. doi:10.1073/pnas.1002747107

Lamas-Toranzo, I., Hamze, J. G., Bianchi, E., Fernández-Fuertes, B., Pérez-Cerezales, S., Laguna-Barraza, R., et al. (2020). TMEM95 Is a Sperm Membrane Protein Essential for Mammalian Fertilization. *Elife* 9, 9. Epub 2020/06/03. doi:10.7554/eLife.53913

Le Naour, F., Rubinstein, E., Jasmin, C., Prenant, M., and Boucheix, C. (2000). Severely Reduced Female Fertility in CD9-Deficient Mice. *Science* 287 (5451), 319–321. eng. Epub 2000/]. Cited in: Pubmed; PMID 10634790. doi:10.1126/science.287.5451.319

Linder, S., Hufner, K., Wintergerst, U., and Aepfelbacher, M. (2000). Microtubule-dependent Formation of Podosomal Adhesion Structures in Primary Human Macrophages. *J. Cell Sci.* 113 (23), 4165–4176. Cited in: Pubmed; PMID WOS:000165975300005. doi:10.1242/jcs.113.23.4165

Liu, Y., DeBoer, K., de Kretser, D. M., O'Donnell, L., O'Connor, A. E., Merriner, D. J., et al. (2015). LRGUK-1 Is Required for Basal Body and Manchette Function during Spermatogenesis and Male Fertility. *PLoS Genet.* 11 (3), e1005090. Epub 2015/03/18. doi:10.1371/journal.pgen.1005090

Lorenzetti, D., Poirier, C., Zhao, M., Overbeek, P. A., Harrison, W., and Bishop, C. E. (2014). A Transgenic Insertion on Mouse Chromosome 17 Inactivates a Novel Immunoglobulin Superfamily Gene Potentially Involved in Sperm-Egg Fusion. *Mamm. Genome* 25 (3-4), 141–148. eng. Epub 2013/11/28Cited in: Pubmed; PMID 24275887. doi:10.1007/s00335-013-9491-x

Massberg, D., and Hatt, H. (2018). Human Olfactory Receptors: Novel Cellular Functions outside of the Nose. *Physiol. Rev.* 98 (3), 1739–1763. Epub 2018/06/14. doi:10.1152/physrev.00013.2017

Miyado, K., Yamada, G., Yamada, S., Hasuwa, H., Nakamura, Y., Ryu, F., et al. (2000). Requirement of CD9 on the Egg Plasma Membrane for Fertilization. *Science* 287 (5451), 321–324. eng. Epub 2000/01/[pii]. Cited in: Pubmed; PMID 10634791. doi:10.1126/science.287.5451.321

Noda, T., Lu, Y., Fujihara, Y., Oura, S., Koyano, T., Kobayashi, S., et al. (2020). Sperm Proteins SOF1, TMEM95, and SPACA6 Are Required for Sperm–oocyte Fusion in Mice. *Proc. Natl. Acad. Sci. U.S.A.* 117, 11493–11502. Epub 2020/05/13. doi:10.1073/pnas.1922650117

Parmentier, M., Libert, F., Schurmans, S., Schiffmann, S., Lefort, A., Eggerickx, D., et al. (1992). Expression of Members of the Putative Olfactory Receptor Gene Family in Mammalian Germ Cells. *Nature* 355 (6359), 453–455. Epub 1992/01/30. doi:10.1038/355453a0

Pausch, H., Kölle, S., Wurmser, C., Schwarzenbacher, H., Emmerling, R., Jansen, S., et al. (2014). A Nonsense Mutation in TMEM95 Encoding a Nondescript Transmembrane Protein Causes Idiopathic Male Subfertility in Cattle. *PLoS Genet.* 10 (1), e1004044. eng. [pii]. Cited in: Pubmed; PMID 24391514. doi:10.1371/journal.pgen.1004044PGENETICS-D-13-02072

Satouh, Y., Inoue, N., Ikawa, M., and Okabe, M. (2012). Visualization of the Moment of Mouse Sperm-Egg Fusion and Dynamic Localization of IZUMO1. *J. Cell Sci.* 125 (Pt 21), 4985–4990. eng. Epub 2012/09/05[pii]. Cited in: Pubmed; PMID 22946049. doi:10.1242/jcs.100867jcs.100867

Sens, K. L., Zhang, S., Jin, P., Duan, R., Zhang, G., Luo, F., et al. (2010). An Invasive Podosome-like Structure Promotes Fusion Pore Formation during Myoblast Fusion. *J. Cell Biol.* 191 (5), 1013–1027. Cited in: Pubmed; PMID WOS: 000284985100013. doi:10.1083/jcb.201006006

Spehr, M., Gisselmann, G., Poplawski, A., Riffell, J. A., Wetzel, C. H., Zimmer, R. K., et al. (2003). Identification of a Testicular Odorant Receptor Mediating Human Sperm Chemotaxis. *Science* 299 (5615), 2054–2058. Epub 2003/03/29. doi:10.1126/science.1080376

Varadi, M., Anyango, S., Deshpande, M., Nair, S., Natassia, C., Yordanova, G., et al. (2021). AlphaFold Protein Structure Database: Massively Expanding the Structural Coverage of Protein-Sequence Space with High-Accuracy Models. *Nucleic Acids Res.* 50, D439–D444. Epub 2021/11/19. doi:10.1093/nar/gkab1061

Veitinger, T., Riffell, J. R., Veitinger, S., Nascimento, J. M., Triller, A., Chandsawangbhuwana, C., et al. (2011). Chemosensory Ca2+ Dynamics Correlate with Diverse Behavioral Phenotypes in Human Sperm. *J. Biol. Chem.* 286 (19), 17311–17325. Epub 2011/04/02. doi:10.1074/jbc.M110.211524

Conflict of Interest: The authors declare that the research was conducted in the absence of any commercial or financial relationships that could be construed as a potential conflict of interest.

Publisher's Note: All claims expressed in this article are solely those of the authors and do not necessarily represent those of their affiliated organizations, or those of the publisher, the editors, and the reviewers. Any product that may be evaluated in this article, or claim that may be made by its manufacturer, is not guaranteed or endorsed by the publisher.

Advantages of publishing in Frontiers

OPEN ACCESS
Articles are free to read for greatest visibility and readership

FAST PUBLICATION
Around 90 days from submission to decision

HIGH QUALITY PEER-REVIEW
Rigorous, collaborative, and constructive peer-review

TRANSPARENT PEER-REVIEW
Editors and reviewers acknowledged by name on published articles

Frontiers
Avenue du Tribunal-Fédéral 34
1005 Lausanne | Switzerland

Visit us: www.frontiersin.org
Contact us: frontiersin.org/about/contact

REPRODUCIBILITY OF RESEARCH
Support open data and methods to enhance research reproducibility

DIGITAL PUBLISHING
Articles designed for optimal readership across devices

FOLLOW US
@frontiersin

IMPACT METRICS
Advanced article metrics track visibility across digital media

EXTENSIVE PROMOTION
Marketing and promotion of impactful research

LOOP RESEARCH NETWORK
Our network increases your article's readership